Loughborough University

This item was submitted to Loughborough University as a PhD thesis by the author and is made available in the Institutional Repository (https://dspace.lboro.ac.uk/) under the following Creative Commons Licence conditions.

creative commons

COMMONS DEED

Attribution-NonCommercial-NoDerivs 2.5

You are free:

- to copy, distribute, display, and perform the work

Under the following conditions:

Attribution. You must attribute the work in the manner specified by the author or licensor.

Noncommercial. You may not use this work for commercial purposes.

No Derivative Works. You may not alter, transform, or build upon this work.

- For any reuse or distribution, you must make clear to others the license terms of this work.
- Any of these conditions can be waived if you get permission from the copyright holder.

Your fair use and other rights are in no way affected by the above.

This is a human-readable summary of the Legal Code (the full license).

Disclaimer

For the full text of this licence, please go to:
http://creativecommons.org/licenses/by-nc-nd/2.5/

BLLID No:- D46583/83

LOUGHBOROUGH
UNIVERSITY OF TECHNOLOGY
LIBRARY

AUTHOR/FILING TITLE

RICHMOND, K M

ACCESSION/COPY NO.

001034/02

VOL. NO.

CLASS MARK

LOAN COPY

date due:-

24 DEC 1986

LOAN 1 MTH + 2
UNLESS RECALLED
BATH UNIV.

-6 JUL 1990

-3 JUL 1992

-2 JUL 1993

18 MAR 1993

26 JUN 1998

-6 JUL 1995

-5 JUL 1985

-4 JUL 1986

-1 JUL 1988

30 JUN 1989

-3 JUL 1987

-8 DEC 1989

000 1034 02

The Characterization and Mechanical Properties of a Series of Fibrous Hybrid Composites

by

Kathryn Richmond B.Sc

A Doctoral Thesis submitted in partial fulfilment of the requirements for the award of Doctor of Philosophy of the Loughborough University of Technology

1983

Supervisor: Dr. M.O.W. Richardson, Department of Materials Engineering and Design

© by Kathryn Richmond, 1983.

Loughborough University
of Technology Library
June 83
Class
Acc. No. 001034/02

SYNOPSIS

Relevant literature on plain and hybrid unidirectional fibrous composites is critically reviewed and the difficulty of assessing previous work due to insufficient data is emphasized.

A systematically varied series of hybrid composites based on vinyl ester resin and unidirectional carbon and E-glass fibre reinforcements is studied and the constituent materials characterized. Particular attention is given to the effect of total and relative fibre volume fractions, geometrical arrangements and fibre surface treatments on the tensile characteristics and interlaminar shear strength of the composites.

Certain hybrid tensile specimens exhibited what is termed a 'hybrid effect', their first failure strain being greater than the expected failure strain of the parent carbon composites. This is discussed in terms of the data and information obtained from the tensile and interlaminar shear strength tests and from a study of the tensile fracture surfaces. Theoretical models for the tensile failure of hybrid composites are critically examined. The tensile fracture mode and the importance of the statistical nature of fibre tensile strength are discussed. Modifications are made to existing statistical failure theory which result in two equations for the ratio of the lower bound on hybrid composite first tensile failure strain to that on the tensile failure strain of the lower elongation fibre parent composite. Comparison between the two equations enables the prediction of the composite failure mode. Where appropriate the theories are applied to the experimental results. Factors controlling the initial failure strain are shown to be the relative volume fractions and statistical characteristics of the two fibre types, the fibre ineffective length and the stress concentrations acting on fibres adjacent to a failed fibre.

ACKNOWLEDGEMENTS.

The author expresses her thanks and gratitude to the following:

Professor I. A. Menzies of the Department of Materials Engineering and Design for the use of laboratory and research facilities;

Dr. M.O.W. Richardson, my supervisor, for guidance and encouragement;

fellow post-graduates in Materials Engineering and Design for helpful discussions;

the technical staff of Materials Engineering and Design and the Institute of Polymer Technology for their practical assistance;

the S.E.R.C. and L.U.T. for the provision of funds;

Mrs. A. Godino for her care and attention in typing this thesis, and,

Arthur Richmond for his patience, understanding and encouragement.

CONTENTS

LIST OF SYMBOLS AND ABBREVIATIONS

1.		INTRODUCTION	1
2.		LITERATURE REVIEW	3
2.1		Tensile Failure of Single Fibre Type Unidirectional Composites.	3
2.2		Tensile Failure of Unidirectional Fibre Hybrid Composites.	22
2.3		The Interfacial/Interphasial Region in Fibrous Composites.	37
2.4		Fibre Surface Treatments.	40
2.5		Composite Constituent Materials.	43
	2.5.1	Carbon and E-Glass Reinforcement Fibres.	43
	2.5.2	Vinyl Ester Resin Matrix.	45
2.6		Factors Affecting the Quality and Comparison of Composite Materials.	47
3.		EXPERIMENTAL PROCEDURE	49
3.1		Choice of Composite System.	50
3.2		Characterization of the Reinforcement Fibres.	51
	3.2.1	Fibre Diameter and Cross-Sectional Area.	52
	3.2.2	Fibre Density.	52
	3.2.3	Fibre Tensile Strength.	52
3.3		Characterization of the Resin Matrix.	54
	3.3.1	The Curing System	54
	3.3.2	Fabrication of Resin Slabs.	55
	3.3.3	Resin Density.	56
	3.3.4	Resin Shear Modulus.	56
	3.3.5	Resin Tensile Strength.	57
3.4		Fibre Surface Treatment.	58
	3.4.1	Fibre Size Content.	59
	3.4.2	Carbon Fibre Surface Treatment.	59
	3.4.3	E-Glass Fibre Surface Treatment.	60
3.5		Fabrication of the Unidirectional Composite Slabs.	62

3.6		Quality Control of the Composite Slabs.	63
3.7		Determination of Composite Interlaminar Shear Strength.	65
3.8		Composite Shear Modulus.	66
3.9		Determination of Composite Longitudinal Tensile Properties.	67
4.		RESULTS AND DISCUSSION	69
4.1		Unidirectional Woven Tapes and Composite Fibre Contents.	71
4.2		Reinforcement Fibre Properties.	72
	4.2.1	Fibre Diameter and Cross-Sectional Area.	73
	4.2.2	Fibre Density.	73
	4.2.3	Fibre Tensile Strength.	74
4.3		Properties of the Derakane 411-45 Vinyl Ester Resin.	77
	4.3.1	The Optimum Curing System for the Resin.	77
	4.3.2	Resin Density.	78
	4.3.3	Resin and E-Glass Composite Shear Modulus.	79
	4.3.4	Resin Tensile Strength.	80
4.4		Fibre Surface Treatment.	81
	4.4.1	Fibre Size Content.	81
	4.4.2	Carbon Fibre Surface Treatments.	82
	4.4.3	E-Glass Fibre Surface Treatments.	83
4.5		Quality Control of the Composite Slabs.	85
4.6		Composite Interlaminar Shear Strength.	87
4.7		Tensile Results of the Parent Composites.	91
	4.7.1	Tensile Properties of the Carbon Fibre Composites of Slabs 1 to 7.	93
	4.7.1.1	The Fracture Surfaces of the Carbon Fibre Composite Tensile Specimens.	93
	4.7.1.2	The Tensile Stress v Strain Curves of the Carbon Fibre Composite Specimens.	93
	4.7.1.3	Comparison of the Experimental and Theoretical Tensile Properties of the Carbon Fibre Composites.	96
	4.7.1.4	Summary of the Tensile Properties of the Carbon Fibre Composites of Slabs 1 to 7.	110
	4.7.2	Tensile Properties of the 600 tex E-Glass Fibre Composites of Slabs 8 to 16.	111

4.7.2.1	The Fracture Surfaces of the 600 tex E-Glass Fibre Composite Tensile Specimens.	111
4.7.2.2	The Tensile Stress v Strain Curves of the 600 tex E-Glass Fibre Composite Specimens.	114
4.7.2.3	Comparison of the Experimental and Theoretical Tensile Properties of the 600 tex E-Glass Fibre Composites.	117
4.7.2.4	Summary of the Tensile Properties of the 600 tex E-Glass Fibre Composites of Slabs 8 to 16.	121
4.7.3	Tensile Properties of the 500 tex E-Glass Fibre Composites of Slabs 17 to 23.	122
4.7.3.1	The Fracture Surfaces of the 500 tex E-Glass Fibre Composite Tensile Specimens.	123
4.7.3.2	The Tensile Stress v Strain Curves of the 500 tex E-Glass Fibre Composite Specimens.	123
4.7.3.3	Comparison of the Experimental and Theoretical Tensile Properties of the 500 tex E-Glass Fibre Composites.	126
4.7.3.4	Summary of the Tensile Properties of the 500 tex E-Glass Fibre Composites of Slabs 17 to 23.	129
4.8	Tensile Results of the Hybrid Composites.	131
4.8.1	Tensile Properties of the 3:1 Tape Hybrid Composites of Slabs 24 to 29.	132
4.8.1.1	The Fracture Surfaces of the 3:1 Tape Hybrid Composite Tensile Specimens.	132
4.8.1.2	The Tensile Stress v Strain Curves of the 3:1 Tape Hybrid Composite Specimens.	133
4.8.2	Tensile Properties of the 1:1 Tape Hybrid Composites of Slabs 30 to 36.	135
4.8.2.1	The Fracture Surfaces of the 1:1 Tape Hybrid Composite Tensile Specimens.	135
4.8.2.2	The Tensile Stress v Strain Curves of the 1:1 Tape Hybrid Composite Specimens.	136
4.8.3	Tensile Properties of the Hybrid Composites of Slabs 37 to 47.	138

4.8.3.1	The Fracture Surfaces of the Hybrid Composite Tensile Specimens from Slabs 37 to 47.	138
4.8.3.2	The Tensile Stress v Strain Curves of the Hybrid Composite Specimens from Slabs 37 to 47.	139
4.8.4	Tensile Properties of the Hybrid Composites of Slabs 46 to 61.	140
4.8.4.1	The Fracture Surfaces of the Hybrid Composite Tensile Specimens from Slabs 46 to 61.	141
4.8.4.2	The Tensile Stress v Strain Curves of the Hybrid Composite Specimens from Slabs 46 to 61.	142
4.8.5	General Points Concerning the Tensile Properties and the Stress v Strain Curves of the Hybrid Composites of Slabs 37 to 61.	143
4.8.6	V_T and the Hybrid Effect.	144
4.8.7	Fibre Geometrical Arrangement and the Hybrid Effect.	145
4.8.8	Ratio of V_g/V_{cf} and the Hybrid Effect.	149
4.8.9	The Hybrid Composite System and the Hybrid Effect	152
4.8.10	Theoretical Carbon/E-Glass/Vinyl Ester Hybrid Composite Failure Process.	156
4.8.10.1	Theoretical Effect of V_T	162
4.8.10.2	Theoretical Effect of Fibre Geometrical Arrangement.	162
4.8.10.3	The Effect of V_g/V_{cf}	165
4.8.10.4	The Effect of the Hybrid Composite System.	167
4.8.11	Quantitative Hybrid Composite Tensile Failure Theories.	170
5.	CONCLUSIONS	181
6.	RECOMMENDATIONS FOR FUTURE WORK	184
REFERENCES		185
APPENDIX 1	The Application of the Weibull Distribution to Fibre Strength.	191
APPENDIX 2	Detailed Experimental Results.	194
FIGURES		254
TABLES		318

LIST OF SYMBOLS AND ABBREVIATIONS

A	cross-sectional area
A_1	effective hybrid composite cross-sectional area in the area of L.E. fibre failure
as rec.	as received
B	specimen width
c.h.s.	cross head speed
c.s.	chart speed
c.s.a.	cross-sectional area
CV	coefficient of variation
CV_{ac}	CV of model composite tensile strength
D	specimen depth
d	diameter
E	elastic modulus
E_1	effective hybrid composite elastic modulus in the area of L.E. fibre failure
Ex_i	expected number of groups of i or more broken fibres in a composite
F	length factor
F_c	composite factor
F_{cf}	fraction of V_{cf} failing in a propagation of carbon fibre failure in one cross-section of a composite
$F(\varepsilon)$	strain cumulative distribution
$F(\sigma)$	strength cumulative distribution
$f(\varepsilon)$	strain distribution
$f(\sigma)$	strength distribution
G	shear modulus
H.E	higher elongation
i.f.s.s.	interfacial shear strength
i.l.s.s.	interlaminar shear strength
J	ratio of composite L to δ
k	stress or strain concentration factor
k_{HE}	stress or strain concentration factor on a H.E. fibre in a hybrid composite due to a failed L.E. fibre
k_{LE}	stress or strain concentration factor on a L.E. fibre in a hybrid composite due to a failed L.E. fibre
k_r	stress or strain concentration factor due to a run of r broken fibres
L	gauge length

L.E.	lower elongation
L_p	fibre positively affected length
L_R	model fibre length for zero debonding
ℓ	effective axial distance over which failed L.E. fibres in a composite can bear no load
l.v.d.t.	linear variable differential transducer
M	number of model composites in a specimen
N	number of fibres
no c.-a.	no coupling-agent
P	applied load
P_1	load at extension ΔL after a failure of L.E. fibres
P_i	probability of at least i broken fibres
p	Weibull constant
q	Weibull constant
r	Weibull constant
S	span
s	Weibull constant
t	slab and composite specimen thickness
V	volume fraction content
ω	weight
α	Weibull constant
α_{LS}	level of significance
β	Weibull constant
Γ	gamma function
ΔL	extension of specimen
δ	ineffective length
ε	tensile strain
ε'_{2HE}	lower bound on the initial fracture strain of a hybrid composite due to failure of H.E. fibres
ε'_{2LE}	lower bound on the initial fracture strain of a hybrid composite due to failure of L.E. fibres
η	length correction factor for mean fibre strength
σ	tensile stress
$\hat{\sigma}_{af}$	mean fibre tensile stress at model composite failure
$\hat{\sigma}_{f(L_R)}$	tensile failure strength of fibre of length L_R
$\hat{\sigma}_n$	mean tensile strength of a fibre of n elements
σ^*	ratio of $\hat{\sigma}_{af}$ to $\hat{\sigma}_{f(L_R)}$
τ	shear strength
ψ	standard deviation
$\psi_{\bar{x}}$	standard error of the mean

Subscripts

b	bundle or tow
c	composite
cf	carbon fibre
e	expected value calculated from range of experimental results
f	fibre
g	glass fibre
g5	500 tex E-glass fibre
g6	600 tex E-glass fibre
h	hybrid
if	interfacial
il	interlaminar
L	lower bound for statistical composite failure mode
M	mean for statistical composite failure mode
m	matrix
T	total fibre
U	upper bound for statistical composite failure mode
W	minimum value for weakest link composite failure mode

Superscripts

E	at elastic limit
'	at initial failure
^	maximum

1. INTRODUCTION

The use of fibrous composite materials with their high strength to weight ratios has been steadily increasing for many years as the efficiency of composite technology has improved. Over the past 8 to 12 years the limitations of single fibre type (plain) composites have been realized, initiating the exploration of the potential of hybrid composites (composites incorporating 2 or more fibre types). Hybrid composites extend the range of application of composite materials and in some cases enable materials to be tailor made for specific purposes. Already hybrid composites are widely used, a popular combination of fibres being glass and carbon. Glass fibre reinforced plastic (g.r.p.) when compared with carbon fibre reinforced plastic (c.f.r.p) is inexpensive, has a high tensile failure strain, a poor elastic modulus but good tensile strength. By combining g.r.p. with c.f.r.p. a hybrid composite is formed which has certain advantages over both its parent composites. For example the hybrid has a lower cost and higher impact resistance than c.f.r.p. and a greater strength to weight ratio, elastic modulus and flexural modulus than g.r.p. A further advantage is that for certain glass to carbon ratios initial tensile failure is not catastrophic. Thus with components in service an early warning of catastrophic failure can be obtained. Present applications of glass and carbon hybrids include sports equipment, car bodies, mine-sweepers, helicopter rotor blades and limb prostheses. Despite this spectrum of usages, neither the failure processes in plain fibre composites nor in hybrid fibre composites are fully understood. A greater knowledge of the behaviour of these materials will clearly promote the efficient use and hybridization of the reinforcing fibres.

It was originally assumed that the mechanical properties of plain unidirectional fibrous composites could be predicted accurately by the rule of mixtures, a summation of the properties of the individual constituent materials multiplied by their volume fractions. The rule of mixtures provides a unique value for the property considered, giving no indication of the degree of scatter to be expected. In the case of the tensile strength of composites this is a drawback, in some fibre/resin systems a coefficient of variation of 15% is not uncommon. For the purposes of design the lower strength limits are of great importance. In addition to this disadvantage the accuracy of the rule of mixtures in predicting the mean tensile strength of some single fibre type composites is questionable. Failure theories based upon the statistical characteristics of fibre tensile strength have been developed by Rosen[1] and Zweben[2] which, when combined, provide

upper and lower limits for composite tensile strength[3]. Barry[4] has also developed a statistical failure model resulting in upper and lower limits for tensile strength. However, these statistical theories are controversial and lack quantitative accuracy. Thus the rule of mixtures is still used widely for predicting composite tensile strength. When the mechanical properties of unidirectional hybrid composites were first considered it was supposed that the use of the properties of the parent composites rather than those of the individual constituents in the rule of mixtures would result in accurate predictions. This was brought into question in 1972 when Hayashi[5] published work on unidirectional carbon/glass/epoxy hybrid composites. Hayashi found that in tension the theoretical and experimental behaviour of the hybrids correlated well, with the notable exception of the primary fracture strengths and corresponding strains. These experimental values were greater than the theoretical, i.e. the apparent strength of the carbon fibre (the lower elongation, L.E., fibre) in the hybrid composite was greater than that in a plain carbon composite. This phenomenon was termed the 'hybrid effect'. Further work on the tensile characteristics of hybrid composites has tended to support the existence of this hybrid effect but in 1977 it was still a subject of controversy. Two types of theories, based on different failure mechanisms, have been postulated in attempts to explain and predict the tensile properties of hybrid composites. Aveston and Sillwood[6] developed a failure theory based on the fracture energy of the hybrid system. A major assumption is that when one L. E. fibre fails all the other L.E. fibres fail and that the failures are coplanar and perpendicular to the fibre direction. In contrast to this Zweben[7] developed a statistical theory in which numerous L.E. fibres may fail at random throughout the composite before any propagation of fibre failure occurs.

The aim of this research is to investigate some longitudinal mechanical properties (elastic modulus, first tensile failure stress and strain and maximum tensile stress and strain) of a unidirectional fibrous hybrid system, study the tensile failure mechanism and determine the importance of five parameters on any hybrid effects observed. These parameters are total and relative fibre contents, the interlaminar shear strength (i.l.s.s.) of the parent composites (and thereby the fibre/resin interfacial properties), the fibre geometrical arrangement and the tensile characteristics of the higher elongation (H.E.) fibre. A brief outline of the experimental work conducted here is as follows:

i) the characterization of the chosen constituent fibres and matrix;

ii) the fabrication of unidirectional parent and hybrid composite

slabs in which the five parameters mentioned above are systematically varied;

iii) quality control monitoring of the composite slabs and

iv) the preparation and testing of i.l.s.s. and tensile specimens from the range of parent and hybrid composite slabs.

An analysis of the results from this work aims at:

i) establishing the existence or otherwise of any hybrid effects in the elastic modulus, first tensile failure stress and strain and maximum tensile stress and strain of the hybrid composites;

ii) determining any dependence of such hybrid effects on the five parameters varied;

iii) clarifying the tensile failure mode of the hybrid composites and

iv) enabling present theoretical tensile failure modes to be critically examined and the appropriate theories to be tested and developed.

2. LITERATURE REVIEW

2.1 Tensile Failure of Single Fibre Type Unidirectional Composites

The tensile failure modes exhibited by unidirectional composites are dependent upon the characteristics of the particular composite system. An understanding of the failure modes adds confidence to the prediction of composite tensile strength and reveals desirable properties of the constituent materials, facilitating the improvement of existing, and the design of future, high strength composite materials.

This section describes the different tensile failure mechanisms observed in fibrous composites and existing failure theories, relating the properties of the fibre matrix interface and the constituent materials to the mechanisms. The theoretical and experimental treatments presented are all applicable to unidirectional brittle, fibrous composites subjected to tensile loading parallel to the fibre direction.

When composite materials were first developed the simplest failure model assumed that the fibres and matrix shared the load with uniform strain throughout the composite. Composite fracture occurred immediately at the failure strain of the fibres, providing that fibre failure strain was less than that of the matrix and that the fibre content was above a critical volume fraction. Thus the failure strength of unidirectional fibrous composites was predicted by the Rule of Mixtures as:

$$\sigma_c = \sigma_f V_f + \sigma_m' V_m \qquad \ldots \quad (1)$$

where $\hat{\sigma}_c$ and $\hat{\sigma}_f$ = composite and fibre tensile strength respectively,

σ_m' = stress in the matrix at the time of fibre fracture.

and V_f and V_m = fibre and matrix volume fractions respectively.

Below a critical fibre volume fraction, V crit, fibre strengthening does not occur and below a 'minimum' fibre volume fraction, V min, the tensile strength of the composite is determined solely by that of the matrix. The above is illustrated in figure 1.

The simple rule of mixtures approach to the tensile strength of composite materials does not take into account the fact that the failure strain of the fibres of a given type is not a unique value but is subject to statistical variations. More detailed failure theories were necessary.

In 1960 Parratt[8] suggested a model for fibre composite failure based on the effect of defects in glass fibres on the strength of plastic mouldings. He postulated that the glass fibres fail throughout the composite at local defects along their lengths but that the failures do not propagate. As the load increases further fibre failures occur, breaking the fibres down into shorter and stronger lengths. This continues until any further increase in the applied load can not be transmitted to the fibres by the matrix because the maximum matrix shear stress is exceeded. The composite failure then occurs due to shear failure of the matrix or the fibre/matrix interface.

In 1964 Rosen[1] produced a paper on composite failure in which he treated the fibres as having a statistical distribution of flaws or imperfections which, as Parratt[8] suggested, result in fibre failure at various stress levels. Here the two theories diverge. Rosen suggested that as the applied load is increased fibre failures occur at randomly distributed flaws throughout the composite to cause cumulative weakening of the composite until the remaining unbroken fibres at the weakest cross-section are unable to support the applied load. The composite then fails by tensile fracture of the remaining intact fibres. Rosen[1] evaluated the composite strength as a function of the statistical strength distribution of the fibres and compared the theory to experimental results for g.r.p. composites, using existing data for the statistical nature of the tensile strength of the glass fibres. In the composite model used he neglects the extensional stress in the matrix relative to the fibres and neglects the shear stresses in the fibres relative to the matrix. It is therefore considered suitable for composites with reinforcing fibres strong and

stiff relative to the matrix. In Rosen's model in the vicinity of a failed fibre end the load carried by the fibre is transmitted through the matrix, by shear, to adjacent fibres. At each end of the broken fibre there is an ineffective portion which is not able to carry the applied load. As the applied load is increased more fibres fracture at points of imperfection and the fractures accumulate until a sufficient number of ineffective fibre lengths combine over a cross-section to result in composite failure. Rosen continues to consider the composite as a series of layers of links of dimension δ (the ineffective length) and the segment of a fibre within a layer as a link in the chain which constitutes the fibre. Thus each layer is a bundle of links and the composite a series of bundles. The applied load is treated as uniformly distributed among the unbroken fibres in each layer. Rosen defines the link length δ as the length of fibre over which the stress is less than a certain fraction, ϕ (Rosen chooses 0.9), of the undisturbed fibre stress, σ_f, and determines the value of δ by considering the shear stress distribution along the fibre/matrix interface, applying a shear-lag type analysis. The final equation for δ is

$$\delta = \frac{d_f}{2}\left[\left(\frac{1 - V_f^{1/2}}{V_f^{1/2}}\right) \times \left(\frac{E_f}{G_m}\right)\right]^{1/2} \times \cosh^{-1}\left[\frac{1 + (1-\phi)^2}{2(1-\phi)}\right] \quad . \quad . \quad (2)$$

where d_f = fibre diameter

E_f = elastic modulus of fibre

and G_m = shear modulus of matrix

In later papers equation 2 is replaced by equation 3[2][9]

$$\delta = d_f\left[\frac{1}{2}\frac{E_f}{G_m}\left(\frac{1 - V_f^{1/2}}{V_f^{1/2}}\right)\right]^{1/2} \quad . \quad . \quad . \quad (3)$$

Rosen[1] proceeded to derive the desired statistical definition of composite strength by defining the fibre strength distribution, $f(\sigma)$, and the associated cumulative distribution, $F(\sigma)$. He then obtained the distribution function for bundle strength which, treating the composite as a chain of bundles and applying the weakest link statistical theorems (i.e. when the weakest bundle fails the composite fails), leads to the statistical definition of composite strength. For fibres with tensile strength characteristics described by a Weibull distribution of the form

$$f(\sigma) = L\alpha\beta\sigma^{\beta-1} \exp(-L\alpha\sigma^{\beta}) \quad \ldots \quad (4)$$

where L = gauge length

σ = applied stress

and α and β = Weibull constants peculiar to the fibre type

Rosen derived the following equation for the most probable fibre stress at composite tensile failure, $\hat{\sigma}_f$.

$$\hat{\sigma}_f = \left[(\alpha\delta\beta e)^{-1/\beta} - \psi_b (2 \log J)^{1/2} + \psi_b \left(\frac{\log \log J + \log 4\pi}{2(2 \log J)^{1/2}}\right)\right] \quad \ldots \quad (5)$$

where J = composite gauge length divided by the ineffective length

e = the exponential, 2.7183

and ψ_b = the standard deviation of the distribution of the average fibre stress at bundle failure and is given by the expression

$$\psi_b = \hat{\sigma}_f \left\{ F(\hat{\sigma}_f) \left[1 - F(\hat{\sigma}_f)\right] \right\}^{1/2} N^{-1/2} \quad \ldots \quad (6)$$

where $\hat{\sigma}_f$ = maximum fibre stress

and N = number of fibres

It is seen from equation 6 that when composite dimensions are large in comparison with fibre cross-sections $N \gg 1$, then $\psi_b \Rightarrow 0$ and equation 5 simplifies to

$$\hat{\sigma}_f = (\alpha\delta\beta e)^{-1/\beta} \quad \ldots \quad (7)$$

α and β can be determined from experimental data on fibre strength versus fibre length. Details of the application of the Weibull distribution to fibre strength are given in Appendix I.

The short comings of Rosen's model are that it neglects to consider the effect of stress concentrations on fibres immediately adjacent to broken fibres and the possibility and effect of fibre debonding in the region of failures. To qualify the analytical model Rosen conducted an experimental study of the mode of failure of glass fibre/epoxy composites. The tensile specimens consisted of one layer of approximately 90 to 100 parallel fibres embedded in an epoxy resin. Still and motion pictures taken during the tensile tests show that individual fibre fractures occurred at less than 50% of the ultimate failure load and that as the load increased further fibre fractures occurred randomly throughout the specimen. The variations in fibre strength initially off-set the stress concentrations in the weakened cross-sections and fibre failures did not

cumulate by propagation.

Complete specimen failure was eventually due to a statistical accumulation of broken fibres across one region, weakening the region beyond the point where it was able to bear the redistributed applied load. Failure did not stem from the existence of fully ineffective fibres, as postulated by Parratt[8]. Upon failure the fibres had broken down typically into what appeared to be lengths an order of magnitude larger than the calculated ineffective length. Rosen[1] concluded that discontinuous fibres may exist in an originally continuous fibre composite at stress levels well below the maximum stress. The composite strength is then affected by the efficiency with which the matrix transmits load around the fibre break. Note that the experimental work above involved specimens of only one reinforcement material in a single resin system and a nearly constant, rather low, fibre volume content of approximately $0.20V_f$.

The validity of Rosen's theory was investigated further by Grinius[10] in 1966. He studied a range of composites, the constituent materials being 5-mil. E-glass (d_f = 0.005 in), S-glass roving and boron fibre reinforcements and Epon 828/1031 epoxy and Epon 815/Versamid (40/60) epoxy matrices. The probable failure strengths for the six different combinations of matrix and fibre were calculated using equation 7, postulated by Rosen[1]. The typical specimen configuration was 25 equally spaced fibres in a single layer within the resin matrix. Fibre volume fractions were low being between 0.060 and 0.094 V_f. One specimen of each composite type was tested initially. The failure modes were resin cracking and catastrophic failures without cumulative fibre fracture at low stress levels. The experimental results, with the exceptions of those of two specimens damaged prior to testing, differed from the predicted values by an average of 23%. Qualitatively the results indicate that increased matrix stiffness increases the strength of the composite. Note that only one specimen of each composite type was tested and that the volume fractions were low. Further sets of specimens were produced for the failure studies. These were S-glass and E-glass both with Epon 828/1031 resin and E-glass with 815/Versamid resin. The volume fractions are not given. The specimen shape was changed from the original rectangular form to a necked specimen with parallel centre gauge length. The composites with Epon 828/1031 resin failed in shear through the ends of the specimens. The E-glass with Epon 815/Versamid resin specimen failed at a very low stress level. Grinius suggested that this was due to the low modulus

resin matrix and concluded that a low yield point resin tends to amplify the failure of a fibre and reduce the composite strength.

In 1968 Zweben [2] investigated two modes of composite failure. The first study is an extension of Rosen's[1] theory. Zweben's model of a two dimensional unidirectional fibrous composite with a load applied in the direction of the fibres is given in figure 2 and is based on Rosen's model. As the load is applied the fibres, due to scattered flaws, break randomly throughout the composite. Whilst Rosen assumed the load in a broken element to be uniformly distributed among the other intact elements in the layer Zweben assumed that the elements adjacent to a broken one are subjected to a load concentration greater than that which is sustained by fibres distant from the fracture site. The equation given for the static stress concentration factor, k, in the two fibres adjacent to a run of r broken fibres is

$$k_r = \frac{4.6.8\ldots(2r+2)}{3.5.7\ldots(2r+1)} \quad \ldots \quad (8)$$

Thus for the most common case of one broken fibre the two adjacent fibres are subjected to a stress $\frac{4}{3}$ times the nominal fibre stress, i.e. the applied load divided by the total fibre area. The increase in average fibre stress due to the initial fractures is neglected since the proportion of broken elements in any given layer immediately prior to composite failure is assumed to be small. The small probability of an adjacent element breaking due to a failure strength less than σ, the applied stress, is also neglected.

Zweben [2] states that the probability that an element adjacent to a broken one will break due to the stress concentration is equal to the probability that the tensile strength of the element lies between σ and $k_1\sigma$, thus the probability is

$$F(k_1\sigma) - F(\sigma) \quad \ldots \quad (9)$$

From this basis Zweben derives the probabilities that:

i) only one of the adjacent fibres breaks;

ii) both adjacent fibres break simultaneously;

iii) if one of the fibres adjacent to a single fibre breaks then only one of the two adjacent fibres now subjected to a stress concentration of k_2 breaks and

iv) if one of the fibres adjacent to a single fibre breaks then both of the adjacent fibres will fail simultaneously.

Zweben continues, taking into account the different possible failure sequences, up to the probability of a multiple fracture of five fibres. He finishes with a general equation for the expected number of groups of i or more broken fibres, Ex_i.

$$Ex_i = JNp_i \qquad \ldots \quad (10)$$

where JN = number of elements

and p_i = probability of a group of at least i broken fibres.

This fracture mode where random fibre failures occur throughout the composite until fibre fracture propagates from one of the fracture sites is called cumulative fracture-propagation. Zweben applied the above theory to and compared the results with experimental data for composites consisting of 3.5mil E-glass fibres in two types of epoxy resin matrices, denoted B and C. The characteristics of the tensile strengths of the 3.5mil. E-glass fibres were derived from tests on the virgin fibres. The Weibull parameters calculated are quoted as $\beta = 9.40$ and $\alpha^{-1/\beta} = 181.5$ k.s.i. When the composites were tested scattered fibre breaks were observed at less than 50% of the ultimate stress, the number increasing with load. Despite the increased stress intensity in the fibres adjacent to the fracture sites few of the overstressed fibres broke. The ineffective lengths obtained from photographs of the tests were 0.7874mm and 2.1844mm for the series B and C respectively. Using the above data the expected number of single broken elements, Ex_1, was calculated from the equation

$$Ex_1 = JNF(\sigma) \qquad \ldots \quad (11)$$

Where $F(\sigma) = \int_0^{\sigma} \alpha\delta\beta\sigma^{\beta-1} \exp(-\alpha\delta\sigma^{\beta})\, d\sigma$

$$= 1 - e^{-\alpha\delta\sigma^{\beta}} \qquad \ldots \quad (12)$$

At low stress levels there were generally more fractures than the theory predicted, possibly a result of damage to the fragile glass fibres during specimen fabrication. In the region of failure loads the agreement was fairly promising considering the experimental uncertainties involved. In general multiple fractures began to appear in the stress range predicted by theory and, consistent with theory, the multiple fractures which occurred at lower stress levels did not propagate immediately to cause composite failure. The rate of formation of multiple fracture groups was quite high in the failure range but composite failure occurred before a large number could form. Although the static failure analysis provides reasonable agreement with experimental data the actual

failure mechanism is more complex. Dynamic load concentration factors may be significant and there is the possibility of fibre debonding and crack propagation in the matrix. However, Zweben[2] suggests that for 2-dimensional composite specimens exhibiting a significant number of scattered breaks before failure a conservative estimate of the fibre failure stress at composite failure is that at which the first multiple break is expected.

$$Ex_2 \left(\hat{\sigma}_f \right) = 1 \qquad \ldots \quad (13)$$

For 3-dimensional composites (multilayer) Zweben predicts that the failure stresses will be greater since the stress concentrations will be shared between more fibres and so be significantly reduced.

The second failure mode considered by Zweben in reference 2 is the noncumulative fracture mode. In some fibre/matrix systems only a few fibre breaks occur before composite failure. This can be explained by cumulative failure theories only if the fibre strength dispersion is particularly small, and Zweben states that this is not the case. He studied the correlation between the theoretical strength of the weakest fibre and the observed failure loads. Again assuming a Weibull distribution for fibre strength the following equation for the mode of the weakest fibre strength ($\hat{\sigma}_{wf}$) distribution is obtained.

$$\hat{\sigma}_{wf} = \left[\frac{(\beta - 1)}{NL\alpha\beta} \right]^{1/\beta} \qquad \ldots \quad (14)$$

Zweben suggests that for noncumulative fracture the fracture of a single fibre propagates through the matrix and causes additional fibres to fail, thus resulting in catastrophic failure of the composite. Zweben compares the theory with data from boron/epoxy specimens and the indication is that using the occurence of the first fibre break as the failure criterion for the noncumulative fracture mode gives a good but conservative estimate of the fibre stress at composite failure. In his conclusions Zweben notes that both the cumulative and noncumulative fracture modes predict a decrease in failure strength with an increase in specimen size, contrary to Rosen's theory where the failure strength is essentially independent of size.

Liptai [11] tested a filament wound NOL S-glass fibre/epoxy ring in tension and the experimental results supported the cumulative fracture theory of Zweben's. Acoustic emission techniques were used to detect fibre failures and again it was found that the first scattered fibre breaks occurred at less than 50% of the ultimate load and the density of the breaks increased with the load.

Blakelock and Lovell[12] also considered the range of failure strength of composites to stem from the statistical nature of the fibres. In 1969 they examined the mechanism by which a carbon fibre composite fails in tension and described a statistical cumulative weakening failure up to the failure of all the fibres in one region due to weakening. The events during the subsequent failure of the matrix were related to the tensile strength of the matrix and the shear strength of the fibre/matrix interface.

In the case of a low interfacial shear strength (τ_{if}) during the increase in local strain, beyond the breaking strain of the reinforcement, the broken but still embedded fibres either debond from the resin and pull-out immediately or break further until they are sufficiently short to debond and pull-out. The failure of the resin propagates through the weakened region of broken and debonded fibres to produce a relatively smooth fracture surface with the ends of the debonded fibres protruding out. The mean height of these exposed fibres can be equated with the shear strength of the interfacial bond between the fibre and resin, τ_{if}

$$\tau_{if} = \frac{d_f \hat{\sigma}_f}{4y} \qquad \ldots \quad (15)$$

where y = pull-out length.

When the interfacial shear strength is lower than the resin tensile strength, failure occurs through shear failure at the fibre/resin interface and is otherwise independent of the mechanical properties of the matrix. In the opposite case, where the interfacial shear strength is greater than the tensile strength of the resin, Blakelock and Lovell[12] state that the failing fibres do not debond from the resin but as they relax at the points of failure they cause extremely high local strains in the resin. These strains may be sufficient to produce small internal cracks at the points of individual fibre failures which propagate and join at ultimate failure. Thus an undulating fracture surface is formed which passes through the individual fibre fractures in the region. In this case the strength of the composite is improved by using a resin with superior properties and not by improving the fibre/resin bond.

The fracture surfaces of a Type I carbon and Type II carbon composite were compared and the results supported the above. The Type II composite had a greater interlaminar shear strength (i.l.s.s.) than the Type I composite. The fracture of the Type II occurred without noticeable separation between the fibre and resin whilst the Type I fractures had a variety of pull-out lengths. There are not sufficient details given to

be able to compare quantitatively the composite strengths with statistical theories of Rosen[1] and Zweben[2].

In 1970 Rosen extended his original ideas on composite failure. In a paper entitled 'Strength of Uniaxial Fibrous Composites'[9] he stated that a single failure mechanism for all fibrous composites did not exist and that failures due to longitudinal and transverse crack propagation, statistical accumulation of internal fractures and matrix flow were all possible. The aim of the paper was to relate several analyses of uniaxial tensile strength which together provide the elements of a rational theory for the tensile failure of fibrous composites. One of the first statements made was that the then general assumption that the average fibre tensile strength measured by testing individual fibres could be directly used in the mixture rule to give composite tensile strength was fallacious. As noted in references 1, 2, 8, 10, and 11 the strength of brittle fibres is not unique but variable. The degree of variation in fibre strengths affects the possible composite failure mechanisms. Rosen again characterizes the fibre strengths with a Weibull distribution function and describes the function in some detail. Here let it suffice to note that the constant β is essentially an inverse measure of the coefficient of variation (CV).

$$CV \simeq \beta^{-0.92} \qquad \ldots \quad (16)$$

For practical fibres $\beta > 1$. $\alpha^{-1/\beta}$ may be regarded as a reference stress level. Figure 3 shows graphically the relationship between β and CV. One aspect of the statistical approach to composite failure is that the composite contains a bundle of filaments and the strength of a bundle is not equal to the mean fibre strength. In general the average strength of the bundle is less than the average strength of the fibres and is a decreasing function of the CV of the fibre strength.

Rosen[9] explains that at the point of a fibre break the extensional stress in the fibre drops to zero, building back up along the fibre away from the break by virtue of the shear transmitted across the interface between the matrix and fibre. The localized shear stresses can be high and, depending on the matrix properties, one may expect either yielding of the matrix or an interface failure. If interfacial failure propagates along the length of the failed fibre that fibre is totally ineffective and the composite acts as a bundle of fibres and the matrix material does not enhance the strength of the composite. Alternatively the crack from the first fibre failure may propagate into the matrix normal to the fibres and local stress concentrations cause other

fibres to fail leading to catastrophic failure of the composite i.e. noncumulative fracture mode. Cumulative damage occurs when both of the above crack propagation modes are suppressed. Rosen examined the question of stress concentrations. He treated the problem in the same manner as Zweben[2], using equation 8 to obtain the stress concentration factors. Rosen considered the dynamic overshoot factors which range from 15% to 27% of the static stress concentration factors as the number of broken fibres range from one to infinity. He assessed the effect of distributed fibre fractures occurring in the same cross-section on the cumulative weakening mode. The interaction of the stress concentration factors where every nth fibre is broken is shown to become significant only when the crack density becomes very high. The stress concentration factor of 1.33 for a single failed fibre increases to 1.50 when the fraction of broken fibres is one in three. The above only applies to a 2-dimensional composite, but in practice the 3-dimensional composite is more important. Rosen considers a 3-dimensional composite to contain a series of elements of seven fibres, a central broken fibre surrounded by six unbroken fibres, and shows the stress concentration factor on the unbroken fibres in each element to be 1.17. This compares with a factor of 1.36 if every 7th fibre in a 2-dimensional composite is broken. For a cumulative fracture mode Rosen[9] repeats the derivation for the statistical composite tensile strength given in reference 1, attaining equation 7 but again does not include the effect of stress concentrations. The equation for the expected fibre stress at composite failure is equal to the mean strength of a bundle of fibres of length δ for a large N. The difference between the strengths of a composite and a bundle of fibres of the same length, L, as the composite is the difference between the strengths of a bundle of length δ and a bundle of length L. The length strength effect is large and therefore the merits of the compositing process are apparent.

From this time onwards there was a greater awareness of the statistical nature of the strength of fibres. However, many people felt, like Harris [13], that the tensile strength of carefully aligned composites is almost always sufficiently accurately predicted by the simple rule of mixtures.

In 1972 Zweben[3] proposed bounds to composite tensile strength. For a composite which fails in the weakest link mode the lower bound on the fibre stress at composite failure is the expected stress at which the first fibre failure will occur, $\hat{\sigma}_{WF}$, as given by equation 14.

$$\hat{\sigma}_{wf} = \left[\frac{\beta-1}{NL\alpha\beta}\right]^{1/\beta} \quad \ldots \quad (14)$$

This is too conservative a stress level for composites in which cumulative damage occurs. Zweben suggests using for the lower bound, $\hat{\sigma}_{Lf}$, the stress level at which the first fibre adjacent to a broken fibre is expected to fail due to the stress concentration factor. For the upper bound, $\hat{\sigma}_{Uf}$, Zweben suggests the equation derived by Rosen in which stress concentration factors are ignored.

$$\therefore \hat{\sigma}_{Uf} = \hat{\sigma}_{f} = (\alpha\delta\beta e)^{-1/\beta} \quad \ldots \quad (7)$$

Zweben tested the validity of this bounding theory by comparing the theory with a number of different sets of experimental data. The majority of results fell within the two bounds for the cumulative fracture mode. The comparison of two of the sets of data, both based on composites of boron fibres in an aluminium matrix is of interest. The two failure bands are significantly different and do not overlap. The first set lies between the predicted $\hat{\sigma}_{Lf}$ and $\hat{\sigma}_{Uf}$ levels and the second set lies below $\hat{\sigma}_{Lf}$. The two sets were manufactured by different methods which resulted in a much stronger fibre/matrix bond in the second set. Experimental observations of the second set showed that fibre breaks initiated matrix cracks, indicating that composite failure was due to the weakest link mode. The weaker fibre/matrix bond in the first set would suppress the weakest link mode of failure, thus the difference in the two sets of data can be explained by the combination of Rosen's and Zweben's theories. The implication is clearly that a strong fibre matrix bond may result in lower tensile strengths than may be obtained with a weaker bond.

In reference 3 Zweben notes that sample calculations show very little difference in $\hat{\sigma}_{Lf}$ values between hexagonal and square array cases but the values of $\hat{\sigma}_{Lf}$ for an equivalent monolayer composite are significantly lower. Thus in thin specimens where the outer layers of fibres with their relatively high stress concentrations are a more significant part of the whole specimen the failure stress levels may be lower than those of a similar composite with a greater number of layers. The question of the influence of composite size on strength is interesting, evidence from experimental data is contradictory. As regards the statistical theories the values of $\hat{\sigma}_{wf}$ and $\hat{\sigma}_{Lf}$ are both size dependent (decreasing with increasing volume of material) but $\hat{\sigma}_{Uf}$ is independent of the volume of the composite.

The tensile failure mechanisms in carbon fibre reinforced plastics were studied, with the aid of acoustic emission monitoring equipment, by Fuwa et al[14] in 1975. They fabricated and tested tensile specimens of:

i) Type I carbon fibre in fully cured epoxy matrix;
ii) Type I carbon fibre in semi-cured epoxy matrix and
iii) Type I carbon fibre bundles.

The acoustic emissions from the specimens due to fibre failure, fibre/matrix debonding, matrix cracking and fibre pull-out were monitored during the tensile testing of the specimens. The stress v strain (σ v ε) curves (see fig. 4) for the cured c.f.r.p. specimens were close to linear with an abrupt brittle failure. In both the semi-cured and bundle specimens the absence of a rigid matrix resulted in a lower initial modulus and the curves became non-linear prior to catastrophic failure. The peak in the frequency distribution of the failure strains of the fully cured c.f.r.p. specimens was close to the strain at which the σ v ε curves of both the bundles and the semi-cured specimens deviated from linearity. Both bundle and semi-cured specimens had fairly constant values of failure strain ($\simeq$ 0.5%) whereas the fully cured specimens had a wide range of failure strains. The greatest extension exceeded the strain at which the bundles failed, indicating that each fibre in the composite had broken at least once. Fuwa et al emphasized the following observations on their results:

i) the weakest fully cured specimen failed at a strain of 0.32%, close to the strain at which the results for bundles and semi-cured samples suggest that significant numbers of fibre failures begin to occur;
ii) about 80% of cured specimens failed before the maximum failure strain for bundle specimens and
iii) some cured specimens survived to strains greater than 0.5% at which level all the fibres in the semi-cured and bundle specimens are expected to have failed.

The fact that 60% of the fully cured specimens failed at a lower strain level than that at which an estimated 10% of fibres in the bundles would have failed indicates that a progressive failure mechanism such as related fibre breakage or crack propagation exists in these fully cured specimens. Alternatively the observation that some samples failed at strains greater than the failure strains of the bundles suggests random fibre failure within the specimens and that ultimate failure is statistically determined. Thus the failure of the fully cured specimens seems to be bounded by upper and lower limits as described by Zweben[3].

The acoustic emission patterns for the fully cured c.f.r.p. showed a sharp increase in emission between 0.35% and 0.40% strain, the critical strain range in which significant numbers of fibres fail in fibre bundles. Similar acoustic emission patterns were obtained from the semi-cured specimens. Microscopic examination of the fractures showed that in both the bundle and semi-cured specimens the fibres failed randomly throughout the gauge length, independent of the failure of others. The soft matrix of the half-cured specimens did not change the mode of failure from that of the bundles since it was not able to support the high shear loads necessary in order to transfer loads from broken fibres to the other fibres in the cross-section. The stiff matrix of the fully cured c.f.r.p. allowed shear stress transfer, thus altering the fracture mode. These specimens failed suddenly, normally into two separate but occasionally into several pieces. By removing the surface layers of the epoxy matrix with sulphuric acid and examining the exposed fibres under the microscope, successions of fibre breaks were observed that were not necessarily associated with the final site of complete failure, although the frequency of the damage was greater near to the final fracture region. In the samples with a tensile strength near to the top of the scatter band the incidence of fibre damage away from the final fracture was much greater than in the lower strength specimens. The fibre fractures observed in the apparently intact portions of the composites frequently ran at angles across a portion of the specimen and small bundles of broken fibres were often linked to neighbouring bundle failures by a final shear failure. In the stronger specimens some random single fibre failure was observed. The conclusion for the failure picture of the fully cured c.f.r.p. was that the basic mechanisms of failure are statistically determined and not a result of straightforward crack propagation. Successive fibre failures occur due to stress concentrations as described by Zweben[2] but the failures are localized, limited to 'sub-bundles', and result in a distribution of weak regions. Shear failure between sub-bundles may be the cause of the limitation of the associated fibre failures. Eventual composite failure is attributed to the statistically determined accumulation of fractured regions across a particular cross-section. It appears that the samples near the bottom of the strength scatter band fail prematurely due to a chance accumulation of weak regions in a given cross-section. In specimens near the upper limit the points of weakness are probably more evenly distributed throughout the specimens so every cross-section is able to sustain higher loads.

The above paper[14] makes a valuable contribution to the field of c.f.r.p. tensile failure mechanisms and is complete within itself but unfortunately the appropriate data for a quantitative analysis of the results using the lower and upper bound theories of Zweben[3] is not supplied.

In 1978 Fukuda and Kawata[15] predicted the statistical strength distribution of unidirectionally reinforced composite materials using Monte Carlo simulation. Unlike Zweben[3][7] they characterized the fibre strength with the normal distribution and not the Weibull distribution. In addition they postulated that the stress concentration factor was dependent upon E_f/E_m and V_f. The work presented in the paper is not used here but note that the relative strength of composites was found to decrease with increasing E_f/E_m, V_f and composite length.

In 1978 Barry[4] presented an extension of the previously proposed statistical theories of Rosen[1][9] and Zweben[2][3] and adopted a computer simulation technique, from the statistical model, to generate a set of generalized scatter limits for the average fibre stress at composite failure. As in references 2 and 9 the model considers the composite to consist of a number of transverse slices, or bundles, of a characteristic thickness and the composite fails when any one of the slices fails. The characteristic fibre length is not δ, the ineffective length, but Lp, the positively affected length. It is a function of the fibre to matrix modulus ratio, E_f/E_m, the volume fraction of fibres, V_f, and the length of debonding that occurs between a failed fibre and the matrix material. From a stress analysis of a 3-dimensional composite Barry derives the relationships of model fibre length, Lp, and the ratio of L_p/L_R, where L_R is the model fibre length for the case of zero debonding (comparable with δ), to the debond length for a composite with modulus ratio of 100 and $V_f = 0.5$. Figure 5 illustrates these relationships. For a composite with differing E_f/E_m and V_f values Barry determined a length factor, F.

$$F = \left[\frac{E_f}{E_m}\left(V_f^{-1/2} - 1\right)\ 0.024\right]^{1/2} \qquad \ldots \quad (17)$$

The model is composed of approximately 4000 fibres and considers the 18 nearest fibres to a failed fibre to be affected by stress concentrations. The 6 nearest fibres and the next 12 nearest fibres to the failed fibre are called primary and secondary fibres respectively. Barry assumes the strength distribution of the fibres to be normal since this was convenient for the computer simulation of the model composite. The fibres

are considered to consist of n elements, each one fibre diameter in length. The strength of the individual fibre elements is taken to be a normal distribution with a mean value of $\hat{\sigma}_e$ and CV of CV_f. If a fibre of n elements is stressed to $\hat{\sigma}_n$, the mean strength of such fibres, the cumulative probability that such a fibre fails during loading to $\hat{\sigma}_n$ is 0.5. From statistical theory Barry arrives at the equation

$$\frac{\hat{\sigma}_n}{\hat{\sigma}_e} = \eta = 1 - CV_f \, A \qquad \ldots \quad (18)$$

A is the number of standard deviations of element strength from the mean of a normal distribution associated with a cumulative probability equal to $1 - 0.5^{1/n}$. η represents the length correction factor for mean fibre strength. An equation similar to the above may then be used to determine mean composite strength from the mean model composite strength.

The static and dynamic stress concentration patterns due to a broken fibre and the effect of debonding on these patterns are considered. In order to obtain a workable distribution model for computer simulation two assumptions were made. Firstly that the stress concentration increases assigned to an intact fibre when more than one nearby fibre fails are additive, and secondly that the sum of the stress concentration increases distributed among the primary intact fibres is constant, and the same for the secondary intact fibres.

The distribution logistics method used in the computer simulation is as follows. When a fibre fails both dynamic and static stress concentration increases are calculated for the intact primary and secondary fibres. The dynamic increases are assigned to the fibres. A check is made to see whether any of these fibres fail. If none fail the dynamic stress concentration is replaced by the static stress concentration increase. Where the dynamic concentration results in one or more fibre failures two possibilities lead to a high and low limit condition. The high limit condition considers completely separate fibre failure with no overlap of dynamic stress concentrations. The low limit condition considers the complete accumulation of dynamic stress concentration increases on the intact fibres. When catastrophic fibre failure occurs the computer programme reports the current value of the average fibre stress. The programme was run several times with varying combinations of CV_f, debond length and limit conditions. The results show that the percentage of fibres failed in a model composite prior to catastrophic failure ranged from $\simeq$ 0.5% for a CV_f of $\simeq$ 10% to $\simeq$ 7% for a CV_f of $\simeq$ 25%. Therefore,

even for a relatively small specimen the number of individual fibre breaks will be very large. The strength results are expressed as a function of the CV_f and the ratio L_p/L_R and the values given are the upper and lower 95% single tail scatter limits and the mean value for the ratio of average fibre stress at model composite failure, $\hat{\sigma}_{af}$ to the mean fibre strength, $\hat{\sigma}_{f(L_R)}$, for a gauge length of L_R. $\hat{\sigma}_{af}/\hat{\sigma}_{f(L_R)}$ is denoted σ^*. The relationships between σ^* and the ratio L_p/L_R, for a range of CV_f, are given in figures 6, 7 and 8. Figure 9 gives the relationship between the CV of the model composite strength (CV_{ac}) and CV_f.

Thus the upper and lower limits for the failure strength of a brittle fibre composite can be calculated using Barry's model providing that the following properties are known: $\hat{\sigma}_{f(L_R)}$; E_f; E_m; V_f; debond length range; d_f; CV_f and L.

Barry compared predicted and experimental ranges of average fibre stress at composite failure for 6 different combinations of carbon fibre/matrix and found the correlation good. The experimental details are presented in reference 16. The predicted minimum composite strength values are very close to the actual values and this emphasized the conservative nature of Zweben's lower bound which utilizes the first multiple fibre break as the failure criterion. Results of Barry's computer model indicate that multiple fibre failure groups containing as many as 5 broken fibres can occur before the composite fails. Two points to note are firstly that the fibre debond lengths are obtained from fibre pull-out lengths and the prediction of the minimum strength of a composite should be based on the maximum fibre pull-out length, and secondly that composite strength is dependent on specimen size.

As the statistical theories for the failure of composites were developed the problem was also considered from the point of view of energy and fracture mechanics. In 1969 Beaumont and Harris[17] evaluated the energy expended during controlled crack propagation in unidirectionally reinforced composites of carbon fibres in an epoxy resin matrix. Important aspects of their work are that the effect of improving the fibre/resin bond and so decreasing the average fibre pull-out length, is to reduce the energy released during crack initiation by approximately a factor of 5, and the resistance of the composite to the propagation of cracks by nearly an order of magnitude. Beaumont and Harris[17] postulated that the energy required to propagate a slowly moving crack in c.f.r.p. is proportional to the fibre critical length and the interfacial shear

stress and that an increase in one is at the expense of the other.

Prior to the above paper Outwater and Murphy[18] considered the fracture energy of unidirectional laminates, concentrating on glass-fibre reinforced plastics (g.r.p.). They too decided that a weaker bond between fibre and matrix reduces the brittleness of a laminate and suggest that a reduction in d_f, V_f, $\widehat{\sigma}_f$, E_m and an increase in E_f all help to increase the brittleness of a composite. Relating this to Zweben's failure modes it is equivalent to saying that the above factors increase the probability of the 'weakest link' failure mode.

Fibre debond lengths also played an important role in Barry's model[4]. As mentioned previously he proposed that both variation in fibre strength and in the debond length of fibres are main sources of variation in composite strength. Composite strength was predicted to increase with decreasing debond length. In his experimental work[16] he assumed that debond length could be observed as the fibre pull-out lengths on the composite fracture surfaces. The carbon/epoxy specimens tested were basically impregnated tows with V_f% between 20% and 25%. In all 6 of the composite systems tested there was a range of tensile strengths and generally the stronger specimens in each system showed smaller fibre pull-out lengths than the weaker specimens. Barry noted that the observations and the strength results were reasonably consistent with the trends predicted by his model[4] and concluded that the fibre pull-out lengths may be used as a guide to the lengths of debonding between fibre and matrix for the purpose of predicting strength. In addition he states that the failure strain of a plastic matrix material may not be a significant factor affecting the short-term composite strength.

To summarize it appears that the mixture rule, using fibre strength data derived from fibres of the same gauge length as those of the composite specimen, generally provides a reasonable approximation to the average composite strength. It can not be used with confidence since it gives no indication of the expected extent of scatter in composite strength and in cases where the weakest link failure mode is dominant the actual composite strengths will be considerably less than predicted.

From the literature reviewed statistical theories predict two major failure modes for fibrous composites and that in practice failure can be a mixture of both, the dominant mode depending on the properties of the system in question. The two modes are the weakest link (or non-cumulative), and the cumulative fracture-propagation mode. The relevant equations for these modes are proposed by Zweben[2] and Rosen [1][9] and form the predictions for lower and upper bounds to composite tensile

strength [3]. The lowest limit, $\hat{\sigma}_W$, for the weakest link mode of failure, the probability of which is increased with increasing composite i.l.s.s. and lower CV_f (i.e. greater β values when described by the Weibull distribution), is taken as the composite stress at which the first fibre fracture is expected. Where cumulative damage occurs the lower bound on composite strength, $\hat{\sigma}_L$, is the stress level at which the first fibre adjacent to a broken fibre is expected to fail. The upper bound, $\hat{\sigma}_U$, is the stress at which failure is expected to occur due to a statistical accumulation of flaws weakening a region, ignoring stress concentrations.

In addition to the above the computer simulation of composite failure evolved by Barry[4], based largely on the failure models of Rosen[1] and Zweben[2], is valuable. The theoretical and experimental data compared correlates well.

The combined works reviewed suggest that potentially important factors influencing the tensile strength and failure mode of unidirectional fibrous composites include:

i) the statistical characteristics of the tensile strength of the reinforcing fibres;
ii) the relative fibre and matrix moduli;
iii) the volumetric fibre content;
iv) the fibre/matrix interfacial bond strength;
v) the matrix shear modulus;
vi) the fibre diameter and
vii) the composite volume.

The composite systems of greatest interest to the author are c.f.r.p. and g.r.p. Cumulative failures have been observed in both types with first fibre failures frequently occurring at less than 50% of the ultimate load. There appears to be a greater tendency in c.f.r.p. than in g.r.p. for related fibre breakage, the c.f.r.p. tending to have higher i.l.s.s. and lower CV_f than g.r.p.

Having achieved a greater understanding of the postulated failure modes in single fibre type composites and their controlling parameters, attention is now turned to hybrid composites. The following section reviews literature on the tensile characteristics and theoretical failure modes for unidirectional hybrid composites.

2.2 Tensile Failure of Unidirectional Fibre Hybrid Composites

The importance of hybrid composites has been explained in the introduction. This section of the literature review concentrates on the experimental results and observations and on the theories evolved in previous work conducted on the tensile strength of hybrid composites. Reviews on this subject are found in references 19, 20 and 21. References 19 and 20 cover the general mechanical properties of fibre composite hybrid systems whilst reference 21 covers most of the area of this review, the tensile strength of hybrid systems containing unidirectional brittle reinforcement fibres.

As with single fibre type composites it was originally assumed that the tensile properties of hybrid composites could be accurately predicted by the rule of mixtures, a summation of the properties of the individual constituents multiplied by their volume fractions, and that initial failure of the hybrid would occur at the failure strain of the lower elongation (L.E.) fibre. When the use of the mixture rule for the prediction of the tensile strength of single fibre type composites was shown to lack accuracy the form of the mixture rule for the prediction of hybrid tensile strengths and other tensile properties was adapted. Instead of regarding the hybrid to be composed of different reinforcing fibres in a resin matrix it came to be regarded as a combination of fibre reinforced plastics. Thus for a hybrid composite, A_f B_f m, containing volume fractions V_{Af}, V_{Bf}, and V_m of fibre A_f, fibre B_f and matrix m respectively, where fibre A_f is the L.E. fibre, the hybrid composite tensile stress at the initial failure, σ_c', can be given by either equation 19 or 20, equation 20 being potentially more reliable.

$$\sigma_c' = \hat{\sigma}_{Af} V_{Af} + \sigma_{Bf}' V_{Bf} + \sigma_m' V_m \quad \ldots \quad (19)$$

$$\sigma_c' = \hat{\sigma}_{Afm} V_{Afm} + \sigma_{Bfm}' V_{Bfm} \quad \ldots \quad (20)$$

where $\hat{\sigma}_{Af}$ = failure stress of A_f,

σ_{Bf}' and σ_m' = stresses in B_f and m respectively at the failure strain of A_f,

$\hat{\sigma}_{Afm}$ = failure stress of composite A_fm with fibre and matrix contents V_{Af} and V_m respectively,

σ_{Bfm}' = stress in the composite B_fm with fibre and matrix contents V_{Bf} and V_m respectively, at the failure strain of composite A_fm

and V_{Afm} and V_{Bfm} = the volume fractions of composites $A_f m$ and $B_f m$ respectively in the hybrid composite $A_f B_f m$.

The first major work on the mechanical properties of hybrid composites was published in 1972 when Hayashi [5] proposed a hybrid design method based on the second form of the mixture rule above. Hayashi postulated the requirement of a hypothetical material X with initial elastic modulus E^*, maximum tensile strength $\hat{\sigma}^*$ and tensile strain $\hat{\varepsilon}^*$, as shown in figure 10. Three different types of unidirectional reinforced materials, A, B and C are considered with elastic moduli, ultimate strengths and ultimate strains of E_A, E_B, E_C, $\hat{\sigma}_{At}$, $\hat{\sigma}_{Bt}$, $\hat{\sigma}_{Ct}$ and $\hat{\varepsilon}_{At}$, $\hat{\varepsilon}_{Bt}$, $\hat{\varepsilon}_{Ct}$, respectively, as shown in their σ v ε curves in figure 11. Hayashi predicts the necessary volume fractions of the three materials A, B and C, using the mixture rule to give the required properties of material X when put into a symmetrically laminated unidirectional hybrid composite. He assumes that the fracture of each material component in the hybrid composite takes place at its normal individual fracture strain. Thus the tensile σ v ε curve for the designed hybrid material and the relevant equations for the elastic modulus (E), tensile stress (σ) and ultimate tensile strength ($\hat{\sigma}$) of the three regions of the curve (I, II, III) are as given in figure 12. It is assumed that once a component material fails it no longer contributes to the strength of the hybrid composite.

In order to verify the theory a hybrid composite was fabricated, consisting of unidirectional carbon/epoxy and unidirectional glass/epoxy material laid up in the order 3 ply g.r.p. + 2 ply c.f.r.p. + 3 ply g.r.p. Tensile tests were conducted on carbon/epoxy specimens, glass/epoxy specimens and the hybrid specimens. The experimental results are compared with those predicted by the proposed hybrid theory. Correlation between the two sets of results is excellent with the exception of the primary fracture stress and strain. The theoretical and experimental curves are given in figure 13. The predicted first fracture stress and strain are 49kg/mm^2 and 0.767% respectively and the experimental values are 67kg/mm^2 and 1.110% respectively. This increase in the primary fracture strength of the hybrid by 37% and increase in the failure strain of the carbon/epoxy part by 45% was unexpected. Hayashi's explanation for this phenomenon, later termed the 'hybrid effect', was that "the occurrence of fracture of c.f.r.p. part will retard under the influence of greater ductility of its surrounded g.r.p. parts and it results in the greater fracture strength and strain for the c.f.r.p. part.".

In the same year as Hayashi's paper[5] Kalnin[22] conducted a more extensive study of the mechanical properties of hybrids using a series of layered unidirectional graphite/glass/epoxy hybrids with varying relative fibre volume fractions. The hybrid composites were tested in shear, flexure, compression and tension. In tension Kalnin found that the initial fracture of the graphite fibres in the glass rich hybrid laminates (less than 2:3 graphite to glass fibre) was not catastrophic for the whole composite. The glass fibre supported the redistributed load and the failure strain of the hybrid was that of the glass fibre. In specimens with graphite to glass ratios greater than 9:11 the initial fracture of the hybrid composite was catastrophic, the amount of glass fibre being insufficient to carry the redistributed load. Comparing the tensile properties of the hybrid composites with those predicted by the mixture rule, Kalnin[22] discovered that the initial fracture strain of the graphite in the hybrid was greater than that of the graphite in its own single fibre type composite. The effect increased with increasing ratio of glass to graphite. In addition Kalnin found that the elastic moduli of the glass rich hybrids were substantially higher than predicted by the rule of mixtures. This contrasts with the glass rich hybrid tested by Hayashi[5] in which only the initial fracture stress and strain were found to deviate from the mixture rule.

In 1974 work conducted by Marshall[23] supported the results of Hayashi[5]. Marshall tested a glass/carbon/resin system with an intraply mixing of the fibre tows and a glass to carbon ratio of 4:1. The first fracture stress and strain was approximately 40% greater than those based upon the rule of mixtures. Marshall tenders two hypotheses for the extension of the initial linear portion of the σ v ϵ curve of the hybrid beyond the point of expected carbon fibre fracture. First is the possibility that before the observed failure strain of the carbon fibres is reached the strain in the glass fibres is greater than that in the carbon, the ends of the comparatively short test pieces becoming non-planar due to shear strain in the matrix allowing the carbon fibre to move relative to the glass fibre. Alternatively the hybrid is considered as carbon fibres in a stiff matrix of glass and resin. Thus weak carbon fibres may fail as their theoretical failure strains are approached but the stiff matrix absorbs a sufficient proportion of the energy released to retard the failure of other stronger fibres in the vicinities. In this case the geometrical configuration of the fibres in the matrix is expected to influence the magnitude of the effect. In both of the above hypotheses Marshall notes that a possible contributory factor to the

increase in initial hybrid failure strain is the different thermal coefficients of expansion of the two types of fibre (carbon fibre Type II and E-glass fibre) since the manufacture of the laminates was completed above room temperature. The effect of different thermal coefficients of expansion is covered in greater detail by Bunsell and Harris[24].

Bunsell and Harris[24] considered the hybrid model of Hayashi[5] in which the L.E. fibre layers bear no load after fracturing and the load-extension behaviour becomes that of the H.E. (higher elongation) components. Bunsell and Harris suggested that in a hybrid with the layers of fibres bonded well together the interlayer bond contributes to the behaviour of the composite and its properties may not correspond to those predicted by the rule of mixtures. For example in a hybrid consisting of well bonded layers of c.f.r.p. and g.r.p. upon the failure of the c.f.r.p. the bond between the c.f.r.p. and g.r.p. may be expected to remain sound and there will be little, if any, debonding of the carbon fibre. In such a case it is only the critical lengths either side of the fractured carbon which are ineffective in a load bearing capacity. As previously described in tensile failure theories of single fibre type composites, multiple fracture of the carbon layer may occur. Bunsell and Harris then postulated the previously reported 'hybrid effect' to be due to differences in the thermal expansion coefficients of the two reinforcing fibres. The L.E. carbon fibre has a lower coefficient of expansion than the H.E. glass fibre. With an effective bond the L.E. carbon is put into compression and the H.E. glass into tension as the hybrid cools from the hot-pressing temperature at which the resin is cured. The hybrid must reach an internal state of equilibrium where the compressive force in the L.E. fibre equals the tensile force in the H.E. fibre. Providing that the tensile and compressive moduli of each fibre are assumed to be the same and the volume fractions of the carbon fibre, V_{cf}, and the glass fibre, Vg are equal then

$$- E_{cf} \Delta\epsilon_{cf} = E_g \Delta\epsilon_g \qquad \ldots \quad (21)$$

where E_{cf} and E_g = the elastic modulus of the carbon and the glass fibres respectively

and $\Delta\epsilon_{cf}$ and $\Delta\epsilon_g$ = the strains induced in the carbon and glass fibres respectively.

Figure 14 shows the proposed effect of the differential thermal contractions on the initial section of the hybrid σ v ϵ curve. The initial hybrid modulus, E_h, is, as Hayashi proposed, calculated by the

rule of mixtures

$$E_h = E_{ofrp} V_{cfrp} + E_{grp} V_{grp} \quad \ldots \quad (22)$$

The above equation should now hold until the strain of the composite is equal to the breaking strain of the c.f.r.p. ($\hat{\varepsilon}_{cfrp}$) plus its original negative strain, i.e. linearity of the σ v ε curve should cease at a strain of $\hat{\varepsilon}_{cfrp} + \Delta\varepsilon_{cf}$.

To test this theory Bunsell and Harris[24] conducted a set of experiments with carbon/glass hybrids consisting of layers of c.f.r.p. and g.r.p. in which :

i) the layers of c.f.r.p. and g.r.p. were unbonded and
ii) the layers of c.f.r.p. and g.r.p. were bonded together.

In the unbonded specimens (which were bonded at their ends) the effect of the differential thermal contraction was clearly visible with buckling of the c.f.r.p. layers. The tensile properties of plain c.f.r.p. and g.r.p. specimens were determined first. The c.f.r.p. specimens failed straight across in a brittle mode and the g.r.p. specimens failed only after extensive splitting. In the hybrid specimens the arrangement of the c.f.r.p. and g.r.p. layers made no obvious difference to their tensile strength or behaviour. For both the bonded and unbonded specimens the initial modulus was rather low, indicating that the g.r.p. layers took the stress until the compressive strain in the c.f.r.p. layers was negated. There was a sharp load drop in the σ v ε curve of the unbonded hybrids at the point of the sudden c.f.r.p. failure. The subsequent curve was characteristic of that of g.r.p. alone. In the bonded hybrids the first drop in load occurred at a strain approximately 48% and 80% greater, for the 1:1 and 2:1 glass to carbon hybrids respectively, than expected from the behaviour of c.f.r.p. alone. The load drop was less than in unbonded specimens and the subsequent curve was jagged. Examination of the failed bonded hybrid specimens showed the c.f.r.p. parts to have failed in many different sections and not straight across. The scatter in the results was large, e.g. the CV of the strain at first failure in the four layer bonded hybrid specimens was approximately 20%. Bunsell and Harris concluded that it was not possible to determine whether the so called hybrid effect was due solely to the residual compressive strains in the c.f.r.p. because of the high degree of scatter.

The acoustic emissions of the specimens were monitored during the tensile testing. Poor acoustic coupling between unbonded layers prevented good detection of activity in the unbonded specimens. In the bonded hybrid specimens some acoustic emissions were monitored in the early stages of loading and the activity increased markedly immediately prior to the first load drop.

In 1976 the controversy concerning the behaviour of hybrid composites was reflected in a paper by Phillips[25] entitled "The Hybrid Effect - Does it Exist?" In the same year Phillips presented a paper[26] at the Reinforced Plastics Conference in Brighton which contained further experimental evidence of the hybrid effect. In a series of hybrids with 60% total fibre volume content, V_T, the initial failure strain ranged from 2% to 20%, for hybrids with 1:1 and 4:1 glass to carbon ratios respectively, greater than the normal failure strain of c.f.r.p. In investigating one of Marshall's theories[23] Phillips[26] found no holographic evidence of differential strain between the carbon and glass fibres in a stressed laminate. Phillips neglected any possible "magical increase in the total extensibility of fibres in the c.f.r.p. phase" and postulated the following two closely linked theories.

i) Fibre Bundle Theory:- The weakest carbon fibres and tows fail at their normal failure strains remaining well bonded to the surrounding glass fibre reinforced resin matrix. The failed fibres act as discontinuous fibres and so still contribute towards composite strength and stiffness. The unbroken fibres are stronger with a breaking strain above the mean for c.f.r.p.

ii) Crack Propagation Theory:- C.f.r.p. with a good i.l.s.s. fails catastrophically, the crack travelling transversely across the composite cross-section. G.r.p. fails with substantial debonding and fibre pull-out giving a rough, jagged fracture surface. The g.r.p. can act as a crack stopper. In a hybrid of g.r.p. and c.f.r.p. the g.r.p. reduces the possibility of a crack, initiated at a weak carbon fibre, propagating through the composite to lead to catastrophic failure.

The two theories are similar, with the g.r.p. suppressing, or retarding, the point at which the failure of one carbon fibre, or one tow, can propagate through the rest of the carbon in that cross-section.

Experimental results do not contradict the theories. It has been shown that in plain c.f.r.p. the carbon fibres may become discontinuous prior to failure[14], following the statistical failure modes described earlier[1][9].

Aveston and Sillwood[6] approached the question of a possible hybrid effect from a synergistic strengthening and fracture energy point of view. They hypothesized that in a hybrid composite a synergistic strengthening of the L.E. fibres occurs and estimated the theoretical $\sigma v \varepsilon$ behaviour of a hybrid composite, regarding the composite as L.E. fibres in a matrix composed of resin and the H.E. fibres. They state that when situated in a composite material the L.E. fibres will only be able to fracture at the failure strain of the L.E. fibres alone if sufficient work to fracture is available from the new fracture surfaces. If composite failure does not occur at the normal failure strain of the L.E. fibres then the potential deformation upon fibre failure may not provide sufficient energy for the failure to proceed. The L.E. fibres must then remain intact until the strain is sufficient to produce the required work of fracture. Aveston and Sillwood assume that wherever a L.E. fibre breaks all the other L.E. fibres break and that the failures are coplanar and perpendicular to the fibres. They estimate and compare the failure strains of the L.E. fibres in a unidirectional hybrid assuming first a perfect fibre/matrix bond and secondly a sliding frictional bond. The derivation of the minimum strain at which L.E. fibre fracture can occur, $\hat{\varepsilon}_{fuc}$, is given in detail for the bonded case. The final equations for the bonded and debonded cases are equations 23 and 24 respectively.

$$\hat{\varepsilon}_{fuc} = \sqrt{\frac{4\,\gamma_f}{E_f\left(1+\frac{1}{\Omega}\right)d_f}\cdot\left(\frac{G_m}{E_f}\right)^{1/2}\cdot\frac{V_f^{1/4}}{(1-V_f^{1/2})^{1/2}}} \qquad \ldots \quad (23)$$

$$\hat{\varepsilon}_{fuc} = \sqrt{\frac{6\,\gamma_f\,\Omega\,V_m}{\delta\,E_c}} \qquad \ldots \quad (24)$$

where γ_f = surface work of fracture of the fibres,
G_m = shear modulus of the matrix (H.E. fibre plus resin)
and $\Omega = \dfrac{E_m V_m}{E_f V_f}$

Multiple fracture of the fibres will occur in both cases providing the matrix can support the additional load in the regions of fibre fracture, i.e.

$$\hat{\varepsilon}_{fuc} E_f V_f + \hat{\varepsilon}_{fuc} E_m V_m \leq \hat{\sigma}_m V_m \qquad \ldots \quad (25)$$

Aveston and Sillwood[6] tested their synergistic strengthening theory with hybrids composed of separate layers of carbon and glass in an epoxy resin. The volume content of carbon, $V_{cf}\%$ was 3.5% and that of glass, $V_g\%$, was 35%. The essential features of their theory were reflected in the σ v ε curve of the hybrid, illustrated in figure 15. One significant difference between the theory and experiment is that multiple failure of the carbon occurred over a stress range instead of at a single value. Carbon failures were marked on the surface of the hybrid specimens by white striations caused by fibre/matrix debonding. The average spacing of the marks was approximately 1.00mm. The mean carbon fibre breaking strain in the hybrids was approximately 116% greater than the normal strain to failure of those carbon fibres, a separation in the order of 10 standard deviations of the strain results. For quantitative comparison of the increase in failure strain with the predictions of the elastic and debonded theories the surface work of fracture of Type I carbon fibre γ_f, was assumed to be 150 Joules/m^2, the value for graphite. The elastic theory proved to be innapplicable, predicting a very low first failure strain. The debonded theory predicted a 1.10% cracking strain compared with the experimental value of 1.08%. Since there was evidence of debonded regions (the white striations) in the specimens it was concluded that the debonded theory was suitable. A major assumption of the bonded and debonded theories is that the fibres in the hybrid are intimately mixed, in practice this is virtually impossible. Although the theoretical (for the debonded case) and the experimental results agree well Aveston and Sillwood[6] put forward the prevention of crack propagation theory postulated by Phillips[26] as an alternative explanation of the hybrid effect. Aveston and Sillwood felt that the validity of their theory could not be truly tested without an exact value for γ_f.

In 1977 Zweben[7] presented an approximate statistical analysis of the tensile strength of hybrid composites. The brief review, in reference 7, of previous work on hybrid composites considered the residual strain theory of Bunsell and Harris[24]. Zweben noted that if the data provided by Bunsell and Harris is assumed to be correct then the residual compressive thermal strain in the carbon phase would not wholly account for the increase in the initial fracture strain of the carbon fibre. The

mean strain at first break in the bonded hybrid composites was 0.48% and that in the plain carbon/epoxy composites was 0.26% . Zweben calculates that approximately 8% of this 80% increase in the carbon failure strain can be explained by residual thermal stresses. Despite the 20% CV of the first failure strains in the hybrid composites the above should be sufficient evidence to conclude that the different thermal expansion coefficients in the two reinforcing fibres does not wholly account for the hybrid effect. This is emphasized by the results of tensile tests on Kevlar 49/graphite/epoxy hybrids presented in reference 7. An analysis of the thermal expansion coefficients of the two fibres predicted an introduction of a positive residual thermal strain in the graphite fibres (L.E. fibres) during curing. Thus, according to Bunsell and Harris's theory[24] the hybrid composite should exhibit a negative hybrid effect in strain to first failure. There was an increase in strain of approximately 4%.

Zweben[7] considered the tensile failure of hybrid composites in the same manner as single fibre type composites, as a complex statistical process involving the fibre strength characteristics and fibre/matrix interfacial properties. However, since hybrids normally contain two types of fibres having quite different mechanical properties then the details of the failure process in the hybrid composites can be expected to differ from those in the single fibre type composites and this may result in differing failure strains. The model used is given in figure 16. The hybrid composite is 2-dimensional, of axial length L and composed of alternating H.E. and L.E. fibres. The moduli and cross-sectional areas are denoted by E_{LE}, E_{HE} and A_{LE}, A_{HE} respectively. The total number of fibres in the composite is N. The axial length L is considered to be divided into M_h layers of δ_h, the ineffective length of a broken fibre in the hybrid composite. The analysis assumes that the fibres support all the load, ignoring the contribution of the matrix. As the composite is strained L.E. fibre breaks occur , subjecting the adjacent H.E. fibres to strain concentration factors, k_h. The analysis follows the approach used in reference 9, postulating that composite failure results from the propagation of fibre breaks caused by local strain concentrations. The lower bound on composite tensile strain is taken as that at which the first overstressed H.E. fibre is expected to break. Representing the cumulative distribution functions of the failure strains of the L.E. and H.E. fibres of length L with Weibull distributions of the form

$$F_{LE}(\varepsilon) = 1 - \exp(-pL\varepsilon^{q}) \quad \ldots \quad (26)$$

and $$F_{HE}(\varepsilon) = 1 - \exp(-rL\varepsilon^{s}) \quad \ldots \quad (27)$$

where p, q, r and s are Weibull parameters, then the expression for the composite strain at which the fracture of the first overstressed H.E. fibre is expected, $\hat{\varepsilon}_{Lh}$, is derived as

$$\hat{\varepsilon}_{Lh} = \left[NLpr\delta_h (k_h^{s} - 1)\right]^{-1/q+s} \quad \ldots \quad (28)$$

The equivalent equation for a composite composed of only LE fibres is:

$$\hat{\varepsilon}_{L} = \left[2NLp^2\delta (k^{q} - 1)\right]^{-1/2q} \quad \ldots \quad (29)$$

The ratio, R_{ε}, of the lower bounds on the failure strain of a L.E. and H.E. fibre hybrid composite to that of a L.E. fibre composite is $\frac{\hat{\varepsilon}_{Lh}}{\hat{\varepsilon}_{L}}$.

$$R_{\varepsilon} = \frac{\left[prNL\,\delta_h (k_h^{s}-1)\right]^{-1/q+s}}{\left[2p^2NL\,\delta (k^{q}-1)\right]^{-1/2q}} \quad \ldots \quad (30)$$

$$\delta = 1.531 \left(\frac{E_{LE} A_{LE}\, g}{G_m t_m}\right)^{1/2} \quad \ldots \quad (31)$$

$$\delta_h = \frac{2}{j^{1/2}} \left(\frac{E_{LE} A_{LE}\, g}{G_m t_m}\right)^{1/2} \frac{m_2^{2} - m_1^{2}}{m_1(2-m_1^{2}) - m_2(2-m_2^{2})} \quad \ldots \quad (32)$$

$$k = 1.293 \quad \ldots \quad (33)$$

$$k_h = 1 + \frac{m_2 - m_1}{m_1(2-m_1^{2}) - m_2(2-m_2^{2})} \quad \ldots \quad (34)$$

where G_m = matrix shear modulus,

t_m = matrix thickness,

g = fibre spacing,

$$j = \frac{E_{LE} A_{LE}}{E_{HE} A_{HE}} \quad \ldots \quad (35)$$

and $$m_{1,2} = \left[\frac{j + 1 \pm (j^2 + 1)^{1/2}}{j}\right]^{1/2} \quad \ldots \quad (36)$$

The above expressions for δ, δ_h, k and k_h are approximate and are derived in Appendix 2 of reference 7.

When the H.E. and L.E. fibres have a similar scatter in failure strains and q≃s, equation 30 simplifies to

$$R_\varepsilon = \left[\frac{\hat{\varepsilon}_{HE}}{\hat{\varepsilon}_{LE}}\right]^{1/2}\left[\frac{\delta_h}{2\delta}\frac{(k_h^q - 1)}{(k^q - 1)}\right]^{-1/2q} \quad \ldots \quad (37)$$

where $\frac{\hat{\varepsilon}_{HE}}{\hat{\varepsilon}_{LE}}$ is the ratio of the average failure strains of the H.E. and L.E. fibres at an arbitrary gauge length L. Furthermore when the CV_f is small (approximately 5% or less) equation 37 reduces to

$$R_\varepsilon = 2^{1/2q}\left(\frac{\hat{\varepsilon}_{HE}}{\hat{\varepsilon}_{LE}}\right)^{1/2}\left(\frac{k}{k_h}\right)^{1/2}\left(\frac{\delta}{\delta_h}\right)^{1/2q} \quad \ldots \quad (38)$$

The model applies to a hybrid with alternating L.E. and H.E. filaments. In practice the fibre tows and not the individual filaments are intimately mixed. To overcome this Zweben assumed that each impregnated yarn can be treated as an individual fibre with an effective fibre cross-sectional area equal to the total cross-sectional area of the fibres in the yarn. The statistical strain characteristics of the fibres are replaced by those of the yarn. Another major assumption is that fibre break propagation in the L.E. fibres is arrested when the crack reaches intact H.E. fibres.

Zweben compared the above statistical theory with experimental data from a Kevlar 49/Thornel 300 system and a high modulus graphite/E-glass system. Tensile failure strain data for neither individual filaments nor impregnated yarns was available and Zweben substituted the data for composite tensile specimens, assuming the effect of composite volume to be small. The Kevlar 49/Thornel 300 hybrids consisted of alternating yarns of the two materials and the Weibull parameters for the materials justified the use of the simplified equation 38 for R_ε. The experimental and theoretical values calculated for R_ε were 1.04 and 1.22 respectively. Hybrid composites composed of balanced Kevlar/Graphite fabrics were also tested in tension and for these the experimental R_ε value was 1.31. The second hybrid system of graphite/E-glass fibres deviated markedly from the model composite. Hybrids of this system consisted of either one or two layers of graphite/epoxy sandwiched between two layers of E-glass/epoxy. No data was given on the Weibull parameters for fibre failure strains and Zweben assumed that the parameters were the same as for the Kevlar 49 and Thornel 300 fibres. Thus when calculating the values of R_ε equation 38 was applicable. Experimental strain ratios were 1.31 and 1.83

for the cases of two layers and one layer of graphite respectively. The theoretical ratio was 2.26. The result for the 3 layer hybrid composite, which more closely fits the assumed model of alternating H.E. and L.E. fibres, is nearest to the theoretical result. Note that the theoretical strain ratio was not adapted for the change in relative volume contents of the two fibres.

Zweben concluded that the agreement between the experimental and theoretical data was not unreasonable when considering the many simplifying assumptions made. However the validity of the failure model is now questioned. Zweben assumes that it is the failure of overstressed H.E. fibres which cause composite failure. Possible explanations for the high theoretical R_ε values are that:

i) crack propagation of L.E. fibres occurs, due to secondary strain concentrations on L.E. fibres, to result in composite failure below the strain at which over strained H.E. fibres are expected to fail and

ii) an extension of Rosen's theory[9] applies, L.E. fibre failures accumulate until one cross-section is seriously weakened and causes further fibre failure, again below the strain at which over strained H.E. fibres are expected to fail.

In either of the above cases the failure of the L.E. fibres may or may not spread to the H.E. fibres, depending on the relative fibre contents. Therefore the first failure strain need not be catastrophic to the whole composite. Zweben's theory does not appear to consider a 'first failure strain'.

In 1978 Marom et al[27] presented evidence to show that the fibre/resin interface is an important factor in the hybrid effect. The main area of research was the effect of hybridization on the ultimate stress (flexural) and fracture energies of a composite. Two systems were used. The first was a carbon/carbon/epoxy hybrid in which the mechanical properties of the carbon fibres differed but the surface characteristics were almost identical. The second system was a carbon/glass/epoxy hybrid, in which both the mechanical properties and surface characteristics of the fibres differed. The experimental results showed a hybrid effect in the carbon/glass/epoxy system. The ultimate strength of the composite was lower than predicted by the rule of mixtures, as found previously by Phillips[26] and Kalnin[22]. A hybrid effect was also observed in the

fracture energies. The important point here is that the hybrid effect was not exhibited by the carbon/carbon/epoxy hybrid where the fibre/resin interfaces were thought to be almost identical. Marom et al noted that in the carbon/glass/epoxy hybrid the pull-out lengths of both fibres were modified. They postulated the existence of two extreme cases resulting in lower and upper bounds in fracture energy:

i) the pull-out length of the glass fibre reduces to that of the carbon fibre and

ii) the pull-out length of the carbon fibre increases to that of the glass fibre.

In 1979 Aveston and Kelly[28] reviewed reference 6 and considered the specific area of the tensile first cracking strain and strength of hybrid composites. They presented a summary of the non-statistical theories of multiple cracking and constrained failure. As previously stated,for multiple cracking of the L.E. phase to occur in a hybrid composite there must be sufficient of the H.E. fibre to bear the applied load when the L.E. fibre fails at the first cracking strain,i.e. assuming no concentration of stress on the H.E. component at the failure of the L.E. component then for multiple fracture

$$V_{HE} \geqslant \frac{\hat{\sigma}_{LE}}{\hat{\sigma}_{HE} + \hat{\sigma}_{LE} - \sigma'_{HE}} \qquad \ldots \quad (39)$$

$$\text{and } \hat{\varepsilon}_{HE} \geqslant \hat{\varepsilon}_{LE}\left(1 + \frac{E_{LE}\,V_{LE}}{E_{HE}\,V_{LE}}\right) \qquad \ldots \quad (40)$$

where σ'_{HE} = stress in the H.E. component at $\hat{\varepsilon}_{LE}$.

Aveston and Kelly postulated that in a hybrid composite, in which the above conditions (equations 39 and 40) are satisfied, as the strain rises above $\hat{\varepsilon}_{LE}$ a series of parallel cracks form in the L.E. phase. Each crack results in an extension, Δl , of the specimen due to local relaxation of the broken L.E. fibres and the additional load bourne by the H.E. phase over a short distance each side of the crack. Where the bond remains intact,i.e. the elastic case, the load transfer length depends on the shear modulus but in the frictional case it is dependant upon the limiting bond strength. The cracking occurs when the strain is sufficient to produce the required work of fracture for the L.E. phase. Equations equivalent to 23 and 24 are produced for the elastic and debonded cases respectively. It is emphasized in reference 28 that by increasing

fibre dispersion, which reduces $\Delta 1$, the first cracking strain can be increased.

In summarizing the hybrid review to date it appears that under certain conditions a hybrid effect can be expected in the tensile stress and strain to first failure. This has been observed by Hayashi[5], Kalnin[22], Marshall[23], Bunsell and Harris[24], Phillips[26], Aveston and Sillwood[6] and Zweben[7]. An increase in initial hybrid tensile modulus, above that predicted by the mixture rule, has been observed, to the author's knowledge, solely by Kalnin[22] and was probably therefore a testing artefact. Two major approaches have been taken to the question of the failure strain of hybrid composites, the statistical theory of Zweben[7] and the non-statistical, energy theories presented by Aveston and Sillwood[6] and Aveston and Kelly[28] involving multiple cracking and constrained failure. The failure models for the two approaches differ. Zweben predicts a random failure of the L.E. fibres, having negligible effect on composite strength, with the H.E. fibres acting as crack arrestors until one H.E. fibre fails due to stress concentrations. The alternative school predicts multiple failures of the L.E. fibres at a specific strain with cracks running right across the composite cross-section normal to the fibres and the crack spacing depending on the load transfer length. The suggestion proffered by Bunsell and Harris[24] that residual differential strains in hybrid composites, cured at elevated temperatures, due to differing thermal coefficients of expansion of the two fibre types is the cause of the hybrid effect has not been substantiated though in a limited number of hybrid systems it may be a contributory factor.

According to the constrained cracking theories the first cracking strains in a hybrid, for the elastic and debonded cases, are given by equations 23 and 24 respectively.

$$\hat{\varepsilon}_{fuc} = \sqrt{\frac{4\gamma_f}{E_f\left(1+\frac{1}{\Omega}\right)d_f}\cdot\left(\frac{G_m}{E_f}\right)^{1/2}\cdot\frac{V^{1/4}}{\left(1-V_f^{1/2}\right)^{1/2}}} \qquad \ldots \quad (23)$$

$$\hat{\varepsilon}_{fuc} = \sqrt{\frac{6\gamma_f \Omega V_m}{\delta E_c}} \qquad \ldots \quad (24)$$

This theory only applies to hybrid composites in which the H.E. component is capable of bearing the additional load upon failure of the L.E. component. The parameters dictating the first cracking strain include the following:

i) fibre dispersion;
ii) the relative stiffness of the L.E. phase and the matrix (H.E. phase + resin);
iii) the L.E. fibre/matrix interfacial characteristics;
iv) the shear modulus of the matrix and
v) L.E. fibre content.

Following the statistical theory of Zweben[7] the lower bound on the failure strain of a hybrid composite containing equal numbers of L.E. and H.E. fibres, i.e. the strain at which the first over stressed H.E. fibre is expected to fail, is given by equation 28.

$$\hat{\varepsilon}_{Lh} = \left[NLpr\,\delta_h\,(k_h^s - 1)\right]^{-1/q+s} \quad \ldots \quad (28)$$

Thus according to Zweben the parameters dictating the failure strain of a hybrid composite, in addition to factors i) to iv) above, include:

i) specimen gauge length and
ii) statistical characteristics of the fibre strength distributions

Both theories assume intimate mixing of the fibre types.

In conclusion although great advancement has been made over the past decade in the field of hybrid composites, none of the existing theories are regarded as completely satisfactory. The proponents themselves advocate care in their use due to the various simplifying assumptions made or the difficulties in obtaining accurate values of the necessary parameters.

The purpose of this research is to further test the hybrid failure theories by manufacturing and tensile testing a series of carbon/E-glass/vinyl ester hybrid composites. The effects of total fibre content, relative fibre content and fibre geometrical arrangements on the tensile properties of the hybrid composites are all investigated. Attention is also paid to the fibre/matrix interfacial characteristics. The surface treatments of both the carbon and the E-glass fibres are varied in an attempt to assess the importance of bond strength on composite tensile properties.

The following section considers the interfacial/interphasial region and outlines problems encountered in determining the effectiveness of different fibre surface treatments.

2.3 The Interfacial/Interphasial Region in Fibrous Composites

The characteristics of the interfacial/interphasial area in a reinforced composite plays an important deterministic role in the mechanical properties of the material. In fibrous composites forces are transmitted between the matrix and fibre across the interface. There is evidence to suggest that extremely good fibre/matrix bonding can reduce composite strength by increasing the chances of catastrophic crack propagation at the failure of a weak fibre[3], i.e. a 'weakest link' mode of failure. However with the majority of fibre/matrix systems the main problem is the opposite, poor fibre/matrix bonding. Low fibre/matrix bond strength does not enable transmission of the necessary forces across the interface. The role of the fibre as a reinforcement is severely limited and the effect on the majority of the mechanical properties is deleterious. Obtaining satisfactory bonding was originally a problem with most g.r.p. systems and, to a lesser degree, with c.f.r.p. systems. G.r.p. is also particularly susceptible to water adsorption due to the hydrophilic nature of the surface of the glass. Water adsorption reduces interfacial bond strength, generally weakening the composite.

It was to improve and stabilize interfacial bonds that coupling-agents were developed. The role of a coupling-agent is to form bonds with both the fibre and matrix, acting as a bridge between the two surfaces, and enabling greater stresses to be carried from one phase to another. The bonds formed between the fibre/coupling-agent/matrix may be either mechanical bonds, due to interlocking of the materials to produce a high coefficient of friction between the surfaces, or chemical bonds. The chemical bonds generally have higher strengths. For this type of bond to form the treated fibre and resin must come into intimate contact, i.e. the resin must 'wet' the fibre.

The optimum fibre/matrix bond strength varies for different fibre/resin systems and on the intended application of the composite. A strong bond is required for stress transmission between the different phases but as already stated this may reduce the resistance of the composite to crack propagation. The accepted explanation for this is that crack growth may be deflected along weaker interfaces, delocalizing stress at the crack tip. With strong interfacial bonds the crack is more likely to pass from fibre to

resin and so propagate through the composite[29], resulting in the catastrophic 'noncumulative' or 'weakest link' fracture mode described by Zweben[3].

It is desirable for the interphasial region to have a modulus between that of the fibre and resin and an adequate toughness to withstand any differential thermal and curing shrinkages between fibres and resin. Note that at the time of writing this complex subject of the interfacial and interphasial region is not wholly understood. Different composite systems should be treated individually. A number of interphasial theories have been proposed after consideration of g.r.p. systems. The theories attempt to correlate the adhesion at the glass/coupling-agent/resin interfaces with the mechanical properties of the composites. Plueddemann[30] and Di Benedetto and Nicolais[31] present short summaries of these theories and more general information on interfaces is given in reference 32.

It is generally accepted that the interlaminar shear strengths (i.l.s.s) of composite materials provide qualitative information on the fibre/resin bond strength and, with high bond strengths, on the general condition of the matrix. Thus the i.l.s.s. is a suitable property by which to compare the effectiveness of different fibre surface treatments. When using the i.l.s.s. of composites for this purpose it is important to be aware of the other factors influencing this property. Slight misalignment of the fibres may increase the composite i.l.s.s. whereas the presence of voids reduces it[33]. In addition it is best to compare composites with similar fibre volume fractions. Prosen et al[34] have shown that the i.l.s.s. of a composite system may decrease with increasing fibre content if the extra fibres impair the efficiency with which the resin wets the fibres.

A popular test for determining the i.l.s.s. of unidirectional continuous fibre composites is the short beam shear test[35][36][37][38], three point bending of a rectangular specimen. The test can be undertaken quickly and cheaply over a range of temperatures. The major problem, given high quality specimens, is in achieving unambiguous results. The span to depth ratio (S:D) of the specimen is crucial. Failure is by a tensile or compressive mode if the ratio is too high and if too low the failure is by combined shear and tensile modes, giving erroneous results. Figure 17 shows the different failure modes possible in short beam shear specimens.

The recommended S:D in A.S.T.M. D. 2344-76[39] for unidirectionally reinforced short beam shear specimens is five or less. The exact ratio depends on the constituent materials, deflection, stiffness and alignment of the test apparatus and on the nature of the load supports, larger diameter load supports tend to give a higher apparent i.l.s.s. The width to depth

ratio also has a significant effect upon the apparent i.l.s.s. The width chosen should be at least twice the specimen thickness. Where possible the specimens should be fabricated with the required thickness of the i.l.s.s. specimen since an extra machined surface may reduce the accuracy of the test. A variety of specimen sizes can be used[39] but are typically close to 2mm x 10mm x 15mm. The cross head speed (c.h.s.) for i.l.s.s. tests should be kept constant for any set of specimens and be approximately 1.2mm/min. The i.l.s.s., τ_{il}, of a composite is calculated using equation 41.

$$\tau_{il} = \frac{3\hat{P}}{4BD} \qquad \ldots \quad (41)$$

where $\hat{P}$ = load at failure

and BD = specimen cross-sectional area.

The equation for the maximum tensile and compressive stresses ($\hat{\sigma}$) at mid span of the specimen is

$$\hat{\sigma} = \frac{3PS}{2BD^2} \qquad \ldots \quad (42)$$

Thus the composite specimen should fail in shear providing that

$$\frac{\hat{\sigma}}{2\tau_{il}} < \frac{S}{D} \qquad \ldots \quad (43)$$

Hancock and Cuthbertson[40] have approximately related the i.l.s.s. of a composite to the fibre/matrix i.f.s.s. (interfacial shear strength), τ_{if}, by considering the shear failure path. The equation derived is

$$\tau_{if} = \frac{\tau_{il} - (1 - x)\tau_m}{x} \qquad \ldots \quad (44)$$

where τ_m = shear strength of the resin

and x = the fraction of the fracture surface area of fibre/resin interface to total surface area of one of the shear fracture planes.

$$x = \frac{(V_f \pi)^{\frac{1}{2}}}{(V_f \pi)^{\frac{1}{2}} + 1 - 2\left(\frac{V_f}{\pi}\right)^{\frac{1}{2}}} \qquad \ldots \quad (45)$$

As previously stated it is the surface treatment of the fibre which determines the potential strength of the fibre/matrix interfacial bond in any given fibrous composite system. Therefore, to assess the importance of the fibre/matrix bond strengths with regards to any possible 'hybrid effects'

in the tensile properties of hybrid composites the author chose to vary the surface treatments of both of the constituent fibres. The fibres used in this research are carbon and E-glass fibres. The following section briefly covers the nature of the glass and carbon fibre with a view to their surface treatments.

2.4 Fibre Surface Treatments

Surface treatments for fibres were originally developed for two reasons and took two forms:

i) sizing, to protect the fibres from damage during handling and.

ii) coupling-agents, to improve the initial fibre/matrix bond strength and its resistance to degradation.

The first types of sizing to be developed had to be removed from the fibres prior to composite fabrication due to incompatability with the common resins. Sizings have been improved and now most need not be removed prior to compositing. Coupling-agents are frequently incorporated into these sizings. The use of suitable coupling-agents enhance the mechanical performance of the majority of fibre reinforced plastics, including g.r.p. and c.f.r.p. As stated in section 2.3, g.r.p. was notorious for poor interfacial bond strength and rapid deterioration of properties in adverse environments due to the hydrophilic nature of the glass. The advent of coupling-agents has therefore been of especial benefit to g.r.p.

This section of the review covers the nature of E-glass and carbon fibre surfaces and the different types of surface treatments for the fibres which are directly applicable to this research.

A comprehensive background to and a review of the developments of glass fibre/resin coupling-agents have been given by Vaughan[41][42]. At present the most widely used glass/resin coupling-agents are silane based. Silane coupling-agents are bifunctional molecules reacting to bond with both glass and resin. The general structure for a silane coupling-agent is $R'Si(OR)_3$. The R' contains the reactive group for the organic resin and the OR is an alkoxy group which reacts with the glass surface (it can also react with many other inorganic surfaces). The OR group is commonly either $-OCH_3$ or $-OC_2H_5$. Immediately prior to the application of the coupling-agent to the glass this alkoxy group is hydrolyzed.

For example, A187 is a Union Carbide silane coupling-agent used largely for epoxy resins and has the structure shown in figure 18. The hydrolysis reaction is as follows

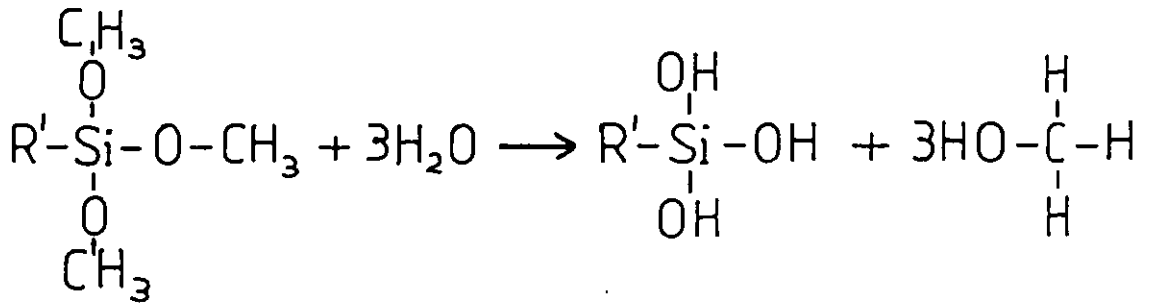

. . . (46)

On subsequent application of the coupling-agent to the glass surface a condensation reaction is thought to occur between the silanols on the glass surface and those of the coupling-agent[29][43], resulting in siloxane bridging (illustrated in figure 19). In addition to the siloxane bridging some hydrogen bonds may form (see figure 20). A further possibility is condensation reactions between the silane coupling-agent molecules, thus forming siloxane polymers which encapsulate the glass.

The decision of which of the many available silane coupling-agents to use in a system is taken by consideration of the resin type. The functional group R' of the coupling-agent should be capable of forming covalent bonds with the resin. Therefore an amino - or epoxy - functional silane is best used with epoxy and vinyl ester resins and a methacrylate - functional silane for a polyester resin. Thus the A187 coupling-agent in figure 18 is ideal for use with epoxy or vinyl ester resins.

Effective coupling appears to require a monomolecular covering or less of the glass surface with the coupling-agent. In practice optimum loading of silane coupling-agents in different systems varies between 0.2% and 2.0% weight per weight of the virgin fibre[44]. Reference 44 describes suitable methods for the application of silane coupling-agents to the fibre surface. Further information on silane coupling-agents is presented in references 45 and 46.

The type of carbon fibre used in this research is produced from polyacrylonitrile (PAN) precursor fibre by a method developed from the original R.A.E. process. The basic procedure is to heat the precursor fibre to remove all the elements except carbon and transform the carbon into the required structure. The process of converting the precursor fibre by pyrolysis to carbon fibre, via a ladder polymer, is described in references 47, 48 and 49. The structure of the fibres is relevant to the potential adhesion between fibres and resin and is therefore mentioned

The structure of carbon fibres [50] has been shown to vary with their precursor fibre and heat treatment[51]. The general structure of the polycrystalline carbon fibres is thought to be as follows: hexagonal crystals form a layer structure with no regularity in stacking; about thirty planar layers group together to form a crystallite; the crystallites form cylindrical fibrils of unknown length and the carbon fibres consist of closely packed fibrils. Carbon fibres formed from acrylic precursors are normally cylindrical. High modulus carbon fibres have greater preferred orientation and crystalline ordering than low modulus carbon fibres. The adhesion of carbon fibres to resin has been found to reduce as the fibre modulus increases[37], implying that in this respect less crystalline ordering is preferable. There are two distinct possible reactive sites in the crystals, firstly those in the basal planes with high bonding energy and therefore low reactivity and secondly the edge sites of the basal planes with high reactivity due to unpaired electrons. Work presented by Clark et al[37] in 1974 shows that the i.l.s.s. of carbon fibres in an epoxy matrix is considerably increased by etching the virgin fibres by oxidation either in air or in sodium hypochlorite solutions. The exact reason for the improvement in the fibre/resin bond strength is not known. It is postulated that the increase is due to the oxidation producing first pitting and then channels on the fibre surface. This results in an increase in the mechanical bonding between fibre and resin. A more favoured hypothesis is that the etching exposes more of the relatively reactive edge sites of the basal planes. Thus groups such as carboxyls (-COOH) and carbonyls ($>C=O$) become attached to these sites. These groups then form chemical bonds with the resin, when at the gelling stage, by means of a condensation reaction to form

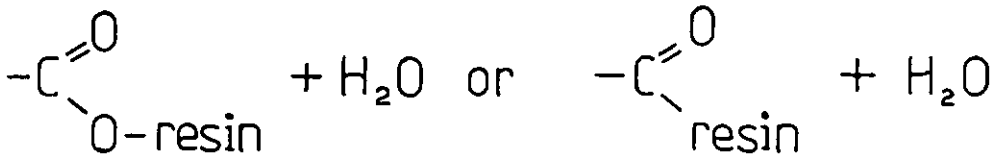

Oxidation, either in air or sodium hypochlorite solutions, is now a standard surface treatment for carbon fibres. Other treatments, suitable mainly for middle modulus carbon fibres, are oxidation by nitric acid[52] and coating with alternating and block copolymers[53].

Theories and experimental work concerning the tensile properties of plain fibre type and hybrid composites have been reviewed. The important parameters for the tensile hybrid effects have been highlighted and attention paid to both the interfacial/interphasial region of composites and the fibre surface treatment. The final two sections of this review concern the materials selected by the author for the experimental work and the quality control of the composites produced.

2.5 Composite Constituent Materials

The material system selected for this research is carbon and E-glass reinforcing fibres and a vinyl ester resin matrix. Reasons for this choice are given in section 3.1. This section deals with characteristics of the reinforcing fibres and the resin matrix.

2.5.1 Carbon and E-glass Reinforcement Fibres

The Hyfil-Torayca (trade name) carbon fibre chosen for this work has not, to the author's knowledge, been used in previous published research on hybrid composites. It is produced from special Toraylon (trade name) 6000 filament PAN fibre by a process involving controlled pyrolysis, in discrete stages, of the precursor fibre. The properties of the carbon fibre, as given by Hyfil[54], are listed in table 1. Two types of E-glass fibre are used in this research, the intention being to assess the effect of H.E. fibres with differing mechanical properties but with similar surface treatments on the tensile properties of a hybrid composite. The types are 600 tex and 500 tex E-glass fibres. The 600 tex E-glass fibre is manufactured by T.B.A. Industrial Products Limited. The sole information available from T.B.A. on the properties of the 600 tex E-glass fibres is that the average filament diameter lies in the range of 12.7μm - 14.0μm[55]. Unfortunately the manufacturers of the 500 tex E-glass fibres could not be traced, the fibre was obtained directly from Carr Reinforcements Limited, the weavers of the fibre tows into unidirectional continuous fibre tapes.

As mentioned in section 2.1 the tensile strength of a fibre type is not a unique value. The fibre strength distributions are attributed to flaws in the fibres. Various types of flaws may exist in both carbon and E-glass fibres[8][56] and can generally be classified as either structural or accidental. Structural faults (e.g. voids, inclusions) are initiated

during the manufacture of the fibres whilst accidental flaws (e.g. surface cracks) occur during subsequent handling of the fibres. Consideration of the severity distribution and density distribution of the flaws explains the length/strength dependence of fibres noted previously. In general the more severe flaws tend to be more widely spaced than the less severe flaws. Thus as the gauge length of a fibre is increased the probability of a severe flaw increases and therefore the tensile strength decreases. Conversely as the gauge length is reduced the tensile strength increases, approaching in the limit the theoretical tensile strength of a flawless fibre.

The statistical characteristics of fibre tensile strengths are particularly pertinent to this research since they are basic to many of the strength theories for composites[2][3][4][9]. The distribution commonly used to describe the fibre tensile strength variations is the Weibull distribution (see Appendix I).

$$f(\sigma) = \alpha L \beta \sigma^{\beta-1} \exp\left(-\alpha L \sigma^{\beta}\right) \quad \ldots \quad (4)$$

The Weibull parameters α and β are characteristic to each individual fibre type.

The relationship between log (fibre strength) and log (gauge length) for both glass and carbon fibres has been found to be linear, as shown in figure 21, and to correspond to a Weibull distribution by a number of researchers[10][16][57]. The Weibull parameters are derived from the log ($\hat{\sigma}_f$) v log (L) plots. Such plots are given in references 15, 57 and 58. The β values calculated from these lie between 6.86 and 10.15. The corresponding $\alpha^{-1/\beta}$ values, sometimes termed the 'reference stress level', are between 1.08 and 3.85 KN/mm$^{(2-1/\beta)}$. Note that the units for $\alpha^{-1/\beta}$ are not those of stress and care must be taken to maintain the correct units. β can be calculated using equation 47.

$$\beta = \frac{\ln\left(\frac{L_1}{L_2}\right)}{\ln\left(\frac{\hat{\sigma}_{f2}}{\hat{\sigma}_{f1}}\right)} \quad \ldots \quad (47)$$

where $\hat{\sigma}_{f1}$ and $\hat{\sigma}_{f2}$ are the average fibre failure stresses at gauge lengths L_1 and L_2 respectively. $\alpha^{-1/\beta}$ can be calculated from equation 48 for $\hat{\sigma}_f$.

$$\hat{\sigma}_f = \alpha^{-1/\beta} L^{-1/\beta} \Gamma\left(1 + \frac{1}{\beta}\right) \quad \ldots \quad (48)$$

where Γ is the gamma function.

Data on the statistical characteristics of carbon fibre tensile strength is not as common as for E-glass fibres. In reference 4 Barry gives the linear log-log plots of average fibre failure stress versus fibre length for Modmor Types IS, IIS and IIIS carbon fibres. The Weibull parameters for the same fibres calculated from data given by Barry in reference 16 are as follows:

Type IS, $\beta = 8.86$, $\alpha^{-1/\beta} = 2.69 \text{KN/mm}^{(2-\frac{1}{\beta})}$;
Type IIS, $\beta = 10.01$, $\alpha^{-1/\beta} = 3.57 \text{KN/mm}^{(2-\frac{1}{\beta})}$;
Type IIIS, $\beta = 9.57$, $\alpha^{-1/\beta} = 3.39 \text{KN/mm}^{(2-\frac{1}{\beta})}$.

The fibres are PAN based and the mechanical properties of Type IIS correspond closely with those of the Hyfil carbon fibre (see Table I) used by the author in this research.

2.5.2 Vinyl Ester Resin Matrix

The definition of a vinyl ester resin is[59] 'a polymerizable resin in which the terminal positions of the resin are vinyl ester groups and in which the main polymeric chain between the terminal portions comprises the residue of a polyepoxide resin'.

The mechanical properties of a vinyl ester resin are generally superior to those of conventional polyester resins and comparable with those of the established epoxy resins[60][61]. Vinyl ester is a relatively new addition to thermosetting resins and has a steadily increasing usage due to its good mechanical properties and high corrosion resistance. The type of vinyl ester used in this research is Derakane 411-45 manufactured by Dow Chemical Company Limited. Its mechanical properties, as given by Dow[62], are presented in Table I.

Vinyl esters are produced by reacting an epoxy with a vinyl group. The reaction is commonly an addition between a bisphenol - A based resin, such as diglycidyl ether of bisphenol - A, and an acrylic acid or derivative (see figure 22). The epoxide ring of the bisphenol - A based epoxy resin is broken and the resultant molecular chain has terminal unsaturation. This results in a relatively low molecular weight and precise polymer structure when compared with the high molecular weight and random structure of polyester resins. The terminal unsaturation and the positioning of the ester groups in the vinyl esters are the keys to their distinguishing properties. During the curing of vinyl ester resins the carbon to carbon double bonds (C=C) at the ends of the chains virtually all react, leaving very few C=C bonds to be

susceptible to oxidation and other chemical attack. The fewer ester groups in vinyl esters[63] compared with polyesters (see figure 23) also contributes towards the superior chemical resistance of vinyl ester resins. The ester groups are particularly susceptible to chemical attack by base catalyzed hydrolysis (see figure 24). For detailed information on the chemical resistance of vinyl esters consult the Dow Technical Bulletin 'Derakane Chemical Resistance Guide' [64].

The high activity of the C=C bonds in vinyl esters gives fast and reproducible gel times and the fibre wetting ability of the resins makes them suitable for wet lay-up fabrication techniques. Both are requirements for this research. A further point in favour of vinyl ester resins when considering them for use in a fibrous hybrid composite system is the occurence of solely terminal cross-linking during the curing process. This produces a relatively uniform polymer which minimizes internal stresses and leaves the whole of the molecular chain free to absorb mechanical and thermal shocks[63].

Another feature of the vinyl ester molecular chain is the secondary hydroxyl groups. It is believed by a number of people that these aid adhesion to reinforcing agents[62][63]. For example, when considering glass it is suggested that the vinyl ester secondary hydroxyl groups react with the hydroxyl groups on the surface of the glass reinforcement, resulting in excellent wetting of and adhesion to the glass by the vinyl ester resin. In this way the resin facilitates the production of high quality laminates.

With styrene present the major curing mechanism of vinyl esters is styrene cross-linking. Free radical initiating catalysts, e.g. organic peroxides (see figure 25), are commonly used to break the C=C bonds and achieve the cross-linking. To generate the free radicals required the catalyst is activated by accelerator(s). The catalyst/accelerator system must be chosen with care. The proportions of each added to the resin can be adjusted to satisfy the various requirements of different resin mixes but it is important that the degree of cure of the resin is checked. Complete curing is important in order to realize the optimum mechanical properties and chemical resistance of the vinyl ester resin. Incomplete curing of the resin matrix in a fibre reinforced composite is just one of a number of parameters which can affect the mechanical properties of the composite. The final section of this review is concerned with the evaluation of composite defects and the correct comparison of experimental data derived from composites with varying composition.

2.6 Factors Affecting the Quality and Comparison of Composite Materials

When comparing the properties of a series of composites it is important to have confidence in the quality of the composites tested. Good quality control reduces the possibility of erroneously assigning special characteristics to a composite which in reality are due to faults originating from the fabrication of the composite. Possible faults in the composites manufactured for this research are inclusion of voids, fibre misalignment and incomplete resin cure. The effect of these faults on the composite tensile and i.l.s.s. are assessed in this section.

A comprehensive paper on the effect of filamentary misalignment was presented by Claus, Jr. in 1972[65]. The bundle strength theory of parallel, non-interacting fibres was extended to incorporate random fibre misalignment. Filament misalignment up to as much as 20° was found to reduce the bundle strength by only a few per cent.

Claus[65] also studied the effect of fibre misalignment on the composite shear strength. The misaligned fibres enhance the composite shear strength since they change the internal state of stress from pure shear to a mixture of shear and tensile stress. Claus considered the misalignment of individual fibres about the mean fibre direction. Another form of misalignment is in the orientation of the mean fibre axis to the stress axis. Slight orientation errors may be made when machining the tensile specimens from the composite slab and in the alignment of the specimen in the testing machine. Phillips and Harris summarize the effect of fibre orientation on tensile strength in reference 66. The critical angle (θ_{cr}) above which composite tensile strength falls significantly and rapidly is that at which the fracture mode changes from fibre tensile fracture to interfacial or matrix shear failure. The value of θ_{cr} is represented by the equation

$$\theta_{cr} = \tan^{-1}\left(\frac{\tau_c}{\sigma_c}\right) \qquad \ldots \quad (49)$$

For untreated fibres, i.e. low τ_c, θ_{cr} may drop to approximately 5°. Fibre misalignment of this extent would be visible to the naked eye in specimens 50mm in length.

In 1970 Lenoe[67] reviewed the theoretical assessments of the effect of voids on mechanical properties of and on crack propagation in fibrous composites and evaluated the various techniques for the measurement and

characterization of voids in graphite/epoxy laminates. The resin burn off and acid digestion techniques of void measurement had both good reproducibility of results with CV's of approximately 2%. Precise values for the fibre and resin densities are important in order to obtain realistic composite void contents and even then extremely small void volume fractions cannot be measured accurately. Various techniques for determining resin and fibre densities are given in references 35, 36, 68, 69 and 70.

In 1972 Olster[33] artificially introduced voids into graphite/epoxy laminates and determined the horizontal shear strengths and tensile properties as a function of void content. For a porosity of 5% (by volume) the composite tensile strength and moduli were found to decrease by approximately 10%. The data indicated that there was a significant degradation at porosities greater than 1%. The strain to failure was highly insensitive to porosity content. The shear strength was highly sensitive to porosity, decreasing by approximately 10% for every 1% increase in porosity.

The question of void content goes hand in hand with fibre content. The resin burn off and acid digestion techniques for void content determination both involve the removal of the resin from the fibres. Knowing the original weight and density of the composite specimen (ω_c, ρ_c), the weight of the residual fibres (ω_f) and the density of the fibres (ρ_f) and the resin (ρ_m) then the void content (V_v %) can be calculated from the equation

$$V_v\% = \frac{\rho_m\left(1-\rho_c\frac{\omega_f}{\omega_c\rho_f}\right)-\rho_c\left(1-\frac{\omega_f}{\omega_c}\right)}{\rho_m} \times 100 \quad \ldots \quad (50)$$

For composites containing two fibre types the equation (50) is replaced by equation (51).

$$V_v\% = \left[1 - \frac{\omega_m\rho_c}{\rho_m\omega_c} - \frac{\omega_{f1}\rho_c}{\rho_{f1}\omega_c} - \frac{\omega_{f2}\rho_c}{\rho_{f2}\omega_c}\right] \times 100 \quad \ldots \quad (51)$$

Where the subscripts f_1 and f_2 denote the two fibre types.

Cilley et al[71] compared a variety of methods of fibre and void measurement in graphite/epoxy composites. These included acid digestion, water take up and quantitative microscopy. The most important

conclusion reached was that the acid digestion technique is as reliable as the more complex quantitative microscopy method for determining total fibre and void contents. Fibre volume fractions are important not only for void content determination but also for accurate comparison of different composites, especially hybrids. Relative fibre contents should always be quoted in terms of volume fraction rather than weight, tow or number fraction since in a stressed system the load bourne by the fibres is a function of their relative volume fractions. In a recent paper by Phillips[72] the importance of the correct definition of hybrid composition is emphasized and some of the consequences of incorrect usage illustrated.

The final source of variation in composite properties considered here is the degree of cure of the resin. Work conducted by Fuwa et al[14] on failure mechanisms in c.f.r.p. showed semi-cured c.f.r.p to have considerably lower tensile strengths than fully cured c.f r.p. (see section 2.1). In addition the density of the resin varies with degree of cure, so incomplete resin cure can also lead to inaccurate void content determination. A differential thermal analysis (D.T.A) technique has been applied successfully to determine the degree of cure of a number of thermosetting resins. This was demonstrated by Creedon[73] in a paper presented in 1970. D.T.A. has been proved to be a quick and reliable method.

The literature relevant to hybrid composites and associated areas has now been reviewed. The following section describes the experimental work undertaken by the author.

3. EXPERIMENTAL PROCEDURE

The literature review has shown the first tensile failure strain and failure mode, in unidirectional hybrid composites to be controversial. The aim of the experimental work is to provide sufficient data to explain the tensile behaviour of hybrid composites, establishing the existence or otherwise of any 'hybrid effects' and determining the controlling parameters. The parameters studied are:

i) total fibre volume content;
ii) relative fibre volume contents;
iii) fibre geometrical arrangement;
iv) fibre/resin interfacial properties and
v) mechanical properties of the H.E. fibre.

Ranges of hybrid composites were fabricated in which the above were varied. iv) was varied by changing the surface treatments of the fibres. v) was varied by using two different H.E. fibres from different manufacturers, keeping the general fibre type constant and therefore enabling the use of the same surface treatments on both H.E. fibres.

Below is a brief outline of the experimental work undertaken:

selection of the hybrid composite L.E. fibre/H.E. fibre/resin system including surface treatments;
characterization of the fibres and matrix;
fabrication of the parent and hybrid composites, varying the appropriate parameters and checking their quality, and,
i.l.s.s. and tensile testing of the composites.

The first step was to choose the constituent materials of the hybrid composites.

3.1 Choice of Composite System

The material requirements for the components of the composites were that:

i) the fibres and resin were compatible;
ii) the mechanical properties of the two types of reinforcing fibres chosen for the hybrid composites were complementary;
iii) the fibres were available in a suitable form for the manufacture of continuous unidirectional fibre composites;
iv) the H.E. fibre type was available from two different manufacturers in the required form;
v) alternative surface treatments were possible for both the L.E. fibre and H.E. fibre and
vi) the viscosity and gel time of the resin were suitable for wet lay-up techniques.

The favourable form for the fibres, considering that their surface treatments were to be changed, was unidirectional woven tape. To facilitate the fabrication of hybrid composites with varying fibre geometrical arrangements both mixed and single fibre type tapes were preferable. This severely limited the fibre choice. Carr Reinforcements Limited (now of Harris Trimmings Limited) were found to weave a range of E-glass fibre and carbon fibre tapes. Therefore this fibre reinforcement system was chosen. The properties of carbon fibre and E-glass fibre are highly complementary. A variety of surface treatments exist for both carbon and glass fibres which are compatible with most common resin matrices. Details of the surface

treatments are given in section 2.4 A final advantage of the system is that glass and carbon composites have good machinability.

The unidirectionally woven tapes obtained from Carr Reinforcements Limited were nominally 150mm. wide and were comprised of continuous warp lengths of carbon and/or E-glass tows held in position by a fine weft thread of E-glass fibre. Five different tapes were used:

i) 6000 filament carbon tow tape;
ii) 600 tex E-glass tow tape;
iii) 500 tex E-glass tow tape;
iv) & v) 600 tex E-glass tow and 6000 filament carbon tow tapes in the E-glass to carbon ratios of iv) 3:1 and v) 1:1.

Tables 2 to 6 give the relevant data on the above unidirectional woven tapes. The equations given for the calculation of the fibre volume fractions in the tape/resin composites are explained in section 4.1. Hybrid tapes of the carbon and 500 tex E-glass tows were not available. As mentioned in section 2.5.1 the 6000 filament carbon is manufactured by Hyfil Limited. The '600' tex E-glass, manufactured by T.B.A. Limited, is actually two tows of 300 tex E-glass. Throughout this work it is referred to as 600 tex E-glass. Epoxy, polyester and vinyl ester resins were all possible matrices for the fibre system. The high corrosion resistant vinyl ester resin Derakane 411-45 (manufactured by Dow Chemical Company) was chosen. In addition to satisfying the material requirements i) and vi) this resin is a cold cure resin with a low shrinkage on curing. Thus internal composite stresses are minimized.

In order to understand the tensile behaviour of the composites and to apply existing tensile failure theories the materials must be thoroughly characterized. Sections 3.2 and 3.3 describe the experimental characterization of the fibres and the vinyl ester resin respectively.

3.2 Characterization of the Reinforcement Fibres

The majority of the fibre properties were determined experimentally. Information provided by the manufacturers was of limited use due to possible variations in fibre properties from batch to batch and possible damage incurred by the fibres during the weaving process. The properties determined here are fibre diameter, fibre density and fibre tensile strength. Section 3.4 is concerned with the fibre surface treatments.

3.2.1 Fibre Diameter and Cross-Sectional Area

The cross-sectional areas (c.s.a.) of the carbon fibres and tows were calculated from the relevant data supplied by Hyfil[54]. The c.s.a. of the 500 tex and 600 tex E-glass fibres were determined experimentally. Two composite rods, approximately 10mm in diameter, were fabricated. One contained 600 tex and the other 500 tex E-glass fibres. Both fibre types were 'clean', the original 'as received' surface treatments having been removed (see section 3.4.3). The rods were sectioned normal to the fibre direction and the cut surfaces polished down to a 1μm finish and prepared for scanning electron microscope (S.E.M.) examination. At known magnifications the projected fibre diameters were measured directly from the screen. The average fibre diameters and the fibre and tow c.s.a. were calculated from the values of forty fibre diameters for both the 600 and 500 tex E-glass fibres. The results are given in section 4.2.1.

3.2.2. Fibre Density

The density bottle technique recommended by Sturgeon[36] was adopted to determine the fibre densities. The weight of a liquid displaced from a density bottle by a specimen of known weight is determined and the specimen's density calculated from the results.

A $100cm^3$ density bottle was weighed. The bottle was filled with distilled water at $21^{\circ}C$ and reweighed. The bottle was emptied, dried, reweighed and filled with bromobenzene at $21^{\circ}C$. The density bottle plus bromobenzene was weighed. A known weight of clean fibre which had been kept in a dessicator for at least 24 hours, was added to the density bottle. Great care was taken to ensure that the fibres were completely wetted by the bromobenzene with no trapped air bubbles. All traces of displaced bromobenzene were carefully removed from the outside of the density bottle and the density bottle was reweighed. The process was repeated ten times for each fibre type and the average of each set of results taken as the fibre densities. The results are given in Section 4.2.2.

3.2.3. Fibre Tensile Strength

The literature review establishes that fibre strengths are statistical in nature and are dependent upon the gauge length of the fibre. Their statistical behaviour can be approximately described by the Weibull

distribution. As previously noted Weibull parameters feature in a number of equations proposed for composite tensile strengths. The manufacturers of the carbon fibres publish only the average fibre tensile strength of the virgin fibres at a gauge length of 23mm, giving no indication of the statistical distribution of the strength. It is almost certain that the sizing and weaving processes cause some damage to the fibres which lowers their average tensile strength to below that quoted by the manufacturers. Therefore the statistical nature and values of the tensile strength of the 6000 filament carbon and 600 tex and 500 tex E-glass fibres were investigated and the appropriate Weibull parameters calculated. Two methods for determining the characteristics of the fibre tensile strengths were considered.

Method I - Single Fibre strength

A brief attempt was made to test single fibres in tension. The intention was to use the window method[35] with fibre gauge lengths of 50mm and 100mm. Unfortunately this method proved unsuitable since the individual filaments, with fibre diameters ranging from 7μm to 14μm, could not be separated from the sized tows without causing damage. Size removal facilitated the separation of the fibres but left them unprotected and far more vulnerable to damage. It was apparent that any results obtained via this method would be unreliable and therefore method II was adopted.

Method II - Fibre Tow Strength

The statistical nature of the strength of fibre bundles, or tows, has been related to that of individual fibres (see Appendix I and reference 57). Therefore the tensile testing of fibre tows provides an alternative method to the tensile testing of single fibres for the determination of the Weibull parameters for the tensile strength of individual fibres.

Tow lengths approximately 50mm greater than the desired specimen gauge lengths were cut. Each tow was gripped at the ends in small clamps and the tow pulled taut. Liquid wax was brushed on the tow at the limits of the gauge length. Cardboard tabs, 25mm square, were glued to the tows with a fast setting epoxy resin. The tabs were positioned at the ends of the specimen, up to the waxed portion of the tow. The purpose of the thin barrier of wax was to prevent any of the epoxy resin travelling along the fibres into the gauge length. The gauge lengths chosen were 50mm and 250mm for the as received fibres. Tows with altered surface treatments were also tested in case they had been damaged by the surface treating process. Such tows were available in lengths up to approximately 230mm. Therefore 50mm and 180mm gauge lengths were used in the tensile testing of these tows. At least 20 specimens were fabricated for each gauge length, fibre type and

fibre surface treatment. The prepared specimens were placed in a dessicator at 50% relative humidity (r.h.) for at least 24 hours prior to testing. The specimens were tensile tested on an Instron testing machine fitted with a 500kg load cell and set at a c.h.s. of 0.1cm/min. The specimens were gripped on the cardboard tabs in self-aligning, self-tightening wedge grips. The results are presented in section 4.2.3.

3.3 Characterization of the Resin Matrix

Table 1 lists the typical room temperature properties of clear cast Derakane 411-45, the vinyl ester resin chosen for the matrix, as given by Dow Chemical Company[62]. However, both the physical and mechanical properties of the vinyl ester resin can vary according to the types, quantity and ratio of the accelerator and catalyst used and to the casting method used. Therefore the properties of the resin relevant to this research were determined experimentally by the author. Tensile, shear and density specimens were taken from vinyl ester slabs fabricated via the same 'leaky mould' technique used for the fabrication of the composite slabs (see sections 3.3.2 and 3.5) and cured under the same conditions and with the same accelerator and catalyst system as used throughout this research. Thus the final properties of the resin specimens were as close as possible to those of the resin in the composite slabs. This section first covers the choice of the curing system and then the fabrication of the resin slabs and the testing for the density, the shear modulus and the tensile strength of the Derakane 411-45 vinyl ester resin.

3.3.1 The Curing System

The desired resin gel time for the fabrication of the composite slabs via the leaky mould technique was 45 to 50 minutes. The optimum resin mix had to have this gel time and give a complete cure. The accelerators and catalyst used were cobalt naphthenate (CoNap), dimethyl amine (DMA) and methyl ethyl ketone peroxide (MEKP), as recommended by Dow Chemicals.

To determine a curing system with the correct gel time a number of resin mixes were prepared with different quantities of catalyst and accelerators. The resin was weighed into polypropylene beakers and the required amounts of accelerators and then catalyst were added, mixing

thoroughly between additions. The addition of the peroxide to vinyl ester resin causes a strong generation of bubbles throughout the mass of the resin. Therefore after the final addition and mixing of the MEKP each mix was placed in a vacuum dessicator and degassed to aid the removal of the bubbles. The gel point of each mix was determined by dipping a glass rod into the mix and immediately removing it[35]. The gel point was reached when a solid string of resin was formed on removal of the rod. The experiments were conducted at room temperature. The results are presented in table 7. Three of the mixes, 3, 9 and 13, gave suitable gel times. The degree of cure of these three mixes was investigated.

D.T.A. (see section 2.6) was used to check the extent of cure. Three batches of resin were mixed with the formulations of mixes 3, 9 and 13 in table 7. Three specimens for D.T.A. analysis were taken from each of these resin mixes. The first specimen from each mix was taken and scanned immediately after mixing to give the complete curing D.T.A. scan of each resin mix. The second specimen from each mix was taken and scanned 24 hours after resin mixing. The final set of three specimens was taken and scanned when the resin had been post-cured, 24 hours after mixing, at 100°C for 2 hours. The temperature range of each D.T.A. scan was 0°C to 200°C. The individual specimen weights were recorded. They were kept to between 4 and 8gms. The results of the D.T.A. scans are given in section 4.3.1.

3.3.2 Fabrication of Resin Slabs

The slabs were fabricated in a leaky mould, see figure 26, with inside dimensions 200mm x 150mm x spacer thickness. The surfaces were treated with Vydax AR release agent. Extreme care in preparing the mould was found to be vital in order to produce resin slabs with satisfactory surface finishes. Prior to the fabrication of a resin or composite slab the mould was thoroughly cleaned. A new coat of release agent, Vydax AR, was then brushed on to the clean grease free surfaces of the mould and left until the solvent had evaporated. The release agent was baked on to the mould at 300°C for approximately 10 minutes to improve its adhesion to the mould. Vydax AR is a trade name for tetrafluoroethane. It is supplied by United Lubricants Limited as a dispersion in Freon TF (trichlorotrifluoroethane) solvent. Details of its properties and recommended modes of application can be found in Vydax trade literature[74].

The prepared mould was placed in a cardboard tray in a fume cupboard and the tray packed to make the mould lie horizontal. Strips of plasticene were positioned along the ends of the mould to act as temporary end walls for the resin and the appropriate spacers were placed on the side walls. The required amount of resin was weighed out and catalyst and accelerators added in the following ratios.

2ml	MEKP	
0.3ml	CoNap	per 100gm of Derakane 411-45 resin.
0.05ml	DMA	

The resin was mixed thoroughly, placed in a vacuum dessicator, degassed for 2 minutes and cast on to the prepared mould. Once the resin began to gel the mould lid was carefully lowered into position and a mass of 20kg placed on the top to force the excess resin out over the plasticene ends until the mould lid and spacers met. After 24 hours the mould was placed in a furnace and slowly heated up to 100°C. After 2 hours it was furnace cooled to room temperature and released from the mould.

3.3.3. Resin Density

The density of the cured vinyl ester resin was determined using the density bottle technique as described in section 3.2.2 with the exception that distilled water and not bromobenzene was used as the displacement medium. The 10 resin samples tested were approximately 0.5gms in weight and were taken from resin slabs, fabricated as described in the previous section 3.3.2. The samples were kept in a dessicator for at least 24 hours prior to their density determination. The results are given in section 4.3.2.

3.3.4 Resin Shear Modulus

The shear modulus of the matrix of a fibre reinforced composite is important when considering the transfer of stresses from fibre to fibre. It is a parameter in a number of equations relating to failure strains in composites. The carbon/E-glass/vinyl ester hybrid composites can be regarded as carbon fibre reinforcement in an E-glass fibre/vinyl ester matrix. Therefore the shear modulus of both the vinyl ester resin and a range of E-glass composites was determined by the method described overleaf. The basis of the method was to apply a known torque to a rectangular bar specimen and measure the resultant deflection.

The standard shear modulus test specimens have the following dimensions: length 125 ± 1mm; width 10.0 ± 0.1mm; thickness 4.0mm ± 0.2mm. The thickness can be reduced but if taken down to less than 2.5mm there is a chance of increasing the error in the measured modulus. The composite specimens were limited to the thickness of their slabs, nominally 2.00mm It was simple to fabricate resin slabs of different thicknesses. Therefore prior to fabricating and testing the composite specimens, the magnitude of the error due to decreasing specimen thickness to below 2.5mm in the case of the resin was investigated by testing resin specimens with the following thicknesses: 2.00mm; 2.50mm; 3.00mm; 4.00mm. Four specimens of each thickness were tested with the length and the width of the standard test specimens.

The specimens were prepared by cutting from the length of the slabs the required number of strips approximately 150mm long and 11mm wide. The strips were routed down to approximately 10.5mm in width and cut down to 125mm in length. The machined edges of the specimens were ground down successively with 400 and 600 grade silicon carbide paper to a width of 10 ± 0.1mm. The specimens were stored in a dessicator and kept at 50% r.h. for 24 hours prior to testing. The thickness and the width of each specimen were measured with a micrometer in five different places along its length and recorded.

A Wallace Clash and Berg Torsion Apparatus was used to test the shear specimens. A specimen was clamped into position in the apparatus. One end was held firmly in a fixed clamp and the other end attached to a rotatable drum. The effective free length of the test piece between the clamps was 100mm. A load of approximately 100gm was applied to the loading wire threaded around the drum. By this means the drum rotated, applying a torque to the specimen. The load applied was recorded, and the resultant deformation of the specimen, in the form of drum rotation, was measured. The results are given in section 4.3.3.

3.3.5 Resin Tensile Strength

In order to calculate the theoretical tensile properties of the composites from the rule of mixtures the tensile behaviour of the matrix must be known.

The resin tensile specimen shape adopted was as shown in figure 27.

Strips of width 27mm were cut from the length of a cast slab. The strips were trimmed to a length of 140mm, placed in the specimen template and routed down to the correct shape. The radius and parallel gauge length of each specimen was polished to 600 grade silicon carbide paper, using a small volume of acetone as the wetting agent. Acetone is a weak solvent for Derakane 411-45 and would therefore tend to close any microscopic cracks remaining on the resin surface. The specimens were placed in a dessicator at 50% r.h. for at least 24 hours prior to testing. Ten specimens were prepared. The thickness and width of each specimen were measured in five places along each gauge length and recorded. The tensile specimens were tested to failure on an Instron testing machine fitted with a 500kg load cell and geared to give a c.h.s. of 0.5cm/min and a chart speed (c.s.) of 5cm/min. The specimens were secured in self-tightening, self-aligning wedge shaped grips. The extension of the specimen was measured up to a 3% strain by means of an extensometer with two linear variable differential transducers (l.v.d.t's.) and a gauge length of 25mm. This extensometer was clipped on to the specimen within the specimen's gauge length. The load v strain was recorded on an XY plotter. The extensometer was removed from the specimen when the l.v.d.t.'s reached the end of their linear range at a strain of approximately 3%. Beyond this point the strain was calculated from the less accurate load v time plot recorded on the Instron's own chart. This was used throughout each test. The results of the tensile tests are given in section 4.3.4.

3.4 Fibre Surface Treatment

As previously stated one of the aims of this research was to investigate the importance of the fibre/matrix interface in hybrid composites. To achieve this the surface characteristics of the glass and carbon fibres in the plain (single fibre type) tapes were changed by varying the fibre surface treatment. The tapes were only available from Carr Reinforcements Limited with one type of surface treatment. Therefore the as received treatments had to be removed from the fibres and alternatives applied. Two alternative treatments were chosen for the 6000 filament carbon fibre and three alternative treatments for both the 600 tex and 500 tex E-glass fibres. This section includes the determination of the type and amount of size (plus coupling-agent) on the as received fibres and describes the size removal processes and the application of the chosen alternative surface treatments.

3.4.1. Fibre Size Content

The weight percentages and volume percentages of sizing on the carbon and E-glass fibres in the as received state were determined. Ten approximately 200mm lengths of fibre tow were cut from each of the carbon, 600 tex and 500 tex E-glass plain tapes. The lengths were kept for 24 hours in a dessicator before being accurately measured and weighed. In the case of the carbon fibre the procedure was repeated with cleaned fibres (see section 3.4.2). The fibre size contents on the as received fibres were calculated from the weights per metre of sized and unsized tow (see section 4.4.1).

3.4.2 Carbon Fibre Surface Treatment

The carbon fibre in the as received unidirectional tapes was treated with an Epikote 828 (Shell trade name) sizing, applied by Hyfil Limited. Information on the removal of the sizing and on possible alternative surface treatments was supplied by Hyfil Limited[75]. The two surface treatments chosen as alternatives to the Epikote 828 sizing were cleaned (hereafter termed no coupling-agent, no c-a) carbon fibre and carbon fibre etched in a solution of ferric chloride in sodium hypochlorite. Thus the three surface treatments of the carbon fibres used in this research are as follows:

i) Shell Epikote 828 sizing (as received, as rec.);
ii) cleaning (no c-a), and
iii) cleaning with subsequent etching to a weight loss of approximately 0.8%, in a solution of ferric chloride in sodium hypochlorite (etched).

The method recommended by Hyfil Limited for the removal of the Epikote 828 sizing was successive leaching in baths of dichloromethane.

The required lengths of carbon tape were cut and immersed for 10 minutes in each of five successive baths of dichloromethane. On removal from the final bath the tapes were rinsed twice in acetone and five times in distilled water. The tapes were hung up to dry in a furnace at 80°C and kept at that temperature until used or treated further. Throughout the process great care was taken not to damage the fibres. In no instance was the clean tapes kept more than 24 hours before use.

The following procedure for the etching of carbon fibres was adopted and produced approximately a 0.8% weight loss of the carbon fibres which in work by Clark et al[37] was found to give good fibre to matrix bonding.

The required number of lengths of tape were cut and cleaned as described above. The tapes were kept at 80°C. 1.25gm of ferric chloride was added to 200ml of sodium hypochlorite and stirred thoroughly for two minutes. The solution was filtered to remove any excess ferric chloride and poured into a glass tray. The tapes were removed from the furnace and placed in the tray, ensuring that all the tapes were completely immersed in the etchant. The tray was left in a fume cupboard for 16 hours. The etchant was poured off and the carbon tapes rinsed in slowly running water until the fibres were clean. The tapes were rinsed five times in distilled water and placed in a furnace at 80°C to dry and kept at that temperature until used a maximum of 24 hours later.

3.4.3 E-glass Fibre Surface Treatment

The 600 tex E-glass fibre was treated by T.B.A. Limited, with a silane coupling-agent incorporated in a polyester size. Unfortunately T.B.A. Limited could not be persuaded to reveal the type of silane coupling-agent used but did say that it was supplied to them by Union Carbide. Information from Union Carbide, along with examination of their trade literature[44] suggested that the incorporated silane coupling-agent was either A172 or A174 (Union Carbide production codes). Union Carbide kindly provided samples of two further types of their silane coupling-agents, A187 and A1100. Nothing was known concerning the surface treatment of the 500 tex E-glass fibres. As with the carbon fibres alternative surface treatments were required for the E-glass fibres. It was decided that both the 600 tex and 500 tex E-glass fibres were to be used in the following four surface treated states, providing that the dressing on the as received 500 tex E-glass was found not to include either A187 or A1100 coupling-agents:

i) as received (as rec.);
ii) cleaned (no c.-a.);
iii) cleaned with A187 coupling-agent applied (A187), and
iv) cleaned with A1100 coupling-agent applied (A1100).

This section covers the experimental investigation into the type of coupling-agent on both the 600 tex and 500 tex E-glass fibres, the method adopted for the removal of the as rec. dressings and the application of the two alternative coupling-agents, A187 and A1100. Two methods were tried to determine which of the two Union Carbide coupling-agents, A172 or A174, was incorporated into the polyester sizing on the 600 tex

E-glass fibres, the first method being unsuccessful. The second method was more involved than the first. Union Carbide's trade literature on silane coupling-agents[44] states that both A172 and A174, under certain conditions, are soluble in water and that the by-products on hydrolysis are 2 methoxy-ethan-1-ol ($CH_3OCH_2CH_2OH$) and methanol (CH_3OH) from A172 and A174 respectively. The aim of the second method was to obtain sufficient of the by-product for analysis.

Method I - The coupling-agent and size was removed from a sample of 600 tex E-glass (as described later in this section). Two KBr disc infra red (I.R.) specimens, A and B, were prepared. Specimen A contained a small amount of the cleaned E-glass and specimen B contained a small amount of the dressed as rec. E-glass. In both cases the glass was chopped up finely, mixed with KBr and pressed into a disc. The specimens were examined on an I.R. analyzer and their spectra compared.

Method II - Approximately 100gms of dressed 600 tex E-glass fibre was simmered for 8 hours in 60ml of distilled water in a 200ml flask. Any condensate was collected and returned to the solution at the end of the 8 hours. A 15ml aliquot of the solution from the flask was measured into a separating funnel and 10ml of Genklene (an I.C.I. trade name for a solvent, the predominant constituent of which is 1-1-1 trichloro-ethane) and a pinch of sodium chloride were added. The sodium chloride was added to enhance separation of the solution and the Genklene. The mixture was shaken thoroughly for 5 minutes and left to settle and separate. A sample of the Genklene (GI) was collected from the separating funnel. A control sample of Genklene (GII) was prepared by repeating the extraction and separating process using distilled water and Genklene. Two further 15ml aliquots were measured from the solution in the 200ml flask and the extraction and separating procedure was repeated using the organic solvents diethyl ether and methyl isobutyl ketone. The samples obtained were labelled DI and MI respectively. The appropriate controls, DII and MII, were prepared in the same manner as the Genklene control. An I.R. analysis was conducted on each of the 6 samples and the spectra compared. The results are presented in section 4.4.3.

The analysis, method II above, of the coupling-agent on the 600 tex E-glass was repeated with the as rec. 500 tex E-glass fibres. The results from this and comparisons between the appearances of the as rec. 600 tex and 500 tex E-glass, the behaviour of the as rec. dressing system at temperature and their composite behaviour are discussed in section 4.4.3 in order to determine the coupling-agent on the as rec. 500 tex E-glass fibres.

The recommended method[55] for the removal of the silane coupling-agent and the polyester sizing from the 600 tex E-glass tapes is to heat the tapes to between 350°C and 600°C until no size or coupling-agent remains. The satisfactory method and conditions for the complete removal of the dressing from both the 600 tex and 500 tex E-glass fibres were found to be identical. The procedure is now described.

The required lengths of glass tapes were cut and placed in a furnace fitted with an extraction tube. The furnace was heated up to 570°C ± 3°C and kept at that temperature for 30 minutes. The glass was furnace cooled to 80°C and kept at that temperature until used or treated further. In no instance was the clean fibres kept more than 24 hours. The clean fibres produced by this treatment were extremely brittle and fragile. Therefore the utmost care was taken not to damage the fibres in subsequent handling of the tapes.

The method for the application of the A187 and A1100 silane coupling-agents to the E-glass fibres was derived from information supplied by T.B.A. Limited[55] and Union Carbide[44]. The method gives the glass fibres a coating of approximately 0.5% by weight of coupling-agent.

The required number of lengths of E-glass tape was cleaned as described above. 80ml of silane coupling-agent was measured out and added to 5000ml of distilled water and stirred thoroughly to form a 1.6% volume solution. The glass tapes were removed from the furnace and immersed in the solution for two minutes. The tapes were removed and hung up to dry in a furnace at 80°C and kept there until used. Throughout the process the silane coupling-agent and its solution were kept in a fume cupboard and the fibres handled as gently as possible. The treated glass was kept a maximum of 24 hours before use.

3.5 Fabrication of the Unidirectional Composite Slabs

Having characterized the constituent materials and determined the methods of application of the alternative surface treatments for the fibres the fibrous composites to be investigated were fabricated. The leaky mould technique was adopted, as for the resin slabs. The following describes the composite slab fabrication.

The required number of 20.5cm lengths of tape was cut from the relevant roll(s) of tape and placed in a furnace at approximately 80°C for at least 3 hours prior to fabrication of the slab. The mould was prepared as described in section 3.3.2. The base was placed in a cardboard tray in

a fume cupboard and positioned to lie horizontally. 2mm spacers were placed on the side walls. These resulted in composite slabs of thickness 1.96 to 2.05mm, depending on the mould used and its preparation. 120gms of resin were weighed out and 0.06ml DMA, 0.36ml CoNap and 2.4ml MEKP were added. The resin was mixed thoroughly after each addition and finally placed in a vacuum dessicator for two minutes to degas. A layer of resin was poured over the prepared surface of the mould base. The appropriate tape length was gently removed from the furnace, allowed to cool and placed on the resin in the mould with the warp threads running the length of the mould. When all the fibres were wet and any air bubbles originally trapped in the fibre bundles had risen and dispersed a further layer of resin was added. The succession of fibre, resin etc. was continued until the desired lay-up sequence and number of layers of tapes had been reached. Great care was taken to position the fibre tows in the different layers parallel to one another. When the final layer of resin had been added and the gel point reached, the mould lid was carefully lowered into position and a mass of 20kg placed on the top to force the excess resin out of the open ends until the mould lid met the spacers. After 24 hours the mould was placed in a furnace, heated up to 100°C and kept at temperature for two hours. The mould was furnace cooled to room temperature and the slab released. Its quality was checked prior to calculating the fibre volume content using the appropriate equation(s) from equations 57 to 65 in section 4.1. Table 8 gives the range of slabs fabricated which passed the quality control tests and lists their fibre volume fractions.

3.6 Quality Control of the Composite Slabs

Occasionally poor quality composites were produced. It was necessary to recognize and reject these to prevent misleading and confusing results. The quality of every slab produced was checked. The following slab properties were monitored: slab thickness; surface finish; void content and degree of cure of the resin.

The thickness of each slab was measured along its length and width upon release from the mould. If the variation in thickness was greater than $\pm$ 1% of the mean thickness the slab was rejected. The cause of this was incorrect settling of the mould lid on to the spacers. The slab surface finish was examined by eye and touch. If either side of the slab looked or felt rough it was rejected. The cause of a poor slab surface finish was inadequate mould surface preparation.

Two methods of void content determination were considered. These were via image analysis microscopy and via composite density and fibre content. Due to problems in the preparation of carbon composite specimens for the image analysis microscopy the second method was preferred. The densities and fibre volume fractions of composite samples were determined and from the results the void content was calculated.

Five samples, each of approximately 0.5gm, were cut from each slab and their edges smoothed down. The samples were placed in a dessicator for at least 24 hours before their densities were determined using the density bottle technique described in section 3.2.2.

Resin burn off and acid digestion techniques were used to determine the fibre volume contents in the composite samples. Control specimens of pure resin, sized glass fibres, no c-a. glass fibres, sized carbon fibres, no c-a. carbon fibres and composites showed that for resin burn-off a temperature of 520°C for 3 hours was required. This removed all the resin and sizing whilst producing no weight loss in no c-a. E-glass. It completely oxidized the carbon fibres. The acid digestion controls showed the technique to remove the resin and sizing with no weight loss of either the clean E-glass or clean carbon fibres. Therefore the resin burn-off method, since it was the simplest to carry out, was used for the plain E-glass composite specimens and the more complicated acid digestion method was used for the plain carbon composite specimens. In the case of hybrid composites the acid digestion technique followed by the resin burn off technique was used in order to produce the separate fibre contents. The accuracy of the techniques for fibre content determination was checked using composite samples of known fibre contents.

For resin burn off a specimen and crucible were weighed and placed in a furnace, with a through air flow, at 520°C for 3 hours. The crucible plus fibres was removed from the furnace, cooled, kept in a dessicator for at least 24 hours and then weighed. The apparatus used for the acid digestion is shown in figure 28. A clean sintered glass filter and a composite specimen were placed in a dessicator for at least 24 hours and weighed. A water pump was attached to the three necked flask in figure 28. The sample was added to the 100ml flask with 20ml of 98% sulphuric acid. The flask was heated gently until the acid was fuming. The heat was removed and 50% weight/volume hydrogen peroxide was added to the flask from the dropping funnel at an approximate rate of one drop every 3 seconds for the first two minutes and then increased to one drop per second until all the resin was digested and the solution was clear. The solution was heated gently for a

further three minutes and allowed to cool. The contents of the flask were thoroughly rinsed out and washed with distilled water through the sintered glass filter until the washing liquid was neutral. The filter with the fibres was dried in a furnace and placed in a dessicator to cool before weighing. The digestion process was carried out in a fume cupboard.

The results are given in section 4.5. Any composite with a void content greater than 1% was likely to give misleading results when tested in tension. Therefore an actual void content of 1% was considered to be the critical rejection level. Due to the difficulties in obtaining precise values at such low void contents it was decided that any composite yielding a value greater than 0.8% would be rejected and composites yielding a void content value of greater than 0.6% would be examined microscopically.

The quality of the liquid resin was checked approximately monthly for deterioration by conducting a D.T.A. immediately after mixing, as described in section 3.3.1. This revealed whether a maximum cure of the resin was possible.

To check the degree of cure of the resin in a composite slab a sample of composite was taken from the slab at the end of the post-cure, weighed and tested by D.T.A. There was no feature in the D.T.A. scan of either the E-glass or carbon fibres over the temperature range of the resin scan. Therefore if the D.T.A. scan obtained for the composite differed from that of mix 3 (shown in figure 36) the cure was unsatisfactory and the slab discarded.

3.7 Determination of Composite Interlaminar Shear Strength

As stated in the literature review the i.l.s.s. of a composite provides qualitative information on the fibre to resin bonding and a relationship between i.l.s.s. and i.f.s.s. (interfacial shear strength), given in equation 44, has been postulated by Hancock and Cuthbertson[40]. The test was therefore used to indicate the relative successes of the different fibre surface treatments and, to a certain extent, to act as a further quality control check on the composites. I.l.s.s. reduces considerably with increase in composite void content (see section 2.6). The short beam shear test method, which is essentially a three-point bending test, was adopted here since it is quick and economical with regard to materials. The recommended specimen span to depth ratio (S:D) for carbon and glass fibre reinforced resins is approximately 5:1[39][76]. The use of the correct ratio is imperative in order for the specimen to fail in shear.

According to B.S. 2782 part 3, method 341A[76] the minimum specimen thickness is 2mm ± 2%, the overall length is 6 times the mean thickness and the width is 10.0 ± 2mm. The specimens were prepared as follows.

Strips approximately 10.6mm wide were cut lengthwise from each composite slab on a diamond cutting wheel. The cut edges were polished down to 1200 grade silicon carbide paper and a width of 10.0 ± 0.02mm, great care being taken to keep edges parallel. The strips were cut into lengths and keeping the corners square were polished down to 1200 silicon carbide paper and a length of 6 times the mean thickness. The specimens were rinsed in distilled water, dried and placed in a dessicator at 50% r.h. for at least 24 hours prior to testing. Six specimens were prepared from each slab.

The specimens were tested on the three-point bending rig shown in figures 29 and 30. The rig has 6mm diameter rollers and was designed to give a span varying in discrete steps of 0.5mm between 9.50mm and 11.50mm. The Instron machine was fitted with a 500kg load cell and geared to give a c.h.s. of 0.1cm/min and c.s. of 10cm/min. The dimensions of the specimen to be tested were measured and the rig set up with the appropriate span. The specimen was positioned in the rig and tested. When specimen failure was not by shear the span was altered and more specimens from the same slab were tested until the correct span to give shear failure was found. The results of the previous specimens from that slab were disregarded and the corrected span used for the remaining specimens. The results are given in section 4.6.

3.8 Composite Shear Modulus

The shear modulus is one of the properties of the composite matrix required for the analysis of the tensile behaviour of the hybrid composites. A hybrid composite can be regarded as the L.E. fibre in a matrix of H.E. fibre and resin. Therefore the shear modulus of a range of E-glass fibre/vinyl ester composites was determined. The specimen shape used and experimental procedure followed was as described in section 3.3.4.

3.9 Determination of Composite Longitudinal Tensile Properties

The tensile stress v strain (σ v ϵ) curves for the composites were obtained and particular attention paid to the initial modulus and the stress and strain at the point of initial fracture. From the results the extent of any hybrid effects with varying composite ratios of glass to carbon, fibre geometric arrangement, fibre volume content, interfacial characteristics and H.E. fibre properties were investigated.

A variety of tensile specimen shapes has been used with unidirectional fibrous composites and three of these are shown in figure 31, all are recommended in B.S. 2782 part 3 [77]. Shape a) was unsuitable since the machining of the waist removes fibres from the outside layers of the composite which, in the case of a hybrid composite composed of plain fibre tapes, would change the carbon to E-glass ratios over the crucial waisted area. Trial specimens with shapes b) and c) were tested. The b) specimens were unsuccessful, failing in shear as shown in figure 32. The rectangular straight sided specimen c) was satisfactory with approximately 90% of the specimens failing within the gauge length. Therefore this specimen shape was chosen and the composite tensile specimens made to the dimensions given in figure 33. The specimens were prepared as follows.

Six strips approximately 13mm wide by 190mm long were cut lengthwise from each slab on a diamond wheel. The specimens were placed in a specimen template and routed down to a width of 10.10±0.10mm. The specimen edges were polished down to 600 grade silicon carbide paper and cut to the required 150mm length. The variation in specimen thickness and width was less than 0.5%. A 50mm centre gauge length was marked on each of the specimens and the outside portions prepared for the bonding of aluminium end tabs. They were abraded in water with 400 grade carbide paper, rinsed thoroughly with distilled water, dried and placed in a dessicator for at least 24 hours. The rectangular end tabs were 50mm x 11mm and were guillotined from a sheet of commercially pure aluminium approximately 0.5mm thick. The tabs were thoroughly degreased in Genklene in an ultra-sonic bath for 15 minutes and etched in a chromic acid bath [36] for 30 minutes. The bath composition was:

10gms	chromium trioxide;
36ml	98% sulphuric acid. and,
160ml	distilled water.

On removal from the bath the tabs were washed thoroughly in distilled water, dried and left in a dessicator for at least 24 hours. Immediately prior to the bonding of the end tabs to the specimens both were wiped quickly with acetone to remove any surface grease. The tabs were bonded to the specimens with a thin layer of fast setting epoxy resin adhesive and left to cure at room temperature under a mass of 1kg. Alternative adhesives were tried but there was frequent debonding of the end tabs during tensile testing. The prepared specimens were placed in a 50% r.h. dessicator for at least 24 hours prior to testing.

The composite specimens were tested on an Instron machine, fitted with a 10,000kg load cell and geared for a c.h.s. of 0.2cm/min and c.s. of 10cm/min.

Prior to the testing of each specimen the specimen's dimensions at 5 equidistant points along its gauge length were measured and recorded. The c.s.a. recorded nearest to the point of actual failure was used in the stress calculations. The specimen was positioned in self-tightening wedge shaped grips and the dynamic strain was recorded against the load on a Bryan's XY plotter. The specimen was pulled to complete failure. The dynamic strain was measured for the first few tensile specimens tested with FLA-30 foil strain gauges (produced by Techni-Measure Limited, gauge length 35mm, gauge factor 211 and nominal resistance 120 ± 0.3ohms). These were applied to the specimens prior to testing and since the specimens were pulled to failure the gauges could only be used once. As the experimental technique developed the strain gauges were replaced by a l.v.d.t. extensometer which clipped straight on to the specimens. This method of strain measurement proved to be both simple and economical. The testing of 6 control specimens showed differences between the strain monitored by the strain gauges and by the extensometer to be insignificant. The initial failure of a specimen disturbed either the strain gauges or extensometer. Therefore where initial failure was not catastrophic, the strain beyond this point was estimated from the Instron plot of load v. time.

The results are presented in section 4.7. The fracture surfaces of the specimens were studied with the aid of S.E.M.

4 RESULTS AND DISCUSSION

This section presents and discusses the results of the experimental work and investigates and develops theories for the tensile failure of hybrid composites. In some cases this section would be unnecessarily encumbered by the inclusion of the data and results for every individual specimen tested. Therefore, where deemed appropriate, only the average results for sets of specimens are detailed here and the complete sets of results are given in Appendix 2 (2A). Where the average, $\bar{x}$, standard deviation, ψ, standard error of the mean, $\psi_{\bar{x}}$, and the coefficient of variation, CV, are reported for any set of results the following formulae have been used:

$$\bar{x} = \frac{\Sigma x}{n} \qquad \ldots \quad (52)$$

$$\psi = \sqrt{\frac{n\Sigma x^2 - (\Sigma x)^2}{n(n-1)}} \qquad \ldots \quad (53)$$

$$\psi_{\bar{x}} = \frac{\psi}{\sqrt{n}} \qquad \ldots \quad (54)$$

$$CV = \frac{\psi}{\bar{x}} \qquad \ldots \quad (55)$$

where x = the value of an observation
and n = the number of observations

In some cases two sets of results are compared to see if there is a 'significant difference' between them. The two-sample t test is applied in these cases using either the 95% or 99% levels of significance (α_{LS} = 0.05 or 0.01). Where the means are found to differ at the 99% level the difference is said to be 'highly significant'. Where means differ only at the 95% level the difference is 'significant'. The t test is used in preference to the simpler z test since $n < 30$. The statistic t for two sets of results is given by the formula:

$$t = \frac{\bar{x}_1 - \bar{x}_2}{\sqrt{\frac{(n_1-1)\psi_1^2 + (n_2-1)\psi_2^2}{n_1+n_2-2} \cdot \left(\frac{1}{n_1} + \frac{1}{n_2}\right)}} \qquad \ldots \quad (56)$$

Table III in reference 78 lists t values for different degrees of freedom and levels of significance.

In cases where the differences amongst more than two means are studied an analysis of variance method in conjunction with an F statistic is adopted. The necessary steps in the calculation are best summarized in the following table:

Source of Variation	Degrees of Freedom	Sum of Squares	Mean Square	F
Treatments	K-1	SS(Tr)	$MS(Tr) = \frac{SS(Tr)}{K-1}$	$\frac{MS(Tr)}{MSE}$
Error	N-K	SS(E)	$MS(E) = \frac{SSE}{N-K}$	
Total	$\overline{N-1}$	$\overline{SST}$		

where Treatments = the K different sets of results being studied,

N = total number of observations

SS(Tr) = treatment sum of squares = $\sum_{i=1}^{K} \frac{T_i^2}{n_i} - \frac{T^2}{N}$,

n_i = number of observations in the ith sample,

T_i = sum of values of the ith sample,

T = grand total = $\sum_{i=1}^{K} T_i$,

SST = total sum of squares = $\sum_{i=1}^{K} \sum_{j=1}^{n_i} x_{ij}^2 - \frac{T^2}{N}$,

x_{ij} = the jth observation of the ith sample ,

SSE = SST - SS(Tr) ,

MS = mean squares = $\frac{\text{respective sum of squares}}{\text{their degrees of freedom}}$

and F = statistic of the F distribution used in the significance test = $\frac{SS(Tr)}{SSE}$

F values are given in Table V of reference 78

4.1 Unidirectional Woven Tapes and Composite Fibre Contents

Section 3.1 gives the reasons for the choices made of constituent materials for the hybrid composites. The materials chosen were Derakane 411-45 vinyl ester resin and 6000 filament carbon and 600 tex and 500 tex E-glass fibres in the form of unidirectional woven tapes. In this section the formulae for fibre volume contents of composites fabricated from the tapes are derived utilizing some of the results presented in the next section, 4.2, on the properties of the reinforcement fibres. Tables 2 to 6 present data on the unidirectional woven tapes. The equations given for composite fibre volume contents were derived as follows.

Consider the plain carbon fibre unidirectional woven tape. The average tape width was 150mm and the warp consisted of 70 tows of 6000 filament carbon fibre. In any composite slab the carbon fibre volume fraction (V_{cf}) due to the layers of the plain carbon tape equals the product of the average carbon c.s.a. per unit width of tape and the number of layers of plain carbon tape divided by the slab thickness (t) in mm.

The average carbon tow c.s.a. = $0.2310mm^2$ (see section 4.2.1). Therefore the average c.s.a. of carbon fibre per unit width of tape = $\frac{70 \times 0.2310}{150}$ which equals $0.1078mm^2$

Therefore the formula for V_{cf} due to n layers of plain carbon tape in a composite slab is:

$$V_{cf} = \frac{0.1078 \times n}{t} \quad . \ . \ . \quad (57)$$

Note that for composites fabricated from etched carbon fibre tapes the carbon content is reduced by 0.8%, i.e. multiply the V_{cf} derived from equation 57 by 0.992.

Parallel calculations for V_{g6} and V_{g5} (volume fractions of the 600 tex and 500 tex E-glass fibres respectively) due to plain 600 tex and plain 500 tex E-glass tapes respectively produce equations 58 and 59.

$$V_{g6} = \frac{0.1117 \times n}{t} \quad . \ . \ . \quad (58)$$

$$V_{g5} = \frac{0.1117 \times n}{t} \quad . \ . \ . \quad (59)$$

In hybrid composites the formulae for composite slab V_T (total fibre content), V_{cf} and V_{g6} due to the hybrid tapes are necessary.

Consider the 3:1 unidirectional woven tape. Tape width was 148mm and of the 71 warp tows every fourth one was carbon. Using the average tow c.s.a.'s given above the average fibre c.s.a. per unit width of tape is calculated as

$$\frac{71 \times 0.2310 \times 1}{148 \times 4} + \frac{71 \times 0.2362 \times 3}{148 \times 4} = 0.1127 mm^2$$

Thus in a composite slab the V_T , V_{cf} and V_{g6} due to n layers of 3:1 hybrid tape are as follows:

$$V_T = \frac{0.1127 \times n}{t} \quad . \ . \ . \quad (60)$$

$$V_{cf} = \frac{0.0277 \times n}{t} \quad . \ . \ . \quad (61)$$

$$V_{g6} = \frac{0.0850 \times n}{t} \quad . \ . \ . \quad (62)$$

Similarly for a composite containing n layers of 1:1 hybrid unidirectional woven tape, in which the warp tows alternate between carbon and 600 tex E-glass tows, the composite V_T , V_{cf} and V_{g6} due to those layers of 1:1 tape are given by equations 63, 64 and 65.

$$V_T = \frac{0.1106 \times n}{t} \quad . \ . \ . \quad (63)$$

$$V_{cf} = \frac{0.0547 \times n}{t} \quad . \ . \ . \quad (64)$$

$$V_{g6} = \frac{0.0559 \times n}{t} \quad . \ . \ . \quad (65)$$

The fibre contents (total, carbon and E-glass) of all the slabs fabricated from the unidirectional woven tapes were calculated using equations 57 to 65 and are given in table 8. In practice slab thickness varied between 1.96 and 2.05 $\pm$ 0.01mm. To facilitate comparison of the tensile results the thickness of all the slabs was taken as 2.0mm in the tensile and fibre content calculations. This simplification is justified by the low variation in thickness between the slabs and the high ratios of fibre to resin tensile strengths and moduli.

4.2 Reinforcement Fibre Properties

The results of the experimental characterization of the constituent fibres in the hybrid composites are presented in this section. The properties concerned are fibre diameters, fibre and tow c.s.a.'s, fibre densities and characteristics of the fibre tensile strengths. The results are summarized in tables 9 and 10.

4.2.1. Fibre Diameter and Cross-Sectional Area

The average fibre diameters, c.s.a.'s and tow c.s.a.'s for the 6000 filament carbon, 600 tex E-glass and 500 tex E-glass are given in table 9. The complete sets of measurements are given in table 2A1.

Hyfil describe the cross-sectional shape of the carbon fibres as off-round. The c.s.a. is calculated using the given average diameter of 7.3μm and the off-round shape factor of 0.92.

$$\text{Carbon filament c.s.a.} = \frac{\pi \times 7.3^2}{4} \times 0.92$$

$$= 38.51\mu m^2$$

$$\text{6000 filament carbon tow c.s.a.} = 6000 \times 38.51\mu m^2 = 0.2310mm^2$$

The S.E.M. examination of both the 600 tex and 500 tex E-glass fibres showed the majority of the fibres to have round cross-sections. A few fibres had irregular cross-sections but their appearance suggested that they had been damaged during the sectioning and preparation of the samples and therefore the diameters of these fibres were discounted. The average diameters for the 600 tex and 500 tex E-glass fibres were 12.82μm and 11.68μm respectively. The corresponding c.s.a.'s are $129.08\mu m^2$ and $107.15\mu m^2$.

The tow c.s.a.'s of the 600 tex and 500 tex E-glass tows, given in table 9 as $0.2362mm^2$ and $0.1969mm^2$ respectively, were calculated using the equation:

$$\frac{\text{weight per unit length of clean tow}}{\text{E-glass density}} \quad . \ . \ . \quad (66)$$

By definition the weight of one metre of virgin 600 tex and 500 tex E-glass tows is 0.6gm and 0.5gm respectively. The densities of the fibres are dealt with in the following section.

4.2.2 Fibre Density

The average densities obtained for the fibres are given in table 9. The complete results are given in table 2A2. The average density of $1.76gm/cm^3$ for the carbon fibre agrees with the value quoted by Hyfil. The average density of $2.54gm/cm^3$ for both the 600 tex and 500 tex E-glass fibres is within the range expected for E-glass material.

The fibre densities were calculated using the equation:

$$\rho_f = \frac{\omega_f \rho_w}{(\omega_{B+Z} - \omega_{B+Z+f} + \omega_f)} \cdot \frac{(\omega_{B+Z} - \omega_B)}{(\omega_{B+W} - \omega_B)} \quad (67)$$

where ρ_f = density of fibre,

ρ_w = density of water at 21°C,

ω_{B+Z} = weight of density bottle plus bromobenzene,

ω_B = weight of empty density bottle,

ω_f = weight of fibre added to density bottle,

ω_{B+Z+f} = weight of density bottle plus bromobenzene plus fibre

and ω_{B+W} = weight of density bottle plus water.

4.2.3 Fibre Tensile Strength

As explained in section 3.2.3 two different methods were considered for the determination of fibre tensile strength characteristics. The first method, based on the testing of individual fibres, proved to be unsuitable and no relevant results were obtained. The second method was more successful.

Method II - Fibre Tow Strength

The average two tensile strengths for all of the sets of tows tested are given in table 10 along with the Weibull parameters and average individual fibre tensile strengths derived from the results. The complete lists of the individual tow strengths are given in table 2A3.

Equation 68 has been successfully used by Zweben et al[57] to predict the mean fibre bundle strengths ($\hat{\sigma}_b$) from the Weibull parameters describing the tensile strength characteristics of the individual fibres.

$$\hat{\sigma}_b = (\alpha L \beta e)^{-1/\beta} \qquad \ldots \quad (68)$$

From equation 68 it is seen that the log - log plot of $\hat{\sigma}_b$ v L has a gradient of $-1/\beta$.

$$\therefore \quad \beta = \frac{\ln\left[\frac{L_1}{L_2}\right]}{\ln\left[\frac{\hat{\sigma}_{b2}}{\hat{\sigma}_{b1}}\right]} \qquad \ldots \quad (69)$$

This equation corresponds to equation 47 used in the case of single fibres rather than fibre tows.

Once β is known the value of $\alpha^{-1/\beta}$ can be calculated by direct substitution into equation 68. The ratio of average bundle strength ($\hat{\sigma}_b$) to average fibre strength ($\hat{\sigma}_f$) is

$$\frac{\hat{\sigma}_b}{\hat{\sigma}_f} = \left[(\beta e)^{1/\beta}\, \Gamma\left(1 + 1/\beta\right)\right]^{-1} \qquad \ldots \quad (70)$$

where $\hat{\sigma}_f = \alpha^{-1/\beta} L^{-1/\beta} \Gamma(1 + 1/\beta)$ . . . (48)

Therefore the tensile characteristics of the single fibres can be calculated from data on fibre bundle strength using equations 68, 69 and 70.

In this research it is assumed that the Weibull distribution adequately describes the statistical behaviour of the 6000 filament carbon fibre, the 600 tex E-glass fibre and the 500 tex E-glass fibre. Work recorded in references 10, 16 and 57 justify this assumption. The Weibull parameters, average bundle and fibre tensile strengths given in table 10 have been calculated from the results of the tensile tests of the fibre tows.

For example, consider the tensile results for the 6000 filament carbon fibre tows. At gauge lengths of 50mm and 253mm the average tow strength is 543.6N/mm^2 and 431.5N/mm^2 respectively. β is calculated by substitution into equation 69.

$$\beta = \frac{\ln\left(\frac{50}{253}\right)}{\ln\left(\frac{431.5}{543.6}\right)} = 7.02$$

Substituting into equation 68 gives the value of $\alpha^{-1/\beta}$

$$543.6 = \alpha^{-1/\beta}\left(50 \times 7.02 \times e\right)^{-1/7.02}$$

$$\therefore \quad \alpha^{-1/\beta} = \frac{543.6}{0.4339 \times 0.8672} = 1.45 \text{ KN/mm}^{1.858}$$

The ratio of $\hat{\sigma}_b$ to $\hat{\sigma}_f$ for the 6000 filament carbon is calculated from equation 70.

$$\frac{\hat{\sigma}_b}{\hat{\sigma}_f} = \left[1.32 \times 1.153 \times 0.9356\right]^{-1} = 0.702$$

Therefore the average tensile strengths for Hyfil carbon fibre with lengths of 50mm and 253mm are 774.4N/mm^2 and 614.7N/mm^2 respectively.

The tensile results for the 600 tex E-glass tows and 500 tex E-glass tows were treated in the same manner.

Consider the results obtained for the carbon fibres. The average fibre tensile strength quoted by Hyfil is 2.35kN/mm^2 at a gauge length of 23mm. The equivalent tensile strength of the as rec. carbon can be calculated from the data in table 10, equation 68 and the ratio of equation 70.

$$\hat{\sigma}_{f(23mm)} = \frac{1450\ (23 \times 7.02 \times e)^{-1/7.02}}{0.702}$$

$$= 868.2\ N/mm^2$$

This is less than 40% of the value quoted by Hyfil. Some variation in properties is expected between fibres from different batches but even when allowing for the possibility that the as rec. fibres came from an inferior batch the difference in tensile strength is still considerable. The reduction in strength may be apparent and, as such, a result of poor specimen preparation. However the author was fully aware of the importance of preparing specimens in which the fibres were of equal length and of careful handling of the specimens throughout the preparation and testing. Great care was taken to minimize damage due to handling. The former source of error is believed to have been eliminated by discarding the results of specimens in which the load v strain plots revealed the specimen to contain fibres of varying lengths. On average there was one such specimen in each set of fibre tows tested. The reduction in carbon fibre strength is therefore attributed to damage incurred by the fibres, due to handling and weaving, between the manufacture and receipt of the fibres in tape form. Both the β value of 7.02 and the $\alpha^{-1/\beta}$ value of 1.45 KN/mm$^{(2-1/\beta)}$ are lower than those values derived for three different types of PAN based fibres from data in reference 16. The values of β and $\alpha^{-1/\beta}$ ranged between 8.86 to 10.01 and 2.69KN/mm$^{(2-1/\beta)}$ to 3.57$^{(2-1/\beta)}$ respectively.

The Weibull parameters calculated for the surface treated fibres (no c-a. and etched) are very close to those of the as rec. carbon fibres. An analysis of the variance amongst the mean fibre strengths of the three groups at the fibre gauge length of 50mm was conducted on the data. The test showed that there is no significant difference amongst the results. Therefore the fibres suffered a negligible amount of damage during the surface treatments.

The results for the as rec. E-glass fibres show both the 600 tex and 500 tex fibres to have noticeably lower tensile strength CV's than the carbon fibres. The β values calculated for the 600 tex and 500 tex E-glass fibres are 14.91 and 11.20 respectively. The average tensile strengths of

the 500 tex E-glass fibres at the gauge lengths tested are slightly greater than the corresponding values for the 600 tex E-glass fibres. It was hoped, for the purpose of investigating the importance of the mechanical properties of H.E. fibres on the tensile properties of a hybrid composite, that this difference would be more marked.

The most important point arising from the results of the tow tensile tests is the difference in the Weibull parameters of the surface treated E-glass fibres. For both types of E-glass the tensile strengths of the no c.-a., A187 and A1100 are considerably lower than the tensile strengths of the as rec. fibres. Despite the care taken during the removal of the original sizing and coupling-agent damage was obviously done to the fragile fibres, reducing their tensile strengths and increasing the strength CV. In the case of the 600 tex E-glass A187 fibres the tensile strength at 50mm is approximately 40% lower than for the equivalent as rec. 600 tex E-glass fibres.

The Weibull parameters for the fibres derived from the tow tensile tests and listed in table 10 are used in sections 4.7 and 4.8 in the comparison of the theories of Rosen[1] and Zweben[2] with the experimental composite tensile strengths.

The properties of the vinyl ester matrix are now considered.

4.3 Properties of the Derakane 411-45 Vinyl Ester Resin

This section deals with the results arising from the experimental work described in section 3.3. These include the determination of a suitable curing system for the resin, the resin density, resin shear modulus and resin tensile strength.

4.3.1 The Optimum Curing System for the Resin

The experimental procedures in the determination of the optimum curing system particular to this research are described in section 3.3.1. Table 7 gives the gel times and formulations of the resin mixes investigated. Out of the 13 formulations tested the following 3 (numbers 3, 9 and 13) gelled within the desired time range of 45 to 50 minutes.

Mix 3: 2.00ml of 50% MEKP; 0.30ml of 10% CoNap and 0.050ml of 100% DMA per 100gms of resin.

Mix 9: 1.00ml of 50% MEKP and 0.60ml of 10% CoNap per 100gms of resin.

Mix 13:0.80ml of 50% MEKP; 0.40ml of 10% CoNap and 0.050ml of 100% DMA per 100gms of resin.

The results of the D.T.A. scans (taken to determine the degree of cure of the resin) of the specimens taken from mixes 3, 9 and 13 are given in figures 34, 35 and 36.

Figure 34 shows that the major curing reaction occurs between 90°C and 120°C. Mix 3 undergoes the greatest exothermic reaction, indicating that mix 3 can be cured to a greater degree than either mixes 9 or 13. The scan of mix 9 shows its potential degree of cure to be minimal, suggesting that for a good cure DMA is necessary. After 24 hours the resin mixes 3 and 13 appeared to have completely hardened. However figure 35 shows mixes 3 and 13 to have only partially cured, making the post-cure treatment necessary. Figure 36 shows mix 3 to respond virtually completely to the post-cure at 100°C for 2 hours whilst the treatment is only partially successful for mix 13. Therefore mix 3 had the optimum formulation for use in this research. The formulation is:

2ml MEKP (50%), 0.30ml CoNap (10%) and 0.05ml DMA (100%) per 100gm of resin.

This mix gives the desired gel time of 45 minutes to 50 minutes and a post-cure treatment of 2 hours at 100°C completes the cure.

4.3.2 Resin Density

The results of the experimental work described in section 3.3.3 are presented in detail in table 2A2 and summarized in table 9. The resin density was calculated using the equation

$$\rho_m = \frac{\omega_m \times \rho_w}{\omega_{B+w} - \omega_{B+w+m} + \omega_m} \quad \ldots \quad (71)$$

where ρ_m = resin density, gm/cm^3,

ρ_w = water density at test temperature, gm/cm^3,

ω_m = weight of resin sample, gm,

ω_{B+w} = weight of density bottle plus water, gm,

and ω_{B+w+m} = weight of density bottle plus water plus resin, gm.

For example, the readings obtained from specimen 1 were as follows:

$\rho_w = 0.99842\ gm/cm^3$; $\omega_m = 0.4810gm$;

$\omega_{B+W} = 85.5778\ gm$; $\omega_{B+W+m} = 85.6362gm$.

Substituting the above values into equation 71 gives $\rho_m = 1.14gm/cm^3$.

The average density of all the specimens was $1.13gm/cm^3$, with a CV of 0.84%. Dow[64] quote the density of Derakane 411-45 as $1.12gm/cm^3$. The slight difference between the two values is probably due to a different formulation and curing cycle adopted for the tested resin by Dow Chemicals compared with those adopted in this work. The density value used throughout this work for the resin is $1.13gm/cm^3$.

4.3.3 Resin and E-Glass Composite Shear Modulus

The average shear modulus for each set of resin and E-glass composite specimens tested (as described in section 3.3.4) is listed in tables 11 and 12. Figure 37 shows the variation in shear modulus with the composite 600 tex and 500 tex E-glass fibre content. Table 2A4 gives the complete results. In every case the shear modulus, G, was calculated from equation 72.

$$G = \frac{L}{Bt^3\mu} \times \frac{T}{\theta} \quad N/mm^2 \qquad \ldots \quad (72)$$

Where L = effective free length of specimen = 100mm,

B = specimen width, mm,

t = specimen thickness, mm,

T = applied torque, N/mm^2 = applied force x drum radius (116mm)

θ = angle of twist, radians

and μ = function dependent on B/t ratio.

Figure 38 shows the relationship between μ and the B/t ratio. The data was obtained from Benham and Warnock[79]. As an example calculation of the shear modulus consider the resin specimen 10 of width 10.00mm and thickness 3.01mm. From figure 38 the B/t ratio of 3.32 gives a μ value of 0.269. For this specimen the applied load of 105gm produced a twist of 0.0747 radians. Substituting into equation 72 gives $G = 2.18KN/mm^2$.

As explained in section 3.3.4 the recommended specimen thickness for the torsion test is 2.5 to 4.0 $\pm$ 0.2mm. However, the composite specimens were taken from the composite slabs with a nominal thickness of 2.0mm. To ascertain the effect of specimen thickness on the resultant experimental

shear modulus the resin specimens of varying thickness were fabricated and tested. The average shear modulus of the 2.00mm thick resin specimens was 2.15KN/mm^2. This is the same value as the overall average shear modulus of the three sets of resin specimens tested with thicknesses of 2.50mm, 3.00mm and 4.00mm. It is therefore concluded that the shear modulus of the vinyl ester Derakane 411-45 resin is 2.15 $\pm$ .01 KN/mm^2, CV 1.29%, and that between the bounds of 2.00mm to 4.00mm the effect of specimen thickness on the shear modulus of the resin is negligible. It is assumed that this can be applied to the composite specimens and that the lower thickness bound can be extended to 1.95mm, the minimum thickness of the composite specimens.

The shear modulus of the composite specimens increased with increasing fibre content. This was expected and is in agreement with results of shear tests conducted by Reynolds and Hancox [80] on carbon fibre reinforced epoxies. Table 12 and figure 37 show the results for the 600 tex and 500 tex E-glass composite specimens to be very similar. The shear modulus for slab 11 (7 G_6, as rec.) and slab 19 (7 G_5, as rec.) is 5.84 KN/mm^2 and 5.51 KN/mm^2 respectively. The shear moduli of the six slabs 14 (7 G_6, A187), 15 (7 G_6, A1100), 16 (7 G_6, no c-a), 21 (7 G_5, A187), 22 (7 G_5, A1100) and 23 (7 G_5, no c-a) all lie between the above values for slabs 11 and 19. Therefore the surface treatment of the E-glass fibres has not affected the shear modulus of their composites. The relationship between the composite shear modulus and the fibre content does not appear to be linear but it is difficult to be certain due to the scatter in the results. The expected shear modulus of 2.15 KN/mm^2 at zero fibre content was considered when fitting the curve to the data points in figure 37. The curve approximates to the data for both the 600 tex and 500 tex E-glass composites. The shear modulus results derived in this section are used in sections 4.7 and 4.8.

4.3.4 Resin Tensile Strength

The tensile test results are presented in table 13 and the stress v strain curve given in figure 39. The average values for the tensile strength (80.5 $\pm$ 1.1N/mm^2), initial modulus (3.37 $\pm$ 0.05 KN/mm^2) and the failure strain (4.90 $\pm$ 0.06%) correspond closely to those quoted by Dow Chemicals [62], 81.4 N/mm^2, 3.38 KN/mm^2 and 5.0% respectively. Some disagreement was expected since, with none of the following information provided by Dow Chemicals, it is probable that the resin composition, testing conditions and specimen size used by Dow Chemicals varied from those used here by the author.

It is interesting to note that the tensile specimens 5, 6 and 7 were machined from a 6 month old resin slab and the other specimens were machined from approximately 3 week old resin slabs. There is no significant difference between the results, suggesting that deterioration in the tensile properties of the cast resin does not occur in the first 6 months.

Figure 39 is the typical stress v strain curve recorded for the Derakane 411-45 resin specimens. It is accurate up to a strain of 3.0% when the extensometer was removed from the specimen. Beyond this point the curve is derived from the Instron chart plot of load v cross-head movement. Fortunately the most relevant portion of the curve is that from 0% to 2.02% strain, 2.02% strain being the expected failure strain of the 600 tex E-glass fibre/resin composites.

The work conducted on the reinforcement fibre surface treatments is now considered.

4.4 Fibre Surface Treatment

The results of the experimental work described in section 3.4 are detailed here.

4.4.1 Fibre Size Content

Table 14 gives the average weight and volume percents of sizing on the as rec. 6000 filament carbon, 600 tex E-glass and 500 tex E-glass tows. The individual results for each tow length weighed and measured are given in table 2A5.

The weight percentage of dressing on a tow was calculated using the equation:

$$wt\% = \frac{\text{gm/m of sized tow} - \text{gm/m of no c.-a. tow}}{\text{gm/m of sized tow}} \times 100\% \quad . \; . \; . \quad (73)$$

The weight of one metre of unsized tow of 600 tex and 500 tex E-glass tow is, by definition, 0.6gm and 0.5gm respectively. In the case of the 6000 filament carbon tow the weight per metre of unsized tow is calculated from the tow volume and carbon density. Thus the weight per metre of unsized carbon tow is 0.2310 x 1.76 = 0.4066 gm/m.

The sized tows had the following weights per metre:

600 tex E-glass	0.6132 gm/m;
500 tex E-glass	0.5130 gm/m;
6000 filament carbon	0.4210 gm/m.

Therefore the weight percentage (wt %) of sizing on the 600 tex E-glass was, using equation 73:

$$\text{wt \%} = \frac{0.6132 - 0.6000}{0.6132} \times 100\% = 2.15\%$$

Similarly the wt % of sizing on the 500 tex E-glass and 6000 filament carbon tows were calculated as 2.53% and 3.42% respectively.

The sizing on both the 600 tex and 500 tex E-glass tows (see section 4.4.3) consisted of an unsaturated polyester resin with a small amount of coupling-agent incorporated. The density of Impol A201, a typical unsaturated polyester resin manufactured by I.C.I., is 1.20gm/cm^3. Therefore, assuming the density of the sizing to be 1.20gm/cm^3 and knowing the density of the E-glass to be 2.54 gm/cm^3 (see section 4.2.2) the volume percent of sizing on the 600 tex tow was:

$$\frac{\left(\frac{0.0132}{1.2}\right)}{\left(\frac{0.6000}{2.54} + \frac{0.0132}{1.2}\right)} \times 100\% = 4.45\%$$

Similarly the volume percent of sizing on the 500 tex E-glass was calculated as 5.21%.

The sizing on the carbon fibre was Epikote 828 which has a density of 1.3gm/cm^3. Therefore the volume percent of sizing on the 6000 filament carbon tow was 4.58%.

The weight percent of size on both the carbon and 600 tex E-glass tows is quoted respectively by Hyfil and T.B.A. Limited as 3% to 5%. However weaving and handling can remove some of the sizing. This obviously happened in the case of the 600 tex E-glass.

4.4.2 Carbon Fibre Surface Treatments

The experimental procedure to produce clean carbon fibres, with the minimum amount of fibre damage, by the removal of the Epikote 828 sizing was straightforward and is described in section 3.4.2. In the etching of the carbon fibres (see section 3.4.2) the care taken over the rinsing stage was crucial. Clark et al[37] found that any deposit on the fibres from the etching solution of ferric chloride in sodium hypochlorite considerably reduced the interfacial bond strength between the fibres and a resin matrix. After etching the carbon fibres Clark et al washed them in running tap water and then in 5 or 6 changes of distilled water, squeezing the fibres to expel

excess water. It was when the squeezing procedure was omitted, leaving some deposits still on the fibres, that the resultant composites had low interlaminar shear strengths. The author, by microscopic examination of the carbon fibres after rinsing in tap water, found that all of the deposit could be removed by prolonging the rinsing time. Therefore the squeezing procedure adopted by Clark et al[37], which could easily damage the wet unprotected fibres, was avoided.

4.4.3 E-Glass Fibre Surface Treatments.

The removal of the as rec. sizing from and application of alternative coupling-agents to the E-glass fibres was straight forward (see section 3.4.3) once the details of the original surface treatments were determined. This section presents the results of the experimental work carried out to determine:

i) the silane coupling-agent in the as rec. dressing on the 600 tex E-glass and
ii) the dressing on the as rec. 500 tex E-glass.

Section 3.4.3 describes the two experimental methods adopted in order to determine the type of silane coupling-agent incorporated in the polyester sizing on the as rec. 600 tex E-glass. The results are as follows.

Method I

The infra red (I.R.) spectra obtained from the no c.-a. 600 tex E-glass and the dressed 600 tex E-glass fibres were identical. As expected the no c.-a. glass blank was highly absorbent, thus the spectrum of the comparatively small amounts of coupling-agent was masked by the glass.

Method II

It was hoped that the solution obtained by boiling the sized E-glass in distilled water for 8 hours would contain a small amount of the by-product from hydrolysis of the coupling-agent and that one or more of the three organic solvents used would extract from the solution sufficient of the by-product to be identified by I.R. analysis.

Identical I.R. spectra were obtained from the GI and GII specimens and from the DI and DII specimens. This suggested that the by-product was not sufficiently soluble in Genklene and diethylether or that there was insufficient of the by-product in the water to be picked up and detected by I.R. analysis or that there was no by-product at all present in the water.

However, a comparison of the spectra of MI and MII showed the MI to have two extra peaks at wave numbers 1070 - 1100 and 710 - 740. The spectra obtained from MI and MII are shown in figures 40 and 41.

The possible by-products from the suspected coupling-agents A172 and A174 were 2 methoxy-ethan-1-ol ($CH_3OCH_2CH_2OH$) and methanol(CH_3OH). The two extra peaks in the MI spectrum do not correspond to peaks in the methanol 'fingerprint'. The absorbance band of 1070 - 1100 indicates the presence of an aliphatic ether (CH_3-O-CH_2-) and the band 710 - 740 indicates the presence of a $-CH_2-$ unit. Thus the two peaks correspond to two units present in 2 methoxy-ethan-1-ol. Other expected peaks in the 2 methoxy-ethan-1-ol 'fingerprint' occur in regions where the methyl isobutyl ketone control strongly absorbed infra red, therefore these peaks due to the 2 methoxy-ethan-1-ol would be masked. For example, a strong absorbance of infra red by 2 methoxy-ethan-1-ol is expected in a band around 3500 due to the C-OH group. The control spectrum has a strong peak at this point due to hydroxyl groups absorbed by the control from the water.

It is therefore concluded from the spectra of the I.R. specimens MI and MII that 2 methoxy-ethan-1-ol was present in MI, having been absorbed by the M.I.B.K. from the water boiled in the flask with the as rec. 600 tex E-glass. Therefore the silane coupling-agent incorporated in the polyester sizing on the as rec. 600 tex E-glass was Union Carbide's A172, vinyl tris (beta-methoxy ethoxy) silane $\left[CH_2 = CHSi(OCH_2CH_2OCH_3)_3\right]$.

When considering the surface treatment of the as rec. 500 tex E-glass fibres the following facts were noted:

i) the appearance of the surface treatment on the as rec. 500 tex E-glass was indistinguishable from that of the as rec. 600 tex E-glass;

ii) the i.l.s.s. values of the as rec. 500 tex E-glass/resin and the as rec. 600 tex E-glass/resin composites are similar (see section 4.6);

iii) the required time at temperature for removal of the dressing on the as rec. 500 tex E-glass tapes was the same as that for the 600 tex E-glass tapes;

iv) the as rec. 500 tex E-glass size content was within the quoted range for the 600 tex E-glass;

v) the results of an I.R. analysis of the by-product of the hydrolysis of the coupling-agent incorporated in the sizing on both the 500 tex and 600 tex E-glass are identical (the analysis was primarily designed to determine whether the coupling-agent incorporated in the sizing on the as rec. 600 tex E-glass was A172 or A174 , it was found to be A172);

vi) the most popular resin for use with E-glass fibres is a polyester resin and

vii) Union Carbide, the major U.K. manufacturer of silane coupling-agents, recommend the use of only two out of their range of sixteen silane coupling-agents for a glass fibre/polyester resin system , these 2 coupling-agents are A172 and A174.

It is probable that the manufacturers of both the 500 tex and 600 tex E-glass fibres were aiming for similar sections of the reinforcement market, i.e. their envisaged applications are similar. If this is so then it is likely that the same dressing system was chosen for both. Therefore, considering the above seven facts it is concluded that the sizing and the coupling-agent on the as rec. 500 tex E-glasswere the same as on the as rec. 600 tex E-glass, i.e. that the dressing on the as rec. 500 tex E-glass fibre consisted of Union Carbide's A172 silane coupling-agent incorporated in a polyester size.

The results of all the experimental work concerning the constituent materials of the composite slabs fabricated and tested have been presented. Results arising from the quality control of the composite slabs are now presented and discussed.

4.5 Quality Control of the Composite Slabs

Consistent quality of specimens is most important for consistent results when testing fibrous composites. As recorded in section 3.6 the thickness, surface finish, void content and degree of cure of each slab were examined. At the outset of this work the slab rejection rate was approximately 25%. This was largely due to inadequate surface finishes and increased attention to the preparation of the mould surface and the application of the release-agent reduced the rejection rate to approximately 10% of the slabs fabricated. The void contents, determined as described in section 3.6, of all the slabs tested are given in 2A6, along with the average density, fibre content and resin content of the five specimens tested from each slab.

The void content of a composite slab is calculated using equation 51.

$$V_v\,\% = \left[1 - \frac{\omega_m \rho_c}{\rho_m \omega_c} - \frac{\omega_{f1} \rho_c}{\rho_{f1} \omega_c} - \frac{\omega_{f2} \rho_c}{\rho_{f2} \omega_c}\right] \times 100 \quad \ldots \quad (51)$$

As an example calculation consider the hybrid slab 28:

$\rho_c = 1.69 gm/cm^3$; $\omega_c = 4.1826 gm$;
$\rho_m = 1.13 gm/cm^3$; $\omega_m = 1.5277 gm$;
$\rho_{cf} = 1.76 gm/cm^3$; $\omega_{cf} = 0.4888 gm$;
$\rho_{gc} = 2.54 gm/cm^3$; $\omega_{gc} = 2.1661 gm$.

$$\therefore V_v\% = \left[1 - \left(\frac{1.5277 \times 1.69}{1.13 \times 4.1826}\right) - \left(\frac{2.1661 \times 1.69}{2.54 \times 4.1826}\right) - \left(\frac{0.4888 \times 1.69}{1.76 \times 4.1826}\right)\right] \times 100\%$$

$$= 0.31\%$$

Unfortunately this method does not give a particularly accurate value for void content. Slight experimental errors have an exaggerated effect since the void content is so low. This explains the negative void contents determined for slabs 5, 16, 26, 39, 41, 42, 44, 47 and 60. However, the results are adequate for the purposes of this research. It is the tensile behaviour of the composites which is of paramount importance to this research. According to Olster[33] significant degradation of the tensile strength and moduli of unidirectional fibrous composites does not occur until the void content is $\geqslant 1\%$ and the strain to failure is less sensitive to void content. The average void content determined of all the slabs is 0.24%, with the maximum being 0.73%. Thus no slabs exceeded the arbitrary rejection level of 0.80% given in section 3.6. As a safety check sections from slabs 1, 9, 34, 37, 40 and 51, which yielded void contents greater than 0.60%, were examined microscopically. This showed the void content to be minimal with no voids at all observed in the majority of the sections. Thus the possibility that any of the slabs had a void content $\geqslant 1\%$ is extremely small. A final check was examination of the composite i.l.s.s. results. Composite shear strength is highly sensitive to voids, decreasing by approximately 10% for every 1% void content. In no case was the i.l.s.s. value of a slab markedly lower than expected. Therefore no slab was rejected on account of its void content.

D.T.A. of all the composite slabs showed the resin to be fully cured.

Table 8 lists the slabs which passed the quality control tests. The volume fractions quoted are calculated from equations 57 to 65. The results for the mechanical tests on the composites are now recorded and discussed.

4.6 Composite Interlaminar Shear Strength

Six i.l.s.s. specimens from each of the slabs in table 8 were prepared and tested in three point bending as described in section 3.7. The full set of results is given in table 2A7. The average i.l.s.s. of each slab is given in table 15. The i.l.s.s. of each specimen was calculated using equation 41.

$$\tau_{il} = \frac{3\hat{P}}{4BD} \qquad \ldots \quad (41)$$

Originally it was hoped to obtain the interfacial shear strengths of the composites from the i.l.s.s. values using equations 44 and 45, proposed by Hancock and Cuthbertson[40].

$$\tau_{if} = \frac{\tau_{il} - (1 - x)\tau_m}{x} \qquad \ldots \quad (44)$$

$$x = \frac{(V_f \pi)^{\frac{1}{2}}}{(V_f \pi)^{\frac{1}{2}} + 1 - 2 (V_f / \pi)^{\frac{1}{2}}} \qquad \ldots \quad (45)$$

This had to be abandoned after obtaining unrealistic results. The equations produced acceptable i.f.s.s. for the higher but not the lower fibre volume content composites. The shear strength of the matrix, τ_m, was estimated after examination of the failed i.l.s.s. specimens from all of the slabs. In composites with i.l.s.s. greater than approximately 104N/mm^2 the fracture surfaces indicated that the shear strength of the specimens was approaching that of the vinyl ester. There was an increasing tendency towards resin shear failure in areas where interfacial failure was expected. The greatest i.l.s.s. of any specimen tested was 109.9 N/mm^2 (see 2A7, specimen 22.2). Therefore the shear strength of the matrix, τ_m, is estimated at 110 N/mm^2.

For example consider the results for slabs 1 and 4. For slab 1 $V_T = V_{cf} = 0.1617$ and i.l.s.s. = 43.3 N/mm^2.

Substituting into equation 45 gives

$$x = \frac{(0.1617\,\pi)^{1/2}}{(0.1617\,\pi)^{1/2} + 1 - 2\left(\frac{0.1617}{\pi}\right)^{1/2}} = 0.5661$$

Substituting into equation 44 gives

$$\tau_{if} = \frac{43.3 - (1-0.5661)\ 110.0}{0.5661} = -7.8 \text{N/mm}^2$$

For slab 4 $V_T = V_{cf} = 0.3773$ and i.l.s.s. = 43.5 N/mm^2

Substituting into equation 45 gives

$$x = \frac{(0.3773\pi)^{\frac{1}{2}}}{(0.3773\pi)^{\frac{1}{2}} + 1 - 2\left(\frac{0.3773}{\pi}\right)^{\frac{1}{2}}} = 0.7801$$

Substituting into equation 44 gives

$$\tau_{if} = \frac{43.5 - (1 - 0.7801)\ 110.0}{0.7801} = 24.8 \text{ N/mm}^2$$

The negative value of τ_{if} for slab 1 is obviously incorrect and therefore no i.f.s.s. value calculated by the above method can be used confidently in this research. Criticism of the equations 44 and 45, as an over simplification, levelled by Phillips and Harris in reference 38 appears to be justified.

Figure 42 gives a typical load v deflection curve for the i.l.s.s. specimens failing in shear. Beyond the peak load the load gradually decreases down to zero. This behaviour was also observed by Prosen et al[34] when testing carbon/epoxy specimens. They found that load v deflection curves similar to that in figure 42 indicated shear failure and that curves without a significant gradual decrease in load prior to an abrupt failure indicated tensile failure. The specimens tested here which failed in modes other than shear had this latter form of curve.

I.l.s.s. specimens from approximately 80% of the slabs tested failed in shear, as illustrated in figure 17, at a span of 10mm. Out of the remaining 20% only specimens from slabs 8 and 57 did not fail in shear when the span was altered. The i.l.s.s. for these two slabs are quoted as being greater than the maximum stresses of the particular specimens tested.

Table 15 shows that there was little variation in the i.l.s.s. of the plain as rec. fibre type composite specimens with the fibre content. Increasing fibre content tends to impede the penetration of the resin and strong interfacial bonds can not be formed if the resin does not wet the fibres. In such a case the i.l.s.s. would be expected to decrease with increasing fibre content[34].

The i.l.s.s. of the hybrid composites generally fell between those of the parent composites. However the results for slabs 41 and 42 are both slightly lower than expected, their i.l.s.s. and geometrical arrangements being 43.3N/mm^2 and 42.3N/mm^2 and G_6 3:1 G_6 3:1 G_6 3:1 G_6 and 1:1 C 1:1 C 1:1 C 1:1 respectively. One of the purposes of evaluating the i.l.s.s. of the composites was as a quality control check on the void contents of the composite

slabs. Inspection of table 2A6 shows that the void contents of slabs 41 and 42, as determined by the density bottle technique (see section 3.6), were both negative, being -0.26% and -0.02% respectively. Therefore it is highly improbable that the slightly low i.l.s.s. results for these slabs should be attributed to a significant void content. It seems more likely that the standard of preparation of the specimens from slabs 41 and 42 was below average or that between preparation and testing the particularly susceptible and important side edges of the specimens were inadvertantly damaged. A further possibility is that the variation is due simply to the inherent inaccuracy of the short beam shear test. Doubts on the ability of the test to give reproducible results except under strictly controlled conditions have been voiced by various people including Harris[13]. The test is correctly termed as the 'apparent' i.l.s.s. of composites, the results being qualitative rather than quantitative. However, the three point bending short beam shear method is still widely used since it is an extremely economic test in terms of both time and materials, the latter being of paramount importance in this work.

Consider the results of the 7 layer parent composites in which the fibre surface treatments vary. The relevant carbon composites are slab 4 (as rec.), slab 6 (etched) and slab 7 (no c.-a.). The results show that the protective sizing applied to the carbon by Hyfil slightly reduced the i.l.s.s. of the carbon/vinyl ester composites from approximately 50.0N/mm^2 for a carbon (no c.-a.) composite to approximately 43.5N/mm^2. This highlights the suitability of vinyl ester resins as a matrix for untreated carbon fibres. The value of 97.8N/mm^2 obtained for the i.l.s.s. of the etched carbon fibres in vinyl ester compares favourably with results obtained by Clark et al[37]. They found that the i.l.s.s. of Type II carbon fibres in an epoxy matrix could be increased up to 90N/mm^2 by liquid-phase oxidation of the carbon fibres in sodium hypochlorite solution. The Type II carbon fibres had a mean elastic modulus of 252KN/mm^2, which is close to the estimated mean elastic modulus of 242.1 KN/mm^2 (see section 4.7.1.2) for the 6000 filament carbon fibre. This is relevant since the i.l.s.s. of carbon/epoxy composites has been shown to vary with the elastic modulus of the constituent carbon fibre[37]. However, comparison between the systems must be guarded since Clark et al do not give details of the i.l.s.s. specimens. It is concluded that the etching of the Hyfil carbon fibre was successful in respect to the improvement of the carbon fibre/resin bond strength and that, as regards i.l.s.s., Derakane 411-45 vinyl ester is at least as suitable in the role of matrix for carbon fibres as the epoxy resin used by Clark et al[37].

The i.l.s.s. results for the E-glass composites show the different surface treatments to be equally effective on both the 600 tex and 500 tex E-glass fibres. This was expected since the surface characteristics of the two fibre types must be virtually identical. The success of the A1100 coupling-agent in promoting adhesion between the E-glass fibres and vinyl ester matrix was the greatest of all the surface treatments. The average apparent i.l.s.s. values for the E-glass/vinyl ester composites with A1100, A187, as rec. (equivalent to A172) and no c.-a. surface treatments are approximately $105N/mm^2$, $59N/mm^2$, $53N/mm^2$ and $46N/mm^2$ respectively. No previous work is known with which the above results may be precisely compared. In general the expected i.l.s.s. of E-glass/polyester resin systems containing untreated fibres is in the range $20N/mm^2$ to $40N/mm^2$, whilst for satisfactorily treated fibres a composite i.l.s.s. greater than about $50N/mm^2$ could be expected. The value of approximately $46N/mm^2$ obtained for the i.l.s.s. of untreated E-glass/vinyl ester specimens is exceptionally high. This supports the theory voiced by Dow Chemicals[62] and Varco and Seamark[63] that the secondary hydroxyl groups on the vinyl ester molecules react with hydroxyl groups on the E-glass surface, promoting excellent adhesion to the glass fibre.

Union Carbide[44] recommend the silane coupling-agent A174 for use with polyester systems and A1100 and A187 for use with epoxy systems but does not mention vinyl ester systems. The i.l.s.s. results of E-glass/vinyl ester composites indicate that though silane coupling-agents used for polyester systems are suitable for vinyl esters the coupling-agents recommended for epoxy systems are preferable. The structures of the three coupling-agents A172, A1100 and A187 are given in figure 18. The silane coupling-agents are believed to bond to the inorganic fibre surfaces via hydrolysis and elimination of the alkoxy groups in the coupling-agents. Union Carbide[44] state that different alkoxy groups only produce minor differences in the overall fibre/coupling-agent bond strength. Thus the variation in the i.l.s.s. of the E-glass/vinyl ester composites is attributable to the different organo-functional (R') groups in the coupling-agents A172, A187 and A1100. Therefore it is the amino functional group of A1100 which makes this coupling-agent more effective than the other two coupling-agents for the vinyl ester system used, the average i.l.s.s. of slabs 15 and 22 being $105N/mm^2$. The considerable difference in the i.l.s.s. of slabs 15 and 22, slabs 14 and 27 (A187), slabs 11 and 19 (A172) and slabs 16 and 23 (no c.-a.) is fortuitous. The purpose of changing the surface treatments of the fibres was to investigate the effect of the strength of the fibre/resin interface on the tensile characteristics of the hybrid composites. The broad range of E-glass fibre/resin bond strengths aids any variation in the tensile properties due to this parameter to be distinguished and not lost in the inherent scatter of the hybrid tensile properties, though this is complicated by the change in the E-glass tensile

strength characteristics with surface treatment (see section 4.2.3). By the same reasoning the extent of variation in the carbon fibre/resin bond strength with the different surface treatments is also pleasing.

The tensile strength properties of the parent composites are now studied.

4.7 Tensile Results of the Parent Composites

The tensile results of the parent, i.e. single fibre type, composites of slabs 1 to 23 are presented, discussed and compared with existing composite strength and failure theories in this section to produce the required information for the analysis of the hybrid tensile results in section 4.8.

The summarized tensile results for all the composite slabs tested are given in table 16. The full tensile results (except those for specimens which failed outside their gauge length which have been discounted) are given in table 2A8. The stress values, σ, quoted were calculated using the equation.

$$\sigma = \frac{\text{load} \times 9.81}{2.00 \times \text{width}} \quad N/mm^2 \qquad \ldots \quad (74)$$

The strain, ε, was taken from the chart recorder plot of either the strain gauge or l.v.d.t. readings up to the initial failure. In some hybrid composites initial failure was not catastrophic. In such cases the strain beyond this point was estimated from the Instron load v time plot. The elastic modulus, E, of the specimens was calculated from the equation

$$E = \frac{\sigma}{\varepsilon} \qquad \ldots \quad (75)$$

σ^E and ε^E define the elastic limit of the specimen tested. They frequently coincide with σ' and ε', the initial failure stress and strain at which the first sudden load drop occurs, and $\hat{\sigma}$, the maximum stress.

A number of graphs have been plotted from the results and, where appropriate, the best straight lines have been fitted to the data by the regression method of least squares. This method defines the constants A and B in the general straight line equation

$$y = Ax + B \qquad \ldots \quad (76)$$

$$\text{where } A = \frac{n\Sigma xy - \Sigma x \Sigma y}{n\Sigma x^2 - (\Sigma x)^2} \qquad \ldots \quad (77)$$

$$\text{and } B = \frac{\Sigma y \Sigma x^2 - \Sigma x \Sigma xy}{n\Sigma x^2 - (\Sigma x)^2} \quad \ldots \quad (78)$$

where n = the number of data points.

When the intercept of the line with the y axis is known, as is occasionally the case in this work, A simplifies to

$$A = \frac{\Sigma xy - B\Sigma x}{\Sigma x^2} \quad \ldots \quad (79)$$

As an example consider the variation in the initial elastic modulus with the fibre volume content of the carbon composites (slabs 1 to 5). E is plotted on the y axis against V_{cf} on the x axis. The value of the intercept on y, i.e. E for a 'composite' with $V_{cf} = 0.00$, is obtained directly from the resin tensile σ v ε curve in figure 39. The initial elastic modulus of the resin is 3.4 KN/mm^2. Therefore the value of B in equation 76 is 3.4. The remaining constant A is calculated using the data in table 16 and the simplified formula A given by equation 79.

E KN/mm^2	V_{cf}	E x V_{cf} KN/mm^2	V_{cf}^2
42.8	0.1617	6.921	0.0262
55.1	0.2156	11.880	0.0465
80.4	0.3234	26.001	0.1046
93.2	0.3773	35.164	0.1424
119.2	0.4851	57.824	0.2353
	Σ 1.5631	Σ 137.790	Σ 0.5550

$$\therefore A = \frac{137.790 - (3.4 \times 1.5631)}{0.5550} = 238.7 \text{ KN/mm}^2.$$

Therefore the relationship between E and V_{cf} in the carbon fibre composites of slabs 1 to 5 calculated by the method of least squares is

$$E = 3.4 + 238.7\ V_{cf} \text{ KN/mm}^2$$

The results of the carbon fibre/vinyl ester resin tensile specimens from slabs 1 to 7 are now studied.

4.7.1 Tensile Properties of the Carbon Fibre Composites of Slabs 1 to 7

The tensile results for slabs 1 to 7 are given in tables 16 and 2A8. Figures 43 and 44 show the variation with V_{cf} of composite elastic modulus and tensile strength respectively. Figure 45 is a typical σ v ϵ curve for a specimen from slab 4. During the testing of some of the higher carbon content specimens occasional faint pings were heard as the ultimate fracture load was approached. No damage was visible on the surface of the specimens at this stage. It is debatable whether the noise originated from fibre failure, fibre/resin debonding within the specimen or debonding of the aluminium tabs from the specimen.

4.7.1.1 The Fracture Surfaces of the Carbon Fibre Composite Tensile Specimens

There was little difference amongst the appearances of the fracture surfaces of the carbon composite specimens from slabs 1 to 7. Figure 46 shows half of the fractured specimen 4.2. Specimens did not fail in a planar manner straight across one cross-section. The fractures had a notched or semi-jagged appearance. The carbon fibres tended to fail in bundles with the different bundles connected by shear failure taking place predominantly at the fibre/resin interface. The fibre surfaces exposed by the shearing, and by fibre pull-out, were almost completely resin free in specimens from slabs 1 to 5 and 7. Only in specimens from slab 6 were portions of resin commonly found adhered to such 'exposed' fibre surfaces. The above is illustrated by figures 47 and 48. The pull-out lengths of the fibres within each specimen varied greatly and were commonly between 0 to 13 fibre diameters. In many cases fibre debonding had continued beneath the failed resin surface (see figure 47). The size of the bundles of failed fibres also varied greatly within each specimen. Typically the bundles consisted of a small fraction of the fibres in one tow although they were not always confined to individual tows. The general trend of the fracture surfaces of these bundles of failed fibres was to run at different angles across the specimen. The varying pull-out lengths of the failed fibres gave the fracture surfaces of the bundles a rough appearance.

4.7.1.2 The Tensile Stress v Strain Curves of the Carbon Fibre Composite Specimens

All the specimens tested from slabs 1 to 7 had linear stress v strain plots up to the catastrophic failure of the composite. Figure 45 is a typical σ v ϵ curve for a composite specimen from slab 4.

Consider the elastic modulus, E, of the carbon composites as given in table 16. Figure 43 is a plot of E v V_{cf} for slabs 1 to 5. The line E_e is the expected elastic modulus of a carbon fibre/vinyl ester resin composite. The equation was calculated to best fit the experimental data by the method of least squares assuming a linear relationship between E and V_{cf}. The value of 3.4KN/mm^2 at V_{cf} = 0.00 is the elastic modulus of the vinyl ester resin matrix, E_m, up to the average failure strain of the carbon composites (0.47% , determined later in this section). The equation derived for E_e is

$$E_e = 3.4 + 238.7\ V_{cf}\ KN/mm^2 \quad . \ . \ . \quad (80)$$

This is equivalent to the familiar rule of mixture form of

$$E_e = 3.4V_m + 242.1\ V_{cf}\ KN/mm^2 \quad . \ . \ . \quad (81)$$

There is little scatter in the results about this line. Extrapolation of the straight line to V_{cf} = 1.00 gives an elastic modulus for the 6000 filament carbon fibre, E_{cf}, of 242.1 KN/mm^2. This compares with the value of 230 KN/mm^2 quoted by Hyfil[54]. This difference of 5% is acceptable since the mechanical properties of carbon fibres are known to vary from batch to batch. Therefore it is concluded that the elastic modulus of the carbon fibres used in this research is 242.1 KN/mm^2 and that the relationship between composite modulus and carbon fibre content is linear, as represented by equations 80 and 81, corresponding to the value predicted by the rule of mixtures.

Consider the elastic modulus of slabs 4, 6 and 7 of 93.2KN/mm^2, 92.6KN/mm^2 and 93.3KN/mm^2 respectively as given in table 16. These are the 7 layer composites containing carbon with varying surface treatments. The value for slab 6, containing etched carbon fibres, is slightly lower than for the other two slabs. However the carbon content of this slab is correspondingly low and normalizing the carbon volume content to 37.73% (that of slabs 4 and 7) gives an elastic modulus of

$$\frac{92.6 \times 37.73}{37.43} = 93.3\ KN/mm^2$$

Therefore the elastic moduli of the three slabs containing carbon fibre in the as rec., etched and no c.-a. surface treated states are in excellent agreement and the appropriate analysis of their variance shows the small difference in their means to be insignificant. It is concluded that these surface treatments of the carbon fibre, and therefore the accompanying changes in the carbon/resin interfacial characteristics, have no effect upon the modulus of the carbon fibre composites.

Consider the failure strains of specimens from slabs 1 to 5 ($\varepsilon^E = \varepsilon' = \hat{\varepsilon}$). Table 16 shows that the average failure strains of slabs 1 to 5 vary between 0.44% and 0.48%. An analysis of the variance amongst the means indicates the differences to be insignificant. Therefore it is assumed that fibre content has no effect on the mean failure strain (within the limits $16.17\% \leq V_{cf}\% \leq 48.51\%$) and that the mean failure strain of the as rec. carbon fibre composites is equal to the grand mean of the failure strains of all the specimens from slabs 1 to 5. The appropriate calculation gives the expected failure strain, $\hat{\varepsilon}_e$, of the carbon fibre/vinyl ester resin composites as $0.47 \pm 0.01\%$.

Now consider the average failure stresses of slabs 1 to 5 ($\sigma^E = \sigma' = \hat{\sigma}$). Figure 44 shows the variation in $\hat{\sigma}$ with V_{cf}. The line $\hat{\sigma}_e$ was calculated to best fit the experimental data by the regression method of least squares assuming a linear relationship. The value of $16 N/mm^2$ plotted at $V_{cf} = 0.00$ is the expected matrix stress at the expected failure strain, 0.47%, of the carbon fibre composites. The equation derived for $\hat{\sigma}_e$ is

$$\hat{\sigma}_e = 16.0 + 1125.0 V_{cf} \ N/mm^2 \quad . \ . \ . \quad (82)$$

This is equivalent to

$$\hat{\sigma}_e = 16.0 \ V_m + 1141.0 \ V_{cf} \ N/mm^2 \quad . \ . \ . \quad (83)$$

It follows that the average carbon fibre failure stress in the composite slabs 1 to 5 is $1141 N/mm^2$. The validity of equations 80 and 82 is checked by substituting 1.00 for V_{cf} and comparing the resultant value of $\hat{\sigma}_e$ divided by the resultant value of E_e with $\hat{\varepsilon}_e = 0.47\%$.

At $V_{cf} = 1.00$

$$\frac{\hat{\sigma}_e}{E_e} = \frac{1141.0}{242.1} = 0.47\% = \hat{\varepsilon}_e$$

The degree of scatter in $\hat{\sigma}$ is similar to that in $\hat{\varepsilon}$, both being considerably greater than that in E. The stress range for each set of specimens is indicated in figure 44. The CV for each set lies between 3.53% and 14.77%. This wide range in CV is attributed to the small number of specimens tested from each slab, one extreme result having an exaggerated effect on the resultant CV.

The effect of the different fibre surface treatments on the carbon composites tensile stress and strain is not marked. There is no significant difference between the mean tensile strengths of the as rec., etched and no c.-a. surface treated carbon fibres (see section 4.2.3) and their $\hat{\varepsilon}$ values

all give similar standard deviations in fibre strengths at a gauge length of 50mm. Thus the tensile results of slabs 4, 6 and 7 can be compared directly with one another and an analysis of the variance between the means is valid (assuming the standard deviation of composite strength to be governed by that of the constituent fibre strength as postulated by Barry[4]). Prior to the analysis the failure stresses of the specimens from slab 6 were appropriately adjusted to normalize the $V_{cf}\%$ from 37.43% to 37.73%. The analysis of the variance of the mean tensile stresses of slabs 4, 6 and 7 shows that the three fibre surface treatments produced no significant difference in either the mean tensile strength or the mean tensile strain of the carbon fibre composites.

The experimental tensile results are now compared with those predicted by existing failure theories.

4.7.1.3 Comparison of the Experimental and Theoretical Tensile Properties of the Carbon Fibre Composites

There is some dispute concerning the tensile behaviour of single fibre type composites and a number of theories have been postulated for composite tensile strength as outlined in the literature review (see section 2.1). This section applies and compares the commonly utilized mixture rule and the more complicated failure theories of Rosen[1], Zweben[3] and Barry[4] to the experimental results of the carbon composite slabs.

i) The Rule of Mixtures - The rule of mixtures predicts a linear relationship between composite fibre content and the property under consideration. According to the rule of mixtures the elastic modulus of a composite is

$$E_{RM} = E_m V_m + E_f V_f \quad . \quad . \quad . \quad (84)$$

It was concluded in section 4.7.1.2 that the elastic modulus of the carbon fibre composites obeys the above rule of mixtures formula, using 242.1 KN/mm^2 as the average modulus of the carbon fibre rather than the value of $230KN/mm^2$ quoted by Hyfil.

In order to compare the average experimental failure stresses of the carbon composites of slabs 1 to 5 with those predicted by the rule of mixtures, it is necessary to know both the average tensile failure stress of the carbon fibres in the unidirectional woven tapes and the stress in the resin composite matrix at the average failure strain of the carbon fibres. According to the results of the carbon fibre tow tests recorded in section 4.2.3 the average tensile strength of the carbon fibres was $774.4N/mm^2$ at a gauge length of 50mm. The elastic modulus of the carbon fibre is taken as $242.1KN/mm^2$. Thus, using the relationship $E = \frac{\sigma}{\epsilon}$, the expected failure strain of the carbon fibres is

$$\hat{\epsilon}_{cf} = \frac{774.4 \times 100}{242.1 \times 10^3} \%$$

$$\therefore \quad \hat{\epsilon}_{cf} = 0.32\%$$

The stress in the vinyl ester matrix at 0.32% ϵ is 11.0N/mm^2 (σ_m'), obtained from figure 39. Therefore the values of 774.4N/mm^2 and 11.0N/mm^2 for $\hat{\sigma}_f$ and σ_m' respectively are substituted into equation 1, the rule of mixtures equation for composite tensile strength, $\hat{\sigma}_{RM}$.

$$\hat{\sigma}_{RM} = 774.4\ V_{cf} + 11.0 V_m \text{ N/mm}^2 \quad . \ . \ . \quad (85)$$

$$\therefore \quad \hat{\sigma}_{RM} = 11.0 + 763.4\ V_{cf} \text{ N/mm}^2 \quad . \ . \ . \quad (86)$$

The relationship determined from the experimental data from slabs 1 to 5 is represented by equation 82.

$$\hat{\sigma}_e = 16.0 + 1125.0\ V_{cf} \text{ N/mm}^2 \quad . \ . \ . \quad (82)$$

Comparison between equations 86 and 82 shows that the average experimental composite failure stress is greater than 140% of that predicted by the rule of mixtures. For example, $\hat{\sigma}_e$ for slab 4 with V_{cf} = 0.3773 is 440.5 N/mm^2 compared with the predicted $\hat{\sigma}_{RM}$ of 298.9 N/mm^2. This result implies that the compositing process has greatly enhanced the failure stress and strain of the carbon fibres in the composites. The composite failure stress is proportional to fibre content so once the average stress and strain of carbon fibres in one composite type at the failure of that composite is known the average failure stress of carbon composites with differing fibre contents can be predicted. In this respect the composite failure stress does follow the mixture rule but $\hat{\sigma}_{cf}$ becomes the average stress of a carbon fibre at composite failure rather than the average failure stress of a free carbon fibre with a gauge length equal to that of the composite under consideration. The average stress in the carbon fibres at the failure of slabs 1 to 5 was 1141.0N/mm^2. Equation 87 defines the average failure stress of the as rec. carbon fibres.

$$\hat{\sigma}_{cf} = 1.45 \times 10^3 \times L^{-1/7.02} \ \Gamma(1 + 1/7.02) \quad . \ . \ . \quad (87)$$

From this equation the expected gauge length of fibres with $\hat{\sigma}_{cf}$ = 1141.0N/mm^2 can be calculated.

$$L^{-1/7.02} = \frac{1141.0}{1.45 \times 10^3 \times \Gamma(1 + 1/7.02)} = 0.84107$$

$$\therefore \quad L = 3.37\text{mm}$$

Thus the apparent failure strength of the 50mm carbon fibres in the composite specimen gauge lengths has increased to the average failure strength of 3.37mm carbon fibres. The theories of Rosen and Zweben consider the statistical characteristics of the fibre tensile strength and the possibility of multiple fibre failure within the composite prior to catastrophic failure.

ii) The Statistical Theories of Rosen and Zweben - The statistical theories of Rosen[1] and Zweben[3] are described in detail in the literature review and are based on the probabilities of random single fibre failures throughout the composite and the probabilities of the propagation of these failures. The different possibilities give rise to three important theoretical fibre stress levels for composite failure:

a) $\hat{\sigma}_{wf}$, the stress at which the first (weakest) fibre is expected to fail;
b) $\hat{\sigma}_{Lf}$, the stress at which the first overstressed fibre (i.e. a fibre subjected to a stress concentration, k, due to a failed adjacent fibre) is expected to fail and
c) $\hat{\sigma}_{Uf}$, the expected stress at which a composite cross-section becomes so weakened by the random fibre failures that the remaining fibres are unable to support the applied load.

These stress levels are calculated for the carbon composites of slabs 1 to 5. Assuming that the carbon fibre strength can be represented by the Weibull distribution of the form

$$F(\sigma) = 1 - e^{-\alpha L \sigma^{\beta}} \qquad \ldots \quad (11)$$

and that the fibre array in the composites approximates to hexagonal then the relevant equations for the three stress levels are

$$\hat{\sigma}_{wf} = \left(\frac{\beta - 1}{NL\alpha\beta}\right)^{1/\beta} \qquad \ldots \quad (14)$$

$$\hat{\sigma}_{Lf} = \alpha^{-1/\beta} \left[6NL\delta(k^{\beta} - 1)\right]^{-1/2\beta} \qquad \ldots \quad (88)$$

$$\hat{\sigma}_{uf} = (\alpha\beta\delta e)^{-1/\beta} \qquad \ldots \quad (7)$$

where N = number of fibres = $\frac{\text{spec. c.s.a.} \times V_{cf}}{\text{carbon fibre c.s.a.}}$,

L = specimen length = 50mm,

$\alpha^{-1/\beta}$ and β = Weibull parameters which for as rec. carbon fibre = $1.45\text{KN/mm}^{(2-1/\beta)}$ and 7.02 respectively (see section 4.2.2)

$k = 1.104$

and δ = ineffective length $= \left[\frac{1}{2}\ \frac{E_f}{G_m}\left(\frac{1 - V_f^{1/2}}{V_f^{1/2}}\right)\right]^{1/2} d_f$ . . (3)

To convert the fibre stress (σ_f) to composite stress (σ_c) without ignoring the stress carried by the matrix it is assumed that the matrix and fibre have the same strain, ϵ . The stress in the matrix, σ_m , is equal to the product ϵE_m. Given that the stress in the fibre is σ_f then $\epsilon = \frac{\sigma_f}{E_f}$. In the case of the carbon fibre composites E_f = 242.1 KN/mm^2 and E_m = 3.4 KN/mm^2. It follows that the stress in the composite is

$$\sigma_c = \sigma_{cf}\ V_{cf} + \frac{E_m}{E_{cf}}\ \sigma_{cf}\left(1 - V_{cf}\right)$$

$$\therefore\ \sigma_c = \sigma_{cf}\ (0.986\ V_{cf} + 0.014)\ N/mm^2$$

Therefore in the case of the carbon composites to convert the stress levels $\hat{\sigma}_{wf}$, $\hat{\sigma}_{Lf}$ and $\hat{\sigma}_{uf}$ to composite stress levels, $\hat{\sigma}_w$, $\hat{\sigma}_L$ and $\hat{\sigma}_u$ the fibre stress levels are multiplied by the composite factor, F_c = (0.986 V_{cf} + 0.014).

The three fibre and composite stress levels were calculated for carbon fibre volume percents of 20%, 40%, 60% and 80%. These are given in table 17 and plotted in figure 44 with the experimental results. As example calculations consider a carbon composite with $V_{cf}\%$ = 40%.

The number of fibres in such a composite is

$$N = \frac{2.00 \times 10 \times 0.4}{38.51 \times 10^{-6}} = 207738$$

δ is calculated using G_m = 2.15KN/mm^2 (see section 4.3.3), E_f = 242.1KN/mm^2 and d_f = 7.3μm. Substituting into equation 3 gives

$$\delta = \left[\frac{1}{2} \cdot \frac{242.1}{2.15}\left(\frac{1 - 0.4^{1/2}}{0.4^{1/2}}\right)\right]^{1/2} 7.3 \times 10^{-3} = 0.0418\text{mm}$$

From equation 14

$$\hat{\sigma}_{wf} = \left(\frac{7.02 - 1}{207738 \times 50 \times 7.02}\right)^{1/7.02} \times 1.45 \times 10^3$$

$$\therefore\ \hat{\sigma}_{wf} = 142.0\text{N/mm}^2 \text{ and } \hat{\sigma}_w = 58.0\text{N/mm}^2$$

From equation 88

$$\hat{\sigma}_{Lf} = 1.45 \times 10^3 \left[6 \times 207738 \times 50 \times 0.0418\ (1.104^{7.02} - 1)\right]^{-\frac{1}{2 \times 7.02}}$$

$$\therefore\ \hat{\sigma}_{Lf} = 506.2\text{N/mm}^2 \text{ and } \hat{\sigma}_L = 206.7\text{N/mm}^2$$

From equation 7

$$\hat{\sigma}_{uf} = 1.45 \times 10^3 \, (7.02 \times 0.0418 \times e)^{-1/7.02}$$

$$\therefore \hat{\sigma}_{uf} = 1497.5 N/mm^2 \text{ and } \hat{\sigma}_u = 611.6 N/mm^2$$

Figure 44 shows all of the experimental failure stresses of the plain carbon composites to fall within the bounds of the upper and lower stress levels, $\hat{\sigma}_u$ and $\hat{\sigma}_L$. The failure stresses predicted by the rule of mixtures also fall within these bounds. The possibility of the weakest link mode of failure, the lower stress bound for which is given by $\hat{\sigma}_w$, applying to the carbon composites can be eliminated. This was expected since for this mode to dominate the distribution in fibre strength must be narrow. This mode is also encouraged by a high fibre/matrix interfacial bond strength so that a crack caused by the failure of one of the weakest fibres may propagate straight across the specimen without being deflected and terminating in fibre/matrix debonding. The 6000 filament carbon fibres in slabs 1 to 7 have a wide distribution in tensile strength and judging by the i.l.s.s. only slab 6 has high fibre/matrix bond strength.

The position of the experimental results between $\hat{\sigma}_u$ and $\hat{\sigma}_L$ indicates, according to the statistical theory, that a considerable number of carbon fibre failures occur in a specimen before catastrophic failure of the composite. It is possible that the faint 'pings' emitted from some of the specimens during the latter stages of their tensile tests originated from carbon fractures. As each additional fibre fails intuitively one expects the tensile strength of the composite to decrease. However, provided that the fractured fibres remain bonded to the matrix, each fractured fibre is only ineffective as reinforcement over the length δ , defined by equation 3. Thus the detrimental effect of single fibre fractures on the tensile strength of the composite is only directly cumulative when they occur in the same composite cross-section, or to be more precise in the same axial layer of length δ . In addition the strength of the discontinuous fibres produced by a fibre fracture is greater than that of the original continuous fibre since the weakest point has been eliminated. Indirectly the single fibre fractures all have a significant effect on the composite tensile strength since neighbouring fibres are subjected to stress concentrations. Thus each single fibre fracture is a potential site for the propagation of fibre fracture leading to the catastrophic failure of the composite. The upper stress limit derived by Rosen[1] ignores the effect of stress concentrations imposed on fibres adjacent to fractured fibres. It is the expected stress level at which complete composite failure

occurs due to the chance accumulation of fibre fractures in one cross-section. The lower stress level considers static but not dynamic stress concentrations. The experimental results for the carbon composites fall in the top half of the area bounded by the upper and lower stress limits. This implies that the stress concentrations on fibres adjacent to broken ones do have a significant effect on the composite failure stress and that numerous single and multiple fibre failures occur before the ultimate composite failure, the lower bound being the stress at which the first multiple fibre fracture is expected. As noted previously all of the experimental carbon composite failure stress levels are above those predicted by the mixture rule. This supports the latter point. It has been calculated that at composite failure the average stress in the carbon fibres is equivalent to the average failure stress of carbon fibres of length 3.37mm. The first point implies that the stress on the fibres which fracture to cause the failure of the whole composite is most likely to be greater than the average carbon fibre stress, due to stress concentrations. If this is so then the strength of the carbon fibres must be equivalent to that of fibres less than 3.37mm in length, implying that the average fibre fails at more than 14 places along its length. However this may be an over estimation since the tensile characteristics of the fibres must improve as failures occur at the weaker points.

The upper, lower and weakest stress levels were calculated for the 7 layer carbon composites with different fibre surface treatments (slabs 4, 6 and 7) and the values are presented in table 18. The slight changes in the Weibull parameters of the etched and no c.-a. carbon fibres account for the small variations ($< 4\%$) in the predicted stress levels for the three slabs.

The statistical failure theories of Rosen and Zweben provide an explanation for the experimental failure stresses of the carbon fibres being greater than predicted by the rule of mixtures but their proposed upper and lower stress levels are very wide apart. Barry's model, presented in reference 4, narrows these stress bounds. He also considered the failure of composite materials from a statistical point of view. Barry's model is a slight variation on and extension to those proposed by Rosen[1] and Zweben[3].

iii) The Statistical Model Proposed by Barry - The composite model and tensile failure theory presented by Barry[4] is covered in detail in the literature review. There are a few basic differences between the models of Zweben and Barry. Firstly Barry's model considers the effect of both dynamic and static stress concentrations caused by a failed fibre, on intact adjacent fibres. Barry obtains upper and lower stress levels. For the upper level he assumes no overlap of dynamic stress concentration increases. For the lower

level he assumes complete accumulation of dynamic stress concentration increases on intact fibres once a dynamic stress concentration causes the failure of one or more fibres. Secondly, instead of dividing the composite into transverse sections of length δ , the ineffective length of a broken fibre, Barry uses the positively affected length, L_p, of adjacent intact fibres. This is calculated in a similar manner to δ but includes the effect of possible debonding of the failed fibre. Thirdly, in considering the effect of fibre debonding on the composite tensile strength Barry obtains two sets of stress levels. One for the case of minimum and one for the case of maximum fibre debonding. A minor difference between the theories is the use of the normal distribution to characterize fibre strength. The complete model is well detailed in reference 4. The information provided in this reference enables the model to be applied to the 6000 filament carbon fibre/vinyl ester resin carbon composites, the stress limits are ultimately derived from the given generalized scatter limits. Section 6 in the reference describes the steps taken in the practical application of the model. Following this method the stress limits were derived for slabs 1 to 7. The results are presented in table 19 and the intermediate steps in table 2A9. An example of the derivation of the stress limits, divided into the main steps, is now given for slab 4.

Step I Determination of $\widehat{\sigma}_{f(L_R)}$:- $\widehat{\sigma}_{f(L_R)}$ is the mean fibre strength of a carbon fibre with a gauge length equal to the model fibre length assuming zero debonding (L_R) in the broken fibre. In the model composite L_R equals 8 fibre diameters (d_f). A correction factor, F, for composites with V_f and $\frac{E_f}{E_m}$ which differ from the model composite is given.

$$F = \left[\frac{E_f}{E_m} \left(V_f^{-\frac{1}{2}} - 1\right) 0.024\right]^{\frac{1}{2}} \quad \ldots \quad (17)$$

For slab 4 $E_f = 242.1 KN/mm^2$, $E_m = 3.37 KN/mm^2$ and $V_f = 0.3773$. Substituting into equation 17:-

$$F = \left[\frac{242.1}{3.37} \left(0.3773^{-\frac{1}{2}} - 1\right) 0.024\right]^{\frac{1}{2}} = 1.041$$

The appropriate carbon fibre gauge length becomes

$$L_R = 1.041 \times 8 \times 7.3 \times 10^{-3} = 0.0608mm$$

The mean fibre strength using equation 48 is

$$\widehat{\sigma}_{f(L_R)} = \alpha^{-1/\beta} L^{-1/\beta} \Gamma\left(1 + 1/\beta\right) \quad \ldots \quad (48)$$

The Weibull parameters for the as rec. carbon fibres are $\alpha^{-1/\beta}$ $= 1.45 KN/mm^{(2-1/\beta)}$ and $\beta = 7.02$.

$$\therefore \quad \hat{\sigma}_{f(L_R)} = 1.45\ (0.0608)^{-1/7.02}\ \Gamma\ (1 + 1/7.02)$$

$$\hat{\sigma}_{f(L_R)} = 2.02 KN/mm^2$$

Step 2. Determination of $\hat{\sigma}_{af}$:- $\hat{\sigma}_{af}$ is the average fibre stress at the failure of the model carbon composite. To determine $\hat{\sigma}_{af}$ it is necessary to estimate the length of fibre debonding in the composite and the fibre strength CV (CV_f). Barry[4][16] found that substituting the fibre pull-out lengths on the composite fracture surfaces for fibre debond lengths gave satisfactory results. The maximum and minimum fibre pull-out lengths for the 6000 filament carbon fibre composite specimens were noted during the microscopic examination of the fractured tensile specimens. In the case of the specimens from slab 4 the pull-out lengths ranged from 0 to 13 fibre diameters. These values are standardized to the model by dividing by F. Thus the equivalent standard debond range is 0 to 12.5 fibre diameters. Figure 5 shows that the corresponding L_p/L_R ratios to the above minimum and maximum standard debond lengths are 1 and 3.7 respectively. CV_f for the as rec. carbon fibre is 16.6% (see table 2A9). The proposed modified value of CV_f in reference 4 is not used here since neither the dependence of the fibre failure strain on the fibre elastic modulus nor the CV of the fibre elastic modulus are known.

σ^* is the ratio of $\hat{\sigma}_{af}$ to $\hat{\sigma}_{f(L_R)}$. Figures 6 to 8 show the variation of the upper and lower 95% single tail scatter limits for σ^* and the mean of σ^* with the ratio of L_p/L_R, as given in reference 4, for fibres with strength CV_f ranging from 10% to 25%. These figures give for slab 4, with $CV_f = 16.6\%$ and $L_p/L_R = 1$, the upper limit, mean and lower limit of σ^* as 0.766, 0.721 and 0.664 respectively. Similarly for $L_p/L_R = 3.7$ the corresponding σ^* values are 0.682, 0.637 and 0.579. Multiplying these values by $\hat{\sigma}_{f(L_R)}$ gives $\hat{\sigma}_{af}$, the predicted values of average fibre stress at model failure. $\hat{\sigma}_{f(L_R)}$ was derived in Step I as $2.02 KN/mm^2$. Thus for the case of zero debonding (i.e. $L_p/L_R = 1$) the upper, mean and lower values for $\hat{\sigma}_{af}$ are $1.55 KN/mm^2$, $1.46 KN/mm^2$ and $1.34 KN/mm^2$ respectively. In the case of maximum debonding (i.e. $L_p/L_R = 3.7$) the corresponding values of $\hat{\sigma}_{af}$ are $1.38 KN/mm^2$, $1.29 KN/mm^2$ and $1.17 KN/mm^2$. The model composite is only a fraction of the real composite. Therefore a composite size factor, η , has to be applied to $\hat{\sigma}_{af}$ to obtain the actual composite strength, $\hat{\sigma}_c$.

Step 3 Determination of η :- It is assumed that the failure of one model composite results in the failure of the whole composite specimen. The specimen is therefore regarded as M times the length of the model composite, where M is the number of model composites in the specimen. The model carbon composite contains approximately 4000 fibres of length 0.0608mm when assuming the case of zero debond length. When assuming maximum debond length the model fibre length becomes 0.0608 x 3.7 = 0.2250mm. The actual test specimens were 50mm in length and contained approximately 196000 fibres. Therefore the number of model carbon composites in the specimen for $L_p/L_R = 1$, M_1, is

$$M_1 = \frac{196000}{4000} \times \frac{50}{0.0608} = 40296$$

Similarly $M_{3.7}$, when $L_p/L_R = 3.7$, is

$$M_{3.7} = \frac{196000}{4000} \times \frac{50}{0.2250} = 10889$$

Figure 9 gives the relationship between CV_f and CV_{ac} (CV of model composite strength). The as rec. carbon fibres have a CV_f of 16.6%, therefore according to figure 9 CV_{ac} is 3.4%.

The computer simulation method of reference 4 assumes the composite specimen to have the same type of strength distribution as the constituent fibres, i.e., in reference 4, a normal distribution. Barry demonstrated that the resultant fibre and composite strength to length relationships deviate from the equivalent relationships predicted by a Weibull distribution by a maximum of 1.5%, provided that M>2 and CV $\leqslant$ 20%. The Weibull distribution has been used throughout this research to represent the strength distribution of the carbon fibres and is therefore, in view of the above, used here to describe the composite strength distribution. As a result of this the formula for η differs from that given in reference 4. η is derived from the equation

$$\beta = \frac{\ln\left(\frac{L_1}{L_2}\right)}{\ln\left(\frac{\sigma_2}{\sigma_1}\right)} \quad \ldots (47)$$

$$\therefore \frac{\sigma_1}{\sigma_2} = \left(\frac{L_1}{L_2}\right)^{-1/\beta} \quad \ldots (89)$$

Substituting M for $\left(\frac{L_1}{L_2}\right)$, $\hat{\sigma}_{af}$ for σ_2 and $\hat{\sigma}_f$ for σ_1 , where $\hat{\sigma}_f$ is the average fibre stress at composite failure it follows that

$$\eta = M^{-1/\beta} \quad \ldots (90)$$

β is determined from the CV of the model composite strength. For slab 4 the equivalent model composite has a CV of 3.4%. Referring to figure 3 and equation 16 the corresponding Weibull parameter, β, for the strength distribution is 36.90. By substitution into equation 90 the size factor, η, can now be determined. For zero debonding $M_1 = 40296$

$$\therefore \quad \eta_1 = (40296)^{-1/36.90} = 0.750$$

Similarly for maximum debonding, $M_{3.7} = 10889$

$$\therefore \quad \eta_{3.7} = (10889)^{-1/36.90} = 0.779$$

To determine $\hat{\sigma}_f$ the size factor is now applied to $\hat{\sigma}_{af}$

Step 4 Determination of $\hat{\sigma}_f$:- The predicted $\hat{\sigma}_f$ values for the real composite are the products of the appropriate η values with their corresponding $\hat{\sigma}_{af}$ values. Thus for the case of zero debonding the upper limit ($\hat{\sigma}_{Uf}$), mean ($\hat{\sigma}_{Mf}$) and lower limit ($\hat{\sigma}_{Lf}$) of the fibre stress at composite failure are:

$$\hat{\sigma}_{Uf} = 1.55 \times 0.750 = 1162.5 \text{N/mm}^2;$$
$$\hat{\sigma}_{Mf} = 1.46 \times 0.750 = 1095.0 \text{N/mm}^2;$$
$$\hat{\sigma}_{Lf} = 1.34 \times 0.750 = 1005.0 \text{N/mm}^2.$$

Similarly for the case of maximum fibre debonding:

$$\hat{\sigma}_{Uf} = 1.38 \times 0.779 = 1075.0 \text{N/mm}^2;$$
$$\hat{\sigma}_{Mf} = 1.29 \times 0.779 = 1004.9 \text{N/mm}^2;$$
$$\hat{\sigma}_{Lf} = 1.17 \times 0.779 = 911.4 \text{ N/mm}^2.$$

Therefore according to Barry's model the fibre stresses at the failure of the specimens from slab 4 are expected to fall within the range 911.4N/mm^2 to 1162.5N/mm^2. To facilitate the comparison of these theoretical results with the experimental results the fibre stresses are converted to composite stresses.

Step 5 Determination of Composite Failure Stress, $\hat{\sigma}_c$:-

To convert $\hat{\sigma}_f$ to $\hat{\sigma}_c$ the $\hat{\sigma}_f$ values for slab 4 are multiplied by the factor $F_c = (0.986\ V_{cf} + 0.014)$ derived earlier in this section when considering the statistical theories of Rosen[1] and Zweben[3]. The general equation for the factor F_c is

$$F_c = V_f \left(1 - \frac{E_m}{E_f}\right) + \frac{E_m}{E_f} \qquad \ldots \quad (91)$$

For slab 4 $V_{cf} = 0.3774$. Therefore $F_c = 0.386$. Thus for the case of zero fibre debonding the expected composite stress levels are:

$$\hat{\sigma}_{U1} = 1162.5 \times 0.386 = 448.7 N/mm^2;$$
$$\hat{\sigma}_{M1} = 1095.0 \times 0.386 = 422.7 N/mm^2;$$
$$\hat{\sigma}_{L1} = 1005.0 \times 0.386 = 387.9 N/mm^2.$$

For the case of maximum fibre debonding are:

$$\hat{\sigma}_{U2} = 1075.0 \times 0.386 = 415.0 N/mm^2;$$
$$\hat{\sigma}_{M2} = 1004.9 \times 0.386 = 387.9 N/mm^2;$$
$$\hat{\sigma}_{L2} = 911.4 \times 0.386 = 351.8 N/mm^2.$$

Table 19 gives the two sets of upper, mean and lower stress values for slabs 1 to 7 and their experimental failure stresses. The theoretical and experimental results are compared graphically in figure 49. The main information and steps in the calculation of the stress levels for slabs 1 to 7 are tabulated in 2A9.

The experimental results are quite close to the stress levels predicted for the case of zero fibre debonding. For all the slabs bar one (slab 4) the failure stress of the strongest specimen exceeds $\hat{\sigma}_{U1}$ with $\hat{\sigma}_e$ (expected composite maximum stress calculated from the experimental results) approximating to $\hat{\sigma}_{U1}$. For example, in the case of slab 4 $\hat{\sigma}_e$ and $\hat{\sigma}_{u1}$ are $440.5 N/mm^2$ and $448.8 N/mm^2$ respectively. $\hat{\sigma}_{U1}$ is defined as the upper 95% scatter limits for the case of zero fibre debonding. Therefore $\hat{\sigma}_{U1}$ is not an absolute limit to composite strength but should rarely be exceeded by an experimental result. The lowest experimental tensile stresses are all above $\hat{\sigma}_{L2}$, commonly falling between $\hat{\sigma}_{M2}$ and $\hat{\sigma}_{U2}$. Again using slab 4 as an example the lowest experimental tensile failure stress is $389.8 N/mm^2$ whereas the corresponding $\hat{\sigma}_{M2}$ and $\hat{\sigma}_{U2}$ levels are $387.9 N/mm^2$ and $415.0 N/mm^2$ respectively. In reference 4 Barry recommended that the estimation of the maximum fibre debond length be based on the maximum fibre pull-out length, even if only a very small number of fibres exhibit such a pull-out length. Examination of the fracture surfaces of specimens from 1 to 7 showed fibre pull-out lengths to be predominantly 0 to 4 fibre diameters in length with only very few fibres exhibiting the maximum pull-out lengths as listed under maximum debond length in table 2A9. Therefore the experimental results are expected to approximate more closely to the $\hat{\sigma}_1$ stress levels than the $\hat{\sigma}_2$ stress levels, as is the case.

As regards the effect of the different surface treatments on composite tensile strength it is interesting to note that Barry's model predicts slightly lower $\hat{\sigma}_1$ and $\hat{\sigma}_2$ levels for slabs 6 and 7 (having normalized the levels of slab 6 to an equivalent $V_{cf}\%$ of 37.73%) than for slab 4 due to the marginally different statistical characteristics of the tensile strengths of the carbon fibres after varying the surface treatments. As stated previously the experimental results from slabs 6 and 7 are slightly greater than those from slab 4 but a statistical analysis shows the variance amongst the means to be insignificant.

In general although the theoretical $\hat{\sigma}_1$ levels are slightly conservative the agreement between the theoretical and experimental results is promising when taking into account the assumptions made in the model and the number of parameters involved in the calculations. The theory is particularly dependent upon the tensile strength characteristics of the constituent fibres since these are necessary for the calculation of the basic mean fibre strength, $\hat{\sigma}_{f(L_R)}$, prediction of CV_{ac} and the size factor η. Unfortunately the statistical characteristics of the carbon fibres were derived from the tensile properties of the fibre tows. Although this has been justified the testing of individual filaments would have been preferable since any interaction between the fibres in the tows tends to mask the basic fibre strength characteristics. The effects of the dynamic stress concentrations in the model should also be considered. Barry's simplified representation of the dynamic stress concentrations may also be partly responsible for the conservative nature of the predicted stress levels. This is questionable though since when Barry applied the model to some carbon/epoxy tensile specimens he found that the experimental results tended towards the lower theoretical stress levels.

One drawback to Barry's model is the method adopted for estimating the maximum fibre debond length. The use of the maximum pull-out length on the composite fracture surface necessitates the testing of the composite before the theoretical lower stress limits can be calculated. In addition it is thought that the maximum fibre pull-out length must frequently overestimate the fibre debond length. Fibre debonding and pull-out of previously failed fibres may occur during the catastrophic failure of the composite rather than at the time of failure of the individual fibre.

In the case of the 6000 filament carbon fibre composites Barry's model[4] has predicted a composite failure stress band considerably narrower than that predicted by the similar statistical theory of Rosen[1] and Zweben[3].

One common criticism of the cumulative fracture propagation mode, upon which the statistical theories are based, is that the random fibre

fractures should result in a non-linear upper portion of the stress v strain curve. In the carbon composites tested in this research and in many other single fibre type systems the stress v strain curves remain linear up to the catastrophic failure of the specimen. This does not mean that the statistical theory is incorrect. In composites containing thousands of fibres (of number N) it is possible for a considerable number of fibre failures to have no determinable effect on the composite elastic modulus. If on failure a fibre is fully ineffective over its entire length then the contribution of that fibre to the elastic modulus of the composite is zero. In this case, assuming the composite elastic modulus obeys the mixture rule (justified for the carbon/vinyl ester composites in section 4.7.1.2), upon the failure of one fibre the reduction in composite elastic modulus, ΔE, is

$$\Delta E = \frac{V_f}{N} . E_f \qquad . . . \quad (92)$$

In the statistical theories, assuming no fibre debonding, the fractured fibres are only ineffective over a length δ . Therefore the reduction in the elastic modulus of a composite of gauge length L when one fibre fails is

$$\Delta E = \frac{V_f E_f \delta}{NL} \qquad . . . \quad (93)$$

Consider a tensile specimen from slab 4 with $V_{cf}\% = 37.73\%$ for which $N = 0.196 \times 10^6$ and $\delta = 43.4 \times 10^{-3}$mm. It follows that

$$\Delta E = 0.405 \times 10^{-6} KN/mm^2$$

From equation 80 the expected modulus of a specimen from slab 4 is $93.5 KN/mm^2 (\pm 0.3)$. It is estimated from the original plots of load v strain recorded during the tensile tests that the minimum detectable change in slope for slab 4, assuming the change to be gradual, is equivalent to a change in modulus of $1.9 KN/mm^2$. Therefore approximately 4.69×10^6 fibre fractures have to occur before the effect on the composite modulus is detectable, each fibre failing an average of 24 times into average lengths of 2.08mm. This demonstrates the feasibility of the cumulative fracture mode for the carbon fibre/vinyl ester composites despite their linear tensile stress v strain curves up to composite failure, i.e. the postulated scattered single and multiple fibre failures have no detectable effect on the tensile stress v strain curve. There is no evidence from the tensile tests to contradict the statistical theory. The apparent increase in the tensile strength of the 50mm constituent fibres from an expected $744.4 N/mm^2$ to an average of $1141.0 N/mm^2$ is supportive. It is consistent with the occurence of random single and multiple fibre failure in the composites, breaking the fibres down into estimated average lengths of

less than 3.37mm, as calculated earlier in this section. The close correlation between the experimental results and the expected stress levels according to Barry, compared with the extremely conservative nature of the lower bound on composite failure stress according to Zweben, indicates that a substantial number of multiple fibre as well as single fibre failures occur prior to the ultimate composite failure. Therefore it is suggested that the tensile failure process of the carbon composites is as follows.

As the applied load is increased single fibre breaks and then single and multiple fibre breaks occur throughout the stressed composite. Initially the broad fibre strength distribution (θ = 7.02) renders unlikely the catastrophic propagation of fibre failure. As the applied load is further increased, but before the upper stress limit as defined by Rosen is reached, i.e. before random fibre failures leave any particular cross-section too weak to support the applied load, a multiple (or single) fibre break eventually becomes unstable. The static or dynamic stress concentrations on fibres adjacent to a fracture causes the fracture to propagate. The sudden failure of more fibres further weakens the cross-section producing dynamic stress concentrations which radiate over a wide region causing further fibres in weakened areas away from the immediate vicinity to fracture and existing multiple fibre fracture groups to enlarge and propagate. The different unstable multiple fracture groups are not all planar and their propagations result in a weak non-planar cross-section which forms the final fracture surface of the composite as some of the failed fibre bundles join together by shear failure. This failure process would result in a fracture surface similar to those of the tested specimens described in section 4.7.1.1. The experimental work of Fuwa, Bunsell and Harris[14] also supports this failure process. Their monitored acoustic emission from Type I carbon fibre/epoxy composites during tensile testing indicated that fibre failures started at the same stress level as in an unimpregnated Type I carbon fibre tow, at less than 50% of the ultimate composite stress. The tensile fracture surfaces of the Type I carbon fibre/epoxy specimens were similar to those described for the 6000 filament carbon/vinyl ester resin tensile specimens. Fuwa et al[14] etched away the surface resin on their failed composite specimens and observed the exposed outer layer of carbon fibres. In all of the specimens groups of broken fibres existed away from the final fracture site with the density of the groups increasing near to the final fracture site and with the failure stress of the specimen. The failures in the fractured fibre groups frequently ran at varying angles to the fibre direction, as observed with the 6000 filament carbon/vinyl

ester composites. Unfortunately quantitative comparisons between the experimental results presented by Fuwa et al and the statistical theories are not possible due to the absence of the necessary data in reference 14.

The experimental results of slabs 1 to 7 and their comparison with existing theories for composite failure are now summarized.

4.7.1.4 Summary of the Tensile Properties of the Carbon Fibre Composites of Slabs 1 to 7

The following points summarize the analyses of the tensile results of the carbon fibre/vinyl ester slabs 1 to 7.

i) The tensile stress v strain plots are linear up to composite failure.

ii) The linear relationship between V_{cf} and E_e follows the rule of mixtures, assuming that E_{cf} is 242.1KN/mm^2

$$E_e = 3.4 + 238.7\ V_{cf}\ \text{KN/mm}^2 \quad . \ . \ . \quad (80)$$

iii) There is no significant variation in the average composite failure strain with V_{cf} within the tested range of $0.16 \leqslant V_{cf} \leqslant 0.49$, the expected composite failure strain being $0.47 \pm 0.01\%$.

iv) The relationship between $\hat{\sigma}_e$ and V_{cf} is linear and is described by the equation

$$\hat{\sigma}_e = 16.0 + 1125.0\ V_{cf}\ \text{N/mm}^2 \quad . \ . \ . \quad (82)$$

v) The three different surface treatments of the carbon fibres produced no significant difference in the mean tensile properties of their composites.*

vi) $\hat{\sigma}_e$ is not estimated satisfactorily by the rule of mixtures when $\hat{\sigma}_{cf}$ is based on the average tensile strength of carbon fibres of the same length as the gauge length of the composite.

vii) The average stress in the carbon fibres at composite failure is 1141.0N/mm^2. This is equivalent to the average tensile strength of carbon fibre 3.37mm in length.

viii) The statistical failure mechanisms described by Rosen[1], Zweben[3] and Barry[4] provide an explanation for the above apparent increase in the tensile strength of the carbon fibres when composited in a vinyl ester matrix.

ix) The extreme conservative nature of the theoretical lower composite failure stress level, $\hat{\sigma}_L$, as defined by Zweben[3], when compared with the experimental results of the carbon composites indicates that a considerable number of multiple fibre failures occur within the composites prior to catastrophic failure.

x) Following the statistical theories the high theoretical upper stress levels, as defined by Rosen, obtained for the composites and the success of Barry's model both indicate that stress concentration effects play a significant.

role in the failure of the carbon composites.

xi) The jagged appearances of the composite fracture surfaces are explained by the statistical theories.

xii) Points vii) and xi) and the general agreement between the experimental results and those predicted by the statistical theories strongly suggest that the failure process of the carbon composites is governed by the statistical nature of the carbon fibre tensile strength.

Points ii), iii) and iv) are of prime importance in establishing the existence or otherwise of any 'hybrid effects' in the carbon fibre/E-glass fibre/vinyl ester resin composites. It is concluded from points ix) and xii) that the failure mechanism of the carbon composites is statistical with random single and multiple (due to stress concentrations) fibre failure occurring throughout the composite prior to the final catastrophic propagation of fibre failure. This forms a base from which to study the failure of the hybrid composites.

The tensile properties and behaviour of the 600 tex E-glass fibre/vinyl ester composites are now studied.

4.7.2 Tensile Properties of the 600 tex E-Glass Fibre Composites of Slabs 8 to 16

The tensile results for slabs 8 to 16 are given in tables 16 and 2A8. Figures 50 and 51 show the variation with V_{g6} of composite elastic modulus and tensile strength respectively. Figure 52 is a typical stress v strain curve for a specimen from slab 11. During the testing of the specimens no acoustic emissions from the specimens were heard or damage observed prior to catastrophic composite failure.

4.7.2.1 The Fracture Surfaces of the 600 tex E-Glass Fibre Composite Tensile Specimens

Figure 53 shows the jagged and spiky appearance of a failed specimen from slab 11 and is typical of all the specimens from slabs 8 to 13. Fibre pull-out is far more extensive in these specimens than in the carbon specimens. The fibre pull-out lengths lie predominantly between 1 and 10 fibre diameters with the full range being 0 to approximately 16 fibre diameters. The fibres have failed in small groups, or bundles, which, as in the carbon specimens, are joined together by shear failure predominantly at the fibre/resin interface. As noted above there was no visible sign of specimen damage immediately prior to the catastrophic failure of the composite. Areas of debonded fibres within

the composites, providing they consist of sufficient fibres, are visible from the surface of the specimens as whitened areas. After composite failure white lines were frequently observed running up to 20mm along a specimen away from the fracture surface. The width of the lines were commonly 0.5 to 1.0 fibre tow width with just a few extremely narrow lines. Very occasionally a short length of debonded fibre tow was visible in the specimen away from the fracture surface. The extent of debonding into the composite from the fracture surfaces varied between specimens from the same slabs. This suggests that the original dressing had not been applied uniformally to the fibre tows. It is postulated that at catastrophic failure large shock waves travel through the composite causing extensive debonding at the weaker fibre/resin interfaces. It seems likely that the small lengths of debonded fibres not connected to the fracture surface also appeared at the moment of, or immediately after, specimen failure since they were not observed prior to failure. These rare debonded areas may be the sites of multiple fibre fractures which extend at composite catastrophic failure but which are too far away from the major site of crack propagation to be incorporated into the final fracture surface. The visible debonding would be caused by shock waves stemming from the catastrophic composite failure.

The general appearance of the fracture surfaces of slabs 14 and 15 was similar to that of slabs 8 to 13. The fibre pull-out ranges were again approximately 0 to 16 fibre diameters but the dominant pull-out lengths seemed slightly less than for slabs 8 to 13, though these were difficult to estimate. The composite specimens were very faintly whitened away from the fracture surfaces up to a distance of approximately 10mm and 6mm for slab 14 and slab 15 respectively. The extent of debonding seemed fairly uniform across the width of each specimen. The average i.l.s.s. of slabs 14 and 15 were $61N/mm^2$ and $103N/mm^2$ respectively. At these high values very little fibre debonding was expected, especially in slab 15, and therefore the presence of the faintly whitened areas suggest that the fibre/resin bond strength was not uniform. In this case the above observations on the intensity and uniform spread across the specimens of the whitened areas implies that variation in the effectiveness of the surface treatment tended to be between fibres rather than along the length of the fibre tows, as appeared to be the case for the as rec. E-glass composites. No debonded area not connected to the fracture surfaces was visible in any of the tested specimens from slabs 14 and 15. The fracture surfaces of the tensile specimens tested from slab 16, containing no c.-a. 600 tex E-glass fibres, were considerably less jagged than those of slabs 8 to 15. The fibre pull-out lengths were predominantly between 0 and 4 fibre diameters with only a small proportion of fibres having the longer pull-out

lengths of 5 to 14 fibre diameters. The spread of the whitened area into the composite body from the fracture surfaces was minimal. This limited amount of debonding was unexpected in the light of the previous results since the average i.l.s.s. of slab 16 was only $46N/mm^2$. The implication is that the fibre/resin bond strength at the weak interfacial areas in slabs 11, 14 and 15 is less than the bond strength between the resin and the no c.-a. E-glass fibres in slab 16. This is possible. The surface of the 600 tex E-glass is extremely smooth and therefore the main contribution to fibre/resin bond strength must be from chemical rather than mechanical bonding. The method chosen for the removal of the dressing from the as rec. fibres (see section 3.4.3) should leave the E-glass fibre clean with the surface hydroxyl groups available for chemical bonding with the secondary hydroxyl groups of the vinyl ester resin (see section 2.5.2). The silane coupling-agents on the surface treated fibres also bond to the E-glass via the surface hydroxyl groups of the fibres. In the cases of the A187 and A1100 treatments it is possible that there was insufficient of the hydrolized coupling-agent, in the solution from which it was applied, to form a complete coating over all the surface area of the fibres. The free hydroxyl groups would have been susceptible to attack by impurities in the solution. In addition impurities may have been attracted to and reached parts of the glass surface before the hydrolized coupling-agent, particularly if the concentration of the coupling-agent in the solution was non-uniform. Therefore it is suggested that a very low proportion of the fibre surface area in slabs 14 and 15 was devoid of coupling-agent and had few free hydroxyl groups with which the resin could bond. The resultant fibre/resin bond strength at these points would be below that of the no c.-a. fibre/resin. Therefore in specimens from slabs 14 and 15 any fibres with a chance accumulation of weak fibre/resin bonding about the fracture surface would debond to a greater extent than expected of fibres with the average interfacial bond strength. Such debonding of only a small percentage of the fibres could result in the faintly whitened areas observed spreading from the fracture surfaces of the specimens. In the case of slab 11 the coupling-agent and sizing is believed to have been applied to the fibre tows as an integral blend. A less than uniform dispersion of the small proportion of the A172 coupling-agent in the sizing would result in varying coupling-agent content along the tow length. Thus the heavily whitened areas in the specimens from slab 11 could be the result of the debonding of groups of fibres in which the fibre surfaces are sized but contain a minimal amount of coupling-agent.

An alternative possibility for the unexpected degrees of fibre debonding in slabs 11, 14, 15 and 16 is that they are in some way connected with the statistical characteristics of the fibre tensile strengths. This is unlikely since the characteristics of the no c.-a. fibres appear similar to those of the A187 and A1100 fibres (see section 4.2.3).

4.7.2.2 The Tensile Stress v Strain Curves of the 600 tex E-Glass Fibre Composite Specimens

All the tensile specimens tested from slabs 8 to 16 had linear stress v strain plots up to the catastrophic failure of the composites. Figure 52 is the average stress v strain curve obtained from the specimens of slab 11.

Consider the elastic modulus, E, of the 600 tex E-glass fibre composites as given in table 16. Figure 50 is a plot of the average elastic modulus of specimens from each of the slabs 8 to 13 against V_{g6}. The line E_e is the expected elastic modulus of the 600 tex E-glass composites calculated from the experimental results. As with E_e for the carbon fibre composites the equation was calculated assuming a linear relationship between E and V_{g6} and using the method of least squares. The value of $3.4 KN/mm^2$ at zero V_{g6} is the elastic modulus of the vinyl ester resin, E_m, up to the average failure strain of the 600 tex E-glass composites (1.96% ε, determined later in this section). The calculated equation for E_e is

$$E_e = 3.4 + 72.2\, V_{g6} \quad KN/mm^2 \qquad . \; . \; . \qquad (94)$$

which is equivalent to

$$E_e = 3.4 V_m + 75.6\, V_{g6} \quad KN/mm^2 \qquad . \; . \; . \qquad (95)$$

There is little scatter in the results about this line, as was found with the results of the carbon composites. Extrapolation of the line E_e to $V_{g6} = 1.00$ predicts an elastic modulus of $75.6 KN/mm^2$ for the as rec. 600 tex E-glass fibre. Therefore E_{g6} is $75.6 KN/mm^2$ with the linear relationship between composite E_e and V_{g6} being accurately represented by the rule of mixtures.

The average elastic modulus of the specimens tested from slabs 11, 14, 15 and 16, containing as rec., A187, A1100 and no c.-a. surface treated fibres respectively, were $31.9 KN/mm^2$, $31.9 KN/mm^2$, $31.4 KN/mm^2$ and $31.4 KN/mm^2$ respectively. An analysis of the variance amongst these means show the differences to be insignificant. Therefore the different surface treatments of the 600 tex E-glass fibres, and the resultant changes in composite i.l.s.s.,

have no significant effect upon the elastic modulus of their composites.

Consider the failure strains ($\varepsilon^F = \varepsilon' = \hat{\varepsilon}$) of specimens from slabs 8 to 13. Table 16 shows that the average failure strains of the sets of specimens tested from these slabs vary between 1.84% and 2.08%. An analysis of the variance amongst the mean strains show the differences to be insignificant. Therefore, within the range $22.34\% \leq V_{g6}\% \leq 51.30\%$, it appears that V_{g6} has no effect on the expected composite failure strain $\hat{\varepsilon}_e$. It follows that the overall average failure strain is equal to the grand mean of all the specimens from slabs 8 to 13. The appropriate calculation gives $\hat{\varepsilon}_e$ equal to $1.96 \pm 0.03\%$.

Now consider the maximum stresses of the specimens. Figure 51 shows the variation in the average composite tensile strength with V_{g6}. The value of $63 N/mm^2$ plotted at zero V_{g6} is the matrix stress (estimated from figure 39) at a strain of 1.96%. Assuming a linear relationship between $\hat{\sigma}_e$ and V_{g6} the following equation for $\hat{\sigma}_e$ was calculated to best fit the experimental data by the regression method of least squares.

$$\hat{\sigma}_e = 63.0 + 1430.0\ V_{g6}\ N/mm^2 \qquad . \ . \ . \qquad (96)$$

This is equivalent to

$$\hat{\sigma}_e = 63.0 V_m + 1493.0 V_{g6} N/mm^2 \qquad . \ . \ . \qquad (97)$$

Substituting 1.00 for V_{g6} it follows that the average 600 tex E-glass fibre stress at composite failure in slabs 8 to 13 was $1493 N/mm^2$. The validity of the proposed equations for E_e and $\hat{\sigma}_e$ is checked by dividing by E_e and comparing the resultant value with $\hat{\varepsilon}_e$.

At $V_{g6} = 1.00$

$$\frac{\hat{\sigma}_e}{E_e} = \frac{1493.0}{75.6 \times 10^3} = 1.97\% \varepsilon$$

1.97% is within the calculated value of $1.96 \pm 0.03\%$ for $\hat{\varepsilon}_e$.

The scatter band for each set of specimens is indicated in figure 51. As with the carbon composites, the degree of scatter in $\hat{\sigma}$ and $\hat{\varepsilon}$ are similar and both are considerably greater than the scatter in E.

The evaluation of the effects of the different surface treatments on the 600 tex E-glass composite tensile properties is complicated by the fact that the surface treatment processes damaged the fibres and altered the statistical characteristics of the tensile strength of the fibres. The differences between the average tensile strengths of the as rec., no c.-a., A187 and A1100 surface treated fibres are highly significant. Thus direct comparison of the stress and strain results of slabs 11, 14, 15 and 16 is

inappropriate. The results are compared indirectly by considering the failure strains of the composites in relation to the failure strains of their constituent fibres at a 50mm gauge length. There is no significant difference amongst the elastic moduli of specimens from slabs 11, 14, 15 and 16 and it is assumed that the surface treatments did not alter the average elastic modulus of the fibres from that of the as rec. fibres of $75.6 KN/mm^2$. Therefore using data given in table 10 the average failure strains of the 600 tex E-glass fibres with different surface treatments at 50mm gauge lengths were

(as rec.) $$\hat{\varepsilon}_{g6} = \frac{1451.6}{75.6 \times 10^3} \times 100\% = 1.92\% ;$$

(A187) $$\hat{\varepsilon}_{g6} = \frac{839.3}{75.6 \times 10^3} \times 100\% = 1.11\% ;$$

(A1100) $$\hat{\varepsilon}_{g6} = \frac{896.3}{75.6 \times 10^3} \times 100\% = 1.19\% .$$

(no c.-a.) $$\hat{\varepsilon}_{g6} = \frac{873.0}{75.6 \times 10^3} \times 100\% = 1.15\%$$

The failure strains of specimens from slabs 11, 14, 15 and 16 are now normalized by dividing by the average failure strain of the constituent fibre as given above:

Slab 11 (as rec.) $$\frac{\hat{\varepsilon}_e}{\hat{\varepsilon}_{g6}} = \frac{1.87}{1.92} = 0.97 ;$$

Slab 14 (A187) $$\frac{\hat{\varepsilon}_e}{\hat{\varepsilon}_{g6}} = \frac{1.04}{1.11} = 0.94 ;$$

Slab 15 (A1100) $$\frac{\hat{\varepsilon}_e}{\hat{\varepsilon}_{g6}} = \frac{1.61}{1.19} = 1.35 ;$$

Slab 16 (no c.-a.) $$\frac{\hat{\varepsilon}_e}{\hat{\varepsilon}_{g6}} = \frac{0.88}{1.15} = 0.77 ;$$

Due to the large degree of scatter in the failure strains of the composites the above ratios must not be regarded as absolute. This is emphasized by considering the ratio for slab 11. The average failure strain for slab 11 was used as the numerator in the strain ratio. Since the numerator represents the average failure strain of a composite containing the fibre under consideration a more accurate value for the numerator is 1.96%, the grand mean of all specimens from slabs 8 to 13. This gives a new ratio of 1.02 compared with the original 0.97. The only reliable conclusions to be drawn are that the strain ratios for slabs 11 and 14 fall between those for slabs 15 and 16, with the ratio for slab 15 being the greatest. Thus in

terms of tensile failure stress and strain the composite containing A1100 surface treated 600 tex E-glass fibres is the most efficient whilst that containing no c.-a. 600 tex E-glass fibres is the least efficient. Examination of table 15 shows that the i.l.s.s. of slab 15 ($103.5 N/mm^2$) was greater than that for slabs 11, 14 and 16, the i.l.s.s. of slab 16 being the lowest at $45.7 N/mm^2$. This suggests that in the composite system of 600 tex E-glass fibres/vinyl ester resin an increase in composite i.l.s.s. increases the tensile failure stress and strain of that composite. Alternatively the varying efficiency of the surface treated fibres could be due to the changes in their tensile strength characteristics (considered further in section 4.7.2.3) and/or to the different degrees of protection which the surface treatments afford the fibres during fabrication of the composites. Logically the most vulnerable fibre is the no c.-a. fibre and its composite, slab 16, has both the lowest i.l.s.s. and the lowest apparent fibre efficiency of the 600 tex E-glass composites.

The relationships between failure stress and fibre content for the different surface treated fibre composites are calculated directly from the results for slabs 14, 15 and 16, assuming the relationships to be linear.

$$\text{(A187)}\quad \hat{\sigma}_e = 35.2 + 752.6\, V_{g6} \quad N/mm^2 \qquad \ldots \quad (98)$$

$$\text{(A1100)}\quad \hat{\sigma}_e = 54.0 + 1158.9\, V_{g6} \quad N/mm^2 \qquad \ldots \quad (99)$$

$$\text{(no c.-a.)}\quad \hat{\sigma}_e = 30.0 + 637.0\, V_{g6} \quad N/mm^2 \qquad \ldots \quad (100)$$

The experimental tensile properties of slabs 8 to 16 are now compared with those predicted by existing theories.

4.7.2.3 Comparison of the Experimental and Theoretical Tensile Properties of the 600 tex E-Glass Fibre Composites

This section compares the commonly utilized mixture rule and the more complicated failure theories of Rosen[1], Zweben[3] and Barry[4] with the experimental results of slabs 8 to 16. The methods of application and sample calculations for the above theories have been given previously in section 4.7.1.3.

i) The Rule of Mixtures – Section 4.7.2.2 demonstrates that the elastic modulus of the 600 tex E-glass composites follows the rule of mixtures, assuming the elastic modulus of the fibres to be 75.6KN/mm^2.

$$E_e = 3.4V_m + 75.6\ V_{g6}\ \ KN/mm^2 \quad . \ . \ . \quad (95)$$

Section 4.7.2.2 also shows $\hat{\sigma}_e$ for the composites from slabs 8 to 13 to be

$$\hat{\sigma}_e = 63.0V_m + 1493.0\ V_{g6}\ N/mm^2 \quad . \ . \ . \quad (97)$$

The corresponding rule of mixtures equation, using the properties of 50mm gauge length 600 tex E-glass fibres is

$$\hat{\sigma}_{RM} = 60.0V_m + 1451.6\ V_{g6}\ \ N/mm^2 \quad . \ . \ . \quad (101)$$

For specimens from slab 11 ($V_{g6}\%$ = 39.09%)equations 97 and 101 predict composite failure stresses of 622.0N/mm^2 and 604.0N/mm^2 respectively. The difference between the two values is less than 3% of $\hat{\sigma}_e$. Therefore the rule of mixtures provides a close approximation for the failure stresses of the as rec. 600 tex E-glass/vinyl ester composites. The alternative surface treatments have been shown to affect the composite failure stress and strain. The strain ratios described and calculated are also ratios of the experimental failure stresses to those predicted by the rule of mixtures. Thus the rule of mixtures underestimates the average failure stress of slab 15 by approximately 35% and overestimates those of slabs 14 and 16 by approximately 6% and 23% respectively and therefore can not be used with confidence for these 600 tex E-glass fibre composites. The average failure stresses of the as rec. A187, A1100 and no c.-a. 600 tex E-glass fibres when in their composites correspond to the average failure stresses of those fibres at gauge lengths of 31.8mm, 70.8mm, 8.4mm and 220.6mm respectively.

The theories of Rosen and Zweben consider the strength characteristics of the fibres.

ii) The Statistical Theories of Rosen[1] and Zweben[3] – The upper ($\hat{\sigma}_U$), lower ($\hat{\sigma}_L$) and weakest ($\hat{\sigma}_W$) stress levels for as rec. 600 tex E-glass fibre composites with V_{g6} values of 0.2, 0.4, 0.6 and 0.8 were calculated using equations 7, 86 and 14 and presented in table 17. Where fibre stress at composite failure was equivalent to a strain of less than 1.58% (elastic limit of the matrix) the conversion to composite failure stress was made using the method described in section 4.7.1.3. Where the fibre failure stress was equivalent to a strain of 1.58% or more the conversion was

made using equation 1 and figure 39. The theoretical stress levels are plotted in figure 51 with the experimental results. $\hat{\sigma}_U$, $\hat{\sigma}_L$ and $\hat{\sigma}_W$ were also calculated for slabs 11, 14, 15 and 16 and are listed in table 18.

Consider figure 51. The $\hat{\sigma}_W$ level is well below the composite failure strengths therefore the composites do not fail by the weakest link mode. This was expected for the same reasons as noted in section 4.7.1.3 for the failure of the carbon composites. The average failure stresses of the specimens from slabs 8 to 13 all fall approximately midway between the stress levels $\hat{\sigma}_U$ and $\hat{\sigma}_L$. The only experimental scatter band to extend beyond this theoretical band is that for slab 12. The appropriate $\hat{\sigma}_L$ value is approximately 570.0N/mm^2. Examination of table 2A8 shows that specimen 12.1 failed at a stress of 552.4N/mm^2. This is an isolated result and it is likely that this specimen was damaged prior to testing. The stress band between $\hat{\sigma}_U$ and $\hat{\sigma}_L$ is considerably narrower than that for the carbon composites, reflecting the lower CV in fibre tensile strength for the as rec. 600 tex E-glass fibres, and taken as a prediction of the expected failure stress range is remarkably accurate. Consider table 18. The experimental failure stresses for slabs 14, 15 and 16 again fall within the predicted $\hat{\sigma}_U$ and $\hat{\sigma}_L$ values. However, the theoretical stress bands are extremely broad due to the reduced β parameter of the constituent fibres. The results from slabs 14 and 16 tend towards the $\hat{\sigma}_L$ values. Therefore, according to the statistical theory, only a limited number of multiple fibre breaks occured in these composites prior to catastrophic failure, whilst more are expected in the as rec. fibre composites. This is contrary to expectations when considering the fibre strength distributions. The as rec. fibres have a narrower distribution than the other surface treated fibres and this is supposed to encourage the catastrophic propagation of fibre failure. However, the damage incurred by the retreated fibres during the retreating process is likely to have resulted in groups of weakened fibres rather than in an even distribution of flawed fibres. These groups must increase the probability of the propagation of fibre breaks and of a non-Weibull distribution of fibre tensile strength.

The general observation from the comparison of the experimental failure stresses of slabs 8 to 16 with the theoretical stresses following Rosen[1] and Zweben[3] is that the experimental results fall within the theoretical $\hat{\sigma}_U$ and $\hat{\sigma}_L$ limits, supporting the statistical theories. The experimental results are now applied to the model proposed by Barry[4].

iii) The Statistical Model Proposed by Barry - The main steps in calculating the predicted range of composite failure stresses for slabs 8 to 16 from Barry's model are given in table 2A9. The σ^* values in this table for slabs 8 to 13 were obtained by a double extrapolation of the plots in figures 6, 7 and 8. The theoretical composite failure stress levels derived are given in table 19. The upper stress levels assuming zero debonding, $\hat{\sigma}_{U1}$, are less than the upper stress levels assuming maximum debonding, $\hat{\sigma}_{U2}$. Figure 6 shows this to be a joint consequence of the low CV ($< 10\%$) of the fibre strength and the large L_p/L_R ratios, determined from the maximum debond lengths. The extreme stress levels $\hat{\sigma}_{U2}$ and $\hat{\sigma}_{L2}$ and the experimental results for the as rec. E-glass composites of slabs 8 to 13 are plotted in figure 54 against V_{g6}. The scatter limits of the experimental results extend beyond the $\hat{\sigma}_{U2}$ and $\hat{\sigma}_{L2}$ values but the average experimental values are all within the theoretical stress band, with a slight bias towards the $\hat{\sigma}_{L2}$ values. Of the 32 specimens tested from slabs 8 to 13, 9 had failure stresses below $\hat{\sigma}_{L2}$ whilst 4 had failure stresses above $\hat{\sigma}_{U2}$. This contrasts with the results from the carbon composites where the theoretical stress values are slightly conservative, 11 of the 28 specimens tested from slabs 1 to 5 had failure stresses greater than $\hat{\sigma}_{U1}$.

Criticism of the theory due to the greater than predicted scatter in the tensile strengths of slabs 8 to 13 is not strictly justified. The model was built to fit composites with a range of L_p/L_R ratios of 1 to 6 and for constituent fibres with a CV of tensile strength between 10% and 25%. To apply the model to the as rec. 600 tex E-glass composites the data provided had to be extrapolated to L_p/L_R ratios greater than 6.8 and fibre strength CV of 8.25%. In the case of slabs 14, 15 and 16 the fibre strength CV is around 20% but the L_p/L_R ratios are still outside the original range. All the results from slabs 14 and 16 are well below the $\hat{\sigma}_{L2}$ levels whilst those of slab 15 are close to $\hat{\sigma}_{L2}$. The theoretical model is based on a random distribution of flaws throughout the fibres. Earlier in this section it was postulated that the removal of the original fibre surface treatment produced large groups of weakened fibres, thus encouraging the catastrophic propagation of fibre failure when in a composite. This would produce the low failure stresses observed in slabs 14 and 16 though the failure stress for slab 15 appears a little high.

The tensile characteristics of the 600 tex E-glass composites calculated and discussed are summarized in the following section.

4.7.2.4 Summary of the Tensile Properties of the 600 tex E-Glass Fibre Composites of Slabs 8 to 16

The following points summarize the analyses of the tensile results of the composite specimens from slabs 8 to 16.

i) The tensile stress v strain plots are linear up to composite failure.

ii) The linear relationship between V_{g6} and E_e follows the rule of mixtures assuming that the average 600 tex E-glass elastic modulus is $75.6 KN/mm^2$.

$$E_e = 3.4 + 72.2\, V_{g6} \quad KN/mm^2 \qquad \ldots \quad (94)$$

iii) There is no significant variation in the average composite failure strain with V_{g6} for slabs 8 to 13. The expected failure strain is $\hat{\varepsilon}_e = 1.96 \pm 0.03\%$.

iv) The relationship between $\hat{\sigma}_e$ and V_{g6} (as rec.) is linear and described by the equation

$$\hat{\sigma}_e = 63.0 + 1430.0\, V_{g6} \quad N/mm^2 \qquad \ldots \quad (96)$$

v) The average stress in the as rec. 600 tex E-glass fibres at the failure of their composites is $1493.0\ N/mm^2$.

vi) The removal of the original fibre dressing from the 600 tex E-glass fibres damaged the fibres, affecting the failure stress and strain, but not the elastic modulus of their composites. $\hat{\sigma}_e$ and $\hat{\varepsilon}_e$ for such composites are given by the following equations.

$$\text{(A187)}\ \hat{\sigma}_e = 35.2 + 752.6\, V_{g6} \quad N/mm^2 \qquad \ldots \quad (98)$$
$$\hat{\varepsilon}_e = 1.04\%$$

$$\text{(A1100)}\ \hat{\sigma}_e = 54.0 + 1158.9\, V_{g6}\ N/mm^2 \qquad \ldots \quad (99)$$
$$\hat{\varepsilon}_e = 1.61\%$$

$$\text{(no c.-a.)}\ \hat{\sigma}_e = 30.0 + 637.0\, V_{g6}\ N/mm^2 \qquad \ldots \quad (100)$$
$$\hat{\varepsilon}_e = 0.88\%$$

vii) The efficiency of the composites containing the different surface treated 600 tex E-glass fibres varied, increasing with increasing composite i.l.s.s., although this may be coincidental (see sec. 4.7.2.2).

viii) The composite tensile strength is roughly approximated by the rule of mixtures (based on the average tensile strength of the 50mm long constituent fibres) in the cases of the as rec. and A187 fibre composites. The rule of mixtures predictions are conservative and non-conservative for the A1100 and no c.-a. fibre composites respectively.

ix) The experimental tensile results of slabs 8 to 13 agree more closely with those predicted by the statistical theories of Rosen[1] and Zweben[3] than with those predicted by the statistical model of Barry[4] which had to be extended to cover the low fibre tensile strength CV and the large L_p/L_R ratios of the 600 tex E-glass/vinyl ester system.

x) The existence of concentrated areas of damaged fibres in the newly surface treated E-glass fibre tapes and the resultant deviation of the fibre tensile strength distributions from the Weibull (and normal) distribution explains the non-conservative nature of the failure stresses predicted by the statistical theories for specimens from slabs 14, 15 and 16, rendering unsuitable the application of the statistical theories to composites containing A187, A1100 or no c.-a. surface treated 600 tex E-glass fibres.

xi) The jagged appearance of the fracture surfaces of the composite specimens is explained by a statistical failure mode.

xii) The above point xi) and the close agreement between the experimental failure strengths of slabs 8 to 13 and the statistical theories of Rosen[1] and Zweben[3] strongly suggest that the failure process in the 600 tex E-glass composites is governed by the statistical nature of the E-glass fibre tensile strength.

The tensile results of the 500 tex E-glass composites are now studied.

4.7.3 Tensile Properties of the 500 tex E-Glass Fibre Composites of Slabs 17 to 23

The tensile results for slabs 17 to 23 are given in tables 16 and 2A8. Figures 55 and 56 show the variation with V_{g5} of composite elastic modulus and tensile strength respectively. Figure 57 is a typical tensile stress v strain curve for a specimen from slab 19. During the tensile testing of the specimens no acoustic emissions from the specimens were noted or damage observed prior to the catastrophic composite failure.

4.7.3.1 The Fracture Surfaces of the 500 tex E-Glass Fibre Composite Tensile Specimens

There was no noticeable difference between the fracture surfaces of the 500 tex E-glass composite specimens and those of the 600 tex E-glass composite specimens as described in section 4.7.2.1. Note that the extent of fibre/resin debonded areas in the specimens from slabs 17 to 23 was similar to that in the corresponding 600 tex E-glass composite slabs. This supports the suggested explanation in section 4.7.2.1 for the surprising relative degrees of debonding in the E-glass composites with different fibre surface treatments.

4.7.3.2 The Tensile Stress v Strain Curves of the 500 tex E-Glass Fibre Composite Specimens

All the specimens tested had linear stress v strain curves up to the catastrophic failure of the composite. Figure 57, as mentioned previously, is the average tensile stress v strain plot obtained from the specimens of slab 19.

Consider the elastic modulus of the 500 tex E-glass fibre composites as given in table 16. Figure 55 is a plot of the average elastic modulus of each set of specimens from slabs 8 to 13 against V_{gs}. The line E_e is the expected elastic modulus of a 500 tex E-glass fibre/vinyl ester resin composite, calculated from the experimental data by the method of least squares, having first assumed a linear relationship between E_e and V_{gs}. The equation derived for E_e is

$$E_e = 3.4 + 80.3\ V_{gs}\ \ KN/mm^2 \quad . \ . \ . \quad (102)$$

This is equivalent to

$$E_e = 3.4V_m + 83.7\ V_{gs}\ \ KN/mm^2 \quad . \ . \ . \quad (103)$$

There is little scatter of the experimental results about this line. The equation predicts an elastic modulus of $83.7 KN/mm^2$ for the as rec. 500 tex E-glass fibres. This is approximately 10% greater than the value of $75.6 KN/mm^2$ predicted for the 600 tex E-glass fibres. This difference is presumably due to differences in the chemical composition and/or the manufacturing process of the two types of E-glass fibres.

The average elastic moduli of the specimens tested from slabs 19, 21, 22 and 23, containing fibres with as rec., A187, A1100 and no c.-a. surface treatments respectively are $34.6 KN/mm^2$, $34.0 KN/mm^2$, $34.9 KN/mm^2$ and $35.1 KN/mm^2$ respectively. An analysis of the variance of these means shows the differences

amongst them to be insignificant. Therefore it is concluded that the various surface treatments of the 500 tex E-glass fibres and the resultant changes in their composite i.l.s.s., had no significant effect upon the elastic modulus of the composites. The above agrees with the findings for both the 600 tex E-glass fibre and carbon fibre composites.

Consider the failure strains of specimens from slabs 17 to 23 (see table 16). The average failure strains of specimens from slabs 17 to 20 range from 1.97% to 2.12%. An analysis of the variance amongst the mean strains shows the differences to be significant at the 95% level. Further analysis shows this to be attributable to the high average failure strain for slab 19. No general trend in composite failure strain with V_{g5} was noted and since neither the carbon nor the 600 tex E-glass composite failure strains had been found to vary with fibre content (within the tested ranges) it is assumed that the failure strain of the 500 tex E-glass composites is also independent of fibre content. The significant, but not highly significant, difference observed in the failure strains is attributed to a chance accumulation of high failure strain specimens in slab 19. $\hat{\varepsilon}_e$ of a 500 tex E-glass composite is therefore taken as the grand mean of all the tensile specimen strain results. This is $2.02 \pm 0.02\%$.

Figure 56 shows the variation in the 500 tex E-glass composite failure stress with V_{g5}. The value of $64.5 N/mm^2$ plotted at zero V_{g5} is the expected matrix stress at a strain of 2.02%. Assuming a linear relationship between the composite failure stress and V_{g5} the following equation 104 was calculated to best fit the data by the regression method of least squares.

$$\hat{\sigma}_e = 64.5 + 1631.9\ V_{g5} \quad N/mm^2 \qquad . \ . \ . \qquad (104)$$

This is equivalent to

$$\hat{\sigma}_e = 64.5 V_m + 1696.4\ V_{g5} \quad N/mm^2 \qquad . \ . \ . \qquad (105)$$

Substituting 1.00 for V_{g5} shows the average stress of the 500 tex E-glass fibres in the composite specimens from slabs 17 to 20 to be $1696.4 N/mm^2$. The expected elastic modulus of the 500 tex E-glass fibres is $83.7 KN/mm^2$. From these values the corresponding failure strain of the 500 tex E-glass fibres in the composites is

$$\frac{1696.4}{83.7 \times 10^3} \times 100\% = 2.03\%$$

This is within the previously calculated range for $\hat{\varepsilon}_e$ of $2.02 \pm 0.02\%$

The stress ranges for the specimens from the slabs 17 to 20 are indicated in figure 56. The degrees of scatter in the failure stresses and strains are similar, both being greater than the scatter in the elastic moduli of the composites. This agrees with the results from both the carbon fibre and 600 tex E-glass fibre composites.

To evaluate the effects of the different fibre surface treatments on the composite tensile properties a direct comparison of the stress and strain results of slabs 19 (as rec.), 21 (A187), 22 (A1100) and 23 (no c.-a.) is inappropriate due to the damage incurred by the fibres during the surface treatment process. The same applied to the 600 tex E-glass composites with varying fibre surface treatments. As described in section 4.7.2.2 the tensile results can be compared by considering the relative failure strains of the composites and the constituent fibres at a 50mm gauge length. There is no significant difference amongst the elastic moduli of specimens from slabs 19, 21, 22 and 23 and therefore it is assumed that the surface treatment processes did not change the average elastic modulus of the 500 tex E-glass fibres from $83.7 KN/mm^2$. From data given in table 10 it follows that the average failure strains of the 500 tex E-glass fibres, with different surface treatments, at 50mm gauge lengths are:

(as rec.) $$\hat{\varepsilon}_{g5} = \frac{1735.6}{83.7 \times 10^3} \times 100 = 2.07\% \;;$$

(A187) $$\hat{\varepsilon}_{g5} = \frac{1297.1}{83.7 \times 10^3} \times 100 = 1.55\% \;;$$

(A1100) $$\hat{\varepsilon}_{g5} = \frac{1306.8}{83.7 \times 10^3} \times 100 = 1.56\% \;;$$

(no c.-a.) $$\hat{\varepsilon}_{g5} = \frac{1293.1}{83.7 \times 10^3} \times 100 = 1.54\% \;.$$

The average failure strains of the specimens from each of the slabs 19, 21, 22 and 23 are normalized by dividing by the appropriate value of $\hat{\varepsilon}_{g5}$ above. The grand mean of the failure strains from slabs 17, 18, 19 and 20 is used instead of the mean for slab 19:

(as rec) $$\frac{\hat{\varepsilon}_e}{\hat{\varepsilon}_{g5}} = \frac{2.02}{2.07} = 0.98;$$

slab 21 (A187) $$\frac{\hat{\varepsilon}_e}{\hat{\varepsilon}_{g5}} = \frac{1.26}{1.55} = 0.81;$$

slab 22 (A1100) $$\frac{\hat{\varepsilon}_e}{\hat{\varepsilon}_{g5}} = \frac{1.63}{1.56} = 1.04;$$

slab 23 (no c.-a.) $$\frac{\hat{\varepsilon}_e}{\hat{\varepsilon}_{g5}} = \frac{1.06}{1.54} = 0.69.$$

Due to the scatter in the failure strains of the composites the ratios can not be regarded as absolute. However, the sequence of order agrees with that found for the 600 tex E-glass ratios calculated in section 4.7.2.2. The discussion in that section on the different surface treated composites is applicable here.

The relationships, assuming linearity, between the expected failure stress and fibre content of the composites containing the different surface treated fibres are calculated from the results of slabs 21, 22 and 23 with reference to figure 39.

$$(A187) \quad \hat{\sigma}_e = 42.5 + 1018.7 V_{gs} \quad N/mm^2 \qquad \ldots (106)$$

$$(A1100) \quad \hat{\sigma}_e = 55.0 + 1310.5\, V_{gs} \quad N/mm^2 \qquad \ldots (107)$$

$$(\text{no c.-a.}) \quad \hat{\sigma}_e = 36.0 + 856.0\, V_{gs} \quad N/mm^2 \qquad \ldots (108)$$

The experimental tensile properties of the 500 tex E-glass composites are now compared with those predicted by existing failure theories.

4.7.3.3 Comparison of the Experimental and Theoretical Tensile Properties of the 500 tex E-Glass Fibre Composites

This section compares i) the commonly utilized mixture rule, and the failure theories of ii) Rosen[1] and Zweben[3] and iii) Barry[4], with the experimental results of the 500 tex E-glass fibre/vinyl ester composites. The methods of application of and the sample calculations for the above theories have been given in section 4.7.1.3

i) The Rule of Mixtures

Section 4.7.3.1 demonstrates that E_e of the 500 tex E-glass fibre composites follows the rule of mixtures, assuming the average elastic modulus of the fibres to be $83.7 KN/mm^2$. E_e is given by equation 103

$$E_e = 3.4 V_m + 83.7\, V_{gs} \quad KN/mm^2 \qquad \ldots (103)$$

Section 4.7.3.2 shows $\hat{\sigma}_e$ for an as rec. 500 tex E-glass fibre composite to follow the equation

$$\hat{\sigma}_e = 64.5 V_m + 1696.4\, V_{gs} \quad N/mm^2 \qquad \ldots (105)$$

This compares with a rule of mixture equation, calculated using the average failure stress of as rec. 500 tex E-glass fibres with a 50mm gauge length ($1735.6 N/mm^2$) and the expected stress in the vinyl ester resin matrix ($65.3 N/mm^2$) at the average failure strain of the fibres (2.07%), of

$$\hat{\sigma}_{RM} = 65.3V_m + 1735.6V_{gs} N/mm^2 \quad \ldots \quad (109)$$

Consider slab 19 with $V_{gs} = 0.3909$. From equations 105 and 109 $\hat{\sigma}_e$ is $702.4N/mm^2$ and $\hat{\sigma}_{RM}$ is $718.2N/mm^2$. The difference between the two is less than 3% of $\hat{\sigma}_e$ and therefore the rule of mixtures can be used to approximate the experimental failure stresses of the as rec. 500 tex E-glass composites. The same conclusion was reached in section 4.7.2.3 concerning the failure stresses of the as rec. 600 tex E-glass composites. There is also a similarity between the results from the different surface treated 500 tex and 600 tex E-glass composites. The strain ratios calculated in section 4.7.3.2 show the rule of mixtures to underestimate the average failure stress of slab 22 (A1100) by approximately 4% and to overestimate the average failure stresses of slabs 21 (A187) and 23 (no c.-a.) by approximately 19% and 31% respectively. Therefore the rule of mixtures,based on the average strength of the constituent fibres of the same gauge length as that of the composite specimens is unreliable as an approximation to the failure stress of 500 tex E-glass fibre/vinyl ester composites. The average failure stresses of the as rec.,A187, A1100 and no c.-a. 500 tex E-glass fibres when composited with vinyl-ester resin correspond to the average failure stresses of those fibres with gauge lengths of 64.7mm, 192.6mm, 37.4mm and 606.3mm respectively.

The theories of Rosen[1] and Zweben[3] are now considered.

ii) The Statistical Theories of Rosen and Zweben

The theoretical upper ($\hat{\sigma}_U$), lower ($\hat{\sigma}_L$) and weakest ($\hat{\sigma}_W$) stress levels were calculated using equations 7, 88 and 14 for as rec. 500 tex E-glass composites with V_{gs}% of 20%, 40%, 60% and 80%. The stress levels are given in table 17 and plotted in figure 56 with the experimental results. The upper, lower and weakest stress levels were also calculated for the slabs 19, 21, 22 and 23 and these are tabulated in table 18.

Consider figure 56. None of the results fall within the stress band between $\hat{\sigma}_L$ and $\hat{\sigma}_W$,therefore the weakest link mode of failure does not apply to the composites. The experimental scatter bands fall well within the band between $\hat{\sigma}_U$ and $\hat{\sigma}_L$ with the line of $\hat{\sigma}_e$ tending slightly towards $\hat{\sigma}_L$ The theoretical stress band between $\hat{\sigma}_U$ and $\hat{\sigma}_L$ is broader than that for the 600 tex E-glass/vinyl ester composites due to the greater tensile strength CV of the 500 tex E-glass fibres. This is not reflected in the scatter in the experimental tensile results of the two composite types. The experimental scatter bands of the 500 tex composites are narrower than those of the 600 tex composites.

Consider table 18. The experimental tensile strengths of slabs 19, 21 and 22 all lie between their respective $\hat{\sigma}_U$ and $\hat{\sigma}_L$ values with those of slabs 21 and 22 tending strongly towards their $\hat{\sigma}_L$ value. Therefore according

to the statistical theories the density of single and multiple fibre failures in the composites containing as rec. 500 tex E-glass fibres is expected to be greater than those in the composites containing A1100, A187 or no c.-a. surface treated 500 tex E-glass fibres. In addition four out of the six specimens tested from slab 23 (no c.-a.) failed below their lower stress level indicating that catastrophic failure is likely to nucleate from the site of a single fibre fracture prior to the occurence of multiple fibre fractures. This supports the hypothesis concerning fibre damage given in section 4.7.2.3 to explain the similar trend in the results from slabs 11, 14, 15 and 16.

The tensile strengths of slabs 17 to 23 are now compared with those predicted by Barry's model[4].

iii) The Statistical Model Proposed by Barry

The main steps in calculating the predicted range of composite failure stresses for slabs 17 to 23 from Barry's model are given in table 2A9 and the six stress levels obtained for each slab are given in table 19. The extreme theoretical stress levels($\hat{\sigma}_{U2}$ and $\hat{\sigma}_{L2}$) and the experimental strength results are plotted for slabs 17 to 20 against V_{gs} in figure 58. Note that for slabs 17 to 20, as with the corresponding 600 tex E-glass composites (see section 4.7.2.3), $\hat{\sigma}_{U1} < \hat{\sigma}_{U2}$. This is again due to both the low CV ($\simeq$ 10%) of fibre tensile strength and the high L_p/L_R ratios, determined by the maximum debond lengths.

Consider figure 58. The composites are substantially weaker than the theory predicts, approximately 70% of the specimens tested from slabs 17 to 20 failed below $\hat{\sigma}_{L2}$. This compares with approximately 30% of the 600 tex E-glass composite specimens from slabs 8 to 13 failing below their $\hat{\sigma}_{L2}$ values. The L_p/L_R ratios of the E-glass composites exceed the L_p/L_R range of 1 to 6 considered in Barry's model and, as noted in section 4.7.2.3, this may contribute to the discrepencies between the theoretical and experimental results.

The results from slabs 21, 22 and 23, containing the specially surface treated fibres, all fall below their predicted stress levels (see table 19). The findings are similar to those for the corresponding 600 tex E-glass composite slabs with the discrepencies between the theoretical and experimental results reducing from slab 23 (no c.-a.) to slab 21 (A187) to slab 22 (A1100). The i.l.s.s. of the slabs increase in that order. The high theoretical stress levels of slabs 21 to 23 again support the suggestion that the removal of the original surface treatment from the E-glass fibres tends to produce groups of weakened fibre, i.e. fibre damage is not random, which increases the probability of the catastrophic propagation of fibre failure in a composite.

The tensile characteristics of the 500 tex E-glass fibre/vinyl ester composites calculated and discussed in this and the previous section are summarized in the following section.

4.7.3.4 Summary of the Tensile Properties of the 500 tex E-Glass Fibre Composites of Slabs 17 to 23

The following points summarize the analyses of the tensile results of the 500 tex E-glass/vinyl ester composites of slabs 17 to 23.

i) The tensile stress v strain plots are linear up to composite failure.

ii) The linear relationship between V_{g5} and E_e follows the rule of mixtures, assuming the average 500 tex E-glass fibre modulus to be 83.7KN/mm^2, and is

$$E_e = 3.4 + 80.3V_{g5} \quad KN/mm^2 \qquad . \; . \; . \qquad (102)$$

iii) The variation in mean failure strains of specimens from slabs 17 to 20 is not highly significant and $\hat{\varepsilon}_e$, calculated as the grand mean of the results from slabs 17 to 20, for as rec. 500 tex E-glass composites is $2.02 \pm 0.02\%$ for the range $27.38\% \leq V_{g5}\% \leq 44.68\%$.

iv) The relationship between the as rec. 500 tex E-glass composite $\hat{\sigma}_e$ and V_{g5} is linear and is described by the equation

$$\hat{\sigma}_e = 64.5 + 1631.9V_{g5} \; N/mm^2 \qquad . \; . \; . \qquad (104)$$

v) The average apparent failure strength of the as rec. 500 tex E-glass fibres in slabs 17 to 20 is 1696.4 N/mm^2.

vi) The removal of the original fibre dressing from the 500 tex E-glass fibres damaged the fibres, affecting the failure stress and strain but not the elastic modulus of their composites. The $\hat{\sigma}_e$ and $\hat{\varepsilon}_e$ values for the composites with the newly surface treated fibres are represented by the following equations.

(A187) $\hat{\sigma}_e = 42.5 + 1018.7\ V_{g5}$ N/mm^2 . . . (106)
$\hat{\varepsilon}_e = 1.26 \pm 0.03\%$

(A1100) $\hat{\sigma}_e = 55.0 + 1310.5\ V_{g5}$ N/mm^2 . . . (107)
$\hat{\varepsilon}_e = 1.63 \pm 0.02\%$

(no c.-a.) $\hat{\sigma}_e = 36.0 + 856.0\ V_{g5}$ N/mm^2 . . . (108)
$\hat{\varepsilon}_e = 1.06 \pm 0.04\%$

vii) The efficiency of the 500 tex E-glass/vinyl ester composites varies with the fibre surface treatment, increasing with composite i.l.s.s. though this may be coincidental (see section 4.7.2.2).

viii) The composite tensile strength is roughly approximated by the rule of mixtures for the as rec. and A1100 fibre surface treated composites but is overestimated by the rule of mixtures for the A187 and no c.-a. 500 tex E-glass composites.

ix) The experimental tensile results of slabs 17 to 20 fall between the upper and lower stress levels calculated from the theories of Rosen[1] and Zweben[3] but 30% of the results lie below the lower scatter limit on the failure stress as derived from Barry's model which had to be extended to cover the large L_p/L_R ratios of the 500 tex E-glass/vinyl ester system.

x) Concentrated areas of damaged fibres in the newly surface treated E-glass fibre tapes and the resultant deviation of the fibre tensile strength distributions from the Weibull distribution (and normal distribution) explains the non-conservative nature of the failure stresses predicted from the statistical theories of Rosen[1] and Zweben[3] and particularly Barry[4] for specimens from slabs 21, 22 and 23, rendering unsuitable the application of these theories to A187, A1100 and no c.-a. surface treated 500 tex E-glass fibre/vinyl ester composites.

xi) The jagged appearances of the fracture surfaces of the composite specimens are explained by a statistical failure mode.

xii) The above point xi) and the approximate agreement between the experimental failure strengths of slabs 17 to 20 and the values predicted by the theories of Rosen and Zweben strongly suggest that the composite failure process is governed by the statistical nature of the 500 tex E-glass fibre tensile strength.

The majority of the above twelve points are in agreement with their parallels listed in section 4.7.2.4 for the 600 tex E-glass composites.

The tensile properties and behaviour of the parent composites have been determined and discussed since they are presumably the keys to the tensile properties and behaviour of their hybrid composites.

The points of prime importance in relation to the carbon/E-glass fibre/vinyl ester resin hybrid composites are points ii), iii), iv) and vi). As with the carbon fibre composites the evidence from the E-glass fibre composites points to a statistical composite failure mechanism.

The tensile results of the hybrid composites are now examined.

4.8 Tensile Results of the Hybrid Composites

The tensile results of slabs 24 to 61 (calculated from the experimental data as described at the beginning of section 4.7) are presented, discussed and compared with various strength and failure theories in this section. It is convenient initially to divide the slabs into 4 groups:

i) slabs 24 to 29, fabricated from 3:1 hybrid tapes;
ii) slabs 30 to 36, fabricated from 1:1 hybrid tapes;
iii) slabs 37 to 47, fabricated from mixtures of the various types of tape and
iv) slabs 46 to 61, fabricated from E-glass fibre and carbon fibre tapes with varying fibre surface treatments.

As the results are presented they are compared with the predicted rule of mixture values derived from the equations describing the properties of their parent composites. As an example of the derivation of one of the rule of mixtures equations for the hybrid composites consider the elastic modulus of a carbon fibre/600 tex E-glass fibre/vinyl ester resin hybrid composite. The equations for E_e of the parent composites, calculated in sections 4.7.1.2 and 4.7.2.2 are

Carbon/vinyl ester: $E_e = 3.4V_m + 242.1V_{cf} KN/mm^2$ . . (81)

600 tex E-glass/vinyl ester: $E_e = 3.4V_m + 75.6V_{g6} KN/mm^2$ . . (95)

~~Therefore,~~ The rule of mixtures equation for the elastic modulus, E_{RM}, of a carbon/600 tex E-glass/vinyl ester hybrid composite is

$$E_{RM} = 3.4V_m + 242.1V_{cf} + 75.6V_{g6}\ KN/mm^2 \quad * \quad . \quad . \quad . \quad (110)$$

The relevant equations for E_{RM}, σ^{E}_{RM} and $\hat{\sigma}_{RM}$ for the hybrid composites tested are listed in table 20. The theoretical rule of mixtures stress v strain curve for each hybrid composite slab is plotted from these equations, following the form given by Hayashi in reference 5.

The initial treatment of the tensile results is designed to determine the extent of any hybrid effects in the tensile properties of the tested hybrid composites. These effects are then considered in relation to the total fibre content, the fibre geometrical arrangement, the ratio of V_g to V_{cf} and the hybrid system (i.e. fibre surface treatment and E-glass type) used. Finally failure processes to explain the hybrid effects are developed and related to statistical theories. Firstly consider the tensile results of the hybrid composites of slabs 24 to 29.

4.8.1 Tensile Properties of the 3:1 Tape Hybrid Composites of Slabs 24 to 29

The tensile results for slabs 24 to 29 are given in tables 16 and 2A8. Figures 63 and 59 show the variation with V_T of composite E and composite σ^E and $\hat{\sigma}$ respectively. The tensile behaviour of all of the specimens tested was similar. Figure 60 shows a stress v strain curve for a typical specimen from slab 27 compared with the theoretical rule of mixture curve. During testing occasional faint pings were heard from some specimens after strains of approximately 0.50% were reached. Beyond ε^E acoustic emissions were frequently noted and often coincided with sudden load drops. After the first few load drops whitened areas (indicative of E-glass/resin debonding) appeared in the specimen. Their subsequent growth occurred predominantly with the later load drops and the line of final specimen fracture tended to cross the largest whitened area.

4.8.1.1 The Fracture Surfaces of the 3:1 Tape Hybrid Composite Tensile Specimens

Figure 61 shows one of the fractured halves of specimen 27.4 and is typical of the other 3:1 hybrid specimens. The fractures are non-planar, commonly involving up to a 15mm band of specimen length. The axial spread in the fracture surface of each carbon tow is normally less than 2mm and the appearance of the carbon tow fracture surfaces is similar to that of the carbon tows in the carbon composite specimens except that the average carbon fibre pull-out length appears to be slightly greater in the hybrids. Figure 62 is a photograph of a fractured carbon tow in a portion of the fracture surface of specimen 25.1.

The high degree of axial spread in the fracture surfaces of the specimens is achieved predominantly by shear failure/debonding at the E-glass fibre/resin interface, shear failure/debonding at the carbon fibre/resin interface being less extensive. The failed E-glass fibres in the 3:1 hybrid specimens give the fracture surfaces their spikey appearance with a few small groups of the E-glass fibres extending up to a maximum of 8mm beyond the general failure plane of their parent tows. Such a group of fibres in the fracture surface of specimen 25.1 is visible on the L.H.S. of figure 62. The extent of E-glass fibre pull-out in the tows in the hybrids appears to be slightly less than that in the 600 tex E-glass composites except for the extensive fibre/resin debonding in the small groups of protruding fibres.

4.8.1.2 The Tensile Stress v Strain Curves of the 3:1 Tape Hybrid Composite Specimens

Figure 60 shows the average stress v strain curve for the specimens from slab 27, the form being typical of the specimens from the other slabs 24 to 29. Each specimen was elastic up to the first stress drop in its stress v strain curve (i.e. $\sigma^E = \sigma'$), after which the curve continued with frequent drops in the stress up to the maximum stress, $\hat{\sigma}$. The size and number of the stress drops and the failure strains varied between specimens. Note the considerable difference between the experimental and the theoretical curves beyond ε^E.

Firstly, consider the elastic modulus of the 3:1 tape hybrid composite specimens. Figure 63 shows the variation in the average elastic modulus of the slabs with the total fibre content, V_T. The relationship is linear and the following equation was calculated for E_e to fit the experimental data by the method of least squares, using $E_e = 3.4 KN/mm^2$ at $V_T = 0.00$.

$$E_e = 3.4 + 113.2V_T \ KN/mm^2 \quad . \ . \ . \quad (112)$$

The equivalent equation in the rule of mixtures form is

$$E_e = 3.4V_m + 242.1V_{cf} + 75.6V_{g6} \ KN/mm^2 \quad . \ . \ . \quad (113)$$

This corresponds exactly to the predicted E_{RM} of equation 110 given in table 20. Therefore the elastic modulus of the 3:1 tape hybrid composites follows the rule of mixtures when based on the elastic moduli of the two parent composites. The CV of E of specimens from the 3:1 hybrid slabs tended to be slightly greater than for the parent composite slabs. An unavoidable source of variation in the 3:1 tape hybrid composite specimens is slightly differing V_{g6}: V_{cf} ratios. This variation is not applicable to the parent composites.

The elastic limits and the first failure stresses and strains of the 3:1 tape hybrid composite specimens coincided, with $\sigma^E = \sigma'$ and $\varepsilon^E = \varepsilon'$. Consider the first failure strains. Table 16 shows that the average values of ε^E for slabs 24 to 29 vary between 0.73% and 0.82%. An analysis of the variance amongst the means show the differences to be insignificant. However, the calculated F statistic of 2.47 is close to the 95% limit given by F = 2.53. Therefore, it is only tentatively concluded that ε^E does not vary with V_T. The expected first failure strain, ε^E_e $(= \varepsilon'_e)$, is taken as $0.78 \pm 0.01\%$, the grand mean of all the specimen ε^E values. This is a highly significant increase in the ε^E_{RM} value of $0.47 \pm 0.01\%$. Consider σ^E. Figure 59 shows the experimental variation in σ^E with V_T and the variation in σ^E_{RM} with V_T. The value of $26.2 N/mm^2$ for σ^E at $V_T = 0.00$ is the expected stress in the vinyl ester resin at a strain of 0.78%. Assuming a

linear equation between σ^{ε} and V_T the following equation was calculated for σ_e^{ε} , to best fit the data.

$$\sigma_e^{\varepsilon} = \sigma_e' = 26.2 + 893.1\ V_T \quad N/mm^2 \qquad . \ . \ . \qquad (114)$$

This is equivalent to

$$\sigma_e^{\varepsilon} = \sigma_e' = 26.2V_m + 919.3V_T \quad N/mm^2 \qquad . \ . \ . \qquad (115)$$

$\sigma_{RM}^{\varepsilon}$ calculated from the tensile results of the parent composites, assuming $\varepsilon^{\varepsilon}$ to be 0.47%,is

$$\sigma_{RM}^{\varepsilon} = \sigma_{RM}' = 16.0V_m + 548.5V_T \quad N/mm^2 \qquad . \ . \ . \qquad (116)$$

The discrepency between equations 115 and 116 is marked. σ_e^{ε} and $\varepsilon_e^{\varepsilon}$ for a 3:1 tape hybrid composite are approximately 65% greater than $\sigma_{RM}^{\varepsilon}$ and $\varepsilon_{RM}^{\varepsilon}$ predicted from the properties of the parent composites. Therefore the 3:1 ratio of 600 tex E-glass to carbon in the hybrid composites of slabs 24 to 29 has produced a positive hybrid effect in their σ_e^{ε} and $\varepsilon_e^{\varepsilon}$ values.

Consider $\hat{\sigma}$. The variation in $\hat{\sigma}$ and $\hat{\sigma}_{RM}$ with V_T is plotted in figure 59. The equation representing the expected ultimate stress, $\hat{\sigma}_e$, was calculated to best fit the experimental data assuming a linear relationship between $\hat{\sigma}$ and V_T .

$$\hat{\sigma}_e = -27.5 + 1406.8V_T \quad N/mm^2 \qquad . \ . \ . \qquad (117)$$

This is equivalent to

$$\hat{\sigma}_e = -27.5V_m + 1379.3V_T \quad N/mm^2 \qquad . \ . \ . \qquad (118)$$

The corresponding rule of mixtures equation is

$$\hat{\sigma}_{RM} = 63.0V_m + 1126.0V_T \quad N/mm^2 \qquad . \ . \ . \qquad (119)$$

The equations 117 and 118, derived for $\hat{\sigma}_e$ cannot be correct since at $V_T < 0.02$ a negative ultimate stress is predicted. Three possible explanations for this are considered:

i) the relationship between $\hat{\sigma}_e$ and V_T is not linear in the range $0.25 < V_T < 0.51$ and therefore the fitting of the straight line to the data is not appropriate;

ii) the relationship between $\hat{\sigma}_e$ and V_T is linear but the experimental average $\hat{\sigma}$ values for slabs 24 to 29 are misleading with chance deviations between the experimental average $\hat{\sigma}$ values and the true $\hat{\sigma}_e$ values resulting in an inaccurate equation for $\hat{\sigma}_e$ and

iii) the relationship between $\hat{\sigma}_e$ and V_T is linear in the range $0.25 < V_T < 0.51$ but becomes non-linear at a lower V_T .

After close examination of the results, equation 118 for $\hat{\sigma}_e$ was accepted between the range $0.25 < V_T < 0.51$ since the scatter in the average

experimental $\hat{\sigma}$ values around the calculated line for $\hat{\sigma}_e$ is small (the coefficient of correlation is 0.996). This reduces the probability of points i) and ii) applying. The results of the 3:1 tape hybrid composites in relation to the results of other hybrid composites are discussed in sections 4.8.6, 4.8.7 and 4.8.8.

4.8.2 Tensile Properties of the 1:1 Tape Hybrid Composites of Slabs 30 to 36

The tensile results of slabs 30 to 36 are presented in tables 16 and 2A8. Figures 64 and 65 show the variation with V_T of composite E and composite σ^E and $\hat{\sigma}$ respectively. The experimental results are compared in the figures with the theoretical results predicted by the rule of mixtures. The general tensile behaviour of all the specimens tested was similar. Figure 66 is a stress v strain curve for a typical specimen from the 7 layer 1:1 hybrid tape composite of slab 34. The detection of acoustic emission during the tensile testing of the specimens was approximately the same as for the 3:1 tape hybrid composite specimens. Rare emissions were noted after strains of approximately 0.50%, the frequency increased after ε^E with the emissions tending to coincide with the drops in stress. The appearance and extension of whitened areas on the specimens, indicating E-glass fibre/resin debonding, coincided with the later stress drops. These areas tended to originate from the region of the final fracture. The debonding was considerably extended after specimen fracture and in some E-glass tows ran almost the whole length of the specimen gauge length.

4.8.2.1 The Fracture Surfaces of the 1:1 Tape Hybrid Composite Tensile Specimens

Figure 67 shows one of the fractured halves of specimen 34.1 and is typical of the other 1:1 hybrid tape composites. The fracture surfaces differ from those of the 3:1 tape specimens in three ways.

i) The non-planar fracture surfaces of the 1:1 composites tend to involve axial bands slightly less than those in the 3:1 specimens.

ii) The carbon fibre pull-out lengths of the 1:1 specimens appear to lie approximately between those of carbon composite and 3:1 hybrid composite specimens whilst the E-glass fibre pull-out lengths appear to be shorter than in either the E-glass composite or the 3:1 hybrid composite specimens.

iii) The fractured sections of the 1:1 specimens appear less 'spikey' than those of the 3:1 specimens. This is due firstly to the lower E-glass fibre volume content and the fewer groups of E-glass fibres extending

beyond the general failure plane of their parent tows (as explained in section 4.8.1.1) and secondly, to the shorter extension (of approximately 4mm) of these groups beyond the general failure plane.

4.8.2.2 The Tensile Stress v Strain Curves of the 1:1 Tape Hybrid Composite Specimens

Figure 66 shows a typical stress v strain curve for the specimens from slab 34. The form of the curve is typical of the specimens from the other slabs 30 to 36. Each specimen was elastic up to the first discontinuity in the stress v strain curve ($\sigma^{\varepsilon} = \sigma'$, $\varepsilon^{\varepsilon} = \varepsilon'$), after which the curve continued with further stress drops to the ultimate stress ($\hat{\sigma}$). The size and number of stress drops and the final failure strains varied between specimens. Occasionally after the initial stress drop the stress did not rise again above σ^{ε}. Generally the initial drop in stress of the 1:1 tape specimens was less than that in the 3:1 tape specimens. As with the 3:1 tape specimens the form of the experimental stress v strain curves beyond σ^{ε}, with the series of stress drops, contrasts with the rule of mixtures theoretical curve in which a secondary modulus continues up to the failure strain of the E-glass fibres.

Consider the elastic modulus, E, of the 1:1 tape hybrid composites. Figure 64 gives the variation in the average modulus of the slabs and the predicted E_{RM} with V_T. The following linear equation for E_e was calculated to best fit the experimental data, with $E_e = 3.4 KN/mm^2$ at $V_T = 0.00$.

$$E_e = 3.4 + 154.7V_T \ KN/mm^2 \quad . \ . \ . \quad (120)$$

The equivalent equation in the rule of mixtures form is

$$E_e = 3.4V_m + 158.1V_T \ KN/mm^2 \quad . \ . \ . \quad (121)$$

The rule of mixtures equation derived from equation 113 is

$$E_{RM} = 3.4V_m + 158.0V_T \ KN/mm^2 \quad . \ . \ . \quad (122)$$

Agreement between the actual (121) and theoretical (122) equations was expected since this had been found for the 3:1 hybrid composites in section 4.8.1.2. The surprising aspect is that despite the experimental errors and variation in the data from which the equations were derived the values of E_{RM} and E_e differ by less than 1%.

Now consider the first failure strains of the specimens given in table 16. The average $\varepsilon^{\varepsilon}$ values vary between 0.56% and 0.64%. An analysis of the variance amongst the means shows the differences to be insignificant. The grand mean of the strains is calculated to give $\varepsilon^{\varepsilon}_e = 0.60 \pm 0.01\%$, compared with $\varepsilon^{\varepsilon}_{RM} = 0.47\%$. The above independence between $\varepsilon^{\varepsilon}$ and V_T in the

tested range for the 1:1 tape hybrid composites supports the tentative conclusion made in section 4.8.1.2 that ε^E does not vary with V_T (in the tested range) in the case of 3:1 tape hybrid composites.

Figure 65 shows the experimental variations in σ^E and $\hat{\sigma}$ with V_T for slabs 30 to 36 and those predicted by the rule of mixtures. Consider σ^E. The value of $\sigma^E = 20.4 N/mm^2$ at $V_T = 0.00$ is the expected stress in the vinyl ester resin matrix at $\varepsilon = 0.60\%$. Assuming a linear relationship between σ^E and V_T the following equation for the σ_e^E of the 1:1 tape hybrid composites best fits the experimental data.

$$\sigma_e^E = \sigma_e' = 20.4 + 935.9V_T \ N/mm^2 \quad . \ . \ . \quad (123)$$

This is equivalent to

$$\sigma_e^E = \sigma_e' = 20.4V_m + 956.3V_T \ N/mm^2 \quad . \ . \ . \quad (124)$$

The equivalent rule of mixtures equation is

$$\sigma_{RM}^E = \sigma_{RM}' = 16.0V_m + 744.1V_T \ N/mm^2 \quad . \ . \ . \quad (125)$$

Therefore there is a positive hybrid effect in the σ_e^E and ε^E of the 1:1 tape hybrid composites, the values being approximately 28% greater than the equivalent values predicted by the rule of mixtures.

Now consider $\hat{\sigma}_e$ and $\hat{\sigma}_{RM}$ depicted in figure 65. The calculated experimental and theoretical equations for $\hat{\sigma}$ are given by equations 126 and 127 respectively.

$$\hat{\sigma}_e = -3.8 + 1065.1V_T = -3.8V_m + 1061.3V_T \ N/mm^2 \quad . \ . \ . \quad (126)$$

$$\hat{\sigma}_{RM} = 63.0V_m + 754.3V_T \ N/mm^2 \quad . \ . \ . \quad (127)$$

Note that assuming a linear relationship between $\hat{\sigma}_e$ and V_T the experimental data predicts a negative $\hat{\sigma}_e$ at $V_T < 0.0036$. In the case of the 3:1 tape hybrid composites a negative $\hat{\sigma}_e$ was predicted from the data at $V_T < 0.02$. Three possibilities to explain this were considered in section 4.8.1.2. The same possibilities are considered here to explain the results for the 1:1 tape hybrid composites. Possibilities i), that the relationship between $\hat{\sigma}_e$ and V_T for $0.16 < V < 0.50$ is non-linear, and ii), that there is a chance bias to the results of slabs 30 to 36, are the least likely to apply since the correlation coefficient for the actual $\hat{\sigma}$ values and $\hat{\sigma}_e$ is 0.994. Therefore it is assumed that in the true relationship between $\hat{\sigma}_e$ and V_T in the range $0.16 < V_T < 0.50$ any deviation from linearity is insignificant and therefore the linear equation 126 derived from the experimental results is accepted for the above V_T range but rejected for 1:1 tape hybrid composites with lower V_T values. The validity of the assumption is supported by the parallel result for the 3:1 tape hybrid composites.

The results of the 1:1 tape hybrid composites are discussed and compared with the tensile results of the other hybrid composites in sections 4.8.6., 4.8.7., and 4.8.8.

4.8.3 Tensile Properties of the Hybrid Composites of Slabs 37 to 47

Slabs 37 to 47 are hybrid composites with varying total fibre contents, fibre geometrical arrangement and E-glass to carbon fibre ratios. The surface treatments of the constituent fibres in all cases are as rec. The tensile results for slabs 37 to 47 are presented in tables 16 and 2A8. The forms of the tensile stress v strain curves typical to each slab are given in figures 68 to 78.

During tensile testing acoustic emissions from the specimens were generally heard beyond a strain of 0.50% as described in sections 4.8.1 and 4.8.2 for the 3:1 and 1:1 tape hybrid composites. The extent of E-glass fibre debonding in the tensile specimens (not possible to observe in slabs 37 and 38 since the outer layers of tape were carbon) both prior to and post composite fracture varied considerably amongst specimens from the same slabs. The only conclusion reached from the comparison of specimens from different slabs is that the incidence of debonded areas of E-glass fibres apparently unconnected with the final site of specimen fracture increased with decreasing carbon fibre content.

4.8.3.1 The Fracture Surfaces of the Hybrid Composite Tensile Specimens from Slabs 37 to 47

The majority of the fractured specimens from slabs 37 to 47 have a spikey appearance (see figure 79) due to fractions of E-glass tows, still resin impregnated, protruding beyond the major fracture surface. The lengths of these spikes varied between specimens from the same slabs more than between slabs. In general terms the 'spikiness' of the specimens was proportional to the E-glass fibre content. Occasionally the fracture appearance of a specimen was uncharacteristic of its composite type. For example figure 80 shows the two halves of the fractured specimen 46.5. Their appearance contrasts with that of specimen 46.6 in figure 79. There is no significant correlation between specimens with uncharacteristic fracture surfaces and extreme tensile properties.

The S.E.M. study of the fracture surfaces of tensile specimens in which the two fibre types are well mixed generally showed a gradual increase in

the average carbon fibre pull-out length in composites with increasing glass fibre to carbon fibre content ratio. Conversely increasing the percentage of carbon fibre reduced the average E-glass fibre pull-out lengths although the maximum pull-out lengths were frequently greater than the 19 fibre diameters expected in their parent E-glass composites. The above trends were not observed in hybrids with a low degree of mixing of the E-glass and carbon fibre tows where the pull-out lengths of the carbon fibres tended towards those expected of the fibres in their parent composites. Slab 37 was such a hybrid with the two outer layers being plain carbon tape. Figure 81 shows a typical portion of the fracture surface of specimen 37.2. Note the range of carbon fibre pull-out lengths in this small area. The variety of both E-glass and carbon fibre pull-out lengths within each hybrid specimen meant that large areas of each fracture surface had to be scanned before the trends in fibre pull-out lengths noted above could confidently be reported. Areas similar to that shown in figure 81 could be found in the fracture surfaces of any of the hybrid composite specimens.

4.8.3.2 The Tensile Stress v Strain Curves of the Hybrid Composite Specimens from Slabs 37 to 47

Table 21 and figures 68 to 78 compare the experimental and theoretical rule of mixtures tensile stress and strain values and stress v strain curves for slabs 37 to 47. Beyond σ^E the forms of the stress v strain curves are varied. In all cases agreement between the experimental and theoretical composite elastic modulus is excellent. Therefore it is concluded that for both the carbon fibre/600 tex E-glass fibre/vinyl ester resin and the carbon fibre/500 tex E-glass fibre/vinyl ester resin systems the elastic modulus is not subject to any 'hybrid effect'.

The variations in the tensile stress v strain curves are considerable beyond σ'. However, the number and magnitude of any stress drops and the approximate failure strains (recall that strains were only measured accurately up to ε') in most cases also differed between specimens from the same slabs. Specimens from slab 42 (containing the lowest $V_g : V_{cf}$ ratio of slabs 37 to 47) failed catastrophically with $\sigma^E = \sigma' = \hat{\sigma}$ (see figure 73) but the combination of 1:1 and plain carbon tapes in this slab did produce a positive hybrid effect on σ^E and ε^E with the experimental and rule of mixture values for ε^E being 0.54% and 0.47% respectively. Positive hybrid effects of varying magnitudes were also observed in slabs 39 to 41 and 43 to 47. Slabs 37 and 38 did not exhibit any hybrid effect in σ^E and ε^E. The major failure of the constituent carbon fibres occurred at approximately the expected strain of 0.47%.

In both of these slabs the outer layers of tape were plain carbon fibre. Hybrid effects are discussed in relation to the $V_g : V_{cf}$ ratios and the constituent tapes and their lay-up sequences in sections 4.8.7 and 4.8.8. For many specimens $\sigma^{\varepsilon} \neq \sigma'$, implying that considerable random fibre failure occurs prior to the first major propagation of fibre failure in these specimens. Table 21 is slightly misleading in respect to σ^{ε} and σ' (and $\hat{\sigma}$) since the quoted average experimental results suggest that all the tensile specimens from one slab behaved in a similar manner with either $\sigma^{\varepsilon} = \sigma'$ or $\sigma^{\varepsilon} \neq \sigma'$. Reference to table 2A8 (the results of the individual specimens) shows that the behaviour of the specimens was mixed within many of the slabs. For example table 21 lists σ^{ε} and σ' for slab 41 as 350.2N/mm^2 and 386.0N/mm^2 respectively but reference to 2A8 shows that for 2 of the 6 specimens tested $\sigma^{\varepsilon} = \sigma'$. Such variations amongst like specimens are noted in figures 68 to 78 along with parallel variations in σ' and $\hat{\sigma}$.

Consider the form of the stress v strain curves beyond σ^{ε} and σ'. The initial stress drop is always less than predicted by the rule of mixtures theory with the carbon fibre continuing to bear some of the stress beyond σ'. There is no obvious secondary modulus. Commonly the stress increases non-linearly (occasionally decreases) with strain between successive drops in stress until complete composite failure occurs. The final failure strain varies with composite type but is in all cases below the failure strain of the high elongation E-glass fibre. For 9 of the 11 slabs under consideration the average $\hat{\sigma}$ value is within $\pm$ 12% of $\hat{\sigma}_{RM}$. The exceptions are the carbon rich slabs 42 and 43 for which $\hat{\sigma}$ is considerably underestimated by $\hat{\sigma}_{RM}$.

It is concluded from this section that the positive hybrid effects observed in σ^{ε} and $\varepsilon^{\varepsilon}$ vary with composite type and that the tensile behaviour beyond σ^{ε} and σ' deviates substantially from that predicted by the rule of mixtures with a negative hybrid effect in the failure strain of the composites. This latter point is explained by strain concentrations around areas of carbon fibre failure.

The following section concerns the tensile results of the GCGCGCG lay-up composites with varying fibre surface treatments.

4.8.4 Tensile Properties of the Hybrid Composites of Slabs 46 to 61

The lay-up sequence in these slabs was GCGCGCG but the fibre surface treatment in the different slabs was varied. Their tensile results are given in tables 16 and 2A8. Typical stress v strain curves for each slab are given and compared with the rule of mixtures curves in figures 77, 78 and 82 to 95.

As with previous hybrid composite specimens during the tensile testing acoustic emissions were generally noted beyond a strain of approximately 0.50%. The extent of visible E-glass fibre debonding prior to and post specimen failure varied considerably between specimens from the same slabs and no difference was detected between the hybrids containing 600 tex E-glass fibre and those containing 500 tex E-glass fibre. Figures 96, 97 and 98 are photographs of seventh specimens from slabs 50, 54 and 57 respectively taken during their tensile testing. They are typical of the tensile failures of specimens from any of the 4G3C slabs except slabs 48, 49, 58 and 59. The final photographs in figures 96 and 98 are close to the maximum and minimum extents respectively of expected E-glass fibre debonding. No debonding in specimens from slabs 48, 49, 58 and 59 was noted prior to specimen failure and very little afterwards. Figures 99 and 100 show specimens from slabs 49 and 58 respectively, before and after the tensile test and figure 101 is a stereozoom photograph of the two halves of the tensile specimen 58.1. This contrasts with figure 102 which shows the spikey appearance of a fractured half of specimen 54.2

4.8.4.1 The Fracture Surfaces of the Hybrid Composite Tensile Specimens from Slabs 46 to 61

The fracture surfaces of all the specimens, except those from slabs 48, 49, 58 and 59 were similar with a spikey appearance due to the E-glass fibre as described in sections 4.8.1.1 and 4.8.2.1. The axial distances of these fracture surfaces were frequently as much as 16mm, compared with a maximum of 8mm in specimens from slabs 48, 49, 58 and 59. Figures 101 and 102 are photographs illustrating the two types of fracture surface. Figure 102 shows a fractured half of specimen 54.2 with spikes of E-glass extending beyond the general fracture surface. Figure 101 shows the two comparatively clean fractured halves of specimen 58.1.

The pull-out lengths of the carbon fibres and E-glass fibres were similar to those of the 1:1 tape hybrid composite specimens except in specimens from slabs 48, 49, 58 and 59. In these the maximum E-glass fibre pull-out lengths were considerably shorter than in the other specimens. This was expected since the longer pull-out lengths were found in the extended spikes of E-glass fibres (illustrated in figure 62) which are not features of the fracture surfaces of slabs 48, 49, 58 and 59. The amount of resin remaining adhered to the surfaces of the pulled-out carbon fibres and E-glass fibres did not vary from the amount expected on such fibres when in their parent composites.

4.8.4.2 The Tensile Stress v Strain Curves of the Hybrid Composite Specimens from Slabs 46 to 61

A typical tensile stress v strain curve for each of the composite types in slabs 46 to 61 is given in figures 77, 78 and 82 to 95, accompanied by the theoretical stress v strain curve according to the rule of mixtures. The experimental and theoretical (rule of mixtures) results are tabulated in table 21. The experimental tensile stress v strain curves show that for the hybrids of slabs 48 to 59 failure was catastrophic at σ' but for the hybrids of slabs 46, 47, 60 and 61 the first drop in stress was not absolute, with subsequent stress drops occuring as the strain increased until composite failure was complete.

Consider the elastic modulus of the hybrid composites of slabs 46 to 61. The above mentioned figures and table 21 show that the agreement between the experimental and the rule of mixture values is excellent in all cases. This is consistent with the findings for the hybrid composites considered in the previous section (4.8.3), i.e. that there is no significant hybrid effect in the elastic modulus of the composites. However, again in agreement with the results of slabs 37 to 45, positive hybrid effects were observed in most σ^{ε} and $\varepsilon^{\varepsilon}$ values. The linear portions of the curves of all the specimens bar one (specimen 58.2) continue beyond the expected failure strain, 0.47%, of a plain carbon composite. The extent of this hybrid effect (illustrated in figures 77, 78 and 82 to 95) varies with the hybrid system. The four slabs with the lowest $\varepsilon^{\varepsilon}$ values are 59 (0.50%), 58 (0.51%), 48 (0.53%) and 49 (0.53%). A common factor in these slabs was the no c.-a. surface treatment of the constituent E-glass fibres. The greatest average $\varepsilon^{\varepsilon}$ values were obtained from slabs 57 (0.70%) and 56 (0.67%). These both contained etched carbon fibres and A1100 treated E-glass fibres (500 tex in slab 57 and 600 tex in slab 56).

Consider the hybrid composites which failed catastrophically at σ' (slabs 48 to 59). The tensile stress v strain curves of all the specimens from slabs 48, 49, 56, 58 and 59 and one specimen from both slabs 51 and 57 are linear up to composite failure ($\sigma^{\varepsilon} = \sigma'$) whilst the other specimens have distinct σ^{ε} and σ' values. In all these slabs the average σ' value ($=\hat{\sigma}$) is greater than the predicted $\hat{\sigma}_{RM}$ value due to the positive hybrid effect in σ'. In slabs 46, 47, 60 and 61, in which failure was not catastrophic at σ', the average experimental σ' and $\hat{\sigma}$ values are within 5% of the predicted $\hat{\sigma}_{RM}$ values. The approximate failure strains of the specimens were generally less than 50% of the predicted failure strains.

The results of all the hybrid composites tested have now been presented and compared with values predicted by the rule of mixtures. The following section briefly summarizes the major points which have arisen.

4.8.5 General Points Concerning the Tensile Properties and the Stress v Strain Curves of the Hybrid Composites of Slabs 37 to 61

There are a variety of stress v strain curves obtained from the hybrid composites tested. In all cases E is accurately estimated from the rule of mixtures equation derived from the properties of the parent composites.

$$E_{RM} = 3.4V_m + 242.1\ V_{cf} + 75.6V_{g6}\ KN/mm^2 \quad . \ . \ . \quad (110)$$

or

$$E_{RM} = 3.4V_m + 242.1V_{cf} + 83.7V_{g5}\ KN/mm^2 \quad . \ . \ . \quad (111)$$

The validity of the rule of mixtures in predicting E is in agreement with the findings of Hayashi[5], Bunsell and Harris[24] and Aveston and Sillwood[6] but differs from those of Kalnin[22]. Kalnin tested glass/graphite hybrids and found the tensile modulus of glass rich laminates to be substantially higher than predicted by the rule of mixtures. Since this result stands on its own it would appear to be a testing artefact.

The result of the most potential practical importance is the extended linear portion of the stress v strain curves found for the majority of the hybrid composites. The magnitude of this positive hybrid effect varied amongst the different composites. Beyond $\sigma^{\epsilon}/\epsilon^{\epsilon}$ the experimental stress v strain curves differ substantially from the predicted rule of mixture curves with no secondary modulus. In cases where $\sigma^{\epsilon} \neq \sigma'$ the slope of the curve gradually decreases until σ' is reached. At σ', if catastrophic failure does not occur, a series of partial composite failures cause sudden drops in stress, between which the stress may or may not rise to above σ', until the failure becomes absolute. There is a substantial negative hybrid effect in the final failure strains of the hybrid composites, the extent of which varies with hybrid type but this is expected due to strain concentrations around groups of failed carbon fibres.

Section 4.7.3.4. concludes that the failure of the single fibre type composites is governed by the statistical failure of their constituent fibres. Therefore statistical failure mechanisms seem likely for the hybrid composites. Such mechanisms are investigated in detail both qualitatively and quantitatively in section 4.8.10 but plausible statistical explanations for the two major features in the stress v strain curves of the hybrid composites are outlined overleaf.

i) A drop in stress at any strain indicates a significant propagation of carbon fibre failure originating from either a single or multiple fibre failure. The greater the extent of propagation of fibre failure the greater the stress drop. Up to complete composite failure only the weaker E-glass fibres are expected to fail.

ii) A decrease in the slope of the stress v strain curve prior to ε' is caused by sufficient random fibre failure accumulating to noticeably weaken the composite prior to any substantial propagation of failure amongst the carbon fibres.

The above two points are expanded in section 4.8.10 and referred to when failure mechanisms are discussed in the following sections which study the dependence of the hybrid effects on V_T, fibre geometrical arrangement, V_g/V_{cf} and the hybrid system used.

4.8.6 V_T and the Hybrid Effect.

The tensile results of the 3:1 and 1:1 tape hybrid composite slabs 24 to 29 and 30 to 36 are used in this study since within both sets of slabs the ratio of V_g/V_{cf}, fibre geometrical arrangement and fibre surface treatments are kept constant whilst V_T is varied. The results have previously been partially discussed in relation to V_T in sections 4.8.1.2 and 4.8.2.2. Consider the positive hybrid effects in ε^E and σ^E (equal to ε' and σ') in both the composite types. ε^E_{RM} is 0.47%. The average ε^E values for specimens from each of the 3:1 slabs range from 0.73% to 0.82%. From the statistical analysis of the significance of the variance amongst the means, as described in section 4.8.1.2, it was tentatively concluded that there was no variation in ε^E with V_T. This conclusion is supported by the results of the 1:1 hybrid slabs in which the variations in ε^E (average ε^E ranged from 0.57% to 0.63%) are found to be insignificant (see section 4.8.2.2). Due to the linear relationship between E and V_T (see figures 63 and 64) the conclusion that the first failure strains of the two sets of 3:1 and 1:1 hybrid composite slabs ($\varepsilon^E = \varepsilon'$) remains constant with changing V_T (within the tested range) establishes the linear relationship between σ^E and V_T for both the hybrid composite types. The linear plots of σ^E v V_T (and $\hat{\sigma}$ v V_T) for the 3:1 and 1:1 tape hybrid slabs are given in figures 59 and 65 respectively.

The general forms of the tensile stress v strain curves of slabs 24 to 29 and 30 to 36 beyond σ^E do not change noticeably with V_T. The validity of the linear equations derived for $\hat{\sigma}$ which predict negative values at very low V_T is discussed in sections 4.8.1.2 and 4.8.2.2. It is concluded that any deviation from linearity in $\hat{\sigma}$ in the tested V_T range of 0.17 to 0.50 is

insignificant. Note that above a V_T of approximately 0.20 $\hat{\sigma}_e$ is greater than $\hat{\sigma}_{RM}$.

The final failure strains of the specimens were not measured accurately but are considerably less than the expected failure strain of the 600 tex E-glass fibre (1.96%). There was no obvious variation with V_T

The major point of importance arising from this section is that the extent of the positive hybrid effect exhibited in $\varepsilon^E = \varepsilon'$ is constant within each of the 3:1 and 1:1 hybrid tape systems for the range of V_T tested.

The importance of the geometrical arrangement of the two fibre types within the hybrid composites is investigated in the following section.

4.8.7 Fibre Geometrical Arrangement and the Hybrid Effect

The tensile results of the slabs 37 to 39, 45 and 46 in conjunction with those of the 3:1 tape and 1:1 tape hybrid composite slabs are used to investigate the influence of the fibre geometrical arrangement on the tensile hybrid effects in the composites. The properties of slabs containing the same ratios of V_g/V_{cf} are compared. It is assumed that the conclusion in the previous section that ε^E of the 1:1 tape and 3:1 tape hybrid composites is constant with varying V_T can be extended to composites with different geometrical arrangements. This enables the comparison of the tensile results of slabs containing different V_T .

Consider slabs 37 (CG_6G_6C), 38 ($CG_6CG_6G_6CG_6C$) and the 1:1 tape slabs. In these slabs $V_{cf} \simeq V_{g6}$ but the geometrical arrangements of the fibres vary. The degree of mixing of the carbon fibre tows and E-glass fibre tows is greatest in the 1:1 tape hybrid composites, where tows alternate within the layers of tape, and is least in slab 37, where all the carbon tows are in the outer layers of the hybrid composite. Consider the tensile stress v strain curves for these slabs in figures 66, 68 and 69. The forms of the three curves are different so it is immediately concluded that the geometrical arrangement of the fibres does affect the tensile characteristics of these hybrid composites. For the three composites considered $\varepsilon^E_{RM} = 0.47\%$. There is no significant hybrid effect in the ε^E of either slab 37 (0.45%) or slab 38 (0.47%) but the $\varepsilon^E_e = \varepsilon'_e$ of the 1:1 tape hybrid composite is 0.60%, an increase over ε^E_{RM} of approximately 28%. Assuming statistical failure of the fibres in the hybrid composites (see section 4.8.5) the following suggestions are postulated.

In the 1:1 tape composites carbon fibres fail randomly but the presence of the evenly distributed E-glass tows suppresses considerable propagation of the carbon fibre failures until $\varepsilon \simeq 0.60\%$. At $\varepsilon^{E} = \varepsilon'$ substantial propagations of carbon fibre failures occur, curtailed by E-glass fibre tows. This produces the recorded drop in stress bourne by the composite at the applied strain. As the stress increases more multiple failures occur until at $\hat{\sigma}$ failure is absolute and propagates through the whole composite. In slab 38 ($CG_6CG_6G_6CG_6C$) the carbon tows and E-glass tows are not as intimately mixed, therefore the E-glass fibres are less effective in suppressing the propagation of the carbon fibre failures. At and beyond ε^{E} sufficient random single fibre failures and multiple fibre failures accumulate to noticeably weaken the hybrid composite and the slope of the stress v strain curve decreases beyond ε^{E}. A sudden drop in stress does not occur at ε^{E} since insufficient fibres are involved in any of the multiple failures. ε' is the limit at and beyond which the substantial propagation of failure within the carbon fibres can not be suppressed and the hybrid composite failure continues in a similar manner to that described above for the 1:1 tape hybrid composites beyond ε^{E}. In slab 37 all of the carbon tows are in the two outer layers of the composite and the influence of the inner E-glass fibres is minimal. At ε^{E} ($\simeq \varepsilon^{E}_{RM}$) multiple carbon failure occurs of sufficient magnitude to produce a small stress drop in the stress v strain curve. The propagation is arrested by the E-glass fibres. The stress and strain increases until another substantial failure occurs producing another drop in stress. This continues until failure is catastrophic..

The above also explains the relative maximum stresses of slabs 37, 38 and the 1:1 tape hybrid composites. The experimental $\hat{\sigma}$ values differ from the predicted $\hat{\sigma}_{RM}$ values in slabs 37, 38 and the 1:1 tape hybrids by -4%, 6% and 27% respectively. A greater degree of carbon fibre failure prior to $\hat{\sigma}$ must reduce the proportion of intact fibres in the cross-section through which complete failure occurs at $\hat{\sigma}$. The order of the relative maximum stresses listed above are as expected since the hypothesis is that the more intimate the mixing of the two fibre types (at least to the limit of alternating tows) the greater the suppression of the propagation of carbon fibre failure. The stress v strain curves in figures 66, 68 and 69 show that substantial failure (ε') occurs at the lowest strain in slab 37 and at the highest in the 1:1 tape hybrid composites. This is attributed to the more extensive propagations of carbon fibre failure possible without the need for the failure of E-glass fibres.

The results of slabs 45 (1:1 1:1 3:1 1:1 3:1 1:1 1:1) and 46 ($G_6CG_6CG_6CG_6$) are now considered. In these slabs the amount of V_{cf} in V_T is approximately 42%. The variances between the two sets of mean σ^{E}, ε^{E}, ε' and $\hat{\sigma}$ (see

table 16) were analysed and no significant differences were found. Examination of the stress v strain curves in figures 76 and 77 show that beyond ε' the behaviours are slightly varied. Possible explanations for the form of the curves are as follows. In slab 45 the accumulation of single and multiple carbon fibre failures start to noticeably weaken the hybrid composite at $\varepsilon^{E} = 0.62\%$ (approximately equal to $\varepsilon^{E} = \varepsilon'$ for the 1:1 tape hybrids). The density of the failures is expected to be greatest in the outer 1:1 layers since these are the most susceptible to damage during the fabrication of the slabs and specimens (also see section 2.1 and reference 3). Substantial propagation of the carbon fibre failures is slightly suppressed by the higher concentration of the E-glass fibre in the 3:1 tapes and ε' occurs at 0.67%, a decrease in gradient being observed between $0.62\% \leq \varepsilon \leq 0.67\%$. Beyond ε' failure occurs in the same manner as described for the 1:1 tape hybrid composites. There are two major features to the lay-up of slab 46 which are contrary to that of slab 45. Firstly the carbon and E-glass tows are segregated into separate layers. Secondly there are no carbon tows in the outside layers. The consequence of the first is a lesser degree of mixing in slab 46 and therefore a tendency to a lower ε^{E} value. However, the second point works towards a higher ε^{E} in slab 46. The result is that the accumulation of failed carbon fibres becomes significant at $\varepsilon^{E} = 0.59\%$, approximately equal to that for slab 45. The layers of E-glass fibres surrounding the three carbon layers suppress substantial carbon fibre failure propagation up to $\varepsilon' = 0.68\%$. Beyond this point only a few further drops in stress occur before final failure. The estimated final failure strain of slab 46, in which more extensive carbon failures are probable, is less than that of slab 45.

Finally consider slab 39 and the 3:1 tape hybrid composites in which the proportion of V_{cf} in V_T is approximately 25%. Their stress v strain curves are given in figures 70 and 60. The following explanations are suggested for the forms of and the differences between the curves. In the 3:1 tape hybrid composites the carbon fibre tows are evenly distributed with both fibre types in all layers. Random single fibre failure occurs up to $\varepsilon^{E} = \varepsilon'$ when substantial carbon fibre failure occurs. Catastrophic propagation is prevented by the surrounding E-glass fibres but is sufficiently extensive to cause a small drop in stress. The numerous subsequent small drops in stress are due to further multiple carbon fibre failures occurring throughout the composite. Propagation is limited due to the isolation of the carbon tows. At $\hat{\sigma}$ (approximately 12% greater than the predicted $\hat{\sigma}_{RM}$) the applied strain is sufficient for failure to propagate from the carbon fibres and spread through the E-glass fibres, resulting in absolute composite failure. In slab 39 the

two layers of carbon tape both have two layers of E-glass tapes on either side of them. As the composite is strained random carbon fibre failures occur. At ε^{ϵ} the continuing accumulation of failures produces a gradual decrease in the gradient of the stress v strain curve. Substantial failure occurs at $\varepsilon' = 0.91\%$. The high proportion and concentration of E-glass fibre limits the failure so the curve continues with a few more drops in stress. Catastrophic failure occurs at a stress approximately 6% lower than the predicted rule of mixtures value and at a slightly lower estimated strain than that for the 3:1 tape hybrid composites. The latter point is attributable to the two all carbon layers in slab 39 increasing the probable extent of multiple carbon failures.

The failure mechanisms postulated to explain the different forms of stress v strain curves rely on the statistical nature of fibre strength and assume that the E-glass fibres impede the propagation of carbon fibre failures. The suggested mechanisms are specifically for the typical stress v strain curves of the appropriate slabs. Since the mechanisms are based on the statistical nature of fibre strength, variations in the failure processes can be expected in identical composite types. As previously noted the stress v strain curves of specimens from the same slabs did vary.

The failure mechanisms for the hybrid composites are discussed in greater detail in section 4.8.10. They have been considered here to aid the investigation into the effect of fibre distribution on the tensile characteristics of the hybrid composites.

The comparison of the results from slabs 37, 38 and the 1:1 tape hybrid composites, slabs 45 and 46, and slab 39 and the 3:1 tape hybrid composites show that the tensile characteristics of the hybrid composites are affected by the geometrical arrangement of the constituent fibres. The following three points are noted:

i) an intimate, evenly distributed mixture of carbon fibre and E-glass fibre tows encourages high ε^{ϵ} (equal to ε'), high $\hat{\sigma}$ and a large number of small stress drops prior to a high final failure strain;

ii) carbon tows in the outer layers of a composite tend to reduce ε^{ϵ} and ε' and

iii) uneven mixes of tows promote the possibility of distinct ε^{ϵ} and ε' values except in cases where one layer of carbon tape bears a high proportion of the applied load (likely to occur in composites with low V_T).

The magnitudes of the above effects are not quantified since they are interacting and are presumably dependent upon the ratio of V_g/V_{cf}. However within the V_g/V_{cf} range investigated for maximum use of the constituent reinforcement fibres the first point is of prime importance.

Previous work on hybrid composites neither supports nor contradicts these results. Kalnin[22], Hayashi[5] and Bunsell and Harris[24] all tested hybrid composites in which the two fibre types were in separate layers and observed positive hybrid effects in the failure stress and strain of the L.E. fibre. Marshall[23] and Phillips[26] tested hybrid composites fabricated from hybrid tapes and also observed positive hybrid effects. The effect of the different fibre geometrical arrangements on the magnitude of the hybrid effects can not be assessed since in the different works different composite systems and fibre ratios were used.

The effects of the ratio of V_g/V_{cf} on the tensile properties of a hybrid composite are now investigated.

4.8.8 Ratio of V_g/V_{cf} and the Hybrid Effect

The effect of the ratio of V_g/V_{cf} on the tensile properties of a hybrid composite is assessed from the tensile results of slabs 24 to 46. Direct comparison amongst all these slabs is inappropriate since the arrangement of the fibres in the slabs varied considerably. In both the 3:1 tape and 1:1 tape hybrid composites the tows of the carbon fibres and the 600 tex E-glass fibres were intimately and evenly mixed. The average experimental properties obtained for these two hybrid composite types are more reliable than those obtained for the hybrid composites of slabs 37 to 46 since they have been derived from the tensile results of specimens from 6 slabs for the 3:1 tape hybrids and from 7 slabs for the 1:1 tape hybrids. In view of this the study of the effect of the V_g/V_{cf} ratio on the tensile properties of a hybrid composite is based mainly on the results of the 3:1 and 1:1 tape hybrid composites.

Figure 103 is a plot of ε^E and ε', for the considered composites, against V_{cf}/V_T (V_{cf}/V_T is inversely proportional to V_g/V_{cf}). The curve is sketched to pass through the dominant points for the 3:1 tape hybrid, 1:1 tape hybrid and the parent carbon composites. Note that the relationship is not linear but that the rate of increase in ε^E increases with decreasing V_{cf}/V_T.

Consider the results of slabs 37 to 39 and 41 to 46 in which the two tow types were not both intimately and evenly distributed. Their strain values, in relation to those expected from a hybrid composite with the same V_{cf}/V_T ratio but with an even and intimate distribution of the two tow types,

are approximately as expected when taking into account their particular fibre geometrical arrangements, as discussed in the previous section 4.8.7. For example, the low ε^{ϵ} value obtained for slab 37 (0.45% compared with 0.60% for the equivalent 1:1 tape hybrid composite) may be attributed to the non-intimate arrangement of the tow types and to the two plain carbon tapes being in the outer layers of the composite. In contrast the high ε^{ϵ} and ε' values of slab 44 may be attributed to the intimate mixing of the tow types and to the low concentration of carbon tows in the outer layers of the hybrid composite.

The major conclusion is that the ratio V_g/V_{cf} does affect the first failure strain of the hybrid composites. The following equation approximates to the sketched curve in figure 103 and was determined by plotting log ε^{ϵ} v log V_{cf}/V_T for the 3:1 tape hybrid, 1:1 tape hybrid and carbon tape composites.

$$\varepsilon^{\epsilon} = \varepsilon' = 0.47\left(\frac{V_{cf}}{V_T}\right)^{-0.36} = 0.47\left(1 + \frac{V_g}{V_{cf}}\right)^{0.36} \% \quad . \; . \; . \quad (128)$$

Consider the effect of V_{cf}/V_T on $\hat{\sigma}$. The experimental values, normalized to correspond to a V_T of 0.40, and the theoretical values ($\hat{\sigma}_{RM}$) are compared in figure 104. The experimental curve is sketched to fit the data for the 3:1 tape and 1:1 tape hybrid composites. In the carbon rich composites $\hat{\sigma}$ is assumed to equal σ^{ϵ} and the latter section of the curve is sketched accordingly. The positive hybrid effect, in $\hat{\sigma}$, above $V_{cf}/V_T \simeq 0.60$ is a direct consequence of the positive hybrid effect in the ε^{ϵ} and σ^{ϵ} of the hybrid composites. The experimental $\hat{\sigma}$ of the glass rich hybrid composites are compared with the equation for $\hat{\sigma}_{RM}$ given in table 20 ($\hat{\sigma}_{RM} = 63.0V_m + 1493.0V_{g6}$)which assumes that beyond σ' the carbon fibres cease to be stress bearing. The positive hybrid effect in this low V_{cf}/V_T range illustrates the error in this assumption. Some carbon fibres must still be contributing to the strength of the hybrid composites up to $\hat{\sigma}$ and therefore in no cross-section can all the carbon fibres have failed. A consequence of this is the increased V_{cf}/V_T ratio at which the minimum $\hat{\sigma}$ is expected to occur. Note that the sketched curve is only for the hybrid composites with intimate and even mixes of the two tow types. The differences in the $\hat{\sigma}$ results of the tested composites in which the above is not the case are again accounted to the differing fibre geometrical arrangements. The $\hat{\sigma}$ for the majority of these slabs lie between the experimental and theoretical curves. The two equations calculated to fit the experimental curve are 129 and 130.

For $0.00 \leqslant \frac{V_{cf}}{V_T} \leqslant 0.50$

$$\hat{\sigma}_e = 63.0 + V_T\left(1430.0 - 1162.5\,\frac{V_{cf}}{V_T}\right) \quad N/mm^2 \qquad . \; . \; . \qquad (129)$$

For $0.60 \leqslant \frac{V_{cf}}{V_T} \leqslant 1.00$

$$\hat{\sigma}_e = \varepsilon^{\varepsilon}\left[3.4 + V_T\left(72.2 + 166.5\,\frac{V_{cf}}{V_T}\right)\right] \times 10^3 \quad N/mm^2 \qquad . \; . \qquad (130)$$

The corresponding theoretical curves, transformed into terms of V_{cf} and V_T are given by equations 131 and 132.

For $0.00 \leqslant \frac{V_{cf}}{V_T} \leqslant 0.53$

$$\hat{\sigma}_{RM} = 63.0 + V_T\left(1430.0 - 1493.0\,\frac{V_{cf}}{V_T}\right) \quad N/mm^2 \qquad . \; . \; . \qquad (131)$$

For $0.54 \leqslant \frac{V_{cf}}{V_T} \leqslant 1.00$

$$\hat{\sigma}_{RM} = 16.0 + V_T\left(342.0 + 783.0\,\frac{V_{cf}}{V_T}\right) \quad N/mm^2 \qquad . \; . \; . \qquad (132)$$

This section has shown that the magnitudes of the hybrid effects in composite $\varepsilon^{\varepsilon}, \varepsilon', \sigma^{\varepsilon}, \sigma'$ and $\hat{\sigma}$ do vary with the ratio of V_g/V_{cf}. The result of the greatest practical importance is the increasing $\varepsilon^{\varepsilon}, \varepsilon', \sigma^{\varepsilon}$ and σ' of a hybrid composite with decreasing V_{cf}/V_T ratio. These results can be compared with those from two previous pieces of work. Marshall[23] fabricated 60% V_T hybrid composites from 4:1, 3:1 and 2:1 600 tex E-glass fibre/5000 filament carbon fibre tapes with either Derakane 411-45 vinyl ester or an epoxy resin as the matrix. When tensile testing the hybrid composites there was deviation from linearity in the stress v strain curves prior to the first failure stress. Marshall ascribed this to partial debonding of the aluminium end tabs from the composite test pieces. Assuming this to be the case and the corrected stress v strain curves to be linear up to their first failure stress then the following $\varepsilon^{\varepsilon} = \varepsilon'$ values were obtained for the hybrids containing 4:1, 3:1 and 2:1 hybrid tapes respectively. With an epoxy resin matrix: 1.26%; 1.24% and 1.20% and with a vinyl ester resin matrix: 1.15%; 1.12% and 1.10%.

The failure strain of a 5000 filament carbon/epoxy composite was 0.89% and that of E-glass/epoxy 2.18%. The trend in both systems is for $\varepsilon^{\varepsilon}$ to increase with decreasing V_{cf}/V_T but this trend is not as marked as in the composites tested here by the author. Further tensile results of 60% V_T glass/carbon hybrid tape/vinyl ester composites are presented in a paper by Phillips[26]. The $\varepsilon^{\varepsilon} = \varepsilon'$

values obtained for all-glass, 4:1, 3:1, 2:1, 1:1 and all-carbon composites were 1.95%, 1.18%, 1.14%, 1.10%, 1.00% and 0.98% respectively. Again $\varepsilon^{\varepsilon}$ increases with decreasing V_{cf}/V_{T} but to a lesser extent than in the composites tested here by the author. An explanation for this may be the different tensile characteristics of the constituent fibres and the relative failure strains of the L.E. and H.E. fibres.

The following section investigates the effect of the hybrid system used on the tensile properties of the composites.

4.8.9 The Hybrid Composite System and the Hybrid Effect

The 'hybrid systems' have been varied in terms of the surface treatment of the carbon fibres, the surface treatment of the E-glass fibres, the E-glass fibre type and, as a result of the latter two, the tensile characteristics of the E-glass fibres.

Firstly consider the effect on the tensile properties of the hybrid composites of varying the surface treatment of the carbon fibres. The relevant slabs are 46 to 61 and all had the tape lay-up sequence GCGCGCG. Thus by pairing the slabs appropriately the tensile results of hybrid composites differing only in respect to the type of carbon fibre surface treatment can be compared. Table 22 presents the average tensile results of these slabs for comparison and briefly indicates the significance or otherwise in any differences in their properties. The elastic moduli of the slabs are omitted from the table since this property has previously been shown to obey the rule of mixtures for all of the slabs tested (see sections 4.8.1.2, 4.8.2.2, 4.8.3.2 and 4.8.4.2) and is therefore not affected by the carbon fibre surface treatment.

There is no significant difference in the properties of slabs 46 and 60 or 51 and 61 or 48 and 58, indicating that any real effect due to changing the carbon fibre surface treatment from as rec. to no c.-a. in a hybrid composite with as rec. 600 tex or 500 tex E-glass fibre or no c.-a. 600 tex E-glass fibre as the second fibre type is negligible. Comparison between the tensile results of slabs 49 and 59 is inconclusive. Here differences in σ^{ε}, σ' $(=\hat{\sigma})$ and ε' are found to be insignificant but the analysis of the $\varepsilon^{\varepsilon}$ values shows $\varepsilon^{\varepsilon}$ of slab 49 to be significantly greater than $\varepsilon^{\varepsilon}$ of slab 59. In practice a true change in $\varepsilon^{\varepsilon}$ with a change in carbon fibre surface treatment means a corresponding change in σ^{ε} since E is independent of fibre surface treatment. Therefore the result of the statistical analysis on either $\varepsilon^{\varepsilon}$ or σ^{ε} is misleading. The conclusion that the effect of the change in carbon fibre surface treatment, from as rec. to no c.-a. in carbon/500 tex (no c.-a.) E-glass/vinyl ester composites, on the tensile properties is negligible (i.e. the results for $\varepsilon^{\varepsilon}$ are misleading) appears to be justified by the following points.

i) The variations in the individual ε^E of specimens from both slabs 49 and 59 are unusually low (see table 2A8). It is likely that the true standard deviations of ε^E in the two composite types are higher than those estimated from the experimental data. This increases the apparent value of the t statistic for the two sets of data. The t value need only drop by 1% for the analysis to show the variations in ε^E as insignificant.

ii) The statistical analysis shows no significant difference between the two sets of data (at the 95% confidence level) if the resultant t statistic is within the range $-2.228 < t < 2.228$. The t statistic for the σ^E data is 1.907, comfortably within this range. The t statistic for ε^E is 2.246, less than 1% greater than the limit.

However, as stated above, the results are inconclusive. Note that the E-glass type in slabs 49 and 59 was 500 tex. Slabs 48 and 58, in which no significant difference in tensile properties was found, contained 600 tex E-glass fibre. The results are reversed in the next group of slabs in table 22. Highly significant differences in the σ^E and ε^E are found for slabs 50 and 56 which contained 600 tex E-glass fibre (A1100), but no significant difference is found in the tensile properties of slabs 51 and 57 which contained 500 tex E-glass fibre. Slab 50 contained as rec. carbon fibres and its specimens exhibited distinct ε^E and ε' values. Slab 56 contained etched carbon fibres and the average ε^E is increased to equal ε'. In slabs 49 and 50 the apparent effect of changing the carbon fibre surface treatment from as rec. to no c.-a. was to reduce the value of ε^E. Ignoring the other results these suggest that the ε^E of the hybrid composites can be increased by changing the surface treatment of the carbon fibre from no c.-a. to as rec. to etched. This order does not correspond to the order of the i.l.s.s. of the carbon composites. The i.l.s.s. of as rec., no c.-a. and etched carbon fibres/vinyl ester resin were $43.7 N/mm^2$, $50.0 N/mm^2$ and $97.8 N/mm^2$ respectively. Thus the apparent changes in ε^E can not be directly attributed to changes in the carbon/resin interfacial shear strength. Slabs 52 and 54, and 53 and 55 were similar to slabs 50 and 56, and 51 and 57 but contained A187 treated E-glass fibre. There is no significant difference between the tensile properties of these slabs 52 and 54, and 53 and 55.

In respect to σ', ε' and $\hat{\sigma}$ of the hybrid composites the results of the comparisons amongst slabs 46 to 61 are all in agreement. These properties were not affected by the surface treatment of the carbon fibres. To reach a definite conclusion concerning the σ^E and ε^E of the hybrid composites more results are needed. Eight pairs of results were examined and the σ^E and ε^E values were found to differ significantly in one and two of these pairs respectively. No link can be found in these variations in σ^E and ε^E with

the effectiveness of the carbon fibre surface treatments (i.e. the i.l.s.s. of their parent carbon composites) or with the type or surface treatment of the E-glass fibre in the hybrid composites. Therefore it is tentatively concluded that any variation in σ^{E} and ε^{E} of the hybrid composites due to the surface treatment of the carbon fibres can be ignored being largely masked by scatter in the individual results.

The other variations in the hybrid systems were the tensile characteristics of the E-glass fibres and their surface treatments. These are linked since for both the 500 tex and 600 tex E-glass fibres the processes of changing their surface treatments damaged the fibres, thereby changing their tensile statistical characteristics. For each type of surface treatment the tensile properties of the 500 tex E-glass fibres were greater than those of the 600 tex E-glass fibres.

Consider the pairs of hybrid composites identical except for the type of constituent E-glass fibre. These are slabs 39 and 40, 46 and 47, 48 and 49, 50 and 51, 52 and 53, 54 and 55, 56 and 57, 58 and 59, and 60 and 61. Their tensile results are given in table 16. The average ε^{E} and ε' values within each pair of slabs reflect the comparative magnitudes of the hybrid effect in the apparent failure strain of the constituent carbon fibres (ε^{E} for the parent carbon composites being 0.47%). Note that in the majority of cases the slab containing 500 tex E-glass fibres has the greater values of ε^{E} and ε'. There are two notable exceptions. The values of ε^{E} and ε' for slabs 48 and 49 are equal and for slabs 58 and 59 both the values of ε^{E} and ε' differ by only 0.01% strain. In both of these pairs of slabs the surface treatment of the E-glass fibres was no c.-a. The trend in the majority of cases for the slab containing 500 tex E-glass fibre to have the greater ε^{E} and ε' values indicates that these properties of the hybrid composites are dependent upon some tensile characteristic(s) of the H.E. fibre. For the dominant characteristic to be the elastic modulus of the fibre one would expect the relative ε^{E} and ε' values to be similar since the fibre elastic modulus varies only with E-glass type and not with surface treatment. The results of the two pairs of slabs containing no c.-a. treated E-glass fibres indicate that the elastic modulus is not the dominant characteristic. The more probable characteristic is the failure strain of the parent H.E. fibre composite. This varies considerably for both E-glass types with the fibre surface treatment, being a maximum for the plain composites containing as rec. fibres and a minimum for those containing no c.-a. fibres. However the degree of scatter in all the strain values and the limited number of results for comparison prevents the drawing of positive conclusions.

Consider the effects of varying the surface treatment and consequently the tensile failure stress and strain of the E-glass fibres. Examination of table 22 shows that in the range of hybrid composites from slabs 46 to 61 containing 600 tex E-glass fibre the general trend of $\varepsilon^{\varepsilon}$ and ε' is to increase as the E-glass fibre surface treatment changes from no c.-a. to A187 to either A1100 or as rec. The same trend is observed in the hybrid composites containing 500 tex E-glass fibres. This corresponds more closely to the order of the failure strain rather than to the order of the i.l.s.s. of the parent E-glass fibre composites. The i.l.s.s. of the parent composites increases as the E-glass fibre surface treatments change from no c.-a. to as rec. to A187 to A1100, the i.l.s.s. of such composites being approximately 46.5N/mm^2, 51.5N/mm^2, 58.5N/mm^2 and 105.0N/mm^2 respectively. This lack of correlation between hybrid composite $\varepsilon^{\varepsilon}$ and ε' values and the i.l.s.s. of their parent E-glass fibre composites is inconclusive. It may be that the surface treatment of the E-glass fibres in the hybrid composites does not affect the expected $\varepsilon^{\varepsilon}$ and ε' of that composite. Alternatively any influence may be masked by i) variations in the effectiveness of the E-glass coupling-agent surface treatments (see section 4.7.2.1), ii) the scatter in the limited number of results considered and iii) any effect due to the varying tensile characteristics of the parent E-glass fibres. Consider the $\varepsilon^{\varepsilon}$ and ε' values of slabs 46 to 61 in relation to the $\varepsilon^{\varepsilon}$ of their parent E-glass fibre composites. These values are plotted in figure 105. This graphical representation indicates that in the hybrid systems considered an increase in the $\varepsilon^{\varepsilon}$ of the parent E-glass composite increases the $\varepsilon^{\varepsilon}$ and ε' values of its hybrid composite. However there is considerable scatter in both the $\varepsilon^{\varepsilon}$ and ε' values of the hybrid composite and the $\varepsilon^{\varepsilon}$ values of the parent E-glass composite.

The tentative conclusion drawn from this section is that the variations in the average $\varepsilon^{\varepsilon}$ and ε' values observed for the hybrid composites of slabs 46 to 61 are predominantly due to changes in the tensile strengths of the constituent E-glass fibres rather than the different moduli of the 600 tex and 500 tex E-glass fibres or the different characteristics of the E-glass/resin interface resulting from the four types of surface treatment. The lower failure strain E-glass fibres, represented in terms of the failure strain of the fibres when in their own composites, produced lower $\varepsilon^{\varepsilon}$ and ε' values in their hybrid composites.

Before considering existing theories for hybrid composite tensile properties the failure process for the carbon/E-glass/vinyl ester hybrid composites is discussed in greater detail than hitherto.

4.8.10 Theoretical Carbon/E-Glass/Vinyl Ester Hybrid Composite Failure Process

At the end of section 4.8.5 an explanation is briefly forwarded, in terms of internal fibre failures, for the two major features of the stress v strain curves of the hybrid composite specimens, i.e. for the gradual decrease in the gradient between the points ($\varepsilon^{\varepsilon}$, σ^{ε}) and (ε' , σ') when these points are distinct and for the drop in stress at (ε' , σ'). The explanation is expanded and its feasability investigated in this section. The suggested failure process is based on the statistical nature of fibre tensile strength.

When fibres in a composite cross-section fail the stress bearing ability of that cross-section is reduced. The effect on the tensile stress v strain curve depends on the extent of the fibre failure and the axial length over which the fibres are ineffective. If random single fibre failures and limited multiple fibre failures accumulate in the composite as the strain increases the elastic modulus of the composite is gradually reduced. This effect of random fibre failures has been shown in section 4.7.1.3 to be so small in the parent fibre composites that catastrophic propagation of fibre failure occurs in these composites before the change in the stress v strain gradient can be detected. In the hybrid composites the E-glass fibres act as a barrier to the propagation of carbon fibre failures. Thus the accumulation of random single and multiple carbon fibre failures prior to a 'substantial' failure of the hybrid composite is much greater than in the parent carbon composites. As the strain in the hybrid composites increases above the normal failure strain of the carbon composites the possibility of a substantial carbon fibre failure, resulting in a stress drop, increases. In a hybrid where $\sigma^{\varepsilon} = \sigma'$ this substantial failure occurs prior to a significant reduction in E due to the accumulated fibre failures. So far the extent of carbon fibre failure necessary to cause a drop in stress has vaguely been described as 'substantial'. By considering the effect of fibre failures on the load bearing ability of the hybrid composites a clearer understanding of the necessary extent of failure is obtained. In the tensile testing of the specimens the total extension of the specimen is controlled. Consider the moment of fibre failure. When a group of fibres fail the extensional stiffness over that cross-section decreases, resulting in a strain concentration over that region. This causes a corresponding strain relaxation in the rest of the composite since the total extension of the specimen must remain the same. Therefore the applied load is reduced. For a hybrid composite specimen of cross-sectional area A, gauge length L and elastic modulus E, when a load P is supported the applied extension ΔL is given by the equation

$$\Delta L = \frac{PL}{AE} \qquad \ldots \quad (133)$$

Suppose at ΔL a quantity of the L.E. fibres fail and can bear no load over an axial distance ℓ. The effective A and E values for the cross-section over this axial distance ℓ change to A_1 and E_1 respectively and the supported load changes to P_1. ΔL is now represented by the equation

$$\Delta L = \frac{P_1 (L-\ell)}{AE} + \frac{P_1 \ell}{A_1 E_1} \qquad \ldots \quad (134)$$

By equating 133 with 134 the ratio of P_1/P is shown to be

$$\frac{P_1}{P} = \frac{LA_1E_1}{A_1E_1(L-\ell) + AE\ell} \qquad \ldots \quad (135)$$

This load ratio is equivalent to the stress ratio. It is now related to the carbon/E-glass/resin composites. The controlling factors are the length ℓ and the number of fibres which fail which dictate the change in A and E to A_1 and E_1. Firstly the variation in $\frac{P_1}{P}$ with changing ℓ is considered for two composites with L = 50mm, V_T = 0.4 and i) V_{g6} = 0.2 , V_{cf} = 0.2, i.e. a 1:1 hybrid composite and ii) V_{g6} = 0.3, V_{cf} = 0.1, i.e. a 3:1 hybrid composite. The model supposes that at ΔL all the carbon fibres in one cross-section fail whilst the E-glass fibres remain intact. The resultant relationships between $\frac{P_1}{P}$ and ℓ are plotted in figure 106. The relationship for the 1:1 hybrid is calculated as follows. E is calculated from equation 110.

$$E = (0.6 \times 3.4) + (242.1 \times 0.2) + (75.6 \times 0.2) = 65.6 KN/mm^2$$

When all the carbon fibres in one cross-section fail A is reduced in that region by 20% and the value of E_1 is given by equation 95.

$$\therefore \quad A_1 = 0.80\ A$$

$$\text{and } E_1 = (3.4 \times 0.6) + (75.6 \times 0.2) = 17.2 KN/mm^2$$

Equation 135 becomes

$$\frac{P_1}{P} = \frac{50 \times 0.80A \times 17.2}{\left[0.80A \times 17.2\ (50-\ell)\right] + \left[65.6\ A\ell\right]}$$

$$= \frac{688.0}{688.0 + 51.8\ell} \qquad \ldots \quad (136)$$

Following the same method the relationship between $\frac{P_1}{P}$ and ℓ for the 3:1 hybrid composite with $V_T = 0.4$ is derived as

$$\frac{P_1}{P} = \frac{1111.5}{1111.5 + 26.7\ell} \quad . \ . \ . \quad (137)$$

Now consider the variation in $\frac{P_1}{P}$ with the fraction of V_{cf} failing (F_{cf}), with $\ell = 0.5$mm, in one cross-section in a i) 1:1 and ii) 3:1 hybrid composite tensile specimen with $V_T = 0.4$ and L = 50mm. The relationships are presented graphically in figure 107. The relationship for the 1:1 hybrid composite is calculated as follows. E is calculated from equation 110.

$E = (3.4 \times 0.6) + (242.1 \times 0.2) + (75.6 \times 0.2) = 65.6 KN/mm^2$

The failure of $F_{cf}V_{cf}$ in one cross-section reduces the A in that region by $0.2F_{cf}A$ and E by $242.1\ F_{cf}V_{cf}$. Therefore

$$A_1 = (1 - 0.2F_{cf})A \ mm^2 \quad . \ . \ . \quad (138)$$

$$E_1 = 65.6 - 48.4F_{cf} \ KN/mm^2 \quad . \ . \ . \quad (139)$$

Substituting for A_1 and E_1 equation 135 becomes

$$\frac{P_1}{P} = \frac{50(1-0.2F_{cf})A\ (65.6-48.4F_{cf})}{49.5\ (1-0.2F_{cf})\ A\ (65.6-48.4F_{cf}) + (65.6 \times 0.5 \times A)}$$

$$\frac{P_1}{P} = \frac{50(65.6-61.5F_{cf} + 9.7F_{cf}^2)}{49.5(65.6-61.5F_{cf} + 9.7F_{cf}^2) + 32.8} \quad . \ . \ . \quad (140)$$

Following the same method the relationship between $\frac{P_1}{P}$ and F_{cf} in a 3:1 hybrid composite with $V_T = 0.4$ when $\ell = 0.5$mm is:

$$\frac{P_1}{P} = \frac{50.0(48.9-29.1F_{cf} + 2.4F_{cf}^2)}{49.5(48.9-29.1F_{cf} + 2.4F_{cf}^2) + 24.5} \quad . \ . \ . \quad (141)$$

Note that the above ignores the effect of carbon fibres in the cross-section under consideration which fracture before ΔL is reached.

In the recorded plots of load v strain obtained for the hybrid specimens drops in load of 1% or more could confidently be distinguished, i.e. the recorded ε' values correspond to the first strain at which a drop in load occurs for which $\frac{P_1}{P} \leqslant 0.9900$. Figures 106 and 107 show the dependence of $\frac{P_1}{P}$ on ℓ and F_{cf} for 3:1 and 1:1 hybrid composites. For both the 3:1 and 1:1 hybrid composites when all carbon fibres in one cross-section fail ℓ must be considerably greater than the estimated ineffective length, δ, of the carbon fibres (approx-

imately 0.05mm), as given by equation 3, for the drop in load to be significant. The values of ℓ and F_{cf} which produce a $\frac{P_1}{P}$ value of 0.9900 are now considered. The following equation for ℓ is obtained from equation 135.

$$\ell = \frac{A_1 E_1 L \left(\frac{P}{P_1} - 1\right)}{AE - A_1 E_1} \quad \ldots \quad (142)$$

For the 1:1 hybrid composite $E = 65.6$, $V_T = 0.4$, $A_1 = (1 - 0.2F_{cf})\,A$ and $E_1 = 65.6 - 48.4F_{cf}$.

Therefore when $\frac{P_1}{P} = 0.9900$

$$\ell = \frac{(1-0.2F_{cf})A(65.6-48.4F_{cf})50(1.0101-1)}{(A65.6)-(1-0.2F_{cf})A(65.6-48.4F_{cf})}$$

$$\therefore \quad \ell = \frac{0.505(65.6-61.5F_{cf} + 9.7F_{cf}^2)}{61.5F_{cf} - 9.7F_{cf}^2} \quad \text{mm} \quad \ldots \quad (143)$$

Similarly for the 3:1 hybrid composite with $V_T = 0.4$ when $\frac{P_1}{P} = 0.9900$

$$\ell = \frac{0.505(48.9-29.1F_{cf} + 2.4F_{cf}^2)}{29.1F_{cf} - 2.4F_{cf}^2} \quad \text{mm} \quad \ldots \quad (144)$$

These equations (143 and 144) are plotted in figure 108. This graph illustrates what the term 'substantial carbon fibre failure' means for the 1:1 and 3:1 hybrid composites with $V_T = 0.4$. In the tensile testing of a specimen any propagation of carbon fibre failure whose combination of F_{cf} and ℓ values lie above the relevant curve in figure 108 results in a significant drop in stress at that point on the stress v strain curve. The necessary values of ℓ, even when $F_{cf} = 1.00$, are an order of magnitude greater than the calculated ineffective lengths, δ, of the carbon fibres when in their parent composites. These high effective ℓ values may be caused by any of or a combination of the following:

i) debonding occuring at the carbon/resin interface;

ii) the propagation of carbon fibre failure in one cross-section sending shock waves through the composite which trigger further carbon fibre failures in another neighbouring cross-section, the effect of these distinct groups of carbon fibre failures being cumulative and

iii) debonding at the E-glass/resin interfaces where the propagation of fibre failure terminates.

The latter is supported by the appearance of whitened areas (indicating E-glass/resin debonding) in the specimens coinciding with the recording of load drops. The axial lengths of these areas were often in the region of mm.

A point not yet considered is that E-glass fibres may also fail up to and at ε'. It is suggested that failure of as rec. E-glass fibres up to ε' is minimal, being confined to the exceptionally weak fibres. Where composite failure at ε' is catastrophic the propagation of carbon fibre failure spreads into and through the E-glass fibres but if the initial load drop is only a few percent of P only a small number of E-glass fibres are expected to fail. Therefore the proposed failure mechanism for the carbon fibre/E-glass fibre hybrid composites is as follows.

As a hybrid tensile specimen is strained, random single carbon fibre failures occur followed by limited multiple failures. When $\varepsilon^{E} \neq \varepsilon'$ these failures accumulate to weaken the composite sufficiently to noticeably reduce the gradient of the stress v strain curve. At ε' a major propagation(s) of carbon fibre failures occurs running through and joining together previously existing multiple failures, as happens at the failure of the parent carbon composites. F_{cf} and ℓ are sufficient to result in a drop in load of 1% or more. If the carbon fibre failures extend into and through the E-glass fibres immediate catastrophic failure of the hybrid composite results. If the failure either terminates at the E-glass fibres or extends only to the weaker E-glass fibres then ε' is marked by a limited drop in stress. Further carbon fibre (and possibly some E-glass fibre) failures occur as the strain increases and where 'substantial' produce further drops in the stress v strain curve until the failure extends to all the carbon and E-glass fibres, probably joining together areas of substantial failure, causing complete composite failure. Figure 109 is a flow chart giving possible tensile failure sequences for a carbon fibre/E-glass fibre/vinyl ester resin hybrid composite and relates three example stress v strain curves to the flow chart.

The failure process described above explains the observed hybrid fracture surfaces. For example consider the fracture surface of a typical 3:1 hybrid specimen as described in section 4.8.1.1. Numerous substantial failures occur prior to complete composite failure. It is suggested that these and multiple carbon failures do not spread significantly into the E-glass tows but cause some debonding at the E-glass/resin interface, especially in the cases of the later substantial failures when the energy of the propagation is greater. This explains the appearance of the whitened areas with the load drops. Failure within the carbon tows occurs through the propagation of single and multiple

carbon fibre failures, as in their parent composites. Therefore the appearance of the carbon tow fracture surfaces in the 3:1 hybrids and the parent carbon composites are similar. Complete composite failure occurs when the composite is weakened by areas of substantial failure and the propagation of failure spreads into and through the E-glass fibres, the weakened areas being joined by debonding at the E-glass/resin interface, probably initiated when the carbon fibre failures first occurred. Thus the fractures have a considerable axial spread. The spikes of E-glass fibres extending beyond the general failure plane are due to debonding at the E-glass/resin interface, caused by carbon fibre failure, reaching a group of weak E-glass fibres. Thus when catastrophic failure occurs this extended group or 'spike' of E-glass fibres forms part of the fracture surface. The slight increase in carbon fibre pull-out length is explained in terms of their debond lengths. Substantial carbon failures occur above the failure strain of the parent carbon composites, therefore more energy is released and the likelihood and extent of debonding at the carbon fibre/resin interface as the broken fibre attempts to contract is increased, thus increasing carbon pull-out lengths when the final failure passes through these points.

The statistical aspect of the failure theory is supported by the acoustic emission recordings of tensile tested bonded c.f.r.p./g.r.p. hybrid composite specimens as monitored by Bunsell and Harris[24]. Acoustic emissions were initially recorded below the expected failure strain of the c.f.r.p. alone. The acoustic activity increased around the first load drop and subsequent drops were accompanied by large bursts of acoustic emission. The failure theory is consistent with these results providing that the majority of the acoustic emissions can be interpreted as fibre failures. Marshall[23] and Phillips[26] both briefly suggest that the presence of the E-glass fibres retards the catastrophic propagation of fibre failure and Marshall comments that if this is so he would "expect the configuration of the glass fibres and the carbon fibres within the matrix to be important". The consequential theoretical effects, assuming the failure process described in this section to be correct, of varying V_T, fibre geometrical arrangement, ratio of V_g/V_{cf} and the hybrid composite system on the hybrid tensile stress v strain curve is now discussed and compared with the appropriate experimental results given in sections 4.8.6 to 4.8.9.

4.8.10.1 Theoretical Effect of V_T

The values of ε^E and ε' in a particular hybrid composite system which exhibits the hybrid effect are only expected to vary with V_T at low V_T values. Theoretically ε^E and ε' decrease slightly at the bottom range of V_T due to changes in the degree of mixing of the carbon fibres and E-glass fibres. The mixing of the two fibre types is limited to the mixing of the tows. Therefore with a very low V_T one carbon fibre tow represents a considerable proportion of the carbon fibres present in the hybrid composite and so a low degree of mixing becomes unavoidable. As described later in section 4.8.10.2 a low degree of mixing is proposed to reduce the magnitude of any hybrid effect in the initial failure strain of the hybrid composites. Consider 3:1 and 1:1 hybrid tape composites. The two fibre types are regarded as intimately and evenly mixed but at some low value of V_T the reduction in the degree of mixing becomes significant and acts to reduce ε^E. Theoretically the V_T range over which ε^E reduces is greater for the 3:1 tape composites since at any V_T one tow represents a larger proportion of the total carbon content than in the 1:1 tape composites.

The values for $\varepsilon^E (= \varepsilon')$ obtained experimentally for the 3:1 and 1:1 tape composites neither support nor contradict the theory. Section 4.8.2.2 concludes that there is no significant difference amongst the mean ε^E $(= \varepsilon')$ values of the 1:1 tape slabs tested (V_T range 0.17 to 0.50). The same conclusion is tentatively reached in section 4.8.1.2 for the 3:1 tape slabs tested (V_T range 0.23 to 0.51). To test the validity of the described theoretical effect of V_T on ε^E, hybrid tape slabs with lower V_T need to be fabricated and tested.

4.8.10.2 Theoretical Effect of Fibre Geometrical Arrangement

The effect of fibre geometrical arrangement on the ε^E and ε' values of the hybrid composites is studied by considering the ease or otherwise with which multiple and substantial carbon fibre failures (as discussed in section 4.8.10) may occur. Firstly the effect of positioning carbon fibres in the outer layers of hybrid composites is briefly considered. Increasing the proportion of carbon fibres in the outer layers of a composite tend to reduce ε^E and ε' values since the failure of any of the outer fibres produces higher stress concentrations on the fewer neighbouring fibres than on those around a failed inner fibre. Thus multiple failures and substantial failures are more likely to occur in the outer layers. In addition any damage incurred by a

composite since fabrication is likely to be concentrated in its outer layers of tape which, as their carbon content increases, increases the number of potential initiation sites for multiple and substantial propagations of carbon fibre failure, thereby tending to reduce ε^{E} and ε' values.

Secondly, the degree of mixing of the carbon and E-glass fibres in their hybrid composite is considered. It is suggested that in a hybrid composite with a very low degree of mixing of the two fibre types substantial propagation of carbon fibre failure is encouraged. Carbon fibre failure is free to propagate through a large proportion of V_{cf} before reaching and being impeded by a large barrier of the H.E. E-glass fibre. Therefore theoretically $\varepsilon^{E} = \varepsilon'$ and any hybrid effect in ε' is minimal.

ε^{E} equal to ε' is also predicted for hybrids with a high degree of mixing. Here the extent of the possible propagation of carbon fibre failure before a barrier of E-glass fibres is reached is minimized, but so is the size of the barrier. The point ε' is suppressed until waves of dynamic stress concentration caused by a multiple carbon fibre failure in one group of carbon fibres are not sufficiently damped by the E-glass fibres to prevent spreading the failure to neighbouring groups of carbon fibres and beyond. Therefore ε' is suppressed (producing a positive hybrid effect) but not to such an extent that the single and minimized multiple carbon failures accumulate sufficiently to produce a distinct ε^{E} value prior to ε'.

It is proposed that an intermediate degree of mixing promotes distinct ε^{E} and ε' values. The groups of carbon fibres are larger than in the above case, increasing the extent of a propagation of carbon fibre failure possible before reaching a barrier of E-glass fibres, which is correspondingly larger. Thus the point ε' is again suppressed until dynamic stress waves from a multiple failure in one group of carbon fibres cause the failure of a neighbouring group(s) of carbon fibres, despite the intervening barrier of E-glass fibres. ε' here is expected to be approximately equal to $\varepsilon^{E} = \varepsilon'$ in the case above for a high degree of fibre mixing. However, for intermediate mixing the increased possible extent of a multiple failure confined to one group of carbon fibres is sufficient for their accumulation prior to ε' to noticeably weaken the composite, producing a distinct ε^{E} value.

Thus for hybrid composites varying only in fibre geometrical arrangement with

i) a low degree of mixing:- $\varepsilon^{E} = \varepsilon'$ and tends towards ε^{E}_{RM}

ii) a high degree of mixing:- $\varepsilon^{E} = \varepsilon'$ and exhibits a positive hybrid effect and

iii) an intermediate degree of mixing:- ε^{E} and ε' have distinct values, that of ε^{E} falling between the ε^{E} values obtained in cases i) and ii) and that of ε' being approximately equal to ε' in case ii).

The majority of the experimental tensile results of slabs 37 to 39, 45 and 46, and 3:1 and 1:1 slabs (as presented in table 16 and discussed in relation to the fibre geometrical arrangements in section 4.8.7) support the above theory. Slab 37 (CG_6G_6C) has the lowest degree of fibre mixing and all the carbon fibres are in the outer layers. The theory predicts $\varepsilon^E = \varepsilon' \simeq \varepsilon^E_{RM}$. The experimental results are $\varepsilon^E = \varepsilon' = 0.45\%$. The difference between this and $\varepsilon^E_{RM} = 0.47\%$ is not significant. The highest degree of mixing of the two tow types occurs in the two series of 3:1 and 1:1 hybrid tape slabs. In agreement with theory both sets have $\varepsilon^E = \varepsilon'$, exhibiting a positive hybrid effect, ε^E being 0.60% and 0.78% for the 1:1 and 3:1 hybrids respectively. Slab 46 ($G_6CG_6CG_6CG_6$) with an intermediate degree of mixing has distinct ε^E and ε' values of 0.59% and 0.68% respectively. The expected value of $\varepsilon^E = \varepsilon'$ for an equivalent intimately mixed hybrid is approximately 0.64% (see figure 103). The slightly high value of $\varepsilon' = 0.68\%$ may be attributed to the lack of carbon fibres in the outer layers of slab 46.

Results of special interest are those for slabs 44 (3:1 1:1 3:1 1:1 3:1 1:1 3:1) and 45 (1:1 1:1 3:1 1:1 3:1 1:1 1:1). Specimens from both these slabs showed mixed behaviour, indicating that the degrees of mixing of the fibre types lie between intermediate and high. From slab 44 three of the six specimens tested have distinct ε^E and ε' values, the average values being $\varepsilon^E = 0.77\%$ and $\varepsilon' = 0.82\%$. The results are rather higher than expected according to figure 103. The lower than average carbon content of the outer layers should act to increase ε^E and ε' and an additional point of note is that the scatter in the ε^E (CV = 8.2%) and ε' (CV = 11.2%) values for slab 44 is greater than that for most other slabs. From slab 45 five of the six specimens tested have distinct ε^E and ε' values. The average ε^E value of 0.62% is approximately equal to that of 0.60% for the 1:1 hybrid tape slabs, suggesting that multiple carbon fibre failures occur in the 1:1 layers of slab 45 in the same manner as in their parent 1:1 tape composites but that the 3:1 layers are successful in limiting the failures until $\varepsilon' = 0.67\%$.

A few of the experimental ε^E and ε' values are slightly different from those expected according to the degree of mixing but these can frequently be related to the proportion of the carbon tows in the outside layers of tape, e.g. ε^E for slab 39 is low at 0.47% but 50% of the carbon fibres are in the two outside layers.

It is concluded that the tensile results of the hybrid slabs with different fibre geometrical arrangements support the proposed failure mechanisms.

4.8.10.3 The Effect of V_g/V_{cf}

Evaluation of the theoretical effect of the ratio of V_g/V_{cf} on the $\varepsilon^{\varepsilon}$ and ε' values of a hybrid composite is approached by considering the changes in fibre geometrical arrangement and the changes necessary for ε' in the quantitative value of the 'substantial' carbon failure as the ratio of V_g/V_{cf} is varied. The following discussion is based on a hybrid composite with a degree of fibre mixing such as occurs when using hybrid tapes and on a V_T value of around 0.4. The ideas apply to alternative hybrids but must be considered in conjunction with the effects of the changes in the other parameters.

First consider the changes in fibre geometrical arrangement with V_g/V_{cf}. In a carbon rich hybrid composite the hybrid may be regarded as isolated E-glass tows in a matrix of the carbon fibres/vinyl ester resin. Therefore the E-glass is ineffective in impeding the propagation of carbon fibre failure so $\varepsilon^{\varepsilon} = \varepsilon' \simeq \varepsilon^{\varepsilon}_{RM}$ is expected. In addition as the V_g/V_{cf} ratio is reduced failure at $\varepsilon^{\varepsilon}$ is more likely to be catastrophic, the E-glass fibres being subjected to greater strain concentrations upon the failure of the carbon fibres. At very high V_g/V_{cf} ratios there are massive barriers of E-glass fibres separating each carbon tow so the propagation of carbon fibre failure is severely limited. If there is sufficient carbon fibre the accumulation of single and multiple carbon fibre failures eventually produce a distinct $\varepsilon^{\varepsilon}$ value. Catastrophic failure at ε' occurs due to the propagation of E-glass fibre failures. ε' is expected to be slightly less than the failure strain of the parent E-glass composites due to strain concentrations around previously failed carbon fibres. The situation for intermediate V_g/V_{cf} ratios is as discussed in section 4.8.10.2 for intimately mixed hybrids. The E-glass limits the extent of carbon fibre propagation until the strain is high enough for any dynamic stress waves from the failure of carbon fibres in one tow, damped by the intervening E-glass fibres, to cause further failure of carbon fibres in another tow. The stress at which this occurs must increase as the size of the E-glass barriers increases. Therefore $\varepsilon^{\varepsilon} = \varepsilon' > \varepsilon^{\varepsilon}_{RM}$ and increases with increasing V_g/V_{cf}.

The above is now summarized. At low V_g/V_{cf} ratios $\varepsilon^{\varepsilon} = \varepsilon' \simeq \varepsilon^{\varepsilon}_{RM}$ Positive hybrid effects are expected to occur when V_g/V_{cf} is increased sufficiently for the E-glass tows to disturb the continuity of the carbon tows (i.e. when the hybrid can no longer be regarded as E-glass tows in a matrix of carbon fibre/vinyl ester). $\varepsilon^{\varepsilon}$ still equals ε'. As V_g/V_{cf} increases through the intermediate range the magnitude of the hybrid effect increases,

until in the high V_g/V_{cf} range carbon failures can not spread between tows. Distinct $\varepsilon^{\varepsilon}$ and ε' values occur, ε' being slightly less than the failure strain of the parent E-glass composite. At very high V_g/V_{cf} ratios $\varepsilon^{\varepsilon}$ and ε' coincide.

Now consider the variation in the extent of carbon fibre failure equalling 'substantial' failure as V_g/V_{cf} varies. At the beginning of section 4.8.10 the ratio of the applied load after to that before (P_1/P) a propagation of carbon fibre failure in a carbon fibre/600 tex E-glass fibre/vinyl ester composite is shown to be given by equation 135.

$$\frac{P_1}{P} = \frac{LA_1E}{A_1E_1(L-\ell) + AE\ell} \quad . \ . \ . \quad (135)$$

Substantial failure is defined as occurring when $\frac{P_1}{P} \leqslant 0.99$. As the ratio of V_g/V_{cf} is increased the minimum fraction of $V_{cf} \cdot F_{cf}$ failing and/or the minimum ineffective length, as given by ℓ, necessary to cause a substantial failure must also increase. The relationship between ℓ and V_{cf} given that $\frac{P_1}{P} = 0.99$, $F_{cf} = 1.00$ and $V_T = 0.40$ is derived from equation 135 by substituting the following: $L = 50mm$; $\frac{P_1}{P} = 0.99$; $A_1 = (1-V_{cf})A\ mm^2$; $E = 32.3 + 166.5V_{cf}\ KN/mm^2$ and $E_1 = 32.3-75.6V_{cf}\ KN/mm^2$. The result is

$$\ell = \frac{16.15-53.95V_{cf} + 37.80V_{cf}^2}{V_{cf}\,(75.6V_{cf} + 274.4)}\ mm \quad . \ . \ . \quad (145)$$

The relationship between F_{cf} and V_{cf} given that $\frac{P_1}{P} = 0.99$, $\ell = 0.5mm$ and $V_T = 0.4$ is derived from equation 135 by substituting the following: $L = 50mm$; $\frac{P_1}{P} = 0.99$; $\ell = 0.5mm$; $E = 32.3 + 166.5V_{cf}\ KN/mm^2$; $E_1 = 32.3 + 166.5V_{cf} - 242.1\ F_{cf}V_{cf}\ KN/mm^2$. The result is

$$F_{cf} = \frac{1.65 + V_{cf} - \sqrt{V_{cf}^2 + 0.40V_{cf} + 2.16}}{2.19V_{cf}} \quad . \ . \ . \quad (146)$$

ℓ and F_{cf} are plotted against V_{cf}/V_T in figure 110. For their fixed conditions both the rate of increase in the minimum required values of ℓ and F_{cf} for a substantial carbon fibre failure increases as V_{cf}/V_T decreases, i.e. as V_g/V_{cf} increases. This suggests that for a hybrid composite the trend in $\varepsilon^{\varepsilon}$ and ε' is to increase with the ratio of V_g/V_{cf}. Note that at low V_{cf}/V_T the possibility of a substantial failure rapidly decreases.

These results are in line with the behaviour of ε^{E} and ε' predicted due to the changes in fibre geometrical arrangement accompanying variations in V_g/V_{cf} as first considered. Thus in the hybrid composites as V_g/V_{cf} increases ε^{E} and ε' are expected to increase due to the E-glass acting more efficiently as a barrier to the propagation of carbon fibre failure and due to the failure of the same proportion of the carbon fibres (with similar ineffective lengths) having a smaller effect on the hybrid tensile stress v strain curve. The theoretical behaviour of ε^{E} and ε' with V_g/V_{cf} is now compared with the results obtained experimentally. These are discussed in section 4.8.8 and figure 103 is a plot of ε^{E} and ε' versus V_{cf}/V_T. Equation 128 is found to approximate to the relationship between $\varepsilon^{E} = \varepsilon'$ and V_{cf}/V_T when using the results from the 3:1 and 1:1 hybrid tape slabs as the dominant points.

$$\varepsilon^{E} = 0.47\left(\frac{V_{cf}}{V_T}\right)^{-0.36}\% = 0.47\left(1 + \frac{V_g}{V_{cf}}\right)^{0.36}\% \quad \ldots \quad (128)$$

As predicted by the theory there is very little increase in ε^{E} above $\varepsilon^{E}_{RM} = 0.47\%$ at high V_{cf}/V_T ratios. The rate of increase in ε^{E} increases with decreasing V_{cf}/V_T and equation 128 predicts $\varepsilon^{E} = 1.96\%$ (the failure strain of the parent 600 tex E-glass composites) at approximately $V_{cf}/V_T = 0.02$. Qualitatively the theoretical and experimental results agree.

4.8.10.4 The Effect of the Hybrid Composite System

In this section the theoretical effects of the changes made to the hybrid composite systems in this research on the hybrid effect are considered. This aspect of the experimental work is discussed in section 4.8.9.

Firstly consider changes in the carbon fibre surface treatment. The changes resulted in a range of carbon fibre/vinyl ester interfacial bond strengths. In theory increasing the interfacial bond strength encourages the propagation of fibre failure since when failures reach strong carbon fibres the propagation is less likely to terminate in debonding at the fibre resin interface. This effect is shown to be minimal in section 4.7.1.2 with no significant difference in the tensile results of the three 7C (as rec.), 7C (etched) and 7C (no c.-a.) slabs. Any effect in the hybrids must be to reduce ε^{E} and ε'. However if the fibre debond length is reduced the ineffective length ℓ of a failed fibre must also be reduced and this acts to increase ε^{E} and ε'. Therefore the theoretical behaviour of ε^{E} and ε' depends on the relative magnitudes of the two opposing effects. The experimental tensile

results for the range of 4G3C slabs tested are inconclusive but there is no obvious trend in the values of ε^{E} and ε' with changes in the carbon fibre surface treatments.

Consider the effect of variations in the tensile characteristics of the E-glass fibres. Theoretically a greater elastic modulus fractionally increases the F_{cf} and ℓ values necessary for a substantial carbon fibre failure and therefore must tend to increase the hybrid ε^{E} and ε' values. The expected failure strain of the E-glass fibres, $\hat{\varepsilon}_g$, in the hybrid composites (i.e. the expected failure strain of the parent E-glass composite) is considered in relation to the expected values of ε^{E} and ε' . When $\hat{\varepsilon}_g$ is considerably greater than the estimated values of ε^{E} and ε' then ε^{E} and ε' are independent of $\hat{\varepsilon}_g$. As $\hat{\varepsilon}_g$ decreases and approaches the expected values of ε^{E} and ε' the 'barriers' of E-glass fibres become more susceptible to the strain concentrations caused by failing carbon fibres (this should tend to increase the V_g/V_{cf} ratio at which catastrophic failure occurs at ε'). Where the CV of $\hat{\varepsilon}_g$ is large weaker E-glass fibres may fail but further propagation be resisted by the stronger E-glass fibres. Thus a large load drop at a reduced ε' value is encouraged. With a low CV of $\hat{\varepsilon}_g$ once the propagation of fibre failure enters the E-glass fibres catastrophic composite failure is likely to result. With very low values of $\hat{\varepsilon}_g$ the hybrid value of ε' may be reduced and equal ε^{E} . Random E-glass failures may contribute to the point ε^{E} if distinct from ε' and, whether distinct or not, carbon failure may propagate into and through the E-glass fibres causing catastrophic failure before ε^{E} would normally occur.

Therefore in theory reducing $\hat{\varepsilon}_g$ has a significant effect on hybrid ε^{E} and ε' when the ability of the E-glass fibres to impede the propagation of fibre failure at or before the expected values of ε^{E} and ε' is impaired. Once this occurs in general as $\hat{\varepsilon}_g$ decreases ε^{E} and ε' decrease and in the extreme case $\varepsilon^{E} = \varepsilon' = \hat{\varepsilon}$ with a minimal hybrid effect.

The theoretical effect of changes in the interfacial bond strength of the E-glass fibre/vinyl ester on the hybrid values of ε^{E} and ε' is considered in the same manner as for the carbon fibres. When a propagation of carbon fibre failures reaches E-glass fibres a low interfacial bond strength encourages the termination of the failure in E-glass/resin debonding, diffusing and absorbing energy of the propagation. Thus the E-glass acts as a more efficient barrier to fibre failure but the debonding tends to increase the effective ℓ values of the failed carbon fibres. These two effects on ε^{E} and ε' are opposing. With a high E-glass/resin bond strength the energy of a propagation of fibre failure is less likely to be diffused by debonding at the

E-glass/resin interface. Therefore the two probabilities of the failure propagating into further carbon fibres and into the E-glass fibres are increased. However the value of ℓ is kept to a minimum with no supplement due to debonding of the E-glass fibres. Therefore according to theory the two effects of varying the E-glass/vinyl ester interfacial bond strength on the ε^E and ε' values of a hybrid composite are opposing and the overall behaviour of ε^E and ε' must depend on the relative magnitudes of these effects.

Comparison of the theoretical effects of changes in the properties of the constituent E-glass fibres on the tensile properties of the hybrid composites with the experimental results (as discussed in section 4.8.9) is only of value in respect to the effect of changes in $\hat{\varepsilon}_g$ on the hybrid ε^E and ε' values. The extent of any influence of the constituent E-glass elastic modulus and the E-glass/resin bond strength on the hybrid ε^E and ε' values is masked partly by scatter in the tensile results but mainly by the effect of changes in the failure strain of the parent E-glass composites which accompanies the changes in bond strength. At the end of section 4.8.9 it is concluded that the general trend of the ε^E and ε' values of a hybrid composite is to decrease as the failure strain of the parent E-glass composite falls below approximately 1.30%. This is illustrated in figure 105. According to the theory the 1.30% strain level must be that at which the efficiency of the E-glass as a barrier to the propagation of fibre failure is impaired. The four hybrid composite slabs 48, 49, 58 and 59, containing no c.a. E-glass fibres [ε^E of G_6 (no c.-a.) and G_5 (no c.-a.) is 0.88% and 1.06% respectively], all have $\varepsilon^E = \varepsilon' \simeq 0.52\%$ whilst slab 47, $4G_5$ (as rec.) 3C (as rec.) [ε^E of G_5 (as rec.) is 2.02%], has distinct ε^E and ε' values with $\varepsilon^E = 0.60\%$ and $\varepsilon' = 0.76\%$. The trend of these results is in agreement with the theory. The effect of different β values of the E-glass failure strain distributions on ε^E and ε' can not be assessed since it was concluded in section 4.7.2.4 [summary point x)] that the failure strains of the A187, A1100 and no c.-a. E-glass fibres do not follow a Weibull distribution due to damage during the treatment processes. A result which looks out of place in figure 105 is that for slab 56 with $\varepsilon^E = \varepsilon' = 0.67\%$ [$\hat{\varepsilon}_g$ for constituent G_6 (A1100) is 1.61%]. However, ε^E equal to ε' may be explained by an unusual distribution of the constituent 600 tex E-glass fibre (A1100) failure strain in conjunction with the high carbon fibre/resin and E-glass fibre/resin bond strengths. Thus in general the qualitative theoretical predictions and experimental results are compatable.

This section has proposed a failure process for the carbon/E-glass hybrid composites and presented supportive experimental evidence. Previous quantitative theories to explain the hybrid effect are now considered and, where appropriate, developed further.

4.8.11 Quantitative Hybrid Composite Tensile Failure Theories

This section considers the value of existing theories in predicting the hybrid effect in the initial tensile failure stress and strain in relation to the E-glass/carbon/vinyl ester hybrid composites tested here and adapts a statistical failure theory for single fibre type composites to hybrid composites. The literature review mentions theories based on fracture energies[6][28] and covers the statistical theory of Zweben[7]. The original intention was to compare quantitatively the results of the hybrid composites tested here with the theory of Aveston and Sillwood[6] (energy based) and Zweben's statistical theory. However for a number of reasons, some arising from the conclusion that failure of the parent composites and the hybrid composites is a statistical process, the energy based theory is not considered suitable. The theoretical hybrid composite tensile stress v strain behaviour postulated by Aveston and Sillwood is limited, being based on a composite in which the failure of the L.E. fibre does not cause catastrophic failure of the whole composite. Their theory assumes that whenever a L.E. fibre failure occurs this is immediately followed by the failure of all the other L.E. fibres and that these failures are coplanar and perpendicular to the fibres. This is not the case for the E-glass/carbon fibres tested here as is shown by their stress v strain curves and their fracture surfaces. In addition the theory applies to composites with an intimate mixture of fibres. Although the carbon and E-glass fibres are evenly distributed in the composites composed of hybrid tapes the fibres are not intimately mixed. The decision not to compare the experimental results with this theory is probably justified solely by the first assumption stated. However further reasons are the unfulfilled prediction of a secondary modulus (equal to $E_g V_g + E_m V_m$) beyond the first failure strain and the fact that the surface work of fracture of the carbon fibre, γ_f, is not known but is a major term in the equations for the first failure strains. As in reference 6, γ_f would have to be estimated at the corresponding value for graphite of 150 Joules/m^2 and so the theory could not be properly tested. For these reasons the experimental hybrid tensile results are not compared with those predicted by the theory of Aveston and Sillwood.

Consider Zweben's work presented in reference 7. This statistical theory for the tensile strength of hybrid composites is modelled on a unidirectional hybrid composite consisting of two dimensional arrays of alternating H.E. and L.E. fibres. Zweben assumes that impregnated yarns can be treated as fibres, hybrid composites usually being a mixture of yarns rather than single fibres. The lower bound for the composite failure strain is taken as the strain at which the first overstressed H.E. fibre is expected to break and the

analysis is based on the assumption that before the failure strain is reached fibre break propagation in the L.E. fibres is arrested when the crack reaches the H.E. fibres. However the tensile results of the carbon/E-glass/vinyl ester hybrid composites show that the first failure strain is usually caused by failure propagating amongst L.E. fibres and only when a low failure strain E-glass fibre is used in the hybrid is the first failure strain due to failure of overstressed H.E. fibres. Both of these failure processes are considered. The process described by Zweben is considered first. The theory is extended to cover the 3-dimensional composites studied here. Consider a hybrid composite fabricated from layers of 1:1 tape. Treating the yarns as fibres the arrangement of the fibres approximates to an hexagonal array. On average each of the L.E. carbon fibres is surrounded by 2 L.E. and 4 H.E. fibres. In this model there are $\frac{N}{2}$ H.E. and $\frac{N}{2}$ L.E. fibres. Following a parallel analysis to that given by Zweben[7] the tensile failure strain distributions for the L.E. and H.E. fibres are:

$$F_{LE}(\varepsilon) = 1 - \exp(-pL\varepsilon^{q}) \quad \ldots \quad (26)$$

$$F_{HE}(\varepsilon) = 1 - \exp(-rL\varepsilon^{s}) \quad \ldots \quad (27)$$

At the strain ε the expected number of L.E. fibre breaks, X_{LE}, is

$$X_{LE} = \frac{N}{2} J F_{LE}(\varepsilon) \quad \ldots \quad (147)$$

where $J = \frac{L}{\delta_h}$, $(\delta_h \equiv \ell)$

The neighbouring L.E. and H.E. fibres are subjected to strain concentrations, $k_{LE}\varepsilon$ and $k_{HE}\varepsilon$, over the ineffective length of the failed L.E. fibre in the hybrid, δ_h. The probability (P_{HE}) that a H.E. fibre fails due to the increase in strain, $(k_{HE}-1)\varepsilon$, given that it did not fail at ε is

$$P_{HE} = \frac{F_{HE}(k_{HE}\varepsilon) - F_{HE}(\varepsilon)}{1 - F_{HE}(\varepsilon)} \quad \ldots \quad (148)$$

The probability that at least one of the four H.E. fibres surrounding a failed L.E. fibre fails is

$$P_{2HE} = 1 - (1 - P_{HE})^{4} \quad \ldots \quad (149)$$

Therefore the expected number of sites where overstressed H.E. fibres have failed is

$$X_{2HE} = X_{LE} P_{2HE} \quad \ldots \quad (150)$$

The strain at which the first overstressed H.E. fibre failure is expected to occur, ε_{2HE}, is derived by equating equation 149 with unity and making certain simplifying assumptions. ε_{2HE} occurs when the magnitude of the cumulative distribution functions is very much less than one, therefore

the term $F_{HE}(\varepsilon)$ is neglected in the denominator of equation 148 as are products and squares of the functions in equation 149. Thus equations 148 and 149 become

$$P_{HE} = \frac{F_{HE}(k_{HE}\varepsilon) - F_{HE}(\varepsilon)}{1} \quad \ldots \quad (151)$$

$$P_{2HE} = 1 - \left[1 - F_{HE}(k_{HE}\varepsilon) + F_{HE}(\varepsilon)\right]^4$$

$$\simeq 4F_{HE}(k_{HE}\varepsilon) - 4F_{HE}(\varepsilon) \quad \ldots \quad (152)$$

Approximating equations 26 and 27 it follows that $\exp(-pL\varepsilon^q) \simeq 1 - pL\varepsilon^q$ and $\exp(-rL\varepsilon^s) \simeq 1 - rL\varepsilon^s$

$$\therefore \quad F_{LE}(\varepsilon) = pL\varepsilon^q \quad \ldots \quad (153)$$

and

$$F_{HE}(\varepsilon) = rL\varepsilon^s \quad \ldots \quad (154)$$

Substituting for X_{LE} and P_{2HE} in equation 150 and equating with unity it follows that

$$1 = 2LNpr\,\delta_h \varepsilon^q \varepsilon^s (k_{HE}^s - 1)$$

$$\therefore \quad \varepsilon'_{2HE} = \left[2LNpr\,\delta_h\,(k_{HE}^s - 1)\right]^{-1/q+s} \quad \ldots \quad (155)$$

This represents the lower bound on the initial hybrid composite failure strain, ε', given that ε' is due to the failure of overstressed H.E. fibres. The expression for the lower bound failure strain of the L.E. parent composite is

$$\hat{\varepsilon}_L = \left[6NLp^2\delta\,(k_q - 1)\right]^{-1/2q} \quad \ldots \quad (156)$$

Therefore the ratio of the failure strains ε'_{2HE} and $\hat{\varepsilon}_L$ is

$$\frac{\varepsilon'_{2HE}}{\hat{\varepsilon}_L} = \frac{\left[2LNpr\,\delta_h\,(k_{HE}^s - 1)\right]^{-1/q+s}}{\left[6NLp^2\delta\,(k^q - 1)\right]^{-1/2q}} \quad \ldots \quad (157)$$

The equations used to calculate δ, δ_h, k and k_{HE} for a two dimensional composite are those given by Zweben in reference 7.

$$\delta = 1.531\left(\frac{E_{LE}\,A_{LE}\,g}{G_m t_m}\right)^{\frac{1}{2}} \quad \ldots \quad (31)$$

$$\delta_h = \frac{2}{f^{\frac{1}{2}}}\left(\frac{E_{LE}\,A_{LE}\,g}{G_m t_m}\right)^{\frac{1}{2}}\left(\frac{m_2^2 - m_1^2}{m_1(2-m_1^2) - m_2(2-m_2^2)}\right) \quad \ldots \quad (32)$$

$$k = 1.293 \quad \ldots \quad (33)$$

$$k_h = k_{HE} = 1 + \left(\frac{m_2 - m_1}{m_1(2-m_1^2) - m_2(2-m_2^2)}\right) \quad \ldots \quad (34)$$

$$\text{where } f = \frac{E_{LE} A_{LE}}{E_{HE} A_{HE}} \qquad \ldots \quad (35)$$

and

$$m_{1,2} = \left[\frac{f + 1 \pm (f^2 + 1)^{\frac{1}{2}}}{f}\right]^{\frac{1}{2}} \qquad \ldots \quad (36)$$

For the three dimensional parent L.E. composite δ is calculated from equation 3 but in the 1:1 hybrid composite the value of δ for a broken carbon fibre is increased due to 4 H.E. fibres, with a lower elastic modulus, replacing 4 of the 6 neighbouring L.E. fibres. In Zweben's model δ changes to δ_h due to the 2 neighbouring L.E. fibres being replaced by 2 H.E. fibres. Therefore in the three dimensional composite δ_h is assumed to be approximated by δ multiplied by $\frac{2}{3}$ x (the ratio of δ_h/δ as defined by Zweben[7]). Similarly for k and k_{HE}, the three dimensional parent L.E. composite $k = 1.104$ and k_{HE} is approximated by $\frac{2}{3}$ x (the ratio of k_{HE}/k as defined by Zweben[7]).

In practice the experimental ratio of the lower bounds of ε' and $\hat{\varepsilon}_L$ approximate to the ratio of the average values of ε' and $\hat{\varepsilon}_L$. Therefore the ratio of the average experimental strain values are used in comparisons between the theory and experiment.

$\frac{\varepsilon'_{2HE}}{\hat{\varepsilon}_L}$ is now calculated for the 1:1 E-glass/carbon/vinyl ester hybrid composite under consideration, with $V_T = 0.4$.

$$\delta = \left[\frac{1}{2} \cdot \frac{242.1}{2.15}\left(\frac{1 - 0.4^{\frac{1}{2}}}{0.4^{\frac{1}{2}}}\right)\right]^{\frac{1}{2}} 0.5423 = 9.32\text{mm}$$

$$\therefore \delta_h = 9.32 \times \frac{2}{3} \times \frac{2}{1.531} \times \frac{1}{f^{\frac{1}{2}}} \times \frac{m_2^2 - m_1^2}{\left[m_1 (2 - m_1^2) - m_2 (2 - m_2^2)\right]}$$

$$\text{where } f = \frac{242.1}{75.6} = 3.20$$

and $m_1 = 1.54$ and $m_2 = 0.52$

$$\therefore \delta_h = 9.25\text{mm}$$

$$k = 1.104$$

$$k_{HE} = 1.104 \times \frac{2}{3} \times 1.693 = 1.246$$

$$N = \frac{\text{c.s.a. specimen}}{\text{c.s.a. carbon tow}} \quad (\simeq \text{c.s.a. 600 tex E-glass tow})$$

$$= 34.6$$

$$L = 50\text{mm}$$

Zweben estimated the Weibull parameters for the L.E. and H.E. 'fibres', p, q, r and s, from the tensile characteristics of their parent composites. In the absence of impregnated tow data the same is done here. For the carbon composites the average failure strain is 0.47% with a CV of 8.10% at L = 50mm. The 600 tex E-glass composites have an average failure strain of 1.96% with a CV of 6.63%. The resultant Weibull parameters calculated from parallel equations to 16 and 48 are:

$$p = 1287.1; \quad q = 15.36; \quad r = 3.07 \times 10^{-8}; \quad s = 19.10.$$

Substituting these values into equation 157 gives the theoretical ratio for the lower bounds of $\frac{\varepsilon'_{2HE}}{\hat{\varepsilon}_L}$

$$\frac{\varepsilon'_{2HE}}{\hat{\varepsilon}_L} = \frac{\left[2.0 \times 50 \times 34.6 \times 1287.1 \times 3.07 \times 10^{-8} \times 9.25\,(1.246^{19.10} - 1)\right]^{-\frac{1}{15.36+19.10}}}{\left[6 \times 34.6 \times 50 \times 1287.1^2 \times 9.32\,(1.104^{15.36} - 1)\right]^{-\frac{1}{2\times 15.36}}}$$

$$= 2.14$$

This is greater than the ratio 0.60/0.47 = 1.28 obtained experimentally for the average failure strains of the 1:1 hybrid and parent carbon composites. This is as expected since the first failure strain for the 1:1 tape hybrids is caused by the propagation of failure amongst the L.E. tows. Therefore $\varepsilon' \equiv \varepsilon'_{2LE}$, the strain at which the first overstressed L.E. tow is expected to fail. This alternative failure process is now considered for the 1:1 hybrids. The hybrid composite is regarded as carbon tows in a matrix of E-glass/vinyl ester resin. Therefore ε'_{2LE} is represented by the same equation 156 as $\hat{\varepsilon}_L$ but with N, δ and k replaced by $\frac{N}{2}$, δ_{LE} and k_{LE}. This gives the ratio of the lower bounds to the failure strains ε'_{2LE} and $\hat{\varepsilon}_L$ as

$$\frac{\varepsilon'_{2LE}}{\hat{\varepsilon}_L} = \frac{\left[3NLp^2\delta_{LE}(k_{LE}^q - 1)\right]^{-1/2q}}{\left[6NLp^2\delta(k^q - 1)\right]^{-1/2q}} = \left[\frac{\delta_{LE}(k_{LE}^q - 1)}{26(k^q - 1)}\right]^{-1/2q} \quad \ldots \quad (158)$$

δ_{LE} is calculated from equation 3 in which G_m is equal to 4.88KN/mm^2, the shear modulus of the 600 tex E-glass/vinyl ester resin matrix, $V_{g6} = 0.25$ (see figure 37).

$$\therefore \quad \delta_{LE} = \left[\frac{1}{2} \cdot \frac{242.1}{3.90}\left(\frac{1 - 0.2^{1/2}}{0.2^{1/2}}\right)\right]^{1/2} 0.5423 = 3.36\text{mm}$$

$\delta = 9.32$mm, $k = 1.104$ and $q = 15.36$

The unknown value is k_{LE}. The strain concentration due to a failed carbon tow acts primarily on the E-glass tows in the 'matrix' and therefore the strain concentration k_{LE} acting on the neighbouring carbon tows must be considerably reduced below k. In order to gain an approximate idea of the validity of equation 158 k_{LE} is estimated. The value chosen for k_{LE} is $\left[1 + \left(\frac{k-1}{3}\right)\right] = 1.035$. The reason for this is that on average each carbon tow is surrounded by six tows, two of which are carbon. It is recognized that this estimate of k_{LE} is a likely source of error. The strain ratio as given by equation 158 is now calculated.

$$\frac{\varepsilon'_{2LE}}{\hat{\varepsilon}_L} = \left[\frac{3.36\ (1.035^{15.36} - 1)}{18.64\ (1.104^{15.36} - 1)}\right]^{-1/30.72}$$

$$\therefore \quad \frac{\varepsilon'_{2LE}}{\hat{\varepsilon}_L} = \left[\frac{2.34}{66.56}\right]^{-1/30.72} = 1.12$$

This is below the experimental ratio for the average strains of 1.28 suggesting that k_{LE} is overestimated by the value 1.035. However, the values obtained for the strain ratios $\frac{\varepsilon'_{2HE}}{\hat{\varepsilon}_L}$ and $\frac{\varepsilon'_{2LE}}{\hat{\varepsilon}_L}$ are promising considering the simplifications adopted and the use of the parent composite tensile results in calculating the Weibull parameters for the carbon and 600 tex E-glass tows. The theory correctly predicts that the first failure strain occurs due to propagation of failure amongst the L.E. tows, since $\frac{\varepsilon'_{2HE}}{\hat{\varepsilon}_L} > \frac{\varepsilon'_{2LE}}{\hat{\varepsilon}_L}$.

So far only the specific case of a 1:1 tape hybrid composite has been considered. If the ratio of H.E./L.E. fibres is increased ε'_{2HE} also increases due to the reduction in the number of L.E. fibres decreasing the expected number of L.E. fibre breaks at a given strain. This effect is greater than the opposing effect of the increase (up to a ratio of 3:1) in the number of H.E. fibres surrounding each L.E. fibre. For example for a 3:1 hybrid tape composite one quarter of the fibres are L.E. but each of these is surrounded by 6 H.E. fibres. The strain ratio calculated in the same manner as for the 1:1 composites becomes

$$\frac{\varepsilon'_{2HE}}{\hat{\varepsilon}_L} = \frac{\left[1.5LNpr\delta_h\left(k_{HE}^{\beta} - 1\right)\right]^{-1/q+s}}{\left[6LNp^2\delta\left(k^q - 1\right)\right]^{-1/2q}} \qquad \ldots \quad (159)$$

Assuming that the values of δ_h and k_{HE} do not change significantly equation 159 for a 600 tex E-glass/carbon/vinyl ester composite with $V_T = 0.4$ produces the value 2.16 compared with 2.14 from equation 157 for 1:1 hybrid composites.

The ratio $\frac{\varepsilon'_{2LE}}{\hat{\varepsilon}_L}$ also increases as the H.E./L.E. fibre ratio increases. For a 3:1 hybrid tape composite the ratio given in equation 158 (for 1:1 composites) becomes

$$\frac{\varepsilon'_{2LE}}{\hat{\varepsilon}_L} = \left[\frac{\delta_{LE}\,(k_{LE}^{q} - 1)}{4\delta\,(k^{q} - 1)}\right]^{-\frac{1}{2}q} \qquad \ldots \quad (160)$$

However, both the values of δ_{LE} and k_{LE} change. δ_{LE} is calculated from equation 3 with (for a 3:1 600 tex E-glass/carbon/vinyl ester hybrid composite with $V_T = 0.4$) G_m equal to that of a composite with $V_{g6} = V_T = 0.33$.

$$\therefore \quad \delta_{LE} = \left[\frac{1}{2} \cdot \frac{242.1}{4.88}\left(\frac{1 - 0.1^{\frac{1}{2}}}{0.1^{\frac{1}{2}}}\right)\right]^{\frac{1}{2}} 0.5423 = 3.97\text{mm}$$

k_{LE} is reduced due to the increase in the average separation of the carbon fibres. Again this value has to be estimated. It is arbitrarily given the value of 1.015. Substituting into equation 160 it follows that

$$\frac{\varepsilon'_{2LE}}{\hat{\varepsilon}_L} = \left[\frac{3.97\,(1.015^{15.36} - 1)}{4 \times 9.32\,(1.104^{15.36} - 1)}\right]^{-\frac{1}{2}q} = 1.17$$

The comparative increases in the $\frac{\varepsilon'_{2HE}}{\hat{\varepsilon}_L}$ and $\frac{\varepsilon'_{2LE}}{\hat{\varepsilon}_L}$ ratios suggest that as the ratio of H.E./L.E. fibre increases the probability of ε' occuring due to the failure of an overstressed H.E. fibre increases. This is logical since ε' of E-glass/carbon/vinyl ester hybrid composites is shown in section 4.8.8 to increase with E-glass (H.E.)/carbon (L.E.) fibre ratio, reducing the difference between ε' and the expected failure strain of the parent E-glass composite.

Rosen's theory[1] for the average fibre stress at the failure of a single fibre type composite, $\hat{\sigma}_f$, is now adapted to hybrid composites. The theory ignores the effect of stress concentrations due to failed fibres and therefore the following equation is regarded as the upper bound on composite strength.

$$\hat{\sigma}_f = (\alpha\beta\delta e)^{-1/\beta} \quad . \ . \ . \quad (7)$$

Composite failure is assumed to occur due to a chance accumulation of fibre failures over one region. The above equation for $\hat{\sigma}_f$ is equal to the mean strength of a bundle of the fibres of length δ. A basic assumption in the theory is that extensional stresses in the matrix are negligible in comparison to those in the fibres. To apply the theory to hybrid composites containing L.E. and H.E. fibres it is first assumed that it is the accumulation of L.E. fibre failures which weaken a region sufficiently to cause further substantial L.E. fibre failure and possibly H.E. fibre failure. It is assumed that up to this point, σ', that failure of H.E. fibres is negligible and the hybrid composite is regarded as L.E. fibres in a matrix of H.E. fibres and resin. The basic assumption of Rosen's theory is no longer valid and the extensional stresses in the H.E. fibres must be considered. To achieve this the H.E. fibres in the hybrid are converted into equivalent L.E. fibres as is outlined below. Firstly the proportion of failed L.E. fibres in a bundle of L.E. fibres of length δ expected to cause the failure of the whole bundle is estimated. This corresponds to the expected proportion of fibre failures in a L.E. fibre composite over a region of length δ which causes the failure of the whole composite.

In a bundle of fibres of length δ the expected proportion of fibre failures at bundle failure is the probability of fibre failure up to or at the failure stress level. The Weibull distribution for fibre strength is given by equation 12 which approximates to equation 161.

$$F(\sigma) = 1 - \exp(-\alpha L \sigma^{\beta}) \simeq \alpha L \sigma^{\beta} \quad . \ . \ . \quad (161)$$

Thus for a fibre of length δ the probability of failure at $\hat{\sigma}_f$ is given by equation (162)

$$F(\sigma) = \alpha\delta\left[(\alpha\delta\beta e)^{-1/\beta}\right]^{\beta} = (\beta e)^{-1} \quad . \ . \ . \quad (162)$$

and is equivalent to the proportion of fibre failures expected to cause composite failure. In a hybrid composite the failure of this same proportion of L.E. fibres in a region of length δ_{LE} can not be expected to cause the rest of the L.E. fibres to fail since the H.E. fibres bear a significant proportion of the redistributed stress from the failed L.E. fibres. The effective number of L.E. fibres, N_{EL}, becomes

$$N_{EL} = N_{LE} + N' \quad . \ . \ . \quad (163)$$

where N_{LE} = the number of L.E. fibres

N' = the number of L.E. fibres which the H.E. fibres are equivalent to

N' is calculated from the extensional properties of the two fibre types and the number of H.E. fibres, N_{HE}.

$$N' = \frac{E_{HE}}{E_{LE}} \times \frac{\text{c.s.a. of H.E. fibres}}{\text{c.s.a. of L.E. fibres}} \times N_{HE} \quad . \; . \; . \quad (164)$$

As previously stated failure of the H.E. fibres up to σ' is assumed to be negligible. Therefore the number of fibre failures expected to cause the first substantial failure of the L.E. fibres (n) must come from the N_{LE} L.E. fibres. n is calculated from the effective number of L.E. fibres.

$$n = N_{EL} \; (\beta e)^{-1} \quad . \; . \; . \quad (165)$$

The stress, σ', at which n fibres of length δ_{LE} are expected to have failed is calculated from the equation

$$\frac{n}{N_{LE}} = \alpha \delta_{LE} \sigma^{\beta}$$

$$\therefore \quad \sigma' = \left(\frac{\alpha N_{LE} \delta_{LE}}{n} \right)^{-1/\beta} \quad . \; . \; . \quad (166)$$

Equation 166 divided by equation 7 gives the ratio of $\frac{\sigma'}{\hat{\sigma}_f}$ which equals $\frac{\varepsilon'}{\hat{\varepsilon}_f}$.

$$\frac{\sigma'}{\hat{\sigma}_f} = \frac{\varepsilon'}{\hat{\varepsilon}_f} = \left[\frac{\alpha N_{LE} \delta_{LE} \beta e}{N_{EL} \alpha \delta \beta e} \right]^{-1/\beta} = \left(\frac{N_{LE} \delta_{LE}}{N_{EL} \delta} \right)^{-1/\beta} \quad . \; . \; . \quad (167)$$

Now consider a 1:1 600 tex E-glass/carbon/vinyl ester resin hybrid composite with $V_T = 0.4$. The tows are again treated as fibres and β in equation 167 is replaced by q = 15.36. $N_{LE} = 17.3$, $N_{EL} = 22.7$, $\delta_{LE} = 3.97$mm and $\delta = 9.32$mm

$$\therefore \quad \frac{\varepsilon'}{\hat{\varepsilon}_f} = \left(\frac{17.3 \times 3.97}{22.7 \times 9.32} \right)^{-1/15.36} = 1.08$$

For a 3:1 600 tex E-glass/carbon/vinyl ester hybrid composite with $V_T = 0.4$, $N_{LE} = 8.7$, $N_{EL} = 16.8$, $\delta_{LE} = 3.97$ and $\delta = 9.32$:

$$\frac{\varepsilon'}{\hat{\varepsilon}_f} = \left(\frac{8.7 \times 3.97}{16.8 \times 9.32}\right)^{-1/15.36} = 1.10$$

This extension of Rosen's theory predicts the correct trend in $\frac{\varepsilon'}{\hat{\varepsilon}_f}$ with V_{gl}/V_{cf} but the errors in the actual values are greater than those in the values of $\frac{\varepsilon'_{2LE}}{\hat{\varepsilon}_L}$ calculated from Zweben's adapted theory. This is not surprising since the failure process assumed when deriving $\frac{\varepsilon'_{2LE}}{\hat{\varepsilon}_L}$ corresponds more closely than that assumed when deriving $\frac{\varepsilon'}{\hat{\varepsilon}_f}$ to the actual failure process suggested for the hybrids in section 4.8.10. It seems that Zweben's adapted theory for the strain ratios has greater potential than Rosen's extended theory.

Inaccuracies in the theoretical ratios $\frac{\varepsilon'_{2HE}}{\hat{\varepsilon}_L}$ and $\frac{\varepsilon'_{2LE}}{\hat{\varepsilon}_L}$ stem largely from the original assumption that the two fibre types are intimately mixed which necessarily led to the treatment of the tows as single fibres. In addition fibre debonding is not considered. A more meaningful test of the ratios requires tensile data for the impregnated tows and accurate values for δ_{LE}, δ_H and k_{HE}.

When comparing the experimental tensile results of the parent composites with the statistical theories, Barry's model[4] appeared more accurate than Rosen's and Zweben's. Unfortunately it is unsuitable for adaptation to the tensile failure of hybrid composites since it considers a unit of approximately 4000 fibres and assumes that when all of these fibres fail (due to stress concentrations within the unit) complete failure of the composite follows. 4000 fibres are equivalent to 0.67 of a carbon tow. In the E-glass/carbon hybrid composites the failure of such a unit may spread through the rest of the tow but the hybrid failure theory predicts the suppression of propagation between carbon tows by the E-glass tows. Therefore the failure of a unit of 4000 fibres is not likely to result in ε'. Treatment of the carbon tows as single fibres is inappropriate since in a parent carbon composite with $V_{cf} = 0.40$ there are 34.6 carbon tows, considerably less than the 4000 fibres in Barry's model.

This section is concluded by reviewing the major points arising from the adaptation of Zweben's thoery.

The adaptation of Zweben's theory produced two equations for the ratios of the lower bound of the first failure strain of a hybrid composite to that of the parent L.E. fibre composite. For a 1:1 hybrid composite the equations are 157 and 158.

$$\frac{\varepsilon'_{2HE}}{\hat{\varepsilon}_L} = \frac{\left[2LNpr\,\delta_h\,(k_{HE}^{s}-1)\right]^{-\frac{1}{q+s}}}{\left[6LNp^2\,\delta\,(k^q-1)\right]^{-\frac{1}{2q}}} \qquad \ldots \quad (157)$$

$$\frac{\varepsilon'_{2LE}}{\hat{\varepsilon}_L} = \left[\frac{\delta_{LE}(k_{LE}^{q}-1)}{2\delta(k^q-1)}\right]^{-\frac{1}{2q}} \qquad \ldots \quad (158)$$

Equation 157 applies when ε' occurs due to the propagation of a L.E. fibre into a H.E. fibre in which case catastrophic failure of the hybrid is expected. Equation 158 applies when ε' occurs due to the propagation of a L.E. fibre failure into another L.E. fibre in which case the failure is not likely (for the 1:1 ratio under consideration) to be catastrophic. Thus comparison between the ratios $\frac{\varepsilon'_{2HE}}{\hat{\varepsilon}_L}$ and $\frac{\varepsilon'_{2LE}}{\hat{\varepsilon}_L}$ enables the prediction of the composite failure mode. The application of equations 157 and 158 to the 1:1 hybrid tape composites tested here predicted the correct failure mode for ε' of propagation amongst the L.E. fibres. Quantitatively when compared with the ratio of the average experimental strains for the 1:1 and the carbon composites the theory is conservative but promising considering the number of possible sources of error in the values used for the parameters. Accurate methods for calculating δ_{LE}, δ_h and k_{HE} are particularly important.

5. CONCLUSIONS

The following conclusions concerning the range of carbon fibre/E-glass fibre/vinyl ester hybrid composites investigated are drawn from the results obtained in this study. The points refer to i) the existence of hybrid effects, ii) the dependence of hybrid effects on the hybrid parameters varied, iii) the tensile failure mode, and, iv) ~~theoretical~~ failure theories for the prediction of the initial failure strain of hybrid composites.

i) Hybrid composites can be fabricated to exhibit positive hybrid effects in initial tensile stress and strain (σ' and ε'), positive or negative hybrid effects in maximum tensile stress ($\hat{\sigma}$) and large negative hybrid effects in maximum tensile strain ($\hat{\varepsilon}$). The elastic modulus (E) of the hybrid composites follows the rule of mixtures. The positive hybrid effect in initial tensile failure is of prime practical importance.

ii) The magnitude of any positive hybrid effect in σ' and ε' is dependent upon the ratio of V_g/V_{cf}, the fibre geometrical arrangement and the tensile characteristics of the E-glass fibres. ε' of the hybrids with an even, intralayer mixing of fibre tow types approximates to equation 128.

$$\varepsilon' = 0.47\left(1 + \frac{V_g}{V_{cf}}\right)^{0.36}\eta \qquad \ldots \quad (128)$$

Changes in the fibre geometrical arrangement alter the values of ε' and σ' and distinct elastic limit and initial failure values can be obtained. The E-glass tensile characteristics become important at low E-glass failure strains ($\hat{\varepsilon}_g$) when reductions in $\hat{\varepsilon}_g$ towards the normal failure strain of the carbon fibres decreases the extent of the hybrid effect in σ'. Total fibre content has no effect on ε' and any effect due to changing fibre/resin interfacial shear strength appears negligible. The magnitude of the hybrid effect in $\hat{\sigma}$ is dependent upon the same parameters as is the hybrid effect in σ' and ε'. In hybrid composites with an intimate and even mixture of fibre tow types there is a positive hybrid effect in $\hat{\sigma}$. In composites with a low V_g/V_{cf} ratio, such that $\hat{\sigma} = \sigma'$, the positive hybrid effect is a direct consequence of that in σ', tending to zero as $V_{cf} \rightarrow V_T$. When V_g/V_{cf} is high the positive hybrid effect is attributed to carbon fibres continuing to bear stress beyond σ', the effect tending to zero as $V_g \rightarrow V_T$. A decrease in the degree of mixing of fibre tow types acts to reduce the positive hybrid effect in $\hat{\sigma}$ and in extreme cases small negative hybrid effects occur. The effect of the tensile characteristics of the E-glass fibres on the

value of $\hat{\sigma}$ is parallel to that on the values of σ' and ε'. The magnitude of the hybrid effect in $\hat{\varepsilon}$ is also dependent upon the ratio V_g/V_{cf}, fibre geometrical arrangement and the E-glass fibre tensile characteristics. The magnitude of the negative hybrid effect is reduced by both increases in the degree of fibre mixing and in the ratio V_g/V_{cf}. The tensile characteristics of the E-glass fibres affect the magnitude of the hybrid effect in $\hat{\varepsilon}$ when the tensile properties of the E-glass are reduced sufficiently for catastrophic hybrid failure to occur at ε' i.e. for the value of $\hat{\varepsilon}$ to equal, and so be controlled in the same manner as, ε'.

iii) The major characteristics of the hybrid composite tensile stress v strain curves are explained by a failure mode based upon the statistical natures of the fibre tensile strengths. The important point is that the H.E. E-glass fibres impede propagation of accumulating single and multiple carbon fibre failures (which in a parent carbon composite could lead to catastrophic failure), so suppressing initial failure.

iv) The energy based hybrid composite tensile failure theory postulated by Aveston and Sillwood[6] is unsuitable for the carbon/E-glass hybrid composites. Adaptations of Rosen's[1] and Zweben's[7] statistical failure theories were considered, with Zweben's showing the greater potential. The modifications to and extension of Zweben's theory produced two equations for the ratio of the lower bound on hybrid composite initial tensile failure strain to that on the L.E. fibre parent composite tensile failure strain. They are applicable to unidirectional hybrid composite systems in which the H.E. and L.E. fibres are intimately and evenly mixed, have an hexagonal array and a ratio of 1:1. Equation 157 applies when initial failure strain is due to the failure of a L.E. fibre failure propagating through a H.E. fibre. Equation 158 applies when initial failure is due to the propagation of fibre failure amongst L.E. fibres.

$$\frac{\varepsilon'_{2HE}}{\hat{\varepsilon}_L} = \frac{\left[2LNpr\,\delta_h\left(k_{HE}^{s}-1\right)\right]^{-\frac{1}{q+s}}}{\left[\delta LNp^2\delta\left(k^q-1\right)\right]^{-1/2q}} \qquad \ldots (157)$$

$$\frac{\varepsilon'_{2LE}}{\hat{\varepsilon}_L} = \left[\frac{\delta_{LE}\left(k_{LE}^{q}-1\right)}{2\delta\left(k^q-1\right)}\right]^{-1/2q} \qquad \ldots (158)$$

Comparison between the two ratios for a composite system enables the prediction of the composite failure mode, indicating whether or not initial failure is expected to be catastrophic. When compared with the experimental results for the 1:1 tape hybrid composites the correct tensile failure mode is predicted but the theoretical strain ratio is conservative, giving a value of 1.12 compared with the experimental value of 1.28. Despite this inaccuracy the theory is promising considering that the hybrid fibre ineffective lengths and strain concentration factors are estimated and that it was necessary to treat the fibre tows in the actual hybrid composites as individual fibres in the model composite.

6. RECOMMENDATIONS FOR FUTURE WORK

Further research directed towards the following is recommended.

i) The effect of L.E. fibre bundle size on hybrid composite properties.

ii) The effect of total composite volume on hybrid composite properties.

iii) The effect of changing the L.E. fibre tensile characteristics (is the initial failure strain of the hybrid composites affected as predicted by the statistical failure theory?).

iv) The development of models for ineffective lengths and stress concentration values in 3-dimensional hybrid composites.

v) The development of the simple hybrid model, upon which the statistical tensile failure theory is based, to fit practical hybrid composites in which fibre tows rather than individual fibres are mixed.

vi) The extension of the quantitative statistical theory for hybrid initial tensile failure strain to include a factor dependent upon the ratio of H.E./L.E. fibres.

vii) The hybrid effects in cross-ply hybrid composites compared with those in unidirectional hybrid composites.

The monitoring of acoustic emission during future testing of hybrid composites is highly recommended. Careful interpretation of the data may provide a valuable picture of the internal failure process and a means of quantifying the extent of L.E. fibre failure occurring prior to the initial tensile failure strain of the hybrid composite.

REFERENCES

1. ROSEN, B.W. "Tensile Failure of Fibrous Composites" AIAA Journal, Vol. 2, No. 11, 1964, pp 1985 - 1991.

2 ZWEBEN, C. "Tensile Failure of Fiber Composites" AIAA Journal, Vol. 6, No. 12, 1968, pp. 2325 - 2331.

3 ZWEBEN, C. "A Bounding Approach to the Strength of Composite Materials" Eng. Frac. Mech., Vol. 4, 1972, pp. 1 - 8.

4 BARRY, P.W. "The Longitudinal Tensile Strength of Unidirectional Fibrous Composites" J. Mat. Sci., Vol.13, 1978, pp. 2177 - 2187.

5 HAYASHI, T. "On the Improvement of Mechanical Properties of Composites by Hybrid Composition" Proc. of 8th Int. Reinf. Plas. Conf., 1972, pp. 149 - 152.

6 AVESTON, J. and SILLWOOD, J.M. "Synergistic Fibre Strengthening in Hybrid Composites" J. Mat. Sci., Vol. 11, 1976, pp. 1877 - 1883.

7 ZWEBEN, C. "Tensile Strength of Hybrid Composites" J. Mat. Sci., Vol. 12, 1977, pp. 1325 - 1337.

8 PARRATT, N. J. "Defects in Glass Fibres and their Effect on the Strength of Plastic Mouldings" Rubber and Plas. Age, March,1960, pp. 263 - 266.

9 ROSEN, B.W. "Strength of Uniaxial Fibrous Composites" Mechanics of Composite Materials, Ed. Wendt, F.W., Liebowits, H. and Perone, N., Pergamon, Oxford, 1970, pp. 621 - 652.

10 GRINIUS, V.G. "Analytical and Experimental Micromechanics Studies" 10th Nat. S.A.M.P.E. Symposium on Advanced Fibrous Reinforced Composites, San Diego, 1966, G1 - G12.

11 LIPTAI, R.G. "Acoustic Emissions from Composite Materials" Comp. Mat. Testing and Des. (2nd Conf.) ASTM STP 497, 1972, pp. 285 - 298.

12 BLAKELOCK, H.D. and LOVELL, D.R. "High Modulus Reinforcing Carbon" 24th Ann. Tech. Conf. Reinf. Plast./Comp. Div., S.P.I., 1969, Section 6B, pp. 1 - 12.

13 HARRIS, B. "The Strength of Fibre Composites" Comps. July, 1972, pp. 152 - 167.

14 FUWA, M., BUNSELL, A.R. and HARRIS, B. "Tensile Failure Mechanisms in Carbon Fibre Reinforced Plastics" J. Mat Sci., Vol. 10, 1975, pp. 2062 - 2070.

15 FUKUDA, H. and KAWATA, K. "On the Strength Distribution of Unidirectional Fibre Composites" Fib. Sci. and Tech., Vol. 10, No. 1, 1977 pp 53 - 63.

16 BARRY, P.W. "Experimental Data for the Longitudinal Tensile Strength of Unidirectional Fibrous Composites - Part 2: Composites" Fib. Sci and Tech., Vol. 11, No. 5. 1978, pp 319 - 327.

17 BEAUMONT, P.W.R. and HARRIS, B. "The Energy of Crack Propagation in Carbon Fibre - Reinforced Resin Systems" J. Mat. Sci., Vol. 7, 1972 pp 1265 - 1279.

18 OUTWATER, J.O. and MURPHY, M.C. "On the Fracture Energy of Uni-Directional Laminates" 24th Ann. Tech. Conf., Reinf. Plast./Comp. Div., S.P.I., 1969, Section 11C, pp 1 - 8.

19 HANCOX, N.L. (Ed.) "Fibre Composite Hybrid Materials" Appl. Sci. Pub.,1981.

20 SHORT, D and SUMMERSCALES, J. "Hybrids - A Review, Part 2. Physical Properties" Comps., Jan., 1980, pp 33 - 38.

21 HARDAKER, K.M. and Richardson, M.O.W. "Hybrid Composites - A Review" 35th Ann. Tech. Conf., Reinf. Plasts./Comp. Inst., S.P.I., 1980, Section 17F, pp. 1 - 5.

22 KALNIN, I.L. "Evaluation of Unidirectional Glass-Graphite Fiber/Epoxy Resin Composites" Comp. Mat: Testing and Des. (2nd Conf.), ASTM STP 497, 1972, pp 551 - 563.

23 MARSHALL, D.A.G. "The Mechanical Properties of Glass/Carbon Composites Manufactured by a Vacuum Box Moulding Technique" M.Sc. Thesis, Lancaster University, 1974.

24 BUNSELL, A.R. and HARRIS, B. "Hybrid Carbon and Glass Fibre Composites" Comps., July, 1974, pp 157 - 164.

25. PHILLIPS, L.N. "The Hybrid Effect - Does It Exist?" Comps., Jan., 1976 pp 7 - 8.

26 PHILLIPS, L.N. "On the Usefulness of Glass Fibre - Carbon Hybrids" Reinf. Pla. Congress, Brighton, 1976, pp 207 - 211.

27 MAROM, G., FISCHER, S., TULER, F.R. and WAGNER, H.D. "Hybrid Effects in Composites: Conditions for Positive or Negative Effects Versus Rule-of-Mixtures Behaviour" J. Mat. Sci., Vol. 13, 1978, pp 1419 - 1426.

28 AVESTON, J. and KELLY, A. "Tensile First Cracking Strain and Strength of Hybrid Composites and Laminates" Phil. Trans. Roy. Soc. London, A294, 1980, pp. 519 - 534.

29 YIP, H.W.C. and SHORTALL, J.B. "The Interfacial Bond Strength in Glass

Surface Treatment" J. Adh., Vol. 8, 1976, pp. 155 - 169.

30 PLUEDDEMANN, E.P. "Catalytic Effects in Bonding Thermosetting Resins to Silane - Treated Fillers "Am. Chem. Soc. Div. Org. Coat. Plast. Chem., Vol. 33 No. 2, 1973, pp 115 - 119.

31 DI BENEDETTO, A.T. and NICOLAIS, L. "Interfaces in Composites" Advances in Composite Materials, Ed. Piatti, G., Appl. Sci. Pub., 1978, pp 153 - 169.

32 McKENNA, "Interlaminar Effects in Fibre Reinforced Plastics" Polym. Plast. Tech. and Eng., Vol. 5, 1975, pp 24 - 53.

33 OLSTER, E.F. "Effect of Voids on Graphite Reinforced Composites" AVCO Corporation, Contract No. NO0019-71-C-0305, 1972.

34 PROSEN, S.P., MUELLER, C.E. and BARNETT, F.R. "Interlaminar Shear Properties of Filament Wound Submergence Vessels" 19th Ann. Tech. Conf. Reinf. Pla. Div., S.P.I., 1974, Section 9D, pp 1 - 9.

35 COURTAULDS LTD., "Grafil Test Methods" 1977.

36 STURGEON, J.B. "Specimens and Test Methods for Carbon Fibre Reinforced Plastics" R.A.E. Tech. Rep., T.R. 71026 (Mat 126), 1976.

37 CLARK, D., WADSWORTH, N.J. and WATT, W. "The Surface Treatment of Carbon Fibres for Increasing the Interlaminar Shear Strength of C.F.R.P." Pla. Inst. Conf. on Carbon Fibres, Their Place in Modern Technology, 1974, Paper No. 7, pp 44 - 51.

38 PHILLIPS, D.C. and HARRIS, B. "The Strength, Toughness and Fatigue Properties of Polymer Composites" Polymer Engineering Composites, Ed. Richardson, M.O.W., App. Sci. Pub., 1977, pp 126 - 128.

39 A.S.T.M. D 2344-76, "Apparent Horizontal Shear Strength of Reinforcement Plastics by Short Beam Shear Method."

40 HANCOCK, P. and CUTHBERTSON, R.C. "The Effect of Fibre Length and Interfacial Bond in Glass Fibre - Epoxy Resin Composites" J. Mat. Sci., Vol. 5, 1970, pp 762 - 768.

41 VAUGHAN, D.J. "The Resin - Glass Interface and Its Role in Reinforced Composites" R.P.G. Conf. on New and Improved Resin Systems, 1973, pp 1 - 12.

42 VAUGHAN, D.J. "A History of Coupling Agent Development" 35th Ann. Conf. S.P.E., 1977, pp 330 - 332.

43 CHAMBERLAIN, D.L. Jr., CHRISTENSEN, M.V. and BERTOLUCCI, M. "A study of Bonding Between Glass and Plastic in Glass Reinforced Plastics (Part II)"

24th Ann. Tech. Conf., Reinf. Plast./Comp. Div., S.P.I., 1969, Section 19C, pp 1 - 12.

44 UNION CARBIDE TRADE LITERATURE "Silanes, Methods of Application."

45 SIDLOVSKY, J. "New Developments in the Application of Silane Glass Finishes" 14th Ann. Meet. of Reinf. Pla. Div., S.P.I., 1959, Section 13F, pp 1 - 3.

46 BASCOM, W.D. "Some Surface Chemical Aspects of Glass-Resin Composites Part I - Wetting Behaviour of Epoxy Resins On Glass Filaments" 20th Ann. Meet. of Reinf. Pla. Div., S.P.I., 1965, Section 15B, pp 1 - 14.

47. DESIGN-ENGINEERING SERIES "Carbon Fibres" Morgan-Grampion Pub. Ltd., 1970, pp 8 - 11.

48 CLARKE, A.J. and BAILEY, J.E. "The Role of Oxidation in Carbon Fibre Formation from Polyacrylonitrile" Plas. Inst. Conf. on Carbon Fibres, Their Place in Modern Technology, 1974, paper 2, pp 12 - 15.

49 WATT. W., JOHNSON, D.J. and PARKER, E. "Pyrolysis and Structure Development in the Conversion of PAN Fibres to Carbon Fibres" Plas. Inst. Conf. on Carbon Fibres, Their Place in Modern Technology, 1974, paper 1, pp 3 - 11.

50 JOHNSON, D.J. "Recent Advances in Studies of Carbon Fibre Structure" Phil. Trans. Roy. Soc. London, A294, 1980, pp 443 - 449.

51 BARNET, F.R. and NORR, M.K. "The Etching of Carbon Fibres to Show Structure" Plas. Inst. Conf. on Carbon Fibres, Their Place in Modern Technology, 1974, paper 6, pp 32 - 43.

52 DONNET, J.B., PAPIRER, E. and DAUKSCH, H. "Surface Modification of Carbon Fibres and Their Adhesion to Epoxy Resins" Pla. Inst. Conf. on Carbon Fibres, Their Place in Modern Technology, 1974, paper 9, pp. 58 - 64.

53 RIESS, G., BOURDEAUX, M., BRIE, M. and JOUQUET, G. "Surface Treatment of Carbon Fibres With Alternating and Block Copolymers" Pla. Inst. Conf. on Carbon Fibres, Their Place in Modern Technology, 1974, paper 8, pp. 52-57.

54 HYFIL LTD. "Hyfil Torayca Carbon Fibre" Technical Data.

55 T.B.A. LTD., Private Communication.

56 SHARP, J.V., BURNAY, S.C., MATTHEWS, J.R. and HARPER, E.A. "Defect Limitations to the Strength of Carbon Fibres" Pla. Inst. Conf. on Carbon Fibres, Their Place in Modern Technology, 1974, paper 5, pp 25-30.

57 ZWEBEN, C., SMITH, W.S. and WARDLE, M.W. "Test Methods for Fibre Tensile Strength, Composite Flexural Modulus, and Properties of Fabric - Reinforced Laminates" Comp. Mat: Testing and Des. (5th Conf.), ASTM STP 674, 1979, pp 228 - 262.

58 LANZA, F. "Statistical Evaluation of the Strength of Composite Materials" Advances in Composite Materials, Ed. G. Piatti, App. Sci. Pub., 1978, pp 238.

59 VETTERS, C.M. "Derakane Vinyl Ester Resins Show Improved Chemical Resistance for Corrosion Control" 25th Ann. Tech. Conf., Reinf. Plasts./Comp. Div., S.P.I., 1970, Section 4B pp 1 - 4.

60 PHILLIPS, L.N. and MURPHY, D.J. "Vinyl Esters as a Matrix For Carbon Fibre Laminates" R.A.E. Tech. Memo, Mat. 201, 1974.

61 ROLSTON, J.A. "Fiberglass Composite Materials and Fabrication Processes" Chem. Eng. Jan. 28, 1980, pp 96 - 110.

62 DOW CHEMICAL COMPANY "General Bulletin Derakane Vinyl Ester Resins" Trade Literature.

63 VARCO, P. and SEAMARK, M.J. "Vinyl Ester Resins" R.P.G. Conf. on New and Improved Resin Systems, Sept., 1973, paper 3.

64 DOW CHEMICAL COMPANY "Derakane Chemical Resistance Guide" Technical Bulletin.

65 CLAUS, W.D. Jr. "Filament Misalignment and Composite Strength" Comp. Mat.: Testing and Des. (2nd Conf.) ASTM STP 497, 1972, pp 564 - 574.

66 PHILLIPS D.C. and HARRIS, B. "The Strength, Toughness and Fatigue Properties of Polymer Composites" Polymer Engineering Composites, Ed. Richardson, M.O.W., App. Sci. Pub. 1977, pp 120 - 121.

67 LENOE, E.M. "The Effect of Voids on the Mechanical Properties of High Modulus Graphite Fibre/Epoxy Reinforced Composites" AVCO Corporation, AVSD-0170-70-RR, 1970.

68 HUSSEY, M.E. "Some Density Measurements on Type I and Type II Carbon Fibre" R.A.E. Test Note, Structures 1742, 1969.

69 ANSI/ASTM D 792 - 66 "Specific Gravity and Density of Plastics by Displacement ".

70 ANSI/ASTM D 1505-68 "Density of Plastics by the Density Gradient Technique".

71 CILLEY, E., ROYLANCE, D. and SCHNEIDER, N. "Methods of Fiber and Void Measurement in Graphite/Epoxy Composites" Comp. Mat.: Testing and Des. (3rd Conf.) ASTM STP 546, 1974, pp 237 - 249.

72 PHILLIPS, M.G. "Composition Parameters for Hybrid Composite Materials" Comp., Vol. 12, No. 2, 1981, pp 113 - 116.

73 CREEDON, J.P. "The Characterization of Thermosetting Polymers (Degree of Cure)" Analytical Chemistry and Applied Spectroscopy Conf., Ohio, 1970, pp 1 - 9.

74 DU PONT "Vydax, Fluorotelomer Dispersions" Du Pont Petroleum Chemicals, Bulletin V - 3.

75 HYFIL LIMITED. Private Communication.

76 B.S. 2782 "Determination of Apparent Interlaminar Shear Strength of Reinforced Plastics" Part 3, Method 341A, 1977.

77 B.S. 2782 "Tensile Strength, Elongation and Elastic Modulus" Part 3, Methods 320A - 320F, 1976.

78 FREUND, J.E. "Statistics A First Course" Prentice-Hall, Inc., New Jersey, 1981.

79 BENHAM, P.P. and WARNOCK, F.V. "Mechanics of Solids and Structures" Pitman Paperbacks, 1973, p. 224.

80 REYNOLDS, W.N. and HANCOX, N.L. "Shear Strength of the Carbon-Resin Bond in Carbon Fibre Reinforced Epoxies" J. Phys., D:Appl. Phys., Vol. 4, 1971, pp 1747 - 1753.

APPENDIX I

The Application of the Weibull Distribution to Fibre Strength

Common reinforcing fibres such as carbon and glass contain numerous flaws along their lengths. These flaws result in a range of fibre strengths, the mean of which varies with fibre length. The distribution most frequently used to describe the statistical characteristics of fibre strengths is the Weibull distribution. The form of the Weibull probability density function applied to fibre strength is

$$f(\sigma) = \alpha L \beta \sigma^{\beta-1} e^{(-\alpha L \sigma^{\beta})} \quad \ldots \quad (i)$$

where $f(\sigma)$ = the probability of fibre failure at stress level σ

L = fibre length

α and β = Weibull constants.

The cumulative probability function for fibre failure, $F(\sigma)$, between the stress levels 0 to σ is obtained by integrating equation (i) with respect to σ

$$F(\sigma) = 1 - e^{(-\alpha L \sigma^{\beta})} \quad \ldots \quad (ii)$$

The mean of the distribution of fibre strengths, $\hat{\sigma}_f$, is dependent upon α, β and L and is defined by the following equation:

$$\hat{\sigma}_f = \int_0^{\infty} \sigma f(\sigma) \, d\sigma$$

$$= \alpha^{-1/\beta} L^{-1/\beta} \Gamma(1+1/\beta) \quad \ldots \quad (iii)$$

where Γ indicates the Gamma function.

For the case of unit length equation (iii) becomes:

$$\hat{\sigma}_f = \alpha^{-1/\beta} \Gamma(1+1/\beta) \quad \ldots \quad (iv)$$

For practical fibres $\beta > 1$ thus

$$0.88 \leq \Gamma(1+1/\beta) \leq 1.00$$

The quantity $\alpha^{-1/\beta}$ is often considered as a reference stress level although its units are not those of stress.

The value of β pertinent to a particular fibre type is commonly obtained from the plot of log (mean fibre strength) v log (fibre length), or from the equation

$$\beta = \frac{\ln\left(\frac{L_1}{L_2}\right)}{\ln\left(\frac{\hat{\sigma}_{f2}}{\hat{\sigma}_{f1}}\right)} \quad \ldots \quad (v)$$

The value of α can then be calculated directly from equation (iii)

The standard deviation, ψ , of the distribution function $f(\sigma)$ is given by the equation:

$$\psi = \alpha^{-1/\beta} L^{-1/\beta} \left[\Gamma(1+2/\beta) - \Gamma^2(1+1/\beta)\right]^{1/2} \quad . \ . \ . \quad (vi)$$

The coefficient of variation, CV, is equal to the standard deviation divided by the mean. From equations (vi) and (iii) it follows that

$$CV = \frac{\alpha^{-1/\beta} L^{-1/\beta} \left[\Gamma(1+2/\beta) - \Gamma^2(1+1/\beta)\right]^{1/2}}{\alpha^{-1/\beta} L^{-1/\beta} \Gamma(1+1/\beta)}$$

$$\therefore \quad CV = \left[\frac{\Gamma(1+2/\beta)}{\Gamma^2(1+1/\beta)} - 1\right]^{1/2} \quad . \ . \ . \quad (vii)$$

The CV is solely reliant upon the value of β . Thus β can be regarded as an inverse measure of scatter. Figure 3 in the main text is a plot of the variation of β with CV. As mentioned previously for practical fibres $\beta > 1$. Values between 2 and 4 correspond to brittle ceramics and a value of around 20 corresponds to a ductile metal. A CV of 12% is roughly equivalent to a β value of 10. Typical CV of glass and carbon fibres lie between 10% and 30%. For $0.05 \leq 0.5$ CV equation (vii) is approximated to within 3% by

$$CV = \beta^{-0.92} \quad . \ . \ . \quad (viii)$$

Extending the application of the Weibull distribution from fibre strength to fibre bundle strength the equation for mean fibre bundle strength ($\hat{\sigma}_b$) has been derived and is given in reference 57 of the main text.

$$\hat{\sigma}_b = (\alpha L \beta e)^{-1/\beta} \quad . \ . \ . \quad (ix)$$

The corresponding CV of bundle strength (CV_b) is

$$CV_b = \left(\frac{1}{n^{1/2}}\right)\left(e^{-1/\beta} - 1\right)^{1/2} \quad . \ . \ . \quad (x)$$

where n = number of fibres in the bundle

For fibres and bundles of the same length the ratio of mean bundle strength to mean fibre strength is derived from equations (iii) and (ix)

$$\frac{\hat{\sigma}_b}{\hat{\sigma}_f} = \left[(\beta e)^{1/\beta}\, \Gamma\left(1 + 1/\beta\right)\right]^{-1} \qquad \ldots \quad \text{(xi)}$$

The practical significance of the above is that $\frac{\hat{\sigma}_b}{\hat{\sigma}_f} < 1$. Typically the mean fibre bundle strength is 70% to 80% of the mean fibre strength.

The Weibull distribution, due to its close approximation to and consequential application to fibre strength distributions, is of great value in the development of composite tensile strength theories. Notable statistical analyses utilizing the Weibull distribution are those of Rosen and Zweben (references 1 and 3 respectively in the main text).

APPENDIX 2.
Detailed Experimental Results

Contents

Table	Title
2A1	Measured Fibre Diameters (d_f) and Cross-Sectional Areas (c.s.a.) of 600 tex and 500 tex E-Glass Fibres.
2A2	Fibre and Resin Densities as Determined by the Density Bottle Technique.
2A3	Fibre Tow Tensile Strength.
2A4	Resin and E-Glass Composite Shear Modulus (G) Results.
2A5	Weight per Length of 6000 Filament Carbon, 600 tex E-Glass and 500 tex E-Glass Fibre Tows.
2A6	Void Volume Percent Content of the Composite Slabs.
2A7	Interlaminar Shear Strength (τ_{il}) Results.
2A8	Tensile Results of the Composite Slabs 1 to 61.
2A9	The Main Steps in calculating the range of Composite Failure Stress and Strain for slabs 1 to 23 following Barry's Model[4].

TABLE 2A1

Measured Fibre Diameters (d_f) and Cross-Sectional Areas (c.s.a.) of 600 tex and 500 tex E-Glass Fibres.

d_f, μm		c.s.a., μm^2	
600 tex	500 tex	600 tex	500 tex
12.98	12.00	132.3	113.1
12.93	11.26	131.3	99.6
12.89	11.41	130.5	102.2
12.70	11.06	126.7	96.1
12.69	11.68	126.5	107.1
12.82	11.89	129.1	111.0
12.80	11.51	128.7	104.0
12.86	11.69	129.9	107.3
12.80	11.86	128.7	110.5
12.81	11.90	128.9	111.2
12.87	11.90	130.1	111.2
12.91	11.90	130.9	111.2
12.81	12.13	128.9	115.6
12.72	11.67	127.1	107.0
12.79	11.68	128.5	107.1
12.76	11.74	127.9	108.2
12.87	11.26	130.1	99.6
12.76	11.47	127.9	103.3
12.75	11.34	127.7	101.0
12.94	12.09	131.5	114.8
12.82	11.27	129.1	99.8
12.82	11.93	129.1	111.8
12.78	11.83	128.3	109.9
13.00	11.90	132.7	111.2
12.84	11.79	129.5	109.2
12.74	11.44	127.5	102.8
12.81	11.58	128.9	105.3
12.84	11.51	129.5	104.0
12.85	11.79	129.7	109.2
12.93	11.20	131.3	98.5
12.68	12.08	126.3	114.6
12.81	11.72	128.9	107.9
12.80	11.46	128.7	103.1
12.77	11.93	128.1	111.8
12.70	11.94	126.7	112.0
12.84	11.68	129.5	107.1
12.84	11.74	129.5	108.2
12.75	11.61	127.7	105.9
12.76	11.62	127.9	106.0
12.89	11.55	130.5	104.8
12.82	11.68	Average	
0.01	0.04	$\psi_{\bar{x}}$	
0.60	2.26	CV %	

TABLE 2A2

Fibre and Resin Densities as Determined by the Density Bottle Technique

Specimen	Density in gm/cm^3			
	6000 filament carbon fibre	600 tex E-Glass Fibre	500 tex E-glass Fibre	Derakane 411-45 Resin
1	1.75	2.54	2.54	1.14
2	1.76	2.54	2.54	1.12
3	1.76	2.53	2.54	1.14
4	1.77	2.54	2.54	1.13
5	1.76	2.55	2.54	1.12
6	1.77	2.54	2.53	1.11
7	1.76	2.54	2.54	1.13
8	1.76	2.54	2.54	1.14
9	1.76	2.54	2.54	1.13
10	1.76	2.54	2.55	1.13
Average	1.76	2.54	2.54	1.13
CV%	0.33	0.19	0.19	0.84

TABLE 2A3

Fibre Tow Tensile Strength

i) 6000 filament carbon tow, as rec. (c.s.a. = 0.2310mm^2)

Specimen	Gauge Length L, mm	Max. Load $\hat{P}$, kg	Failure Stress $\hat{\sigma}$, N/mm^2
1	253	9.4	399.2
2	253	10.1	428.9
3	253	10.5	445.9
4	253	10.1	428.9
5	253	11.1	471.4
6	253	10.3	437.4
7	253	10.3	437.4
8	253	10.2	433.2
9	253	9.6	407.7
10	253	10.9	462.9
11	253	10.5	445.9
12	253	10.1	428.9
13	253	10.6	450.2
14	253	9.4	399.2
15	253	10.2	433.2
16	253	9.7	411.9
17	253	9.9	420.4
18	253	10.0	424.7
19	253	10.1	428.9
20	253	10.2	433.2
		Average	431.5
21	50	14.0	594.6
22	50	12.5	530.8
23	50	12.5	530.8
24	50	12.0	509.6
25	50	13.0	552.1
26	50	12.6	535.1
27	50	13.6	577.6
28	50	13.2	560.6
29	50	12.7	539.3
30	50	12.4	526.6
31	50	12.2	518.1
32	50	13.8	586.1
33	50	12.9	547.8
34	50	12.7	539.3
35	50	13.0	552.1
36	50	12.2	518.1
37	50	12.7	539.3
38	50	12.9	547.8
39	50	13.2	560.6
40	50	11.9	505.4
		Average	543.6

TABLE 2A3

ii) 6000 Filament carbon tow, no c.-a. (c.s.a. =0.2310mm^2)

Specimen	L, mm	$\hat{P}$, kg	$\hat{\sigma}$, N/mm^2
1	180	11.1	471.4
2	180	10.7	454.4
3	180	11.3	479.9
4	180	10.5	445.9
5	180	10.6	450.2
6	180	9.9	420.4
7	180	10.5	445.9
8	180	10.9	462.9
9	180	11.4	484.1
10	180	11.3	479.9
11	180	11.1	471.4
12	180	10.8	458.6
13	180	10.1	428.9
14	180	10.7	454.4
15	180	10.8	458.6
16	180	10.8	458.6
17	180	11.3	479.9
18	180	10.7	454.4
19	180	10.4	441.7
20	180	9.9	420.4
		Average	456.1
21	50	11.8	532.3
22	50	11.5	518.8
23	50	12.4	559.4
24	50	12.6	568.4
25	50	12.0	541.3
26	50	12.4	559.4
27	50	11.6	523.2
28	50	11.7	527.8
29	50	12.2	550.3
30	50	12.4	559.4
31	50	11.8	532.3
32	50	11.9	536.8
33	50	12.1	545.9
34	50	12.5	563.8
35	50	11.9	536.8
36	50	11.8	532.3
37	50	12.6	568.4
38	50	12.0	541.3
39	50	13.0	586.4
40	50	11.4	514.2
		Average	544.9

TABLE 2A3

iii) 6000 Filament carbon tow, etched (c.s.a. = 0.2292mm^2)

Specimen	L, mm	$\hat{P}$, kg	$\hat{\sigma}$, N/mm^2
1	180	10.0	428.0
2	180	10.2	436.6
3	180	10.4	445.1
4	180	11.0	470.8
5	180	10.6	453.7
6	180	10.8	462.3
7	180	10.5	449.4
8	180	10.7	458.0
9	180	9.7	415.2
10	180	9.9	423.7
11	180	11.0	470.8
12	180	11.1	475.1
13	180	10.8	462.3
14	180	10.7	458.0
15	180	11.1	475.1
16	180	10.3	440.9
17	180	10.2	436.6
18	180	10.7	458.0
19	180	10.6	453.7
20	180	10.9	466.5
		Average	452.0
21	50	12.1	517.9
22	50	12.6	539.3
23	50	12.2	522.2
24	50	13.1	560.7
25	50	13.0	556.4
26	50	13.0	556.4
27	50	12.3	526.5
28	50	12.5	535.0
29	50	13.1	560.7
30	50	12.2	522.2
31	50	12.8	547.9
32	50	12.9	552.1
33	50	11.9	509.3
34	50	12.7	543.6
35	50	12.9	552.1
36	50	13.0	556.4
37	50	13.5	577.8
38	50	11.4	487.9
39	50	12.8	547.9
40	50	12.9	552.1
		Average	541.2

TABLE 2A3

iv) 600 tex E-glass tow, as rec. (c.s.a. = 0.2362mm^2)

Specimen	L, mm	$\hat{P}$, kg	$\hat{\sigma}$, N/mm^2
1	253	24.0	996.8
2	253	27.2	1129.6
3	253	24.1	1000.9
4	253	26.6	1104.8
5	253	26.7	1108.9
6	253	25.7	1067.4
7	253	23.9	992.6
8	253	23.0	955.2
9	253	25.9	1075.6
10	253	24.5	1017.5
11	253	27.1	1125.5
12	253	26.7	1108.9
13	253	26.4	1096.5
14	253	25.4	1054.9
15	253	25.8	1071.5
16	253	24.7	1025.9
17	253	24.9	1034.2
18	253	26.0	1079.8
19	253	23.3	967.7
20	253	24.9	1034.2
		Average	1052.4
21	50	27.0	1121.4
22	50	26.9	1117.2
23	50	27.5	1142.1
24	50	27.3	1133.8
25	50	27.5	1142.1
26	50	28.4	1179.5
27	50	29.5	1225.2
28	50	28.2	1171.2
29	50	29.5	1225.2
30	50	28.9	1200.3
31	50	28.5	1183.7
32	50	28.3	1175.4
33	50	29.4	1221.1
34	50	29.0	1204.4
35	50	27.0	1121.4
36	50	27.6	1146.3
37	50	28.5	1183.7
38	50	28.2	1171.2
39	50	28.2	1171.2
40	50	29.6	1229.4
		Average	1173.3

TABLE 2A3

v) 600 tex E-glass tow, no c.-a. (c.s.a. = 0.2362mm^2)

Specimen	L, mm	$\hat{P}$, kg	$\hat{\sigma}$, N/mm^2
1	180	11.8	490.1
2	180	11.2	465.2
3	180	11.4	473.5
4	180	11.0	456.9
5	180	11.3	469.3
6	180	10.4	431.9
7	180	10.7	444.4
8	180	11.2	465.2
9	180	10.6	440.2
10	180	10.2	423.6
11	180	11.4	473.5
12	180	10.6	440.2
13	180	10.5	436.1
14	180	10.7	444.4
15	180	11.0	456.9
16	180	11.0	456.9
17	180	10.8	448.6
18	180	11.2	465.2
19	180	11.9	494.2
20	180	11.3	469.3
		Average	457.3
21	50	13.4	556.5
22	50	13.7	569.0
23	50	13.8	573.1
24	50	13.5	560.7
25	50	13.0	539.9
26	50	13.2	548.2
27	50	14.0	581.5
28	50	14.0	581.5
29	50	13.8	573.1
30	50	14.5	602.2
31	50	13.5	560.7
32	50	14.7	610.5
33	50	14.6	606.4
34	50	14.0	581.5
35	50	13.7	569.0
36	50	14.1	585.6
37	50	14.8	614.7
38	50	14.5	602.2
39	50	13.9	577.3
40	50	13.6	564.8
		Average	577.9

TABLE 2A3

vi) 600 tex E-glass tow, A187 (c.s.a. = 0.2362mm^2)

Specimen	L, mm	$\hat{P}$, kg	$\hat{\sigma}$, N/mm^2
1	180	11.2	465.2
2	180	10.6	440.2
3	180	10.7	444.4
4	180	11.2	465.2
5	180	11.1	461.0
6	180	10.5	436.1
7	180	10.9	452.7
8	180	11.0	456.9
9	180	10.4	431.9
10	180	11.3	469.3
11	180	10.8	448.6
12	180	11.2	465.2
13	180	10.8	448.6
14	180	10.3	427.8
15	180	10.0	415.3
16	180	10.5	436.1
17	180	11.2	465.2
18	180	11.1	461.0
19	180	11.7	485.9
20	180	10.9	452.7
		Average	451.5
21	50	13.5	560.7
22	50	13.8	573.1
23	50	13.5	560.7
24	50	12.7	527.5
25	50	14.1	585.6
26	50	12.8	531.6
27	50	12.6	523.3
28	50	14.4	598.1
29	50	13.9	577.3
30	50	12.8	531.6
31	50	13.7	569.0
32	50	13.8	573.1
33	50	13.1	544.1
34	50	14.3	593.9
35	50	14.0	581.5
36	50	14.1	585.6
37	50	13.9	577.3
38	50	13.4	556.5
39	50	13.6	564.8
40	50	13.2	548.2
		Average	563.2

TABLE 2A3

vii) 600 tex E-glass tow, A1100 (c.s.a. = 0.2362mm^2)

Specimen	L, mm	$\hat{P}$, kg	$\hat{\sigma}$, N/mm^2
1	180	11.8	490.1
2	180	11.5	477.6
3	180	11.2	465.2
4	180	12.3	510.9
5	180	12.0	498.4
6	180	12.7	527.5
7	180	12.1	502.5
8	180	11.4	473.5
9	180	12.0	498.4
10	180	11.3	469.3
11	180	12.5	519.2
12	180	11.7	485.9
13	180	12.1	502.5
14	180	12.3	510.9
15	180	11.9	494.2
16	180	10.8	448.6
17	180	11.7	485.9
18	180	11.0	456.9
19	180	11.5	477.6
20	180	11.9	494.2
		Average	489.5
21	50	15.0	623.0
22	50	14.8	614.7
23	50	14.6	606.4
24	50	14.2	589.8
25	50	14.5	602.2
26	50	14.7	610.5
27	50	15.1	627.1
28	50	15.4	639.6
29	50	14.6	606.4
30	50	15.2	631.3
31	50	13.8	573.1
32	50	14.8	614.7
33	50	14.0	581.5
34	50	14.6	606.4
35	50	14.8	614.7
36	50	14.0	581.5
37	50	14.5	602.2
38	50	14.7	610.5
39	50	14.7	610.5
40	50	14.2	589.8
		Average	606.8

TABLE 2A3

viii) 500 tex E-glass tow as rec. (c.s.a. = 0.1969mm^2)

Specimen	L, mm	$\hat{P}$, kg	$\hat{\sigma}$, N/mm^2
1	252	23.0	1145.9
2	252	24.7	1230.6
3	252	23.1	1150.9
4	252	22.2	1106.1
5	252	23.8	1185.8
6	252	22.0	1096.1
7	252	21.4	1066.2
8	252	23.8	1185.8
9	252	24.2	1205.7
10	252	23.3	1160.8
11	252	22.2	1106.1
12	252	23.1	1150.9
13	252	23.4	1165.8
14	252	25.3	1260.5
15	252	22.5	1121.0
16	252	22.4	1116.0
17	252	21.8	1086.1
18	252	24.9	1240.6
19	252	24.1	1200.7
20	252	23.6	1175.8
		Average	1157.9
21	50	27.1	1350.2
22	50	26.7	1330.3
23	50	25.2	1255.5
24	50	27.3	1360.1
25	50	27.4	1365.1
26	50	26.3	1310.3
27	50	27.8	1385.1
28	50	27.4	1365.1
29	50	26.5	1320.3
30	50	28.5	1419.9
31	50	26.6	1325.3
32	50	27.7	1380.1
33	50	26.6	1325.3
34	50	27.4	1365.1
35	50	25.6	1275.4
36	50	27.3	1360.1
37	50	25.9	1290.4
38	50	25.8	1285.4
39	50	27.6	1375.1
40	50	26.6	1325.3
		Average	1338.5

TABLE 2A3

ix) 500 tex E-glass tow, no c.-a. (c.s.a. = 0.1969mm^2)

Specimen	L, mm	$\hat{P}$, kg	$\hat{\sigma}$, N/mm^2
1	180	14.5	722.4
2	180	14.9	742.4
3	180	14.6	727.4
4	180	15.3	762.3
5	180	15.2	757.3
6	180	14.0	697.5
7	180	15.7	782.2
8	180	15.4	767.3
9	180	15.1	752.3
10	180	14.7	732.4
11	180	14.6	727.4
12	180	15.5	772.2
13	180	15.1	752.3
14	180	15.4	767.3
15	180	14.9	742.4
16	180	14.6	727.4
17	180	14.7	732.4
18	180	15.3	762.3
19	180	14.8	737.4
20	180	14.6	727.4
		Average	744.6
21	50	18.6	926.7
22	50	18.2	906.8
23	50	17.6	876.9
24	50	18.7	931.7
25	50	17.8	886.8
26	50	18.5	921.7
27	50	18.1	901.8
28	50	17.1	852.0
29	50	17.8	886.8
30	50	17.9	891.8
31	50	18.5	921.7
32	50	17.8	886.8
33	50	18.7	931.7
34	50	18.2	906.8
35	50	18.0	896.8
36	50	18.1	901.8
37	50	17.9	891.8
38	50	17.5	871.9
39	50	18.3	911.7
40	50	18.0	896.8
		Average	900.0

TABLE 2A3

x) 500 tex E-glass tow, A187 (c.s.a. = 0.1969mm^2)

Specimen	L, mm	$\hat{P}$, kg	$\hat{\sigma}$, N/mm^2
1	180	14.4	717.4
2	180	14.6	727.4
3	180	15.0	747.3
4	180	15.1	752.3
5	180	15.5	772.2
6	180	14.9	742.2
7	180	15.5	772.2
8	180	14.7	732.4
9	180	14.7	732.4
10	180	14.1	702.5
11	180	15.3	762.3
12	180	14.6	727.4
13	180	15.7	782.2
14	180	14.9	742.4
15	180	14.8	737.4
16	180	14.9	742.4
17	180	15.3	762.3
18	180	15.2	757.3
19	180	14.9	742.4
20	180	15.0	747.3
		Average	745.1
21	50	18.7	931.7
22	50	18.4	916.7
23	50	17.8	886.8
24	50	18.6	926.7
25	50	18.4	916.7
26	50	17.8	886.8
27	50	17.5	871.9
28	50	17.1	852.0
29	50	18.0	896.8
30	50	17.9	891.8
31	50	18.1	901.8
32	50	17.7	881.9
33	50	17.9	891.8
34	50	18.3	911.7
35	50	18.0	896.8
36	50	18.3	911.7
37	50	18.9	941.6
38	50	18.0	896.8
39	50	18.3	911.7
40	50	18.2	906.8
		Average	901.5

TABLE 2A3

xi) 500 tex, E-glass tow, A1100 (c.s.a. = 0.1969mm^2)

Specimen	L, mm	$\hat{P}$, kg	$\hat{\sigma}$, N/mm^2
1	182	14.7	732.4
2	182	14.3	712.5
3	182	15.6	777.2
4	182	14.5	722.4
5	182	14.9	742.4
6	182	15.0	747.3
7	182	15.1	752.3
8	182	15.1	752.3
9	182	15.7	782.2
10	182	14.9	742.4
11	182	14.6	727.4
12	182	15.4	767.3
13	182	14.6	727.4
14	182	15.5	772.2
15	182	14.6	727.4
16	182	14.8	737.4
17	182	14.9	742.4
18	182	15.1	752.3
19	182	15.0	747.3
20	182	14.9	742.4
		Average	745.3
21	51	18.6	926.7
22	51	18.2	906.8
23	51	17.9	891.8
24	51	18.7	931.7
25	51	17.9	891.8
26	51	17.8	886.8
27	51	17.4	866.9
28	51	17.7	881.9
29	51	17.9	891.8
30	51	18.5	921.7
31	51	18.6	926.7
32	51	18.0	896.8
33	51	18.1	901.8
34	51	18.2	906.8
35	51	18.5	921.7
36	51	17.8	886.8
37	51	19.0	946.6
38	51	18.1	901.8
39	51	17.7	881.9
40	51	18.4	916.7
		Average	904.3

TABLE 2A4

Resin and E-Glass Composite Shear Modulus (G) Results

Specimen	Thickness t, mm	Width B, mm	$\frac{B}{t}$	Function μ	Load P, kg	Twist θ, rad	G KN/mm^2		
1	2.00	10.02	5.01	0.292	110	0.2444	2.19	Average 2.15 ± 0.01 1.34% CV	
2	2.00	10.02	5.01	0.292	110	0.2501	2.14		
3	2.00	10.00	5.00	0.292	105	0.2401	2.13		
4	2.00	10.00	5.00	0.292	105	0.2401	2.13		
5	2.50	10.06	4.02	0.281	115	0.1413	2.10	Average 2.14 ± 0.01 1.35% CV	Average 2.15 ± 0.01 1.29% CV
6	2.51	10.02	3.99	0.281	110	0.1315	2.14		
7	2.50	10.06	4.02	0.281	105	0.1270	2.13		
8	2.51	10.02	3.99	0.281	105	0.1237	2.17		
9	3.01	10.00	3.32	0.269	110	0.0785	2.10	Average 2.15 ± 0.02 1.58% CV	
10	3.01	10.00	3.32	0.269	105	0.0747	2.18		
11	3.00	10.04	3.35	0.270	110	0.0792	2.16		
12	3.00	10.04	3.35	0.270	105	0.0774	2.15		
13	4.00	10.00	2.50	0.250	115	0.0386	2.12	Average 2.16 ± 0.01 1.22% CV	
14	3.99	10.01	2.51	0.250	115	0.0384	2.15		
15	3.99	10.04	2.52	0.251	120	0.0392	2.18		
16	4.01	9.98	2.49	0.250	120	0.0392	2.17		
8.1	2.02	10.03	4.97	0.292	75	0.0928	3.81	Average 3.75 ± 0.03 1.74% CV	
8.2	2.02	10.02	4.96	0.292	90	0.1160	3.66		
8.3	2.03	10.03	4.94	0.292	120	0.1490	3.74		
8.4	2.02	10.01	4.96	0.292	90	0.1125	3.78		
9.1	2.03	10.00	4.93	0.292	90	0.0955	4.39	Average 4.45 ± 0.04 1.79% CV	
9.2	2.04	10.00	4.90	0.291	90	0.0946	4.38		
9.3	2.04	10.02	4.91	0.291	140	0.1430	4.50		
9.4	2.03	10.01	4.93	0.292	70	0.0718	4.54		

Contd/....

Table 2A4 Continued

Composite Specimen	Thickness t, mm	Width B, mm	$\frac{B}{t}$	Function μ	Load P, kg	Twist θ, rad	G KN/mm^2	
10.1	1.97	10.01	5.08	0.293	95	0.0980	4.92	
10.2	1.95	10.01	5.13	0.293	100	0.1074	4.87	Average
10.3	1.97	10.02	5.09	0.293	105	0.1086	4.90	4.92 ± 0.02
10.4	1.97	10.02	5.09	0.293	110	0.1120	4.98	0.95% CV
11.1	2.00	10.02	5.01	0.292	95	0.0781	5.91	
11.2	2.00	10.01	5.01	0.292	75	0.0625	5.84	Average
11.3	2.00	10.01	5.01	0.292	95	0.0796	5.81	5.84 ± 0.02
11.4	2.01	10.02	4.99	0.292	90	0.0743	5.80	0.85% CV
12.1	2.00	10.02	5.01	0.292	140	0.1052	6.47	
12.2	2.00	10.01	5.01	0.292	105	0.0781	6.54	Average
12.3	2.00	10.00	5.00	0.292	110	0.0822	6.52	6.51 ± 0.01
12.4	2.00	10.01	5.01	0.292	85	0.0635	6.51	0.45% CV
13.1	2.04	10.04	4.92	0.291	100	0.0640	7.17	
13.2	2.05	10.01	4.88	0.291	140	0.0728	7.15	Average
13.3	2.05	10.02	4.89	0.291	120	0.0749	7.26	7.20 ± 0.03
13.4	2.05	10.03	4.89	0.291	80	0.0501	7.23	0.71% CV
14.1	1.99	10.01	5.03	0.293	95	0.0862	5.71	
14.2	1.99	10.00	5.03	0.293	100	0.0869	5.67	Average
14.3	1.99	10.03	5.04	0.293	125	0.1048	5.86	5.74 ± 0.04
14.4	1.99	10.03	5.04	0.293	90	0.0776	5.70	1.48% CV
15.1	1.99	10.02	5.04	0.293	130	0.1082	5.91	
15.2	1.99	10.03	5.04	0.293	125	0.1046	5.87	Average
15.3	1.99	10.02	5.04	0.293	90	0.0761	5.82	5.85 ± 0.03
15.4	1.98	10.01	5.06	0.293	115	0.0994	5.78	0.97% CV
16.1	1.97	10.03	5.09	0.293	115	0.1035	5.63	
16.2	1.96	10.03	5.12	0.293	100	0.0885	5.81	Average
16.3	1.98	10.00	5.05	0.293	95	0.0855	5.56	5.66 ± 0.05
16.4	1.97	10.03	5.09	0.293	135	0.1217	5.62	1.91% CV

Cont/....

Table 2A4 Continued

Composite Specimen	Thickness t, mm	Width B, mm	$\frac{B}{t}$	Function μ	Load P, kg	Twist θ, rad	G KN/mm^2	
17.1	2.01	10.02	4.99	0.292	75	0.0891	4.03	
17.2	2.00	10.01	5.01	0.292	105	0.1246	4.10	Average
17.3	2.00	10.02	5.01	0.292	100	0.1240	3.92	3.99 ± 0.05
17.4	2.01	10.01	4.98	0.292	100	0.1232	3.89	2.44% CV
18.1	2.05	10.02	4.89	0.291	140	0.1297	4.89	
18.2	2.05	10.01	4.88	0.291	85	0.0768	5.02	Average
18.3	2.05	10.01	4.88	0.291	120	0.1069	5.09	5.00 ± 0.04
18.4	2.05	10.02	4.89	0.291	100	0.0904	5.01	1.66% CV
19.1	2.00	10.00	5.00	0.292	105	0.0918	5.57	
19.2	2.00	10.02	5.01	0.292	75	0.0664	5.49	Average
19.3	2.00	10.02	5.01	0.292	85	0.0760	5.44	5.51 ± 0.03
19.4	2.00	10.02	5.01	0.292	120	0.1057	5.52	0.99% CV
20.1	2.00	10.02	5.01	0.292	100	0.0729	6.67	
20.2	1.99	10.00	5.03	0.293	90	0.0661	6.71	Average
20.3	1.99	10.00	5.03	0.293	110	0.0824	6.58	6.65 ± 0.03
20.4	2.00	10.01	5.01	0.292	105	0.0772	6.62	0.86% CV
21.1	2.03	10.01	4.93	0.292	125	0.1035	5.62	
21.2	2.02	10.01	4.96	0.292	80	0.0678	5.57	Average
21.3	2.03	10.01	4.93	0.292	80	0.0658	5.66	5.65 ± 0.04
21.4	2.03	10.01	4.93	0.292	110	0.0892	5.74	1.27% CV
22.1	2.04	10.00	4.90	0.291	110	0.0865	5.80	
22.2	2.04	10.02	4.91	0.291	110	0.0882	5.73	Average
22.3	2.05	10.00	4.88	0.291	105	0.0823	5.79	5.74 ± 0.04
22.4	2.04	10.02	4.91	0.291	105	0.0859	5.62	1.00% CV
23.1	2.03	10.02	4.94	0.292	90	0.0730	5.73	
23.2	2.04	10.01	4.91	0.291	90	0.0734	5.64	Average
23.3	2.03	10.01	4.93	0.292	70	0.0579	5.63	5.68 ± 0.02
23.4	2.04	10.00	4.90	0.291	100	0.0808	5.70	0.85% CV

TABLE 2A5

Weight Per Length of 6000 Filament Carbon, 600 tex E-Glass and 500 tex E-Glass Fibre Tows

Carbon (as rec.)		Carbon (no c.-a.)		600 Tex E-Glass (as rec.)		500 Tex E-Glass (as rec.)	
Length mm	Weight gm	Length mm	Weight gm	Length mm	Weight gm	Length mm	Weight gm
199	0.0840	198	0.0808	200	0.1225	200	0.1019
200	0.0842	198	0.0806	200	0.1223	197	0.1021
200	0.0841	199	0.0811	201	0.1230	200	0.1025
200	0.0842	201	0.0815	200	0.1226	201	0.1030
200	0.0845	199	0.0808	201	0.1229	200	0.1029
200	0.0839	199	0.0810	202	0.1226	202	0.1030
202	0.0850	200	0.0812	198	0.1233	201	0.1029
200	0.0841	198	0.0809	200	0.1222	200	0.1027
200	0.0842	201	0.0816	200	0.1225	200	0.1024
200	0.0846	201	0.0813	199	0.1229	199	0.1026
2001	0.8428	1994	0.8108	2001	1.2268	2000	1.0260
0.4210 gm/m		0.4066 gm/m		0.6132 gm/m		0.5130 gm/m	

TABLE 2A6

Void Volume Percent Content of the Composite Slabs Calculated from the Equation

$$V_v\,\% = \left(1 - \frac{\omega_m \rho_c}{\rho_m \omega_c} - \frac{\omega_{cf} \rho_c}{\rho_{cf} \omega_c} - \frac{\omega_g \rho_c}{\rho_g \omega_c}\right) \times 100$$

Where ω and ρ = weight and density respectively and subscripts m, c, cf, and g denote resin, composite, carbon fibre and glass fibre respectively.

Slab	ρ_c gm/cm^3	ω_c gm	ω_g gm	ω_{cf} gm	ω_m gm	V_v %
1	1.22	3.0298	-	0.6797	2.3501	0.71
2	1.26	5.3697	-	0.6797	3.7986	0.15
3	1.33	4.7174	-	1.5731	2.7754	0.25
4	1.37	5.9934	-	1.9420	3.0030	0.41
5	1.45	3.8582	-	2.9904	1.4939	-0.17
6	1.36	4.9606	-	2.3643	2.6174	0.00
7	1.37	4.9930	-	2.3432	2.5471	0.02
8	1.45	3.3158	1.3261	2.4459	1.9897	0.17
9	1.48	3.6000	1.5639	-	2.0361	0.61
10	1.60	5.8073	3.0890	-	2.7183	0.22
11	1.69	6.9990	4.1978	-	2.8012	0.24
12	1.76	5.7913	3.7515	-	2.0398	0.26
13	1.84	8.9886	6.2786	-	2.7120	0.27
14	1.69	6.3125	3.7689	-	2.5436	0.01
15	1.64	5.5240	3.1338	-	2.3902	0.57
16	1.72	6.3256	3.9073	-	2.1401	-0.02
17	1.55	6.3767	1.2267	-	2.8857	0.04
18	1.54	6.0394	1.1573	-	3.0999	0.54
19	1.62	7.9586	4.3588	-	3.5998	0.22
20	1.77	8.3211	5.4421	-	2.8790	0.23
21	1.63	7.0533	3.9452	-	3.1081	0.54
22	1.67	6.8151	3.9720	-	2.8431	0.03
23	1.75	8.0808	5.1776	-	2.9032	0.22
24	1.30	5.6784	1.8805	0.4247	3.8117	0.30
25	1.49	7.2958	2.8173	0.6081	3.8704	0.34
26	1.55	7.3747	3.1159	0.7311	3.5277	-0.13
27	1.60	7.3046	1.3398	0.8012	3.1003	0.59

Table 2A6 Continued

Slab	ρ_c gm/cm^3	ω_c gm	ω_g gm	ω_{cf} gm	ω_m gm	V_v %
28	1.69	4.1826	2.1661	0.4888	1.5277	0.31
29	1.75	9.7083	5.4887	1.1185	3.1011	0.12
30	1.30	5.0636	0.8153	0.5992	3.6491	0.11
31	1.35	5.6078	1.1674	0.8082	3.6322	0.50
32	1.40	5.6312	1.2932	1.0502	3.2878	0.17
33	1.45	6.5454	1.7632	1.3304	3.4518	0.21
34	1.51	7.3290	2.4040	1.5258	3.3992	0.66
35	1.61	7.9798	3.0789	1.8992	3.0017	0.18
36	1.62	8.1536	3.0203	2.2623	2.8710	0.36
37	1.37	4.9312	1.0604	0.6861	3.1847	0.73
38	1.68	7.8059	2.7496	2.0757	2.9806	0.26
39	1.65	7.2768	3.6492	0.7512	2.8764	-0.05
40	1.70	7.9848	4.3234	0.8682	2.7931	0.63
41	1.65	6.4719	3.4599	0.2976	2.7144	-0.26
42	1.48	5.8533	1.1565	2.0706	2.6262	-0.02
43	1.50	5.8126	1.6237	1.5341	2.6548	0.38
44	1.60	8.1890	3.5054	1.2753	3.4084	-0.05
45	1.56	6.6690	2.5408	1.2245	2.9037	0.22
46	1.54	6.2276	2.2831	1.1329	2.8116	0.33
47	1.53	5.6160	1.9417	1.0816	2.5927	-0.08
48	1.55	6.0305	2.2508	1.1302	2.6495	0.46
49	1.55	6.3101	2.3184	1.1916	2.8001	0.08
50	1.54	6.9974	2.5023	1.3491	3.1460	0.18
51	1.54	6.5497	2.4147	1.2205	2.9145	0.70
52	1.54	6.7903	2.4994	1.2319	3.0590	0.41
53	1.56	6.0491	2.2501	1.1659	2.6331	-0.02
54	1.53	5.3627	1.8741	1.0308	2.4578	0.19
55	1.56	6.0581	2.2210	1.2498	2.5873	0.24
56	1.53	5.2078	1.7990	1.0507	2.3581	0.34
57	1.55	6.3041	2.3411	1.1686	2.7944	0.21
58	1.54	5.7661	2.0563	1.1263	2.5835	0.23
59	1.55	6.6486	2.4889	1.2237	2.9360	0.38
60	1.55	5.3827	1.9561	1.0331	2.3935	-0.07
61	1.54	4.5767	1.6681	0.8391	2.0695	0.23

TABLE 2A7

Interlaminar Shear Strength (τ_{il}) Results

Specimen	Max Load $\hat{P}$, kg	Failure mode	τ_{il} N/mm^2	
1.1	118	Shear	43.4	
1.2	120	Shear	44.1	Average
1.3	117	Shear	43.0	43.3 ± 0.2
1.4	116	Shear	42.6	CV
1.5	118	Shear	43.3	0.94%
1.6	118	Shear	43.4	
2.1	118	Shear	43.0	
2.2	119	Shear	43.3	Average
2.3	120	Shear	43.9	43.4 ± 0.2
2.4	121	Shear	43.9	CV
2.5	119	Shear	43.2	1.07%
2.6	117	Shear	42.8	
3.1	120	Shear	44.0	
3.2	119	Shear	44.1	Average
3.3	122	Shear	45.2	44.5 ± 0.3
3.4	120	Shear	44.5	CV
3.5	124	Shear	45.4	1.49%
3.6	120	Shear	43.8	
4.1	121	Shear	44.2	
4.2	121	Shear	44.2	Average
4.3	119	Shear	43.4	43.5 ± 0.3
4.4	116	Shear	42.2	CV
4.5	120	Shear	43.6	1.26%
4.6	120	Shear	43.6	
5.1	99	Mixed	>35.4	
5.2	122	Shear	43.7	Average
5.3	125	Shear	45.0	44.0 ± 0.3
5.4	123	Shear	44.2	CV
5.5	122	Shear	43.7	1.56%
5.6	120	Shear	43.2	

Table 2A7 Continued

Specimen	Max. Load $\hat{P}$, kg	Failure mode	τ_{il} N/mm^2	
6.1	262	Shear	95.8	
6.2	269	Shear	98.5	Average
6.3	271	Shear	99.1	97.8 ± 0.6
6.4	250	Mixed	>91.0	CV
6.5	269	Shear	98.5	1.45%
6.6	267	Shear	97.2	
7.1	136	Shear	50.4	
7.2	139	Shear	51.0	Average
7.3	117	Mixed	>43.6	50.0 ± 0.3
7.4	135	Shear	49.6	CV
7.5	134	Shear	49.4	1.43%
7.6	134	Shear	49.4	
8.1	104	Mixed	>38.0	
8.2	108	Mixed	>39.4	Average
8.3	87	Mixed	>31.6	>42.0
8.4	115	Mixed	>42.0	
8.5	104	Mixed	>38.0	
8.6	104	Mixed	>38.0	
9.1	140	Shear	50.6	
9.2	146	Shear	52.8	Average
9.3	139	Shear	50.5	51.5 ± 0.4
9.4	144	Shear	52.3	CV
9.5	142	Shear	51.8	1.92%
9.6	140	Shear	51.1	
10.1	134	Shear	50.2	
10.2	102	Mixed	>38.4	Average
10.3	137	Shear	51.3	50.9 ± 0.5
10.4	139	Shear	52.1	CV
10.5	132	Shear	49.4	2.13%
10.6	136	Shear	51.5	

Table 2A7 Continued

Specimen	Max. Load $\hat{P}$, kg	Failure mode	τ_{il} N/mm^2	
11.1	140	Shear	51.6	
11.2	142	Shear	52.3	Average
11.3	145	Shear	53.4	52.3 ± 0.3
11.4	143	Shear	52.4	CV
11.5	143	Shear	52.7	1.31%
11.6	140	Shear	51.6	
12.1	137	Shear	50.5	
12.2	140	Shear	51.6	Average
12.3	136	Shear	50.1	50.5 ± 0.2
12.4	136	Shear	50.1	CV
12.5	136	Shear	50.1	1.20%
12.6	138	Shear	50.9	
13.1	125	Mixed	>45.0	
13.2	148	Shear	53.3	Average
13.3	150	Shear	53.8	54.0 ± 0.2
13.4	152	Shear	54.8	CV
13.5	150	Shear	54.1	1.01%
13.6	150	Shear	54.0	
14.1	167	Shear	61.9	
14.2	164	Shear	60.8	Average
14.3	168	Shear	62.4	61.3 ± 0.4
14.4	168	Shear	62.3	CV
14.5	164	Shear	60.9	1.72%
14.6	161	Shear	59.7	
15.1	280	Shear	103.7	
15.2	240	Mixed	> 89.4	Average
15.3	288	Shear	106.9	103.5 ± 1.2
15.4	283	Shear	105.1	CV
15.5	271	Shear	100.8	2.54%
15.6	272	Shear	101.0	

Table 2A7 Continued

Specimen	Max Load $\hat{P}$, kg	Failure mode	τ_{il} N/mm^2	
16.1	120	Shear	45.2	
16.2	98	Mixed	>36.9	Average
16.3	118	Shear	44.2	45.7 ± 0.7
16.4	123	Shear	46.1	CV
16.5	102	Mixed	>38.2	3.15%
16.6	126	Shear	47.3	
17.1	135	Shear	49.5	
17.2	138	Shear	50.6	Average
17.3	134	Shear	49.5	49.5 ± 0.4
17.4	130	Shear	47.7	CV
17.5	135	Shear	49.5	2.01%
17.6	136	Shear	50.2	
18.1	134	Shear	48.0	
18.2	125	Mixed	>45.0	Average
18.3	140	Shear	50.4	49.2 ± 0.8
18.4	132	Shear	47.3	CV
18.5	142	Shear	50.9	3.38%
18.6	119	Mixed	>42.8	
19.1	150	Shear	55.3	
19.2	146	Shear	53.9	Average
19.3	148	Shear	54.7	54.2 ± 0.7
19.4	146	Shear	53.8	CV
19.5	139	Shear	51.3	3.24%
19.6	153	Shear	56.5	
20.1	132	Shear	48.6	
20.2	142	Shear	52.3	Average
20.3	139	Shear	51.7	51.4 ± 0.6
20.4	141	Shear	52.1	CV
20.5	140	Shear	52.0	2.72%
20.6	140	Shear	51.8	

Table 2A7 Continued

Specimen	Max Load $\hat{P}$, kg	Failure mode	τ_{il} N/mm^2	
21.1	150	Shear	54.5	
21.2	150	Shear	54.2	Average
21.3	152	Shear	55.1	56.5 ± 0.9
21.4	160	Shear	58.3	CV
21.5	160	Shear	58.0	3.73%
21.6	162	Shear	59.1	
22.1	267	Mixed	>95.8	
22.2	308	Shear	109.9	Average
22.3	287	Shear	103.5	106.6 ± 1.0
22.4	296	Shear	106.2	CV
22.5	296	Shear	106.2	2.14%
22.6	298	Shear	106.8	
23.1	103	Mixed	>37.2	
23.2	132	Shear	47.8	Average
23.3	129	Shear	46.8	47.0 ± 0.3
23.4	103	Mixed	>37.6	CV
23.5	130	Shear	47.0	1.41%
23.6	128	Shear	46.2	
24.1	101	Shear	37.8	
24.2	107	Shear	40.1	Average
24.3	107	Shear	39.9	39.1 ± 0.4
24.4	105	Shear	39.0	CV
24.5	105	Shear	38.9	2.35%
24.6	91	Mixed	>34.0	
25.1	99	Mixed	>35.7	
25.2	111	Shear	40.0	Average
25.3	110	Shear	39.8	39.7 ± 0.4
25.4	107	Shear	38.4	CV
25.5	115	Shear	41.3	2.52%
25.6	109	Shear	39.1	

Table 2A7 Continued

Specimen	Max. Load $\hat{P}$, kg	Failure mode	τ_{11} N/mm^2	
26.1	115	Shear	42.3	
26.2	114	Shear	41.7	Average
26.3	115	Shear	42.3	41.6 ± 0.3
26.4	110	Shear	40.7	
26.5	110	Shear	40.9	CV
26.6	113	Shear	41.7	1.63%
27.1	115	Shear	43.2	
27.2	118	Shear	44.3	Average
27.3	116	Shear	43.5	44.2 ± 0.4
27.4	121	Shear	45.5	
27.5	116	Shear	43.6	CV
27.6	119	Shear	44.8	2.00%
28.1	115	Shear	43.3	
28.2	116	Shear	43.6	Average
28.3	116	Shear	43.6	43.6 ± 0.1
28.4	117	Shear	43.9	
28.5	115	Shear	43.3	CV
28.6	117	Shear	44.0	0.67%
29.1	121	Shear	44.6	
29.2	115	Shear	42.6	Average
29.3	122	Shear	45.0	44.2 ± 0.6
29.4	114	Shear	42.3	
29.5	124	Shear	45.8	CV
29.6	121	Shear	44.7	3.16%
30.1	96	Shear	36.3	
30.2	103	Shear	38.9	Average
30.3	78	Mixed	>29.6	36.4 ± 0.6
30.4	98	Shear	37.0	
30.5	93	Shear	34.9	CV
30.6	93	Shear	35.1	3.99%

Table 2A7 Continued

Specimen	Max. Load $\hat{P}$, kg	Failure mode	τ_{il} N/mm^2	
31.1	109	Shear	40.2	
31.2	112	Shear	41.3	Average
31.3	114	Shear	42.0	40.8 ± 0.4
31.4	108	Shear	39.5	CV
31.5	84	Mixed	>31.0	2.37%
31.6	110	Shear	40.8	
32.1	112	Shear	40.6	
32.3	119	Shear	43.1	Average
32.3	124	Shear	44.9	43.2 ± 0.6
32.4	121	Shear	43.9	CV
32.5	117	Shear	42.5	3.53%
32.6	122	Shear	44.2	
33.1	127	Shear	46.0	
33.2	124	Shear	44.9	Average
33.3	119	Shear	43.1	45.1 ± 0.5
33.4	122	Shear	44.2	CV
33.5	129	Shear	46.7	2.89%
33.6	126	Shear	45.6	
34.1	112	Mixed	>40.2	
34.2	120	Shear	42.9	Average
34.3	123	Shear	43.8	43.6 ± 0.4
34.4	109	Mixed	>39.1	CV
34.5	124	Shear	44.2	1.53%
34.6	110	Mixed	>39.4	
35.1	120	Shear	45.1	
35.2	116	Shear	43.6	Average
35.3	108	Shear	40.6	42.5 ± 0.7
35.4	112	Shear	42.0	CV
35.5	110	Shear	41.4	3.81%
35.6	112	Shear	42.2	

Table 2A7 Continued

Specimen	Max. Load $\hat{P}$, kg	Failure mode	τ_{il} N/mm^2	
36.1	120	Shear	43.3	
36.2	102	Mixed	>36.8	Average
36.3	124	Shear	44.9	43.8 ± 0.6
36.4	117	Shear	42.3	
36.5	124	Shear	44.9	CV
36.6	110	Mixed	>39.9	2.92%
37.1	120	Shear	44.0	
37.2	117	Shear	43.1	Average
37.3	102	Mixed	>37.6	43.2 ± 0.5
37.4	119	Shear	43.9	
37.5	114	Shear	42.0	CV
37.6	104	Mixed	>38.4	2.15%
38.1	125	Shear	45.5	
38.2	118	Shear	43.0	Average
38.3	120	Shear	43.4	44.1 ± 0.4
38.4	123	Shear	44.8	
38.5	121	Shear	43.9	CV
38.6	121	Shear	44.0	2.08%
39.1	135	Shear	49.2	
39.2	135	Shear	49.2	Average
39.3	118	Mixed	>43.0	49.7 ± 0.3
39.4	120	Mixed	>43.8	
39.5	138	Shear	50.6	CV
39.6	136	Shear	49.6	1.33%
40.1	146	Shear	53.0	
40.2	149	Shear	54.4	Average
40.3	147	Shear	53.9	54.0 ± 0.3
40.4	150	Shear	54.9	
40.5	148	Shear	53.6	CV
40.6	149	Shear	54.2	1.22%

Table 2A7 Continued

Specimen	Max. Load $\hat{P}$, kg	Failure mode	τ_{il} N/mm^2	
41.1	132	Shear	49.2	
41.2	136	Shear	50.4	Average
41.3	135	Shear	50.6	50.5 ± 0.3
41.4	138	Shear	51.4	CV
41.5	138	Shear	51.2	1.63%
41.6	134	Shear	49.9	
42.1	113	Shear	42.0	
42.2	115	Shear	42.7	Average
42.3	111	Shear	41.2	42.3 ± 0.3
42.4	113	Shear	42.0	CV
42.5	114	Shear	42.4	1.91%
42.6	118	Shear	43.6	
43.1	130	Shear	46.8	
43.2	116	Mixed	>41.8	Average
43.3	134	Shear	48.0	46.9 ± 0.4
43.4	132	Shear	47.6	CV
43.5	130	Shear	46.6	2.01%
43.6	127	Shear	45.5	
44.1	116	Shear	43.1	
44.2	115	Shear	42.7	Average
44.3	116	Shear	43.1	43.3 ± 0.2
44.4	119	Shear	44.0	CV
44.5	118	Shear	43.6	1.28%
44.6	107	Mixed	>39.8	
45.1	117	Shear	43.1	
45.2	121	Shear	44.5	Average
45.3	118	Shear	43.4	43.7 ± 0.4
45.4	120	Shear	44.6	CV 2.03%
45.5	119	Shear	44.0	
45.6	115	Shear	42.3	

Table 2A7 Continued

Specimen	Max.Load $\hat{P}$, kg	Failure mode	τ_{il} N/mm^2	
46.1	138	Shear	50.3	
46.2	135	Shear	49.0	Average
46.3	133	Shear	48.7	49.9 $\pm$ 0.4
46.4	136	Shear	49.9	CV
46.5	140	Shear	51.3	1.89%
46.6	138	Shear	50.2	
47.1	130	Shear	47.4	
47.2	127	Shear	46.6	Average
47.3	104	Mixed	>37.8	47.2 $\pm$ 0.2
47.4	127	Shear	46.6	CV
47.5	130	Shear	47.4	1.14%
47.6	131	Shear	47.8	
48.1	126	Shear	46.2	
48.2	134	Shear	49.1	Average
48.3	133	Shear	48.5	48.6 $\pm$ 0.4
48.4	135	Shear	49.5	CV
48.5	135	Shear	50.0	2.13%
48.6	130	Shear	48.0	
49.1	130	Shear	48.7	
49.2	132	Shear	49.3	Average
49.3	132	Shear	49.2	48.7 $\pm$ 0.2
49.4	130	Shear	49.0	CV 1.10%
49.5	129	Shear	47.9	
49.6	129	Shear	48.4	
50.1	250	Mixed	>89.8	
50.2	278	Shear	99.9	Average
50.3	275	Shear	98.9	99.9 $\pm$ 0.5
50.4	281	Shear	101.1	CV
50.5	280	Shear	100.8	1.03%
50.6	275	Shear	98.9	

Table 2A7 Continued

Specimen	Max. Load $\hat{P}$, kg	Failure mode	τ_{il} N/mm^2	
51.1	266	Shear	98.9	
51.2	264	Shear	97.2	Average
51.3	264	Shear	97.3	97.9 ± 0.4
51.4	263	Shear	97.0	
51.5	268	Shear	99.3	CV
51.6	263	Shear	97.5	1.10%
52.1	202	Shear	73.9	
52.2	203	Shear	75.0	Average
52.3	203	Shear	74.3	74.4 ± 0.2
52.4	202	Shear	73.9	
52.5	203	Shear	75.0	CV
52.6	201	Shear	74.2	0.68%
53.1	193	Mixed	>69.1	
53.2	218	Shear	77.7	Average
53.3	216	Shear	77.4	78.3 ± 0.3
53.4	222	Shear	79.1	
53.5	220	Shear	78.8	CV 0.88%
53.6	220	Shear	78.3	
54.1	180	Shear	66.4	
54.2	181	Shear	66.5	Average
54.3	182	Shear	67.4	66.7 ± 0.3
54.4	179	Shear	65.8	
54.5	180	Shear	66.2	CV
54.6	184	Shear	67.8	1.14
55.1	169	Shear	62.0	
55.2	174	Shear	64.2	Average
55.3	174	Shear	64.2	63.4 ± 0.4
55.4	172	Shear	63.5	
55.5	170	Shear	62.8	CV
55.6	173	Shear	63.9	1.57%

Table 2A7 Continued

Specimen	Max Load $\hat{P}$, kg	Failure mode	τ_{11} N/mm^2	
56.1	270	Shear	100.7	
56.2	275	Shear	102.0	Average
56.3	276	Shear	102.4	101.8 $\pm$ 0.5
56.4	276	Shear	103.5	CV
56.5	268	Shear	100.4	1.12%
56.6	273	Shear	101.9	
57.1	250	Mixed	>89.3	
57.2	240	Mixed	>86.0	Average
57.3	251	Mixed	>90.1	>90.7
57.4	253	Mixed	>90.7	
57.5	249	Mixed	>88.8	
57.6	253	Mixed	>90.4	
58.1	137	Shear	50.2	
58.2	133	Shear	48.8	Average
58.3	132	Shear	48.4	49.3 $\pm$ 0.4
58.4	131	Shear	48.1	CV
58.5	135	Shear	49.8	2.13%
58.6	138	Shear	50.7	
59.1	136	Shear	49.3	
59.2	140	Shear	50.4	Average
59.3	135	Shear	48.4	49.3 $\pm$ 0.3
59.4	121	Mixed	>43.4	CV
59.5	136	Shear	49.0	1.48%
59.6	137	Shear	49.4	
60.1	132	Shear	48.5	
60.2	134	Shear	48.9	Average
60.3	131	Shear	47.8	48.1 $\pm$ 0.2
60.4	129	Shear	47.6	CV
60.5	130	Shear	47.7	1.00%
60.6	132	Shear	48.2	

Table 2A7 Continued

Specimen	Max. Load $\hat{P}$, kg	Failure mode	τ_{II} N/mm^2	
61.1	144	Shear	52.7	
61.2	139	Shear	50.8	Average
61.3	136	Shear	49.5	50.9 ± 0.5
61.4	137	Shear	49.9	CV
61.5	142	Shear	51.9	2.36%
61.6	140	Shear	50.9	

TABLE 2A8

Tensile Results of the Composite Slabs 1 to 61

E = elastic modulus; σ^E and ε^E = elastic limit; σ' and ε' = initial failure stress and strain; $\hat{\sigma}$ = maximum stress.

SLAB 1 3C, $V_r\% = V_{cf}\% = 16.17\%$

Specimen	E KN/mm^2	σ^E N/mm^2	ε^E %	σ' N/mm^2	ε' %	$\hat{\sigma}$ N/mm^2
1.1	40.8	189.0	0.46			
1.2	44.5	186.9	0.42			
1.3	43.5	202.7	0.47			
1.4	42.0	175.9	0.42	σ^E	ε^E	σ^E
1.5	42.9	172.9	0.40			
1.6	43.2	208.3	0.48			
Average	42.8	189.3	0.44			
$\psi_{\bar{x}}$	0.5	5.8	0.01			
CV%	3.03	3.06	6.82			

SLAB 2 4C, $V_r\% = V_{cf}\% = 21.56\%$

2.1	53.2	234.0	0.44			
2.2	53.2	315.8	0.59			
2.3	55.4	266.1	0.48	σ^E	ε^E	σ^E
2.4	56.6	271.5	0.48			
2.5	57.0	215.6	0.38			
Average	55.1	260.6	0.47			
$\psi_{\bar{x}}$	0.8	17.2	0.04			
CV%	3.27	14.77	17.02			

SLAB 3 6C, $V_r\% = V_{cf}\% = 32.34\%$

3.1	79.9	405.2	0.51			
3.2	79.8	370.1	0.46			
3.3	81.8	378.1	0.46	σ^E	ε^E	σ^E
3.4	79.7	394.1	0.50			
3.5	80.8	386.6	0.48			
Average	80.4	386.8	0.48			
$\psi_{\bar{x}}$	0.4	6.1	0.01			
CV%	1.12	3.54	4.17			

Table 2A8 Continued

SLAB 4 7C, $V_T\% = V_{cf}\% = 37.73\%$

Specimen	E KN/mm^2	σ^E N/mm^2	ε^E %	σ' N/mm^2	ε' %	$\hat{\sigma}$ N/mm^2
4.1	93.7	420.7	0.45			
4.2	93.0	389.8	0.42			
4.3	93.9	448.0	0.48	σ^E	ε^E	σ^E
4.4	92.5	427.6	0.46			
4.5	93.1	427.6	0.47			
Average	93.2	422.7	0.46			
$\psi_{\bar{x}}$	0.3	9.4	0.01			
CV%	0.64	4.99	4.35			

SLAB 5 9C, $V_T\% = V_{cf}\% = 48.51\%$

5.1	119.2	603.4	0.51			
5.2	117.8	629.6	0.53			
5.3	119.5	545.6	0.46	σ^E	ε^E	σ^E
5.4	120.7	602.1	0.50			
5.5	118.2	538.7	0.46			
5.6	120.0	521.4	0.43			
Average	119.2	573.5	0.48			
$\psi_{\bar{x}}$	0.4	17.8	0.02			
CV%	0.90	7.62	8.33			

SLAB 6 7C (etched) $V_T\% = V_{cf}\% = 37.43\%$

6.1	91.2	461.7	0.51			
6.2	93.9	420.0	0.45			
6.3	92.3	446.5	0.48	σ^E	ε^E	σ^E
6.4	93.3	478.5	0.51			
6.5	92.6	426.8	0.46			
6.6	92.1	484.7	0.52			
Average	92.6	453.0	0.49			
$\psi_{\bar{x}}$	0.4	10.9	0.01			
CV%	0.97	5.9	6.12			

Table 2A8 Continued

SLAB 7 7C (no c.-a.) $V_T\% = V_{cf}\% = 37.73\%$

Specimen	E KN/mm^2	σ^E N/mm^2	ε^E %	σ' N/mm^2	ε' %	$\hat{\sigma}$ N/mm^2
7.1	93.7	368.0	0.39			
7.2	93.3	428.1	0.46			
7.3	94.4	469.8	0.50	σ^E	ε^E	σ^E
7.4	92.4	446.9	0.48			
7.5	93.7	482.1	0.51			
7.6	92.3	451.4	0.49			
Average	93.3	441.4	0.47			
$\psi_{\bar{x}}$	0.3	16.5	0.02			
CV%	0.86	9.16	8.51			

SLAB 8 $4G_6$ $V_T\% = V_{g6}\% = 22.34\%$

8.1	19.3	320.0	1.66			
8.2	19.9	384.5	1.93			
8.3	19.4	330.6	1.70	σ^E	ε^E	σ^E
8.4	19.1	401.5	2.10			
8.5	19.5	355.6	1.82			
Average	19.4	358.4	1.84			
$\psi_{\bar{x}}$	0.1	14.1	0.07			
CV%	1.55	9.65	9.78			

SLAB 9 $5G_6$ $V_T\% = V_{g6}\% = 27.38\%$

9.1	23.7	526.2	2.22			
9.2	23.1	496.4	2.15			
9.3	22.6	463.2	2.05	σ^E	ε^E	σ^E
9.4	24.0	469.5	1.96			
9.5	23.0	460.7	2.00			
9.6	22.3	469.0	2.10			
Average	23.1	480.8	2.08			
$\psi_{\bar{x}}$	0.2	10.5	0.04			
CV%	2.60	5.32	4.81			

Table 2A8 Continued

SLAB 10 $6G_6$ $V_r\% = V_{g6}\% = 33.51\%$

Specimen	E KN/mm^2	σ^E N/mm^2	ε^E %	σ' N/mm^2	ε' %	$\hat{\sigma}$ N/mm^2
10.1	27.2	521.8	1.92			
10.2	28.9	635.5	2.20			
10.3	27.9	564.2	2.02	σ^E	ε^E	σ^E
10.4	28.3	617.5	2.18			
10.5	27.0	490.9	1.82			
Average	27.9	566.0	2.03			
$\psi_{\bar{x}}$	0.4	27.5	0.07			
CV%	2.87	10.85	7.88			

SLAB 11 $7G_6$ $V_r\% = V_{g6}\% = 39.09\%$

11.1	32.1	597.3	1.86			
11.2	32.8	658.4	2.01			
11.3	31.1	525.1	1.69			
11.4	31.5	567.3	1.80	σ^E	ε^E	σ^E
11.5	31.1	535.3	1.72			
11.6	32.7	690.5	2.11			
Average	31.9	595.7	1.87			
$\psi_{\bar{x}}$	0.3	27.3	0.07			
CV%	2.51	11.23	9.09			

SLAB 12 $8G_6$ $V_r\% = V_{g6}\% = 45.60\%$

12.1	35.2	552.4	1.57			
12.2	36.5	730.1	2.00			
12.3	36.9	867.6	2.35	σ^E	ε^E	σ^E
12.4	36.4	786.4	2.16			
12.5	36.3	631.6	1.74			
Average	36.3	713.6	1.96			
$\psi_{\bar{x}}$	0.3	55.7	0.14			
CV%	1.65	17.45	7.14			

TABLE 2A8 Continued

SLAB 13 $9G_6$ $V_T\% = V_{g6}\% = 51.30\%$

Specimen	E KN/mm^2	σ^{ε} N/mm^2	$\varepsilon^{\varepsilon}$ %	σ' N/mm^2	ε' %	$\hat{\sigma}$ N/mm^2
13.1	40.7	773.6	1.90			
13.2	39.3	754.5	1.92			
13.3	40.4	820.1	2.03	σ^{ε}	$\varepsilon^{\varepsilon}$	σ^{ε}
13.4	39.9	807.3	2.02			
13.5	40.8	839.0	2.06			
Average	40.2	798.9	1.99			
$\psi_{\bar{x}}$	0.3	15.4	0.03			
CV%	1.49	4.31	3.52			

SLAB 14 $7G_6$ (A187) $V_T\% = V_{g6}\% = 39.09\%$

14.1	31.3	326.0	1.04			
14.2	32.9	335.9	1.02			
14.3	31.9	338.3	1.06	σ^{ε}	$\varepsilon^{\varepsilon}$	σ^{ε}
14.4	31.9	322.9	1.01			
14.5	31.5	323.9	1.05			
Average	31.9	329.4	1.04			
$\psi_{\bar{x}}$	0.3	3.2	0.01			
CV%	1.88	2.19	1.92			

SLAB 15 $7G_6$ (A1100) $V_T\% = V_{g6}\% = 39.09\%$

15.1	31.2	515.4	1.65			
15.2	31.7	494.8	1.56			
15.3	30.9	445.2	1.44	σ^{ε}	$\varepsilon^{\varepsilon}$	σ^{ε}
15.4	32.0	554.0	1.72			
15.5	31.3	507.8	1.62			
15.6	31.6	524.9	1.66			
Average	31.4	507.0	1.61			
$\psi_{\bar{x}}$	0.2	14.8	0.04			
CV%	1.27	7.14	6.21			

TABLE 2A8 Continued

SLAB 16 $7G_6$ (no c.-a.) $V_T\% = V_{g6}\% = 39.09\%$

Specimen	E KN/mm^2	σ^E N/mm^2	ε^E %	σ' N/mm^2	ε' %	$\hat{\sigma}$ N/mm^2
16.1	31.4	291.9	0.93			
16.2	32.3	294.0	0.91			
16.3	31.9	254.8	0.80	σ^E	ε^E	σ^E
16.4	31.6	255.8	0.81			
16.5	31.7	298.3	0.94			
Average	31.8	279.0	0.88			
$\psi_{\bar{x}}$	0.1	9.7	0.03			
CV%	0.94	3.48	7.95			

SLAB 17 $5G_5$ $V_T\% = V_{g5}\% = 27.38\%$

17.1	25.3	546.1	2.16			
17.2	25.1	543.7	2.17			
17.3	25.9	515.9	1.99	σ^E	ε^E	σ^E
17.4	26.3	508.5	1.93			
17.5	26.4	490.9	1.86			
17.6	24.8	520.4	2.10			
Average	25.6	520.9	2.03			
$\psi_{\bar{x}}$	0.3	8.6	0.05			
CV%	2.73	4.05	6.40			

SLAB 18 $6G_5$ $V_T\% = V_{g5}\% = 33.51\%$

18.1	30.7	613.3	2.00			
18.2	30.7	543.8	1.77			
18.3	30.9	615.5	1.99	σ^E	ε^E	σ^E
18.4	29.7	630.1	2.12			
18.5	30.4	574.8	1.89			
18.6	30.3	597.0	1.97			
Average	30.5	595.7	1.96			
$\psi_{\bar{x}}$	0.2	12.9	0.02			
CV%	1.31	5.32	1.89			

Table 2A8 Continued

SLAB 19 $7G_5$ $V_T\% = V_{g5}\% = 39.09\%$

Specimen	E KN/mm^2	σ^E N/mm^2	ε^E %	σ' N/mm^2	ε' %	$\hat{\sigma}$ N/mm^2
19.1	34.4	707.6	2.06			
19.2	34.1	732.1	2.15			
19.3	35.3	762.0	2.16	σ^E	ε^E	σ^E
19.4	34.2	739.0	2.16			
19.5	34.6	727.8	2.10			
19.6	34.9	740.7	2.12			
Average	34.6	734.9	2.12			
$\psi_{\bar{x}}$	0.2	7.3	0.02			
CV%	1.45	2.42	1.89			

SLAB 20 8_{G5} $V_T\% = V_{g5}\% = 44.68\%$

20.1	38.6	749.9	1.94			
20.2	39.8	824.9	2.07			
20.3	38.7	789.9	2.04	σ^E	ε^E	σ^E
20.4	40.0	732.8	1.83			
20.5	38.3	746.8	1.95			
20.6	39.5	782.3	1.98			
Average	39.2	771.1	1.97			
ψ_R	0.3	14.0	0.03			
CV%	1.79	4.45	4.06			

SLAB 21 $7G_5$ (A187) $V_T\% = V_{g5}\% = 39.09\%$

21.1	34.2	403.6	1.18			
21.2	35.5	471.5	1.33			
21.3	34.5	406.6	1.18	σ^E	ε^E	σ^E
21.4	35.4	449.1	1.27			
21.5	35.4	435.0	1.23			
21.6	35.0	478.8	1.37			
Average	35.0	440.8	1.26			
$\psi_{\bar{x}}$	0.2	13.0	0.03			
CV%	1.43	7.21	6.35			

Table 2A8 Continued

SLAB 22 $7G_5$ (A1100) $V_r\% = V_{g5}\% = 39.09\%$

Specimen	E KN/mm^2	σ^{ε} N/mm^2	$\varepsilon^{\varepsilon}$ %	σ' N/mm^2	ε' %	$\hat{\sigma}$ N/mm^2
22.1	35.7	600.3	1.68			
22.2	34.1	542.2	1.59			
22.3	34.3	562.9	1.64	σ^{ε}	$\varepsilon^{\varepsilon}$	σ^{ε}
22.4	34.5	580.5	1.68			
22.5	35.8	551.2	1.54			
22.6	34.8	567.3	1.63			
Average	34.9	567.4	1.63			
$\psi_{\bar{x}}$	0.3	8.5	0.02			
CV%	2.01	3.67	3.07			

SLAB 23 $7G_5$ (no c.-a.) $V_r\% = V_{g5}\% = 39.09\%$

23.1	35.5	365.7	1.03			
23.2	34.9	416.3	1.19			
23.3	34.8	390.4	1.12	σ^{ε}	$\varepsilon^{\varepsilon}$	σ^{ε}
23.4	35.2	366.1	1.04			
23.5	34.3	315.2	0.92			
23.6	35.6	370.7	1.04			
Average	35.1	370.7	1.06			
$\psi_{\bar{x}}$	0.2	13.6	0.04			
CV%	1.42	9.01	8.49			

SLAB 24 4 x 3:1 $V_r\% = 22.54$ $V_{c\ell}\% = 5.54\%$ $V_{g6}\% = 17.00\%$

24.1	28.4	199.1	0.70			289.1
24.2	26.5	195.0	0.74			253.5
24.3	26.6	218.0	0.82	σ^{ε}	$\varepsilon^{\varepsilon}$	304.7
24.4	29.2	239.3	0.82			271.7
24.5	29.8	214.2	0.72			356.2
24.6	28.4	210.4	0.74			273.3
Average	28.1	212.7	0.76			291.4
$\psi_{\bar{x}}$	0.5	6.4	0.02			14.8
CV%	4.79	7.41	6.74			12.41

Table 2A8 Continued

SLAB 25 5 x 3:1 $V_T\% = 28.18\%$ $V_{cf}\% = 6.93\%$ $V_{g6}\% = 21.25\%$

Specimen	E KN/mm^2	σ^E N/mm^2	ε^E %	σ' N/mm^2	ε' %	$\hat{\sigma}$ N/mm^2
25.1	36.8	293.4	0.80			354.5
25.2	35.8	272.0	0.76			330.3
25.3	34.4	247.7	0.72	σ^E	ε^E	408.0
25.4	34.8	226.1	0.65			360.2
25.5	36.1	281.7	0.78			435.3
25.6	35.2	236.1	0.67			332.5
Average	35.5	259.5	0.73			370.1
$\psi_{\bar{x}}$	0.4	11.0	0.02			17.4
CV%	2.50	10.34	8.31			11.48

SLAB 26 6 x 3:1 $V_T\% = 33.81\%$ $V_{cf}\% = 8.31\%$ $V_{g6}\% = 25.50\%$

26.1	41.5	265.4	0.64			447.2
26.2	42.7	316.0	0.74			491.5
26.3	42.5	348.5	0.82	σ^E	ε^E	388.9
26.4	42.6	349.3	0.82			485.7
26.5	41.9	318.8	0.76			440.4
26.6	43.2	319.0	0.74			447.6
Average	42.4	319.5	0.75			450.2
$\psi_{\bar{x}}$	0.3	12.5	0.03			15.1
CV%	1.43	9.56	8.87			8.21

SLAB 27 7 x 3:1 $V_T\% = 39.45\%$ $V_{cf}\% = 9.70\%$ $V_{g6}\% = 29.75\%$

27.1	47.2	391.8	0.83			609.5
27.2	49.0	406.7	0.83			627.3
27.3	47.5	337.6	0.71	σ^E	ε^E	433.7
27.4	47.4	369.4	0.78			497.3
27.5	48.6	398.4	0.82			560.8
27.6	48.8	409.5	0.84			451.7
Average	48.1	385.6	0.80			530.0
$\psi_{\bar{x}}$	0.3	11.2	0.02			33.3
CV%	1.67	7.13	6.25			15.38

Table 2A8 Continued

SLAB 28 — 8 x 3:1 — $V_r\% = 45.08\%$ — $V_{cf}\% = 11.08\%$ — $V_{g6}\% = 34.00\%$

Specimen	E KN/mm^2	σ^{ε} N/mm^2	$\varepsilon^{\varepsilon}$ %	σ' N/mm^2	ε' %	$\hat{\sigma}$ N/mm^2
28.1	54.4	397.4	0.73			549.9
28.2	54.0	431.7	0.80			618.8
28.3	55.3	471.5	0.85	σ^{ε}	$\varepsilon^{\varepsilon}$	505.5
28.4	54.6	464.1	0.85			649.7
28.5	54.1	460.2	0.85			597.2
28.6	53.5	438.9	0.82			575.2
Average	54.3	444.0	0.82			582.8
$\psi_{\bar{x}}$	0.2	11.2	0.02			20.9
CV%	1.13	6.18	5.75			8.78

SLAB 29 — 9 x 3:1 — $V_r\% = 50.72\%$ — $V_{cf}\% = 12.47\%$ — $V_{g6}\% = 38.25\%$

29.1	60.8	499.0	0.82			741.1
29.2	61.4	503.9	0.82			657.1
29.3	61.6	517.1	0.84	σ^{ε}	$\varepsilon^{\varepsilon}$	802.8
29.4	60.4	453.1	0.75			659.9
29.5	60.2	445.7	0.74			645.9
29.6	59.7	477.3	0.80			708.5
Average	60.7	482.7	0.79			702.6
$\psi_{\bar{x}}$	0.3	11.8	0.02			24.9
CV%	1.20	5.99	5.17			8.70

SLAB 30 — 3 x 1:1 — $V_r\% = 16.59\%$ — $V_{cf}\% = 8.21\%$ — $V_{g6}\% = 8.38\%$

30.1	28.5	148.2	0.52			157.9
30.2	28.3	170.0	0.60			170.0
30.3	29.8	167.1	0.56	σ^{ε}	$\varepsilon^{\varepsilon}$	167.1
30.4	27.8	157.2	0.57			159.7
30.5	29.4	161.7	0.55			161.7
30.6	30.4	182.4	0.60			186.1
Average	29.0	164.4	0.57			167.1
$\psi_{\bar{x}}$	0.4	4.8	0.01			4.2
CV%	3.43	7.12	5.40			6.21

Table 2A8 Continued

SLAB 31 4 x 1:1 $V_r\% = 22.12\%$ $V_{cf}\% = 10.94\%$ $V_{g6}\% = 11.18\%$

Specimen	E KN/mm^2	σ^E N/mm^2	ε^E %	σ' N/mm^2	ε' %	$\hat{\sigma}$ N/mm^2
31.1	37.2	201.1	0.54			201.1
31.2	36.8	209.8	0.57			209.8
31.3	36.1	198.5	0.55	σ^E	ε^E	215.8
31.4	37.2	215.8	0.58			215.8
31.5	37.2	230.5	0.62			241.0
31.6	37.5	221.2	0.59			221.2
Average	37.0	212.9	0.57			217.5
$\psi_{\bar{x}}$	0.2	5.0	0.01			5.5
CV%	1.34	5.73	5.05			6.17

SLAB 32 5 x 1:1 $V_r\% = 27.65\%$ $V_{cf}\% = 13.68\%$ $V_{g6}\% = 13.97\%$

32.1	46.8	332.5	0.71			353.3
32.2	46.2	277.1	0.60			308.4
32.3	46.9	276.3	0.59	σ^E	ε^E	300.7
32.4	45.8	270.4	0.59			270.4
32.5	46.2	256.8	0.56			309.1
32.6	46.1	262.5	0.57			262.5
Average	46.3	279.3	0.60			300.7
$\psi_{\bar{x}}$	0.2	11.1	0.02			13.3
CV%	0.92	9.76	9.00			10.80

SLAB 33 6 x 1:1 $V_r\% = 33.18\%$ $V_{cf}\% = 16.41\%$ $V_{g6}\% = 16.77\%$

33.1	55.0	285.9	0.52			340.2
33.2	54.8	318.3	0.58			369.0
33.3	54.2	325.6	0.60	σ^E	ε^E	340.6
33.4	55.2	348.1	0.63			367.7
33.5	54.7	371.8	0.68			371.8
33.6	54.5	343.8	0.63			384.7
Average	54.7	332.2	0.61			362.3
$\psi_{\bar{x}}$	0.1	12.0	0.02			7.4
CV%	0.65	8.86	8.85			4.98

Table 2A8 Continued

Specimen	E KN/mm^2	σ^E N/mm^2	ε^E %	σ' N/mm^2	ε' %	$\hat{\sigma}$ N/mm^2
SLAB 34	7 x 1:1	$V_r\%$ = 38.71%	$V_{cf}\%$ = 19.15%	$V_{g6}\%$ = 19.56%		
34.1	64.4	412.5	0.64			442.5
34.2	63.6	394.4	0.62			394.4
34.3	63.4	374.0	0.59	σ^E	ε^E	438.6
34.4	62.7	401.5	0.64			421.8
34.5	63.0	421.9	0.67			448.4
34.6	65.1	416.6	0.64			433.8
Average	63.7	403.5	0.63			429.9
$\psi_{\bar{x}}$	0.4	7.2	0.01			8.0
CV%	1.41	4.36	4.22			4.55
SLAB 35	8 x 1:1	$V_r\%$ = 44.24%	$V_{cf}\%$ = 21.88%	$V_{g6}\%$ = 22.36%		
35.1	72.6	450.3	0.62			469.9
35.2	72.4	477.8	0.66			492.5
35.3	71.0	439.9	0.62	σ^E	ε^E	439.9
35.4	71.0	354.8	0.50			431.3
35.5	71.9	381.2	0.53			441.9
35.6	71.8	408.6	0.57			452.1
Average	71.8	418.8	0.58			454.6
$\psi_{\bar{x}}$	0.3	18.7	0.03			9.3
CV%	0.94	10.96	10.52			5.01
SLAB 36	9 x 1:1	$V_r\%$ = 49.77%	$V_{cf}\%$ = 24.62%	$V_{g6}\%$ = 25.15%		
36.1	80.8	540.6	0.67			540.6
36.2	81.1	527.3	0.65			527.3
36.3	80.4	490.5	0.61	σ^E	ε^E	524.8
36.4	80.0	504.0	0.63			516.5
36.5	79.6	461.2	0.58			461.2
36.6	80.4	434.4	0.54			521.3
Average	80.4	493.0	0.61			515.3
$\psi_{\bar{x}}$	0.2	16.3	0.02			11.3
CV%	0.67	8.12	7.87			5.38

Table 2A8 Continued

SLAB 37 CG_6G_6C $V_T\% = 21.95\%$; $V_{cf}\% = 10.78\%$ $V_{g6}\% = 11.17\%$

Specimen	E KN/mm^2	σ^{ε} N/mm^2	$\varepsilon^{\varepsilon}$ %	σ' N/mm^2	ε' %	$\hat{\sigma}$ N/mm^2
37.1	37.2	156.2	0.42			182.0
37.2	37.9	185.5	0.49			241.6
37.3	37.7	169.5	0.45	σ^{ε}	$\varepsilon^{\varepsilon}$	191.2
37.4	37.4	175.6	0.47			234.0
37.5	37.0	159.0	0.43			226.4
37.6	36.7	165.3	0.45			207.7
Average	37.3	168.5	0.45			213.8
$\psi_{\bar{x}}$	0.2	4.4	0.01			9.8
CV%	1.19	6.46	5.78			11.26

SLAB 38 $CG_6CG_6G_6CG_6C$ $V_T\% = 43.90\%$ $V_{cf}\% = 21.56\%$ $V_{g6}\% = 22.34\%$

38.1	72.2	324.7	0.45	407.1	0.68	419.6
38.2	71.2	313.4	0.44	398.0	0.64	398.0
38.3	70.7	374.5	0.53	423.3	0.65	428.2
38.4	70.9	368.9	0.52	408.8	0.61	418.8
38.5	71.5	321.7	0.45	430.6	0.63	430.6
38.6	71.2	313.1	0.44	323.0	0.48	333.0
Average	71.3	336.0	0.47	398.5	0.62	404.7
$\psi_{\bar{x}}$	0.2	11.4	0.02	15.8	0.03	15.1
CV%	0.74	8.35	8.87	9.74	11.29	9.13

SLAB 39 $G_6G_6CG_6G_6CG_6G_6$ $V_T\% = 44.29\%$ $V_{cf}\% = 10.78\%$ $V_{g6}\% = 33.51\%$

39.1	53.9	403.9	0.75	440.6	0.85	440.6
39.2	53.7	429.5	0.80	483.2	0.95	541.9
39.3	52.9	397.0	0.75	484.1	0.95	484.1
39.4	54.5	461.4	0.85	529.4	1.00	597.4
39.5	53.4	436.6	0.82	436.6	0.82	566.4
39.6	53.6	363.2	0.68	426.1	0.90	440.6
Average	53.7	415.3	0.78	466.7	0.91	511.8
$\psi_{\bar{x}}$	0.2	14.1	0.02	16.1	0.03	27.2
CV%	0.99	8.31	7.81	8.43	7.46	13.00

Table 2A8 Continued

SLAB 40 $G_5G_5CG_5G_5CG_5G_5$ $V_r\% = 44.29\%$ $V_{cf}\% = 10.78\%$ $V_{g5}\% = 33.51\%$

Specimen	E KN/mm^2	σ^E N/mm^2	ε^E %	σ' N/mm^2	ε' %	$\hat{\sigma}$ N/mm^2
40.1	55.8	479.5	0.86	517.8	0.97	585.0
40.2	56.5	502.5	0.89	531.2	0.96	603.0
40.3	56.5	463.3	0.82	544.5	0.99	644.8
40.4	55.8	468.9	0.84	536.4	1.00	575.1
40.5	57.0	524.5	0.92	548.8	0.99	660.5
40.6	56.5	486.1	0.86	510.4	0.93	583.3
Average	56.3	487.5	0.86	531.5	0.97	608.6
$\psi_{\bar{x}}$	0.2	9.3	0.02	6.1	0.01	14.6
CV%	0.82	4.67	4.19	2.82	2.68	5.86

SLAB 41 $G_63{:}1G_63{:}1G_63{:}1G_6$ $V_r\% = 39.15\%$ $V_{cf}\% = 4.16\%$ $V_{g6}\% = 34.99\%$

41.1	39.0	362.5	0.93	362.5	0.93	582.4
41.2	39.6	372.7	0.94	407.9	1.06	614.3
41.3	39.0	349.6	0.90	367.1	0.95	568.4
41.4	39.1	340.3	0.87	402.9	1.07	468.9
41.5	38.7	367.9	0.95	367.9	0.95	613.0
41.6	38.2	308.4	0.81	407.9	1.13	616.8
Average	38.9	350.2	0.90	386.0	1.02	577.3
$\psi_{\bar{x}}$	0.2	9.7	0.02	9.1	0.03	23.1
CV%	1.18	6.78	5.89	5.77	8.08	9.82

SLAB 42 1:1Cl:1Cl:1Cl:1 $V_r\% = 38.29\%$ $V_{cf}\% = 27.11\%$ $V_{g6}\% = 11.18\%$

42.1	76.2	449.5	0.59			
42.2	78.2	445.6	0.57			
42.3	75.9	394.5	0.52	σ^E	ε^E	σ^E
42.4	76.2	426.6	0.56			
42.5	75.0	367.6	0.49			
42.6	76.1	411.0	0.54			
Average	76.3	415.8	0.54			
$\psi_{\bar{x}}$	0.4	12.8	0.01			
CV%	1.38	7.56	6.70			

Table 2A8 Continued

SLAB 43 3:1C3:1C3:1C3:1 $V_T\% = 38.71\%$ $V_{cf}\% = 21.71\%$ $V_{g6}\% = 17.00\%$

Specimen	E KN/mm^2	σ^E N/mm^2	ε^E %	σ' N/mm^2	ε' %	$\hat{\sigma}$ N/mm^2
43.1	67.7	331.8	0.49	374.2	0.54	409.2
43.2	67.5	344.3	0.51	424.2	0.66	424.2
43.3	67.2	409.6	0.61	422.1	0.64	422.1
43.4	66.9	334.0	0.50	408.8	0.64	408.8
43.5	67.8	318.6	0.47	358.1	0.55	370.5
43.6	68.0	360.4	0.53	360.4	0.53	380.4
Average	67.5	349.8	0.52	391.3	0.60	402.5
$\psi_{\bar{x}}$	0.2	13.2	0.02	12.5	0.02	9.04
CV%	0.60	9.28	9.42	7.82	8.90	5.50

SLAB 44 3:1 1:1 3:1 1:1 3:1 1:1 3:1 $V_T\% = 39.13\%$ $V_{cf}\% = 13.75\%$ $V_{g6}\% = 25.38\%$

44.1	53.6	370.1	0.69	370.1	0.69	
44.2	54.3	380.4	0.70	415.9	0.79	
44.3	55.0	462.2	0.84	462.2	0.84	σ'
44.4	55.4	454.3	0.82	518.2	0.96	
44.5	54.4	424.4	0.78	424.4	0.78	
44.6	54.6	436.7	0.80	444.1	0.83	
Average	54.6	421.4	0.77	439.2	0.82	
$\psi_{\bar{x}}$	0.3	15.6	0.03	20.3	0.04	
CV%	1.13	9.07	8.15	11.33	11.22	

SLAB 45 1:1 1:1 3:1 1:1 3:1 1:1 1:1 $V_T\% = 38.82\%$ $V_{cf}\% = 16.45\%$ $V_{g6}\% = 22.37\%$

45.1	57.9	370.8	0.64	388.1	0.69	455.0
45.2	58.4	367.9	0.63	385.0	0.67	407.9
45.3	58.4	385.4	0.66	385.4	0.66	412.5
45.4	58.0	365.4	0.63	377.7	0.65	387.5
45.5	59.6	351.8	0.59	371.6	0.65	470.7
45.6	58.7	352.1	0.60	395.5	0.69	419.7
Average	58.5	365.6	0.62	383.9	0.67	425.5
$\psi_{\bar{x}}$	0.3	5.2	0.01	3.4	0.01	12.7
CV%	1.05	3.48	4.17	2.16	2.74	7.33

Table 2A8 Continued

SLAB 46 $G_6CG_6CG_6CG_6$ $V_T\% = 38.51\%$ $V_{cf}\% = 16.17\%$ $V_{g6}\% = 22.34\%$

Specimen	E KN/mm^2	σ^{ϵ} N/mm^2	ϵ^{E} %	σ' N/mm^2	ϵ' %	$\hat{\sigma}$ N/mm^2
46.1	58.5	315.8	0.54	370.1	0.66	370.1
46.2	58.0	394.2	0.68	394.2	0.68	394.2
46.3	57.9	347.2	0.60	384.4	0.69	391.7
46.4	58.9	359.2	0.61	376.4	0.65	403.1
46.5	58.1	302.0	0.52	391.4	0.71	391.4
46.6	58.6	346.0	0.59	379.1	0.67	418.4
Average	58.3	344.1	0.59	382.6	0.68	394.8
	0.2	13.3	0.02	3.8	0.01	6.5
CV%	0.67	9.48	9.59	2.40	3.18	4.02

SLAB 47 $G_5CG_5CG_5CG_5$ $V_T\% = 38.51\%$ $V_{cf}\% = 16.17\%$ $V_{g5}\% = 22.34\%$

47.1	59.3	397.0	0.67	447.8	0.80	447.8
47.2	60.3	404.3	0.67	448.2	0.77	448.2
47.3	59.5	333.1	0.56	415.3	0.75	415.3
47.4	60.0	329.9	0.55	402.7	0.72	407.6
47.5	60.0	329.1	0.55	390.1	0.69	390.1
47.6	59.6	345.4	0.58	446.6	0.81	458.9
Average	59.8	356.5	0.60	425.1	0.76	428.0
	0.2	14.2	0.02	10.5	0.02	11.2
CV%	0.63	9.76	9.65	6.07	6.09	6.41

SLAB 48 $G_6CG_6CG_6CG_6$(G_6 no c.-a.) $V_T\% = 38.51\%$ $V_{cf}\% = 16.17\%$ $V_{g6}\% = 22.34\%$

48.1	58.8	323.5	0.55			
48.2	58.5	292.4	0.50			
48.3	58.0	278.2	0.48	σ^{ϵ}	ϵ^{E}	σ^{E}
48.4	59.3	332.2	0.56			
48.5	58.5	321.8	0.55			
48.6	58.7	316.8	0.54			
Average	58.6	310.8	0.53			
	0.2	8.5	0.01			
CV%	0.73	6.71	5.67			

Table 2A8 Continued

SLAB 49 $G_5CG_5CG_5CG_5$ (G_5 no c.-a.) $V_T\% = 38.51\%$ $V_{cf}\% = 16.17\%$ $V_{g5} = 22.34\%$

Specimen	E KN/mm^2	σ^ϵ N/mm^2	ϵ^ϵ %	σ' N/mm^2	ϵ' %	$\hat{\sigma}$ N/mm^2
49.1	59.5	309.6	0.52			
49.2	60.2	337.1	0.56			
49.3	59.5	339.3	0.57	σ^ϵ	ϵ^ϵ	σ^ϵ
49.4	60.2	300.9	0.50			
49.5	59.9	301.3	0.50			
49.6	59.0	306.6	0.52			
Average	59.7	315.8	0.53			
$\psi_{\bar{x}}$	0.2	7.2	0.01			
CV%	0.79	5.60	5.65			

SLAB 50 $G_6CG_6CG_6CG_6$ (G_6 A1100) $V_T\% = 38.51\%$ $V_{cf}\% = 16.17\%$ $V_{g6}\% = 22.34\%$

50.1	57.6	333.9	0.58	375.6	0.67	
50.2	58.2	314.1	0.54	386.7	0.69	
50.3	57.7	369.1	0.64	384.0	0.68	σ'
50.4	57.5	345.1	0.60	372.2	0.67	
50.5	58.4	356.0	0.61	386.5	0.68	
50.6	58.8	352.8	0.60	404.3	0.71	
Average	58.0	345.2	0.60	384.9	0.68	
$\psi_{\bar{x}}$	0.2	7.8	0.01	4.6	0.01	
CV%	0.89	5.56	5.55	2.92	2.21	

SLAB 51 $G_5CG_5CG_5CG_5$ (G_5 A1100) $V_T\% = 38.51\%$ $V_{cf}\% = 16.17\%$ $V_{g6}\% = 22.34\%$

51.1	59.0	371.7	0.63	429.6	0.76	
51.2	60.3	446.4	0.74	446.4	0.74	
51.3	60.9	383.4	0.63	454.7	0.77	σ'
51.4	59.6	369.8	0.62	447.4	0.78	
51.5	60.8	383.2	0.63	431.8	0.73	
51.6	60.0	336.1	0.56	377.6	0.65	
Average	60.1	381.8	0.63	431.2	0.74	
$\psi_{\bar{x}}$	0.3	14.7	0.02	11.4	0.02	
CV%	1.21	9.45	9.24	6.49	6.36	

Table 2A8 Continued

SLAB 52 $G_6CG_6CG_6CG_6$ (G_6 A187) $V_T\% = 38.51\%$ $V_{cf}\% = 16.17\%$ $V_{g6}\% = 22.34$

Specimen	E KN/mm^2	σ^E N/mm^2	ε^E %	σ' N/mm^2	ε' %	$\hat{\sigma}$ N/mm^2
52.1	58.4	333.0	0.57	342.9	0.60	
52.2	57.8	329.3	0.57	356.8	0.65	
52.3	58.1	331.0	0.57	348.2	0.63	σ'
52.4	57.7	340.3	0.59	345.3	0.61	
52.5	57.2	319.8	0.56	330.7	0.60	
52.6	57.9	341.5	0.59	350.8	0.63	
Average	57.9	332.5	0.57	345.8	0.62	
$\psi_{\bar{x}}$	0.2	3.2	0.01	3.6	0.01	
CV%	0.70	2.39	2.15	2.55	3.23	

SLAB 53 $G_5CG_5CG_5CG_5$ (G_5 A187) $V_T\% = 38.51\%$ $V_{cf}\% = 16.17\%$ $V_{g5}\% = 22.34$

53.1	60.2	331.1	0.55	397.3	0.69	
53.2	60.4	326.3	0.54	333.5	0.57	
53.3	60.1	336.4	0.56	389.5	0.68	σ'
53.4	59.2	485.0	0.82	527.7	0.91	
53.5	60.7	352.1	0.58	403.5	0.69	
53.6	60.9	359.6	0.59	399.6	0.68	
Average	60.2	365.1	0.61	408.5	0.70	
$\psi_{\bar{x}}$	0.2	24.5	0.04	26.1	0.04	
CV%	0.99	16.46	17.4	15.65	15.90	

SLAB 54 $G_6CG_6CG_6CG_6$ (G A187, C etched) $V_T\% = 38.38\%$ $V_{cf}\% = 16.04\%$ $V_{g6}\% = 22.34\%$

54.1	58.8	305.6	0.52	322.9	0.57	
54.2	57.9	295.5	0.51	349.7	0.66	
54.3	58.5	363.0	0.62	412.0	0.73	σ'
54.4	57.6	328.6	0.57	333.5	0.59	
54.5	58.5	322.0	0.55	356.7	0.65	
54.6	57.9	318.4	0.55	356.4	0.67	
Average	58.2	322.2	0.55	355.2	0.65	
$\psi_{\bar{x}}$	0.2	9.5	0.02	12.6	0.02	
CV%	0.79	7.22	7.15	8.70	8.90	

Table 2A8 Continued

SLAB 55 $G_5CG_5CG_5CG_5$ (G_5 A187, C etched) $V_f\% = 38.38\%$ $V_{cf}\% = 16.04\%$ $V_{g5}\% = 22.34\%$

Specimen	E KN/mm^2	σ^E N/mm^2	ε^E %	σ' N/mm^2	ε' %	$\hat{\sigma}$ N/mm^2
55.1	59.5	315.5	0.53	352.5	0.61	
55.2	59.7	364.4	0.61	411.2	0.71	
55.3	59.5	321.4	0.54	388.1	0.68	σ'
55.4	60.2	348.9	0.58	396.3	0.68	
55.5	60.0	341.7	0.57	419.6	0.74	
55.6	59.1	331.0	0.56	377.5	0.66	
Average	59.7	337.2	0.56	390.9	0.68	
$\psi_{\bar{x}}$	0.2	7.4	0.01	9.9	0.02	
CV%	0.66	5.40	5.14	6.19	6.51	

SLAB 56 $G_6CG_6CG_6CG_6$ (G_6 A1100, C etched) $V_f\% = 38.38\%$ $V_{cf}\% = 16.04\%$ $V_{g6}\% = 22.34\%$

56.1	58.6	386.8	0.66			
56.2	58.2	395.5	0.68			
56.3	57.3	365.6	0.64	σ^E	ε^E	σ^E
56.4	57.1	399.8	0.70			
56.5	57.9	388.0	0.67			
56.6	57.1	393.8	0.69			
Average	57.7	388.3	0.67			
$\psi_{\bar{x}}$	0.3	4.9	0.01			
CV%	1.09	3.12	3.22			

SLAB 57 $G_5CG_5CG_5CG_5$ (G_5 A1100, C etched) $V_f\% = 38.38\%$ $V_{cf}\% = 16.04\%$ $V_{g5}\% = 22.34\%$

57.1	60.3	416.1	0.69	443.2	0.75	
57.2	60.1	394.8	0.66	409.6	0.69	
57.3	59.0	348.3	0.60	430.6	0.75	σ'
57.4	60.8	533.4	0.88	533.4	0.88	
57.5	59.4	398.0	0.67	456.9	0.79	
57.6	59.6	417.2	0.70	451.6	0.78	
Average	59.9	418.0	0.70	454.2	0.77	
$\psi_{\bar{x}}$	0.3	25.2	0.04	17.3	0.02	
CV%	1.10	14.79	11.55	9.32	8.16	

Table 2A8 Continued

SLAB 58 $G_6CG_6CG_6CG_6$ (G_6 no c.-a., C no c.-a.) $V_T\% = 38.51\%$, $V_{cf}\% = 16.17\%$, $V_{g6}\% = 22.34\%$

Specimen	E KN/mm^2	σ^E N/mm^2	ε^E %	σ' N/mm^2	ε' %	$\hat{\sigma}$ N/mm^2
58.1	57.7	271.2	0.47			
58.2	58.3	250.7	0.43			
58.3	59.0	336.3	0.57	σ^E	ε^E	σ^E
58.4	57.0	302.1	0.53			
58.5	58.2	291.0	0.50			
58.6	58.5	321.9	0.55			
Average	58.1	295.5	0.51			
$\Psi_{\bar{x}}$	0.3	12.9	0.02			
CV%	1.19	10.73	10.26			

SLAB 59 $G_5CG_5CG_5CG_5$ (G_5 no c.-a., C no c.-a.) $V_T\% = 38.51\%$, $V_{cf}\% = 16.17\%$, $V_{g5}\% = 22.34\%$

59.1	59.8	305.1	0.51			
59.2	59.8	299.0	0.50			
59.3	59.3	284.7	0.48	σ^E	ε^E	σ^E
59.4	60.2	300.9	0.50			
59.5	59.9	299.6	0.50			
59.6	60.1	312.6	0.52			
Average	59.9	300.3	0.50			
$\Psi_{\bar{x}}$	0.1	3.7	0.01			
CV%	0.53	3.05	2.65			

SLAB 60 $G_6CG_6CG_6CG_6$ (C no c.-a.) $V_T\% = 38.51\%$; $V_{cf}\% = 16.17\%$ $V_{g6}\% = 22.34\%$

60.1	58.6	333.8	0.57	377.3	0.67	
60.2	58.9	329.9	0.56	402.6	0.72	
60.3	57.8	341.3	0.59	431.6	0.78	σ'
60.4	58.4	338.5	0.58	421.3	0.76	
60.5	59.2	331.7	0.56	372.9	0.65	
60.6	58.2	331.9	0.57	392.9	0.70	
Average	58.5	334.5	0.57	399.8	0.71	
$\Psi_{\bar{x}}$	0.2	1.8	0.01	9.6	0.02	
CV%	0.85	1.33	2.05	5.88	7.04	

Table 2A8 Continued

SLAB 61 $G_5CG_5CG_5CG_5$ (C no c.-a.) $V_r\% = 38.51\%$; $V_{cf}\% = 16.17\%$, $V_{g5}\% = 22.$

Specimen	E KN/mm^2	σ^E N/mm^2	ε^E %	σ' N/mm^2	ε' %	$\hat{\sigma}$ N/mm^2
61.1	60.8	340.6	0.56	403.9	0.68	411.2
61.2	59.7	417.7	0.70	437.1	0.74	437.1
61.3	60.4	374.3	0.62	422.9	0.72	439.9
61.4	60.0	389.9	0.65	446.3	0.76	446.3
61.5	59.7	382.1	0.64	432.9	0.75	435.4
61.6	60.2	427.3	0.71	454.8	0.77	454.8
Average	60.1	388.7	0.65	433.0	0.74	437.4
$\psi_{\bar{x}}$	0.2	12.8	0.02	7.4	0.01	6.0
CV%	0.71	8.05	8.46	4.15	4.41	3.36

Table 2A9

The Main Steps in Calculating the Range of Composite Failure Stress and Strain for Slabs 1 to 23, Following Barry's[4] Model

Slabs 1 to 7	1	2	3	4	5	6	7
E_f/E_m ratio	71.84	71.84	71.84	71.84	71.84	71.84	71.84
Average V_f, %	16.17	21.56	32.34	37.73	48.51	37.43	37.73
Length Factor, F	1.601	1.410	1.144	1.041	0.867	1.046	1.041
Mean fibre diameter, d_f, μm	7.3	7.3	7.3	7.3	7.3	7.3	7.3
Fibre gauge length, mm	0.0935	0.0823	0.0668	0.0608	0.0506	0.0611	0.0608
Fibre strength, $\hat{\sigma}_{f(L_R)}$, KN/mm^2	1.90	1.94	1.99	2.02	2.08	1.96	1.97
Debond length, d_f	0 - 13	0 - 12	0 - 14	0 - 13	0 - 13	0 - 11	0 - 12
Equivalent debond length, d_f	0 - 8.1	0 - 8.5	0 - 12.2	0 - 12.5	0 - 15	0 - 10.5	0 - 11.5
L_p/L_R	1 - 2.6	1 - 2.7	1 - 3.7	1 - 3.7	1 - 4.4	1 - 3.2	1 - 3.5
CV_f %	16.6	16.6	16.6	16.6	16.6	16.4	16.5
σ^* for $L_p/L_R = 1$							
Upper	0.766	0.766	0.766	0.766	0.766	0.764	0.764
Mean	0.721	0.721	0.721	0.721	0.721	0.723	0.723
Lower	0.664	0.664	0.664	0.664	0.664	0.667	0.666
σ^* for $L_p/L_R > 1$							
Upper	0.689	0.689	0.682	0.682	0.679	0.685	0.684
Mean	0.646	0.645	0.637	0.637	0.631	0.643	0.639
Lower	0.591	0.590	0.579	0.579	0.572	0.587	0.583
$\hat{\sigma}_{af}$ for $L_p/L_R = 1$							
Upper	1.46	1.49	1.52	1.55	1.59	1.50	1.51
Mean KN/mm^2	1.37	1.40	1.43	1.46	1.50	1.42	1.42
Lower	1.26	1.29	1.32	1.34	1.38	1.31	1.31
$\hat{\sigma}_{af}$ for $L_p/L_R > 1$							
Upper	1.31	1.34	1.36	1.38	1.41	1.34	1.35
Mean KN/mm^2	1.23	1.25	1.27	1.29	1.31	1.26	1.26
Lower	1.12	1.14	1.15	1.17	1.19	1.15	1.15
Number of model elements, M							
$L_p/L_R = 1$	11230	17011	31437	40296	62253	40098	40296
$L_p/L_R > 1$	4319	6300	8496	10889	14148	12531	11513
CV_{ac} %	3.4	3.4	3.4	3.4	3.4	3.3	3.3

Cont/....

Slabs 1 to 7	1	2	3	4	5	6	7
f_{ac}	36.90	36.90	36.90	36.90	36.90	37.00	37.00
Size factor, η							
$L_p/L_R = 1$	0.779	0.770	0.754	0.750	0.742	0.751	0.750
$L_p/L_R > 1$	0.798	0.788	0.782	0.779	0.771	0.775	0.777
$\hat{\sigma}_f$ for $L_p/L_R = 1$							
Upper	1137.9	1147.0	1146.9	1162.5	1180.0	1126.1	1132.5
Mean N/mm^2	1067.4	1077.9	1078.8	1095.1	1113.2	1066.0	1065.2
Lower	982.0	993.0	996.0	1005.0	1024.1	983.4	982.5
$\hat{\sigma}_f$ for $L_p/L_R > 1$							
Upper	1045.1	1056.6	1064.0	1075.0	1087.0	1038.2	1048.5
Mean N/mm^2	981.4	985.6	993.5	1004.9	1009.9	976.2	978.5
Lower	893.6	898.9	899.8	911.4	917.5	891.0	893.2
F_c	0.173	0.227	0.333	0.386	0.492	0.383	0.386
$\hat{\sigma}_c$ for $L_p/L_R = 1$							
Upper, $\hat{\sigma}_{U1}$,	196.9	260.4	381.9	448.8	580.6	431.3	437.1
Mean, $\hat{\sigma}_{M1}$, N/mm^2	184.7	244.7	359.2	422.7	547.7	408.3	411.2
Lower, $\hat{\sigma}_{L1}$,	169.9	225.4	331.7	387.9	503.9	376.6	379.2
$\hat{\sigma}_c$ for $L_p/L_R > 1$							
Upper, $\hat{\sigma}_{U2}$,	180.8	239.8	354.3	415.0	534.8	397.6	404.7
Mean, $\hat{\sigma}_{M2}$, N/mm^2	169.8	223.7	330.8	387.9	496.9	373.9	377.7
Lower, $\hat{\sigma}_{L2}$,	154.6	204.1	299.6	351.8	451.4	341.3	344.8
$\hat{\varepsilon}_c$ for $L_p/L_R = 1$							
Upper, $\hat{\varepsilon}_{U1}$,	0.47	0.47	0.47	0.48	0.49	0.47	0.47
Mean, $\hat{\varepsilon}_{M1}$, %	0.44	0.45	0.45	0.45	0.46	0.44	0.44
Lower, $\hat{\varepsilon}_{L1}$,	0.41	0.41	0.41	0.42	0.42	0.41	0.41
for L_p/L_R 1							
Upper, $\hat{\varepsilon}_{U2}$,	0.43	0.44	0.44	0.45	0.45	0.43	0.43
Mean, $\hat{\varepsilon}_{M2}$, %	0.41	0.41	0.41	0.42	0.42	0.40	0.40
Lower, $\hat{\varepsilon}_{L2}$,	0.37	0.37	0.37	0.38	0.38	0.37	0.37

Cont/....

Slabs 8 to 16	8	9	10	11	12	13	14	15	16
E_f/E_m ratio	22.43	22.43	22.43	22.43	22.43	22.43	22.43	22.43	22.43
Average V_f, %	22.34	27.38	33.51	39.09	45.60	51.30	39.09	39.09	39.09
Length factor, F,	0.775	0.700	0.626	0.568	0.509	0.462	0.568	0.568	0.568
Mean fibre diameter, d_f, μm	12.82	12.82	12.82	12.82	12.82	12.82	12.82	12.82	12.82
Fibre gauge length	0.0795	0.0718	0.0642	0.0583	0.0522	0.0474	0.0583	0.0583	0.0583
Fibre strength, $\sigma_{f(L_R)}$, KN/mm^2	2.23	2.25	2.26	2.28	2.29	2.31	2.69	2.78	3.01
Debond length, d_f	0 - 19	0 - 18	0 - 16	0 - 16	0 - 15	0 - 14	0 - 16	0 - 16	0 - 14
Equivalent debond length, d_f	0 - 24.5	0 - 25.7	0 - 25.6	0 - 28.2	0 - 29.5	0 - 30.3	0 - 28.2	0 - 28.2	0 - 24.6
L_p/L_R	1 - 6.8	1 - 7.1	1 - 7.1	1 - 7.8	1 - 8.1	1 - 8.3	1 - 7.8	1 - 7.8	1 - 6.8
CV_f, %	8.25	8.25	8.25	8.25	8.25	8.25	20.00	19.50	21.10
σ^* for $L_p/L_R = 1$									
Upper	0.797	0.797	0.797	0.797	0.797	0.797	0.750	0.752	0.746
Mean	0.774	0.774	0.774	0.774	0.774	0.774	0.695	0.699	0.687
Lower	0.741	0.741	0.741	0.741	0.741	0.741	0.630	0.635	0.620
σ^* for $L_p/L_R > 1$									
Upper	0.802	0.806	0.806	0.816	0.818	0.819	0.620	0.628	0.605
Mean	0.746	0.746	0.746	0.747	0.748	0.749	0.553	0.560	0.542
Lower	0.687	0.681	0.681	0.681	0.679	0.664	0.478	0.486	0.472
$\hat{\sigma}_{af}$ for $L_p/L_R = 1$									
Upper	1.78	1.79	1.80	1.82	1.83	1.84	2.02	2.09	2.25
Mean KN/mm^2	1.73	1.74	1.75	1.76	1.77	1.79	1.87	1.94	2.07
Lower	1.65	1.67	1.67	1.69	1.70	1.71	1.69	1.76	1.87
$\hat{\sigma}_{af}$ for $L_p/L_R > 1$									
Upper	1.79	1.81	1.82	1.86	1.87	1.89	1.67	1.75	1.82
Mean KN/mm^2	1.66	1.68	1.69	1.70	1.71	1.73	1.49	1.56	1.63
Lower	1.53	1.53	1.54	1.55	1.55	1.53	1.29	1.35	1.42
Number of model elements, M									
$L_p/L_R = 1$	5444	7388	10113	12991	16925	20969	12991	12991	12991
$L_p/L_R > 1$	801	1041	1424	1666	2090	2526	1666	1666	1910
CV_{ac}, %	1.7	1.7	1.7	1.7	1.7	1.7	4.0	3.9	4.2

Cont/....

Slabs 8 to 16	8	9	10	11	12	13	14	15	16
β_{ac}	70.4	70.4	70.4	70.4	70.4	70.4	30.6	32.0	29.4
Size factor, η									
$L_p/L_R = 1$	0.886	0.880	0.877	0.875	0.871	0.867	0.734	0.744	0.724
$L_p/L_R > 1$	0.909	0.906	0.901	0.900	0.897	0.895	0.785	0.793	0.773
$\hat{\sigma}_f$ for $L_p/L_R = 1$									
Upper,	1577.1	1575.2	1578.6	1592.5	1593.9	1595.3	1482.7	1555.0	1629.0
Mean, N/mm^2	1532.8	1531.2	1534.8	1540.0	1541.7	1551.9	1372.6	1443.4	1498.7
Lower,	1461.9	1469.6	1464.6	1478.8	1480.7	1482.6	1240.5	1309.4	1353.9
$\hat{\sigma}_f$ for $L_p/L_R > 1$									
Upper,	1627.1	1639.9	1639.8	1674.0	1677.4	1691.6	1310.9	1387.8	1406.9
Mean, N/mm^2	1508.9	1522.1	1522.7	1530.0	1533.9	1548.4	1169.7	1237.1	1260.0
Lower,	1390.8	1386.2	1387.5	1395.0	1390.4	1369.4	1012.7	1070.6	1097.7
F_c	0.257	0.305	0.364	0.417	0.480	0.534	0.418	0.418	0.418
$\hat{\sigma}_c$ for $L_p/L_R = 1$									
Upper, $\hat{\sigma}_{u1}$,	403.2	478.7	572.5	662.6	762.6	850.4	618.0	647.4	677.3
Mean, $\hat{\sigma}_{M1}$, N/mm^2	392.5	466.1	557.2	641.4	738.2	827.7	573.1	602.0	624.5
Lower, $\hat{\sigma}_{L1}$,	375.1	447.9	532.5	616.5	709.5	791.3	518.5	547.2	565.3
$\hat{\sigma}_c$ for $L_p/L_R > 1$									
Upper, $\hat{\sigma}_{u2}$,	415.1	497.4	593.8	695.5	801.7	900.9	547.8	579.3	587.1
Mean, $\hat{\sigma}_{M2}$, N/mm^2	386.6	463.2	552.8	637.3	734.5	825.9	488.9	517.2	526.8
Lower, $\hat{\sigma}_{L2}$,	357.6	423.3	505.1	582.2	666.9	731.6	423.3	447.5	458.8
$\hat{\varepsilon}_c$ for $L_p/L_R = 1$									
Upper, $\hat{\varepsilon}_{u1}$,	2.09	2.08	2.08	2.11	2.11	2.11	1.96	2.06	2.15
Mean, $\hat{\varepsilon}_{M1}$, %	2.03	2.03	2.03	2.04	2.04	2.05	1.82	1.91	1.98
Lower, $\hat{\varepsilon}_{L1}$,	1.93	1.94	1.94	1.96	1.96	1.96	1.64	1.73	1.79
$\hat{\varepsilon}_c$ for $L_p/L_R > 1$									
Upper, $\hat{\varepsilon}_{u2}$,	2.15	2.17	2.17	2.21	2.22	2.24	1.73	1.84	1.86
Mean, $\hat{\varepsilon}_{M2}$, %	2.00	2.01	2.01	2.02	2.03	2.05	1.55	1.64	1.67
Lower, $\hat{\varepsilon}_{L2}$,	1.84	1.83	1.83	1.85	1.84	1.81	1.34	1.42	1.45

Cont/....

Slabs 17 to 23	17	18	19	20	21	22	23
E_f/E_m ratio,	24.84	24.84	24.84	24.84	24.84	24.84	24.84
Average V_f, %	27.38	33.51	39.09	44.68	39.09	39.09	39.09
Length factor, F	0.737	0.659	0.598	0.544	0.598	0.598	0.598
Mean fibre diameter, d_f, μm	11.68	11.68	11.68	11.68	11.68	11.68	11.68
Fibre gauge length, mm	0.0689	0.0616	0.0559	0.0508	0.0559	0.0559	0.0559
Fibre strength, $\hat{\sigma}_{f(L_R)}$, KN/mm^2	3.12	3.15	3.18	3.21	3.57	3.69	3.53
Debond length, d_f	0 - 20	0 - 18	0 - 18	0 - 16	0 - 17	0 - 16	0 - 15
Equivalent debond length, d_f	0 - 27.1	0 - 27.3	0 - 30.1	0 - 29.4	0 - 28.4	0 - 26.8	0 - 25.1
L_p/L_R	1 - 7.5	1 - 7.5	1 - 8.2	1 - 8.1	1 - 7.8	1 - 7.4	1 - 7.0
CV_f %	10.80	10.80	10.80	10.80	17.40	17.80	17.30
σ^* for $L_p/L_R = 1$							
Upper,	0.787	0.787	0.787	0.787	0.760	0.759	0.761
Mean,	0.757	0.757	0.757	0.757	0.713	0.710	0.714
Lower,	0.718	0.718	0.718	0.718	0.656	0.652	0.657
σ^* for $L_p/L_R > 1$							
Upper,	0.767	0.767	0.767	0.767	0.661	0.655	0.663
Mean,	0.704	0.704	0.704	0.704	0.594	0.589	0.601
Lower,	0.639	0.639	0.639	0.639	0.521	0.519	0.532
$\hat{\sigma}_{af}$ for $L_p/L_R = 1$							
Upper,	2.46	2.48	2.50	2.53	2.71	2.80	2.69
Mean, KN/mm^2	2.36	2.38	2.41	2.43	2.55	2.62	2.52
Lower,	2.24	2.26	2.28	2.30	2.34	2.41	2.32
$\hat{\sigma}_{af}$ for $L_p/L_R > 1$							
Upper,	2.39	2.42	2.46	2.48	2.36	2.42	2.34
Mean, KN/mm^2	2.20	2.22	2.24	2.26	2.12	2.17	2.12
Lower,	1.99	2.01	2.01	2.03	1.86	1.92	1.88
Number of model elements, M							
$L_p/L_R = 1$	9274	12695	16320	20526	16320	16320	16320
$L_p/L_R > 1$	1237	1693	1990	2534	2092	2205	2331
CV_{ac}, %	2.2	2.2	2.2	2.2	3.5	3.6	3.5

Cont/....

Slabs 17 to 23	17	18	19	20	21	22	23
β_{ac}	57.2	57.2	57.2	57.2	35.5	34.8	35.5
Size factor, η							
$L_p/L_R = 1$	0.851	0.848	0.844	0.842	0.760	0.760	0.760
$L_p/L_R > 1$	0.884	0.877	0.875	0.873	0.806	0.801	0.803
$\hat{\sigma}_f$ for $L_p/L_R = 1$							
Upper,	2093.5	2103.0	2110.0	2130.3	2059.6	2128.0	2044.4
Mean, N/mm^2	2008.4	2018.2	2034.0	2046.1	1938.0	1991.2	1915.4
Lower,	1906.2	1916.5	1924.3	1936.6	1778.4	1831.6	1763.2
$\hat{\sigma}_f$ for $L_p/L_R > 1$							
Upper,	2112.8	2122.3	2152.5	2165.0	1902.2	1938.4	1879.0
Mean, N/mm^2	1944.8	1946.9	1960.0	1973.0	1708.7	1738.2	1702.4
Lower,	1759.2	1762.8	1758.8	1772.2	1499.2	1537.9	1509.6
F_c	0.299	0.358	0.412	0.465	0.412	0.412	0.412
$\hat{\sigma}_c$ for $L_p/L_R = 1$							
Upper, $\hat{\sigma}_{u1}$,	625.0	752.1	868.3	991.5	848.2	875.5	842.2
Mean, $\hat{\sigma}_{m1}$, N/mm^2	600.8	723.0	838.0	953.3	799.6	820.9	790.5
Lower, $\hat{\sigma}_{l1}$,	571.7	687.9	794.1	903.3	735.5	756.8	729.3
$\hat{\sigma}_c$ for $L_p/L_R > 1$							
Upper, $\hat{\sigma}_{u2}$,	630.4	758.9	885.2	1007.2	785.2	799.7	775.9
Mean, $\hat{\sigma}_{m2}$, N/mm^2	582.6	698.4	808.4	920.0	707.3	719.2	704.8
Lower, $\hat{\sigma}_{l2}$,	529.3	634.5	727.5	828.3	621.9	638.0	626.3
$\hat{\varepsilon}_c$ for $L_p/L_R = 1$							
Upper, $\hat{\varepsilon}_{u1}$,	2.50	2.51	2.52	2.55	2.46	2.54	2.44
Mean, $\hat{\varepsilon}_{m1}$, %	2.40	2.41	2.43	2.44	2.32	2.38	2.29
Lower, $\hat{\varepsilon}_{l1}$,	2.28	2.29	2.30	2.31	2.12	2.19	2.11
$\hat{\varepsilon}_c$ for $L_p/L_R > 1$							
Upper, $\hat{\varepsilon}_{u2}$,	2.52	2.54	2.57	2.59	2.27	2.32	2.24
Mean, $\hat{\varepsilon}_{m2}$, %	2.32	2.33	2.34	2.36	2.04	2.08	2.03
Lower, $\hat{\varepsilon}_{l1}$,	2.10	2.11	2.10	2.12	1.79	1.84	1.80

Figure 1

The Relationship Between Composite Tensile Strength, $\hat{\sigma}_c$, and Fibre Volume Fraction, V_f, According to the Rule of Mixtures.

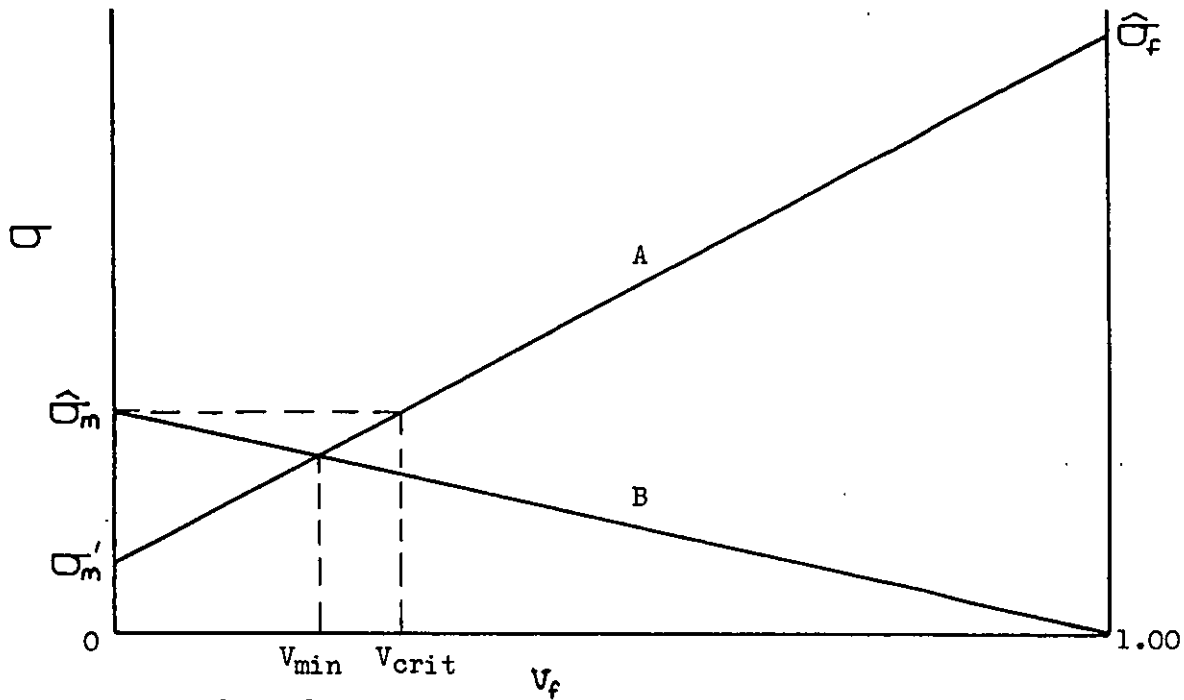

A $\hat{\sigma}_c = \hat{\sigma}_f V_f + \sigma_m' V_m$

B $\hat{\sigma}_c = \hat{\sigma}_m V_m$

Figure 2

The Unidirectional Fibre Composite Tensile Failure Model, After Zweben[2].

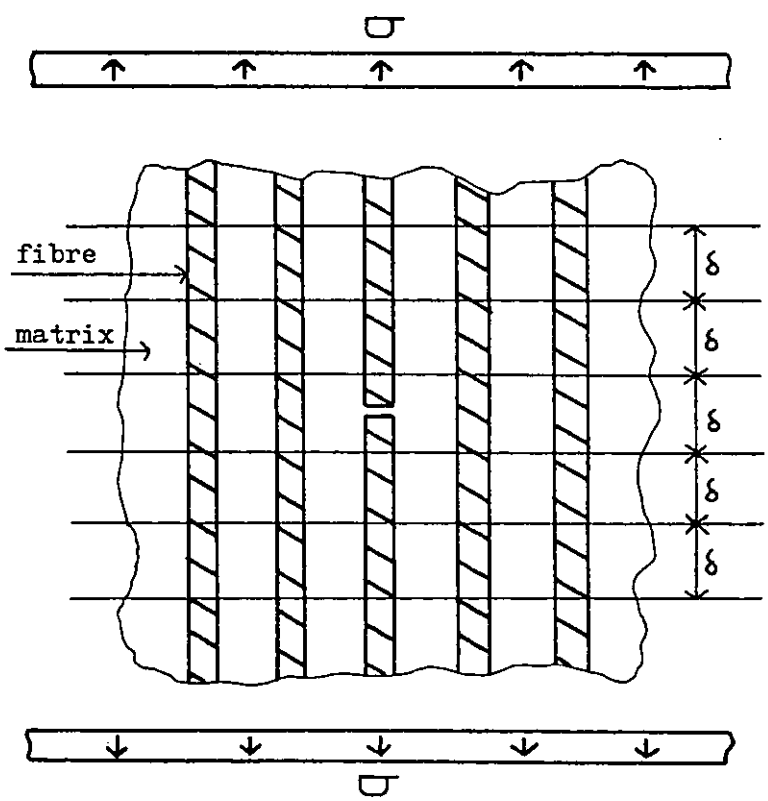

Figure 3 The Relationship between the Weibull Parameter β and the Coefficient of Variation, CV, of a Weibull Distribution $CV = \left[\frac{\Gamma(1+2/\beta)}{\Gamma^2(1+1/\beta)} - 1\right]^{1/2}$

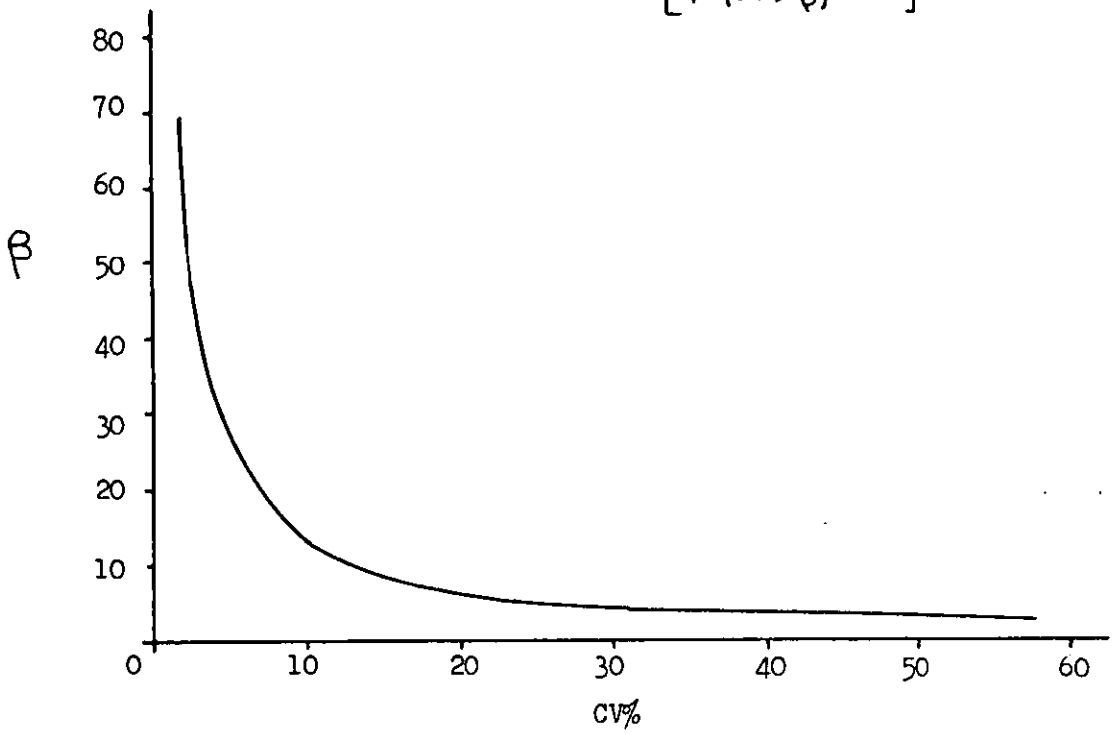

Figure 4 Stress v Strain Curves Obtained For Type I Carbon Fibre in Cured and Semi-Cured Epoxy Resin and Type I Carbon Fibre Bundle Tensile Specimens By Fuwa et al[14]

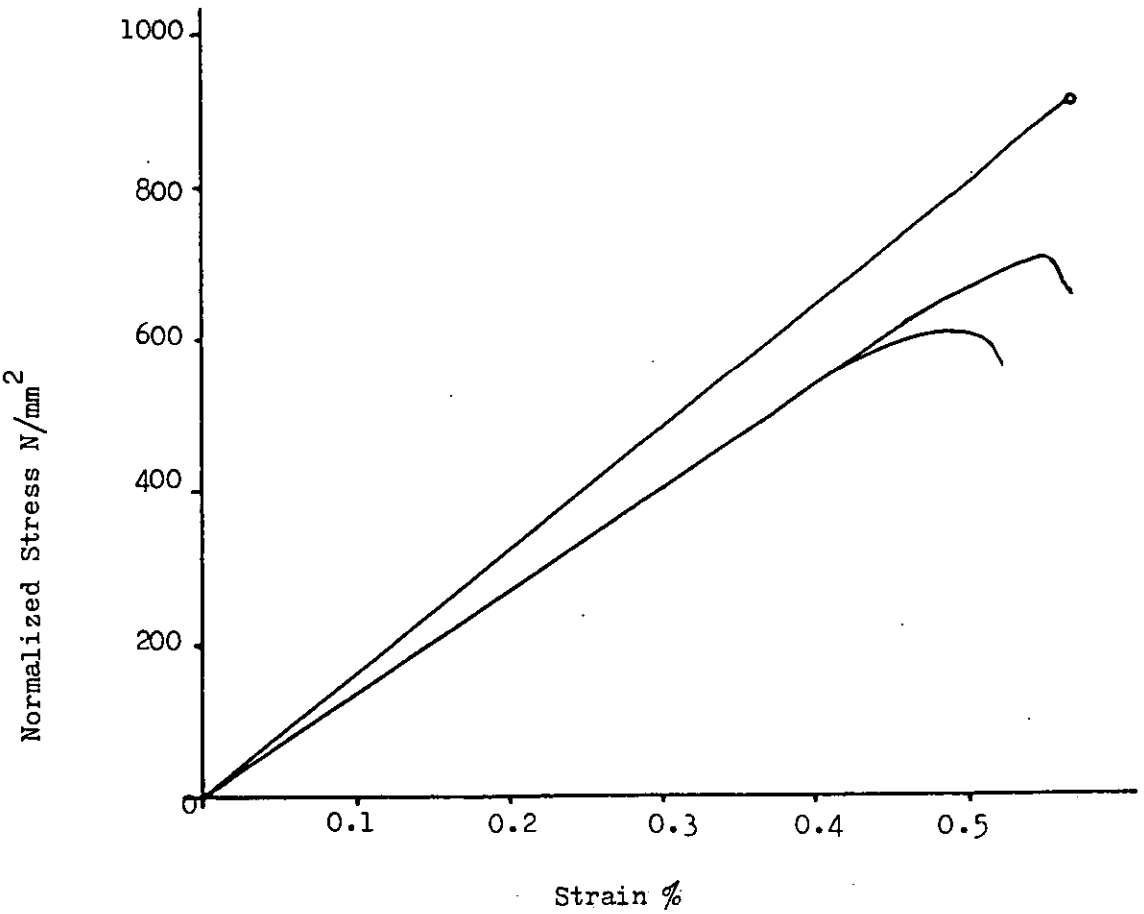

Figure 5.

The Relationships of the Model Fibre Length L_p and the Ratio $\frac{L_p}{L_R}$ to the Fibre Debond Length, After Barry[4].

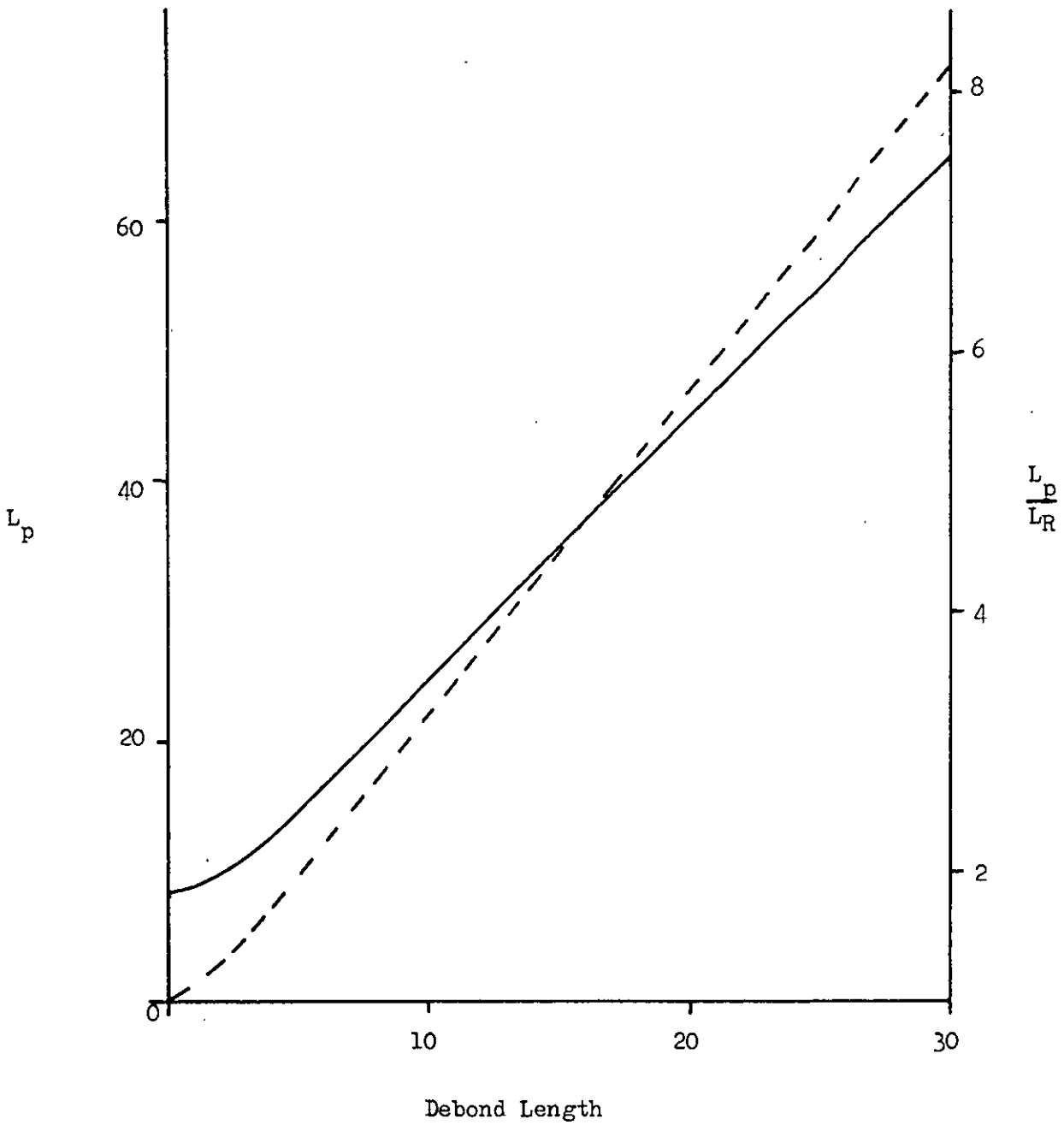

Figure 6

The Upper 95% Single Tail Scatter Limits for σ^* from the Model Composite, After Barry[4].

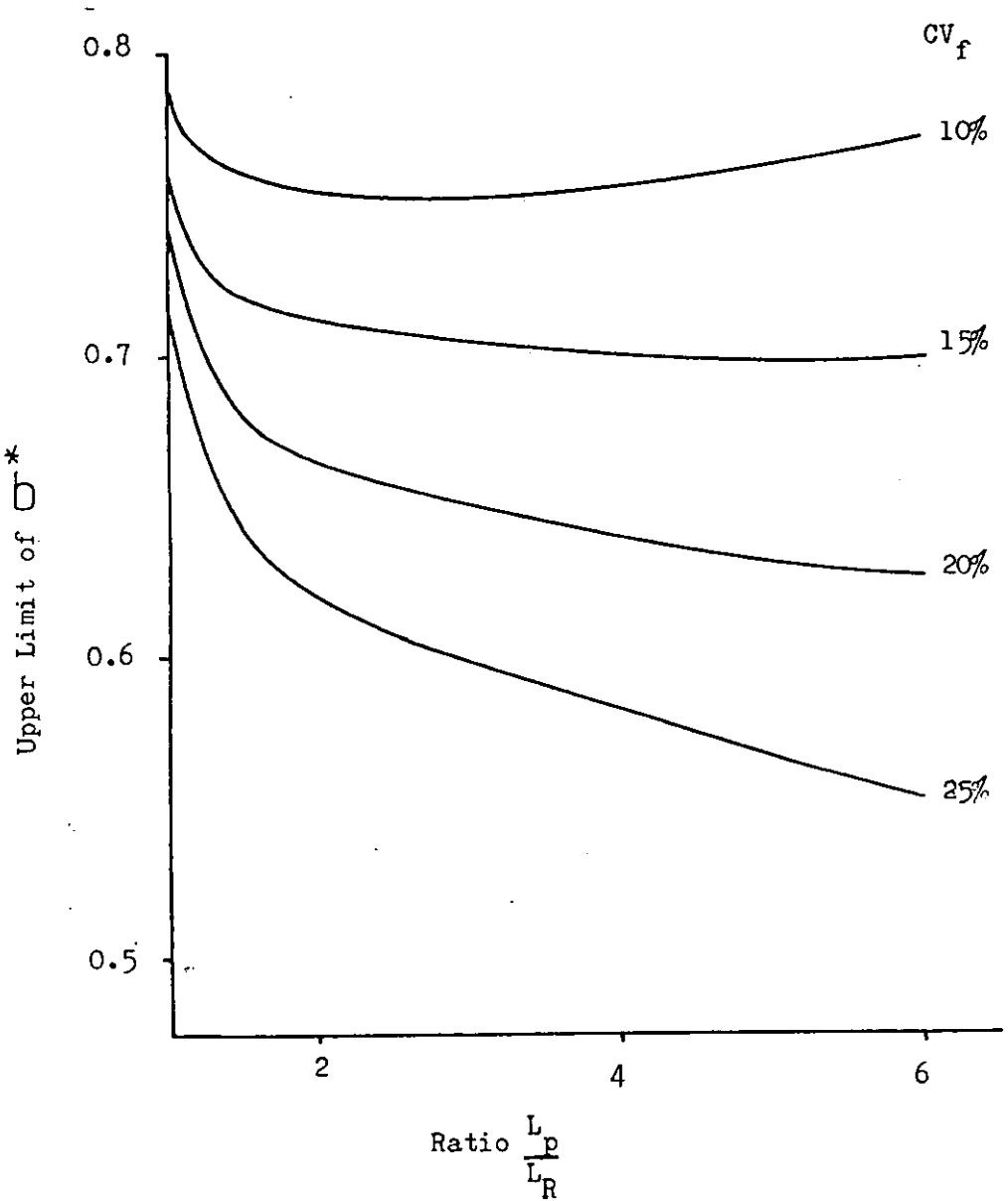

Figure 7

The Mean Values of σ^* from the Model composite, After Barry[4].

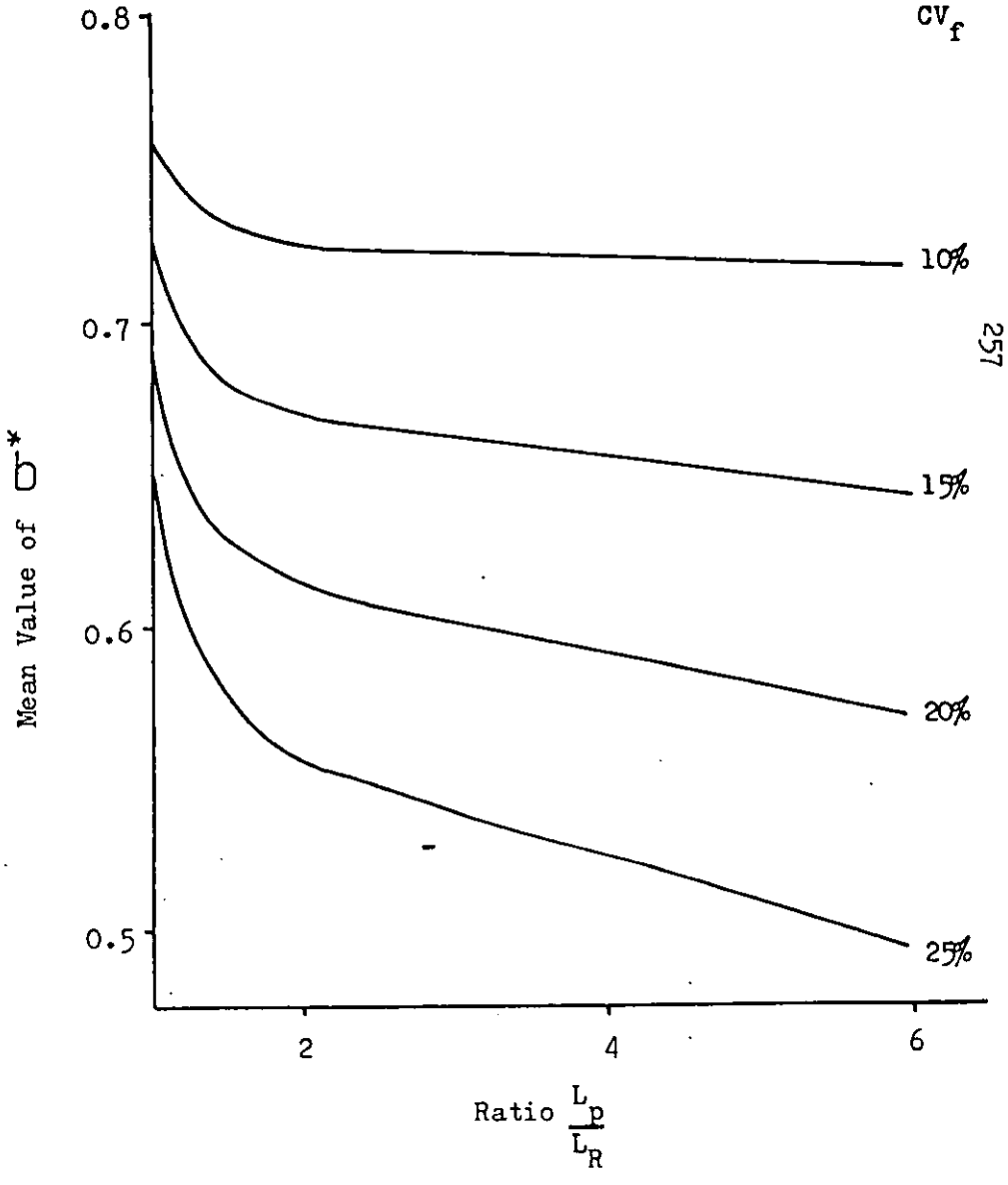

Figure 8

The Lower 95% Single Tail Scatter Limits for σ^* from the Model Composite, After Barry[4].

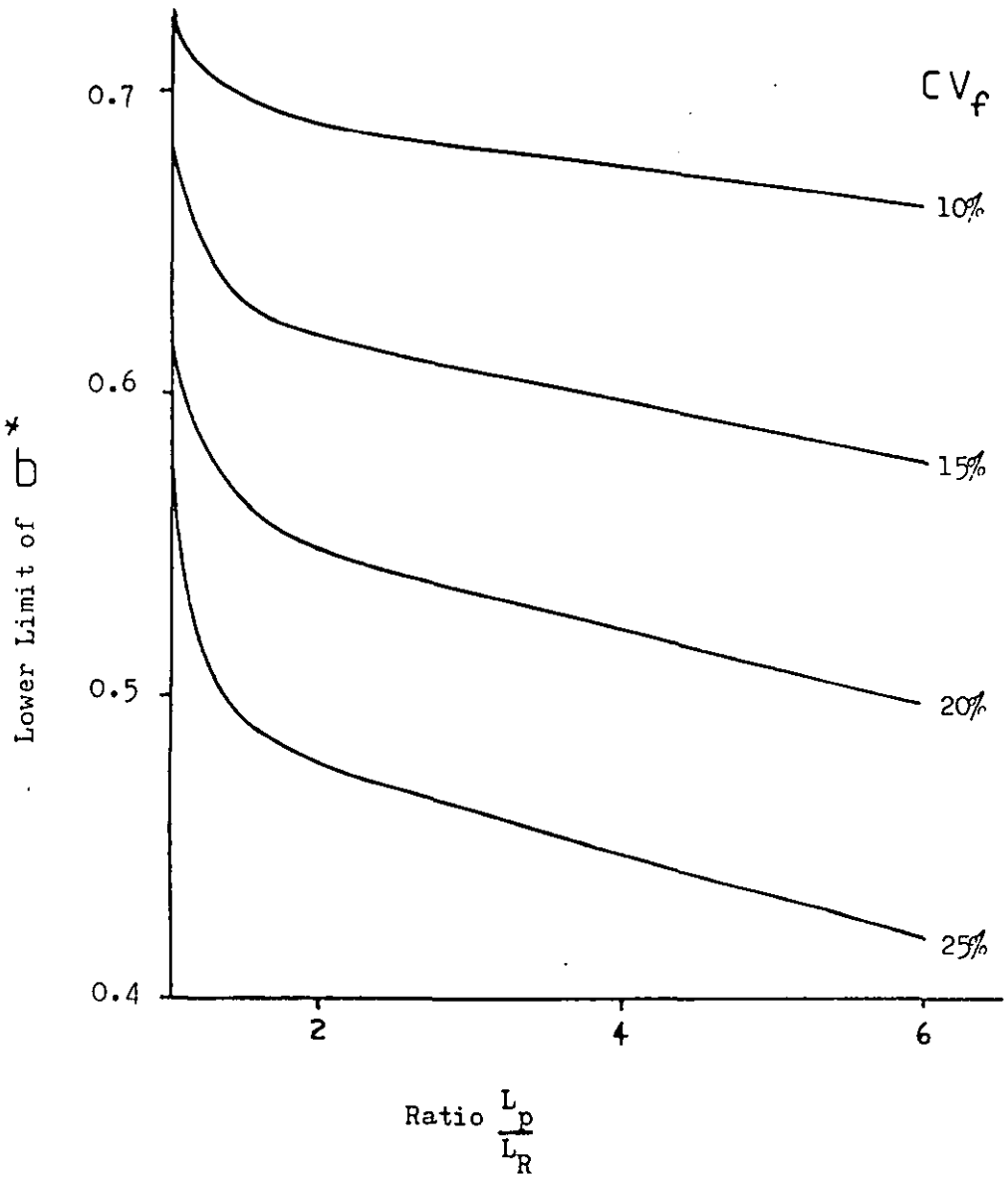

Figure 9

The Relationship Between the CV of the Model Composite Strength (CV_{ac}) and the CV of Fibre Strength (CV_f), After Barry[4].

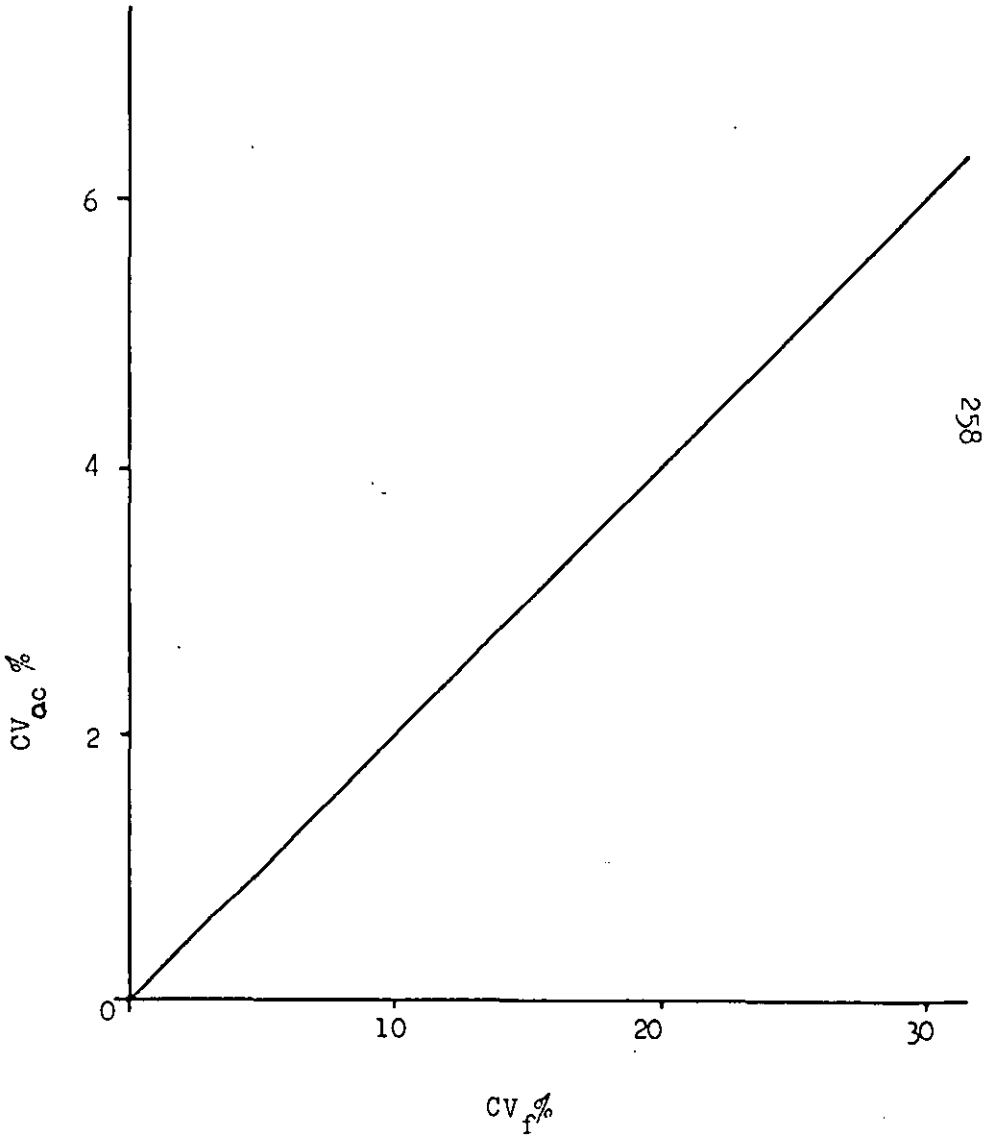

Figure 10

Tensile Property Requirements of a Material X (Hayashi[5]).

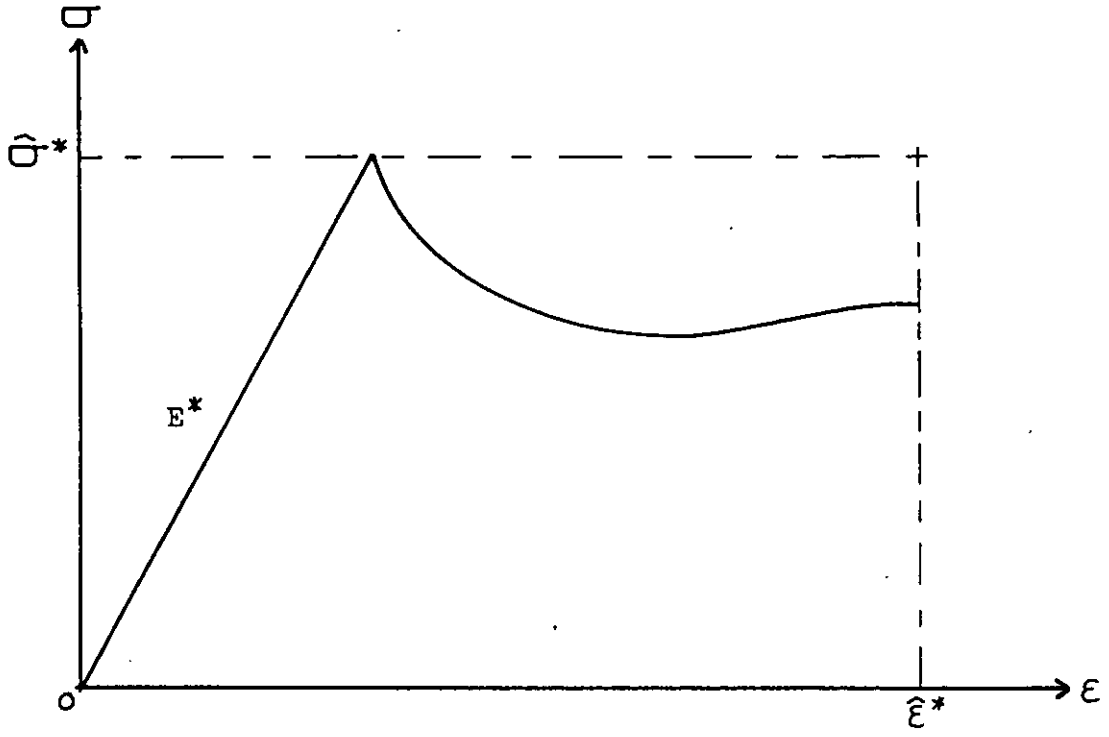

Figure 11

Tensile Properties of Materials A, B and C (Hayashi [5]).

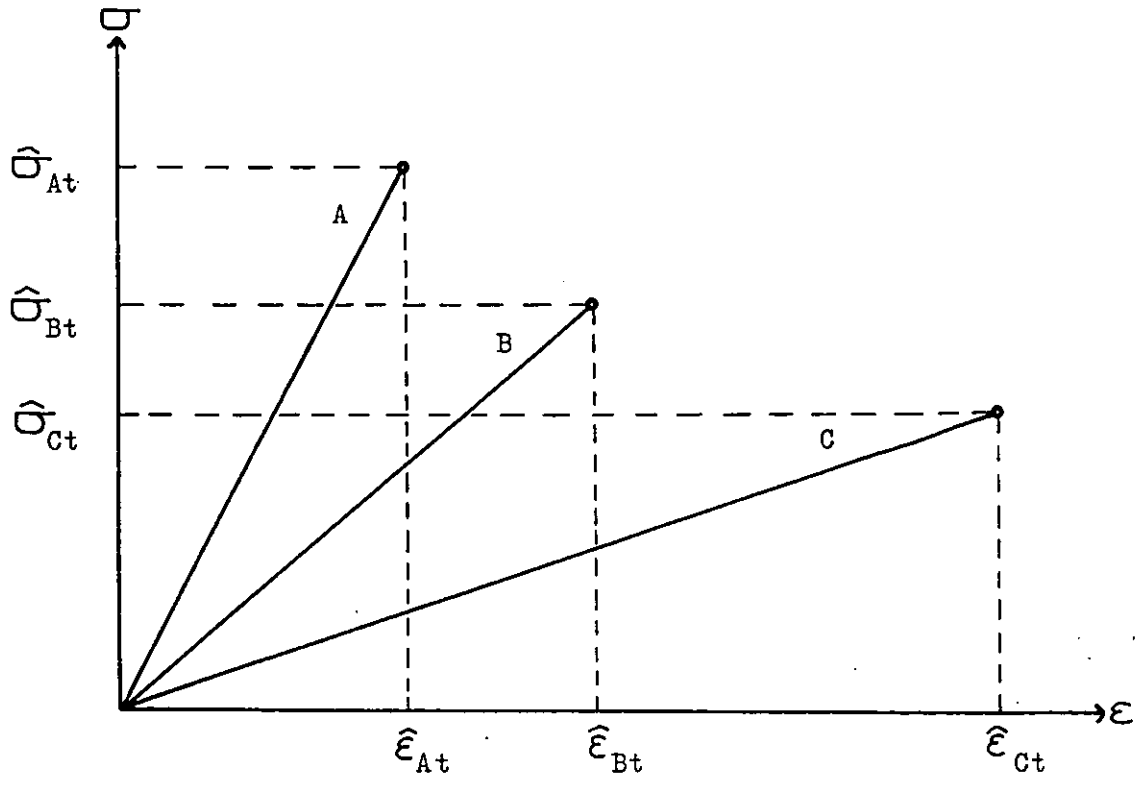

Figure 12

Theoretical Tensile Properties of the Hybrid Composite Designed from Materials A, B and C (Hayashi[5]).

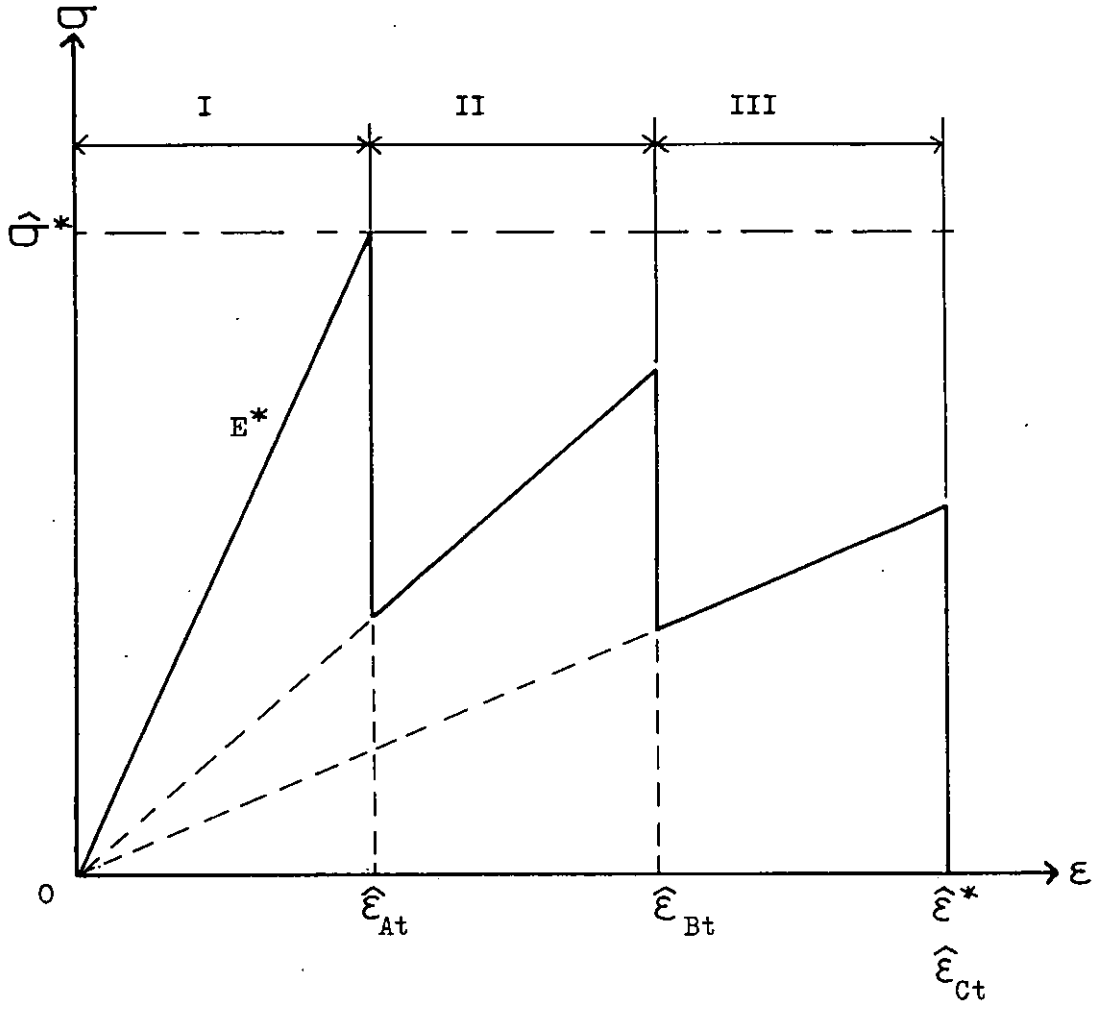

In Region I ($0 < \varepsilon \leq \hat{\varepsilon}_{At}$)

Initial Elastic Modulus = $E_I = E_A V_A + E_B V_B + E_c V_c = E^*$

Tensile Stress = $\sigma_I = E_I \varepsilon$

Ultimate Tensile Strength = $\hat{\sigma}_I = E_I \hat{\varepsilon}_{At} = \hat{\sigma}^*$

In Region II ($\hat{\varepsilon}_{At} < \varepsilon \leq \hat{\varepsilon}_{Bt}$)

Elastic Modulus = $E_{II} = E_B V_B + E_c V_c$

Tensile Stress = $\sigma_{II} = E_{II} \varepsilon$

Ultimate Tensile Strength = $\hat{\sigma}_{II} = E_{II} \hat{\varepsilon}_{Bt}$

In Region III ($\hat{\varepsilon}_{Bt} < \varepsilon \leq \hat{\varepsilon}_{Ct}$)

Elastic Modulus = $E_{III} = E_c V_c$

Tensile Stress = $\sigma_{III} = E_{III} \varepsilon$

Ultimate Tensile Strength = $\hat{\sigma}_{III} = E_{III} \hat{\varepsilon}_{Ct} = E_{III} \hat{\varepsilon}^*$

Figure 13

Comparison of the Theoretical and Experimental Stress v Strain Curves for Carbon/Epoxy, Glass/Epoxy Hybrid Composites, Obtained by Hayashi[5].

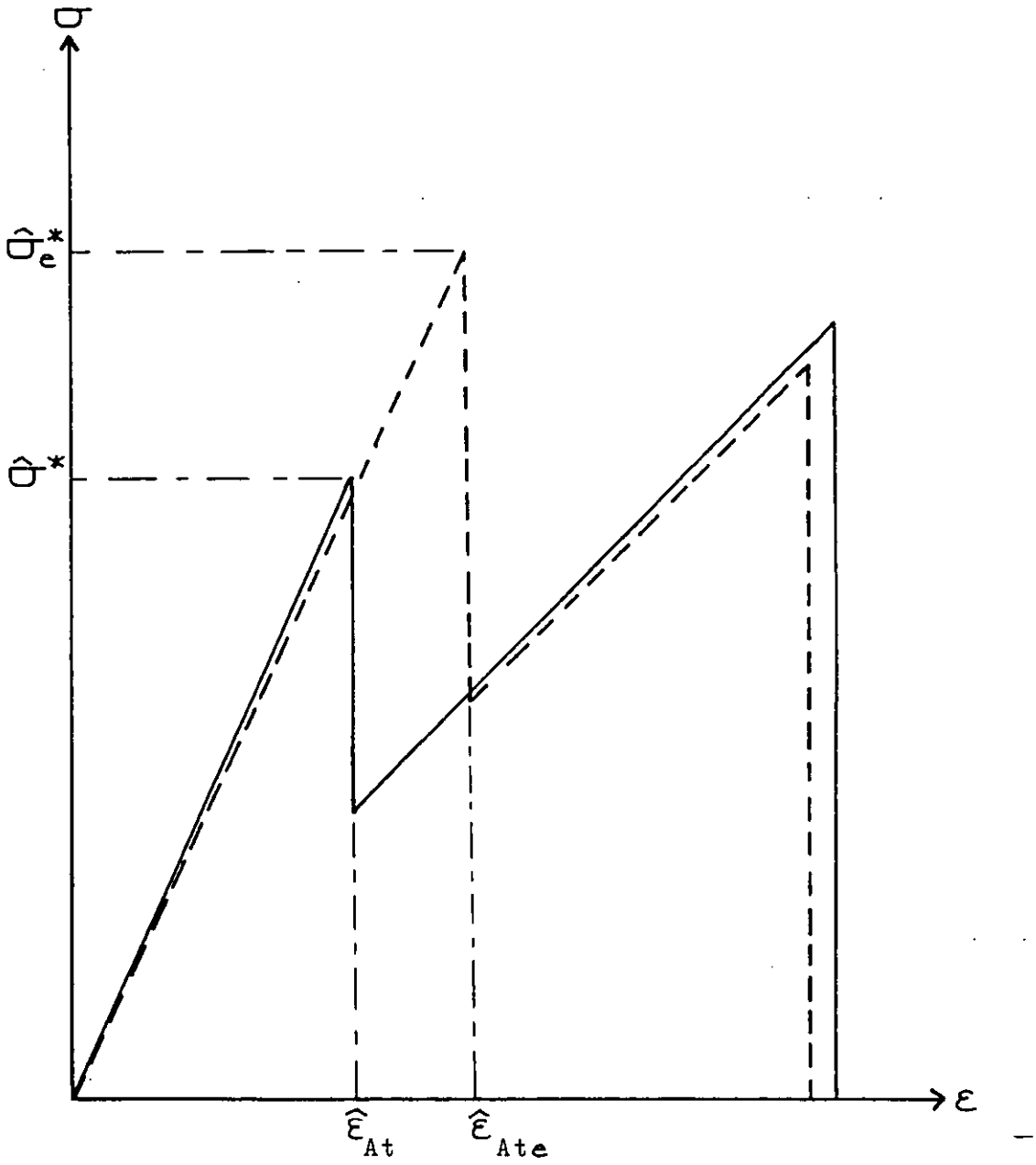

– – – Experimental curve

——— Theoretical curve

Figure 14

The Stress v Strain Diagram Obtained when Combining C.F.R.P. and G.R.P. to Form a Hybrid Composite, Showing the Effect of Differential Thermal Contraction Between the Layers, After Bunsell and Harris[24].

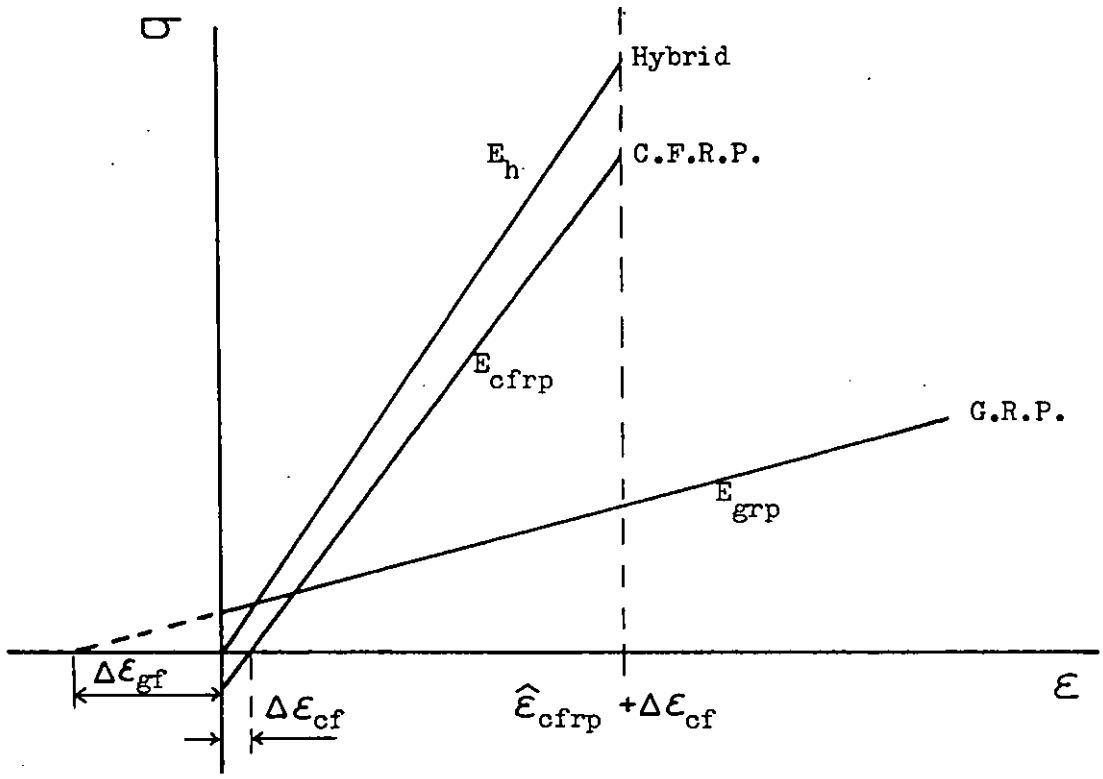

Figure 15

Tensile Stress v Strain Diagram for a Carbon/Glass/Epoxy Hybrid Composite, After Aveston and Sillwood[6].

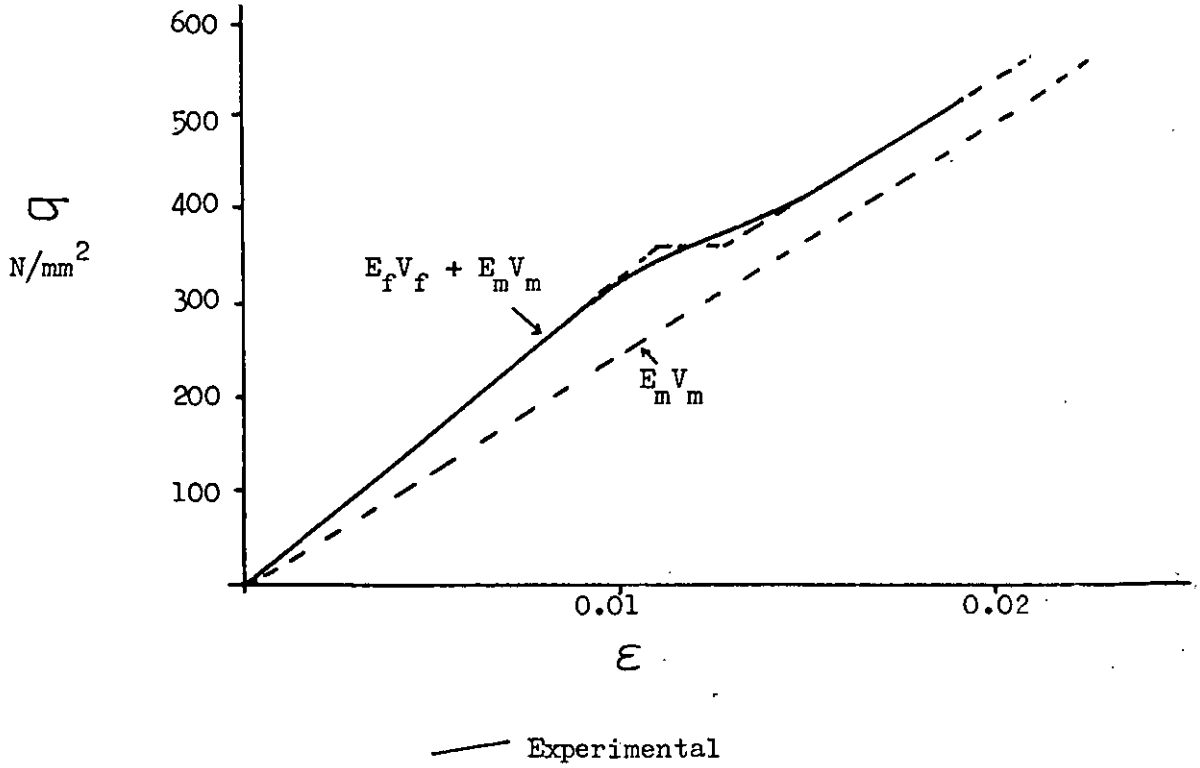

Figure 16 Zweben's[7] Model for the Tensile Strength Analysis of Hybrid Composites

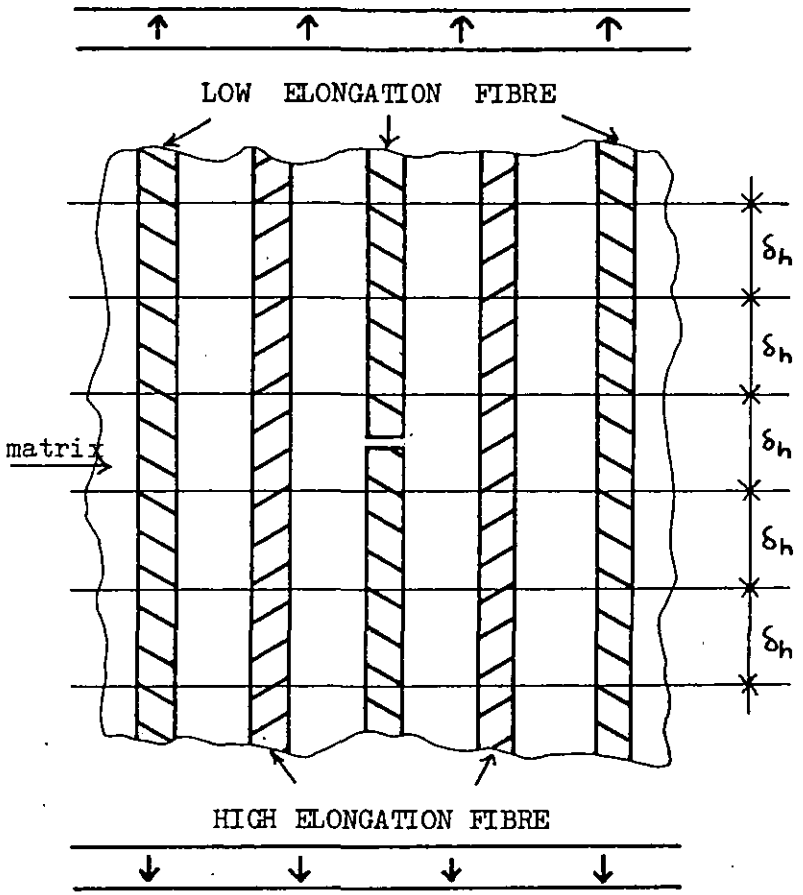

Figure 17 Possible Modes of Failure in Short Beam Shear Specimens

a) Shear Failure

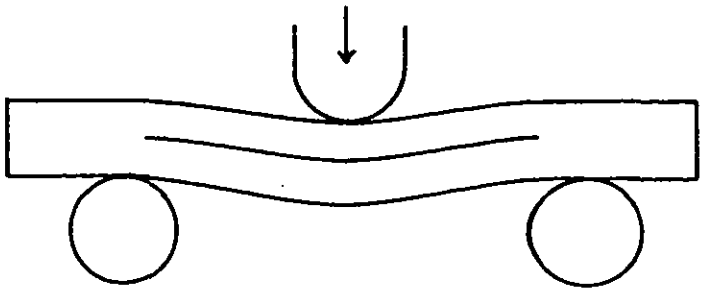

b) Complex Failure Mode

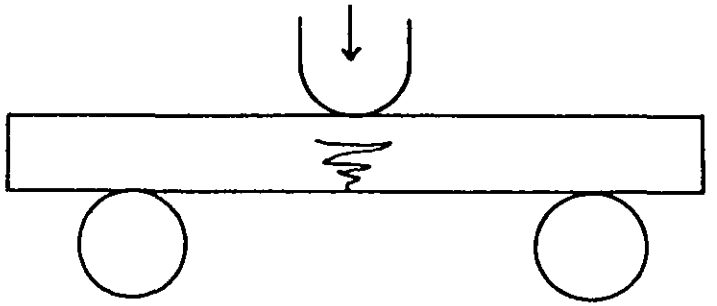

c) Tensile Failure

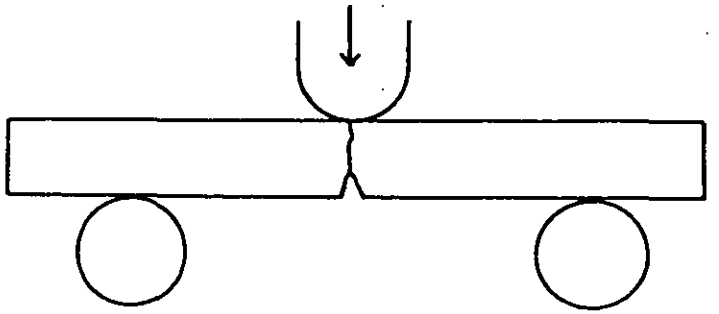

Figure 18

The Structure of A172, A187 and A1100 Union Carbide Coupling Agents.

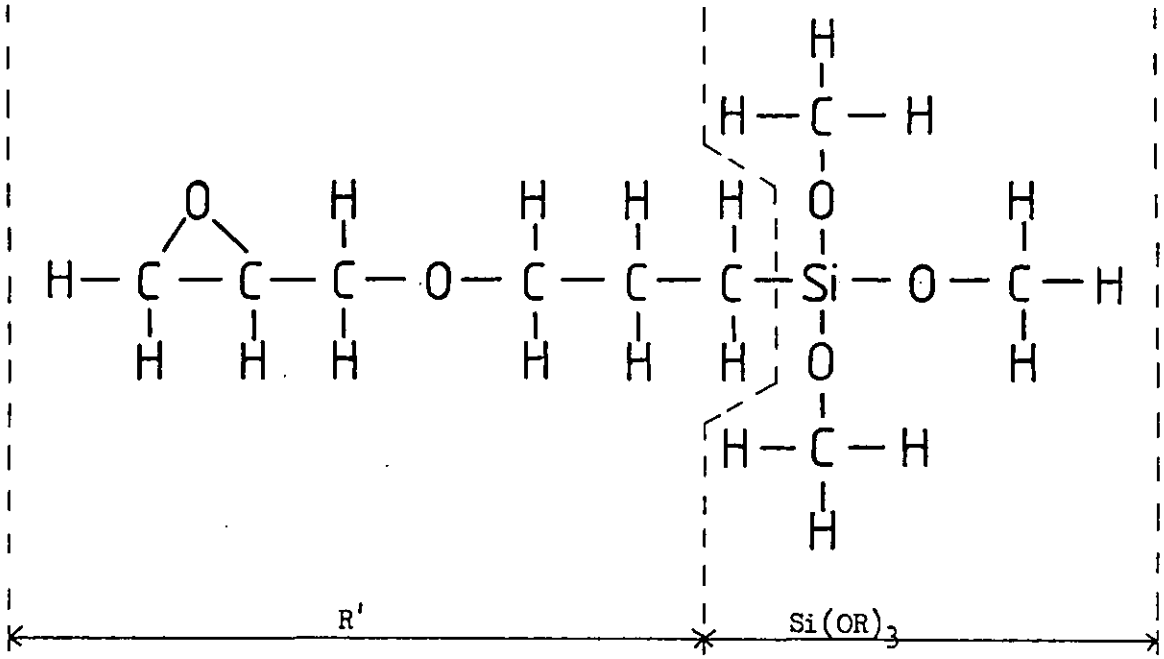

A187 gamma-glycidoxypropyl - trimethoxy silane

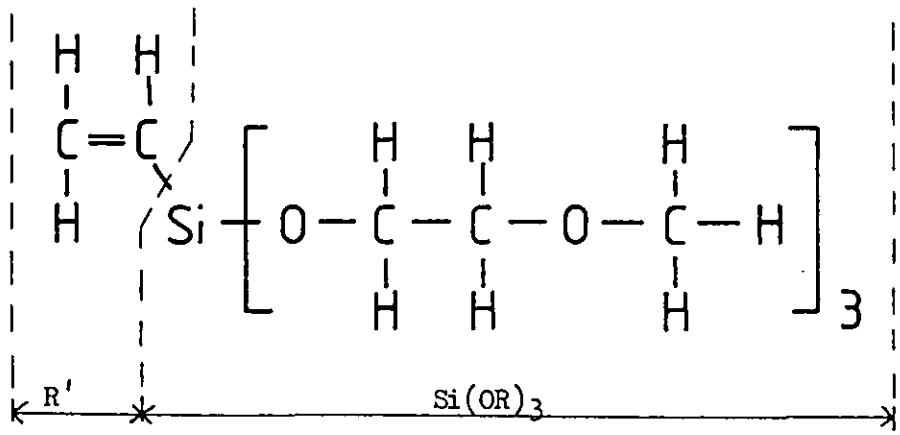

A172 vinyl - tris (beta-methoxyethoxy) silane

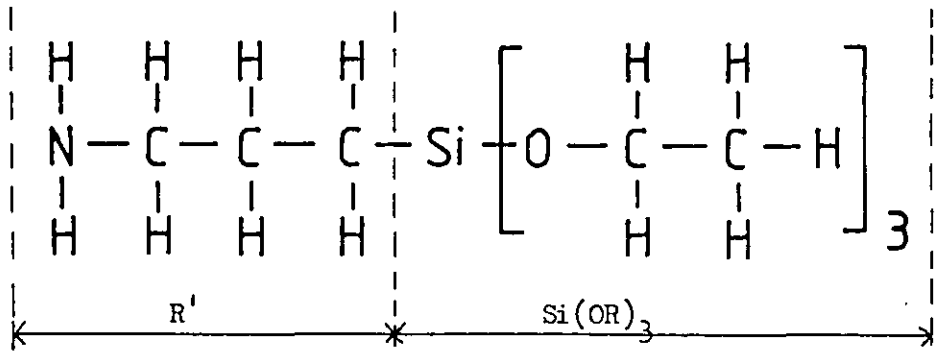

A1100 gamma-aminopropyl triethoxy silane

Figure 19

Silane Bridging Between Silane Coupling-Agents and a Glass Surface

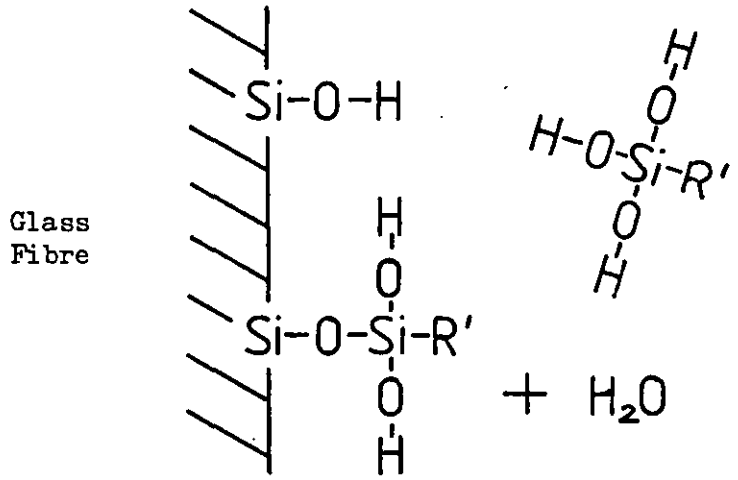

Figure 20

Hydrogen Bonding Between Silane Coupling-Agents and a Glass Surface

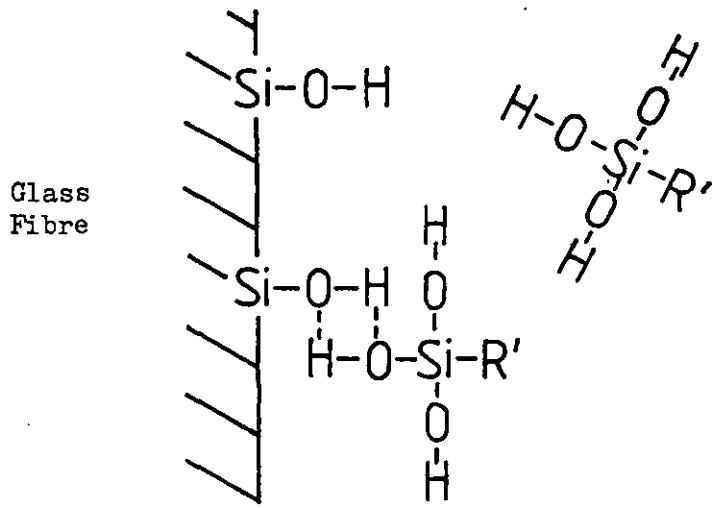

Figure 21

The Variation of the Mean Strength of E-Glass Fibres ($\hat{\sigma}_g$) with their Length (L) After Lanza(58).

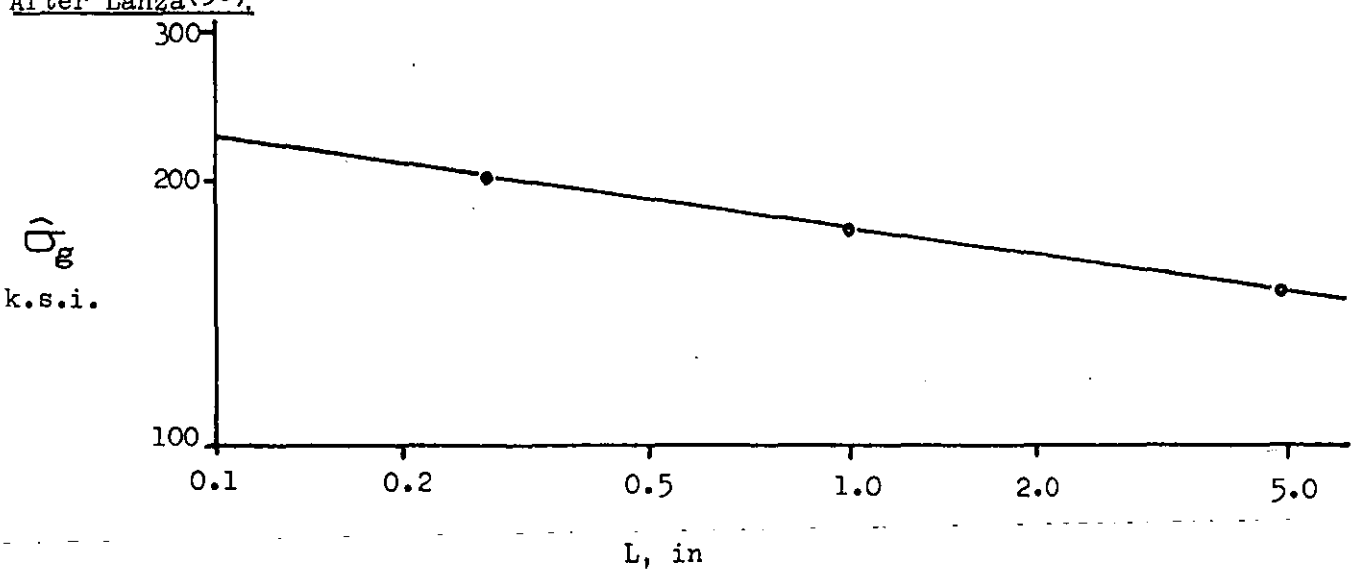

Figure 22 Reaction of Diglycidyl Ether of Bisphenol A and Acrylic Acid to Form a Vinyl Ester[63]

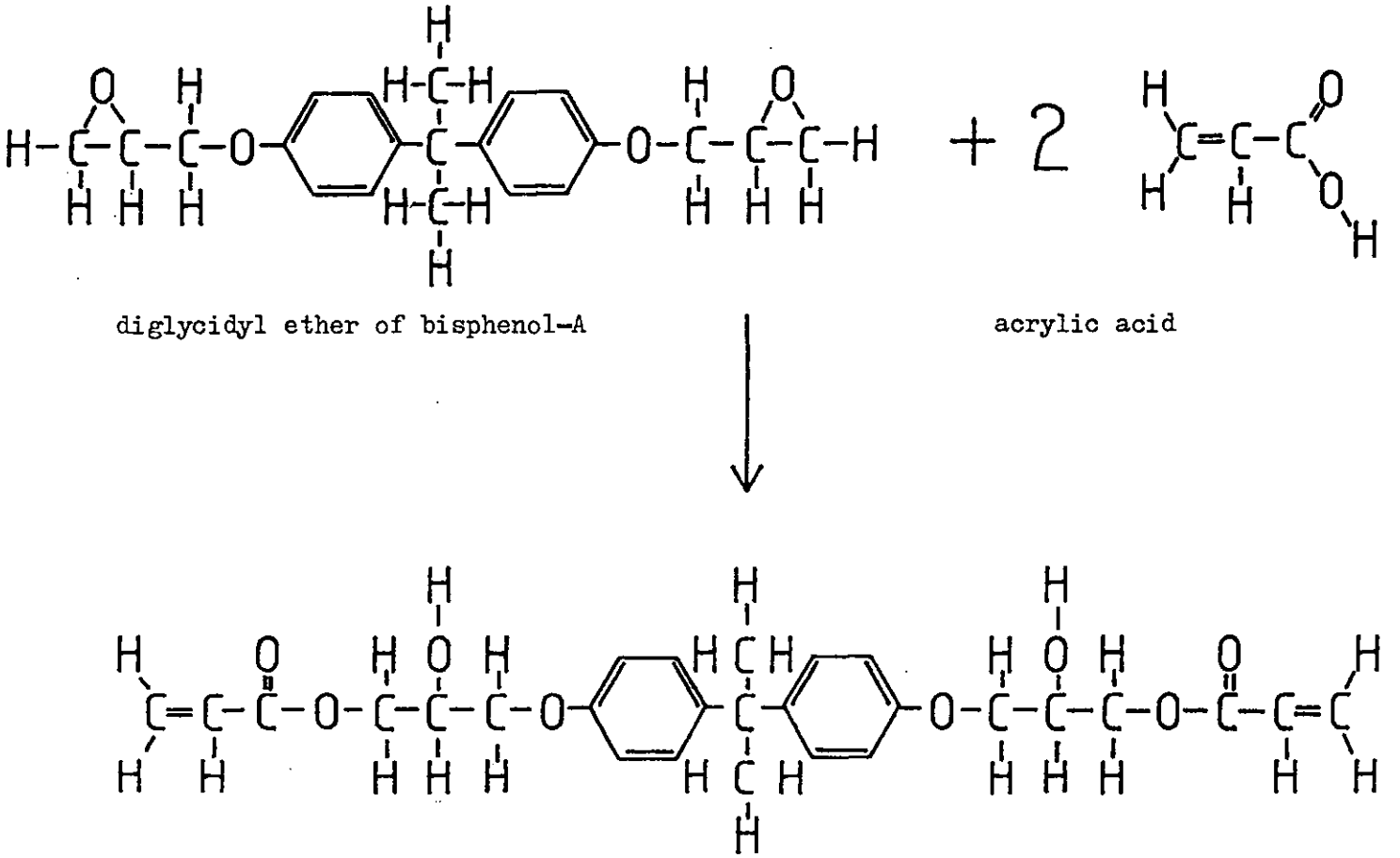

diglycidyl ether of bisphenol-A

acrylic acid

vinyl ester

Figure 23 The Chemical Resistance of Resins (63)

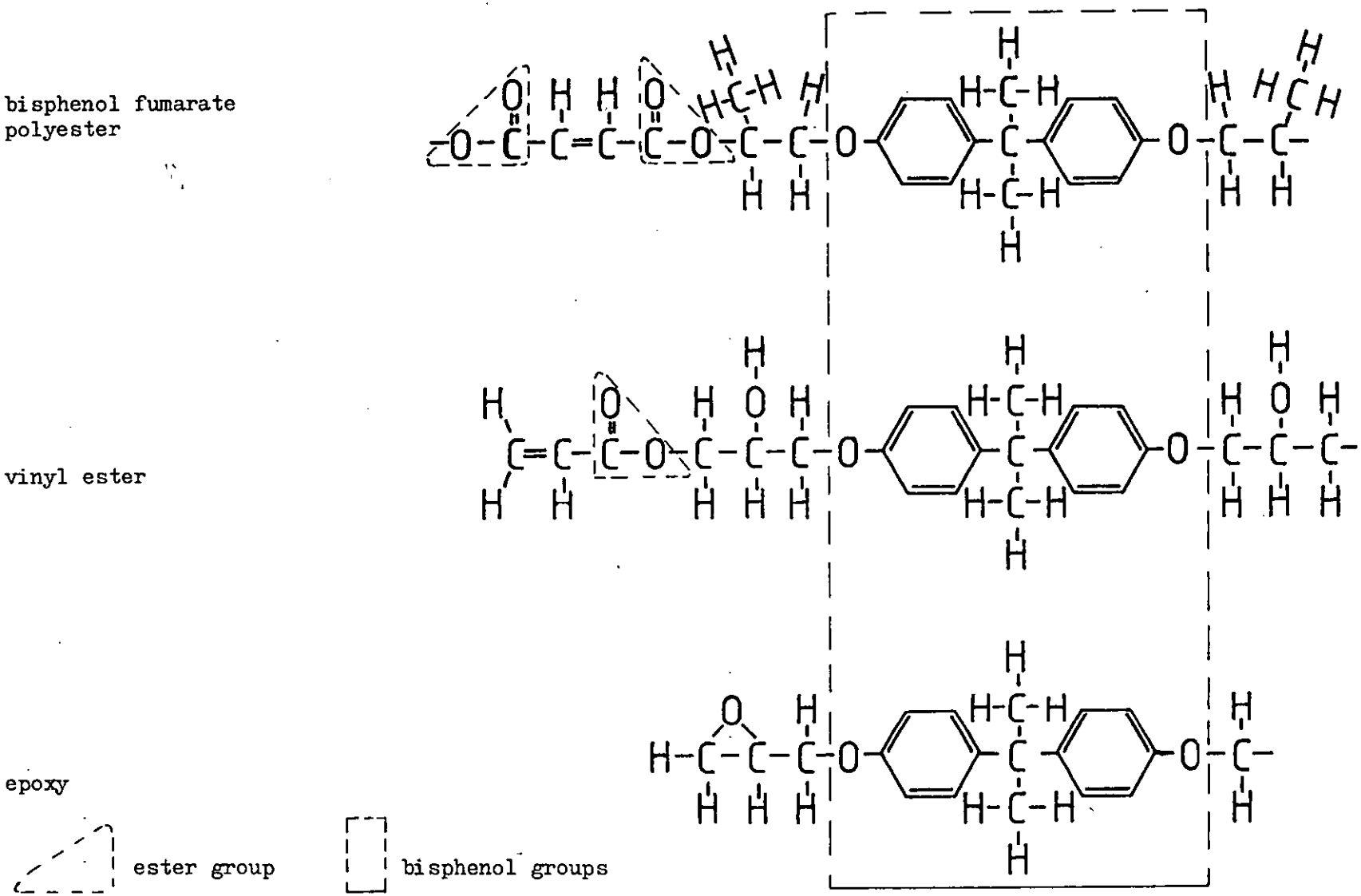

Figure 24

Base Catalyzed Hydrolysis of an Ester Group.

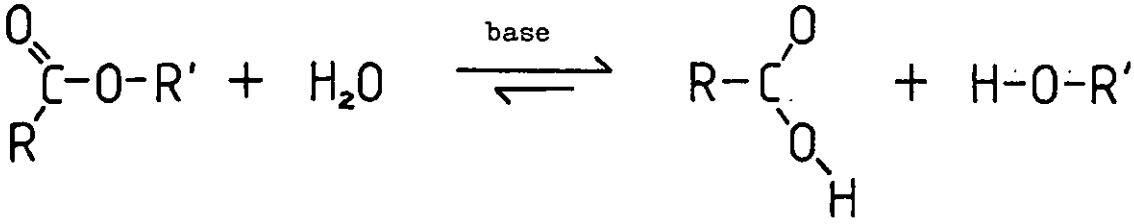

Figure 25

The Decomposition of Methyl Ethyl Ketone Peroxide Producing Free Radicals.

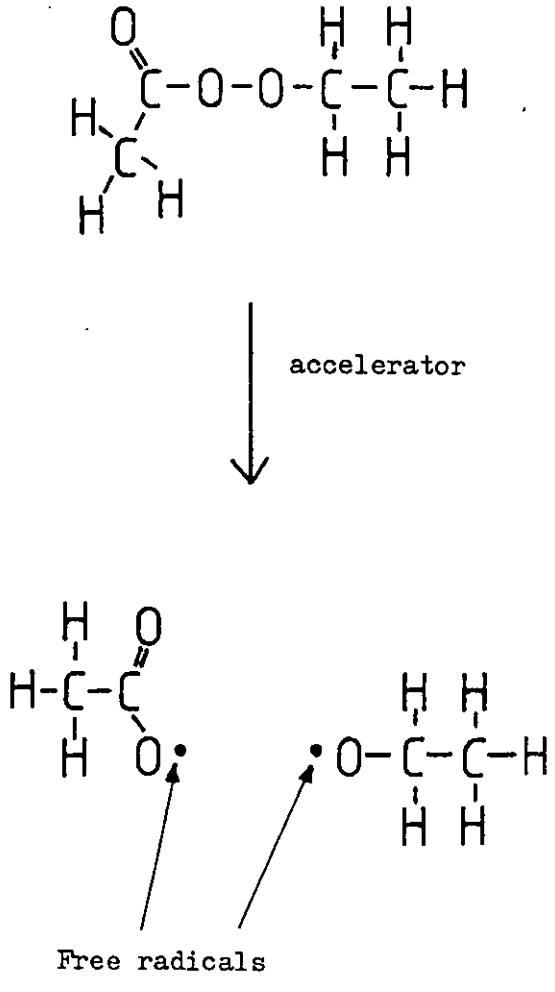

Figure 26 Diagram of the 'Leaky' Mould Used for the Fabrication of Resin and Composite Slabs

Dimensions in mm

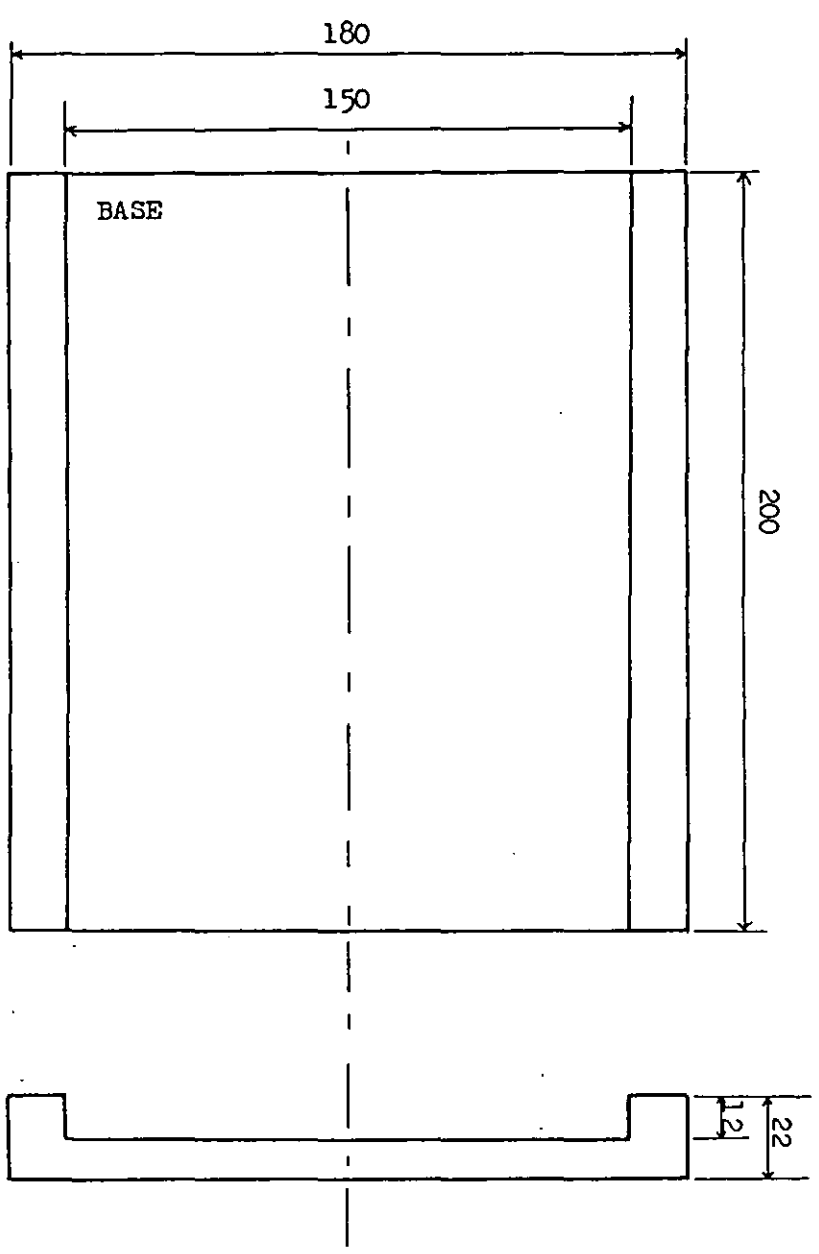

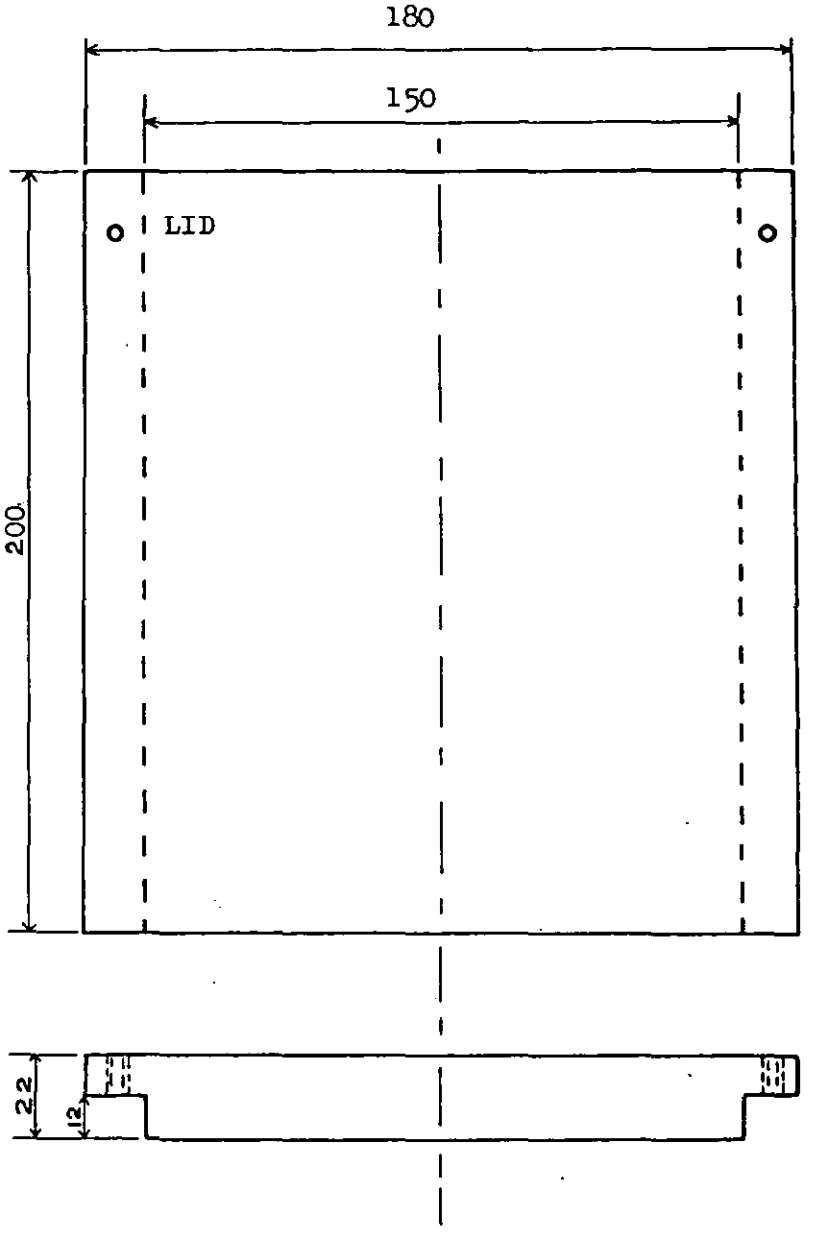

Figure 27

Diagram of the Resin Tensile Specimen Shape.

Dimensions in mm.

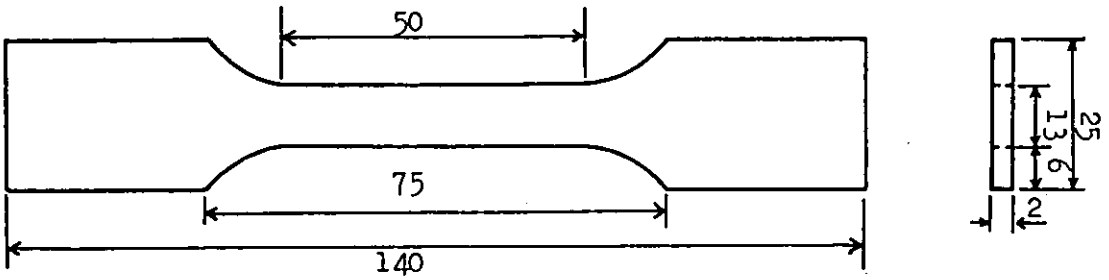

Figure 31

Different Specimen Shapes Commonly Used in the Tensile Testing of Unidirectional Composites[77].

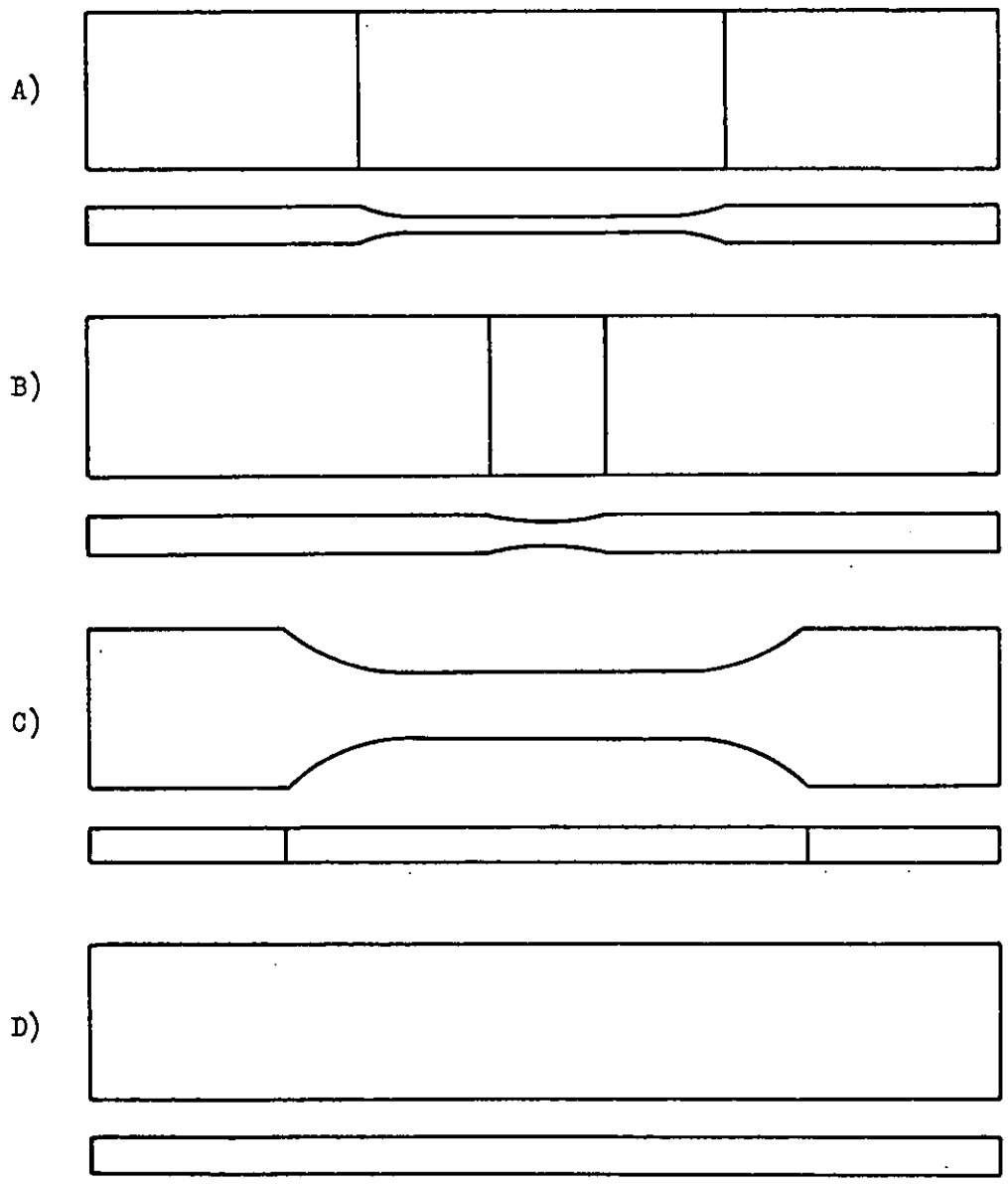

Figure 28

Diagram of the Acid Digestion Apparatus.

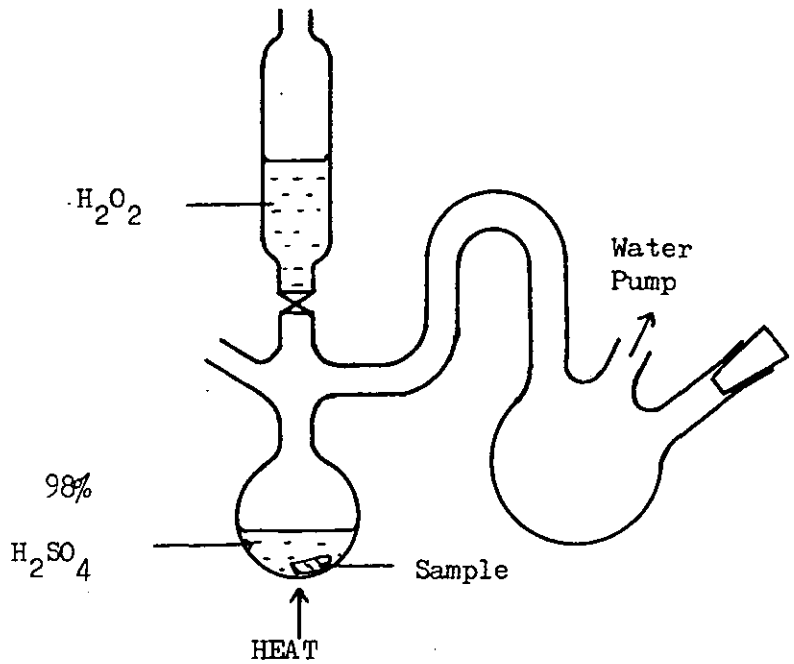

Figure 29

The Separated I.L.S.S.
3-Point Bending Rig.

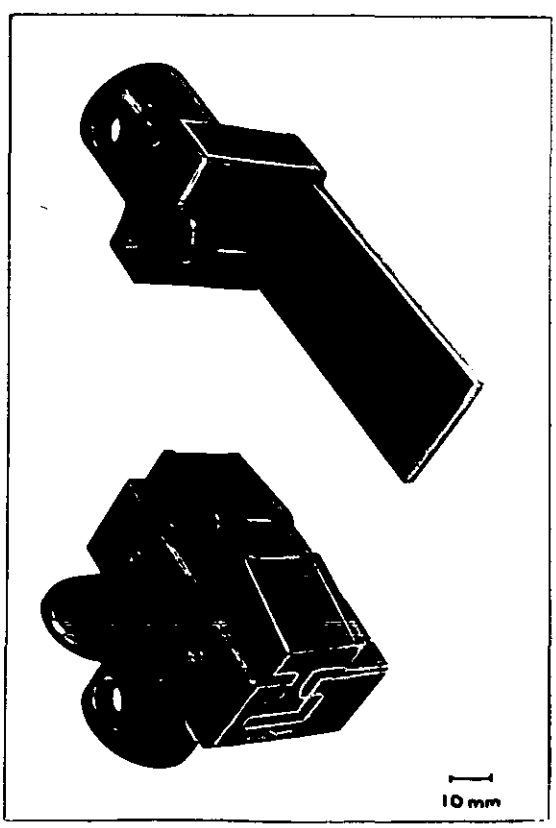

Figure 30

The I.L.S.S. 3-Point Bending Rig
with a Composite Specimen in Position.

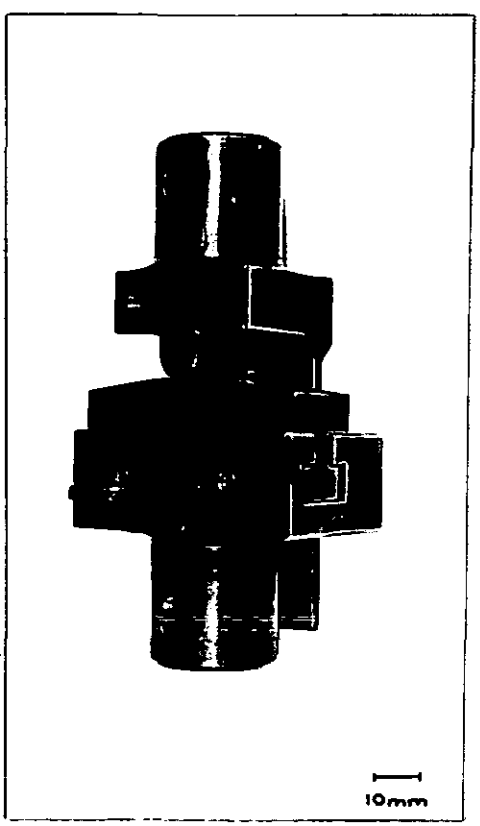

Figure 32

Shear Failure of Waisted Tensile Specimen.

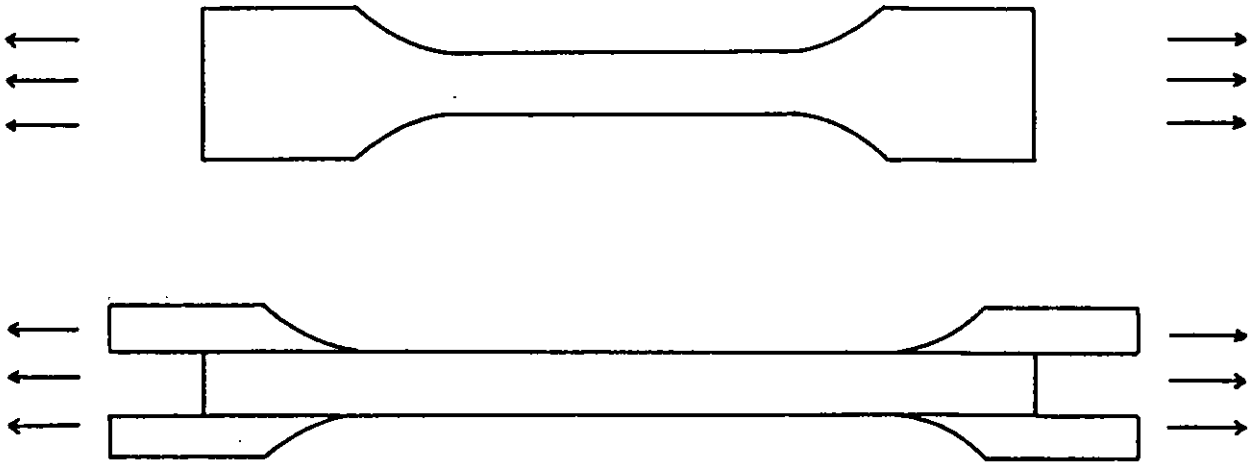

Figure 33

Composite Tensile Specimen Shape.

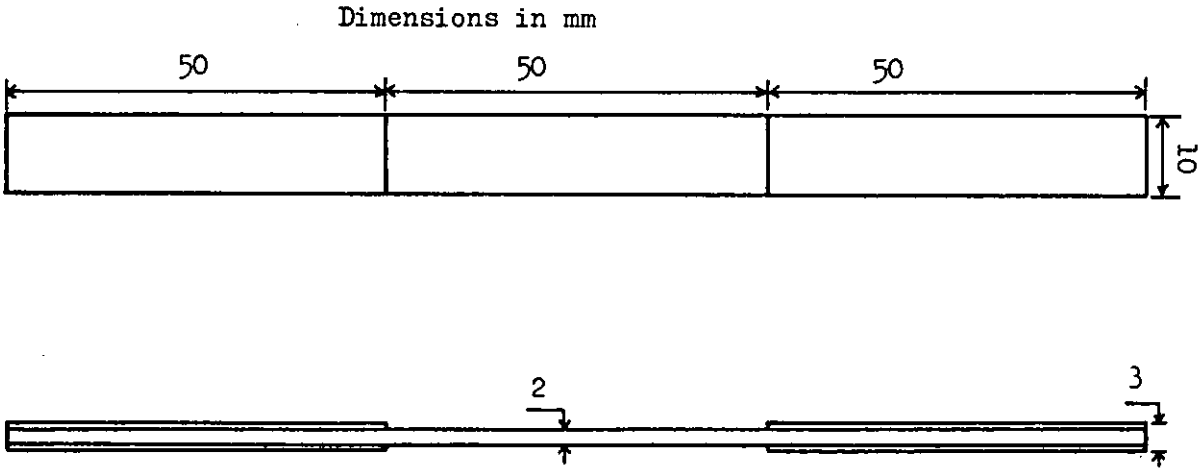

Figure 34 D.T.A. Scan of Resin Mixes 3, 9 and 13 Taken Immediately after Mixing

Figure 35 D.T.A. Scan of Resin Mixes 3, 9 and 13 Kept for 24 hours at Room Temperature after mixing

Figure 36 D.T.A. Scan of Resin Mixes 3, 9 and 13 Post Cured at 100°C for 2 Hours 24 Hours After Mixing

Fig 34

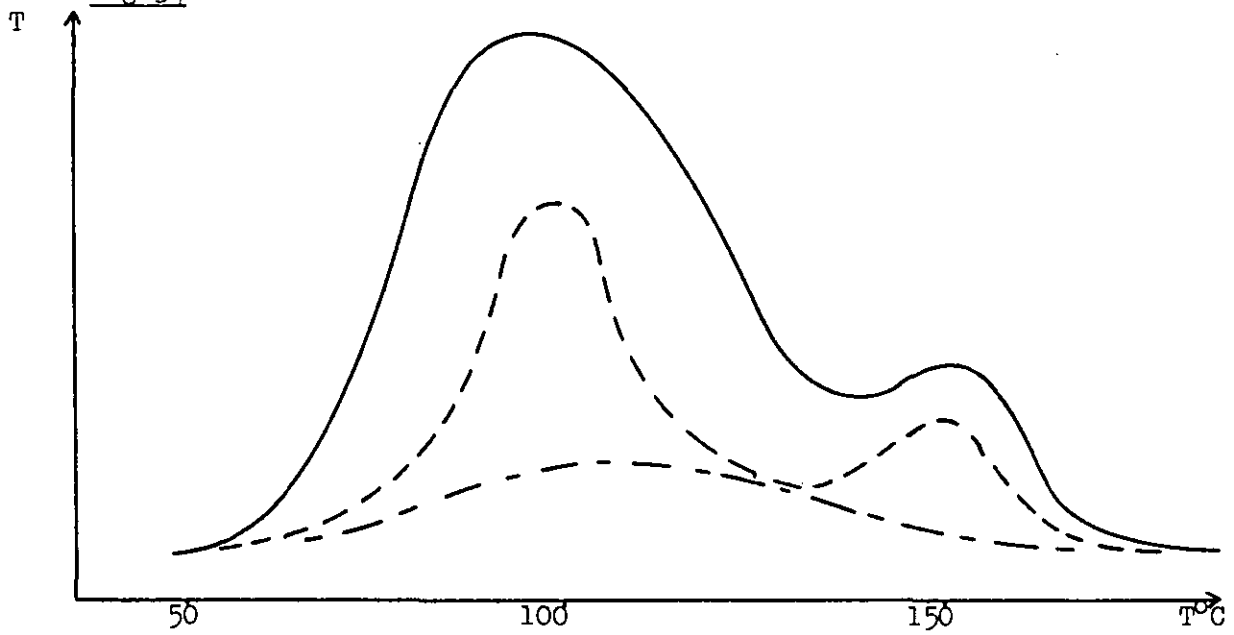

Fig 35

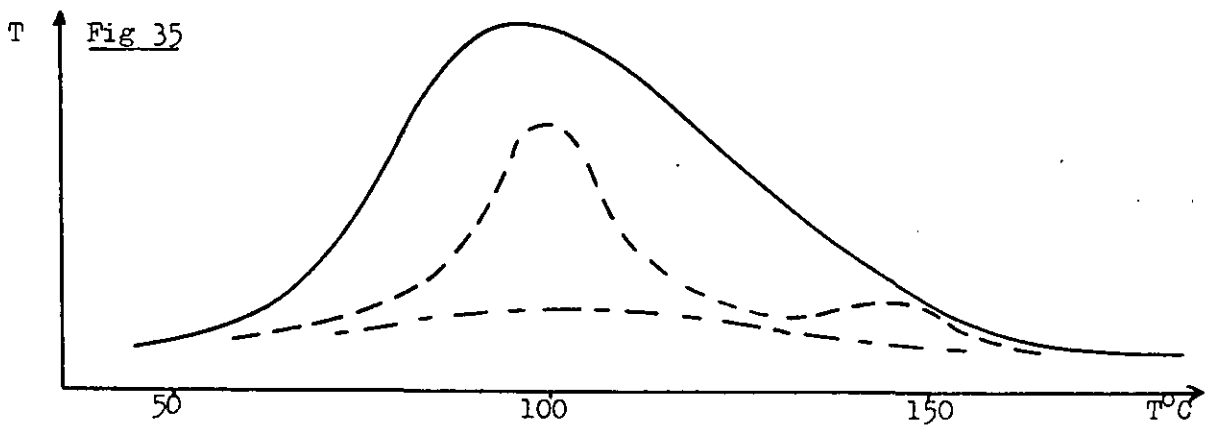

Fig 36

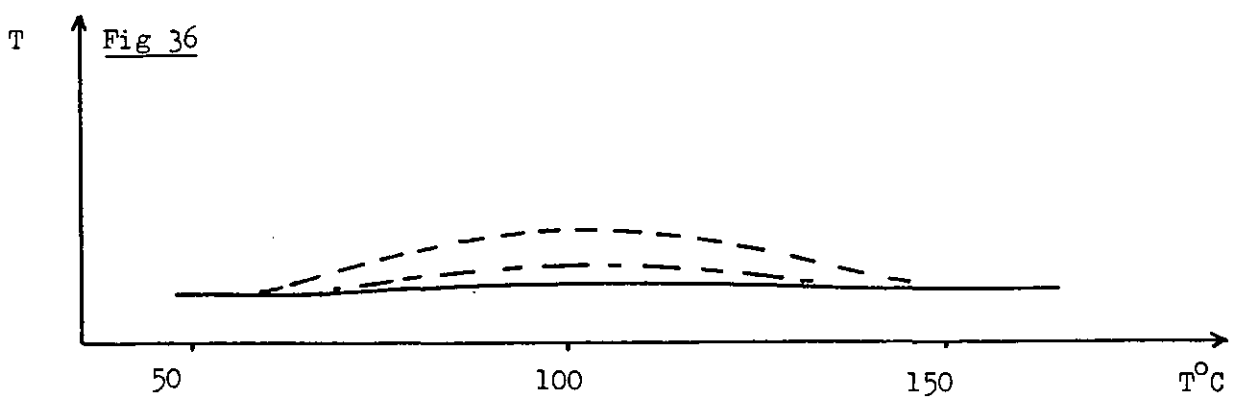

scans from mixes

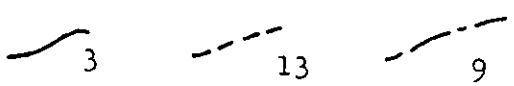

Figure 37 Variation in Composite Shear Modulus (G) with E-Glass Fibre Content (V_g)

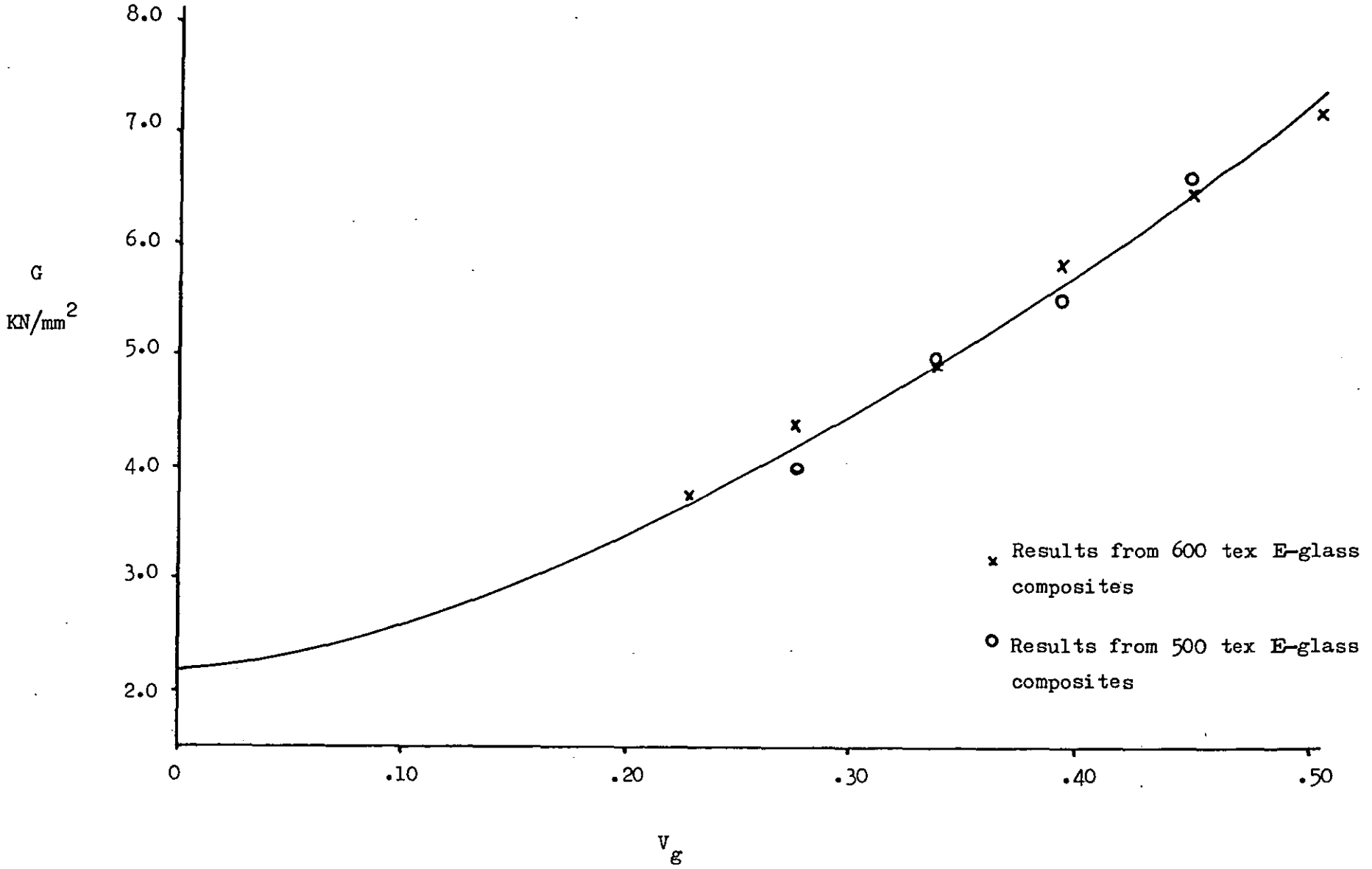

Figure 38

The Relationship Between the Width to Thickness Ratio (B/t) of a Shear Specimen and the Factor μ in the Equation

$$G = \frac{L}{Bt^3\mu} \cdot \frac{T}{\theta} \quad N/mm^2$$

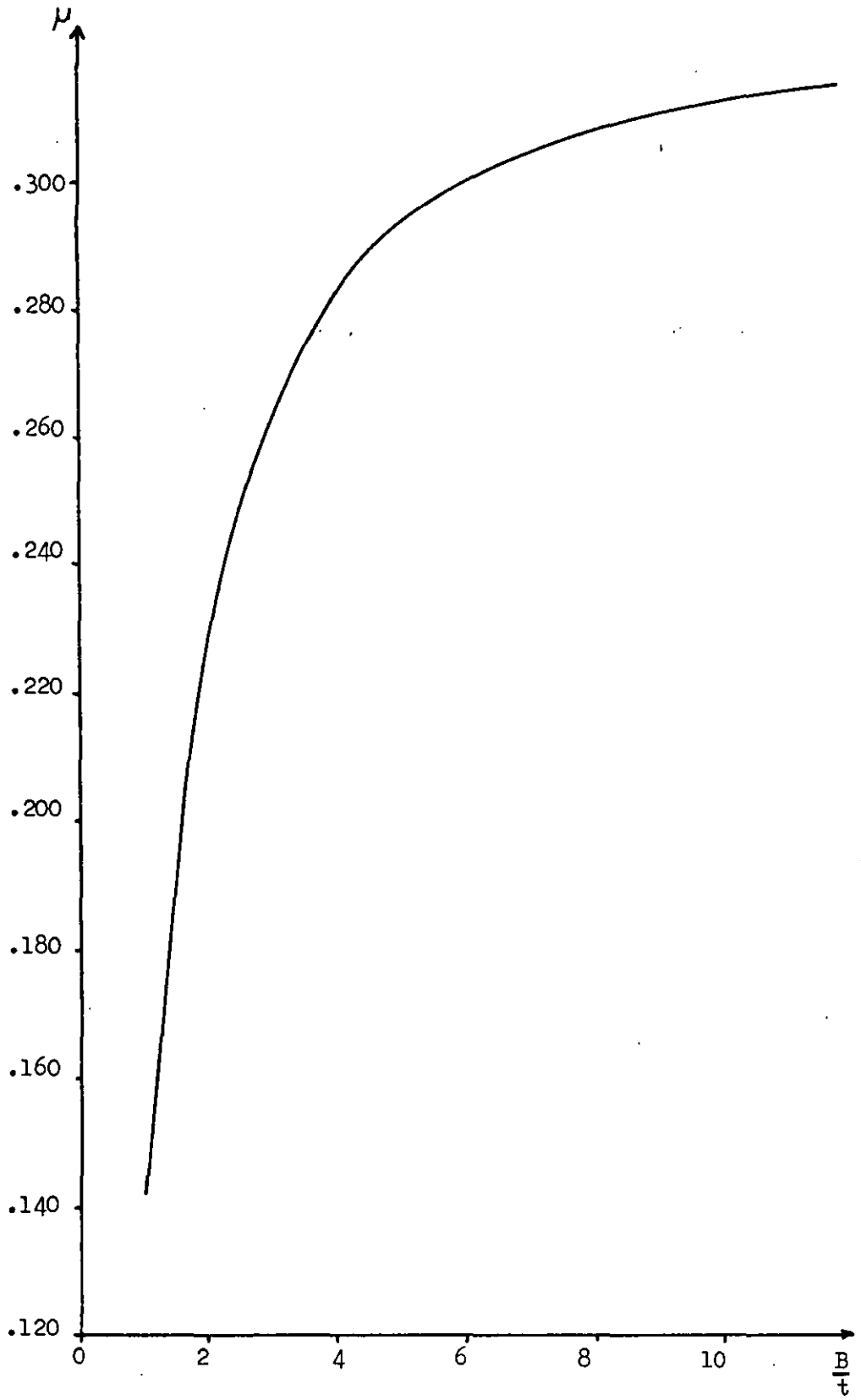

Figure 39 The Stress v Strain Curve of Derakane 411-45 Vinyl Ester Resin

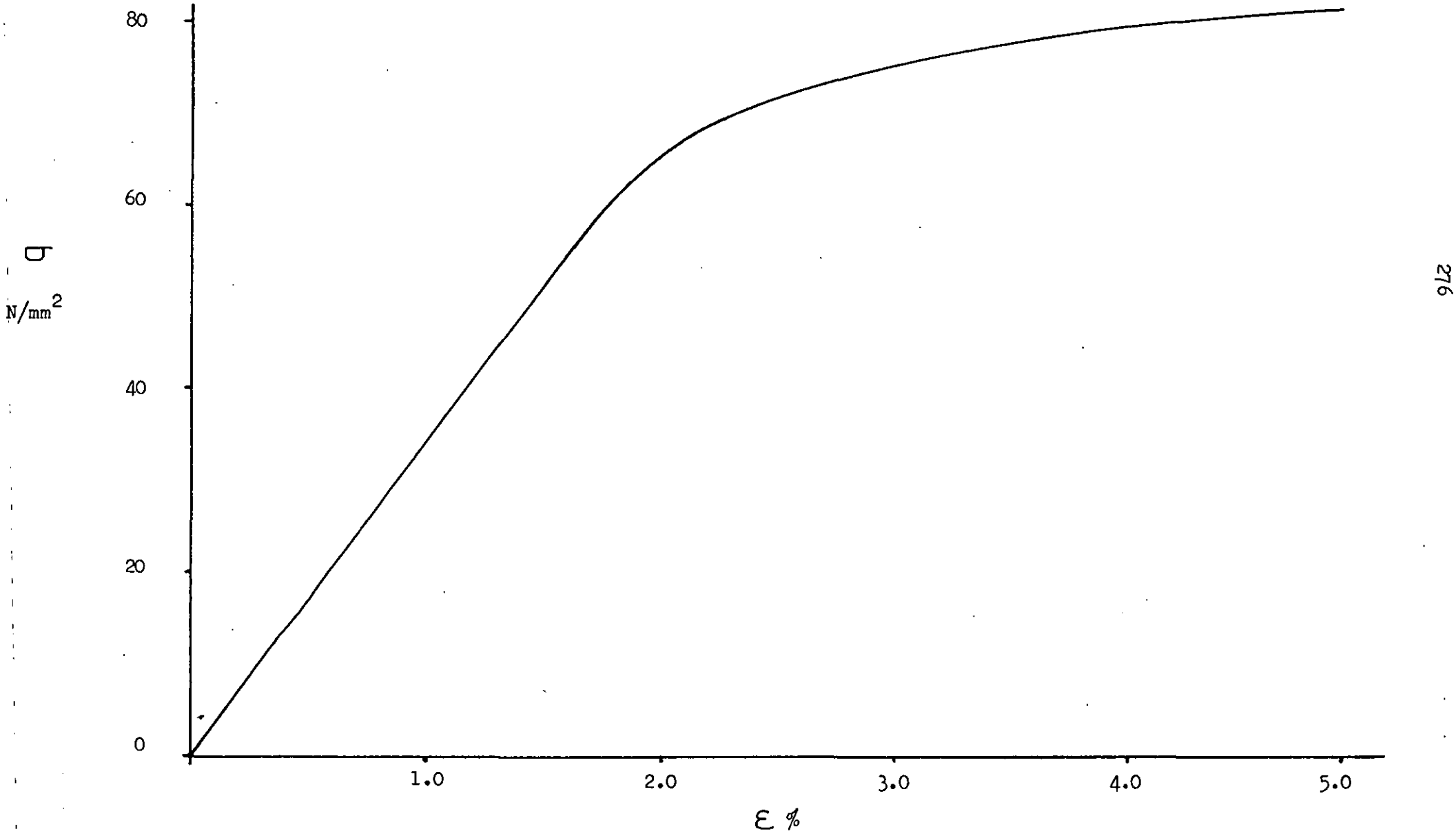

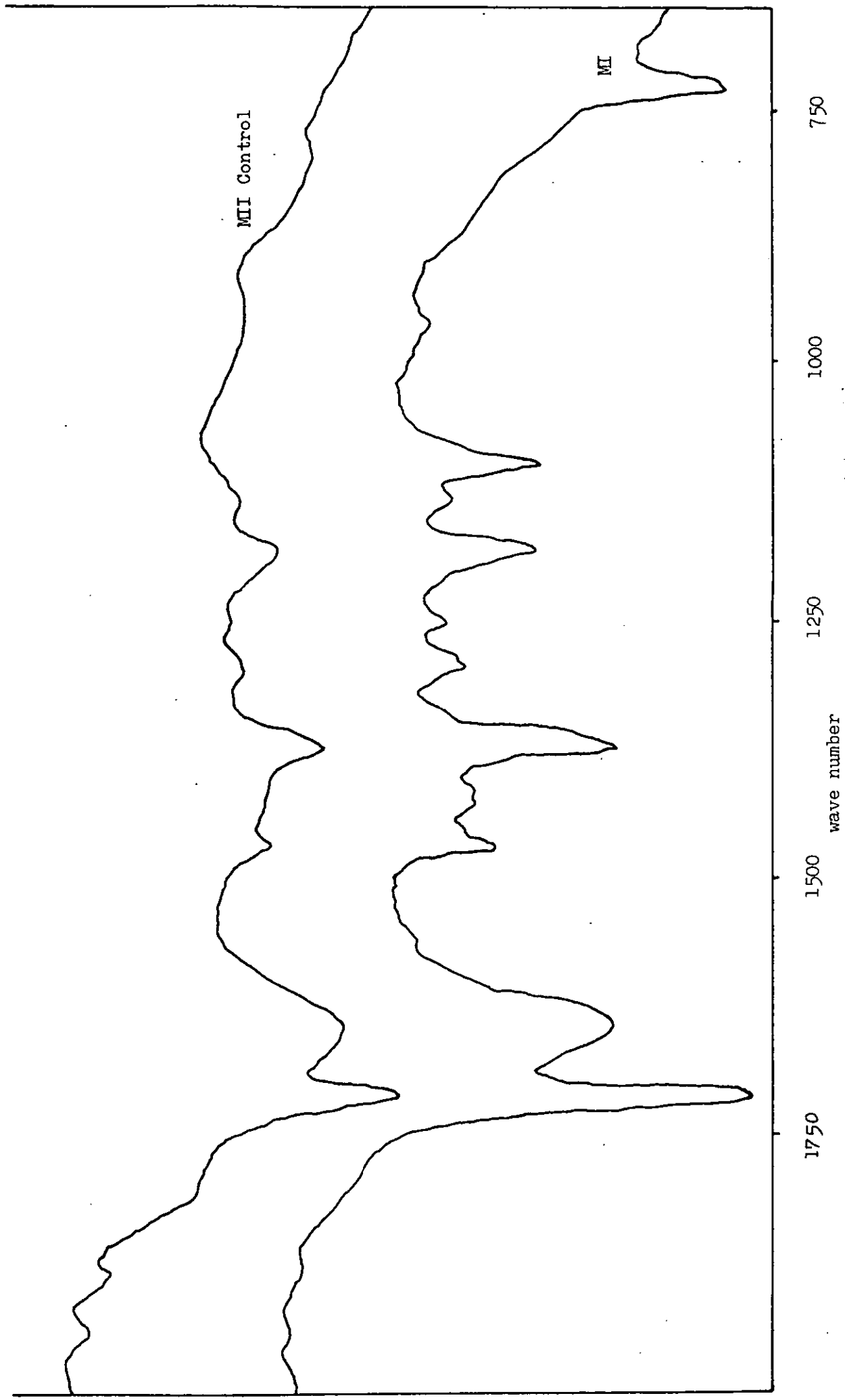

Figure 40 Infra Red Spectra for MI and MII

Figure 41 Infra Red Spectra for MI and MII

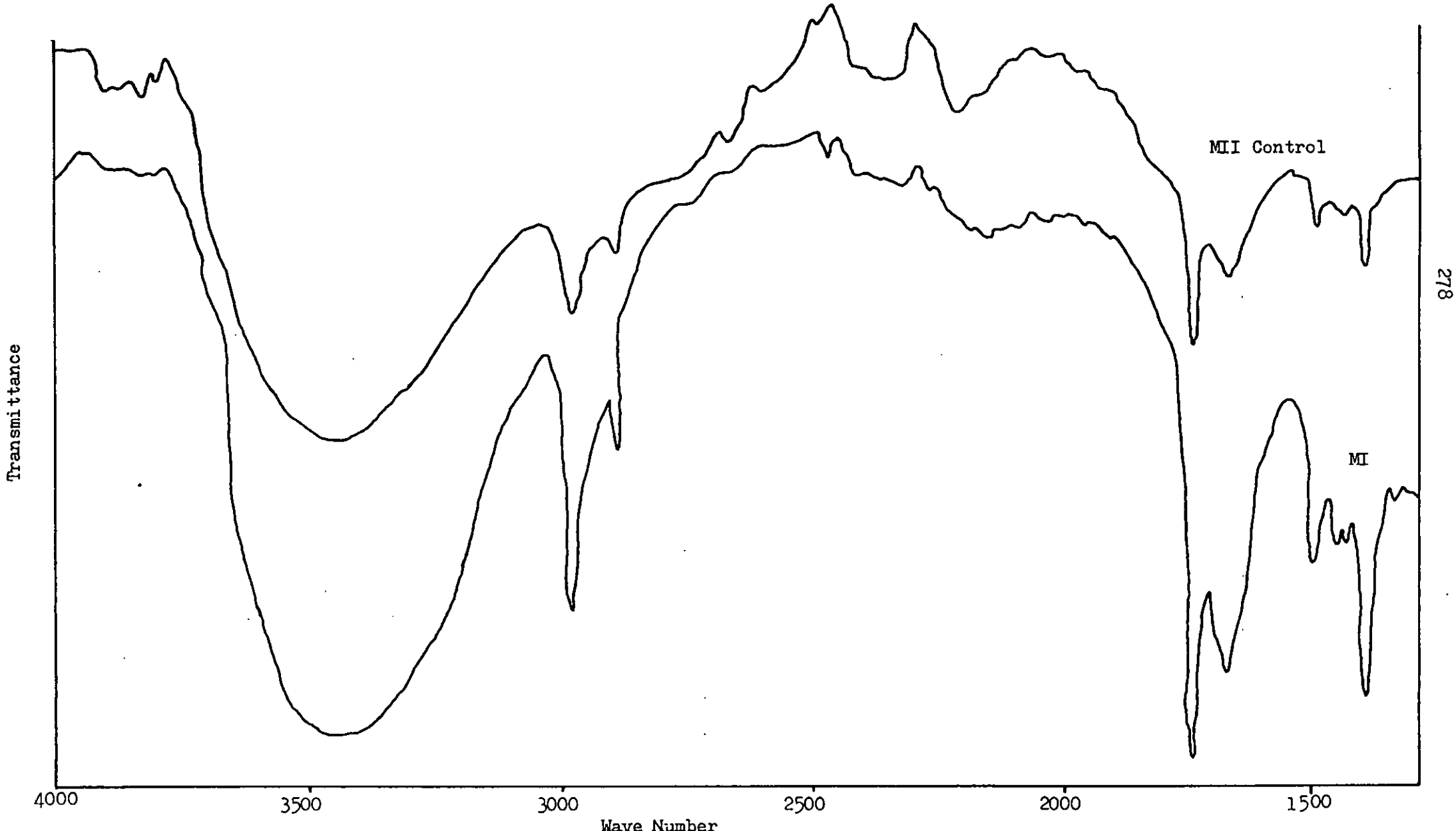

Figure 42

Typical Load Deflection Curve for I.L.S.S. Composite Specimens Failing in Shear.

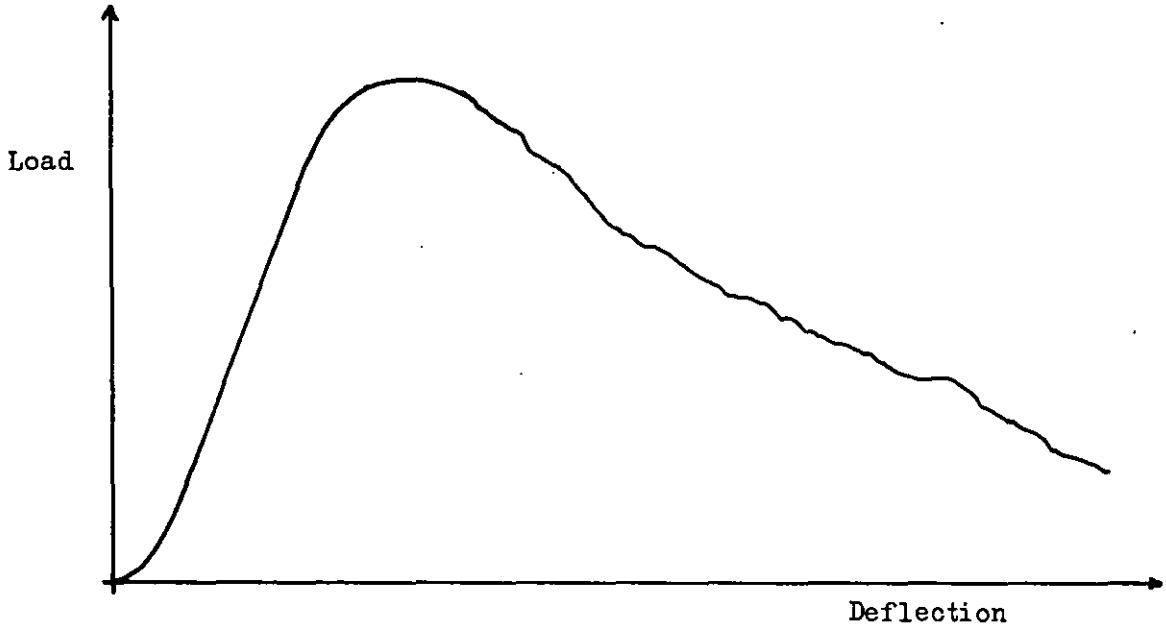

Figure 43

The Variation in the Elastic Modulus, E, of Carbon Composites with Carbon Volume Fraction Content, V_{cf}.

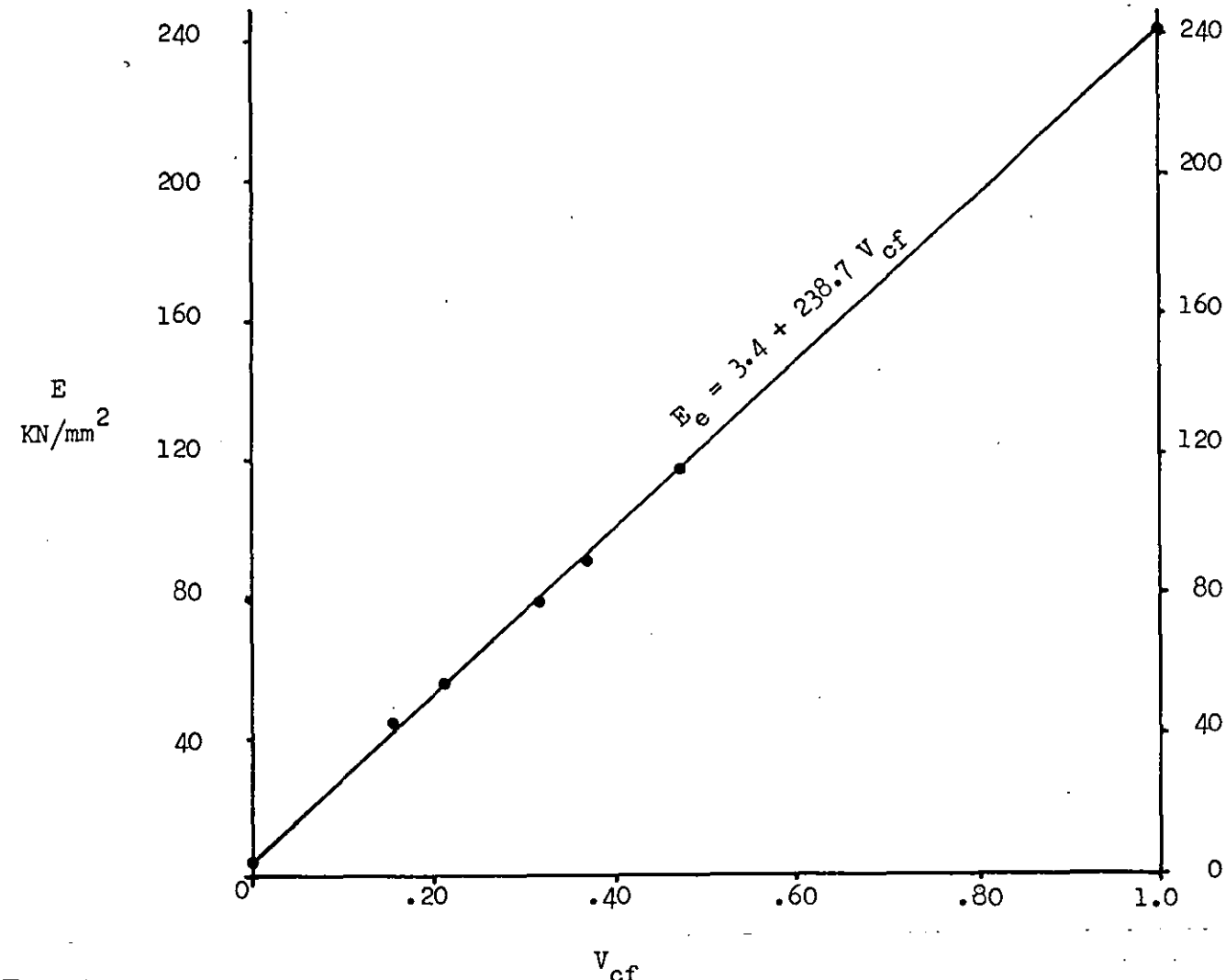

Figure 44 The Variation in the Experimental Tensile Strength of Carbon Composites ($\hat{\sigma}_e$) with Carbon Volume Fraction Content (V_{cf}) and the Predicted Rule of Mixtures ($\hat{\sigma}_{RM}$), Upper ($\hat{\sigma}_u$), Lower ($\hat{\sigma}_L$) and Weakest ($\hat{\sigma}_w$) Stress Levels following the Theory of Rosen[1] and Zweben[3].

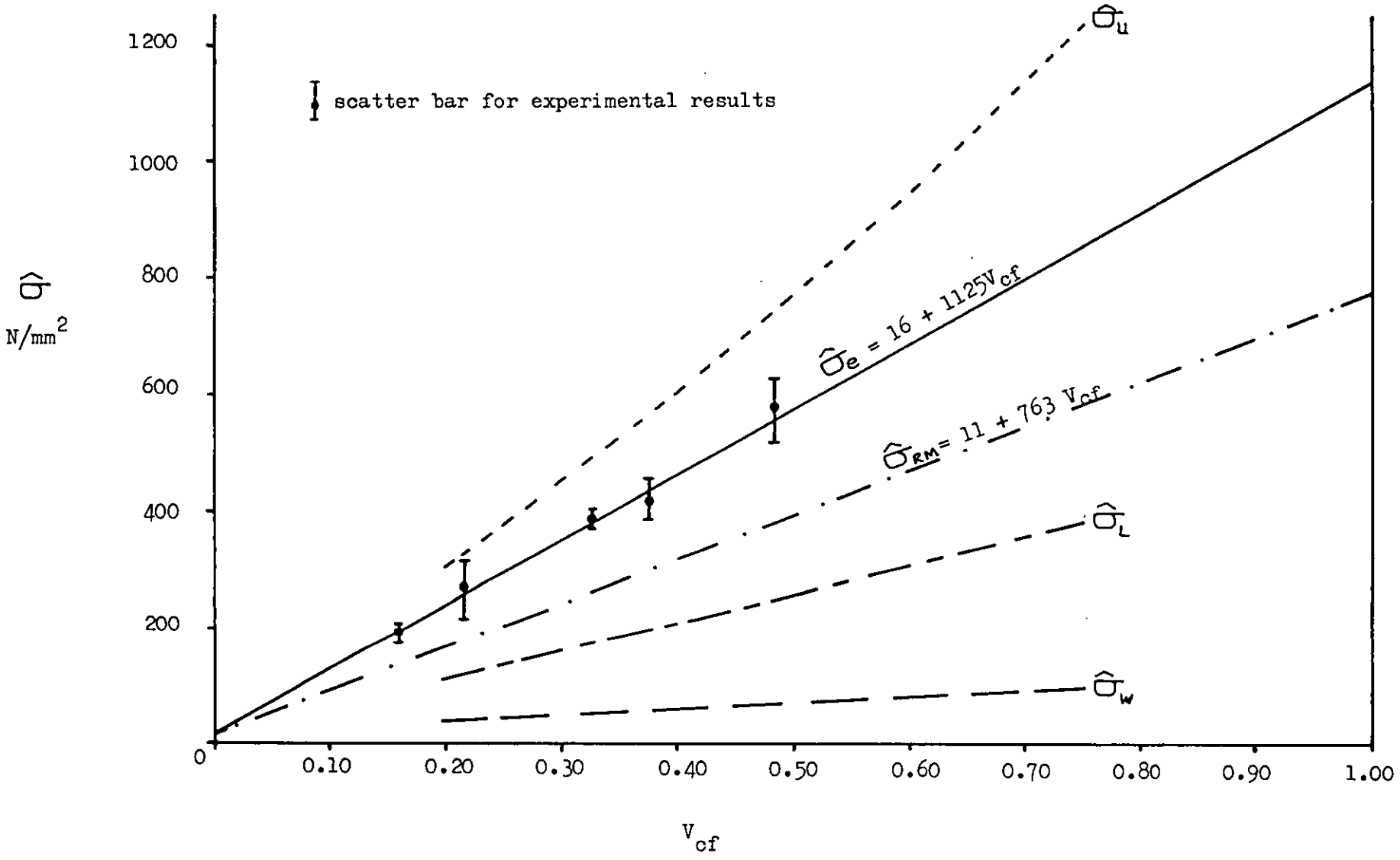

Figure 45

A Typical Tensile Stress v Strain Curve for a Carbon Composite Specimen from Slab 4 (7C, $V_{cf} \simeq 0.38$).

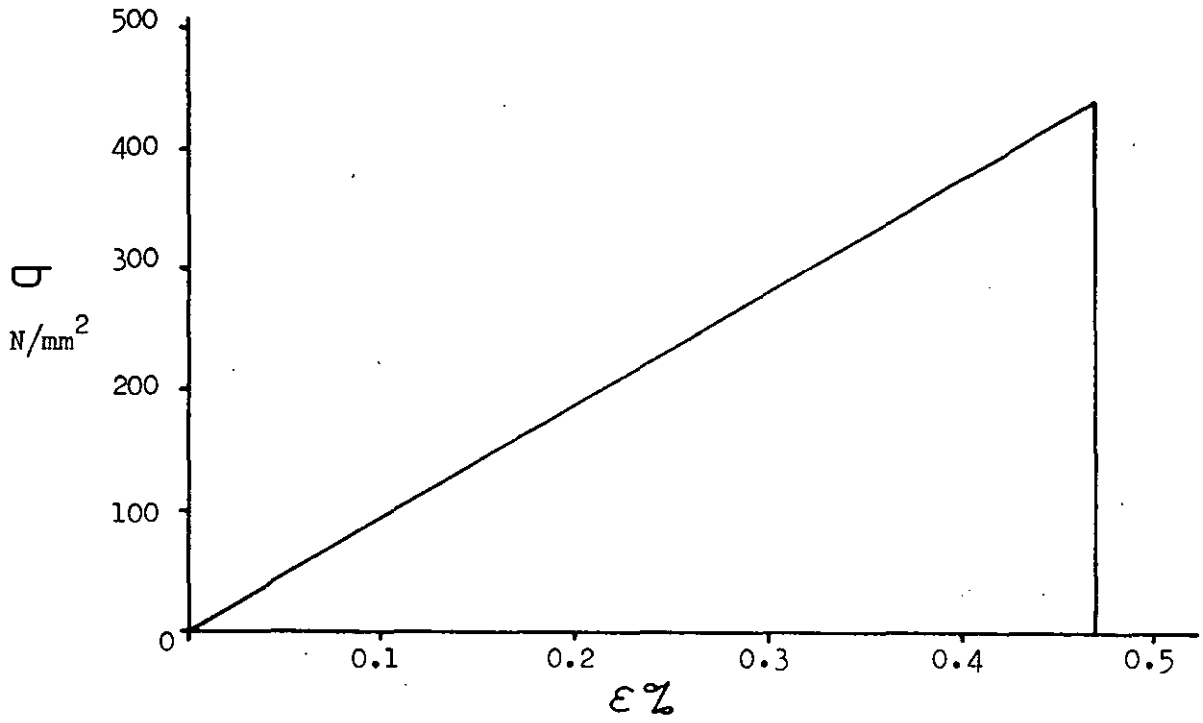

Figure 46

Half of the Fractured Carbon Composite Tensile Specimen 4.2.

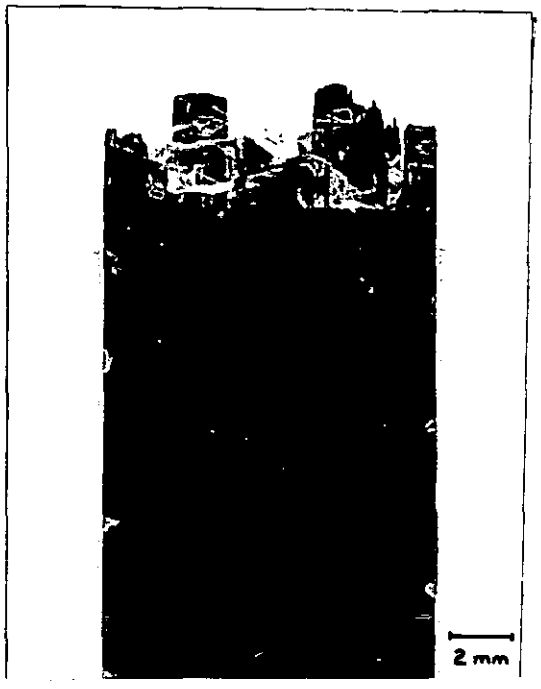

Figure 47

Scanning Electron Micrograph of a Portion of the Fracture Surface of Specimen 4.3, an As Recieved Carbon Fibre/Resin Composite. Note the clean fibre/resin interfacial failure and the continuation of the debonding beneath the fracture surface of the resin.

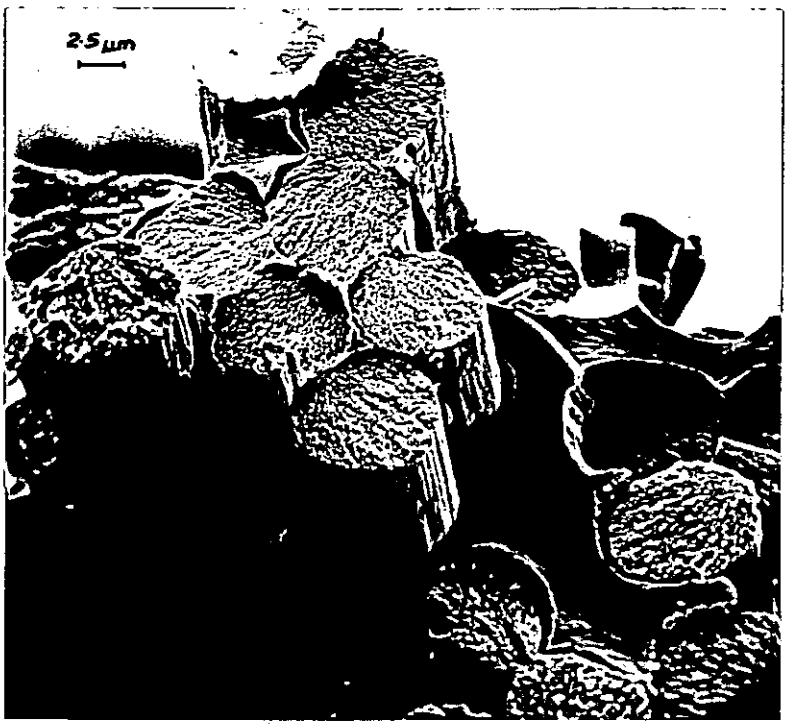

Figure 48

Scanning Electron Micrograph of a Portion of the Fracture Surface of Specimen 6.1, an Etched Carbon Fibre/Resin Composite. Note the resin adhering to the 'exposed' carbon fibre surface

Figure 49

Comparison Between the Experimental and Theoretical (After Barry[4]) Failure tresses of the Carbon Composites from Slabs 1 to 5

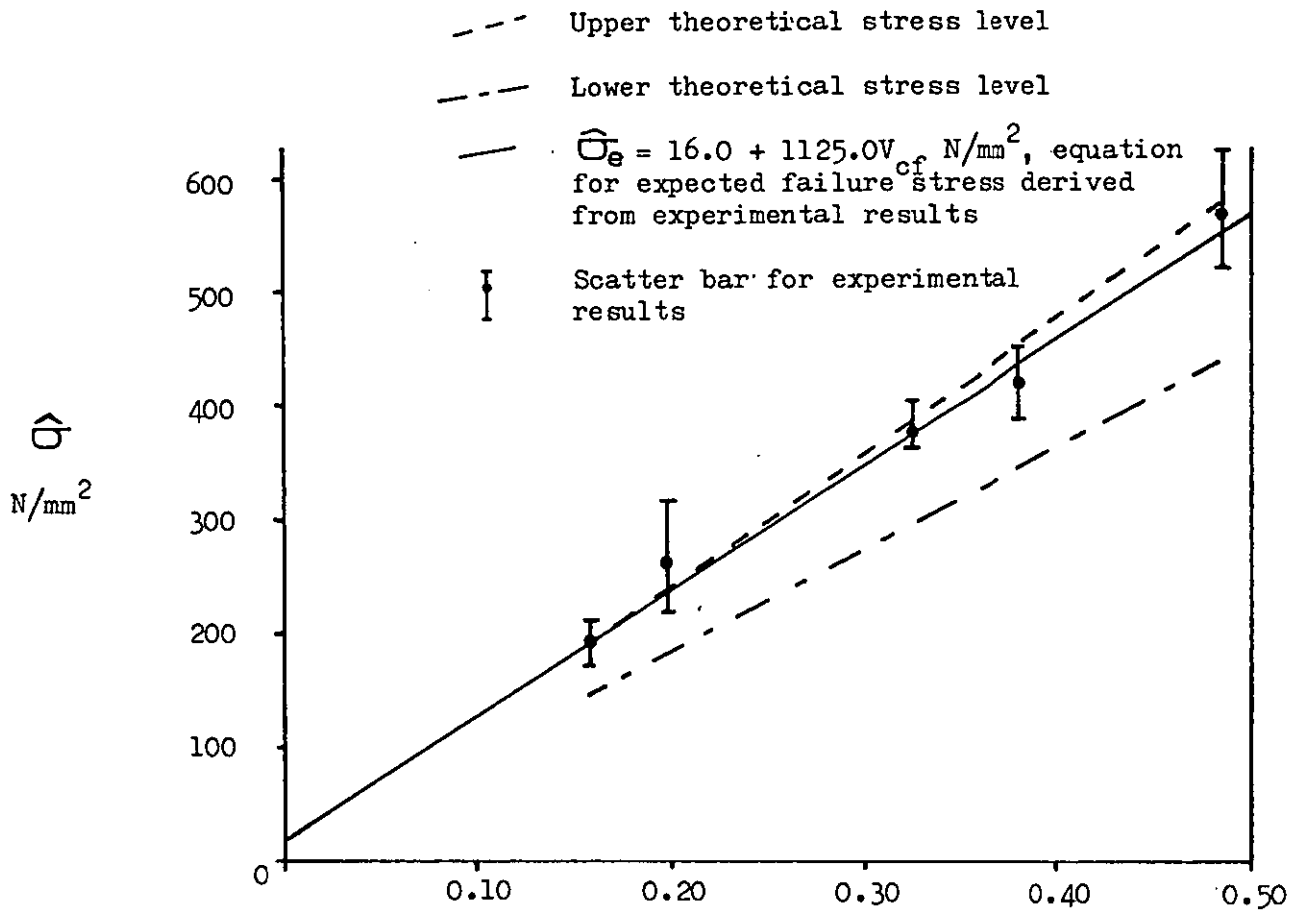

Figure 50

The Variation in the Elastic Modulus (E) of 600 tex E-glass Composites with 600 tex E-Glass Volume Fraction Content (V_{g6})

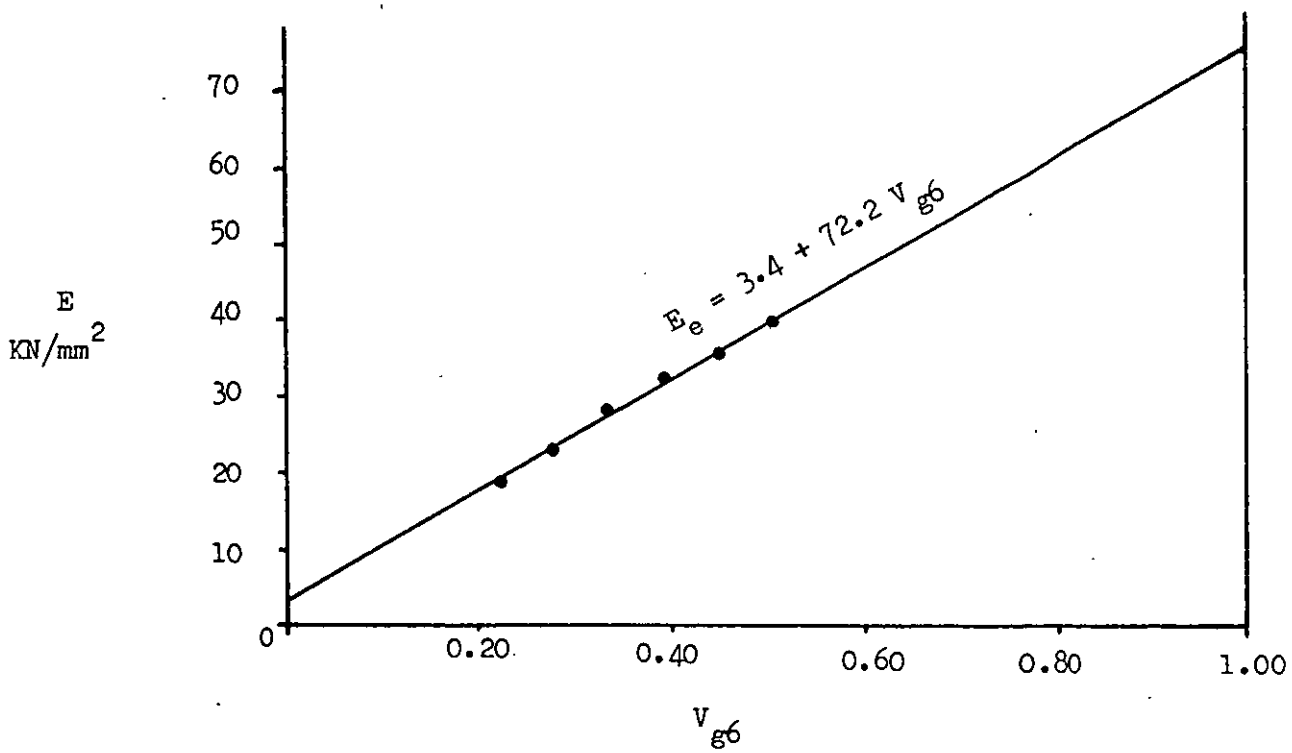

Figure 51 The Variation in the Tensile Strength ($\hat{\sigma}_e$) of 600 tex E-Glass Composites with 600 tex E-Glass Volume Fraction Content (V_{g6}) and the Predicted Upper ($\hat{\sigma}_u$) Lower ($\hat{\sigma}_L$) and Weakest ($\hat{\sigma}_w$) Stress Levels Following the Theory of Rosen[1] and Zweben[3].

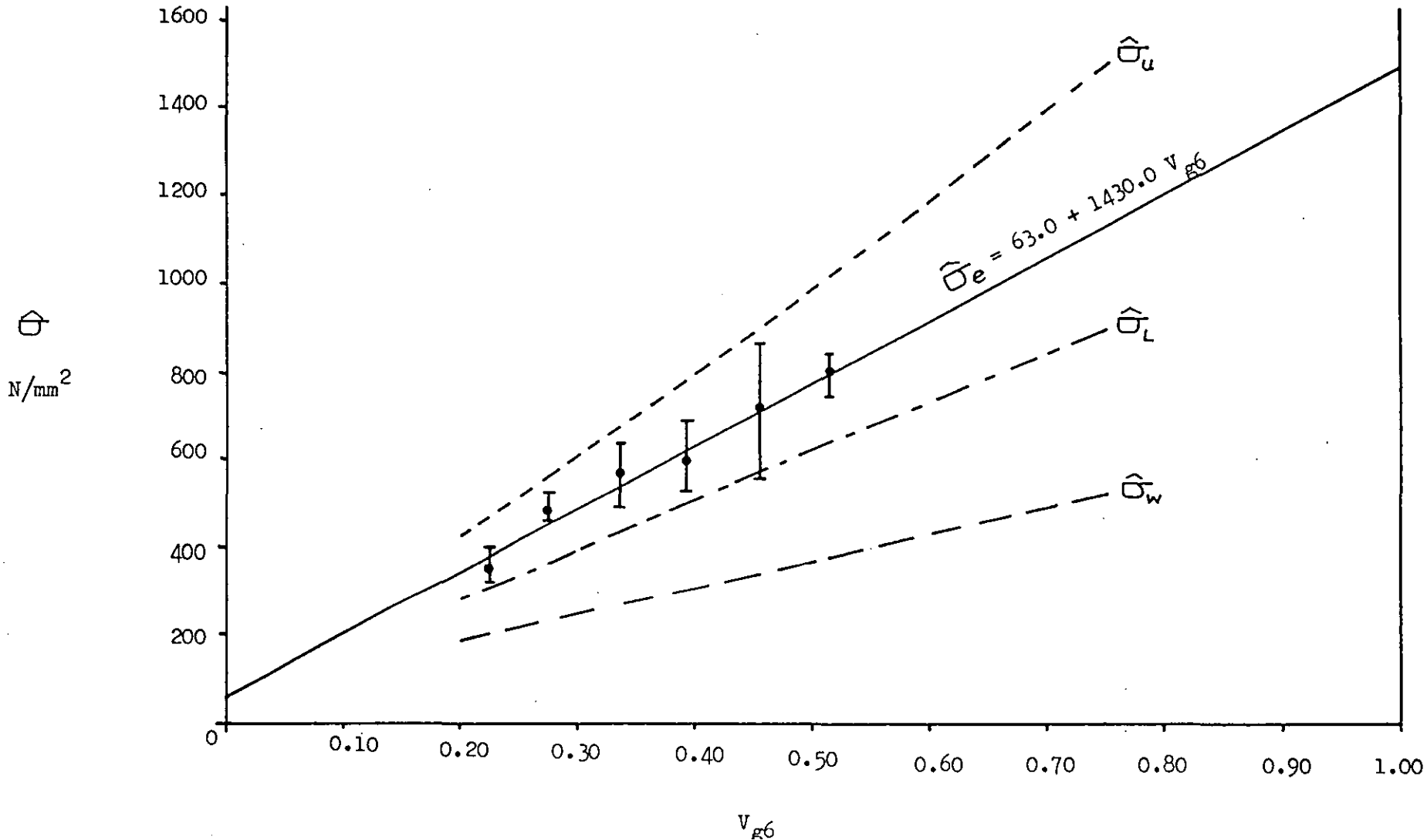

Figure 52

A Typical Tensile Stress v Strain Curve for a 600 tex E-Glass Composite Specimen From Slab 11 ($7G_6$, $V_{g6} \simeq 0.39$).

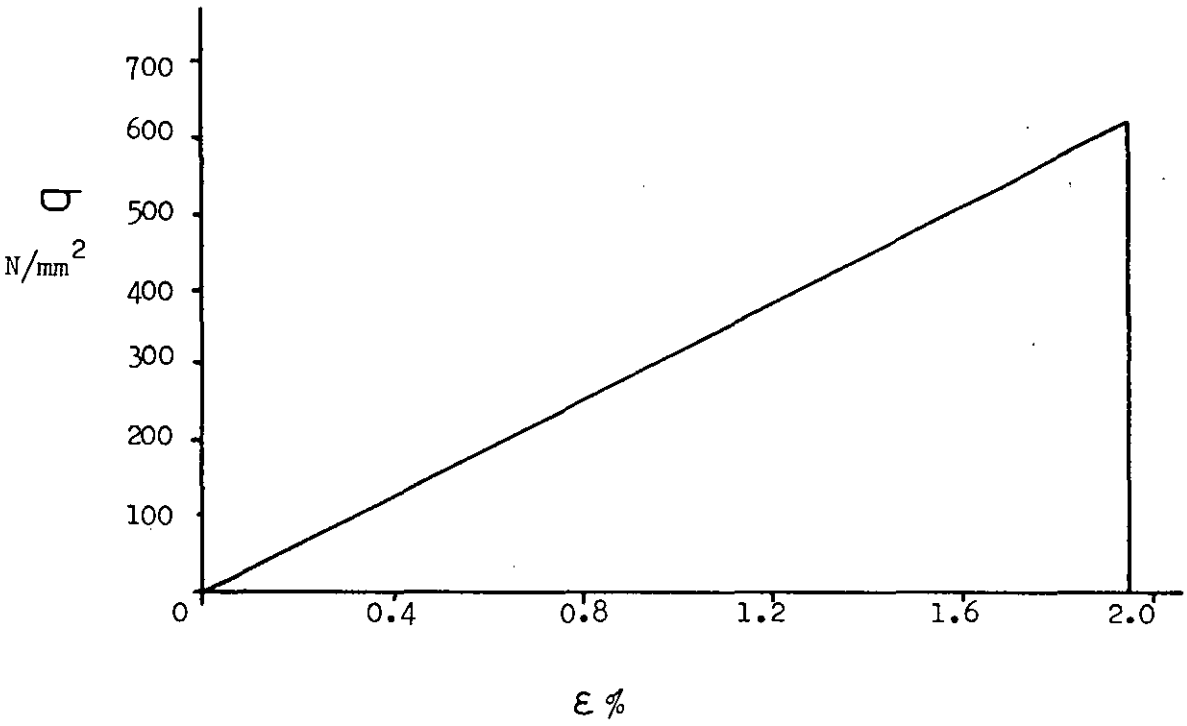

Figure 53

Half of the Fractured 600 tex E-Glass Composite Tensile Specimen 11.4.

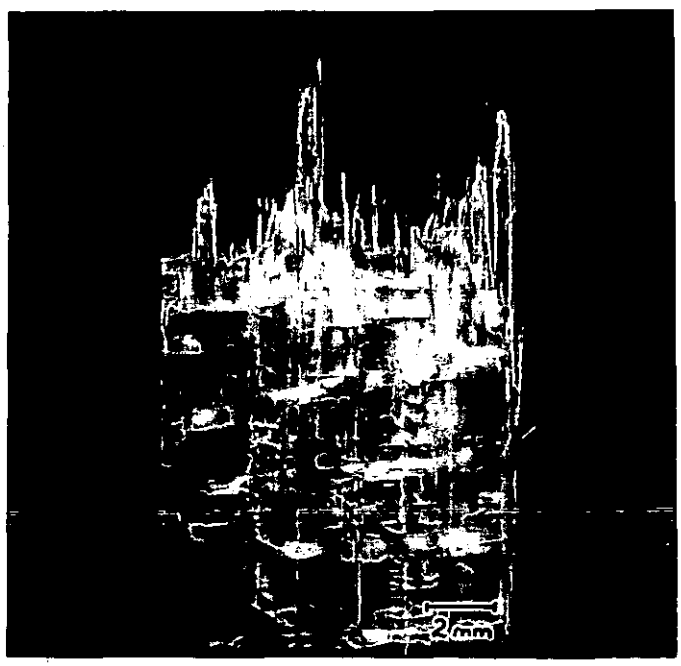

Figure 54

Comparison Between the Experimental and Theoretical (After Barry[4]) Failure Stresses of the 600 tex E-Glass Composites from Slabs 8 to 13.

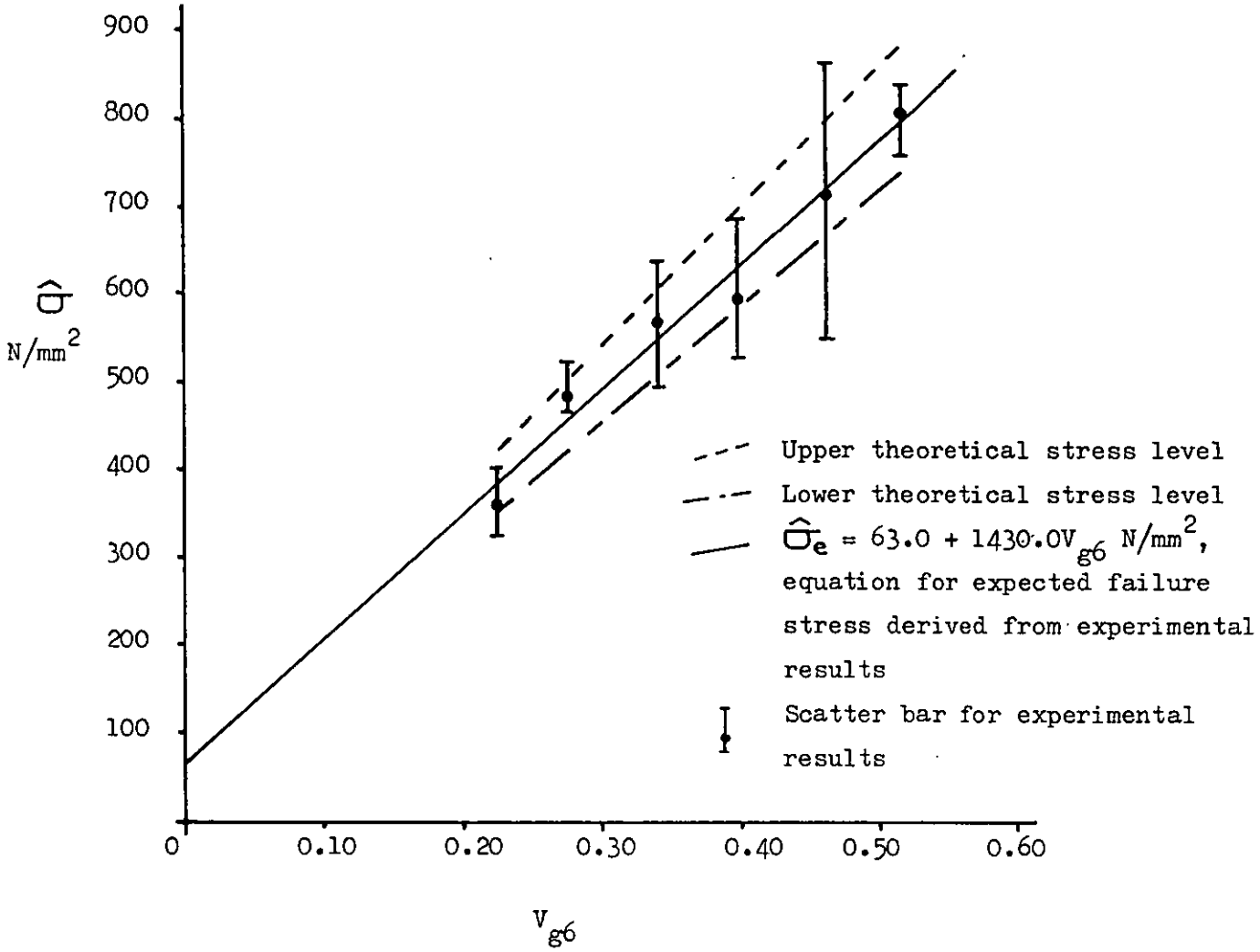

Figure 55

The Variation in the Elastic Modulus (E) of 500 tex E-Glass Composites with 500 tex E-Glass Volume Fraction Content (V_{g5}).

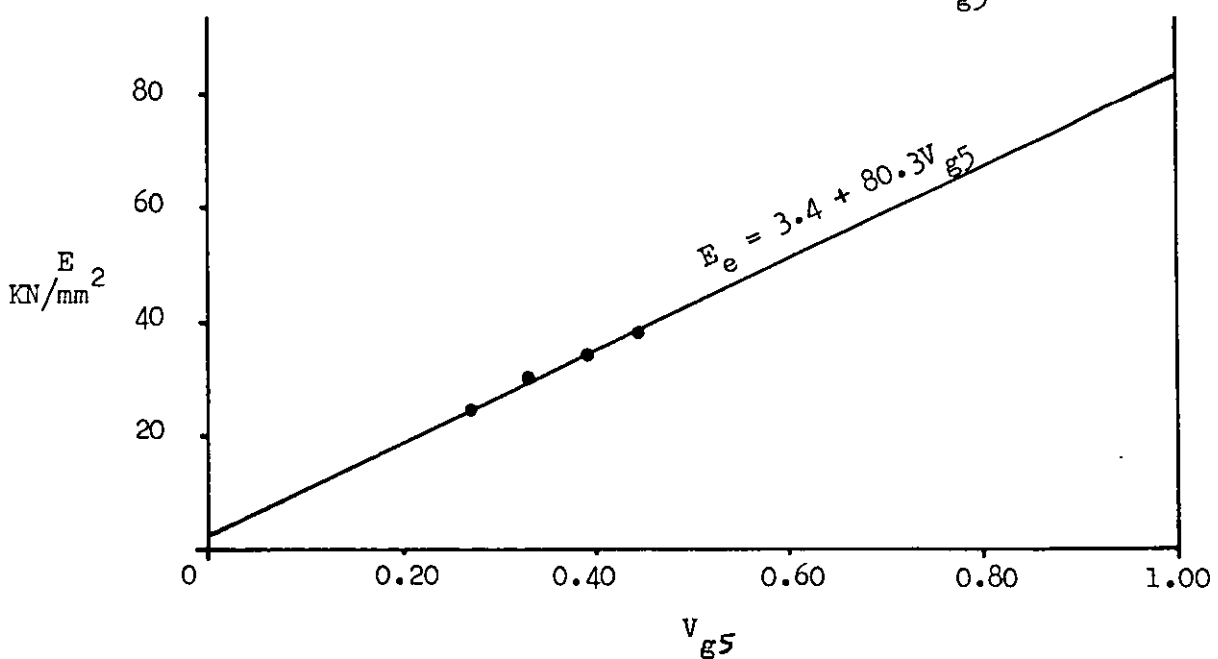

Figure 56 The Variation in the Tensile Strength ($\hat{\sigma}_e$) of 500 tex E-Glass Composites with 500 tex E-Glass Volume Fraction Content (V_{g5}) and the Predicted Upper ($\hat{\sigma}_u$) Lower ($\hat{\sigma}_L$) and Weakest ($\hat{\sigma}_w$) Stress Levels Following the Theory of Rosen[1] and Zweben[3].

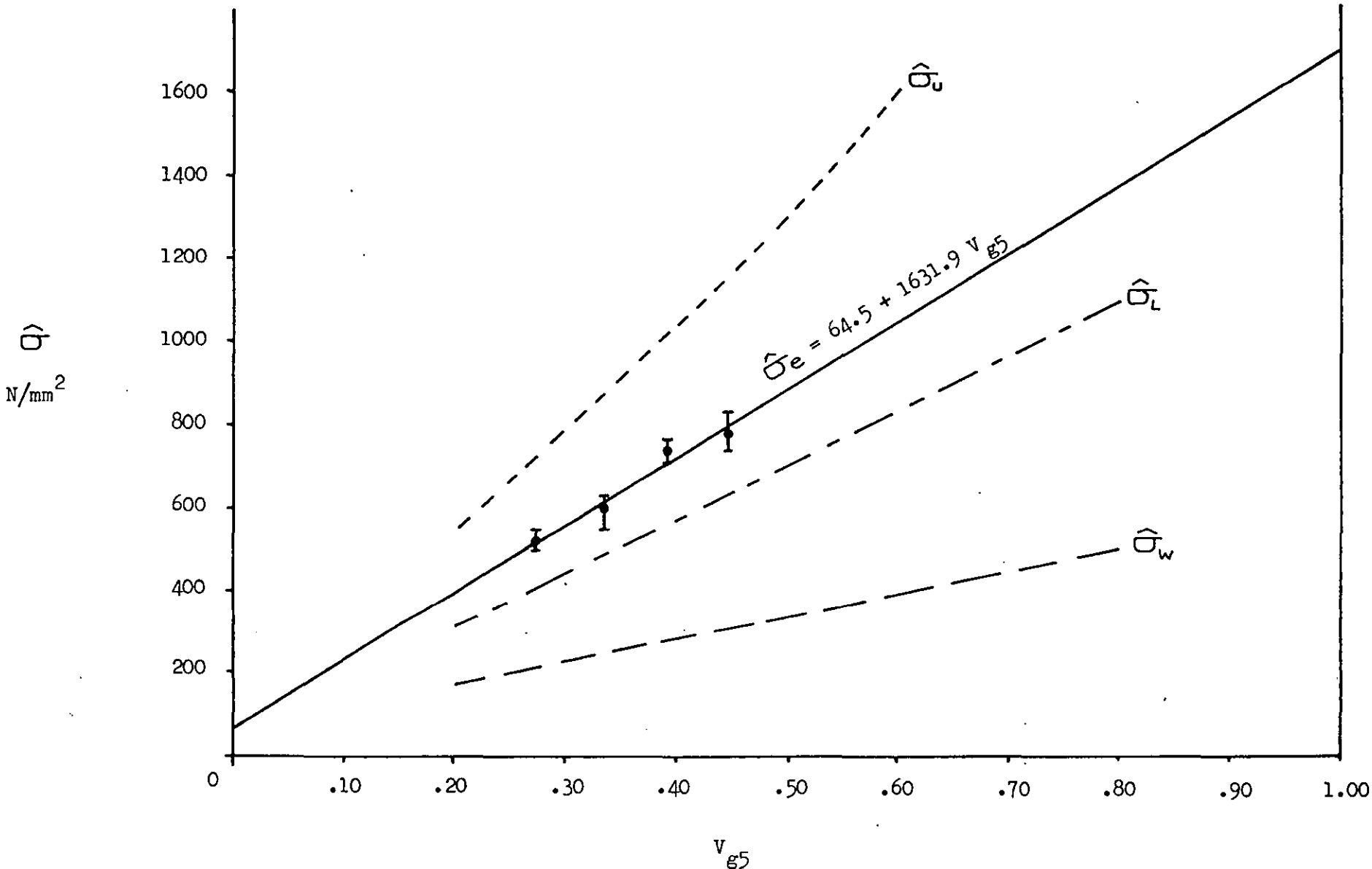

Figure 57

A Typical Tensile Stress v Strain Curve for a 500 tex E-Glass Composite Specimen from slab 19 ($7G_5$, $V_{g5} \simeq 0.39$)

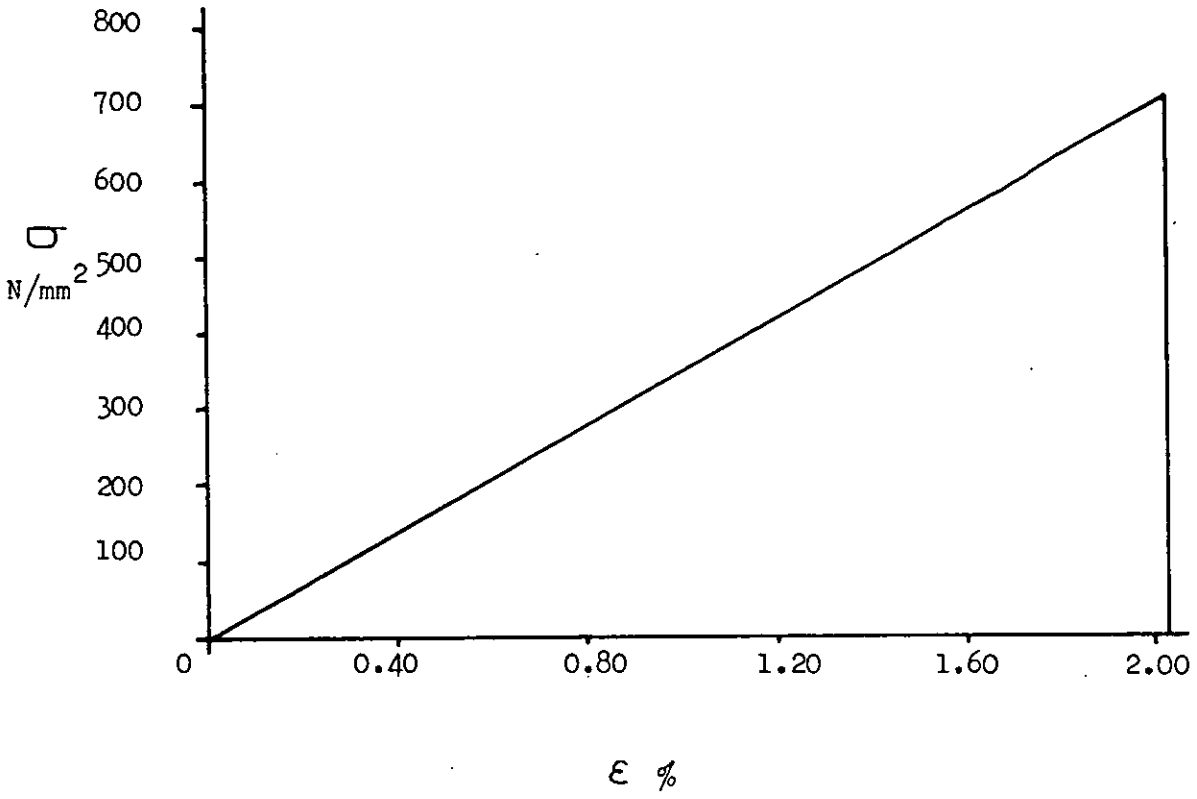

Figure 58

Comparison Between the Experimental and Theoretical (After Barry[4]) Failure Stresses of the 500 tex E-Glass Composites from Slabs 17 to 20.

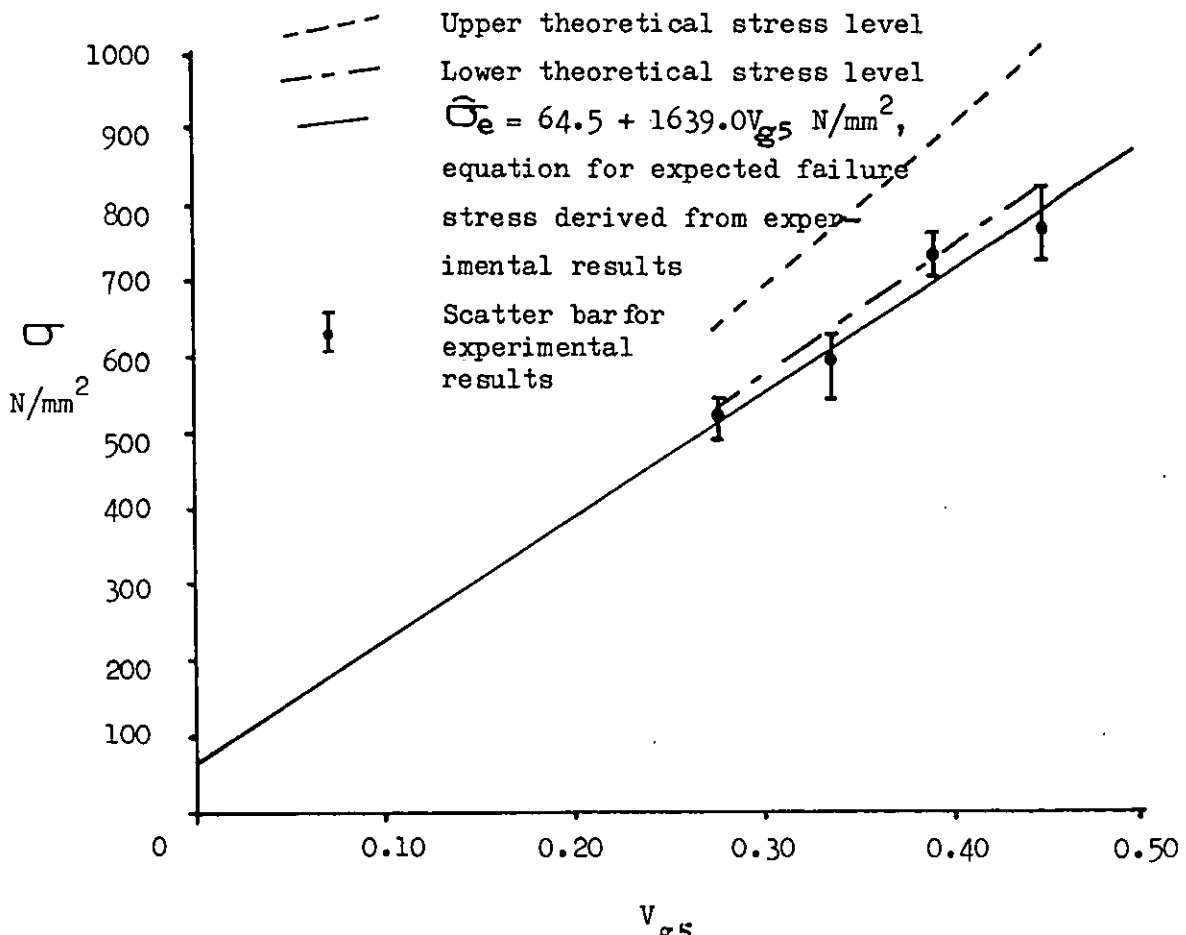

Figure 59 The Variation in the Experimental Tensile Stress at the Elastic Limit (in this case equal to the initial failure stress), σ^{E}, and the Maximum stress, $\hat{\sigma}$, of the 3:1 Tape Hybrid Composites with Total Fibre Volume Fraction Content, V_T, Compared with the Rule of Mixtures Values (σ^{E}_{RM} and $\hat{\sigma}_{RM}$).

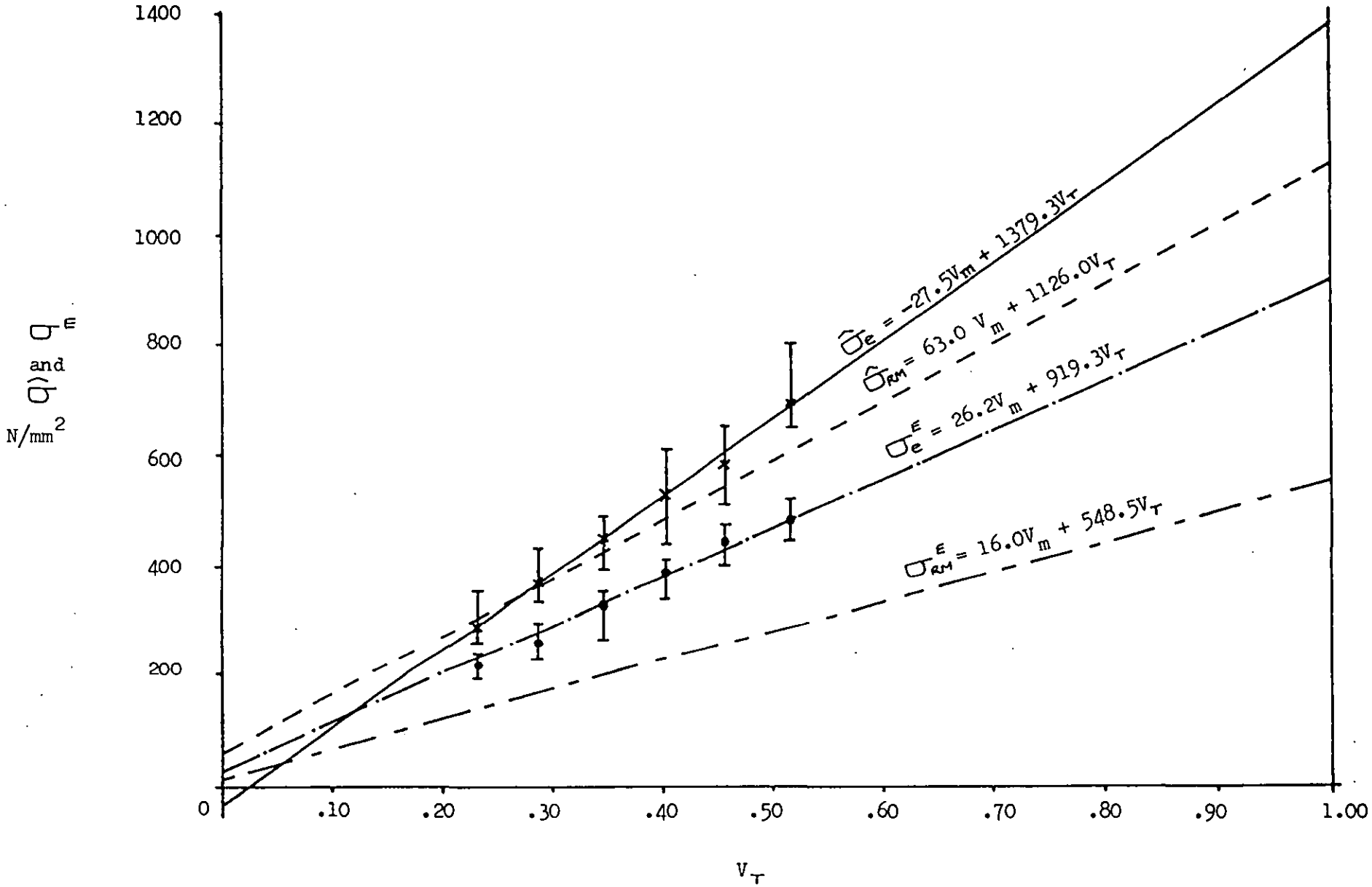

Figure 60 A Typical Experimental Tensile Stress v Strain Curve (—~—) for a 3:1 Tape Hybrid Composite Specimen from Slab 27 (7 x 3:1, $V_f \simeq 0.39$) and the Theoretical Rule of Mixtures curve (- - -)

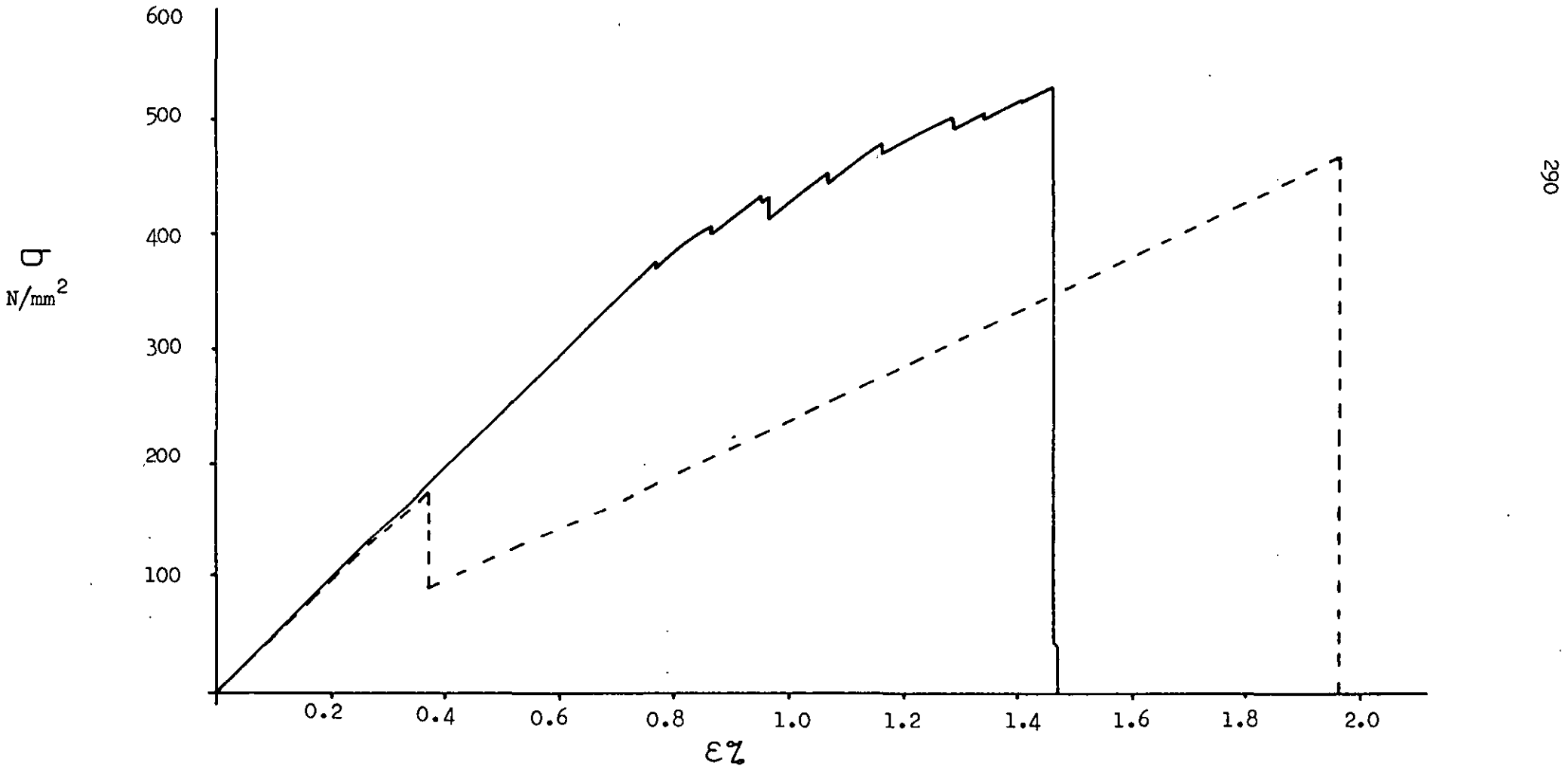

Figure 61

Half of the Fractured 3:1 Tape Hybrid Composite Tensile Specimen 27.4.

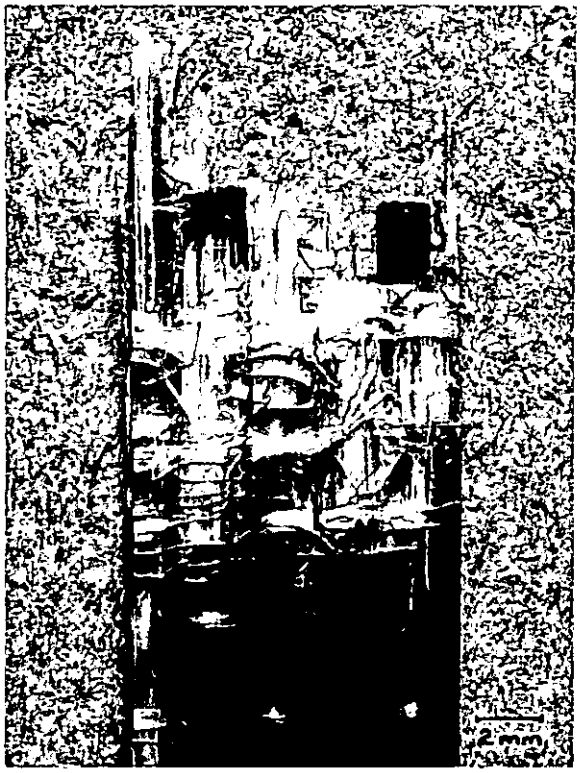

Figure 62

Stereozoom Photograph of a Portion of the Fracture Surface of the 3:1 Tensile Specimen 25.1. Note the profile of the fractured carbon tow and the spike of E-glass on the L.H.S.

Figure 63

The Variation in the Elastic Modulus, E, of the 3:1 Tape Hybrid Composites with Total Fibre Volume Fraction Content, V_T.

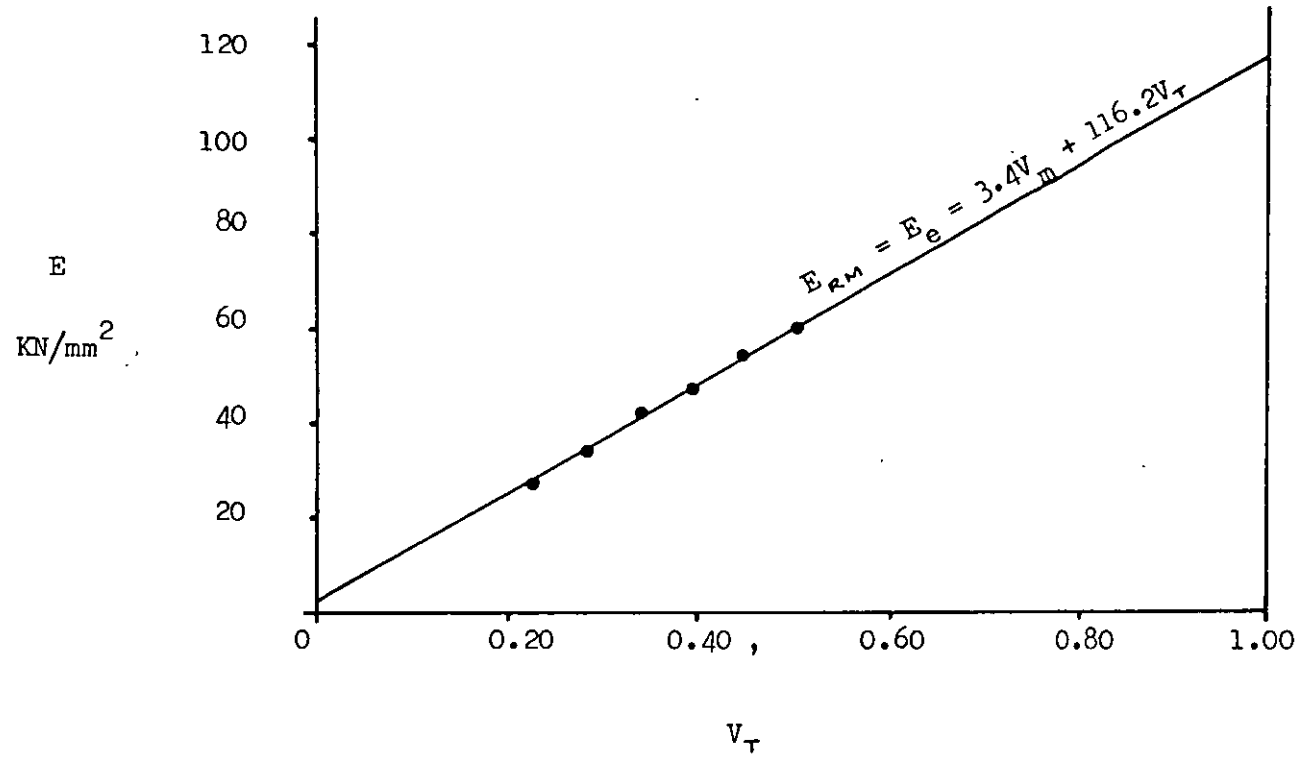

Figure 64

The Variation in the Elastic Modulus, E, of the 1:1 Tape Hybrid Composites with Total Fibre Volume Fraction Content, V_T.

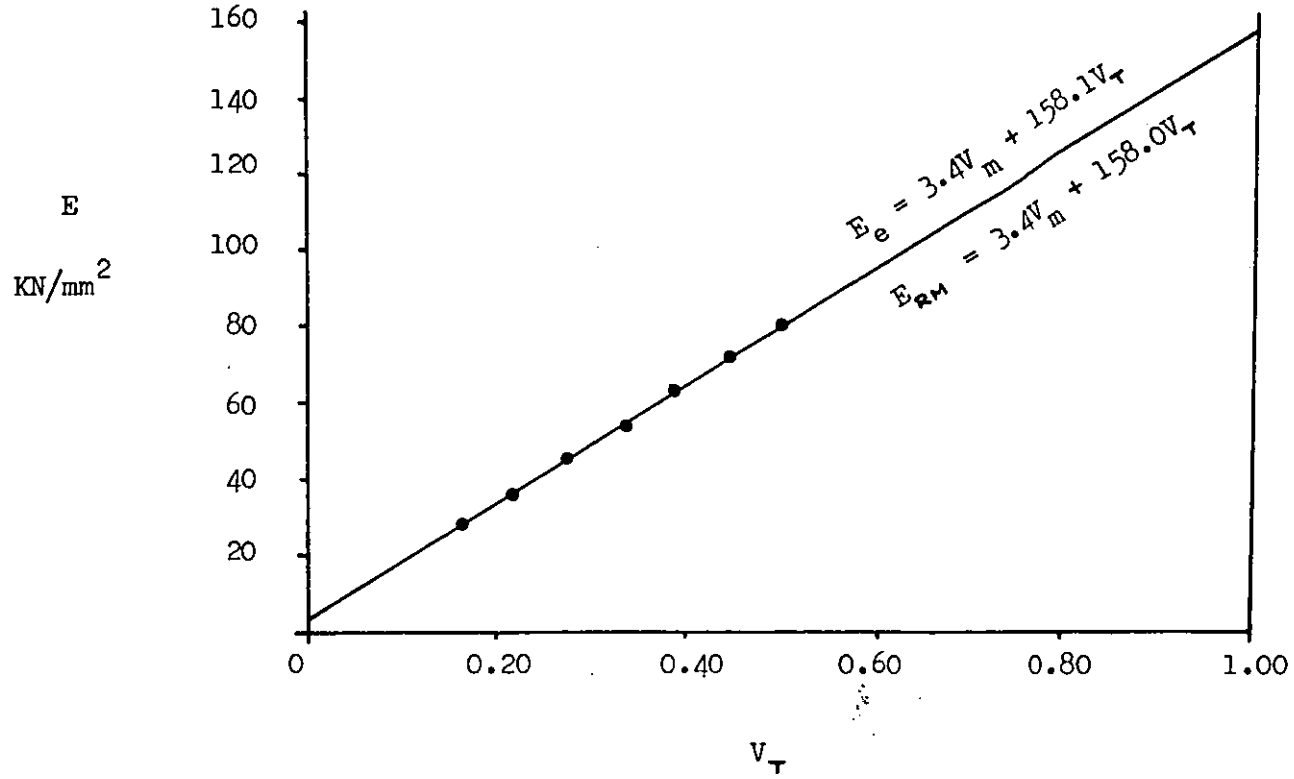

Figure 65 The Variation in the Experimental Tensile Stress at the Elastic Limit (in this case equal to the initial failure stress), σ^{ε}, and the Maximum stress, $\hat{\sigma}$, of the 1:1 Tape Hybrid Composites with Total Fibre Volume Fraction Content, V_T, Compared with the Rule of Mixtures Values ($\sigma^{\varepsilon}_{RM}$ and $\hat{\sigma}_{RM}$).

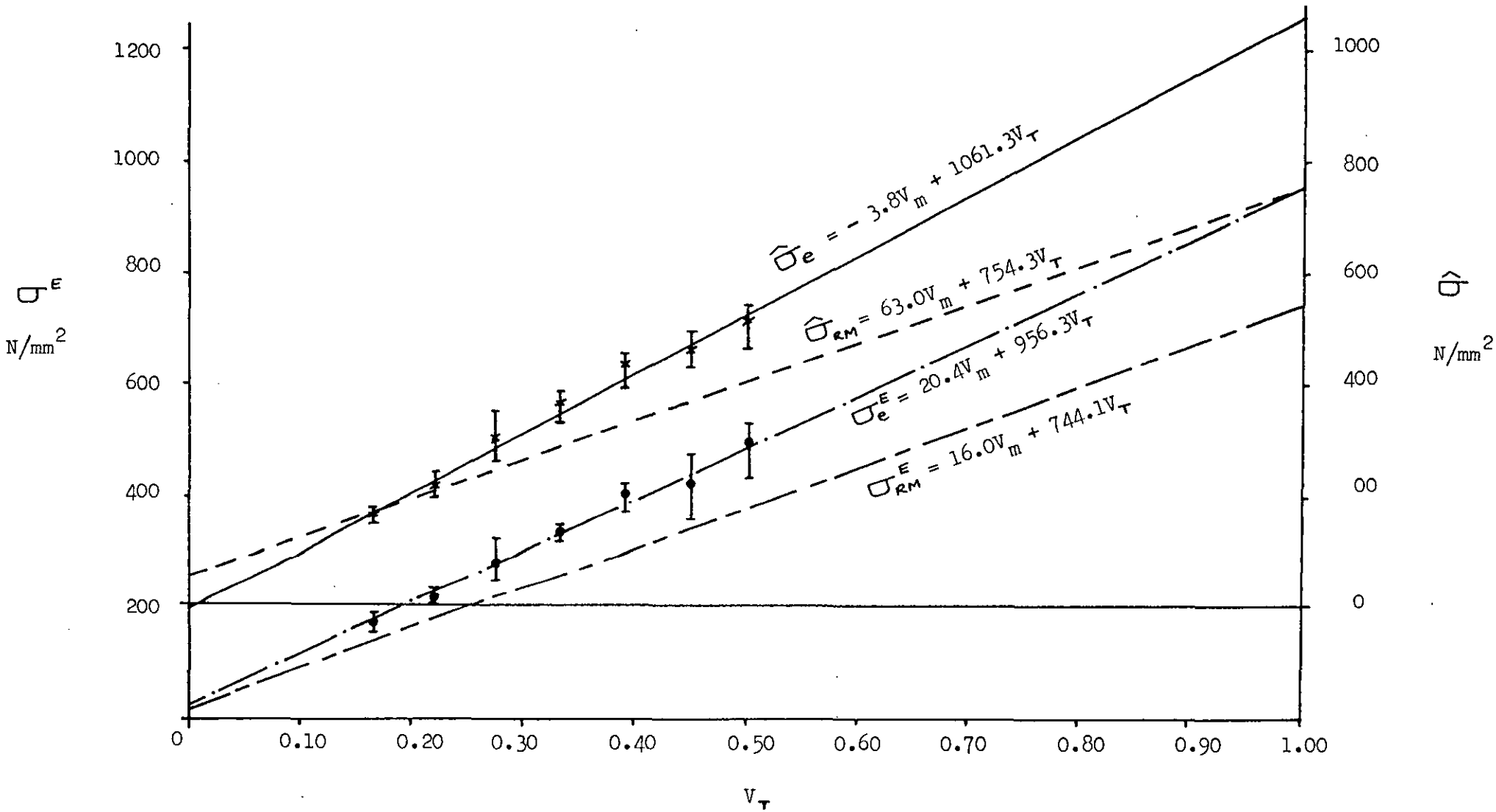

Figure 66

A Typical Tensile Stress v Strain Curve for a 1:1 Tape Hybrid Composite Specimen from Slab 34 (7 x 1:1, $V_f \simeq 0.39$) and the Theoretical Rule of Mixtures Curve.

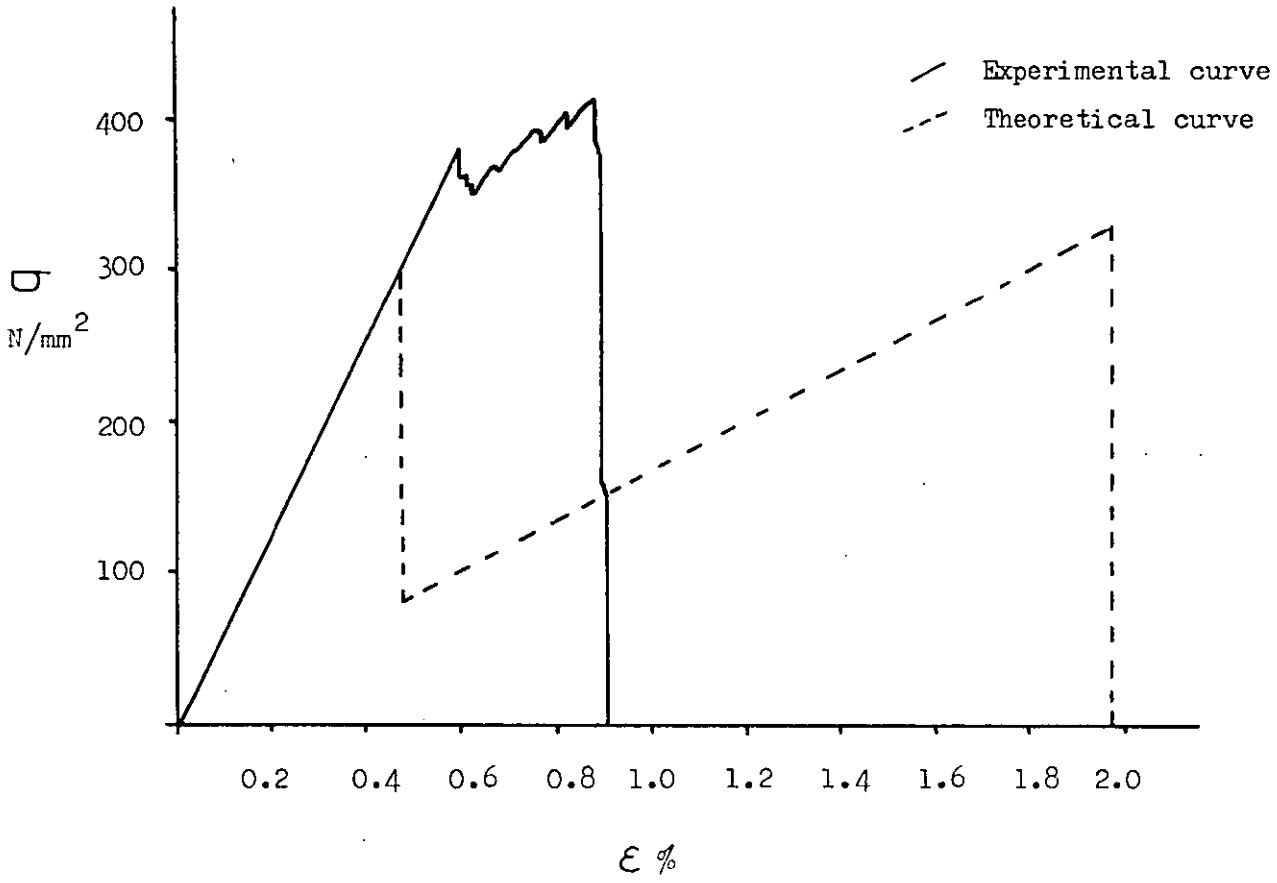

Figure 67

Half of the Fractured 1:1 Tape Hybrid Composite Tensile Specimen 34.1

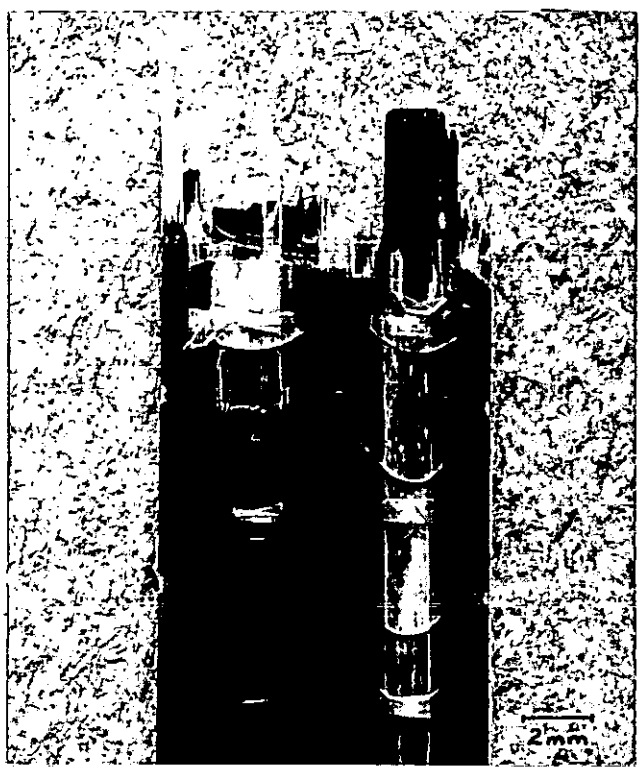

Figures 68 to 78

Typical Tensile Stress v Strain Curves (———) for specimens from Slabs 37 to 47 Compared with the Theoretical Rule of Mixtures Curves (- - -).

Figure 68 Slab 37, CG_6G_6C, $V_T \simeq 0.22$

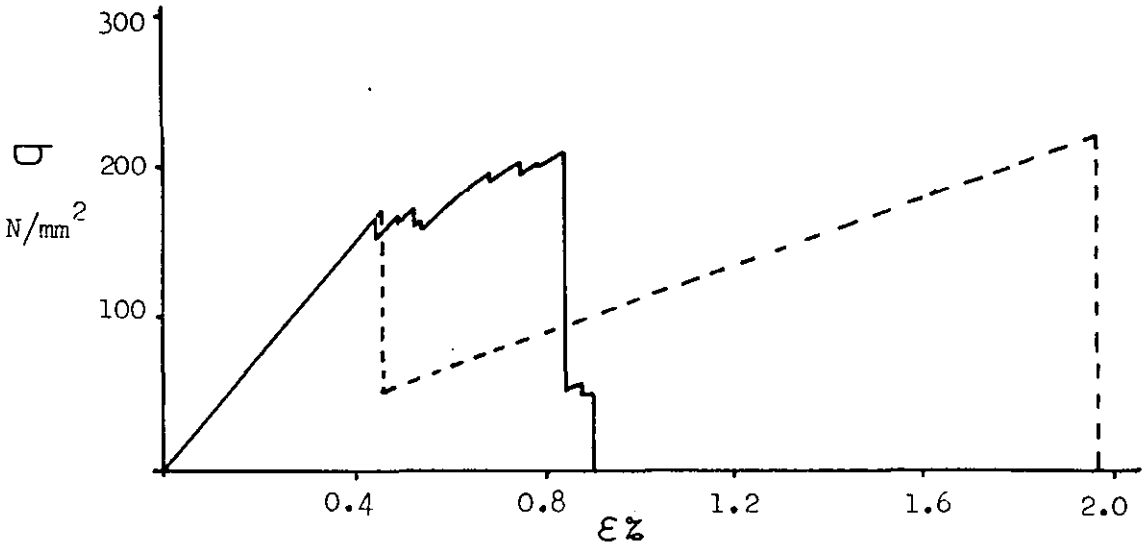

Figure 69 Slab 38, $CG_6CG_6G_6CG_6C$, $V_T \simeq 0.44$

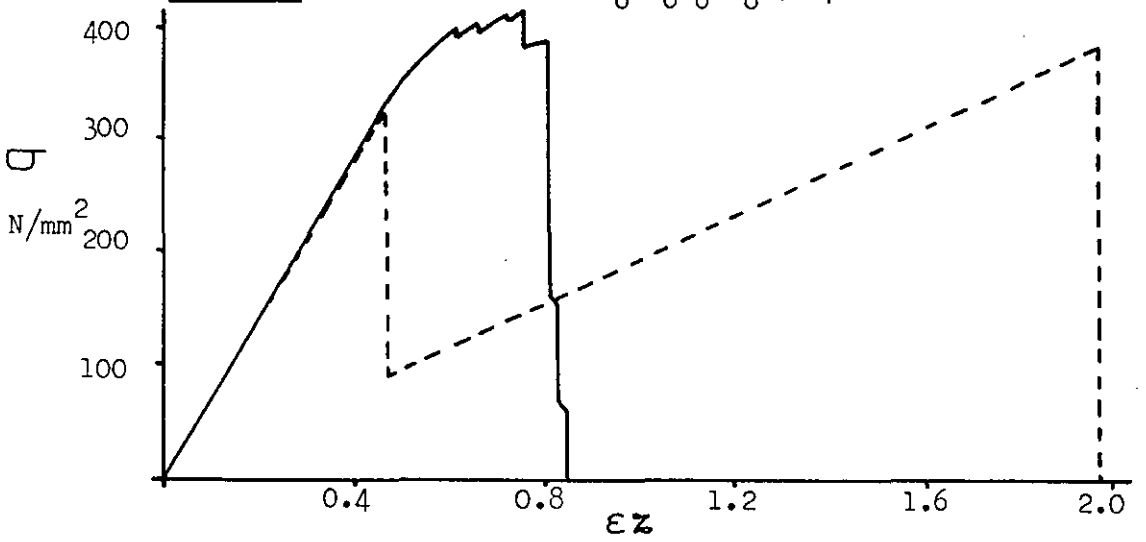

of 6 specimens tested 2 had $\sigma' = \hat{\sigma}$

Figure 70 Slab 39, $G_6G_6CG_6G_6CG_6G_6$, $V_T \simeq 0.44$

Of 6 specimens tested 1 had $\sigma^E = \sigma'$ and 2 had $\sigma' = \hat{\sigma}$

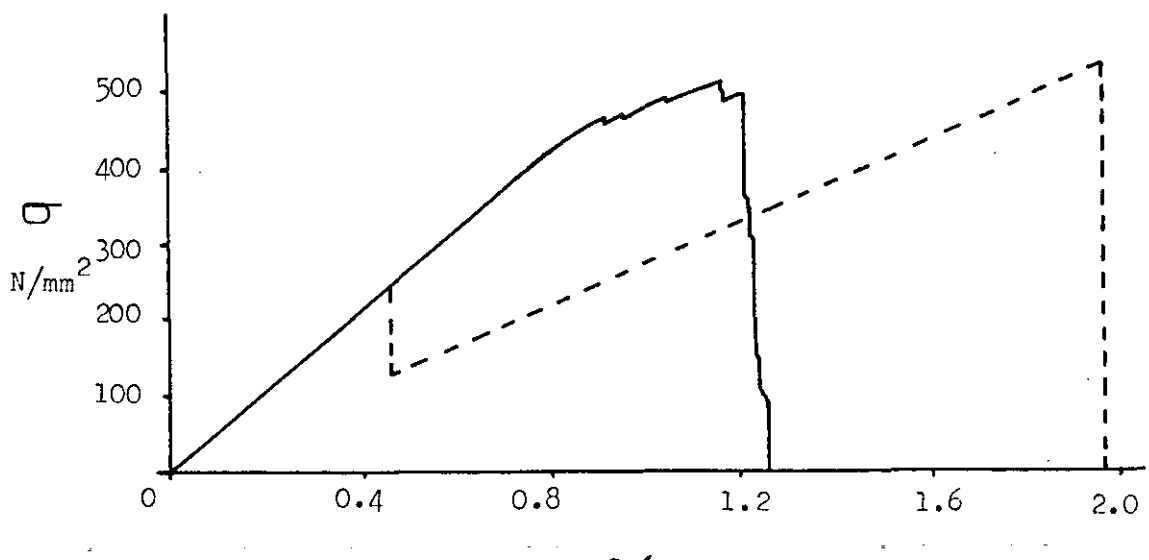

Figure 71 Slab 40, $G_5G_5CG_5G_5CG_5G_5$, $V_T \simeq 0.44$

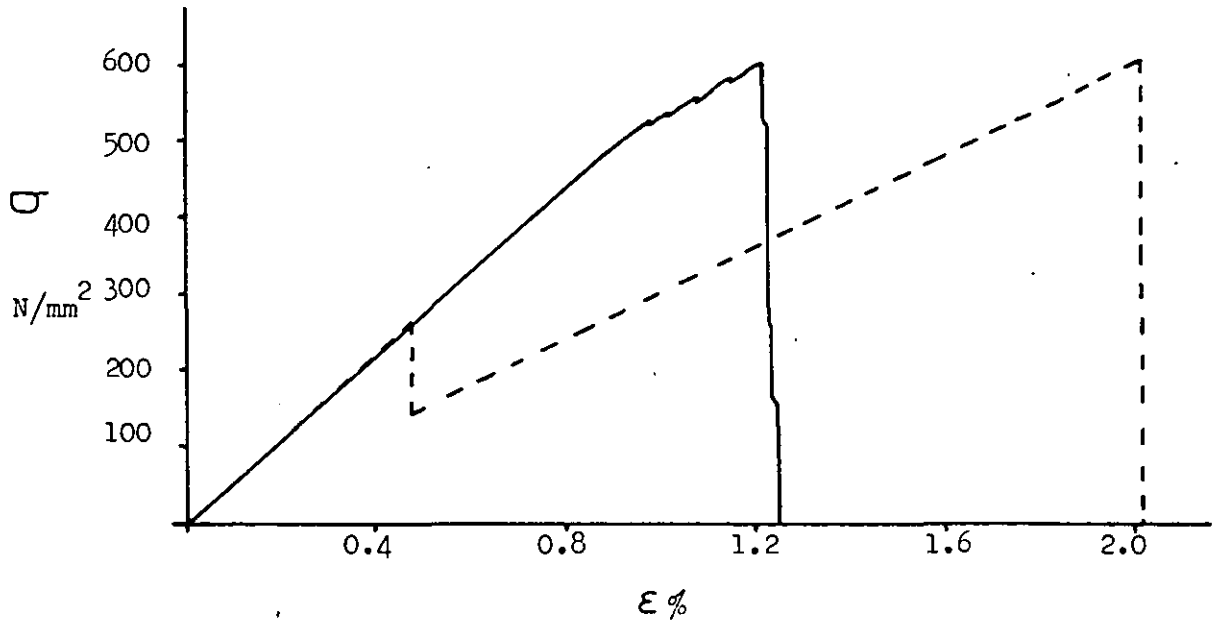

Figure 72 Slab 41, G_6 3:1 G_6 3:1 G_6 3:1 G_6, $V_T \simeq 0.39$
of 6 specimens tested 2 had $\sigma^E = \sigma'$

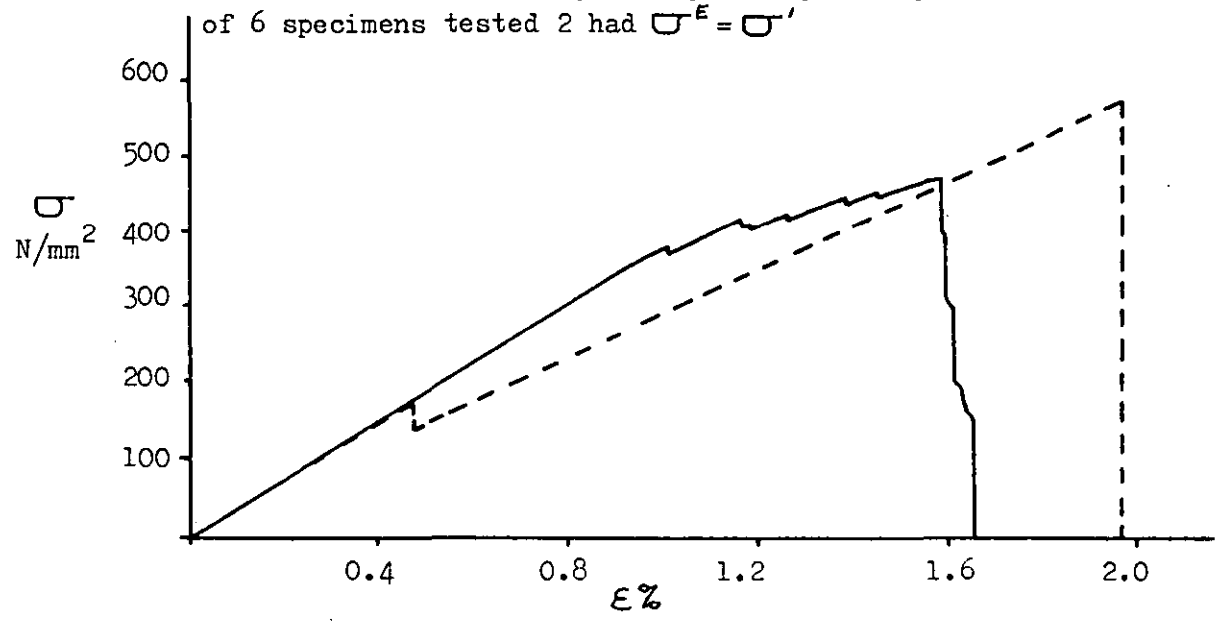

Figure 73 Slab 42, 1:1 C 1:1 C 1:1 C 1:1, $V_T \simeq 0.38$

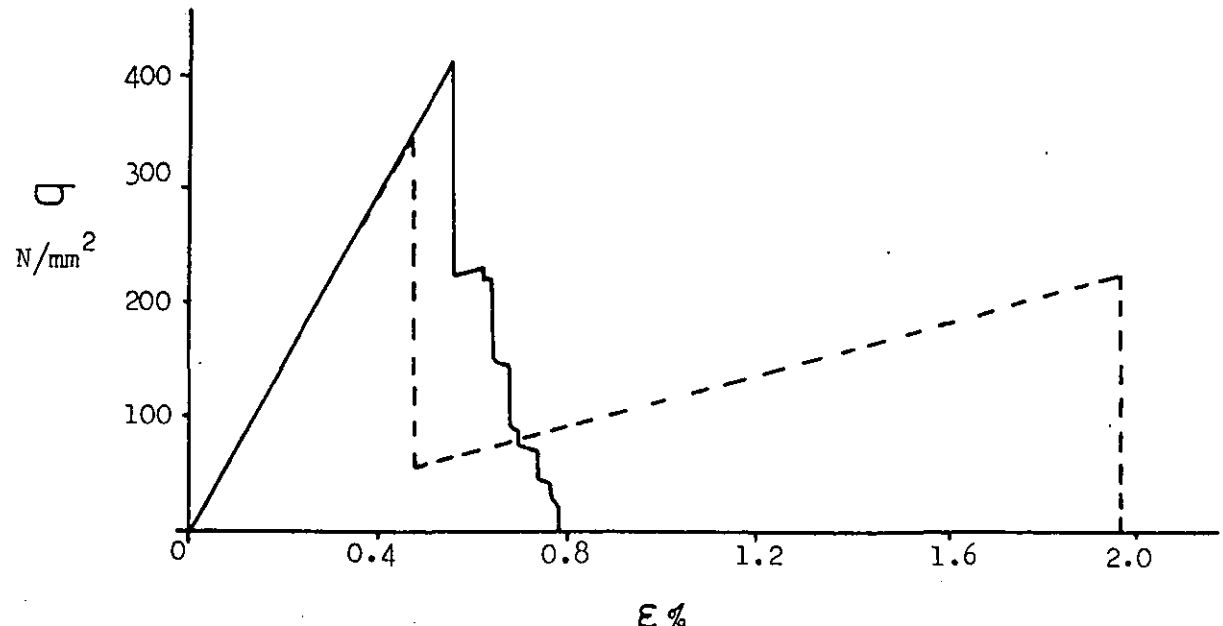

Figure 74 Slab 43, 3:1 C 3:1 C 3:1 C 3:1, $V_T \simeq 0.39$
Of 6 specimens tested 1 had $\sigma^{\epsilon} = \sigma'$ and 3 had $\sigma' = \hat{\sigma}$

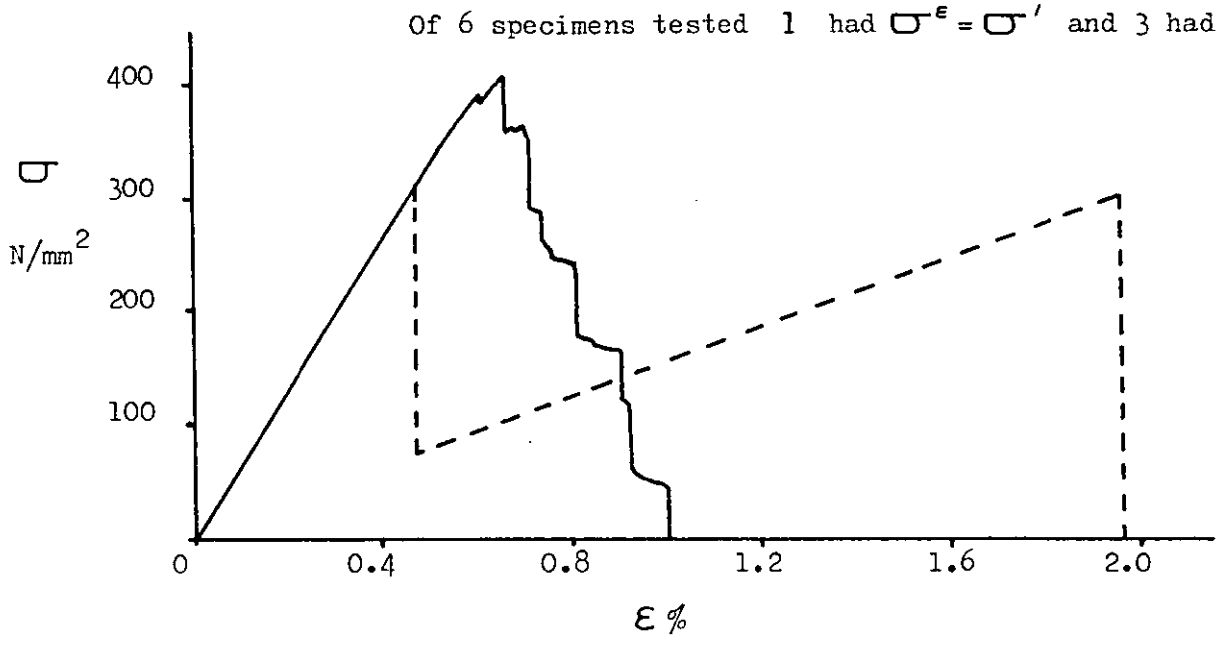

Figure 75 Slab 44, 3:1 1:1 3:1 1:1 3:1 1:1 3:1, $V_T \simeq 0.39$
Of 6 specimens tested 3 had $\sigma^{E} = \sigma' = \hat{\sigma}$

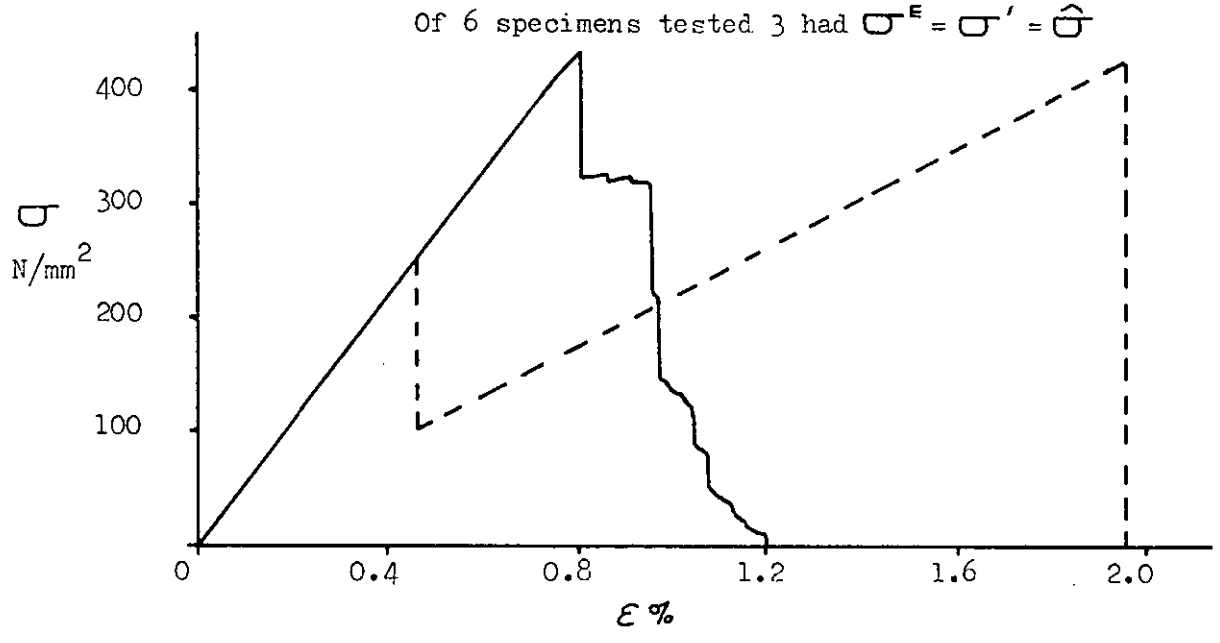

Figure 76 Slab 45, 1:1 1:1 3:1 1:1 3:1 1:1 1:1, $V_T \simeq 0.39$
Of 6 specimens tested 1 had $\sigma^{E} = \sigma'$

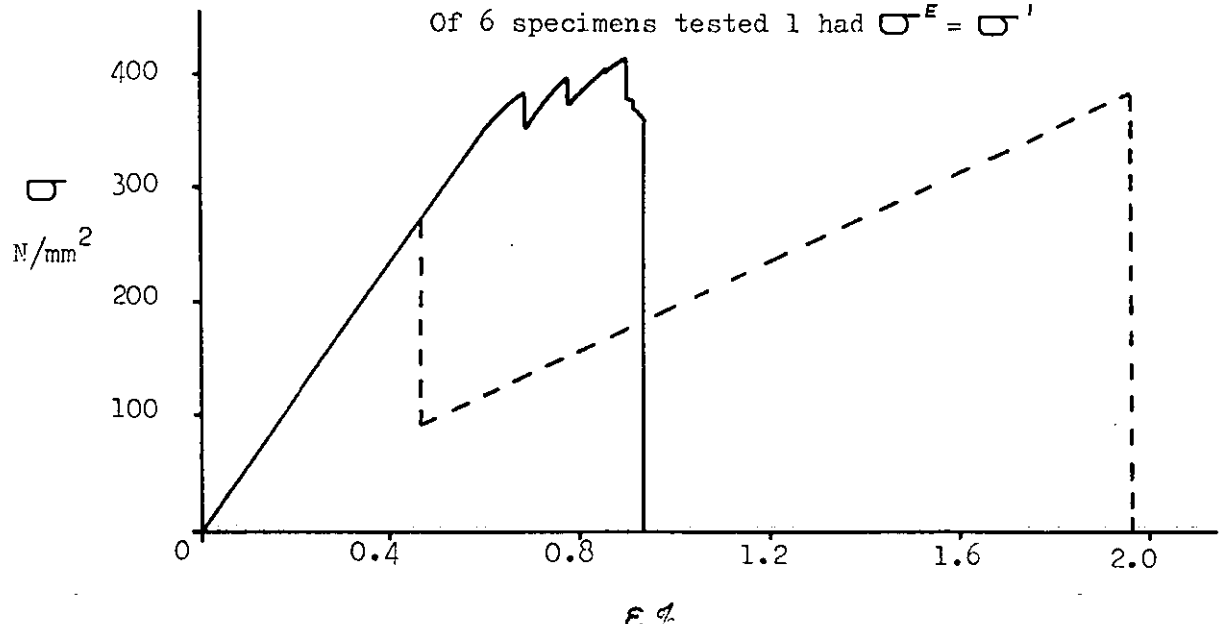

Figure 77 Slab 46, $G_6CG_6CG_6C$, $V_T \simeq 0.39$
Of 6 specimens tested 1 had $\sigma^{\varepsilon} = \sigma' = \hat{\sigma}$ and 2 had $\sigma^{\varepsilon} \neq \sigma' = \hat{\sigma}$

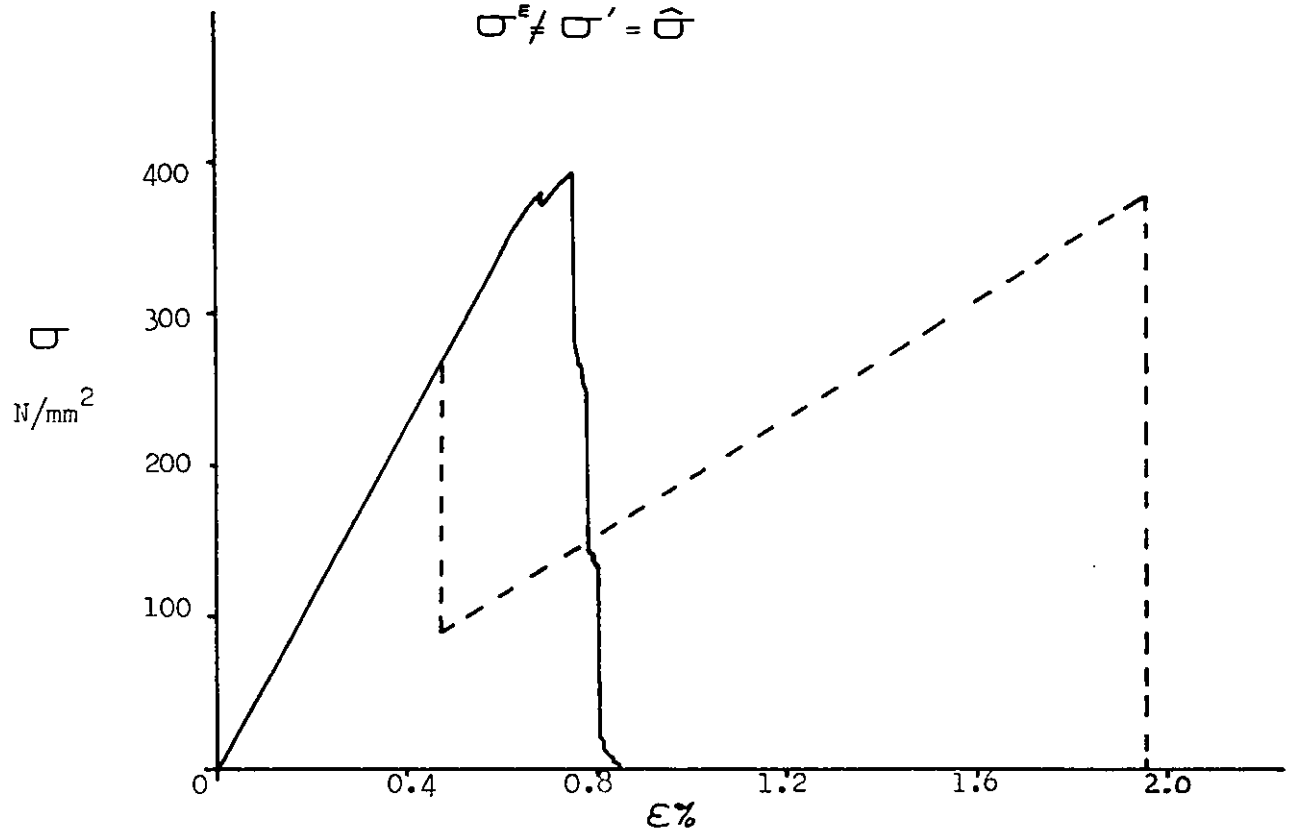

Figure 78 Slab 47, $G_5CG_5CG_5CG_5$ $V_T \simeq 0.39$
Of 6 specimens tested 4 had $\sigma' = \hat{\sigma}$

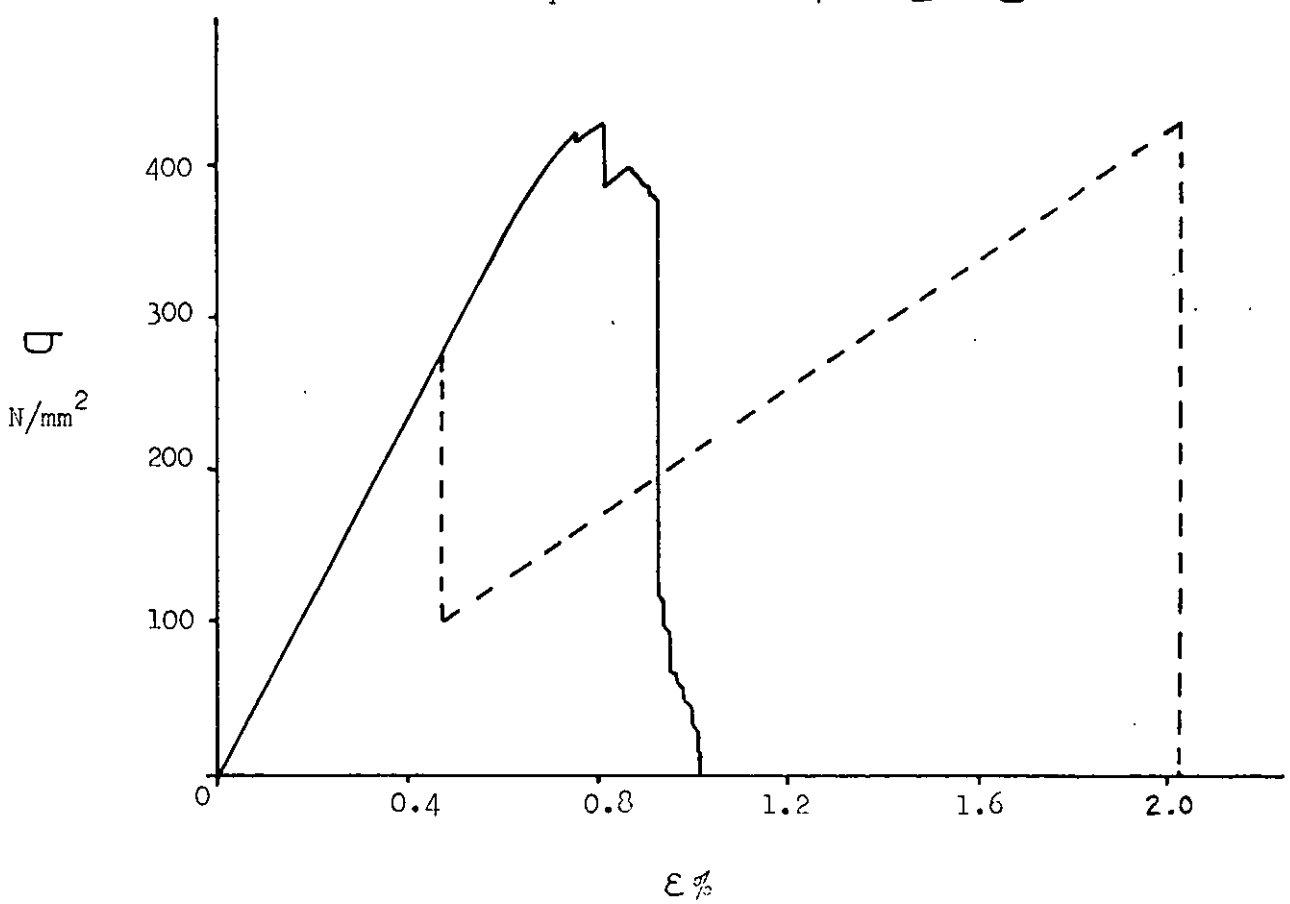

Figure 79

Stereozoom Photograph of a Section of the Fractured Hybrid Tensile Specimen 46.6. Note the 'spikey' appearance of the fracture.

Figure 80

Stereozoom Photograph of the Fractured Hybrid Tensile Specimen 46.5. Note the contrast between this fracture and the one in figure 79.

Figure 81

Scanning Electron Micrograph of a Typical Portion of the Fracture Surface in a Carbon Fibre area of the Hybrid Tensile Specimen 37.2. Note the range of carbon fibre pull-out lengths.

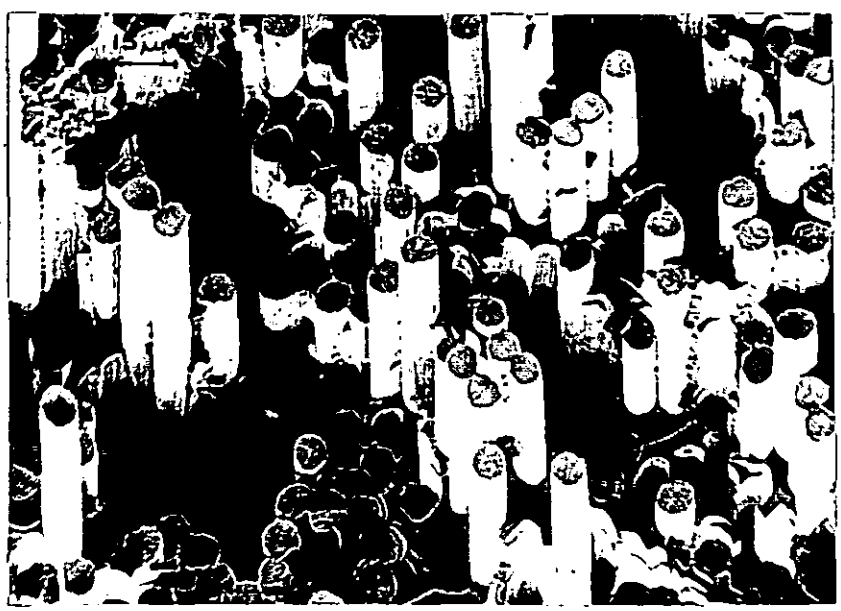

Figures 82 to 95

Typical Tensile Stress v Strain Curves (—) for Specimens from Slabs 48 to 61 Compared with the Theoretical Rule of Mixtures Curves (- - -). For all slabs $V_f \simeq 0.39$

Figure 82 Slab 48, $G_6CG_6CG_6CG_6$, G_6 = no c.-a., C = as rec.

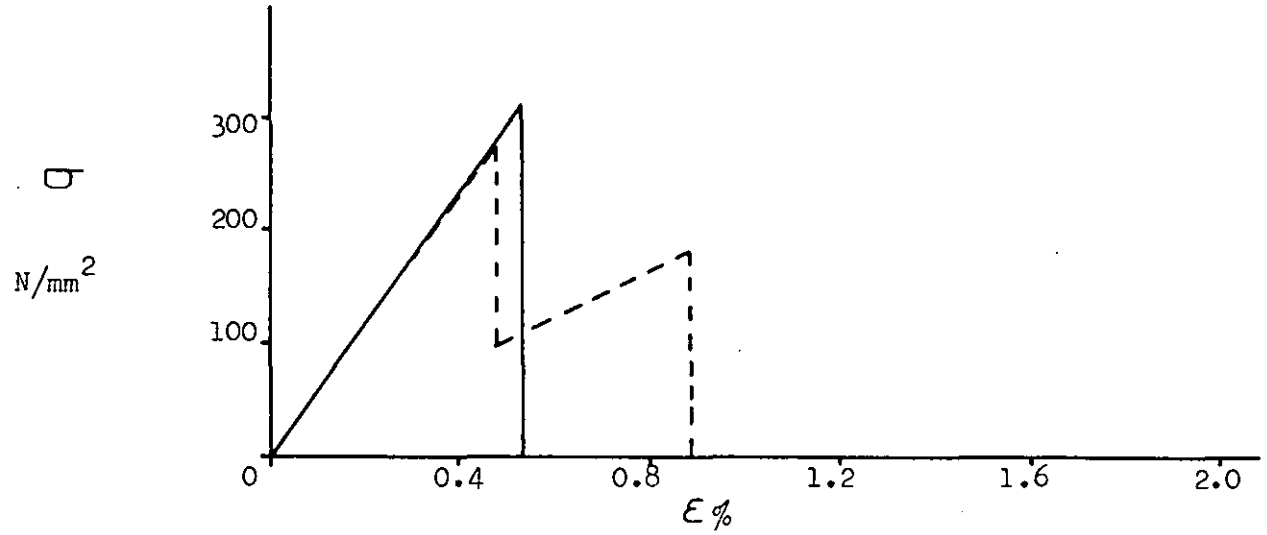

Figure 83 Slab 49, $G_5CG_5CG_5CG_5$, G_5 = no c.-a., C = as rec.

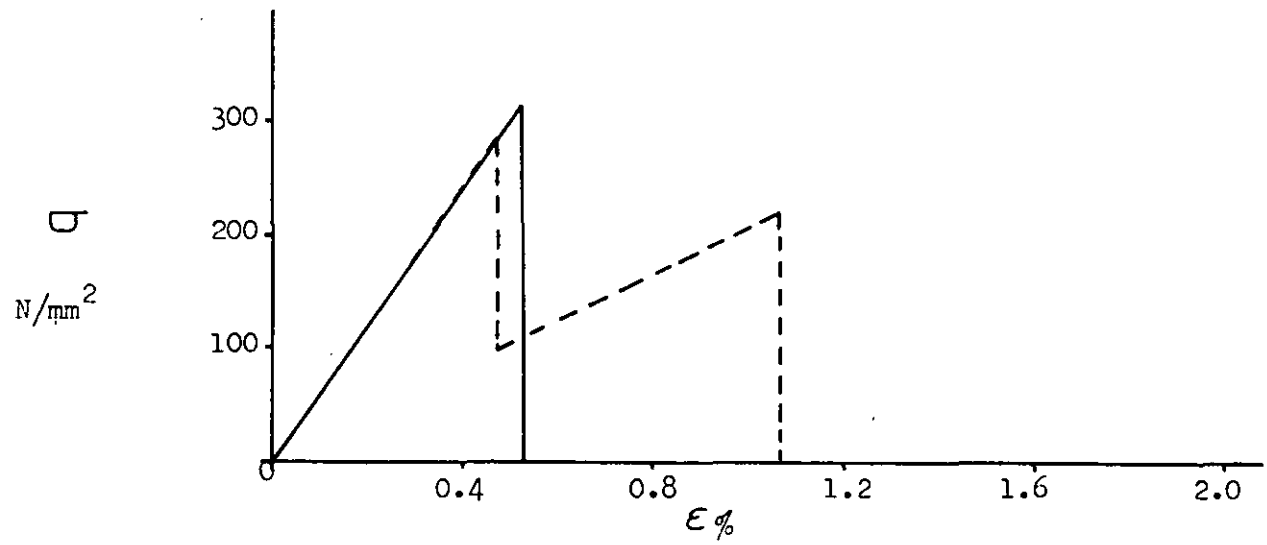

Figure 84 Slab 50, $G_6CG_6CG_6CG_6$, G_6 = A1100, C = as rec.

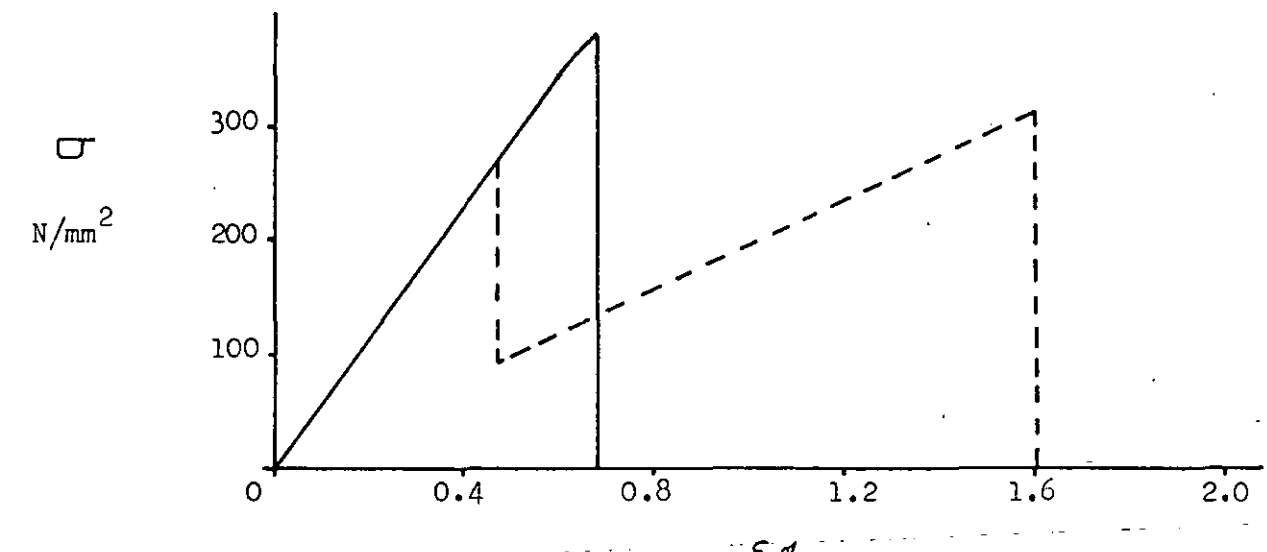

Figure 85 Slab 51, $G_5CG_5CG_5CG_5$, G_5: A1100, C: as rec.
Of 6 specimens tested 1 specimen had $\sigma^{\varepsilon} = \sigma' = \hat{\sigma}$

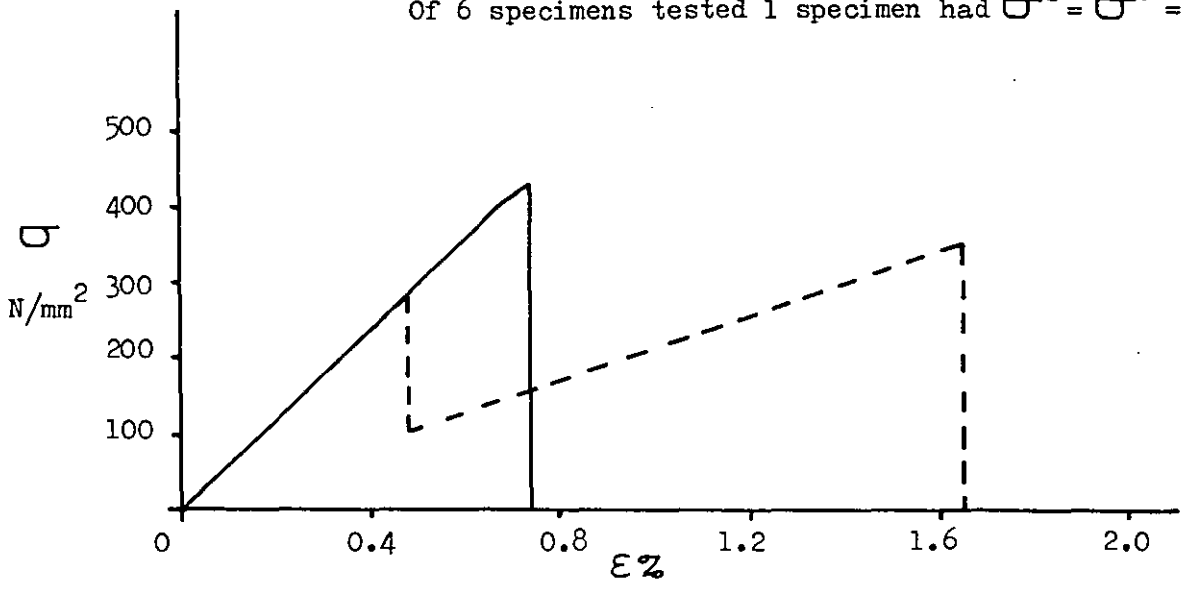

Figure 86 Slab 52, $G_6CG_6CG_6CG_6$, G_6: A187, C: as rec.

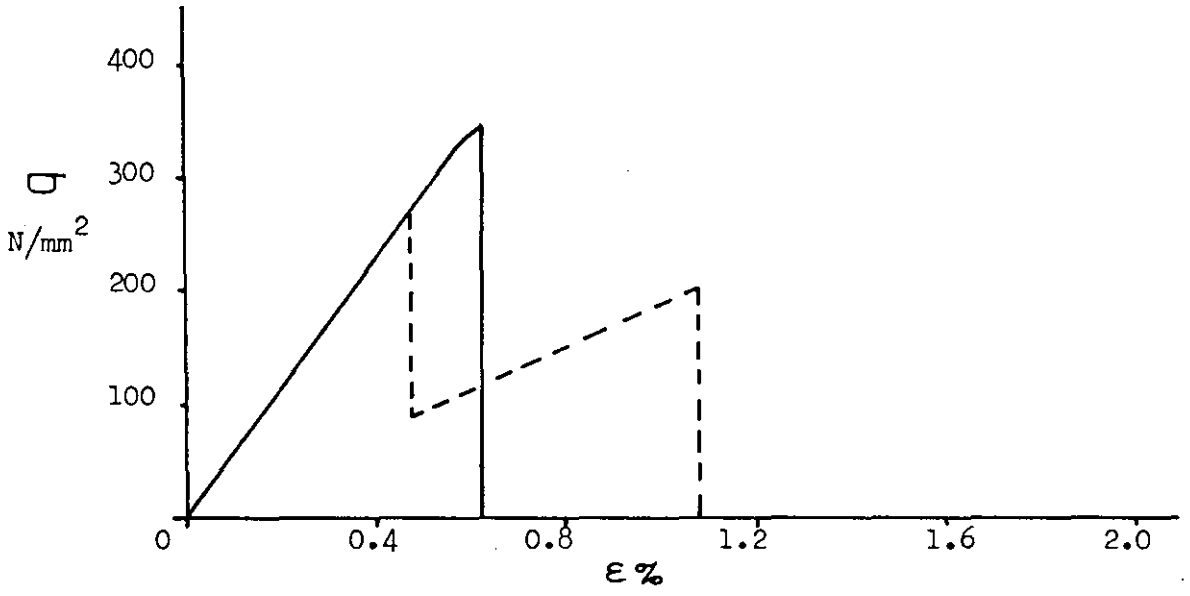

Figure 87 Slab 53, $G_5CG_5CG_5CG_5$, G_5: A187, C: as rec.

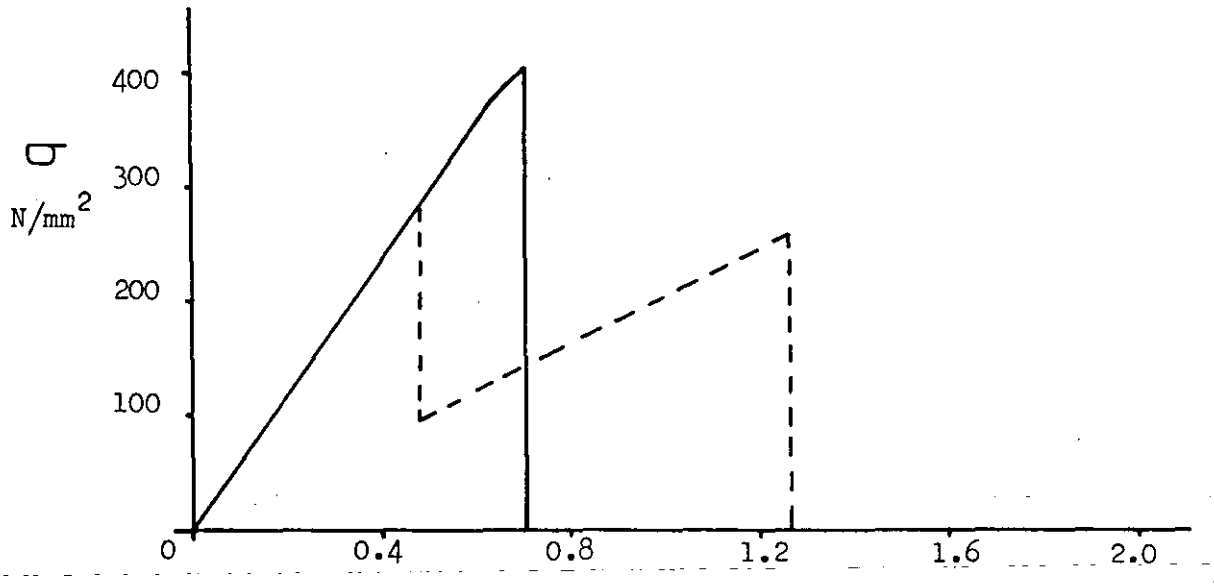

Figure 88 Slab 54, $G_6CG_6CG_6CG_6$, G_6: A187, C:etched

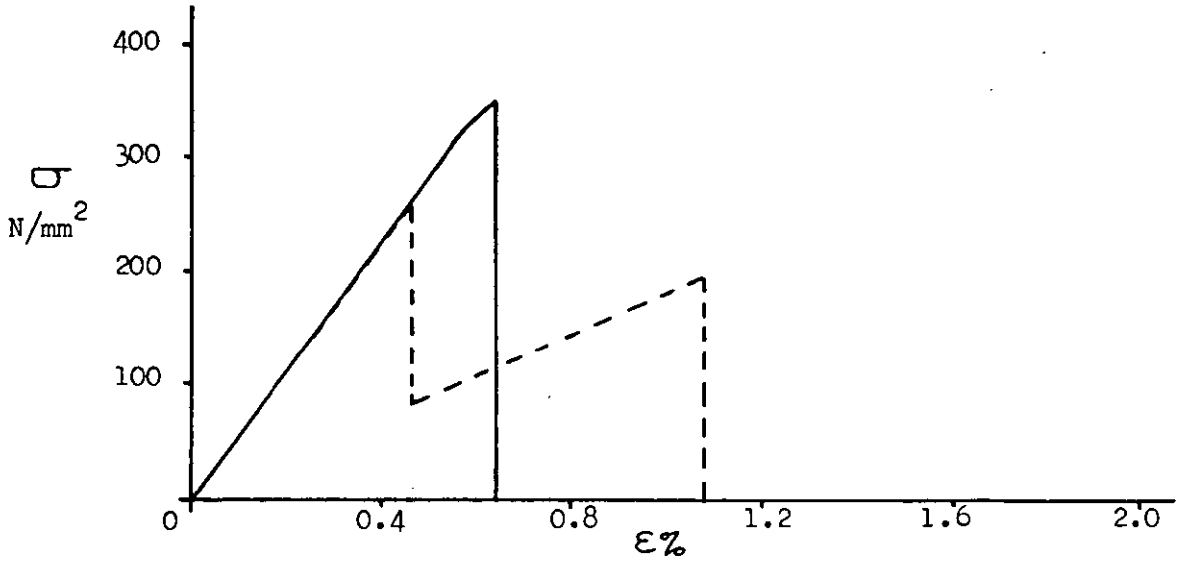

Figure 89 Slab 55, $G_5CG_5CG_5CG_5$, G_5: A187, C: etched

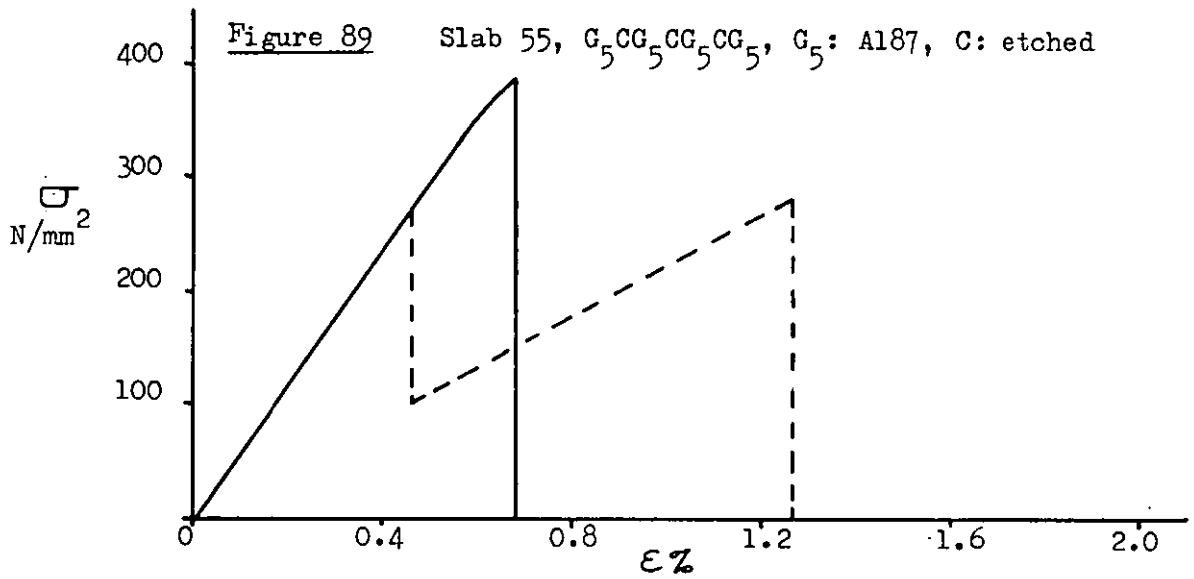

Figure 90 Slab 56, $G_6CG_6CG_6CG_6$, G_6; A1100, C: etched

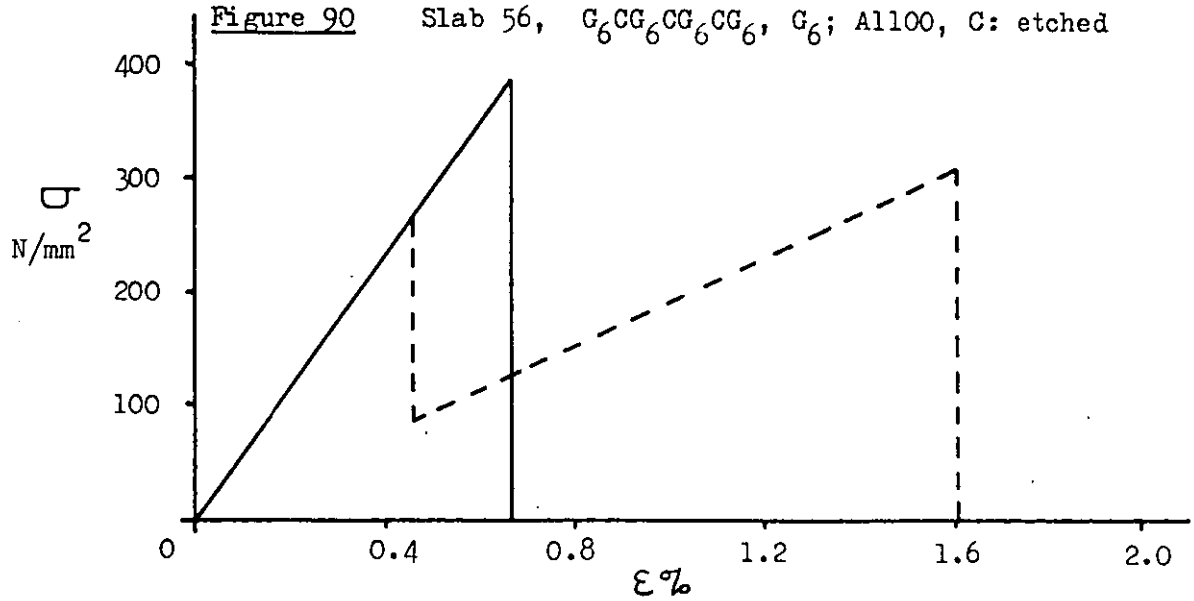

Figure 91 Slab 57, $G_5CG_5CG_5CG_5$, G_5: Al100, C: etched

Of six specimens tested 1 had $\sigma^{\varepsilon} = \sigma' = \hat{\sigma}$

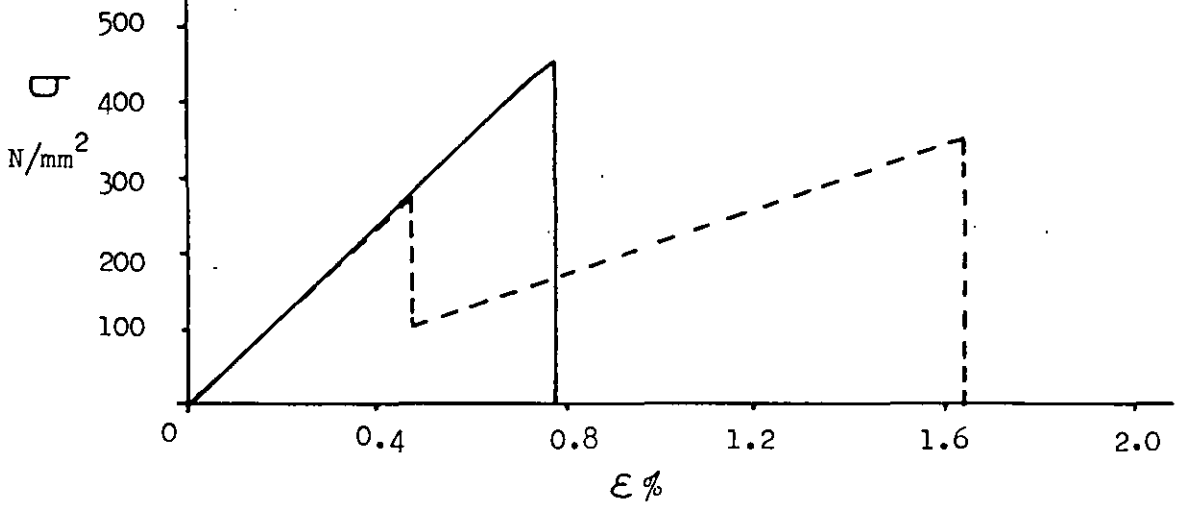

Figure 92 Slab 58, $G_6CG_6CG_6CG_6$, G_6:no c.-a., C: no c.-a.

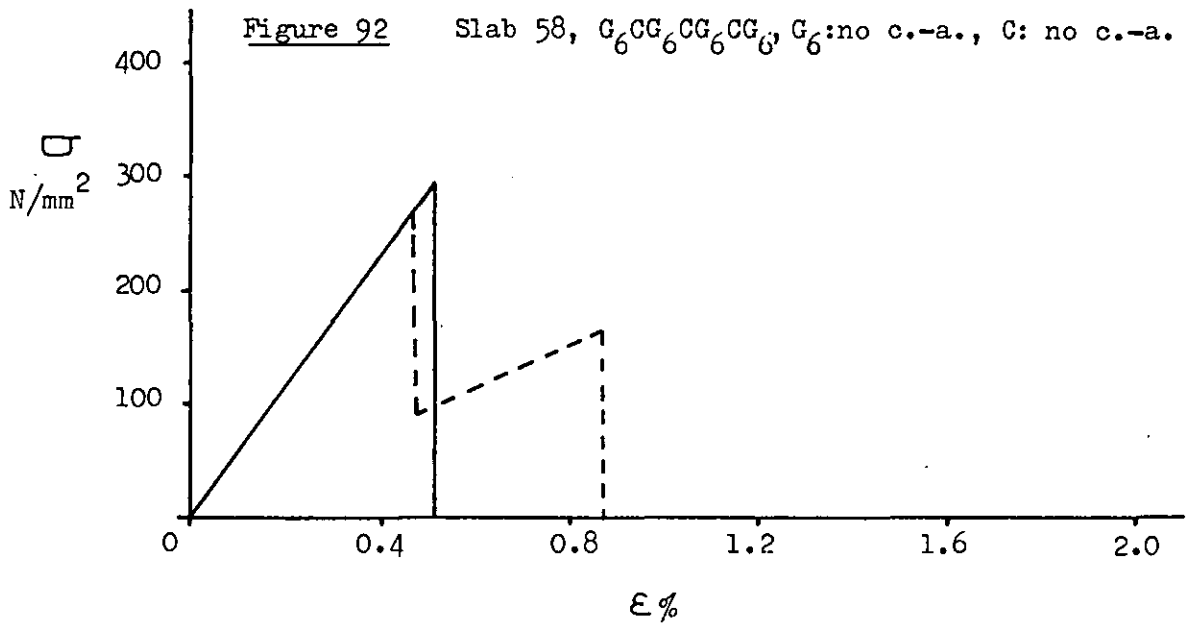

Figure 93 Slab 59, $G_5CG_5CG_5CG_5$, G_5: no c.-a., C: no c.-a.

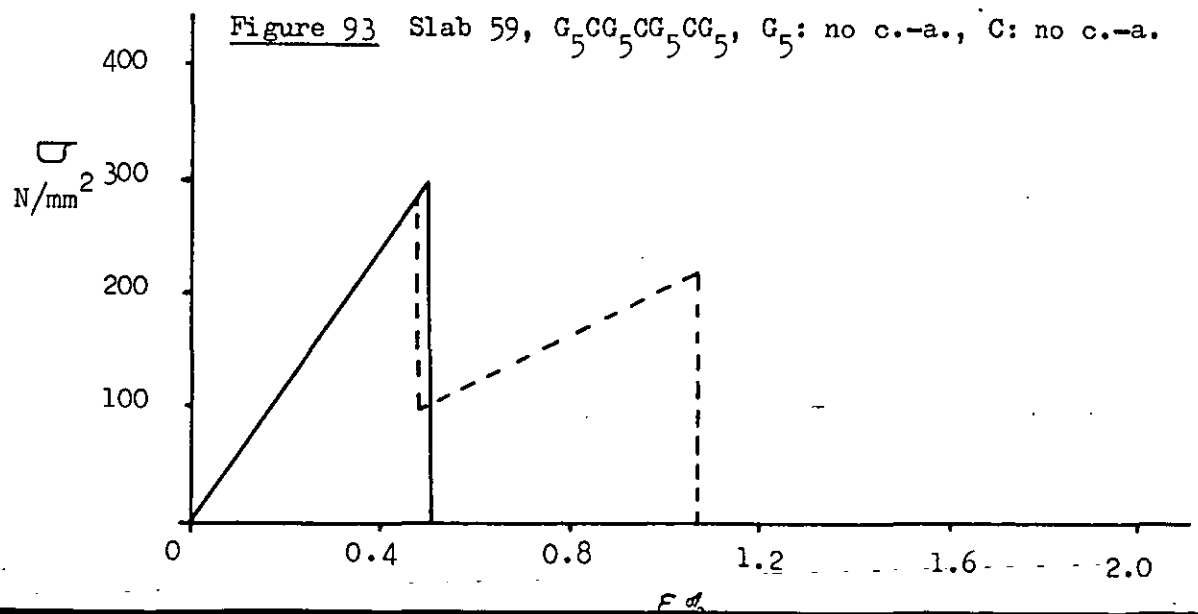

Figure 94 Slab 60 $G_6CG_6CG_6CG_6$, G_6: as rec. C: no c.-a.

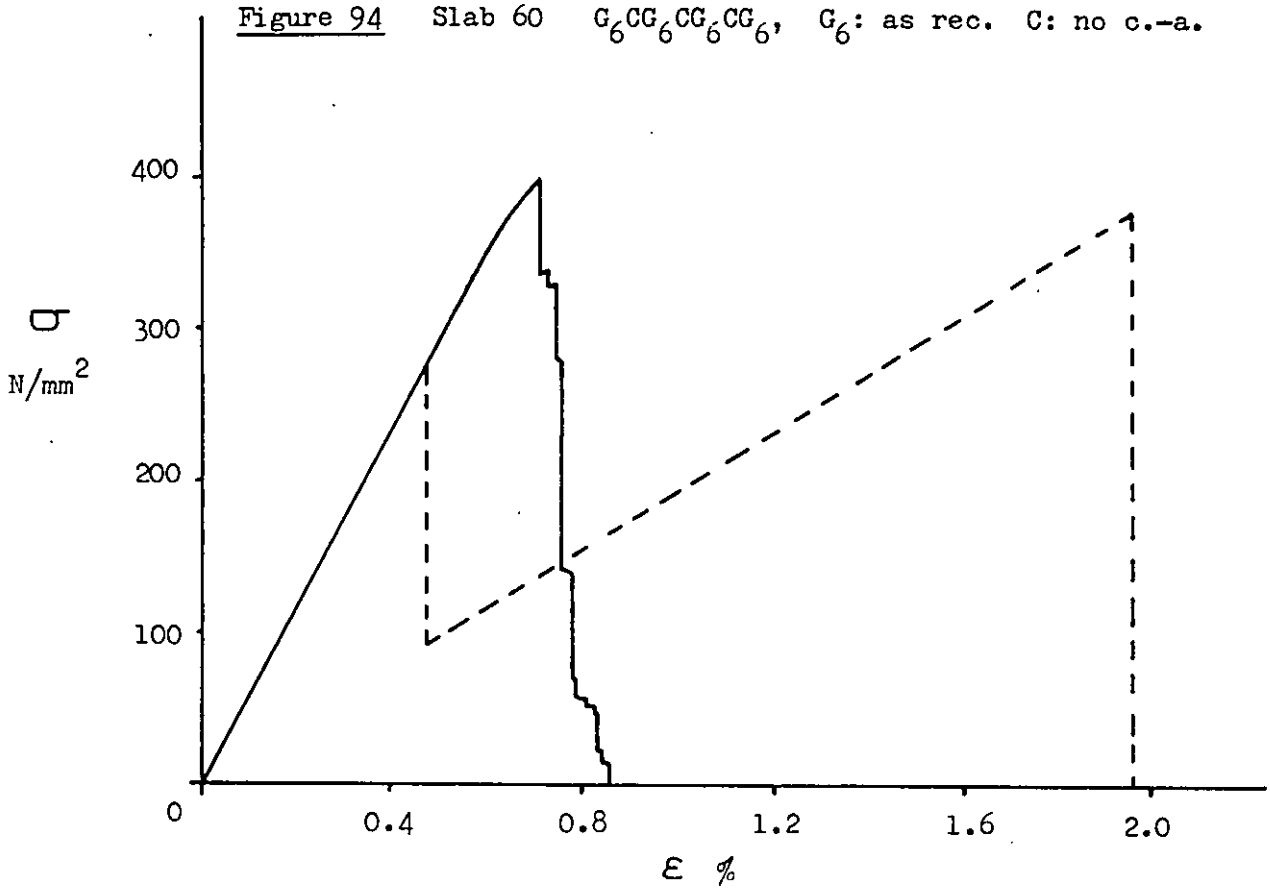

Figure 95 Slab 61, $G_5CG_5CG_5CG_5$ G : as rec, C = no c.-a.
of 6 specimens tested 3 had $\sigma' = \hat{\sigma}$

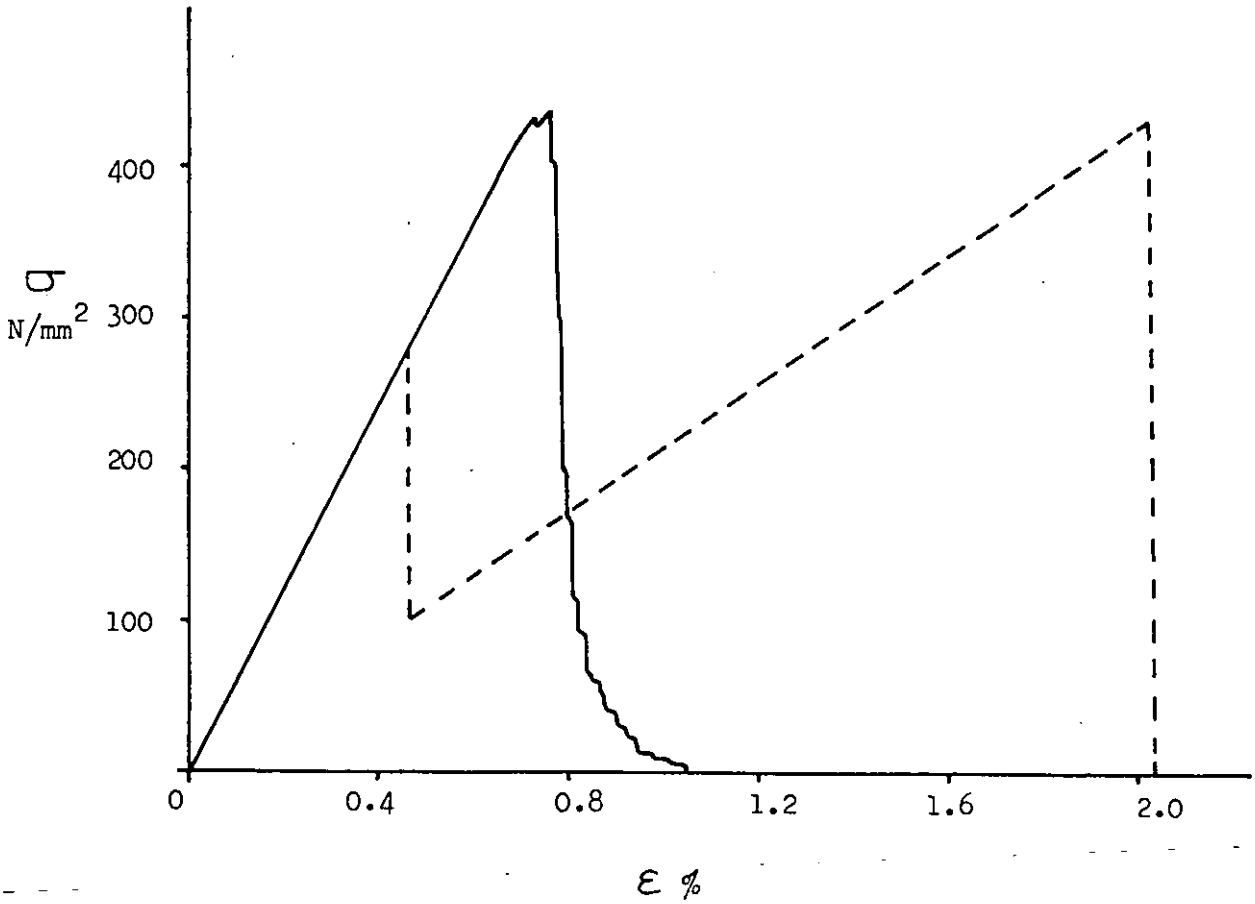

Figure 96

Photographs of Specimen 50.7 Taken During Tensile Testing.

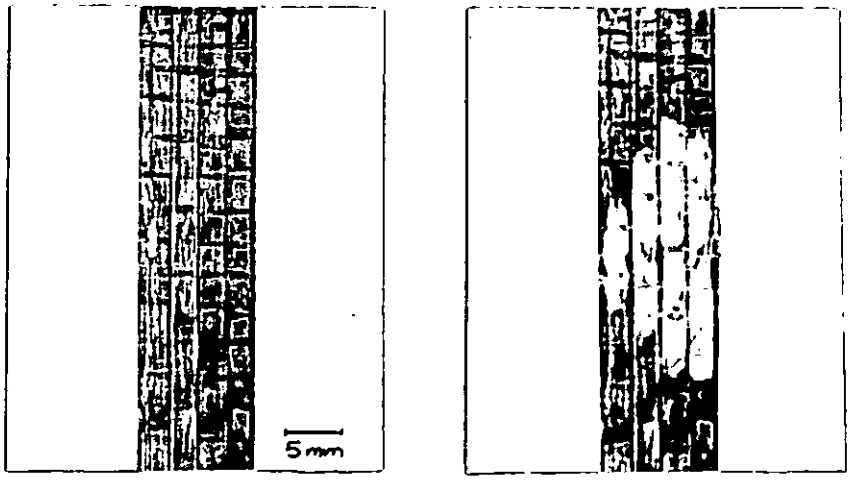

Figure 97

Photographs of Specimen 54.7 Taken During Tensile Testing.

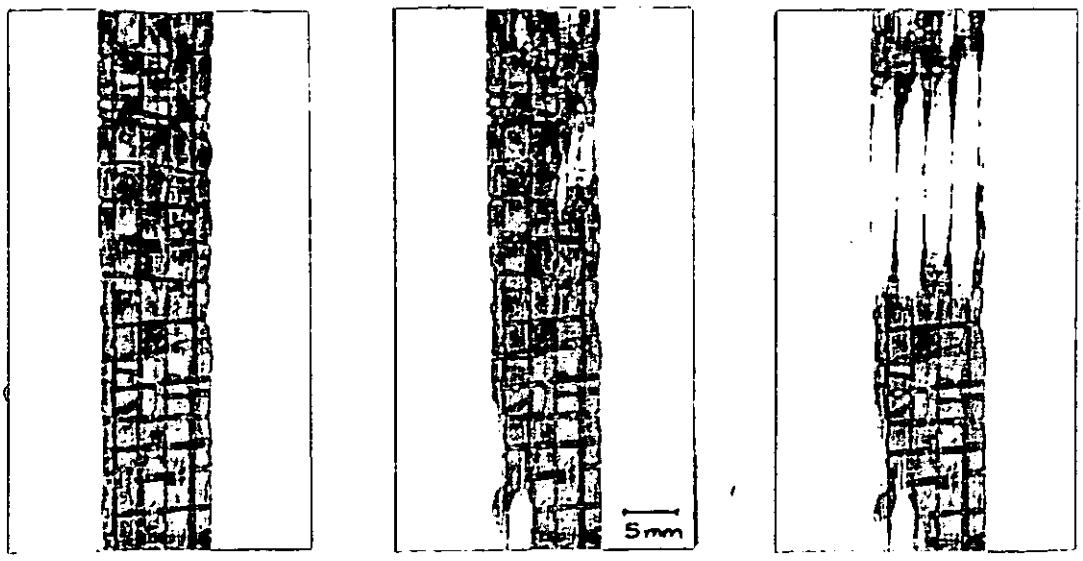

Figure 98

Photographs of specimen 57.7
Taken during Tensile Testing

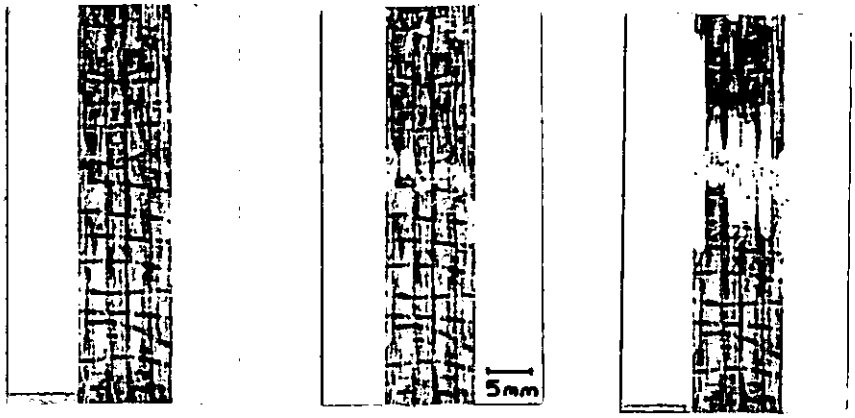

Figure 99

Photographs of specimen 49.7
Taken During Tensile Testing

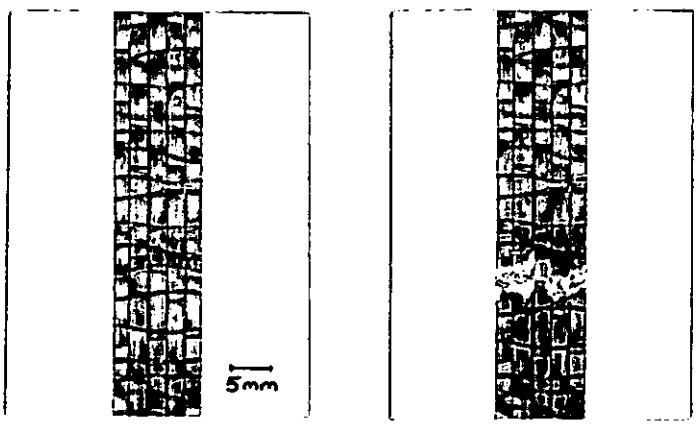

Figure 100

Photographs of Specimen 58.7
Taken During Tensile Testing

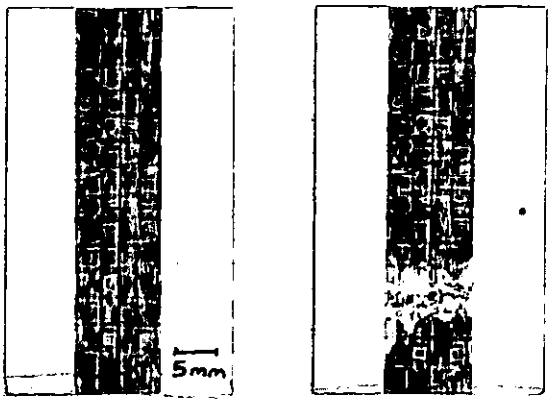

Figure 101

Stereozoom Photograph of the Fractured Tensile Specimen 58.1

Figure 102

Stereozoom Photograph of Half of the Fractured Tensile Specimen 54.2

Figure 103 Plot of the Elastic Strain Limit, ε^{E} (×) and the Initial Failure Strain, ε' (•), Against the Ratio of Carbon Fibre to Total Fibre Volume Fraction Content, V_{cf}/V_{T}, for a Range of Hybrid Composite Slabs.

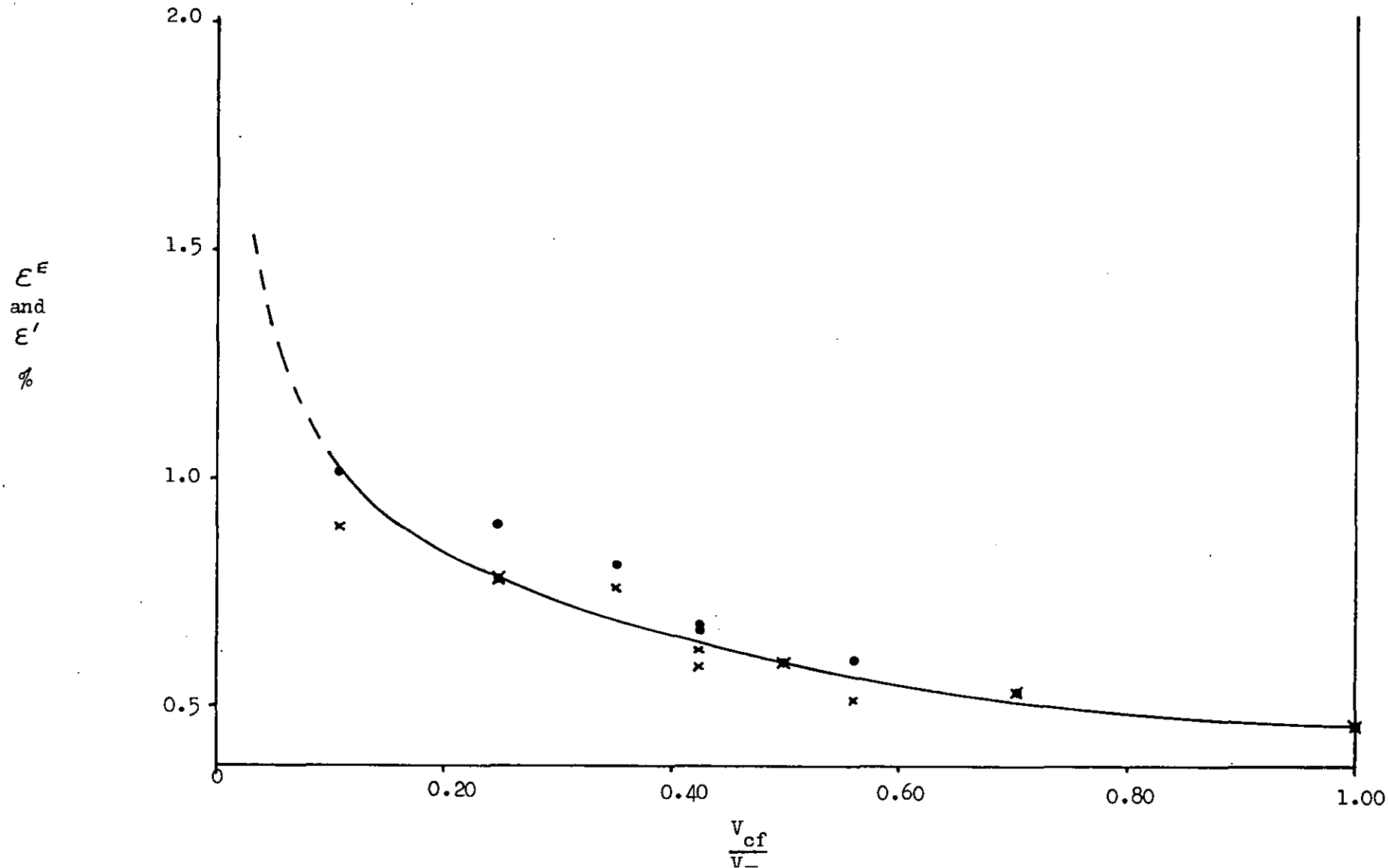

Figure 104

Plot of Maximum Tensile Stress, $\hat{\sigma}$, Against the Ratio of Carbon Fibre to Total Fibre Volume Fraction Content, V_{cf}/V_T, for a Range of Hybrid Composite Slabs with V_T Normalized to 0.40 compared with the Theoretical Rule of Mixtures, $\hat{\sigma}_{RM}$, Plot.

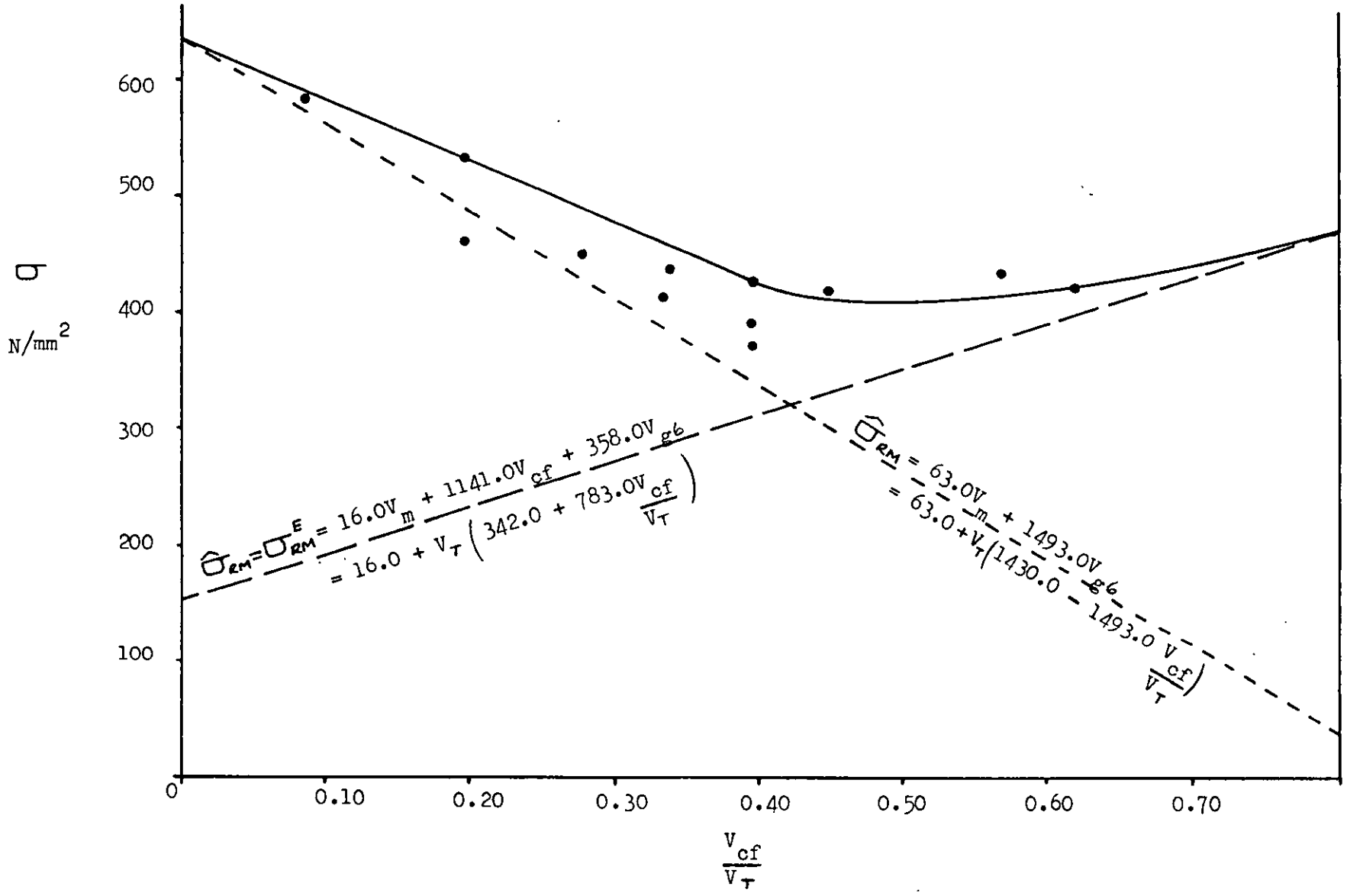

Figure 105 The Elastic Strain Limit, $\mathcal{E}^{E}$(×), and Initial Failure Strain, $\mathcal{E}'$(o), Values of the Hybrid Composites of Slabs 46 to 61 Against the Expected $\mathcal{E}^{E}$ of Their Parent E-Glass Composites

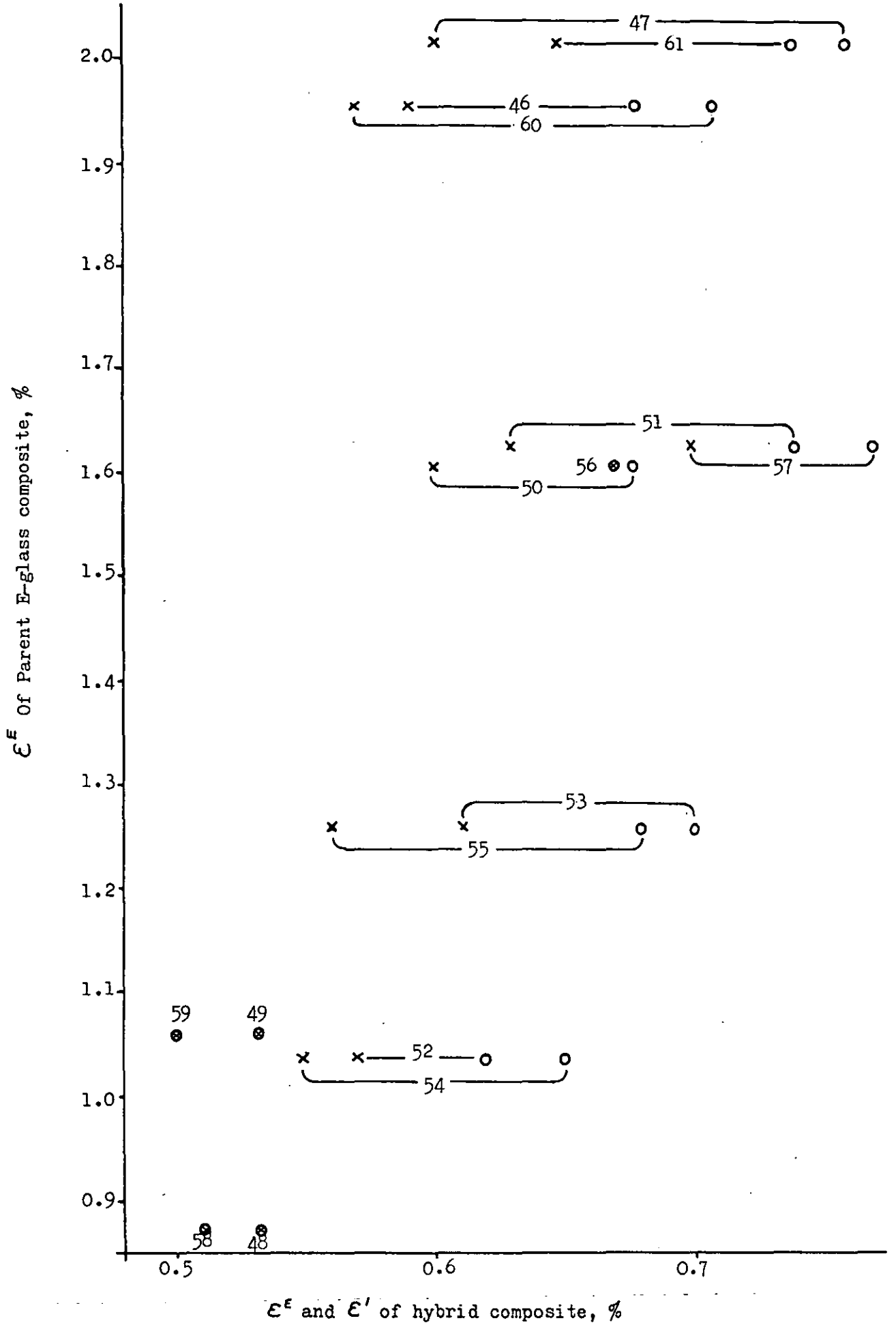

Figure 106 The Relationship Between the Ratio of the Load After to the Load Before (P_1/P) the Failure of all the Carbon Fibres in one Cross-Section of two Hybrid Carbon / 600 tex E-Glass/Vinyl Ester Composites and the Effective Axial Length over which the Failed Fibres Bear No Load (ℓ) in a Tensile Specimen. With Extension $\triangle$L and Gauge Length 50mm.

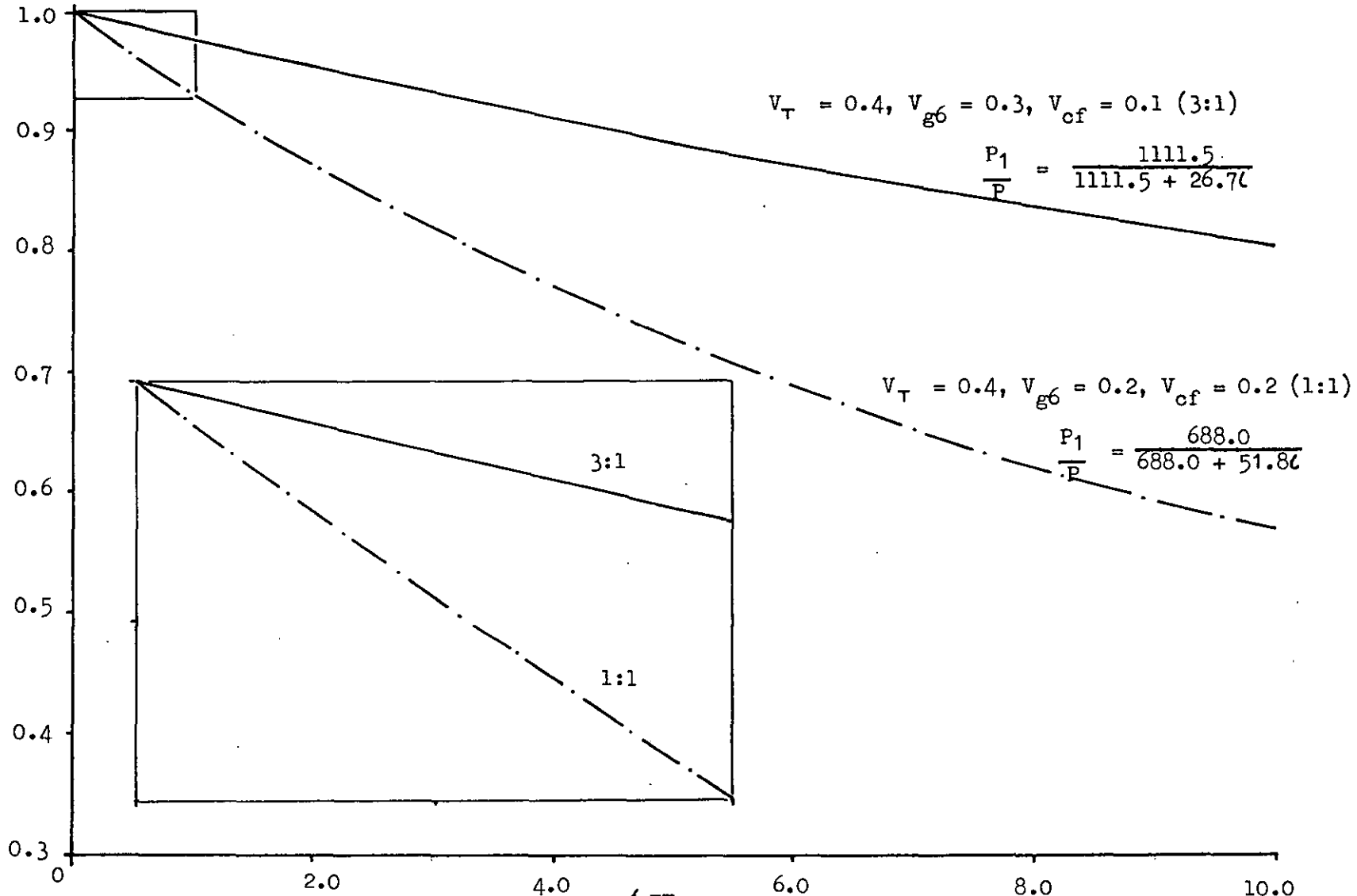

Figure 107 The Relationship Between the Ratio of the Load After to the Load Before (P_1/P) the Failure of Carbon Fibres and the Fraction of V_{cf} Failed (F_{cf}) in one Composite Cross-Section For Two Types of Hybrid Carbon/600 tex E-Glass/Vinyl Ester Composite Tensile Specimens. The axial length over which the failed fibres bear no load is 0.5mm, specimen extension is ΔL and specimen gauge length is 50mm.

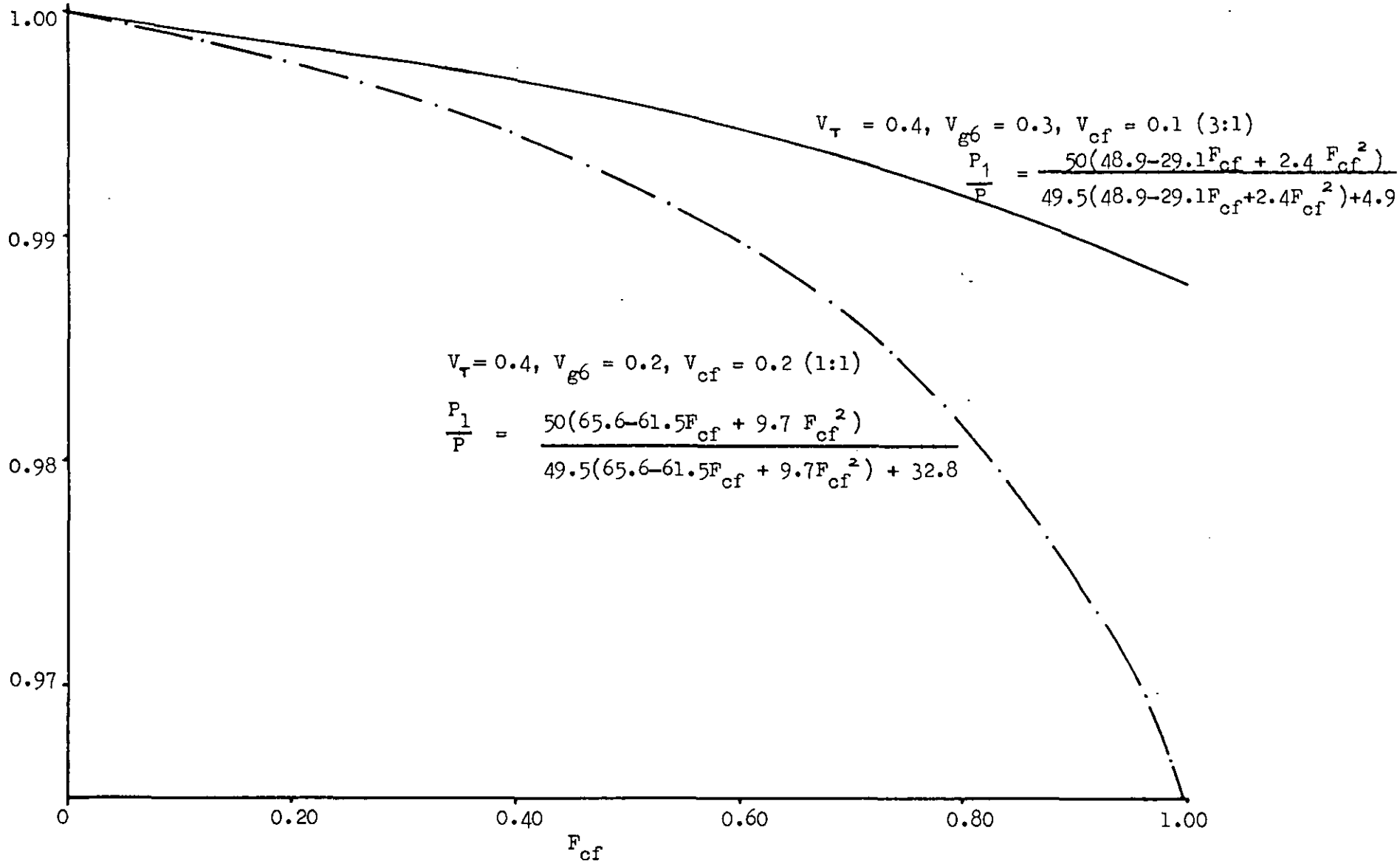

Figure 108 The Relationship Between the Axial Length over which Failed Fibres are Ineffective, ℓ, and the Fraction, F_{cf}, of the Carbon Fibre Content, V_{cf}, Failing in 1:1 and 3:1 E-Glass/Carbon/Vinyl Ester Composites with Total Fibre Fraction Content $V_T = 0.4$, given that the Ratio of the Load After, P_1, to the Load Before Failure, P, is $\frac{P_1}{P} = 0.9900$.

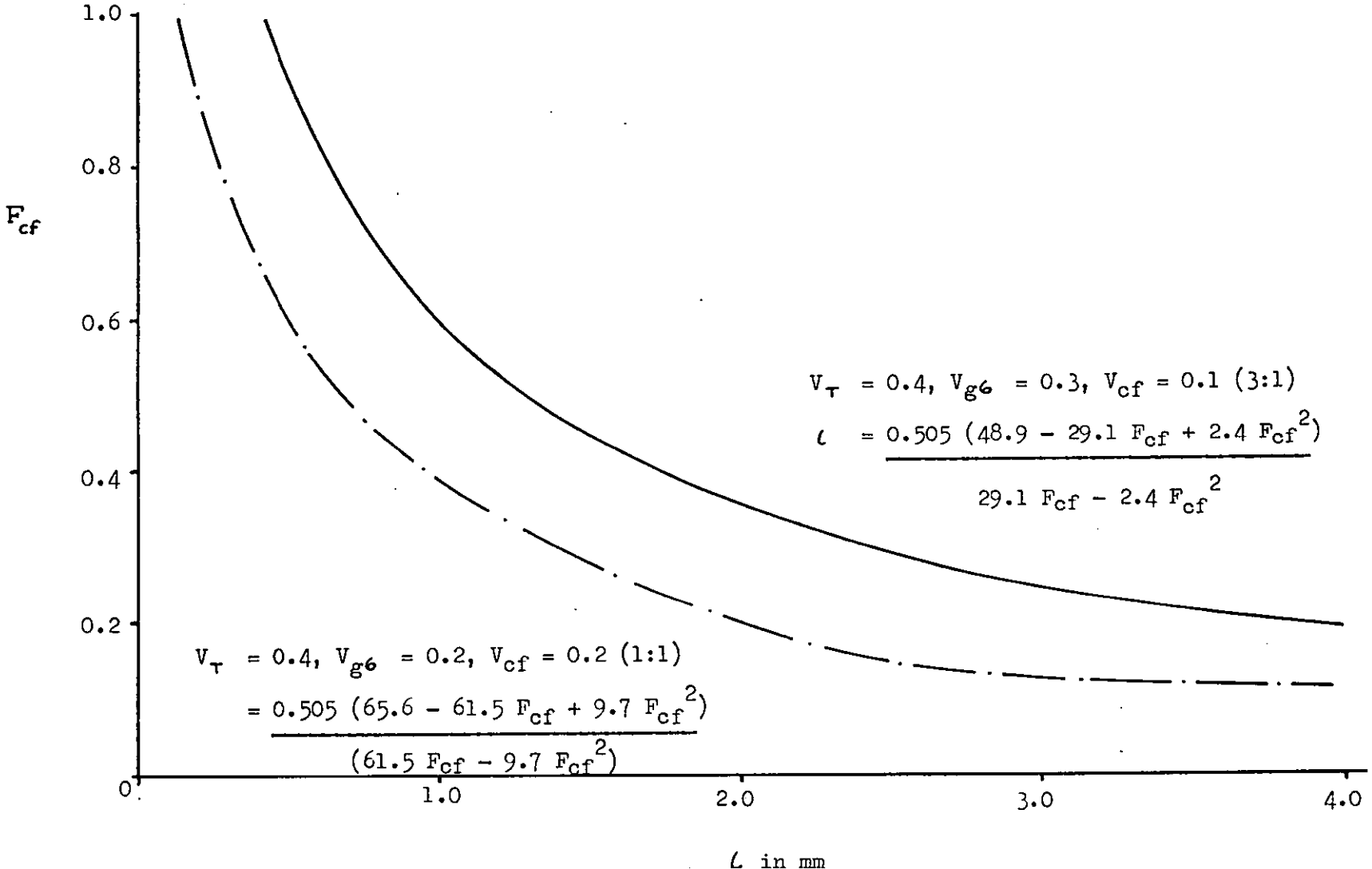

Figure 109

Tensile Failure Chart for the Carbon Fibre/E-glass Fibre/Vinyl Ester Hybrid mposites and the Relation of the Different stages in the Failure Process to ree Typical Hybrid Composite Stress v Strain Curves.

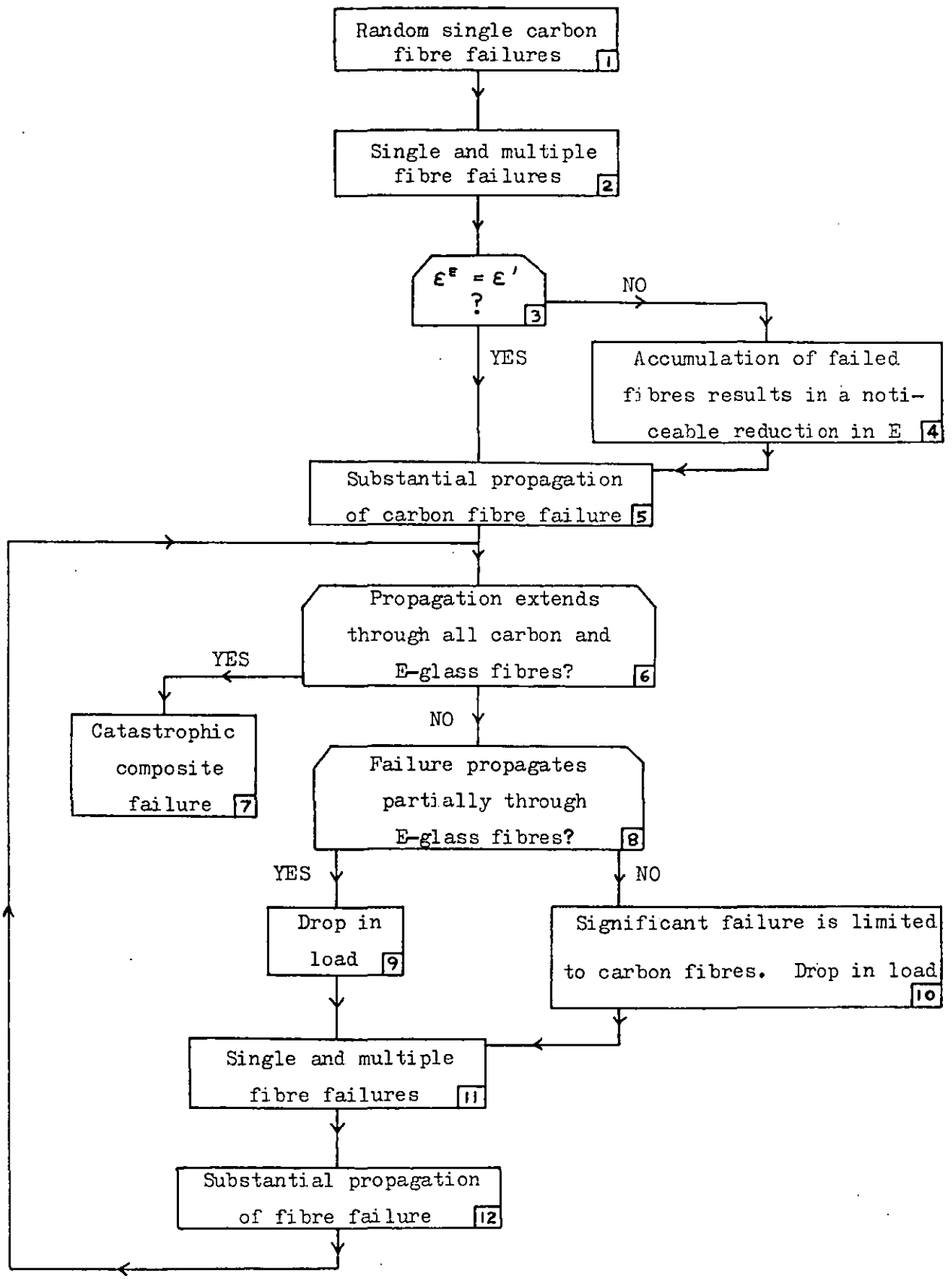

cont.

i)

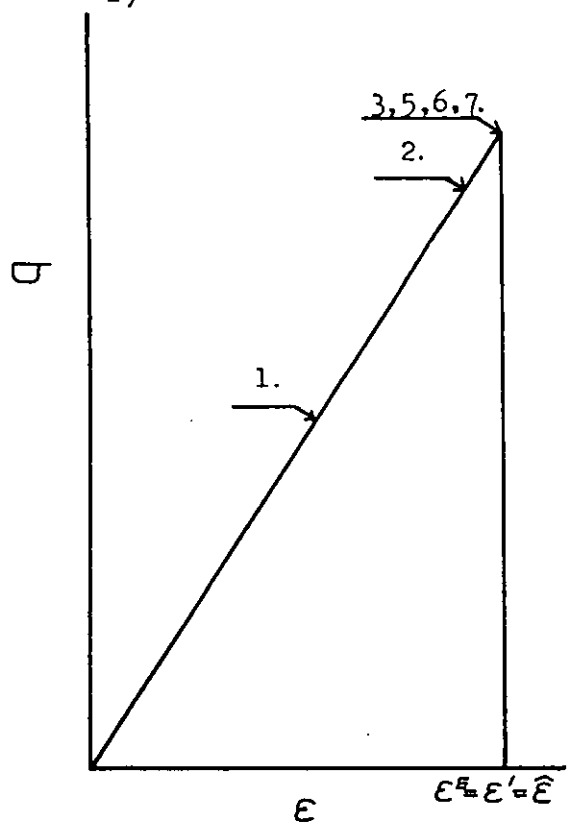
σ
3,5,6,7.
2.
1.
ε
ε^E = ε' = ε̂

ii)

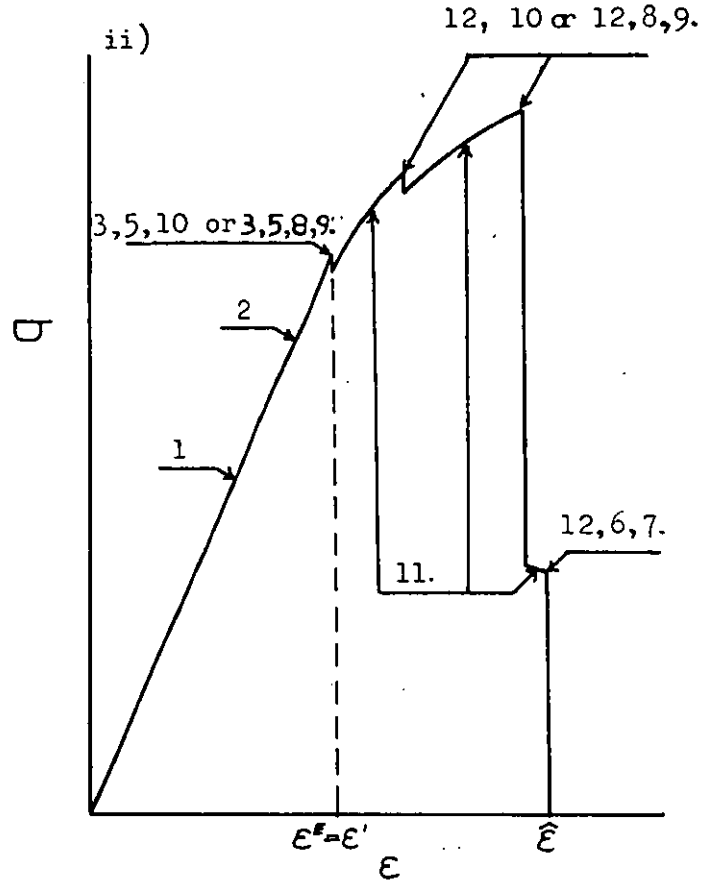
12, 10 or 12,8,9.
σ
3,5,10 or 3,5,8,9.
2
1
12,6,7.
11.
ε^E = ε'
ε̂
ε

iii)

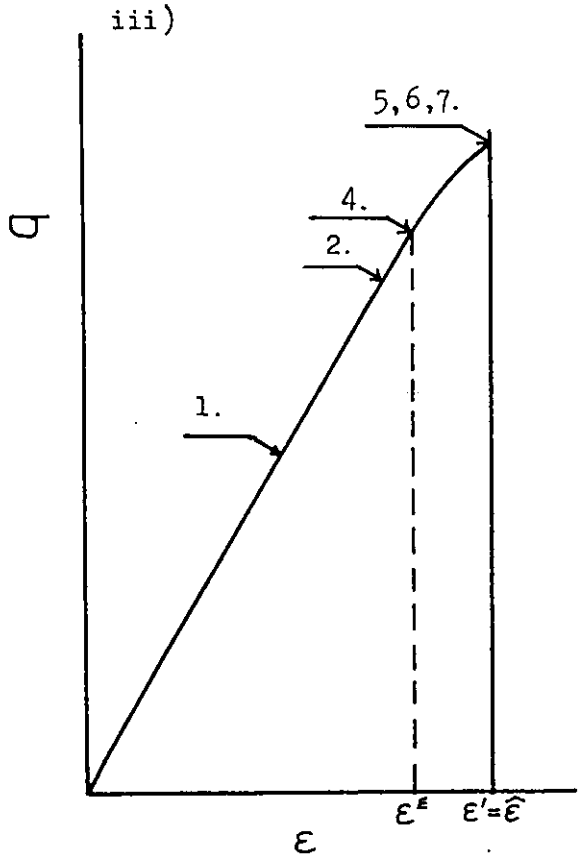
σ
5,6,7.
4.
2.
1.
ε^E
ε' = ε̂
ε

Figure 110 The Relationship Between the Ratio of Carbon Fibre to Total Fibre Volume Fraction Content, V_{cf}/V_T, and i) the Minimum Ineffective Length, ℓ, of V_{cf} Failing Carbon Fibres in a Hybrid Composite Necessary to Produce a Drop in Load on the Tensile Curve and ii) the Minimum Fraction, F_{cf}, of V_{cf} Carbon Fibres Necessary to Fail In a Hybrid Composite In order to Produce a Drop in Load on the Tensile Curve. In both cases $\ell = 0.5$mm, $V_T = 0.40$ and specimen gauge length L = 50mm

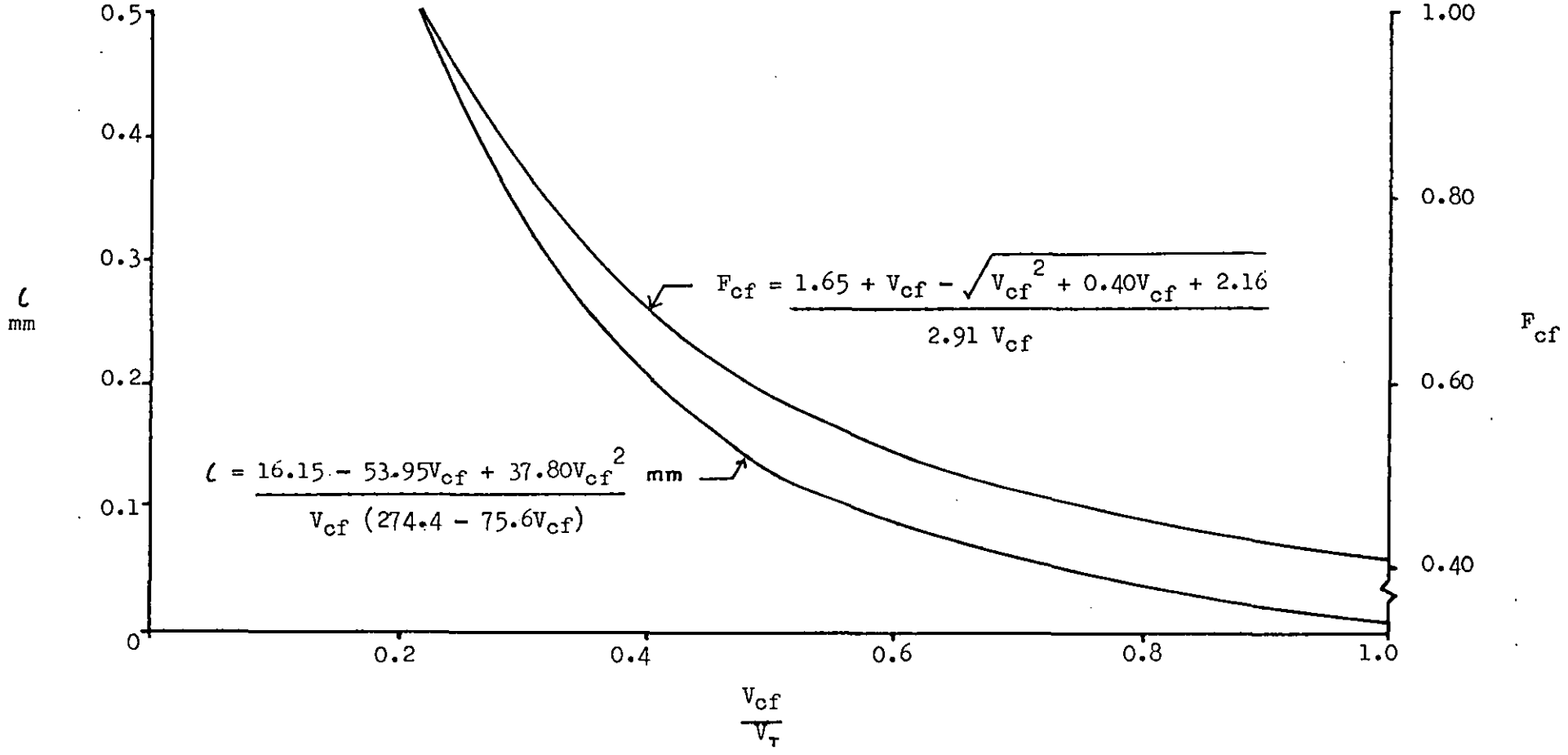

TABLE 1

Properties of Hyfil 6000 Filament Carbon Fibres[54], T.B.A. 600 tex E-Glass Fibres[55] and Derakane 411-45 Vinyl Ester Resin[62] as quoted by their Respective Manufacturers.

	Hyfil Carbon Fibre	600 tex E-Glass Fibre	Derakane 411-45 Vinyl Ester Resin
Tensile Strength $\hat{\sigma}$, N/mm²	2350 23mm L*	-	81.4
Tensile Modulus E, KN/mm²	230 23mm L*	-	3.37
Failure Strain $\hat{\varepsilon}$, %	1.02	-	5.00
Specific Gravity ρ, gm/cm³	1.76	-	1.12
Fibre Diameter d_f, μm	7.3 shape factor 0.92	12.7 - 14.0	-

* L = gauge length

TABLE 2

Data for Plain Carbon Fibre Unidirectional Woven Tape (C).

Warp	6000 filament carbon, continuous tow
Tows in warp	70
Weft	44 tex E-glass strand
Weft picks per metre	394
Tape Width	150mm
Carbon fibre volume fraction in a tape/resin composite (V_{cf})	$\frac{0.1078 \times \text{number of layers of C}}{\text{slab thickness}}$

TABLE 3

Data for Plain 600 tex E-Glass Fibre Unidirectional Woven Tape (G_6).

Warp	600 tex E-glass, continuous tow
Tows in warp	70
Weft	44 tex E-glass strand
Weft picks per metre	394
Tape Width	148mm
600 tex E-glass fibre volume fraction in a tape/resin composite (V_{g6})	$\frac{0.1117 \times \text{number of layers of } G_6}{\text{slab thickness}}$

TABLE 4

Data for Plain 500 tex E-Glass fibre Unidirectional Woven Tape (G_5).

Warp	500 tex E-glass, continuous tow
Tows in warp	84
Weft	44 tex E-glass strand
Weft picks per metre	394
Tape Width	148mm
500 tex E-glass fibre volume fraction in a tape/resin composite (V_{g5})	$\frac{0.1117 \times \text{number of layers of } G_5}{\text{slab thickness}}$

TABLE 5

Data for Hybrid 75% 600 tex E-Glass Fibre and 25% Carbon Fibre Unidirectional Woven Tape (3:1).

Warp	75% 600 tex E-glass, continuous tow 25% 6000 filament carbon, continuous tow
Tows in warp	54 E-glass, 17 carbon
Weft	44 tex E-glass strand
Weft picks per metre	394
Tape Width	148mm
Total fibre volume fraction in a tape/resin composite (V_T)	$\frac{0.1127 \times \text{number of layers of 3:1}}{\text{slab thickness}}$
V_{cf}	$\frac{0.0277 \times \text{number of layers of 3:1}}{\text{slab thickness}}$
V_{g6}	$\frac{0.0850 \times \text{number of layers of 3:1}}{\text{slab thickness}}$

TABLE 6

Data for Hybrid 50% 600 tex E-Glass Fibre and 50% Carbon Fibre Fibre Unidirectional Woven Tape (1:1).

Warp	50% 600 tex E-Glass, continuous tow 50% 6000 filament carbon, continuous tow
Tows in warp	36 E-glass, 35 carbon
Weft	44 tex E-glass strand
Weft picks per metre	394
Tape width	150mm
V_T	$\frac{0.1106 \times \text{number of layers of 1:1}}{\text{slab thickness}}$
V_{cf}	$\frac{0.0547 \times \text{number of layers of 1:1}}{\text{slab thickness}}$
V_{g6}	$\frac{0.0559 \times \text{number of layers of 1:1}}{\text{slab thickness}}$

TABLE 7

The Gel Time of Derakane 411-45 Vinyl Ester Resin with Varying Curing Agent Formulations.

Mix Number	Addition in ml per 100gm of resin			gel time in minutes
	MEKP 50%	CoNap 10%	DMA 100%	
1	2.00	0.30	—	78
2	2.00	0.30	0.025	60
*3	2.00	0.30	0.050	45
4	2.00	0.30	0.075	33
5	0.80	0.40	0.075	41
6	2.00	—	0.050	127
7	2.00	0.50	0.050	39
8	2.00	0.70	0.050	39
*9	1.00	0.60	—	48
10	—	0.30	0.050	>480
11	1.00	0.30	0.050	67
12	1.50	0.30	0.050	54
*13	0.80	0.40	0.050	50

* Mixes producing the desired gel time

TABLE 8

The Composite Slabs Fabricated.

Slab Number	Slab Type	Fibre Volume Percent and Surface Treatment			
		V_T %	V_{cf}%	V_{g6}%	V_{g5}%
1	3C	16.17	16.17	-	-
2	4C	21.56	21.56	-	-
3	6C	32.34	32.34	-	-
4	7C	37.73	37.73	-	-
5	9C	48.51	48.51	-	-
6	7C	37.43	37.43 etched	-	-
7	7C	37.73	37.73 no c.-a.	-	-
8	$4G_6$	22.34	-	22.34	-
9	$5G_6$	27.38	-	27.38	-
10	$6G_6$	33.51	-	33.51	-
11	$7G_6$	39.09	-	39.09	-
12	$8G_6$	44.68	-	44.68	-
13	$9G_6$	50.27	-	50.27	-
14	$7G_6$	39.09	-	39.09 A187	-
15	$7G_6$	39.09	-	39.09 A1100	-
16	$7G_6$	39.09	-	39.09 no c.-a.	-
17	$5G_5$	27.38	-	-	27.38
18	$6G_5$	33.51	-	-	33.51
19	$7G_5$	39.09	-	-	39.09
20	$8G_5$	44.68	-	-	44.68
21	$7G_5$	39.09	-	-	39.09 A187
22	$7G_5$	39.09	-	-	39.09 A1100
23	$7G_5$	39.09	-	-	39.09 no c.-a.
24	4 x 3:1	22.54	5.54	17.00	-
25	5 x 3:1	28.18	6.93	21.25	-
26	6 x 3:1	33.81	8.31	25.50	-
27	7 x 3:1	39.45	9.70	29.75	-

Contd/...

Table 8 Continued.

Slab No	Slab Type	V_T %	V_{cf}%	V_{g6}%	V_{g5}%
28	8 x 3:1	45.08	11.08	34.00	—
29	9 x 3:1	50.72	12.47	38.25	—
30	3 x 1:1	16.59	8.21	8.38	—
31	4 x 1:1	22.12	10.94	11.18	—
32	5 x 1:1	27.65	13.68	13.97	—
33	6 x 1:1	33.18	16.41	16.77	—
34	7 x 1:1	38.71	19.15	19.56	—
35	8 x 1:1	44.24	21.88	22.36	—
36	9 x 1:1	49.77	24.62	25.15	—
37	CG_6G_6C	21.95	10.78	11.17	—
38	$CG_6CG_6G_6CG_6C$	43.90	21.56	22.34	—
39	$G_6G_6CG_6G_6CG_6G_6$	44.29	10.78	33.51	—
40	$G_5G_5CG_5G_5CG_5G_5$	44.29	10.78	—	33.51
41	$G_6$3:1$G_6$3:1$G_6$3:1G_6	39.15	4.16	34.99	—
42	1:1 C 1:1 C 1:1 C 1:1	38.29	27.11	11.18	—
43	3:1 C 3:1 C 3:1 C 3:1	38.71	21.71	17.00	—
44	3:1 1:1 3:1 1:1 3:1 1:1 3:1	39.13	13.75	25.38	—
45	1:1 1:1 3:1 1:1 3:1 1:1 1:1	38.82	16.45	22.37	—
46	$G_6CG_6CG_6CG_6$	38.51	16.17	22.34	—
47	$G_5CG_5CG_5CG_5$	38.51	16.17	—	22.34
48	$G_6CG_6CG_6CG_6$	38.51	16.17	22.34 no c.-a.	—
49	$G_5CG_5CG_5CG_5$	38.51	16.17	—	22.34 no c.-a.
50	$G_6CG_6CG_6CG_6$	38.51	16.17	22.34 A1100	—
51	$G_5CG_5CG_5CG_5$	38.51	16.17	—	22.34 no c.-a.
52	$G_6CG_6CG_6CG_6$	38.51	16.17	22.34 A187	—
53	$G_5CG_5CG_5CG_5$	38.51	16.17	—	22.34 A187
54	$G_6CG_6CG_6CG_6$	38.38	16.04 etched	22.34 A187	—
55	$G_5CG_5CG_5CG_5$	38.38	16.04 etched	—	22.34 A187
56	$G_6CG_6CG_6CG_6$	38.38	16.04 etched	22.34 A1100	—
57	$G_5CG_5CG_5CG_5$	38.38	16.04 etched	—	22.34 A1100
58	$G_6CG_6CG_6CG_6$	38.51	16.17 no c.-a.	22.34 no c.-a.	—

Contd /....

Table 8 Continued

Slab No.	Slab Type	V_T %	V_{cf}%	V_{g6}%	V_{g5}%
59	$G_5CG_5CG_5CG_5$	38.51	16.17 no c.-a.	-	22.34 no c.-a.
60	$G_6CG_6CG_6CG_6$	38.51	16.17 no c.-a.	22.34	-
61	$G_5CG_5CG_5CG_5$	38.51	16.17 no c.-a.	-	22.34

* Where no surface treatment is given below V% the treatment was as rec.

TABLE 9

Average Fibre Diameters, Fibre and Tow Cross-Sectional Areas and Fibre and Resin Densities as Determined Experimentally by the Author.

Property	6000 filament carbon	600 tex E-Glass	500 tex E-Glass	Derakane 411-45 Vinyl Ester
Fibre diameter, μm	7.3 (shape factor = 0.92)	12.82	11.68	—
Fibre c.s.a., μm^2	38.51	129.08	107.15	—
Tow c.s.a., mm^2	0.2310	0.2362	0.1969	—
Density, gm/cm^3	1.76	2.54	2.54	1.13

TABLE 10

The Statistical characteristics of the Fibre Tensile Strengths, when Described by a Weibull Distribution, obtained from Tow Strengths.

Fibre Type	Gauge Length L, mm	Tow Strength $\hat{\sigma}_b$, N/mm^2	Fibre Strength $\hat{\sigma}_f$, N/mm^2	Weibull β	Parameters $\alpha^{-1/\beta}$, N/mm$^{(2-1/\beta)}$	$\hat{\sigma}_b / \hat{\sigma}_f$
Carbon (as rec.)	50 253	543.6 431.5	774.4 614.7	7.02	1.45	0.702
Carbon (no c-a.)	50 180	544.9 456.1	771.8 646.0	7.20	1.42	0.706
Carbon (etched)	50 180	541.2 452.0	768.8 642.0	7.11	1.42	0.704
600 tex E-glass (as rec.)	50 253	1173.3 1052.4	1451.6 1302.0	14.91	1.95	0.808
600 tex E-glass (no c-a.)	50 181	577.9 457.3	873.0 690.8	5.47	1.94	0.662
600 tex E-glass (A1100)	50 180	606.8 489.5	896.3 723.0	5.96	1.87	0.677
600 tex E-glass (A187)	50 180	563.2 451.5	839.3 672.9	5.79	1.78	0.671
500 tex E-glass (as rec.)	50 252	1338.5 1157.9	1735.6 1501.4	11.20	2.57	0.771
500 tex E-glass (no c-a.)	50 180	900.0 744.6	1293.1 1069.8	6.76	2.47	0.696
500 tex E-glass (A1100)	51 182	904.3 745.3	1306.8 1077.0	6.58	2.55	0.692
500 tex E-glass (A187)	50 180	901.5 745.1	1297.1 1072.1	6.72	2.49	0.695

TABLE 11

The Average Experimental Shear Modulus of Derakane 411-45 Vinyl Ester Resin Determined From Torsion Specimens of Varying Thickness

Specimens	Thickness t, mm	Shear Modulus G, KN/mm^2	Coefficient of Variation
1 – 4	2.00 ± 0.01	2.15 ± 0.01	1.34
5 – 8	2.50 ± 0.01	2.14 ± 0.01	1.67
9 – 12	3.00 ± 0.01	2.15 ± 0.02	1.34
13 – 16	4.00 ± 0.01	2.16 ± 0.01	1.25
1 – 16		2.15 ± 0.01	1.29

TABLE 12

The Average Experimental Shear Modulus of E-Glass Composites Determined from Torsion Specimens

Slab Number (and lay-up)	Fibre Volume Content V_f, %	Shear Modulus G, KN/mm^2	Coefficient of Variation CV, %
8 ($4G_6$)	22.34	3.75 ± 0.03	1.74
9 ($5G_6$)	27.38	4.45 ± 0.04	1.79
10 ($6G_6$)	33.51	4.92 ± 0.02	0.95
11 ($7G_6$)	39.09	5.84 ± 0.02	0.85
12 ($8G_6$)	44.68	6.51 ± 0.01	0.45
13 ($9G_6$)	50.27	7.20 ± 0.03	0.93
14 ($7G_6$, A187)	39.09	5.74 ± 0.04	1.49
15 ($7G_6$, A1100)	39.09	5.85 ± 0.03	0.98
16 ($7G_6$, no c.-a.)	39.09	5.66 ± 0.05	1.89
17 ($5G_5$)	27.38	3.99 ± 0.05	2.45
18 ($6G_5$)	33.51	5.00 ± 0.04	1.66
19 ($7G_5$)	39.09	5.51 ± 0.03	0.99
20 ($8G_5$)	44.68	6.65 ± 0.03	0.86
21 ($7G_5$, A187)	39.09	5.65 ± 0.04	1.27
22 ($7G_5$, A1100)	39.09	5.74 ± 0.04	1.00
23 ($7G_5$, no c.-a.)	39.09	5.68 ± 0.02	0.85

TABLE 13

Results of the Tensile Testing of Derakane 411-45 Vinyl Ester Resin Specimens.

Specimen	Tensile Strength $\hat{\sigma}_m$, N/mm^2	Initial Elastic E_m, KN/mm^2	Failure Strain $\hat{\varepsilon}_m$, %
1	80.6	3.38	4.90
2	80.1	3.14	4.95
3	76.8	3.22	4.88
4	85.7	3.29	5.17
5	85.1	3.34	5.12
6	85.2	3.62	4.73
7	78.3	3.31	5.01
8	75.4	3.53	4.61
9	77.9	3.39	4.93
10	80.1	3.48	4.70
Average	80.5	3.37	4.90
$\psi_{\bar{x}}$ (±)	1.1	0.05	0.06
CV %	4.5	4.3	3.7

TABLE 14

Size Content on As Received 600 tex E-Glass, 500 tex E-Glass and 6000 Filament Carbon Tows.

	Weight/metre of sized tow gm/m	Weight/metre of unsized tow gm/m	Weight % sizing	Volume % sizing
600 tex E-glass	0.6132	0.6000	2.15	4.45
500 tex E-glass	0.5130	0.5000	2.53	5.21
6000 filament carbon	0.4210	0.4066	3.42	4.58

TABLE 15

The Average Interlaminar Shear Strengths (τ_{il}) of Composite Slabs 1 - 61

Slab	τ_{il} N/mm^2	Slab	τ_{il} N/mm^2
1 (3C)	43.3	32 (5 x 1:1)	43.2
2 (4C)	43.4	33 (6 x 1:1)	45.1
3 (6C)	44.5	34 (7 x 1:1)	43.6
4 (7C)	43.5	35 (8 x 1:1)	42.5
5 (9C)	44.0	36 (9 x 1:1)	43.8
6 (7C - etched)	97.8	37 (2C, 2G_6)	43.2
7 (7C - no c.-a.)	50.0	38 (4C 4G_6)	44.1
8 (4G_6)	>42.0	39 (2C, 6G_6)	49.7
9 (5G_6)	51.5	40 (2C, 6G_5)	54.0
10 (6G_6)	50.9	41 (3 x 3:1, 4G_6)	43.3
11 (7G_6)	52.3	42 (3C, 4 x 1:1)	42.3
12 (8G_6)	50.5	43 (3C, 4 x 1:1)	46.9
13 (9G_6)	54.0	44 (3 x 1:1, 4 x 3:1)	50.5
14 (7G_6 - A187)	61.3	45 (5 x 1:1, 2 x 3:1)	43.7
15 (7G_6 - A1100)	103.5	46 (3C, 4G_6)	49.9
16 (7G_6 - no c.-a.)	45.7	47 (3C, 4G_5)	47.2
17 (5G_5)	49.5	48 (3C, 4G_6 - no c.-a.)	48.6
18 (6G_5)	49.2	49 (3C, 4G_5 - no c.-a.)	48.7
19 (7G_5)	54.2	50 (3C, 4G_6 - A1100)	99.9
20 (8G_5)	51.4	51 (3C, 4G_5 - A1100)	97.9
21 (7G_5 - A187)	56.5	52 (3C, 4G_6 - A187)	74.4
22 (7G_5 - A1100)	106.6	53 (3C, 4G_5 - A187)	78.3
23 (7G_5 - no c.-a.)	47.0	54 (3C - etched, 4G_6 - A187)	66.7
24 (4 x 3:1)	39.1	55 (3C - etched, 4G_5 - A187)	63.4
25 (5 x 3:1)	39.7	56 (3C - etched, 4G_6 - A1100)	101.8
26 (6 x 3:1)	41.6	57 (3C - etched, 4G_5 - A1100)	>90.4
27 (7 x 3:1)	44.2	58 (3C - no c.-a., 4G_6 - no c.-a.)	49.3
28 (8 x 3:1)	43.6	59 (3C - no c.-a., 4G_5 - no c.-a.)	49.3
29 (9 x 3:1)	44.2	60 (3C - no c.-a., 4G_6)	48.1
30 (3 x 1:1)	36.4	61 (3C - no c.-a., 4G_5)	50.9
31 (4 x 1:1)	40.8		

TABLE 16

Tensile Properties of the Composite Slabs 1 to 61

Slab	Fibre Volume Contents				Elastic Modulus E, KN/mm^2	Elastic Limits		Initial Failure		Maximum Stress $\hat{\sigma}$, N/mm^2
	V_T %	V_{cf} %	V_{g6} %	V_{g5} %		σ^E, N/mm^2	ε^E, %	σ', N/mm^2	ε', %	
1 3C	16.17	16.17	–	–	42.8 ± 0.5 40.8-44.5	189.3 ± 5.8 172.9-208.3	0.44±0.01 0.40-0.48	σ^E	ε^E	σ^E
2 4C	21.56	21.56	–	–	55.1 ± 0.8 53.2-57.0	260.6 ± 17.2 215.6-315.8	0.47±0.04 0.38-0.59	σ^E	ε^E	σ^E
3 6C	32.34	32.34	–	–	80.4 ± 0.4 79.7-81.8	386.8 ± 6.1 370.1-405.2	0.48±0.01 0.46-0.51	σ^E	ε^E	σ^E
4 7C	37.73	37.73	–	–	93.2 ± 0.3 92.5-93.9	422.7 ± 9.4 389.8-448.0	0.46±0.01 0.42-0.48	σ^E	ε^E	σ^E
5 9C	48.51	48.51	–	–	119.2 ± 0.4 117.8-120.7	573.5 ± 17.8 521.4-629.6	0.48±0.02 0.43-0.53	σ^E	ε^E	σ^E
6 7C	37.43	37.43 etched	–	–	92.6 ± 0.4 91.2-93.9	453.0 ± 10.9 420.0-484.7	0.49±0.01 0.45-0.52	σ^E	ε^E	σ^E
7 7C	37.73	37.73 no c.-a.	–	–	93.3 ± 0.3 92.3-94.4	441.1 ± 16.5 368.0-482.1	0.47±0.02 0.39-0.51	σ^E	ε^E	σ^E
8 4G	22.34	–	22.34	–	19.4 ± 0.1 19.1-19.9	358.4 ± 14.1 320.0-401.5	1.84±0.07 1.66-2.10	σ^E	ε^E	σ^E
9 5G	27.38	–	27.38	–	23.1 ± 0.2 22.3-24.0	480.8 ± 10.5 460.7-526.2	2.08±0.04 1.96-2.22	σ^E	ε^E	σ^E
10 6G	33.51	–	33.51	–	27.9 ± 0.4 27.0-28.9	566.0 ± 27.5 490.9-635.5	2.03±0.07 1.82-2.20	σ^E	ε^E	σ^E
11 7G	39.09	–	39.09	–	31.9 ± 0.3 31.1-32.8	595.7 ± 27.3 525.1-690.5	1.87±0.07 1.69-2.11	σ^E	ε^E	σ^E

Cont/....

Table 16 Continued

	V_T %	V_{cf} %	V_{g6} %	V_{g5} %	E, KN/mm^2	σ^{ϵ}, N/mm^2	ε^E, %	σ', N/mm^2	ε', %	$\hat{\sigma}$, N/mm^2
12 8G	44.68	–	44.68	–	36.3± 0.3 35.2-36.9	713.6±55.7 552.4-867.6	1.96±0.14 1.57-2.35	σ^{ϵ}	ε^E	σ^E
13 9G	49.72	–	49.72	–	40.2± 0.3 39.3-40.8	798.9±15.4 754.5-839.0	1.99±0.03 1.90-2.06	σ^{ϵ}	ε^E	σ^E
14 7G	39.09	–	39.09 A187	–	31.9± 0.3 31.3-32.9	329.4± 3.2 322.9-338.3	1.04±0.01 1.01-1.06	σ^{ϵ}	ε^E	σ^E
15 7G	39.09	–	39.09 A1100	–	31.4± 0.2 30.9-32.0	507.0±14.8 445.2-554.0	1.61±0.04 1.44-1.73	σ^{ϵ}	ε^E	σ^E
16 7G	39.09	–	39.09 no c.-a.	–	31.8± 0.1 31.4-32.3	279.0± 9.7 254.8-298.3	0.88±0.03 0.80-0.94	σ^{ϵ}	ε^E	σ^E
17 5G	27.38	–	–	27.38	25.6± 0.3 24.8-26.4	520.9± 8.6 490.9-546.1	2.03±0.05 1.86-2.17	σ^{ϵ}	ε^E	σ^E
18 6G	33.51	–	–	33.51	30.5± 0.2 29.7-30.9	595.7±12.9 543.8-630.1	1.96±0.05 1.77-2.12	σ^{ϵ}	ε^E	σ^E
19 7G	39.09	–	–	39.09	34.6± 0.2 34.1-35.3	734.9± 7.3 707.6-762.0	2.12±0.02 2.06-2.16	σ^{ϵ}	ε^E	σ^E
20 8G	44.68	–	–	44.68	39.2± 0.3 38.3-40.0	771.1±14.0 732.8-824.9	1.97±0.03 1.83-2.07	σ^{ϵ}	ε^E	σ^E
21 7G	39.09	–	–	39.09 A187	35.0± 0.2 34.2-35.5	440.8±13.0 403.6-478.8	1.26±0.03 1.18-1.37	σ^{ϵ}	ε^E	σ^E
22 7G	39.09	–	–	39.09 A1100	34.9± 0.3 34.1-35.8	567.4± 8.5 542.2-600.3	1.63±0.02 1.59-1.68	σ^{ϵ}	ε^E	σ^E
23 7G	39.09	–	–	39.09 no c.-a.	35.1± 0.2 34.3-35.6	370.7±13.6 315.2-416.3	1.06±0.04 0.92-1.19	σ^{ϵ}	ε^E	σ^E

Cont/....

	V_T %	V_{cf} %	V_{g6} %	V_{g5} %	E, KN/mm^2	σ^{ε}, N/mm^2	$\varepsilon^{\varepsilon}$, %	σ', N/mm^2	ε', %	$\hat{\sigma}$, N/mm^2
24 4 x 3:1	22.54	5.54	17.00	-	28.1 ± 0.5 26.5-29.5	212.7 ± 6.4 195.0-239.3	0.76±0.02 0.72-0.81	σ^{ε}	$\varepsilon^{\varepsilon}$	291.4±14.8 253.5-356.2
25 5 x 3:1	28.18	6.93	21.25	-	35.5 ± 0.4 34.4-36.8	259.5±11.0 226.1-293.4	0.73±0.02 0.65-0.80	σ^{ε}	$\varepsilon^{\varepsilon}$	370.1±17.4 330.3-435.3
26 6 x 3:1	33.81	8.31	25.50	-	42.4 ± 0.3 41.5-43.2	319.5±12.5 265.4-349.3	0.75±0.03 0.64-0.82	σ^{ε}	$\varepsilon^{\varepsilon}$	450.2±15.1 388.9-491.5
27 7 x 3:1	39.45	9.70	29.75	-	48.1 ± 0.3 47.2-49.0	385.6±11.2 337.6-409.5	0.80±0.02 0.71-0.84	σ^{ε}	$\varepsilon^{\varepsilon}$	530.2±33.3 433.7-609.5
28 8 x 3:1	45.08	11.08	34.00	-	54.3 ± 0.2 53.5-55.3	444.0±11.2 397.4-471.5	0.82±0.02 0.73-0.85	σ^{ε}	$\varepsilon^{\varepsilon}$	582.8±20.9 505.5-649.7
29 9 x 3:1	50.72	12.47	28.25	-	60.7 ± 0.3 59.7-61.6	482.7±11.8 445.7-517.1	0.79±0.02 0.74-0.84	σ^{ε}	$\varepsilon^{\varepsilon}$	702.4±24.9 645.9-802.8
30 3 x 1:1	16.59	8.21	8.38	-	29.0 ± 0.4 27.8-30.4	164.4 ± 4.8 148.2-182.4	0.57±0.01 0.52-0.60	σ^{ε}	$\varepsilon^{\varepsilon}$	167.1 ± 4.2 157.9-186.1
31 4 x 1:1	22.12	10.94	11.18	-	37.0 ± 0.2 36.1-37.5	212.9 ± 5.0 198.5-230.5	0.57±0.01 0.54-0.62	σ^{ε}	$\varepsilon^{\varepsilon}$	217.5 ± 5.5 201.1-241.0
32 5 x 1:1	27.65	13.68	13.97	-	46.3 ± 0.2 45.8-46.9	279.3±11.1 256.8-332.5	0.60±0.02 0.56-0.71	σ^{ε}	$\varepsilon^{\varepsilon}$	300.7±13.3 262.5-353.3
33 6 x 1:1	33.18	16.41	16.77	-	54.7 ± 0.1 54.2-55.2	332.2±12.0 318.3-348.1	0.61±0.02 0.52-0.68	σ^{ε}	$\varepsilon^{\varepsilon}$	362.3 ± 7.4 340.2-384.7
34 7 x 1:1	38.71	19.15	19.56	-	63.7 ± 0.4 62.7-65.1	403.5 ± 7.2 374.0-421.9	0.63±0.01 0.59-0.67	σ^{ε}	$\varepsilon^{\varepsilon}$	429.9 ± 8.0 394.4-448.4
35 8 x 1:1	44.24	21.88	22.36	-	71.8 ± 0.3 71.0-72.6	418.8±18.7 354.8-477.8	0.58±0.03 0.50-0.66	σ^{ε}	$\varepsilon^{\varepsilon}$	454.6 ± 9.3 431.3-492.5

Cont/....

	V_r %	V_{cf} %	V_{g6} %	V_{g5} %	E, KN/mm^2	σ^ε, N/mm^2	ε^ε, %	σ', N/mm^2	ε', %	$\hat{\sigma}$, N/mm^2
36 9 x 1:1	49.77	24.62	25.15	–	80.4 ± 0.2 79.6-81.1	493.0 ± 16.3 434.4-527.3	0.61±0.02 0.54-0.67	σ^ε	ε^ε	515.3 ± 11.3 461.2-540.6
37 CG_6G_6C	21.95	10.78	11.17	–	37.3 ± 0.2 36.7-37.9	168.5 ± 4.4 156.2-185.5	0.45±0.01 0.43-0.49	σ^ε	ε^ε	213.8 ± 9.8 182.0-241.6
38 $CG_6CG_6G_6CG_6C$	43.90	21.56	22.34	–	71.3 ± 0.2 70.7-72.2	336.0 ± 11.4 313.1-374.5	0.47±0.02 0.44-0.53	398.5 ± 15.8 323.0-430.6	0.62±0.03 0.48-0.68	404.7 ± 15.1 333.0-430.6
39 $G_6G_6CG_6G_6CG_6G_6$	44.29	10.78	33.51	–	53.3 ± 0.2 52.6-53.9	415.3 ± 14.1 363.2-461.4	0.78±0.02 0.69-0.86	466.7 ± 16.1 426.1-529.4	0.91±0.03 0.82-1.00	511.8 ± 27.2 440.6-597.4
40 $G_5G_5CG_5G_5CG_5G_5$	44.29	10.78	–	33.51	56.3 ± 0.2 55.8-57.0	487.5 ± 9.3 463.3-524.5	0.86±0.02 0.82-0.92	531.5 ± 6.1 510.4-548.8	0.97±0.01 0.93-1.00	608.6 ± 14.6 575.1-660.5
41 $G_6$3:1$G_6$3:1$G_6$3:1G_6	39.15	4.16	34.99	–	38.9 ± 0.2 38.2-39.6	350.2 ± 9.7 308.4-372.7	0.90±0.02 0.81-0.92	386.0 ± 9.1 362.5-407.9	1.02±0.03 0.93-1.13	577.3 ±23.1 468.9-616.8
42 1:1C1:1C1:1C1:1	38.29	27.11	11.18	–	76.3 ± 0.4 75.0-78.2	415.8 ±12.8 367.6-449.5	0.54±0.01 0.49-0.59	σ^ε	ε^ε	σ^ε
43 3:1C3:1C3:1C3:1	38.71	21.71	17.00	–	67.5 ± 0.2 66.9-68.0	349.8 ± 13.2 318.6-409.6	0.52±0.02 0.47-0.61	391.3 ± 12.5 358.1-424.2	0.60±0.02 0.53-0.66	402.1 ± 9.04 370.5-424.2
44 3:1 1:1 3:1 1:1 3:1 1:1 3:1	39.13	13.75	25.38	–	54.6 ± 0.3 53.6-55.4	421.4 ±15.6 370.1-454.3	0.77±0.03 0.69-0.84	439.2 ± 20.3 370.1-518.5	0.82±0.04 0.69-0.96	σ'
45 1:1 1:1 3:1 1:1 3:1 1:1 1:1	38.82	16.45	22.37	–	58.5 ±0.3 57.9-59.6	365.6 ± 5.2 351.8-385.4	0.62±0.01 0.59-0.66	383.9 ± 3.4 371.6-395.5	0.67±0.01 0.65-0.69	425.5 ± 12.7 387.5-470.7
46 $G_6CG_6CG_6CG_6$	38.51	16.17	22.34	–	58.3 ± 0.2 57.9-58.9	344.1 ± 13.3 302.0-394.2	0.59±0.02 0.52-0.68	382.6 ± 3.8 370.1-394.2	0.68±0.01 0.65-0.71	394.8 ± 6.5 370.1-418.4
47 $G_5CG_5CG_5CG_5$	38.51	16.17	–	22.34	59.8 ± 0.2 59.3-60.3	356.5 ±14.2 329.1-404.3	0.60±0.02 0.55-0.67	425.1 ± 10.5 390.1-448.2	0.76±0.02 0.69-0.81	428.0 ± 11.2 390.1-458.9
48 $G_6CG_6CG_6CG_6$	38.51	16.17	22.34 no c.-a.	–	58.6 ± 0.2 58.0-59.3	310.8 ± 8.5 278.2-332.2	0.53±0.01 0.48-0.56	σ^ε	ε^ε	σ^ε

Cont/.....

	V_r %	V_{cf} %	V_{g^6} %	V_{g^5} %	E, KN/mm^2	σ^ε, N/mm^2	ε^ε, %	σ', N/mm^2	ε', %	$\hat{\sigma}$, N/mm^2
49 $G_5CG_5CG_5CG_5$	38.51	16.17	–	22.34 no c.-a.	59.7± 0.2 59.0-60.2	315.8 ± 7.2 301.3-339.3	0.53±0.01 0.50-0.57	σ^ε	ε^ε	σ^ε
50 $G_6CG_6CG_6CG_6$	38.51	16.17	22.34 A1100	–	58.0± 0.2 57.5-58.8	345.2 ± 7.8 314.1-369.1	0.60±0.01 0.54-0.64	384.9 ± 4.6 375.6-404.3	0.68±0.01 0.67-0.71	σ'
51 $G_5CG_5CG_5CG_5$	38.51	16.17	–	22.34 A1100	60.1± 0.3 59.0-60.9	381.8 ±14.7 336.1-446.4	0.63±0.02 0.56-0.74	431.2 ±11.4 377.6-454.7	0.74±0.02 0.65-0.78	σ'
52 $G_6CG_6CG_6CG_6$	38.51	16.17	22.34 A187	–	57.9± 0.2 57.2-58.4	332.5 ± 3.2 319.8-341.5	0.57±0.01 0.56-0.59	345.8 ± 3.6 330.7-356.8	0.62±0.01 0.60-0.65	σ'
53 $G_5CG_5CG_5CG_5$	38.51	16.17	–	22.34 A187	60.2± 0.2 59.2-60.9	365.1± 24.5 326.3-485.0	0.61±0.04 0.54-0.82	408.5 ±26.1 333.5-527.7	0.70±0.04 0.57-0.91	σ'
54 $G_6CG_6CG_6CG_6$	38.38	16.04 etched	22.34 A187	–	58.2± 0.2 57.6-58.8	322.2 ± 9.5 295.5-363.0	0.55±0.02 0.51–0.62	355.2± 12.6 322.9-412.0	0.65±0.02 0.57-0.73	σ'
55 $G_5CG_5CG_5CG_5$	38.38	16.04 etched	–	22.34 A187	59.7± 0.2 59.1-60.2	337.2 ± 7.4 315.5-364.4	0.56±0.01 0.54-0.61	390.9 ± 9.9 352.5-419.6	0.68±0.02 0.61-0.74	σ'
56 $G_6CG_6CG_6CG_6$	38.38	16.04 etched	22.34 A1100	–	57.7± 0.3 57.1-58.6	388.3 ± 4.9 365.6-399.8	0.67±0.01 0.64-0.70	σ^ε	ε^ε	σ^ε
57 $G_5CG_5CG_5CG_5$	38.38	16.04 etched	–	22.34 A1100	59.9± 0.3 59.4-60.8	418.0 ±25.2 348.3-533.4	0.70±0.04 0.60-0.88	454.2 ±17.3 409.6-533.4	0.77±0.02 0.69-0.88	σ'
58 $G_6CG_6CG_6CG_6$	38.51	16.17 no c.-a.	22.34 no c.-a.	–	58.1± 0.3 57.0-59.0	295.5 ±12.9 250.7-336.3	0.51±0.02 0.43-0.57	σ^ε	ε^ε	σ^ε
59 $G_5CG_5CG_5CG_5$	38.51	16.17 no c.-a.	–	22.34 no c.-a.	59.9± 0.1 59.3-60.2	300.3 ± 3.7 284.7-312.6	0.50±0.01 0.48-0.52	σ^ε	ε^ε	σ^ε
60 $G_6CG_6CG_6CG_6$	38.51	16.17 no c.-a.	22.34	–	58.5± 0.2 58.2-59.2	334.5 ± 1.8 329.9-341.3	0.57±0.01 0.56-0.59	399.8 ± 9.6 372.9-431.6	0.71±0.02 0.65-0.78	σ'
61 $G_5CG_5CG_5CG_5$	38.51	16.17 no c.-a.	–	22.34	60.1± 0.2 59.7-60.8	388.7 ±12.8 340.6-427.3	0.65±0.02 0.56-0.71	433.0 ± 7.4 403.9-454.8	0.74±0.01 0.68-0.76	437.4 ± 6.0 411.2-454.8

TABLE 17

The Weakest Lower and Upper Stress Levels (Theory According to Rosen[1] and Zweben[3]) for fibres in Parent Composites and the Parent Composites With Fibre Volume Fraction (V_f) of 0.20, 0.40, 0.60 and 0.80.

	V_f	N	Ineffective Length δ, mm	Fibre Failure Stress Levels $\hat{\sigma}_{WF}$, N/mm^2	$\hat{\sigma}_{LF}$, N/mm^2	$\hat{\sigma}_{UF}$, N/mm^2	Composite Failure Stress Levels $\hat{\sigma}_W$, N/mm^2	$\hat{\sigma}_L$, N/mm^2	$\hat{\sigma}_U$, N/mm^2
6000 filament carbon/vinyl ester resin composites	0.2	103869	0.0609	155.8	516.1	1414.3	32.9	109.0	298.7
	0.4	207738	0.0418	142.0	506.2	1497.5	58.0	206.7	611.6
	0.6	311607	0.0296	133.6	502.3	1567.5	80.9	304.2	949.3
	0.8	415476	0.0188	128.3	508.2	1671.9	103.0	408.0	1342.2
600 tex E-glass/vinyl ester resin composites	0.2	31008	0.0598	751.5	1204.5	1842.5	177.1	283.8	425.0
	0.4	61967	0.0409	714.0	1191.8	1889.8	304.6	508.4	798.6
	0.6	92951	0.0290	695.0	1189.3	1934.0	429.2	734.5	1189.1
	0.8	123935	0.0185	681.6	1195.9	1993.0	551.2	967.0	1608.9
500 tex E-glass/vinyl ester resin composites	0.2	37331	0.0573	702.0	1371.0	2445.5	163.1	318.4	548.6
	0.4	74662	0.0393	660.0	1351.5	2529.3	280.0	573.3	1056.7
	0.6	111993	0.0278	636.5	1348.0	2608.5	392.3	830.6	1595.3
	0.8	149324	0.0177	620.4	1357.9	2715.9	501.5	1097.3	2187.9

TABLE 18

The Upper ($\hat{\sigma}_u$), Lower ($\hat{\sigma}_L$) and Weakest Link ($\hat{\sigma}_w$), According to the Theories of Rosen[1] and Zweben[3], and Experimental ($\hat{\sigma}$) Tensile Failure Stresses for 7 Layer Single Fibre Type Composites With Varying Fibre Surface Treatments

Slab	$\hat{\sigma}_u$ N/mm^2	$\hat{\sigma}_L$ N/mm^2	$\hat{\sigma}_w$ N/mm^2	$\hat{\sigma}$ N/mm^2
4 7C as rec.	574.5	195.5	55.2	422.7 389.8-448.0
7 7C no c.-a.	560.3	187.1	57.3	441.1 368.0-482.1
6 7C etched	556.7	193.8	55.3	453.0 420.0-484.7
11 7G as rec.	778.9	497.0	298.2	595.7 525.1-690.5
16 7G no c.-a.	873.0	242.6	51.1	279.0 254.8-298.3
14 7G A187	792.5	220.0	54.7	329.4 323.9-338.3
15 7G A1100	825.3	255.7	62.0	507.1 445.2-554.0
19 7G as rec.	1033.3	562.0	274.9	734.9 707.6-762.0
23 7G no c.-a.	1057.0	374.7	107.3	370.7 315.2-416.3
21 7G A187	1066.5	377.1	106.6	440.8 403.6-478.8
22 7G A1100	1095.7	377.3	104.0	567.4 542.2-600.3

TABLE 19

The Theoretical Range for Composite Failure Stresses ($\hat{\sigma}_1$ and $\hat{\sigma}_2$) following Barry's Model[4] and the Experimental Failure Stresses ($\hat{\sigma}$) of slabs 1 to 23. The subscripts e, u, M and L denote expected (calculated from experimental results), upper, mean and lower stress levels respectively.

Slab	Stress Level	$\hat{\sigma}_1$ (zero fibre debonding) N/mm^2	$\hat{\sigma}_2$ (max. fibre debonding) N/mm^2	$\hat{\sigma}$ N/mm^2	$\hat{\sigma}_e$ N/mm^2
1	$\hat{\sigma}_u$	196.9	180.8	208.3	197.9
	$\hat{\sigma}_M$	184.7	169.8	189.3	
	$\hat{\sigma}_L$	169.9	154.6	172.9	
2	$\hat{\sigma}_u$	260.4	239.8	315.8	258.6
	$\hat{\sigma}_M$	244.7	223.7	260.6	
	$\hat{\sigma}_L$	225.4	204.1	215.6	
3	$\hat{\sigma}_u$	381.9	354.3	405.2	379.8
	$\hat{\sigma}_M$	359.2	330.8	386.8	
	$\hat{\sigma}_L$	331.7	299.6	370.1	
4	$\hat{\sigma}_u$	448.8	415.0	448.0	440.5
	$\hat{\sigma}_M$	422.7	387.9	422.7	
	$\hat{\sigma}_L$	387.9	351.8	389.8	
5	$\hat{\sigma}_u$	580.6	534.8	629.6	561.7
	$\hat{\sigma}_M$	547.7	496.9	573.5	
	$\hat{\sigma}_L$	503.9	451.4	521.4	
6	$\hat{\sigma}_u$	431.3	397.6	484.7	437.1
	$\hat{\sigma}_M$	408.3	373.9	453.0	
	$\hat{\sigma}_L$	376.6	341.3	420.0	
7	$\hat{\sigma}_u$	437.1	404.7	482.1	440.5
	$\hat{\sigma}_M$	411.2	377.7	441.1	
	$\hat{\sigma}_L$	379.2	344.8	368.0	
8	$\hat{\sigma}_u$	403.2	415.1	401.5	382.5
	$\hat{\sigma}_M$	392.5	386.6	358.4	
	$\hat{\sigma}_L$	375.1	357.6	320.0	
9	$\hat{\sigma}_u$	478.7	497.4	526.2	454.5
	$\hat{\sigma}_M$	466.1	463.2	480.8	
	$\hat{\sigma}_L$	447.9	423.3	460.7	
10	$\hat{\sigma}_u$	572.5	593.8	635.5	542.2
	$\hat{\sigma}_M$	557.2	552.8	566.0	
	$\hat{\sigma}_L$	532.5	505.1	490.9	
11	$\hat{\sigma}_u$	662.6	695.5	690.5	622.0
	$\hat{\sigma}_M$	641.4	637.3	595.7	
	$\hat{\sigma}_L$	616.5	582.2	525.1	
12	$\hat{\sigma}_u$	762.6	801.7	867.6	715.1
	$\hat{\sigma}_M$	738.2	734.5	713.6	
	$\hat{\sigma}_L$	709.5	666.9	552.4	

Table 19 Continued

Slab	Stress Level	$\hat{\sigma}_1$ (zero fibre debonding) N/mm^2	$\hat{\sigma}_2$ (max fibre debonding) N/mm^2	$\hat{\sigma}$ N/mm^2	$\hat{\sigma}_e$ N/mm^2
13	$\hat{\sigma}_U$	850.5	900.9	839.0	796.6
	$\hat{\sigma}_M$	827.7	825.9	798.9	
	$\hat{\sigma}_L$	791.3	731.6	754.5	
14	$\hat{\sigma}_U$	618.0	547.8	338.3	
	$\hat{\sigma}_M$	573.1	488.9	329.4	
	$\hat{\sigma}_L$	518.5	423.3	322.9	
15	$\hat{\sigma}_U$	647.4	579.3	554.0	
	$\hat{\sigma}_M$	602.0	517.2	507.0	
	$\hat{\sigma}_L$	547.2	447.5	445.2	
16	$\hat{\sigma}_U$	677.3	587.1	298.3	
	$\hat{\sigma}_M$	624.5	526.8	279.0	
	$\hat{\sigma}_L$	565.3	458.8	254.8	
17	$\hat{\sigma}_U$	625.0	630.4	546.1	511.3
	$\hat{\sigma}_M$	600.8	582.6	520.9	
	$\hat{\sigma}_L$	571.7	529.3	490.9	
18	$\hat{\sigma}_U$	752.1	758.9	630.1	611.3
	$\hat{\sigma}_M$	723.0	698.4	595.7	
	$\hat{\sigma}_L$	687.9	634.5	543.8	
19	$\hat{\sigma}_U$	868.3	885.2	762.0	702.4
	$\hat{\sigma}_M$	838.0	808.4	734.9	
	$\hat{\sigma}_L$	794.1	727.5	707.6	
20	$\hat{\sigma}_U$	991.5	1007.2	824.9	793.6
	$\hat{\sigma}_M$	953.3	920.0	771.1	
	$\hat{\sigma}_L$	903.3	828.3	732.8	
21	$\hat{\sigma}_U$	848.2	785.2	478.8	
	$\hat{\sigma}_M$	799.6	707.3	440.8	
	$\hat{\sigma}_L$	735.5	621.9	403.6	
22	$\hat{\sigma}_U$	875.5	799.7	600.3	
	$\hat{\sigma}_M$	820.9	719.2	567.4	
	$\hat{\sigma}_L$	756.8	638.0	542.2	
23	$\hat{\sigma}_U$	842.2	775.9	416.3	
	$\hat{\sigma}_M$	790.5	704.8	370.7	
	$\hat{\sigma}_L$	729.3	626.3	315.2	

TABLE 20

Summary of the Expected Tensile Properties of the Parent Composites (Subscript e) and the Theoretical Rule of Mixture Properties (Subscript RM) of their Hybrid Composites.

Composite System	Elastic Modulus E_e KN/mm^2	Elastic Limit σ_e^E N/mm^2	ε^E %
C (any)*/V.-E.	$3.4V_m + 242.1\ V_{cf}$	$16.0V_m + 1141.0\ V_{cf}$	0.47
G_6 (as rec.)/V.E.	$3.4V_m + 75.6V_{g6}$	$63.0V_m + 1493.0\ V_{g6}$	1.96
G_6 (A187)/V.E.		$35.2V_m + 787.8\ V_{g6}$	1.04
G_6 (A1100)/V.E.		$54.0V_m + 1212.9V_{g6}$	1.61
G_6 (no c.-a.)/V.E.		$30.0V_m + 667.0V_{g6}$	0.88
G_5 (as rec.)/V.E.	$3.4V_m + 83.7V_{g5}$	$64.5V_m + 1696.4\ V_{g5}$	2.02
G_5 (A187)/V.E.		$42.5V_m + 1061.2V_{g5}$	1.26
G_5 (A1100)/V.E.		$55.0V_m + 1365.5V_{g5}$	1.63
G_5 (no c.-a.)/V.E.		$36.0V_m + 892.0V_{g5}$	1.06
	E_{RM} KN/mm^2	σ_{RM}^E N/mm^2	ε_{RM}^E %
C (any)/G_6 (any)/V.E.	$3.4V_m + 242.1V_{cf} + 75.6V_{g6}$	$16.0V_m + 1141.0V_{cf} + 358.0\ V_{g6}$	0.47
C (any)/G_5 (any)/V.E.	$3.4V_m + 242.1V_{cf} + 83.7V_{g5}$	$16.0V_m + 1141.0V_{cf} + 394.7V_{g5}$	0.47
		Maximum Stress $\hat{\sigma}_{RM}$ N/mm^2	Maximum Strain $\hat{\varepsilon}_{RM}$ %
C (any)/G_6 (as rec.)/V.E.		$63.0Vm + 1493.0V_{g6}$	1.96
C (any)/G_6 (A187)/V.E.		$35.2V_m + 787.8V_{g6}$	1.04
C (any)/G_6 (A1100)/V.E.		$54.0V_m + 1212.9V_{g6}$	1.61
C (any)/G_6 (no c.-a.)/V.E.		$30.0V_m + 667.0\ V_{g6}$	0.88
C (any)/G_5 (as rec.)/V.E.		$64.5V_m + 1696.4V_{g5}$	2.02
C (any)/G_5 (A187)/V.E.		$42.5V_m + 1061.2V_{g5}$	1.26
C (any)/G_5 (A1100)/V.E.		$55.0V_m + 1365.5V_{g5}$	1.63
C (any)/G_5 (no c.-a.)/V.E.		$36.0V_m + 892.0V_{g5}$	1.06

* The contents of the brackets after the fibre type indicates the fibre surface treatment

TABLE 21

The Average Experimental (Exptal) and the Theoretical, According to the Rule of Mixtures (R.M.), Tensile Properties of the Hybrid Composite Slabs 37 to 61

Slab Number and Lay-up Sequence		Elastic Modulus E, KN/mm^2	Elastic Limit		Initial Failure		Maximum Stress $\hat{\sigma}$, N/mm^2
			σ^E, N/mm^2	ε^E, %	σ', N/mm^2	ε', %	
37	Exptal	37.3	168.5	0.45	σ^E	ε^E	213.8
CG_6G_6C	R.M.	37.2	173.8	0.47	σ^E_{RM}	ε^E_{RM}	222.7
38	Exptal	71.2	336.0	0.47	398.5	0.62	404.7
$CG_6CG_6G_6CG_6C$	R.M.	71.0	331.5	0.47	σ^E_{RM}	ε^E_{RM}	382.5
39	Exptal	53.3	415.3	0.78	466.7	0.91	511.8
$G_6G_6CG_6G_6CG_6G_6$	R.M.	53.3	250.2	0.47	σ^E_{RM}	ε^E_{RM}	542.2
40	Exptal	56.3	487.5	0.86	531.5	0.97	608.6
$G_5G_5CG_5G_5CG_5G_5$	R.M.	56.0	262.5	0.47	σ^E_{RM}	ε^E_{RM}	611.3
41	Exptal	38.9	350.2	0.90	386.0	1.02	577.3
G_6 3:1 G_6 3:1 G_6 3:1 G_6	R.M.	38.6	181.8	0.47	σ^E_{RM}	ε^E_{RM}	563.4
42	Exptal	76.3	415.8	0.54	σ^E	ε^E	σ^E
1:1 C 1:1 C 1:1 C 1:1	R.M.	76.2	354.9	0.47	σ^E_{RM}	ε^E_{RM}	σ^E_{RM}
43	Exptal	67.5	349.8	0.52	391.3	0.60	402.1
3:1 C 3:1 C 3:1 C 3:1	R.M.	67.5	314.9	0.47	σ^E_{RM}	ε^E_{RM}	σ^E_{RM}
44	Exptal	54.6	421.4	0.77	439.2	0.82	σ'
3:1 1:1 3:1 1:1 3:1 1:1 3:1	R.M.	54.5	255.3	0.47	σ^E_{RM}	ε^E_{RM}	425.9
45	Exptal	58.5	365.6	0.62	383.9	0.67	425.5
1:1 1:1 3:1 1:1 3:1 1:1 1:1	R.M.	58.8	274.9	0.47	σ^E_{RM}	ε^E_{RM}	382.9

Cont/....

Slab Number and Lay-up Sequence		Elastic Modulus E, KN/mm^2	Elastic Limit		Initial Failure		Maximum Stress
			σ^E, N/mm^2	ε^E, %	σ', N/mm^2	ε', %	$\hat{\sigma}$, N/mm^2
46	Exptal	58.3	344.1	0.59	382.6	0.68	394.8
$G_6CG_6CG_6CG_6$	R.M.	58.1	271.7	0.47	σ^E_{RM}	ε^E_{RM}	382.5
47	Exptal	59.8	356.5	0.60	425.1	0.76	428.0
$G_5CG_5CG_5CG_5$	R.M.	59.9	279.9	0.47	σ^E_{RM}	ε^E_{RM}	429.1
48 (G_6 = no c.-a. C = as rec.)	Exptal	58.6	310.8	0.53	σ^E	ε^E	σ^E
$G_6CG_6CG_6CG_6$	R.M.	58.1	271.7	0.47	σ^E_{RM}	ε^E_{RM}	σ^E_{RM}
49 (G_5 = no c.-a. C = as rec.)	Exptal	59.7	315.8	0.53	σ^E	ε^E	σ^E
$G_5CG_5CG_5CG_5$	R.M.	59.9	279.9	0.47	σ^E_{RM}	ε^E_{RM}	σ^E_{RM}
50 (G_6 = A1100 C = as rec.)	Exptal	58.0	345.2	0.60	384.9	0.68	σ'
$G_6CG_6CG_6CG_6$	R.M.	58.1	271.7	0.47	σ^E_{RM}	ε^E_{RM}	312.9
51 (G_5 = A1100 C = as rec.)	Exptal	60.1	381.8	0.63	431.2	0.74	σ'
$G_5CG_5CG_5CG_5$	R.M.	59.9	279.9	0.47	σ^E_{RM}	ε^E_{RM}	347.8
52 (G_6 = A187 C = as rec.)	Exptal	57.9	332.5	0.57	345.8	0.62	σ'
$G_6CG_6CG_6CG_6$	R.M.	58.1	271.7	0.47	σ^E_{RM}	ε^E_{RM}	σ^E_{RM}
53 (G_5 = A187 C = as rec.)	Exptal	60.2	365.1	0.61	408.5	0.70	σ'
$G_5CG_5CG_5CG_5$	R.M.	59.9	279.9	0.47	σ^E_{RM}	ε^E_{RM}	σ^E_{RM}
54 (G_6 = A187 C = etched)	Exptal	58.2	322.2	0.55	355.2	0.65	σ'
$G_6CG_6CG_6CG_6$	R.M.	57.8	270.3	0.47	σ^E_{RM}	ε^E_{RM}	σ^E_{RM}
55 (G_5 = A187 C = etched)	Exptal	59.7	337.2	0.56	390.9	0.68	σ'
$G_5CG_5CG_5CG_5$	R.M.	59.6	278.5	0.47	σ^E_{RM}	ε^E_{RM}	σ^E_{RM}

Cont/....

Slab Number and Lay-up Sequence		Elastic Modulus E, KN/mm^2	Elastic Limit		Initial Failure		Maximum Stress
			σ^{ϵ}, N/mm^2	ϵ^{ϵ}, %	σ', N/mm^2	ϵ', %	$\hat{\sigma}$, N/mm^2
56 (G_6 = Al100 C = etched)	Exptal	57.7	388.3	0.67	σ^{ϵ}	ϵ^{ϵ}	σ^{ϵ}
$G_6CG_6CG_6CG_6$	R.M.	57.8	270.3	0.47	σ^{ϵ}_{RM}	ϵ^{ϵ}_{RM}	312.9
57 (G_5 = Al100 C = etched)	Exptal	59.9	418.0	0.70	454.2	0.77	σ'
$G_5CG_5CG_5CG_5$	R.M.	59.6	278.5	0.47	σ^{ϵ}_{RM}	ϵ^{ϵ}_{RM}	347.8
58 (G_6 = no c.-a. C = no c.-a.)	Exptal	58.1	295.5	0.51	σ^{ϵ}	ϵ^{ϵ}	σ^{ϵ}
$G_6CG_6CG_6CG_6$	R.M.	58.1	271.7	0.47	σ^{ϵ}_{RM}	ϵ^{ϵ}_{RM}	σ^{ϵ}_{RM}
59 (G_5 = no c.-a. C = no c.-a.)	Exptal	59.9	300.3	0.50	σ^{ϵ}	ϵ^{ϵ}	σ^{ϵ}
$G_5CG_5CG_5CG_5$	R.M.	59.9	279.9	0.47	σ^{ϵ}_{RM}	ϵ^{ϵ}_{RM}	σ^{ϵ}_{RM}
60 (G_6 = as rec. C = no c.-a.)	Exptal	58.5	334.5	0.57	399.8	0.71	σ'
$G_6CG_6CG_6CG_6$	R.M.	58.1	271.7	0.47	σ^{ϵ}_{RM}	ϵ^{ϵ}_{RM}	382.5
61 (G_5 = as rec. C = no c.-a.)	Exptal	60.1	388.7	0.65	433.0	0.74	437.4
$G_5CG_5CG_5CG_5$	R.M.	59.9	279.9	0.47	σ^{ϵ}_{RM}	ϵ^{ϵ}_{RM}	429.1

TABLE 22

Comparison of the Average Tensile Properties and the Interlaminar Shear Strengths (τ_{il}) of Pairs of Hybrid Composites from Slabs 46 to 61 Differing in Respect to the Surface Treatment of Their Constituent Carbon Fibres.

Slab	E-Glass Type	Surface Treatment G	Surface Treatment C	Elastic Limit σ^E N/mm^2	Elastic Limit ε^E %	First Failure σ' N/mm^2	First Failure ε' %	Maximum Stress N/mm^2	τ_{il} N/mm^2	Comments
46	G_6	as rec.	as rec.	344.1	0.59	382.6	0.68	394.8	49.9	
60	G_6	as rec.	no c-a	334.5	0.57	399.8	0.71	399.8	48.1	There is no significant difference in the tensile properties of either slabs 46 and 60 or slabs 47 and 61.
47	G_5	as rec.	as rec.	356.5	0.60	425.1	0.76	428.0	47.2	
61	G_5	as rec.	no c-a	388.7	0.65	433.0	0.74	437.4	50.9	
48	G_6	no c-a	as rec.	310.8	0.53	310.8	0.53	310.8	48.6	There is no significant difference in the tensile properties of slabs 48 and 58. The analysis of the variance of the data for slabs 49 and 59 shows the differences in ε' σ^E, σ' and $\hat{\sigma}$ to be insifnificant but the difference in ε^E values to be significant at the 95% level.
58	G_6	no c-a	no c-a	295.5	0.51	295.5	0.51	295.5	49.3	
49	G_5	no c-a	as rec.	315.8	0.53	315.8	0.53	315.8	48.7	
59	G_5	no c-a	no c-a	300.3	0.50	300.3	0.50	300.3	49.3	
50	G_6	A1100	as rec.	345.2	0.60	384.9	0.68	384.9	99.9	The differences in σ^E and ε^E for slabs 50 and 56 are highly significant. There is no significant difference in σ', ε' or $\hat{\sigma}$ or in any of the tensile properties of slabs 51 and 57.
56	G_6	A1100	etched	388.3	0.67	388.3	0.67	388.3	101.8	
51	G_5	A1100	as rec.	381.8	0.63	431.2	0.74	431.2	97.9	
57	G_5	A1100	etched	418.0	0.70	454.2	0.77	454.2	>90.4	
52	G_6	A187	as rec,	332.5	0.57	345.8	0.62	345.8	74.4	There is no significant difference between the tensile properties of either slabs 52 and 54 or slabs 53 and 55.
54	G_6	A187	etched	322.2	0.55	355.2	0.65	355.2	66.7	
53	G_5	A187	as rec.	365.1	0.61	408.5	0.70	408.5	78.3	
55	G_5	A187	etched	337.2	0.56	390.9	0.68	390.9	63.4	